Romanian Journal of MINERALOGY

continuation of

DĂRI DE SEAMĂ ALE ŞEDINŢELOR INSTITUTULUI DE GEOLOGIE ŞI GEOFIZICĂ
COMPTES RENDUS DES SÉANCES DE L'INSTITUT DE GÉOLOGIE ET GÉOPHYSIQUE
(1. Mineralogie-Petrologie)

Founded 1906 by the Geological Institute of Romania

ISSN 1220-5621

Vol. 79

CONTENTS

(Contents continued on outside back cover)

Institutul Geologic al României
Bucureşti – 1999

GEOLOGICAL INSTITUTE OF ROMANIA
Director General Dr. **G. Udubaşa** Member of the Romanian Academy

The **Geological Institute of Romania** is now publishing the following periodicals:

Romanian Journal of Mineralogy
Romanian Journal of Petrology
Romanian Journal of Mineral Deposits
Romanian Journal of Paleontology
Romanian Journal of Stratigraphy
Romanian Journal of Tectonics and Regional Geology
Romanian Journal of Geophysics
Anuarul Institutului Geologic al României
Memoriile Institutului Geologic al României

Romanian Journals supersede "Dări de Seamă ale Şedinţelor" and "Studii Tehnice şi Economice", whose apparition goes back to 1910. Besides regular volumes, each series may occasionally contain Supplements (for abstracts and excursion guides to congresses and symposia held in Romania) and Special Issues (for larger papers of special interest). "Anuarul Institutului Geologic al României" appears in a new form, containing both the annual activity report and review papers.

Editorial Board: Gheorghe Udubaşa (chairman), Şerban Veliciu (vice-chairman), Tudor Berza, Marcel Mărunţiu, Grigore Pop, Gheorghe Popescu, Vlad Roşca, Anatol Rusu, Mircea Săndulescu

Managing Editor: Cecilia Vamvu

Executive Secretary: Georgeta Borlea

Editorial Office:
Geological Institute of Romania
Str. Caransebeş Nr. 1, RO – 79678 Bucureşti – 32
Tel. (+40) 1 - 224 20 91, 1 - 224 20 93, 1 - 224 15 30
Fax (+40) 1 224 04 04
e-mail geol@ns.igr.ro
http://www.igr.ro

The editor has changed the name as follows: Institutul Geologic al României (1906–1952), Comitetul Geologic (1953–1966), Comitetul de Stat al Geologiei (1967–1969), Institutul Geologic (1970–1974), Institutul de Geologie şi Geofizică (1975–1993), Institutul Geologic al României (since 1994).

ROMANIAN JOURNAL OF MINERALOGY supersedes "Dări de seamă ale Şedinţelor", Series 1/Mineralogie-Petrologie - the last volume with this title being No. 74.

Scientific Editor: Gheorghe Udubaşa

Volume editorial work: Gabriela Ioane

Rom. J. Mineralogy is also the Bulletin of the Mineralogical Society of Romania, a member of the EMU and IMA. Thus, this journal follows the rules of the Commission on New Minerals and Mineral Names of the IMA in all the matters concerning mineral names and nomenclature.

The manuscripts should be sent to the scientific editor and/or executive secretary. Correspondence concerning advertisments, announcements and subscriptions should be sent to the Managing Editor.

ISSN 1220-5621
Classification index for libraries 55(058)

Printed by the Geological Institute of Romania
Bucharest

CONTENTS

Rom. J. Mineralogy, 79, p. 3-30, Bucureşti, 1999

ADVANCES IN MINERALOGY OF ROMANIA

Gheorghe UDUBAŞA

Institutul Geologic al României, str. Caransebeş 1, 78344, Bucureşti

Key words: Mineral species inventory. Type localities.

Abstract: To date over 700 valid mineral species are known in Romania, to which many mineral varieties add. In addition, about 70 mineral names are directly related to the development of mineralogy in the country (Udubaşa et al., 1992). Several minerals have the type localities in Romania. There are also many occurrences bearing rare and very rare minerals, such as bannisterite, cymrite, greigite, hetaerolite, nambulite, zoubekite etc., which were recently identified. Among the more common minerals there are a lot showing either uncommon frequency, abundance and crystal forms, e.g. stibnite in the Baia Mare mining area, or unusual mode of presentation, e.g. greigite concretions, hydrothermal vein ilvaite at Turţ, biotite "balls" within the medium grade metamorphic rocks of the Sebeş Mts. etc.

Some characteristic mineral associations

Alongwith the rock salt and oil, the Au-Ag-Te minerals, the Bi sulphosalts, the skarn and manganese minerals form typical associations and occurrences in Romania, some of them being or becoming celebrated, at least in Europe. All these associations occur in areas with old mining activity. In the last time many minerals were also identified in caves. The Au-Ag-Te minerals typically occur in the Metaliferi Mts./ siebenbürgisches Erzgebirge, in relation with Miocene volcanics of dominant andesitic composition. The celebrated "Golden Quadrangle" belongs here, having the four "pillars" at Săcărâmb, Zlatna, Baia de Arieş and Căraciu. Săcărâmb / Nagyag is the type locality of many tellurides, nagyagite included, for which many modern investigations have been undertaken, e.g. Mössbauer spectroscopy, showing the gold to be trivalent (Udubaşa et al., 1993), microprobe analyses and microhardness measurements (Lupulescu et al., 1993; Popescu, Simon, 1995), crystal structure determination (Stanley et al., 1994). The old problem of two or even three nagyagite phases, suspected by Giuşcă as early as 1937, has been partly solved by the discovery of the arsenian nagyagite (Simon et al., 1994). Outside the "Golden Quadrangle" the telluride minerals were scarcely reported in isolated occurrences and minor amounts: at Stânceni, Călimani Mts. (hessite, petzite; Peltz et al., 1982), Rodna (hessite; Constantiniuc et al., 1987) and Băiţa, Baia Mare area (altaite, hessite, petzite, sylvanite; Butucescu et al., 1963).

The Bi minerals typically develop within the skarns formed in connection with subduction related magmatites of K_3-Pg_1 age and dominant granodioritic composition. The associated ores are either copper-rich (Moldova Nouă, Sasca Montană) or iron-rich (Ocna de Fier, Băişoara) as well as with dominant polymetallic associations (Dognecea, Băiţa Bihor, Tincova, Ruşchiţa).

However, the presence of the Bi minerals is a common feature, which allows a "Bi line" to trace in West Romania. The Bi minerals are extremely fine grained and generally show unusual complex intergrowths, a fact long time preventing the true identification of minerals species. The "rezbanyite" case story is significant in this respect, it being proved to represent a fine intergrowth of several phases with dominant paderaite as a new mineral (Mumme, Zak, 1985). The progress made in knowing these minerals was shown in the review paper of Cioflica et al. (1995), new identifications including pekoite, cupropavonite, krupkaite, kobellite etc. Lupulescu et al. (1993) repoted ingodite at Valea Seacă near Băiţa Bihor. New data on the Bi minerals at Oraviţa-Ciclova and Băiţa Bihor and Valea Seacă, respectively are critically presented by Ilinca (1992) Ilinca et al. (1993), Ilinca, Cook (1995), Ilinca, Marincea (1996). A new mineral, makovickyite, was also described at Băiţa Bihor (Zak et al., 1994).

In the last case, very fine intergrowths of bismuthinite derivatives chemically corresponding to hammarite-friedrichite, hodrushite, cuprobismutite and a Cu-rich makovickyite have been identified, as well as many still problematic phases which are now further investigated.

Other Bi bearing occurrences of minor importance were recently studied, proving the presence of lillianite at Ditrău (Damian et al., 1992), of bismuthinite associated with native bismuth and a Bi_3S_2 phase within the shear zone related gold ores at Costeşti, South Carpathians (Udubaşa, Ţopa, 1995), of berryite, izoklakeite, nuffieldite etc. in the ores at Baia Borşa - Toroiaga (Cook, 1997), of wittichenite, bismuthinite and native bismuth in the Leaota Mts. (Udubaşa, 1988) etc.

Significant data were also obtained concerning the distribution and properties of the skarn related endogene borates (Marincea, 1993; 1997; Marincea, Cristea, 1995; Marincea, Guy, 1997). Ludwigite is the dominant borate at Ocna de Fier and Băişoara whereas szaibelyite typically develops at Băiţa Bihor and Pietroasa.

Two major belts of Mn ores are known in the East and in the South Carpathians, forming stratiform bodies in medium grade metamorphics. Isolated deposits are also known at Răzoare, Preluca Mts., and at Delineşti, Semenic Mts.

Significant results as concerns the mineralogical aspects were obtained in studying especially the Mn occurrences in the Bistriţa Mts. (Hârtopanu, in Nedelcu et al., 1997; Hârtopanu et al., 1996; Hartopanu, Scott, 1997). Numerous Mn-silicates, sometimes Li-containg such as nambulite, bannisterite, kozulite, norrishite, kelyite were thus identified as major phases in which a large number of other minerals have been found: silicate-arsenates (schallerite, nelenite), Zn-Be-Ti-Ba silicates (genthelvite, fraipontite, bafertisite), rare sulphides: stannite, chatkalite, carrolite, cobaltite, rare oxides: akhtensite, vernadite, ashanite etc.

A further fertile field of investigation is the study of cave minerals. The recently described minerals in such environments include bobierrite, barrandite, vivianite, wawellite, brushite, romanéchite, huntite, mirabilite, thenardite etc. An overview hereupon has been given by Onac (1996).

Is there a real progress?

The progress made in the mineralogical reconnaissance of Romania can be shown at least by a significant increase of number of minerals identified; in 1966 there were about 450 mineral species whereas in 1998 over 700 minerals are known, i.e. an increase by 25% (Fig. 1). The foundation of the Mineralogical Society of Romania (MSR) in 1992 contributed much to the stimulation of mineralogical research in our country. New occurrences were described, many novelties in old occurrences were reported either by investigation of old mining "remnants" or of museum materials. The achievements were noted at every SMR symposia (Udubaşa, 1992, 1993, 1995, 1997).

There is a number of mineral occurrences in Romania for which the term "sacred monsters" was proposed (Udubaşa, 1994). The selection was based both on the number of the mineral species and on their rarity, as well as on some crystallographic features. Figure 2 shows the distribution of mineral occurrences in Romania and the position of several "sacred monsters".

It is expected that the alkaline massif of Ditrău will soon produce an important growth of mineral species, as about 1/5 of the minerals approved by the CNMMN-IMA in the last years originate in such environments. The same is true for several Mn occurrences.

As shown above, the most interesting and characteristic mineral associations or occurrences in Romania are the gold-silver tellurides, the Bi minerals, the skarn minerals with associated borates and the manganese minerals, to which also the cave minerals add. The important Baia Mare mining district contains base metal ore deposits of prime importance in which the abundance of Sb is obvious. Besides the "Bi line" in West Romania, related to skarn ores occurred in connection with K_3-Pg_1 magmatites, a "Sb line" can be delineated in North Romania, containing both unusual amounts of stibnite and numerous Sb sulphosalts. Such occurrences are related to Neogene volcanics resulted from the down break-off a subduction slab. They contrast the Neogene volcanics in the Metaliferi Mts., that represent extensional magmatites, emplaced in grabens connected with Badenian back-arc riftogenesis (Balintoni et al., 1996). Here the unusual gold richness and the abundance of porphyry coppers are very characteristic features. It is perhaps not a pure coincidence that all or nearly all the significant mineral occurrences in Romania lie beneath the contacts between the cratons (as defined by Balintoni, 1996). However, the Major Tethysian Suture - MTS (Săndulescu, 1984) represents the most important primary source of metals. The MTS is largely developed in the SW part of Romania, where a first order "gold spot" and a significant number of porphyry copper systems occur on a relatively limited area. The "Bi-line" in West and the "Sb-line" in North are related to convergent plate

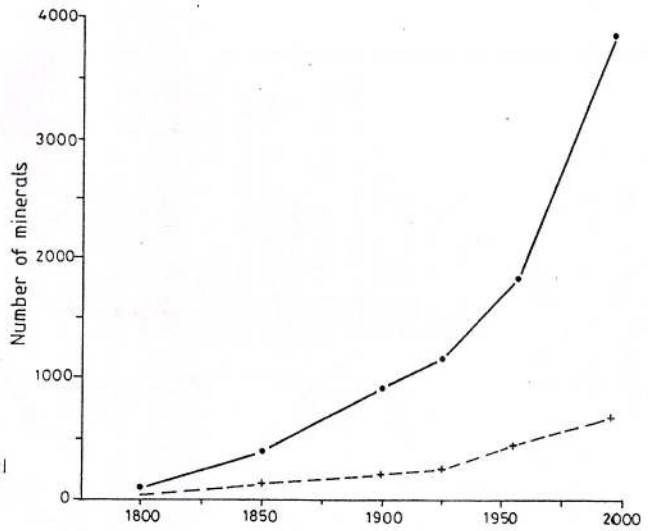

Fig. 1 – Increase of the minerals number in the world (solid line) and in Romania (dashed line)

boundaries, showing however significant differences in age of the associated igneous rocks and in the type of plate convergence. The geochemical features of the banatitic, i.e. K_3-Pg_1 ores (Bi rich) and the Miocene ores (Sb rich) might suggest different depths of generating magmas (and thus the ores), seemingly greater in the case of banatites.

Some problems of mineralogical nomenclature

The following list of minerals includes practically all the mineral names used up to now in Romania. Some inconsistencies in writing the mineral names mostly related to etymology should be therefore corrected according to the recommendations of IMA, especially of CNMMN. Old names and varietal names appear together with discredited mineral species, in the last case by specifying the new status of the mineral, either mixtures or synonyms. Minerals having type localities in Romania appear in bold capital letters (e.g. **NAGYAGITE**) as against the discredited mineral names (e.g. MONSMEDITE). Formulas are given only in a limited number of cases, especially for "persistent errors" such as valleriite. Romanian mineral names were added only for words significantly differing from English. Names of mineral groups are italicized (in paranthesis - mineral species found in Romania).

Although an attempt was made to collect all the names of the mineral species found or used in Romania it was quite impossible to cover all the literature data. Old German mineral names are still missing except some few more common names such as Fahlerz, Rädelerz etc.

The pyroxenes and amphiboles are presented according to the IMA nomenclature and classifications (Morimoto et al., 1978; Leake et al., 1997). For the REE containing minerals it was not always possible to give the correct formula, e.g. monazite - (La) as a result of missing data. If any indetermination exists, the mineral name is marked with a question mark. The priority of a mineral name or of the locality is marked with an exclamation mark if the status is still obscure (presumed, not surely proved).

Acanthite (Rom.: acantit)
Acerdese (= manganite)
Acmite (= aegirine)
Actinolite
Aedelfosite = Laumontite
Adularia (Rom.: adular, var. ortoză)
Aegirine (Rom.: egirin)
Aeschynite - (Y)
Agalmatolite (= fine-grained variety of pyrophillite; var. fin granulară de pirofilit)
Agate (= banded chalcedony; calcedonie rubanată)
Aikinite
ALABANDITE (!) (Săcărâmb? described as "schwarze Blende" by M. von Reichenstein in 1784; other syn.: Manganblende, Manganglanz. The origin of the name alabandine is questionable. See Mârza et al. (1993) for details.)
Albite

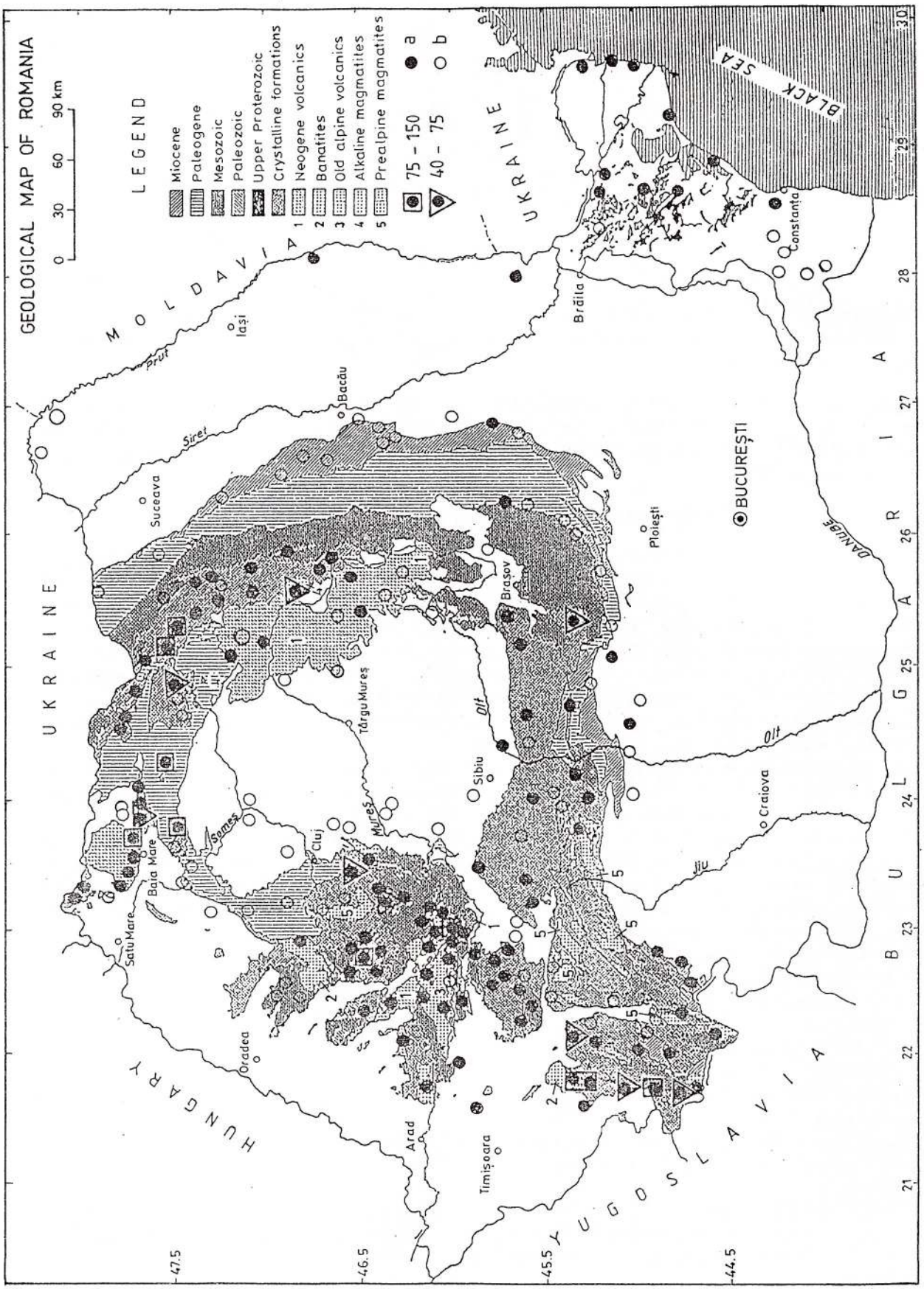

Fig. 2 – Distribution of metalliferous (•) and nonmetalliferous (o) occurrences and "sacred monsters" with a large number of minerals (more than 40 species).

Aleksite
Algodonite
Aliettite (interstratificaţie regulată talc - smectit trioctaedric)
Allanite - (Ce)
Alleghanyite
Allemontite (= stibarsen)
Allochroite (= andradite)
Alloclase (= alloclasite)
ALLOCLASITE (Oraviţa)
Allophane (Rom.: alofan)
Alluaudite
Almandine
Almashite (var. amber; var. chilimbar)
Altaite
Alumino - winchite (= winchite)
Aluminite
Alunite
Alunogen
Amber
Ambligonit (Engl.: amblygonite)
Amblygonite (Rom.: ambligonit)
Amesite
Ametist (Engl.: amethyst)
Amethyst (Rom.: ametist; var. cuarţ)
Amiant (fibrous variety of amphiboles; var. fibroase de amfiboli)
Analcime
Anatase
Andalusite
Andesine
ANDORITE (Baia Sprie)
Andradite
Anglesite
Anhydrite (Rom.: anhidrit)
Ankerite
Annabergite
Annite
Anorthite (Rom.: anortit)
Anorthoclase (Rom.: anortoză)
Anortoză (= anorthoclase)
Anosovit (Ti_3O_5; meteorites, synthetic product; meteoriţi, produs sintetic)
Antigorite
Antimonite (syn. stibnite; Rom.: stibină)
Antimony (Rom.= antimoniu; stibin)
Anthophyllite (Rom.= antofilit)
Apatite group (chlorapatite, fluorapatite, hydroxylapatite, carbonate - chlorapatite, carbonate - hydroxylapatite)
Aphrosiderite (var. chamoisite; var. chamosit)
Aphtitalite
Apophyllite group (Rom.: apofilit) (fluorapophyllite, hydroxyapophyllite)
Aragonite
Arakawaite (= veszelyite)
ARDEALITE (Cioclovina cave)
Arfvedsonite
Argentite (dimorph of acanthite, stable above 179^{0}C; matter of natural argentite is still open. Argentite occurrences in Romania have been transfered to acanthite; dimorf al acantitului, stabil

peste 179^{0}C; problema a. natural rămâne deschisă. Ocurenţele de a. din Romania au fost transferate acantitului.)

Argentopyrite (Rom.: argentopirita)

Argint (Engl.: silver)

Argyrodite (Rom.: argirodit)

Argyropyrite (Rom.: argiropirită) (stenbergite paramorphosis after argentopyrite; paramorfoză de sternbergit după argentopirită)

Argyrose (= argentite)

Arizonite

Armalcolite (Săbău et al., 1997)

Arsenic (Rom.: arsen)

Arsenolite

Arsenopyrite (Rom.: arsenopirită; syn.: mispichel)

Arsenosulvanite

Artinite

Asbolane

Ashanite (Hârtopanu, Scott, 1997)

Ascharit (syn. szaibelyit)

Astrophyllite (Rom.: astrofilit)

Attapulgite (= palygorskite)

Augite

Aur (Engl.: Gold)

Aurichalcite

Auripigment (Engl.: orpiment)

Autunite

Awaruite

Axinite group (ferro-axinite)

Azbest (fibrous varieties of serpentine minerals and amphiboles; var. fibroase de minerale serpentinice şi amfiboli)

Azurite

Baddeleyite

BADENITE (= mixture of bismuth, safflorite and modderite; amestec bismut, safflorit şi modderit) (Bădeni, Leaota Mts.)

Bafertisite (Hârtopanu, Scott, 1997)

Bannisterite

Barite (Rom.: baritină)

Barkevicit (= ferro-pargasitic hornblende; hornblendă fero-pargasitică)

Barrandit (intermediary between strengite and variscite; interm. între strengit şi variscit)

Barroisite

Bassanite

Bastite (coplex alteration product of enstatite, formed of serpentine minerals and talc; produs complex de alteraţie a enstatitului, alcătuit din min. serpentinice şi talc)

Bastnäsite - (La)

Bauerite (altered biotite, colourless; partly amorphous; biotit alterat, decolorat; în parte amorf)

Becquerelite

Beidellite

Bementite

Benavidesite

Benjaminite

Bentonite (rock mostly formed of montmorillonite; rocă alcătuită predominant din montmorillonit)

Beril (Engl.: Beryl)

Berryite

Berthierine

Berthierite

Beryl (Rom.: beril)

Betekhtinite
BIHARIT (Băiţa Bihor; mixture of magnesium silicates, calcite, dolomite etc.; see Papp, 1992; amestec de silicaţi magnezieni, calcit, dolomit etc.)
Biotite
Birnessite
Bismite
Bismuth
Bismuthinite (Rom.: bismutină)
Bismutite
Bixbyite
Blenda (Engl.: Sphalerite; e. am.: sfalerite)
Blödite
Bobierrite
Böhmite
Bol, bolus (mixture of halloysite and "limonite"; amestec de halloysit şi "limonit")
Bornite
Bosjemanit (= Mn pickeringite; pickeringit cu Mn)
BOTESITE (= hessite from Boteş)
Botryogen
Boulangerite
Bournonite
Brannerite
Braunite
Bravoite (nickeloan pyrite; pirită nicheliferă)
Breunnerite (magnezit ferifer, cu 5 - 30 % moli $FeCO_3$)
Brochantite
Bronzite (ferriferous enstatite; enstatit ferifer)
Brookite
BROSTENITE (mixture of birnessite and todorokite; amestec de birnessit şi todorokit) (Broşteni)
Brucite
Brushite
Bursaite
Bustamite
Bytownite
Calaverite
Calcantit (Engl.: Chalcanthite)
Calcedonie (Engl.: chalcedony; fine-grained variety of quartz; var. fin granulară de cuarţ)
Calcite
Calcofilit (Engl.: Chalcophyllite)
Calcopirita (Engl.: Chalcopyrite)
Calcopirotină (= isocubanite; isocubanit)
Calcostibit (Engl.: Chalcostibite)
Calderite
Caledonite
Cancrinite
Canfieldite
Cannizzarite
Capnite (= ferriferous smithsonite; Smithsonit ferifer)
Carbonate - chlorapatite
Carbonate - hydroxylapatite
Carinthin (= paragasit)
Carnallite
Carpholite (Hârtopanu, Scott, 1997)
Carrolite
Caryopilite (Hârtopanu, Scott, 1997)

Cassiterite
Cattierite
Celadonite
Celestite (Rom.: celestina)
Celsian
Cerussite
Cesarolite
Chabasite
Chalcanthite (Rom.: calcantit)
Chalcedony (Rom.: calcedonie)
Chalcocite (Rom.: calcozina)
Chalcophyllite (Rom.: calcofilit)
Chalcopyrite (Rom.: calcopirita)
Chalcopyrrhotite (= isocubanite)
Chalcostibite (Rom.: calcostibit)
Chamosite
Chevkinite
Chihlimbar (Engl.: amber)
Chloantite (= nickel - skutterudite)
Chlorapatite (Rom.: Clorapatit)
Chlorargyrite (Rom.: Clorargirit)
Chloritoid (Rom.: Cloritoid)
Chlorophäite (Rom.: clorofeit)
Chondrodite
Chromite (Rom.: cromit)
Chrysocolla (Rom.: crizocol)
Chrysolith (Rom.: crizolit; 10–30 mole % fay).
Chrysotile subgroup (ortocrysotile, clinochrysotile)
Cinabru
Cinnabar (Rom.: cinabru)
Clausthalite
Cleiofan (Engl.: Cleiophane; iron poor sphalerite; var. de ZnS săracă în fier)
Clevelandite - albit tabular
Clinochlore
Clinochrysotile
Clinoenstatite
Clinohumite
Clinoptilolite
Clinozoizite
Clintonite
Cloantit (Engl.: chloantite; = nickel-skutterudite)
Clorapatit (Engl.: chlorapatite)
Clorargirit (Engl.: chlorargyrite)
Cloritoid (Engl.: chloritoide)
Clorofeit (Engl.: chlorophäite)
Coalingite
Cobaltite
Cobaltpentlandite
Coeruleolactite
Coesite
Coffinite
Coloradoite
Columbite - group (Ferrocolumbite)
Colusite
CONIFEITE (=cobalt pentlandite) (Baia de Aramă)

Copiapite
Copper (Rom.: cupru)
Cordierite
Corindon (Engl.: corundum)
Coronadite
Correnšite
Corundum
Cosalite
Cotunnite
Covellite (Rom.: covellină; scrierea "covelină" este incorectă).
Crandallite
Crednerite
Criptomelan (Engl.: Cryptomelane)
CRISITE (a recently described cave mineral, not approved by CNMMN of IMA). A hydrous silicate of Al and K. (Peşterile Bolhac şi Izvor, M. Apuseni, Onac, 1997)
Cristobalite
Crizolit (Engl.: Chrysolite; forsterit cu 10-30% mol de Fe_2SiO_4)
Crizotil (subgrup; Engl.: Chrysotile)
Crizocol (Engl.: Chrysocolla)
Crocidolite (asbestos variety of riebeckite; var. azbestiformă de riebeckit; Germ.: Krokydolith)
Crocoite
Cromit (Engl.: Chromite)
Cronstedtite
Crossite (= glaucophane or riebeckite; glaucofan sau riebeckit)
Cryptomelane (Rom.: criptomelan)
CSIKLOVAITE (= mixture of tetradymite, galenobismuthite and bismuthite; amestec de tetradimit, galenobismutină şi bismutină) (Ciclova)
Cuarţ (Engl.: Quarz; Germ.: Quartz)
Cubanite
CUBOSILICITE (Trestia near Cavnic; blue cubes of chalcedony pseudomorph after melanophlogite; early presented to be pseudomorph after fluorite)
Cummingtonite
Cuprite
Cuprobismutite
Cupropavonite
Cuprosklodowskite
Cupru (Engl.: copper; Germ.: Kupfer; Fr.: cuivre)
Cupru gri (translation of the French word "cuivre gris", used as a generic term for the tetrahedrite group; traducere a cuvântului francez "cuivre gris" folosit ca termen generic pentru grupul tetraedritului).
CYANOTRICHITE (Moldova Nouă?) Type locality doubtful; see Clark (1993)
Cymrite
Dahllite (= carbonate - hydroxylapatite)
Damourite (= fine-grained muscovite; muscovit fin granular)
Danaite (= arsenopyrite with 9–12% Co; arsenopirită cu 9–12% Co)
Danburite
Dannemorite(= mangano - grünerite)
Daphnite (= chamosite)
Datolite
Davidite
Davyne
Dawsonite
Delessite (Syn. Melanolite; ferro-ferri chamosite)
Demantoid (greenish-yellowish variety of andradite; var. verzui - gălbuie de andradit)

Desmine (= Stilbite)
Deweyllite (mixture of talc and serpentine)
Diadochite
Diallag (= diopside with cleavage on (100); diopsid cu clivaj (100)).
Dialogite (= syn. rhodochrosite)
Diamant. (Diamond) Former references, e.g. Fichtel (1972) on diamond presence at Osdola concern, in fact, ultra-pure quartz grains (Ackner, 1855). Referirile vechi, e.g. Fichtel (1792) privind prezenţa d. la Osdola privesc de fapt cristale de cuarţ foarte curate (Ackner, 1855)
Diaphorite
Diaspore
Dickite
DIETRICHITE (Baia Sprie)
Digenite
Diopside
Dioptase
Dipyre (intermediary term in the scapolite series, with 50–80% marialite; termen intermediar în seria scapolitului, cu 50–80% marialit)
Discrasit (Engl.: Dyscrasite)
Disten (Engl.: Kyanite)
Djurleite
Doelterite (colloidal TiO_2, specific to laterites; $TiO_2.nH_2O$ natural alpha titanic acid; TiO_2 coloidal, specific lateritelor; $TiO_2 .nH_2O$; acidul alfa titanic natural).
DOGNACSKAITE (Dognecea); mixture of bismuthnite, chalcopyrite and chalcocite
Dolomite
Domeykite
Donbassite
Dravite
Dumortierite
Dyscrasite (Rom.: discrasit)
Ebelmenite (= mixture of Mn oxides or variety of psilomelane with K; syn.: pyrolusite; amestec de oxizi de Mn sau varietate de psilomelan cu K; sin. piroluzit).
Eclarite (!)
Eggonite (= syn.: sterretite; initially considered Cd silicate, later Al hydrated phosphate; sin.: sterretit; iniţial considerat silicat de Cd, apoi fosfat hidratat de Al).
Egirin (Engl.: aegirine)
Ehlite (= pseudomalachite)
Elaterite (= variety of ozokerite; elastic bitumen with 32–86%C, 11–13%H, 1–5%O; var. de ozocherită; bitumen elastic, cu 32–86%C, 11–13%H, 1–5%O).
Elbaite
Electrum
Eleolite (= variety of nepheline, turbid, with exsolved potash component; var. nefelin, tulbure, cu componentă potasică exsolvită)
Emplectite
Empressite
Enargite
Enstatite
Epidote
Epistilbite
Epsomite
Erionite
Eritrină (Engl.: erythrite)
Erubescite (= bornite)
Erythrite (= eritrină)
Eucairite

Euchroite
Eulytite
Evansite
Fahlerz (= German denomination for the tetrahedrite group; denumire germană pentru grupul tetraedritului)
Fahlore (= English translation of the German denomination; traducerea în engleză a denumirii germane).
Famatinite
Fassaite (= aluminous ferriferous diopside or augite; diopsid ferifer aluminos sau augit)
Faujasite
Fayalite
Federerz (= fibrous jamesonite, heteromorphite)
FELSÖBANYITE (Baia Sprie)
Fengit (Engl.: phengite; var. de muscovit cu Si în exces; mică potasică dioctaedrică)
Ferberite
Fergustonite - (Y)
Fergusonite - beta - (Y)
Ferri - ferrotschermakite
Ferro-anthophyllite (Rom.: fero-antofilit)
Ferro-axinite
Ferrocolumbite
Ferroedenite
Ferroglaucophane
Ferrohornblende
Ferrosalite (= hedenbergite)
Ferrosilite
Ferrotantalite
Fersmite
Fier (Engl.: iron; Germ.: Eisen)
Fischerite (= wawellite)
FIZELYITE (Herja)
Fletcherite
Flogopit (Engl.: Phlogopite)
Fluoborite
Fluorapatite
Fluorapophyllite (Rom.: fluorapofilit)
Fluorina (Engl.: Fluorite)
Fluorite (Rom.: Fluorina)
Forsterite
Fraipontite (Hârtopanu, în Nedelcu et al., 1997)
Francolite (= carbonate-fluorapatite)
Franklinite
Freibergite
Freieslebenite
Friedelite
Friedrichite
Frieseite (= mixture of pyrite and sternbergite or a precursor of decomposition in these minerals; amestec de pirită şi sternbergit sau un precursor al descompunerii în aceste minerale)
Frohbergite
Fuchsite (= chrome muscovite; muscovit cromifer)
FÜLÖPPITE (Dealul Crucii)
Gahnite
Galaxite
Galena
Galenobismutite

Ganophyllite
Garnierite (= generic term for Ni hydrated silicates, especially of antigorite or chrysotile type; termen generic pentru silicaţi hidrataţi cu Ni, în special de tip antigorit sau crizotil).
Gedrite
Gehlenite
Geikielite
Genthelvite
Geocronite
Germanite
Gersdorffite
Gheaţa (Engl.: ice)
Gibbsite
Gilbertit (= muscovite + nacrite and kaolinite, pseudomorph after topaz; muscovit + nacrit şi kaolinit, pseudomorf după topaz)
Giobertit (= magnezit)
Gips (Engl.: Gypsum)
Gismondine
Gladite
Glagerite (= var. halloysite)
Glaserite (= aphthitalite)
Glaucodot
Glauconite
Glaucophane
Gmelinite
Goethite
Gold (Rom.: aur)
Goldfieldite
Goongarite (= mixture of cosalite and galena; amestec de cosalit şi galenă)
Gorceixite
Görgeyite
Goslarite
Grammatite (= var. tremolit)
Graphite
Gratonite
Greenalite
Greenockite
Greigite
Grossular
Groutite
Grünerite
Grünlingite (= mixture of joseite + bismuthinite; amestec joseit + bismutină)
Guanajuatite (!)
Gustavite
Gymnite (deweylite = talc+serpentine)
Gypsum (Rom.: Gips)
Haapalaite (!)
Haidingerite
Halite
Halloysite- 7 Å
Halloysite-10 Å
Halotrichite
Hammarite
Harmotome
Hastingsite
Hauerite

Hausmannite
Heazlewoodite
Hedenbergite
Helvite
Hematite
HEMIMORPHITE (Rom.: hemimorfit) (Băiţa Bihor, Clark, 1983)
Hercinit (Engl.: hercynite)
Hercynite (Rom.: hercinit)
Hessite
Hessonit (= ferriferous grossular, transparent, used as ornamental stone; diverse colours - red, brown, greenish; grosular ferifer, transparent, utilizat ca piatră de podoabă; culori diverse - roşu, brun, verzui)
Hetaerolite
Heteromorphite (Rom.: heteromorfit; fibrous var.: plumosite)
Heulandite
Hexahydrite (Rom.: hexahidrit)
Heyrovskite
Hialofan (Engl.: hyalophane)
Hialosiderit (Engl.: hyalosiderite; intermediate member of forsterite-fayalite sol.sol. series with 30–50% moles; termen intermediar al sol. sol. forsterit-fayalit cu 30–50% moli fay)
Hibschite
Hidrargilit (Engl.: hydrargilite; = gibbsit)
Hidrobiotit (Engl.: hydrobiotite; regular interbedding 1=1 biotite-vermiculite; interstratificaţie regulată 1=1 biotit-vermiculit)
Hidrogranaţi (Engl.: hydrogarnet; garnets in which a part of SiO_2 is replaced by $(OH)_4$; granaţi în care o parte din SiO_4 este înlocuită cu $(OH)_4$).
Hidrogrosular (Engl.: hydrogrossular; group denomination for hibschite-katoite series, with formula Ca_3Al_2 $(SiO_4)3\text{-}x$ $(OH)4x$); denumire de grup pentru seria hibschit-katoit, cu formula Ca_3Al_2 $(SiO_4)3\text{-}x$ $(OH)4x$)
Hidromagnezit (Engl.: hydromagnesite)
Hidromice (Engl.: hydromica; possibly group denomination for brammalite, hydrobiotite, illite; eventual denumire de grup, pentru brammalit, hidrobiotit, illit).
Hidrotalcit (Engl.: hydrotalcite)
Hidrotroilit (Engl.: hydrotroilite; colloidal Fe sulphide; sulfură de Fe coloidală)
Hidrotungstite (Engl.: hydrotungstite)
Hidrougrandit (Engl.: hydrougrandite; generic denomination for hydrogarnets; denumire generică pentru hidrogranaţi).
Hidroxiapofilit (Engl.: hydroxyapohyllite)
Hidroxilapatit (Engl.: hydroxylapatite)
Hidroxil - szaibelyit (Engl.; hydroxyl-szaibelyite)
Hidrozincit (Engl.: hydrozincite)
Hipersten (Engl.: hypersthene; intermediate member of the enstatite-ferrosilite sol.sol. series; termen intermediar al sol.sol. enstatit-ferosilit)
Hisingerite
Hodrushite
Högbomite
Holdawayite
Hollandite
HÖRNESITE (Oraviţa - Ciclova)
Hortonolite (= magnesium ± manganese fayalite; fayalit magnezian ± manganifer)
Hübnerite
Humite
Huntilite (intermediate member of the Ag-As sol.sol. series; termen intermediar al sol. sol. Ag - As).
Huntite
Huréaulite

. **Hyalophane (Rom.: hialofan)**
Hyalosiderite (Rom.: hialosiderit)
Hydrargilite (Rom.: hidrargilit)
Hydrobiotite (Rom.: hidrobiotit)
Hydrogarnet (Rom.: hidrogranaţi)
Hydrogrossular (Rom.: hidrogrosular)
Hydromagnesite (Rom.: hidromagnezit)
Hydromica (Rom.: hidromice)
Hydrotalcite (Rom.: hidrotalcit)
Hydrotroilite (Rom.: hidrotroilit)
Hydrotungstite (Rom.: hidrotungstit)
Hydrougrandite (Rom.: hidrougrandit)
Hydroxyapophyllite (Rom.: hidroxiapofilit)
Hydroxylapatite (Rom.: hidroxilapatit)
Hydroxyl - szaibelyite (Rom.: hidroxil - szaibelyit)
Hydrozincite (Rom.: hidrozincit)
Hypersthene (Rom.: hipersten)
Ice (Rom.: gheaţă)
Idaite
Iddingsite (= pseudomorphosis of serpentinic minerals after olivine; pseudomorfoză de min. serpentinice după olivină)
Idocrase (= verzuvianite)
Ilbaite (= var. allophane)
Illite (a NH_4 - bearing illite was identified within the clay mineral assemblages at Harghita-Băi, Boboş, 1997)
Ilmenite
Ilsemannite
Ilvaite
Inesite
Ingodite
Iron (Rom.: fier)
Iserine (var. ilmenite; pseudomorphs of ilmenite after rutile).
Isocubanite (= replaces the poorly defined chalcopyrrhotite)
Iwakiite ($Mn^{+2}(Fe^{+3},Mn^{+3})_2O_4$)
Ixiolite
Izoklakeite
Izortoză (= var. black-grey orthose; var. ortoză, culoare negru-gri)
Jacobsite
Jadeite (mostly as jadeite component of some eclogite pyroxenes)
Jalpaite
Jamesonite; fibrous var.: plumosite
Jarosite
Jasp (Engl.: Jasper; fine-grained, red quartz; cuarţ fin granular colorat roşu)
Jerrygibbsite
Johannsenite
Johnstonite (var. galena; var. galenă)
JOLOTCAITE (a new sulphosalt, $PbBi_3Te_4S_3$, not approved by the CNMMN of IMA; from Jolotca, Ditrău alk. massif, East Carpathians).
Jordanite
Joseite - A

Joseite - B
Junoite
Kaersutite
Kainite
Kalinite
Kamacite
Kämmererite (= chromian clinochlore)
Kandite (subgroup of kaolinite-serpentine group, including dickite, kaolinite and macrite; subgrup al gr. kaolinit - serpentine, incluzând dickitul, kaolinitul şi nacritul)
Kaolinite
Kapnicite (= syn. wavellite)
Kapnikite (syn. rhodonite, but also of wavellite)
Kapnite (= ferriferous smithsonite, with 10–30% mol. $FeCO_3$; smithsonit ferifer, cu 10–30% mol. $FeCO_3$)
Karinthin (= pargasite)
Katophorite
Keeleyite (= zinkenite)
Kellyite (Hârtopanu, Scott, 1997)
KENNGOTTITE (= Pb - bearing miargyrite from Baia Sprie).
Kerargyrite
Kermesite
Kerolithe (= chrysotile or saponite)
Kieserite
Klaprothite (= mixture of wittichenite and emplektite, described at Cavnic, also found as Klaprotholit or Klaprothin, also syn. of Beudant lazurite; amestec de wittichenit şi emplektit, descris la Cavnic; apare şi sub forma Klaprotholit sau Klaprothin; folosit şi ca sinonim al lazuritului de Beudant)
KLEBELSBERGITE (Baia Sprie)
Knebelite (= manganoan fayalite or ferroan tephroite)
Kobellite
Kolophonite (= brownish andradite, described in the Rodna Mts; andradit bruniu, descris în Munţii Rodnei)
Kostovite (!)
KOTOITE (Băiţa Bihor and Hol Col, Korea)
Kozulite
KRAUTITE (Săcărâmb and Cavnic)
KRENNERITE (Săcărâmb)
Krupkaite
Kupholith (= serpentine)
Kutnohorite
Kyanite (Rom.: disten)
Langbeinite
Laumontite
Lautite (!)
Lawsonite
Lead (Rom.: plumb)
Leadhillite
Lennilenapeite (Hârtopanu, Scott, 1997)
Leonite
Lepidocrocite
Lepidolite
Lepidomelane (= ferriferous biotite; biotit ferifer)
Leptochlorite (= ferriferous chlorites, usually fibrous; clorite ferifere, de regulă fibroase)
Lettsomite (= cyanotrichite)
Leuchtenbergite (= var. clinochlore)
Leucite

Leucophoenicite
Leucopyrite (= löllingite)
Leucoxene (= fine-grained mixture of titanite, rutile and anatase; amestec fin granular de titanit, rutil şi anatas)
Libethenite
Liebenerite (= muscovite - fine grained - pseudomorph after nepheline)
Lievrite (= ilvaite)
Lillianite
Lindströmite
Linnaeite
Linarite
Lithionite (= lepidolite)
Lithiophilite
Lithiophorite
Lizardite
Löllingite
Loparite - (Ce)
LOTRITE (Urdele peak, similar to pumpellyite, to which it has priority (lost for the time being); vf. Urdele; similar pumpellyitului, faţă de care are prioritate, pierdută pentru moment)
Lublinite (= fibrous calcite, apparently hydrous)
LUDWIGITE (Ocna de Fier)
Lunnite (= pseudomalachite)
Luzonite
Mackinawite, $(Fe,Ni)_9S_8$ sau $Fe_{1+x}S$, tetragonal; fine exsolutions in chalcopyrite and pentlandite replacing "valleriite" described in the period 1935–1960 as $Cu_2Fe_4S_7$, later redefined; exsoluţii fine în calcopirită şi pentlandit înlocuind "valleriitul" descris în perioada 1935-1960 ca fiind $Cu_2Fe_4S_7$, ulterior redefinit.
Maghemite
Magnesiochromite
Magnesioferrite
Magnesiohastingsite
Magnesiohornblende
Magnesiolaumontite (= laumonite with Mg; laumontit cu Mg)
Magnesioriebeckite
Magnesiotaramite
Magnesite (Rom.: magnezit)
Magnetite
Magnezit (Engl.: magnesite)
MAKOVICKYITE (Băiţa Bihor) (Zak et al., 1994)
Malachite
Malacolite (= diopside)
Maldonite
Mallardite
Manganapatite (= manganoan apatite; apatit manganifer)
Manganite
Mangano-grünerite (dannemorite)
Manganhumite
Manganocalcite (= manganoan calcite; calcit manganifer)
Manganofilit (Engl.: manganophyllite, = manganoan biotite; biotit manganifer)
Manganpyrosmalite (Rom.: manganpirosmalit)
Manjiroite
Marcasite
Margarite
Marialite
Marmatit (= iron sphalerite; sfalerit ferifer)

Marmolith (= serpentine)
Martit (= pseudomorphosis of hematite after magnetite; pseudomorfoză de hematit după magnetit)
Maskelynit (= glass with plagioclase composition, especially in meteorites; sticlă cu compoziţie de plagioclaz, în special în meteoriţi)
Massicot
Matildite
Maucherite
Mcgillite
Meionite
Melaconite (= tenorite)
Melanite (= titaniferous andradite; andradit titanifer)
Melanocerite - (Ce)
Melanolite (syn. delessite; ferriferous chlorite; clorit ferifer)
Melanophlogite, $C_2H_{17}O_5.Si_{48}O_{92}$, tetrag.; precursor of Trestia blue chalcedony; precursor al calcedoniei bleu de la Trestia.
Melanterite
Melilite - akermanite - gehlenite series
Melinite (Germ.: Gelberde; a mixture of argillaceous minerals (bol) and iron hydroxides; un amestec de minerale argiloase (bol) şi hidroxizi de fier)
Melinophane (= meliphanite)
Meliphanite
Mellite $Al_2[C_6(COO)_6].18H_2O$
Meneghinite
Mercury (Rom.: mercur)
Merrilite (whithlockite found in meteorites)
MERRIHUEITE (Mezö - Madaras meteorite)
Meroxene (= biotite, poor in Fe)
Merumite (= mixture of CrOOH trimorphs bracewellite, guyanalite, grimaldiite; found within Au-As ores at Costeşti - Horezu).
Mesitine (= intermediate member of magnesite-siderite sol.sol. series with 30–50% moles $FeCO_3$; termen intermediar al sol.sol. magnezit-siderit, cu 30–50% moli $FeCO_3$).
Mesolite
Meta-alunogen
Metacinnabar
Metahalloysite (= halloysite - 7A)
Metalaumontite (= partly dehydrated laumontite; laumontit parţial deshidratat; syn.: leonhardite)
Metaxite (= var. chrysotile)
Miargyrite (Rom.: Miargirit)
Microcline
Miharaite (Zak et al., 1994)
Millerite
Millisite
Mimetesite (= mimetite; preferred usage)
Mimetite (= mimetesite)
Minamiite (Ghergari et al., 1994)
Minnesotaite
Minium
Mirabilite
Mispichel (= arsenopyrite)
Mizzonit (intermediate member in the scapolite series, with 20–50% marialite; termen intermediar în seria scapolitului, cu 20–50% marialit)
Modderite
Moissanite
MOLDOVITE (= var. of ozocerite)
Molybdenite (mainly 2H)

Monazite - (Ce)
MONSMEDITE (Baia Sprie, Săsar) (= Tl - bearing voltaite; Zemann, 1993)
Montbrayite
Montebrasite
Monticelite
Montmorillonite
Mordenite
MRAZECITE (= mixture of saponite, stevensite and talc)
Mullite
MUNTENITE (= var. of amber, from Olăneşti)
MURGOCITE (= mixture of saponite, swelling chlorite, and stevensite)
Muriacite (= anhydrite)
Muscovite
Musketovite (= pseudomorph of magnetite after hematite)
MUTHMANNITE (Săcărâmb)
Nacrite
NAGYAGITE (Săcărâmb / Nagyag; recently an As- nagyagite was found in the material from the type locality; Şimon et al., 1994)
Nambulite
Natroalunite
Natrolite
Natron (Rom.: Soda)
Natronambulite
Nasturan (= pitchblende, uraninite)
Nelenite
Neotocite
Nepheline
Nesquehonite
Nicheline
Nickel - skutterudite
Nimite
Niobite (= columbite)
Niter (Rom.: nitronatrit)
Nitrammite, NH_4NO_3
Nitrite (= niter)
Nitronatrit (Engl.: niter)
Nitrocalcite
Nontronite
Norbergite
Norrishite
Nsutite
Nuffieldite
Nukundamite
Nyboite (Săbău, Negulescu, 1997)
OCHRAN (clay mineral with Fe; probably a mixture, Oraviţa; mineral argilos cu Fe; probabil amestec).
Okenite
Oldhamite (meteorite Mesö Madaraş)
Oligiste (= syn. hematite; Eisenglimmer - Germ.)
Oligoclase
Oligonite, Oligonsiderite, Oligonspar, Oligonspath (= interm. member of the sol. sol. series $MnCO_3$ - $FeCO_3$ with up to 40% $MnCO_3$)
Omphacite
Opal
ORAVICZITE (= halloysite with Zn; Oraviţa)
Orpiment (Rom.: auripigment)

Orthite (= allanite - (Ce))
Orthochrysotile
Osbornite (meteorite mineral; Mocs / Moci)
Owyheeite
PADERAITE (Băiţa Bihor) (Mumme, Zak, 1985)
Palygorskite
Paracelsian
Paragonite
PARAJAMESONITE (Herja)
Parankerite (= Mg - rich ankerite)
Paraspurrite (Piret et al., 1997)
Pargasite
Parisite - (Ce)
Parsettensite
PARTSCHIN / PARTSCHINITE (Pianu de Jos; anisotropic spessartine)
Paulingite
Pavonite
Pearceite
Pechblenda (Engl.: pitchblende; = uraninite)
Pectolite
Pekoite
Pennantite
Pentlandite
Periclase
Perovskite (Meteorite mineral; Mesö Madaraş)
Perrierite
PETZITE (Săcărâmb)
Pharmacolite
Pharmacosiderite
Phengite (Rom.: fengit; potassic dioctahedral micas; Si-rich muscovite)
Phillipsite
Phlogopite (Rom.: flogopite)
Pickeringite
Picotite (= chromian spinel)
Picrochromite (= magnesiochromite)
Picrolite (= var. antigorite)
Picromerite
Piemontite
PIETRICIKITE (= var. ozocerite)
Pigeonite
Pilsenite
Pinnite (= pseudomorph of mica after cordierite)
Pirargirit (Engl.: pyrargyrite)
Pirită (Engl.: pyrite)
Piroaurit (Engl.: pyroaurite)
Pirochroit (Engl.: pyrochroite)
Pirofanit (Engl.: pyrophanite)
Pirofilit (Engl.: pyrophyllite)
Piroclor (Engl.: pyrochlore)
Piroluzit (Engl.: pyrolusite)
Piromorfit (Engl.: pyromorphite)
Pirop (Engl.: pyrope)
Pirostipnit (Engl.: pyrostilpnite)
Pirosmalit (Engl.: pyrosmalite)
Pirotină (Engl.: pyrrhotite)

Piroxmangit (Engl.: pyroxmangite)
Pisanite (= cuprian melanterite)
Pistacite / Pistazite (= epidote, green fibrous aggregates)
Pistomesite (= intermediate member of the sol. sol. series magnesite - siderite, with 30-50% mols $MgCO_3$)
Pitticite, (Fe, AsO_4.SO_4.H_2O)?, amorphous, of variable composition.
Plagionite
Planerite
Platina (Engl.: platinum)
Platinum
Pleonaste (= ferroan spinel)
Plumb (Engl.: lead; Germ.: Blei)
Plumbogummite
Plumbojarosite
Plumosite (= fibrous sulphosalts, not only boulangerite, as given in many text and handbooks, but also jamesonite and robinsonite). German: Federerz, Zunderz)
Polianite (= syn. of pyrolusite)
Polibazit (Engl.: polybasite)
Polihalit (Engl.: polyhalite)
Polybasite (Rom.: polibazit)
Polyhalite (Rom.: polihalit)
PONITE (Broşteni; iron- rich rhodochrosite; up to 20% $FeCO_3$)
Pre-graphite / graphitoide (= partly ordered carbonaceons matter, sometimes found in sheared authracite)
Prehnite
Prochlorite (= syn. of ripidolite, i.e. ferroan clinochlore).
PROTOCALCITE (Comarnic cave; acicular calcite or perhaps a hydrate; see also lublinite)
Proustite
PSEUDOBROOKITE (Măgura Uroi / Aranyer Berg)
Pseudomalachite
Pseudorutile (= arizonite)
Psilomelane (= partly romanèchite)
Pumpellyite - (Fe^{2+})
Purpurite
Pyrantimonite (= kermesite)
Pyrargyrite (Rom.: pirargirit)
Pyrite (Rom.: pirita)
Pyroaurite (Rom.: piroaurit)
Pyrochlore (Rom.: piroclor)
Pyrochroite (Rom.: pirochroit)
Pyrolusite (Rom.: piroluzit)
Pyromorphite (Rom.: piromorfit)
Pyrope (Rom.: pirop)
Pyrophanite (Rom.: pirofanit)
Pyrophyllite (Rom.: pirofilit)
Pyrosmalite (manganpyrosmalite)
Pyrostilpnite (Rom.: pirostilpnit)
Pyroxmangite (Rom.: piroxmangit)
Pyrrhotite (Rom.: pirotină)
Quartz (Rom.: cuarţ)
Quenstedtite
RÄDELERZ (Cavnic; wheel ore; twinned bournonite crystals, first described from Cavnic)
Ramdohrite
Rammelsbergite
Ramsdellite

Rancieite
Realgar
Rectorite
Renardite
REZBANYITE (Băiţa Bihor / Rezbanya; mixture of bismuthinite, hammarite, cosalite, paderaite)
RHODOCHROSITE (Cavnic may be given as type locality as the name first appeared by analyzing material from this locality (Hausmann, 1813). Previously known as "luftsaures Brauneisenerz" (Lenz, 1794) manganèse oxyde carbonate (Haüy, 1809). In the 18-th century confused with rhodonite. (Anterior a fost cunoscut ca "luftsaures Brauneisenerz" (Lenz, 1794). In sec. XVIII confundat cu rodonitul. Rom.: rodocrozit.).
RHODONITE (Rom.: rodonit; Cavnic? var. kapnikite (Huot))
Rhönite
Ribbeite
Richterite
Riebeckite
Ripidolite (= ferroan clinochlore; name often given to chlorites of worms-like appearance)
Robinsonite
RODOCROZIT (Cavnic; Engl.: Rhodochrosite; see the comments under rh.)
RODONIT (Cavnic; Engl.: rhodonite)
Romanèchite
ROMANITE (Name given both to a var. of amber and more recently to a Pb-bearing davidite)
Roscoelite
Rozenite
Rubellan (= altered / oxidized biotite of red colour)
RUMÄNITE (var. of amber with 1-30% succinic acid)
Rutile
Săcărâmbite (translation of the name NAGYAGITE)
Safflorite
Sagenit (= accicular rutile, developed/exsolved in biotite; rutil acicular, dezvoltat / exsolvit în biotit)
Samsonite
Sal ammoniac (Rom.: salmiac)
Salite (= iron-rich diopside)
Salmiac (Engl.: sal ammoniac)
Salpetru de potasiu (sin. nitrit, nitrokalit) (Engl.: Niter)
Samarskite
Samoite (var. montmorillonite)
Sanidine
Saponite
Sarkinite
Sauconite
Scapolite group (**marialite, meionite**; *mizzonite, dipyre*)
Scawtite (Piret et al., 1997)
Schallerite
Scheelite
Schefferite (= manganoan augite)
Schirmerite
Schorl
SCHRAUFITE (Vama; var. of amber, high in oxygen; low content of succinic acid)
Schreibersite (meteorite Tăuţi)
Schuchardite (= nickeloan clinochlore)
Schwarze Blende (initial name given by Müller von Reichenstein to the Săcărâmb MnS (1784); denumire inițială dată de Müller von Reichenstein pentru MnS de la Săcărâmb (1784))
Schweizerite (mixture of chrysotile and lizardite, with fibrous character and polygonal parting)
Switzerite (Hârtopanu, Scott, 1997)

Scolecite
Scorodite
SEBESITE (Sebeş Mts.; name of lost priority over tremolite)
Seligmanite
SEMSEYITE (Baia Sprie)
Sepiolite
Sericite (fine grained muscovite - $2M_1$, paragonite - 2M, or illite)
Serpentine group
Sfen (= titanite is the favourite term; titanit este termenul preferat)
Sheridanite (= var. of clinochlore)
Siderite
Sideroplesite (= Mg rich siderite with 11-12 mol% $MgCO_3$)
Siegenite
Sillimanite
SILVANIT (Engl.: Sylvanite; Baia de Arieş)
Silver (Rom.: argint)
SINKALITE (mixture of galena, anglesite and sulphur, from Şinca / Făgăraş Mts)
Skutterudite
Smaltine / smaltite (= skutterudite)
Smaragdite (= actinolite)
Smectite group
Smithsonite
Soda (Engl.: natron)
Sodalite
Sommarugaite (= a gold-bearing gersdorffite from Băiţa Bihor)
Sonolite
Specularite (= syn. hematite, well developed lamellae)
Sperrylite
Spessartine
Sphalerite (Rom.: blendă, sfalerit)
Sphene (= titanite)
Spinel
Spionkopite, $Cu_{39}S_{28}$, hex. (!)
Spodumene
Spurrite
Stannina (Engl.: stannite)
Stannite
Staurolite
Steatite (= fine grained, compact talc)
Steinmannite (= galena, with some As and Sb, of octahedral habit, sometimes forming spheroidal aggregates)
Steinmark (= kaolinite and halloysite mostly pseudomorphs after feldspar)
Stephanite
Sternbergite
Sterrettite (= hydrated aluminium phosphate; no relation to kolbeckite, $ScPO_4 . 2H_2O$; syn.: eggonite)
Stevensite
Stibarsen
Stibiconite
Stibiu (Engl.: antimony)
Stibnite (Rom.: stibină)
Stilbite
Stilpnomelane
Stilpnosiderite (= nearly amorphous limonite)
Strahlstein (= tremolite, in German)
Stromeyerite

Strontianite
Strüverite
STÜTZITE (Săcărâmb)
Suanite
Succinite (= var. of amber)
Sulf (Engl.: sulphur; e. am.: sulfur)
Sulfur (Rom.: sulf)
SYLVANITE (Baia de Arieş / Offenbanya; modified by Necker from Sylvane of Beudant)
Sylvite (Rom.: silvina)
Symplesite
SZABOITE (= altered/oxidized, red hypersthene from pseudobrookite-bearing andesites from Uroiu)
SZAIBELYITE (Baiţa Bihor; Syn.: ascharite)
SZASZKAITE (= smithsonite from Sasca Montană, of special morphology)
SZMIKITE (Baia Sprie)
Szomolnokite
Taeniolite (!)
Taenite (meteorite Mocs/Moci)
Tafelspat (= wollastonite; may be a precursor of wollastonite-1T)
Tainiolite(= taeniolite)
Takanelite, $(Mn,Ca)Mn_4O_9.3H_2O$, hex. (Perseil et al., 1995)
Talc
Tantalite (ferrontantalite)
Tapalpite (= mixture of acanthite and tetradymite)
Taramite
Taranakite
Tavorite
Teallite
TELEGDITE (an amber-like sulfur-bearing resin but with no succinic acid, from Săsciori, Apuseni Mts)
Tellurantimony, Sb_2Te_3. (A compound of the formula $SbTe_2$ was also recently found in the Au-Te ores of the Metaliferi Mts.)
TELLURITE (Faţa Băii / Facebanya)
TELLURIUM (Faţa Băii)
Tellurobismuthite
Tennantite
Tenorite
Tephroite
Tetradymite
Tetrahedrite
Thaumasite
Thenardite
Theophrastite
Thomsonite
Thorianite
Thorite
Thrombolite (Baiţa Bihor; pseudomalachite)
Thucholite (= anisotropic carbonaceous matter associated with uraninite)
Thuringite (= ferrian chamosite)
TIBISCUMITE (Caransebes; var. of montmorillonite or a mixture)
Tilleyite
Tirolit (Engl.: tyrolite)
Titanite
Titanomagnetite: (= titaniferous magnetite)
Tochilinite
Toddite (= uranium-bearing columbite and/or a mixture of columbite and samarskite)
Todorokite

Topaz
Torbernite
Tosudite
Tourmaline group (Rom.: turmalina) (elbaite, dravite, schorl)
Tremolite
Tridymite (Rom.: tridimite)
Triphylite
Troilite (meteorite mineral)
Tschermakite
Tschermigite
Tungstite
Twinnite (Damian, Cook, 1997)
Tyrolite (Rom.: tirolit)
Ullmannite
Ulvöspinel
Umohoite
Uralite (= amphibole pseudomorph after pyroxene)
Uraninite
Uranofan (Engl.: uranophane)
Uranophane (Rom.: uranofan)
Vaesite
Valachite (= mixed-layer clay mineral from soils; probably illite)
Valentinite
Valleriite, 4(Fe,Cu)S,3(Mg,Al)$(OH)_2$,hex. (Formula $Cu_3Fe_4S_7$ este eronată, dar a mai apărut în lucrări publicate, la noi, in 1996!)
Variscite
Vaterite
Veenite (Damian, Cook, 1997)
Vermiculite
Vernadite
Vesuvian (Engl.: vesuvianite)
Vesuvianite (Rom.: vesuvian)
VESZELYITE (Ocna de Fier/Vask / Moravicza)
Vezuvian (= vesuvian)
Villyaellenite (Ghergari et al., 1994)
Violarite
Vivianite
Voltaite
Voltzite (= mixture of wurtzite with an organometallic compound)
Vredenburgite (= mixture of jacobsite and hausmannite)
Wad (= soft manganese oxides)
Wairakite
Wakabayashilite
Warthaite (= mixture of cosalite and galena; = goongarite)
Wavellite
Weissite
Whewellite, $CaC_2O_4.H_2O$, mon.
Whitlockite (meteorite mineral initially described as merrilite)
Whitneyite (= copper with some 10–12% As)
Willemseite
Winchite
Witherite
Wittichenite
Wittite
Wöhlerite

Wolframite (= ferberite, hübnerite)
Wollastonite
Wulfenite
Wurtzite
Wüstite (in extraterrestrial spherules)
Xanthoconite
Xenotime - (Y)
Xylotile (= iron sepiolite)
Yarrowite, Cu_9S_8, Rhomb
Zaratite
Zeofilit (Engl.: zeophyllite)
Zeophyllite (Rom.: zeofilit)
ZINKFAUSERITE (Baia Sprie; a Zn variety of fauserite; fauserite = a Mn variety of epsomite, thus zinkfauserite is a Mn and Zn-bearing epsomite)
Zincite
Zincocopiapite
Zinkenite / zinckenite
Zircon
Zoizite
Zoubekite (Popescu, Şimon, 1995)
Zundererz (= impure plumosite)
Zunyite

Acknowledgements. A comprehensive list of papers concerning mineralogy development in Romania during the last years (1991–1998) could not be given. This is why apology is necessary to many colleagues not having found their papers here. However, the reference list of the book "Minerals of the Carpathians" (by G. Udubaşa, S. Szakall, R. Duda, V. Kvasnytsya, M. Novak), which will soon appear at the GRANIT Publ. House in Prague, includes all the significant papers on mineralogy in Romania, especially after the book "Topographic mineralogy of Romania" by D. Rădulescu and R. Dimitrescu (1966, Edit. Acad. Rom.) and the paper of Udubaşa et al. (1992) were printed. Nevertheless, the author wishes to thank to his colleagues Paulina Hartopanu, Gheorghe Ilinca, Ştefan Marincea and Mihai Tatu, who agreed to include in the list of minerals some still unpublished or partly published data.

The responsability for any errors is, however, solely of the author. In addition, by publishing this paper no claim for first mention is required.

References

Ackner, M. J. (1855) Mineralogie Siebenbürgens, mit geognostischen Andeutungen. Steinhaussen, 391 p., Hermannstadt. (Sibiu).

Balintoni, I., Seghedi, I., Szakacs, Al. (1996) Geotectonic framework of the Neogene calc - alkaline magnetism in the intracarpathian area with an emphasis on the Romanian territory. *An. Inst. Geol. Rom.*, 69, Suppl. 1, p. 15–16, Bucureşti.

Boboş, I. (1997) Hydrothermal ammonium - bearing illite from Harghita Băi area: XRD, IR spectroscopy, DTA and chemical analysis. *Rom. J. Mineralogy*, 77, Suppl. 1, p. 10–11, Bucureşti.

Butucescu, N., Bonea, L., Botnarencu, A., Stoicescu, Gh., Stoicescu, Fl. (1963) Mineralizaţia cu telururi auro-argentifere din zăcământul Băiţa - Nistru (Baia Mare). *Rev. Minelor*, XIV, 5, p. 214–221.

Cioflica, G., Jude, R., Lupulescu, M., Şimon, Gr. (1995) New data on the Bi - minerals from the mineralizations related to Paleocene magmatites in Romania. *Rom. J. Mineralogy*, 76, Part 2, p. 9–23, Bucureşti.

Clark, A. M. (1993) Hey's mineral index. Mineral species, varieties and synonyms. Chapman & Hall, London, 852 p.

Constantiniuc, V., Constantiniuc, E., Mârza, I., Ghergari, L., Bojin, D. (1987) La présence des tellurures dans le gisements polymétalliques néogènes de Rodna Veche (Monts de Rodna). *Rev. roum. géol., géophys., géogr, Géologie*, 31, p. 15–18, Bucureşti.

Cook, N. J. (1997) Bismuth and bismuth - antimony sulphosalts from Neogene vein mineralisation, Baia Borşa area, Maramureş, Romania. *Mineralog. Magazine*, 61, p. 387–409.

— , **Damian, Gh. (1997)** Bismuth sulphosalts within Neogene polymetallic vein mineralisation, NW Romania. (abs.). *Rom. J. Mineralogy*, 78, Suppl. 1, p. 15–16, Bucureşti.

Damian, Gh., Pop, N., Garbaşevschi, N. (1992) Sur la presence de la lillianite dans les minéralisations de Jolotca - Ditrău. *Rom. J. Mineralogy*, 75, p. 87–90, Bucureşti.

— , **Cook, N. J. (1997)** New data on Pb - Sb, Ag - Sb, Ag - Pb - Sb, Pb - As sulphosalts and related minerals. Herja polymetallic vein deposit, Baia Mare, Romania. (abs.) *Rom. J. Mineralogy*, 78, Suppl. 1, p. 17–18, Bucureşti.

Fichtel, J. E. (1791) Mineralogische Bemerkungen von den Karpathen. I - II, Wein, 730 p.

Ghergari, L., Forray, F., Gál, A., Fărcaş, T. (1994) Arsenic minerals from Săcărâmb ore deposit: arsenic, arsenolite, villyaellenite and krautite (Transylvania, Romania). *Studia Univ. "Babeş - Bolyai", Cluj - Napoca, Ser. geol. geogr.*, p. 127–140.

— , **Strusievicz, R. O., Dumitrescu, S. (1994)** Minamiite in the hydrothermal alteration zone of the Fâncel - Lăpuşna caldera (Gurghin Mts., East Carpathians): first record in Romania. *Studia Univ. "Babeş - Bolyai", Cluj - Napoca, Ser. geol. geogr.*, p. 93–103.

Giuşcă, D. (1937) Le chimisme de la nagyagite. *Bul. Soc. Rom. Geol.*, III, p. 118–121.

Hausmann, J. F. (1813) Handbuch der Mineralogie, I–III, Göttingen.

Hârtopanu, P., Hârtopanu, I., Cristea, C., Stelea, G., Udrescu, C. (1996) Mineralogy study of the metamorphosed manganese accumulation in the Bistriţa Mts., Dadu deposit. *An. Inst. Geol. Rom.*, 69, part 1, p. 95–98, Bucureşti.

— , **Scott, P. (1997)** Paragenetical evolution of metamorphosed Mn - deposits from Romania (abs.). *Rom. J. Mineralogy*, 78, Suppl. 1 , p. 34–35, Bucureşti.

Ilinca, Gh. (1992) Bismuth sulphosalt assemblages in copper ore deposits at Oraviţa - Ciclova, South - Western Banat. *Rom. J. Mineralogy*, 75, Suppl. 1, p. 19–20, Bucureşti.

— , **Marincea, St., Russo-Săndulescu, D., Iancu, V., Seghedi, I. (1993)** Mineral occurrences in Southwestern Banat, Romania. Excursion guide, 2nd Symp. Mineralogy, Timişoara 5–11 July 1993. *Rom. J. Mineralogy*, 76, Suppl. 2, 40 p., Bucureşti.

— , **Cook, N. J. (1995)** Note on the Cu-Ag-Pb / Bi sulphosalts from Băiţa Bihor and Valea Seacă (abs.). *Rom. J. Mineralogy*, 77, Suppl. 1, p. 23, Bucureşti.

— , **Marincea, St. (1996)** Bismuth minerals in Romania . Valea Seacă area. *An. Inst. Geol. Rom.*, 69, part 1, p. 83–84, Bucureşti.

Leake, B. E. et al. (1997) Nomenclature of amphiboles. *American Mineralogist*, 82, p. 1019–1037.

Lupulescu, M., Şimon, Gr., Alderton, D. H. M., Watson, E. B. (1993) Preliminary data on ingodite from Valea Seacă - Băiţa Bihor area; a first occurrence in Romania. *Rom. J. Mineralogy*, 76, Suppl. 1, p. 27–28, Bucureşti.

— , **Watson, E. B., Wark, D. (1993)** New chemical and mineralogical data on nagyagite from the type locality. (abs.) AGU Spring Meeting, Baltimore, May 24–28, EOS Suppl., p. 167.

Marincea, St. (1993) Mineralogical data concerning szaibelyite from Romania: the Gruiului Hill occurrence (Aleului Valley, Bihor Mountains). *Rom. J. Mineralogy*, 75, p. 69–85, Bucureşti.

— , **Cristea, C. (1995)** Ludwigite, szaibelyite and pyroaurite at Cacova Ierii (Gilău Mountains): new occurrences in the Banatitic province in Romania. *Rom. J. Mineralogy*, 76, part 2, p. 67–84, Bucureşti.

— , **Guy, B. (1996)** New data on kotoite from the co-type locality Băiţa Bihor, Romania. *An. Inst. Geol.*, 69, Suppl. 1, p. 122–124, Bucureşti.

— **(1997)** Kotoite in Romania: a third occurrence Cacova Ierii (Gilău Mountains) and review. (abs.) *Rom. J. Mineralogy*, 78, Suppl. 1, p. 52–53, Bucureşti.

Mârza, I., Pop, D., Dărăban, L. (1993) L'alabandite dans les gisements de Roumanie. *Rom. J. Mineralogy*, 76, part 1, p. 71–78, Bucureşti.

Morimoto, N. (1988) Nomenclature of pyroxenes. *Schweiz. Min. Petr. Mitt.*, 68, p. 95–111.

Mumme, W. G., Zak, L. (1985) Padéraite, $Cu_{5.9}Ag_{1.3}Pb_{1.6}Bi_{11.2}S_{22}$, a new mineral of the cuprobismutite - hodrushite group. *N. Jb. Miner. Mh.*, p. 557–567.

Nedelcu, L., Hârtopanu, P., Szakács, Al., Moga, C., Podaşcă, I. (1997) Field trip (guide), 4th nat. Symp. Mineralogy, October 1997, Iaşi. *Rom. J. Mineralogy*, 78, Suppl. 2, 40 p., Bucureşti.

Onac, B. P. (1998) Formaţiuni stalagmitice în peşterile Pădurii Craiului. Edit. Acad. Române, 175 p.

Papp, G. (1992) The reinvestigation of "biharite" of Peters (1861) (abs.). *Rom. J. Mineralogy*, 75, Suppl. 1, p. 31–32, Bucureşti.

Peltz, S., Stanciu, C., Balla, Z., Gheorghiu, A., Niţulescu, I., Pomârleanu, V., Udrescu, C., Anastase, S. (1982) Date noi privind mineralizaţia hidrotermală de la Stănceni (Munţii Călimani de sud). *D. S. Inst. Geol. Geof.*, LXVII/2, p. 113–159, Bucureşti.

Perseil, E. A., Giovanoli, R., Vodă, Al. (1995) Les concentrations ferro-manganésiféres des Carpates orientales: le gisement de Oiţa (Roumanie). *Bull. Mus. Nation. Hist. Nat. Paris*, 4e série, 16, p. 383–401.

Piret, R., Verkaeren, J., Marincea, St. (1997) Mineralogy and geochemistry of the high - temperature calc - skarns of Cornet Hill and Măgureaua Vaţei (Apuseni Mountains). Discovery of scawtite and paraspurrite. *Rom. J. Mineralogy*, 78, Suppl. 1, p. 74–75, Bucureşti.

Popescu, Gh. C., Şimon Gr. (1995) Zoubekite, ($AgPb_4S_{10}$) from Cioclovina shear-zone mineralization, România. (abs.) *Rom. J. Mineralogy*, 77, Suppl. 1, p. 37–38, Bucureşti.

— , **Şimon, Gr. (1995)** Contribution to the study of tellurides from Săcărâmb (Nagyag), Romania. *Rom. J. Mineralogy*, 76, Part 2, p. 37–42, Bucureşti.

Săbău, G., Castelli, D., Ferraris, G., Mărunţiu, M. (1997) Unusual Al- armalcolite and apparently low-symmetry TiO_2 inclusions in pyrope from the Foltea garnet - periodite (South Carpathians); some preliminary data and petrological implications (abs.). *Rom. J. Mineralogy*, 78, Suppl. 1, p. 87–88, Bucureşti.

— , **Negulescu, E. (1997)** Exotic amphibole compositions in the Leaota massif UHP eclogites (abs.) *Rom. J. Mineralogy*, 78, Suppl. 1, p. 91–92, Bucureşti.

Săndulescu, M. (1984) Geotectonica României. Edit. Tehnică, 334 p.

Stanley, C. J., Roberts, A. C., Harris, D. C. (1994) New data on nagyagite. *Mineralogical Magazine*, 58, p. 477–480.

Şimon, Gr., Alderton, D. H. M., Bleser, T. (1994) Arsenian nagyagite from Săcărâmb, Romania, a possible new mineral species. *Mineral. Magazine*, 58, p. 473–478.

Udubaşa, G. (1988) Metalogeneza masivului Leaota. *Bul. inf. teh. şt.* - Centrala Departament a Geologiei, No. 3, p. 5–14.

— , **Ilinca, Gh., Marincea, Şt., Săbău, G., Rădan, S. (1992)** Minerals in Romania: the state of art 1991. *Rom. J. Mineralogy*, 75, p. 1–51, Bucureşti.

— **(1992)** Introductory talk. *Rom. J. Mineralogy*, 75, Suppl. 1, p. 1–2, Bucureşti.

— , **Wagner, F., Friedl, F. (1993)** Nagyagite: some features of its composition and Mössbauer spectra (abs.). *Rom. J. Mineralogy*, 76, Suppl. 1, p. 1–51, Bucureşti.

— **(1993)** Introductory talk. *Rom. J. Mineralogy*, 76, Suppl. 1, p. 1–2, Bucureşti.

— **(1994)** Sacred monsters of mineral occurrences in Romania: past, present, future (abs.). *Anal. Univ. Bucureşti*, XLIII, Suppl., p. 34–35, Bucureşti.

— **(1995)** 3rd Symposium on mineralogy: introductory talk. *Rom. J. Mineralogy*, 77, Suppl. 1, p. 1–6, Bucureşti.

— **, Ţopa, D. (1995)** Arsenopyrite composition, microinclusions, and parageneses, Costeşti gold - occurrence, Căpăţâna Mts. (abs.). *Rom. J. Mineralogy*, 77, Suppl. 1, p. 47–48, Bucureşti.

— **(1997)** Is there still place for mineralogy? Foreword to the 4th Symposium of the Mineralogical Society of Romania. *Rom. J. Mineralogy*, 78, Suppl. 1, p. 1–2, Bucureşti.

Zak, L., Fryda, I., Mumme, W. G., Paar, W. H. (1994) Makovickyite, $Ag_{1.5}Bi_{5.5}S_9$, from Băiţa Bihorului, Roumania: the 4P natural mineral member of the pavonite series. *N. Jb. Miner. Abh.*, 168, p. 147–169.

Zemann, J. (1993) What is monsmedite? *Rom. J. Mineralogy*, 76, part 1, p. 97–98, Bucureşti.

Rom. J. Mineralogy, 79, p. 31-34, Bucureşti, 1999

PRESENT AND FUTURE OF IMPACT MINERALOGICAL SCIENCES

Yasunori MIURA

Department of Earth Sciences, Faculty of Science Yamaguchi University,

Yoshida, Yamaguchi 753, Japan. E-mail: yasmiura @ po. cc. yamaguchi-u.ac.jp

Key words: Impact minerals. Shocked minerals. Characterization.

Abstract: A new field of impact mineralogical sciences is discussed on materials in the Solar System. In order to make clear significance of new terminology, present and future situations are compared with normal mineralogy (by terrestrial tectonic and sedimentary activities) and impact mineralogical sciences (by catastrophic collision by meteoritic impact).

Introduction

Minerals on the Earth are considered to be formed by tectonic activity on the Earth. Various minerals from minor to large sizes and from rock-forming minerals to precious and economic ore minerals are originating from related formation processes within the Earth.

If the Earth is considered to be closed planet of the Earth, minerals on the Earth should be interpretated by the tectonic activity of the Earth. However, the Earth has many impact craters and catastrophic events originated by the extraterrestrial bodies of meteoroids, which suggests that the Earth is not a closed planet anymore. This is new epoch-making interpretation of Earth and mineralogical sciences field, which is similar new interpretation of the Earth movement in the Solar system.

The main purposes of the present paper are to discuss new field of impact mineralogy by making clear significance of new terminology, present and future situations of normal mineralogy (by terrestrial tectonic and sedimentary activities) and impact mineralogical sciences (by catastrophic collision by meteoritic impact).

1. Present and future of impact mineralogical sciences

Mineralogical sciences are total science by the following characterization (Miura, 1992, 1997):

Time (microseconds to years), space (localized on planet to whole solar system);

Reaction (static and closed, or dynamic open), Pressure and Temperature conditions P/T (magmatic high or impact high P/T).

Impact mineralogy should be extended to planetary mineralogical sciences, by using mathematics, physics, chemistry, biology, earth sciences, and engineering sciences (Tab. 1).

2. Impact mineralogical sciences on the Earth

Impact mineralogy includes new terminology of impact and shock wave application to the Earth and solar system, as follows (Miura, 1992, 1994a, 1994b, 1997).

2.1. Terminology of impact and shock waves

Shock wave in rocks and minerals is a dynamic process which travels at supersonic velocities and is capa-

Table 1

Comparison of past and future of mineralogical sciences (Miura, 1992)

	Time	Space	Reaction	P/T conditions
Present (Past)	Long (m,h,y)	Localized	Static, Closed	Magma (high P/T)
Future	Short (ms)	Solar system	Dynamic, Open	Impact (high P/T)

ble of vaporing, melting, mineralogical transforming, or strongly deforming rock materials (French, 1968; Miura, 1992). In meteorite collision, wide meaning of shock wave can be applied to natural hypervelocity collision of a body such as a meteorite (Chao, 1967), as listed in Table 2. Collision shock wave can be found at meteorites, terrestrial rocks, and Lunar and Martian rocks, though collisionless shock waves are reported to observe at cosmic space formed by electric (by solar wind) and magnetic (by Earth's magnetism) fields (Miura, 1992; Miura and Kato, 1993; Miura, 1994a, 1994b, 1997).

2.2. Present and future of impact geology on the Earth

The Earth consists of continental land (ca. 30 vol. %) and ocean (ca. 70 vol. %), whose topography is originally formed by giant impact between proto-Earth and Mars-size parent body, and by its fragments produce at giant impacts (Table 3). Main erosion process of the land is glacial movement, volcanos, or earthquake, whereas that of the ocean is plate-tectonics and mantle convection with new field of mantle plume Earth sciences.

2.3. Significance of impact mineralogical sciences

Significance of impact mineralogical sciences can be summarized as the following three points (Miura, 1994a, 1994b, 1997).

a) Ocean impact on water planet. Major impacts to water planets of the earth are estimated on ocean as 70 volume % of the Earth which has thin crust layer easily broken by impact. Large impact reached to upper mantle produces catastrophic event of mantle convection, plate movements, and explosion with volcanic activity. Such impact makes "impact winter" by stopping sunlight energy. This is very important for five major geological boundaries formed by iron-rich meteoritic impacts mainly on oceanic regions. Sixth extinction on the Earth will be estimated by stopping circulation system by human being who uses huge fossil energy from the crust. Environmental sciences based on mineralogical sciences are important to deal with dynamic circulation system of the Earth (Table 4).

b) New materials by impact sedimentation. Shock wave produces shock metamorphosed materials formed by vapor-liquid-solid reaction. Plasma conditions of impact process reveal new types of materials which are purified iron-spherules in lunar agglutinates, or carbon materials of limestone target-rock (Miura , 1994b). Terrestrial evolved rocks and minerals are also mixed from impact-generated evolved materials on the crust or upper mantle of the Earth (Table 4).

c) Effect of collision and shock impact. Planetary formation of the solar system originated from collisions of dust, and planetesimals, asteroids, planets, and Moon, which can be treated by planetary mineralogical sciences (Table 4).

3. Impact mineralogical sciences in the Solar System

Impact mineralogical sciences can be expanded to the whole space of the solar system.

Table 2
Comparison of terminology of impact and shock waves (Miura, 1992)

Terminology	Time	Changes	Style	Projectiles	Remarks
Shock waves	Short (ms)	P, C, Min, Mor	Collision/ Collisionless	All	SW,Met,Td, Vol, EQ, Life
Impact	Short (ms)	P, C, Min, Mor	Collision	Meteoroids	Meteorites
	Shock waves ≫ Impact				

Table 3
*Comparison of present and future of impact Earth sciences on the Earth**

Time	Area	Information	Erosion	Importance
Present (Past)	Land (30%)	30%	Glacial, Volcano Earthquake	Oil-gas, metallic, water sources; plate-tectonics
Future	Ocean (70%)	70%	Plate, Mantle	Mantle plume Earth Sciences

**Continents* are first uneven surface formed by Giant impact and Earth ring.
Ocean impact: produces catastrophe of the Earth (mantle plume, subduction, continental drift, volcano, and mass extinction; Miura, 1994a).

Table 4
Application of impact mineralogical sciences in the solar system (Miura, 1992, 1994a, 1994b, 1997; Miura and Okamoto, 1995)

Events	New formation	Remarks
Ocean impact	Catastrophic explosion from mantle,	Mantle plume Earth sciences
	Plate-movements	Plate-tectonics
New materials	Purified reduced materials (Fe, C)	VLS reaction, shocked features
	Impact-generated evolved rocks	Mixed in the interior
Collision impact	Dust, planetesimals, asteroids,	Planetary sciences
	Planets, Moon	Moon Geological sciences

3.1. Formation of solar system by impact reaction

Impact reaction can be found at various materials of the solar system, as follows:

a) Earth-type planets: Metallic and silicate materials are originally formed by impact collision and progressive evolution to make Earth-type planets of large core (in Mercury) to small core planets (in Mars). These planets are interpreted by heavy portion of iron-rich fragments after numerous collisions (Miura, 1994a; Miura and Okamoto, 1995).

b) Gas-rich (Jupiter) type planets: From numerous impacts and solar gravitational relations, light portion of solar system materials is concentrated to gas-rich (Jupiter) type planets staring from Jupiter. Such light materials of ice, CHON-rich elements and water ice can be observed at many satellites and planets beyond Jupiter. Characteristic of water ice are based on its crystal structure of OH_4 tetrahedra (similar to hard SiO_4 structure), which is hard as target rock but easily melt and vaporized after heating or impact (Miura, 1994b).

c) Fundamental events of planetary mineralogy. Circulation system between small and large materials can be found on the Earth. In fact, impact growth from small to large sizes, and from amorphous to crystalline materials of minerals is observed in the Moon and planet formation, whereas impact destruction from large to small sizes is found in meteoroids, asteroids, dusts, and spherules. Chemical separation by vapor-liquid-solid reaction can be found at formation of solar system by impact evolution to heavy and light elements. Circulation of elements can be found in cosmic system (from big-bang or supernova to blackhole), in the solar system (from dust, planetesimas, to planets and finally return to dusts), and in the Earth (from vapor in air, water molecules to solid rocks expressed by carbon elements, or CHO or CHON system in total composition). Impact process by shock wave is fundamental dynamic process not only in materials formation of the solar system, but also in organic material formation connected to origin of the life from inorganic to organic compounds (Miura, 1994b).

3.2. New data planetary geology

New interpretation of planetary surfaces is obtained by Venus (as molten mantle without crust), and possible molten mantle surface in Mars (based on EETA84001 Martian meteorites), impact craters without regolith materials or soft materials on three asteroids by remote-sensing techniques. Real impact process can be observed by Shoemaker-Levy comet 9 (SL9) to Jupiter from Olt clouds around the solar system planets. Impacts on planet Earth can be discussed by continents and ocean floors, which are connected to ring materials and origin of the life formation (Miura, 1994b, 1997).

4. Summary

The present results can be summarized as follows:

1. Impact mineralogical sciences have wide new fields and application to the solar system especially to the Earth.

2. Shock wave impacts to the fundamental events of impact mineralogical sciences reveal significant process of dynamic reaction by meteoritic collision.

3. Further development of the Moon, various planets and asteroids feed back to unsolved problems of the Earth's land, ocean, and life origin and evolution.

4. Buried deformed impact craters on the Earth will be the next interesting research projects on the terrestrial surfaces.

5. Global circulation system is significant project on planetary impact sciences (esp. size, chemicals, separation, and copying process).

References

Chao, E.T.C. (1967) Impact metamorphism. Researches in geochemistry (Wiley), 2, p. 204-233.

French, B. (1968) Shock Metamorphism as a geological process. Shock Metamorphism of Natural Materials. 1, p. 1–17.

Miura, Y. (1992) Robotic exploration of the Moon and Mars. Proc. Missions, Technologies and Design of Planetary Mobile Vehicles (Toulouse, CNES), 1, p. 115–124.

— , **Kato, T. (1993)** Shock waves in cosmic space and planetary materials. American Institute of Physics (AIP) Conf. Proc., 283, p. 488–492.

— **(1994)** Global phenomena induced by asteroid impacts on the Earth's ocean-origins of mantle plume, marine biomass extinction and primitive life. *Astron. Soc. Pacific (ASP) Conf. Series*, 63, p. 259–264.

— **(1994)** Material evidence for compositional change of dusts by collision applied to the Solar System formation and asteroid belt. *Astron. Soc. Pacific (ASP) Conf. Series*, 63, p. 286–288.

— , **Okamoto, M. (1995)** Compositional changes of Moon and Earth by impacts. *Proc. Int. Symp. of shock waves (Pasadena, USA)*, 20, p. 1473–1478.

Received: March 1998
Accepted: June 1998

Rom. J. Mineralogy, 79, p. 35-48, Bucureşti, 1999

MÖSSBAUER SPECTROSCOPY IN MINERALOGY AND GEOCHEMISTRY
Part 1: PRINCIPLES AND METHODS

(review paper)

[1]S. CONSTANTINESCU, [2]G. UDUBAŞA, [3]S. CALOGERO
[1]National Institute of Materials Physics, P.O.Box: Mg-07, Bucharest, Romania
[2] Geological Institute of Romania, 78344, Bucharest, Romania
[3]Universita Ca'Foscari di Venezia, Dipt. Chimico - Fisica, 30123, Venezia, Italy

Key words: Mössbauer spectroscopy. Principles. Methods. Applications.

Abstract: In this review paper, the authors pointed out the importance of Mössbauer spectroscopy as a useful tool to investigate the minerals. In the first part of the paper, we introduced the basic principles and methods of the Mössbauer effect. A survey of the hyperfine interactions between the Mössbauer probe and its vicinity and a description of the extracted parameters from most types of Mössbauer experimental spectra are done. The authors evidenced the correlation between these parameters and the hyperfine interaction parameters. They insisted on the Mössbauer information that can be obtained about the local hyperfine fields around the probe. The experimental equipment and other experimental aspects (as the computational aspects to fit the experimental spectra and errors of the extracted spectral parameters) are given too.

1. NUCLEAR GAMMA RESONANCE (MÖSSBAUER EFFECT)

1.1. Resonance process and its energetic spectrum

The resonance processes have been evidenced experimentally by Wood (Wood, 1954) at sodium optical spectra. In these optical spectra, some discrete lines, for the given energies, are shown to be more intense as the rest of spectra. These processes could be explained by the Bohr's atomic theory, which considered the atomic stationary states and the possibility of the electrons to jump between them. In these processes an electromagnetic radiation (optical photons) is emitted or absorbed. The nuclear resonance processes have been evidenced later than 1958, by Mössbauer, due to the experimental difficulties. The principles and methods have been explained in detail in many books and papers, but the authors considered to be useful the works of Mössbauer (1958, 1963), Fraunfelder (1962), Abragam (1964), Wertheim (1964), Matthias (1968), Barb (1973, 1980), Gonser (1975), Gutlich (1975) etc.

In a nuclear resonance process, the nucleus jumping from initial state to final one emits or absorbs an electromagnetic radiation, so called nuclear gamma-radiation (γ -photon) (Figure 1.1). The energy $\hbar\omega_\gamma$ and momentum $\hbar\vec{k}_\gamma$ of absorbed or emitted γ-photon are given by the laws of conservation.

$$\left.\begin{aligned} &\vec{p}_i = \vec{p}_f \pm \hbar\vec{k}_\gamma ;\ \vec{p}_i = 0 \\ &E_i + \frac{p_i^2}{2M} = E_f + \frac{p_f^2}{2M} \pm \hbar\omega_\gamma \end{aligned}\right\} \Rightarrow \hbar\omega_\gamma = E'_o \cong E_o \pm R; E_o = \left|E_i - E_f\right|; R \cong \frac{E_o}{2Mc^2};$$

$+ \rightarrow$ *absobtion case* (1.1)

$- \rightarrow$ *emission case*

Here E_o and R are the energies difference of initial and final states and the recoil energy respectively.

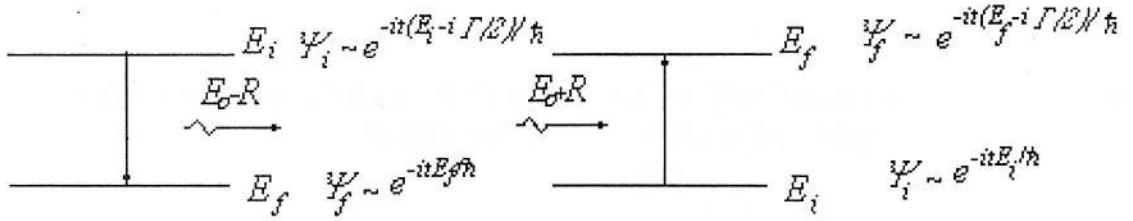

Fig. 1.1 - Emission and absorption of quantum systems

The gamma radiation of the nuclear decay is a superposition of monochromatic electromagnetic waves emitted to $E'_o \pm \Gamma/2$, where Γ is the half - line-width corresponding to life time of the excited nuclear state τ.

$$P_i \propto |\Psi_i|^2 \propto e^{-\frac{t}{\tau}} = e^{-\frac{\Gamma t}{\eta}} \rightarrow \vec{A} = \vec{A}_o e^{-\frac{it}{\hbar}(E_o - i\frac{\Gamma}{2})}$$

$$I(E) \propto \left| \int_o^{\infty} e^{\frac{it}{\hbar}\left[(E-E'_o)-\frac{\Gamma}{2}\right]} dt \right|^2 \propto \frac{\frac{\Gamma}{2\pi}}{(E-E'_o)^2 + \frac{\Gamma^2}{4}} \rightarrow \int_{-\infty}^{+\infty} I(E)dE = 1 \qquad (1.2)$$

The spectrum intensity $I(E)$ is a Lorenz function centered on E_o and with a half - line-width Γ. The energies implied in the nuclear transitions are high energies (~KeV), so the recoil energies of free nuclei are greater than Γ and as a consequence the absorption and emission spectrum intensities are not superposed. That means the emitted γ -photon cannot be absorbed by an identical nucleus (Figure 1.2). As a consequence, the nuclear resonance process is out for free nuclei. In the optical case the resonance processes have been observed due to $R << \Gamma$ (Wood, 1954). Table 1.1 evidences the important differences between the optical and the nuclear transitions.

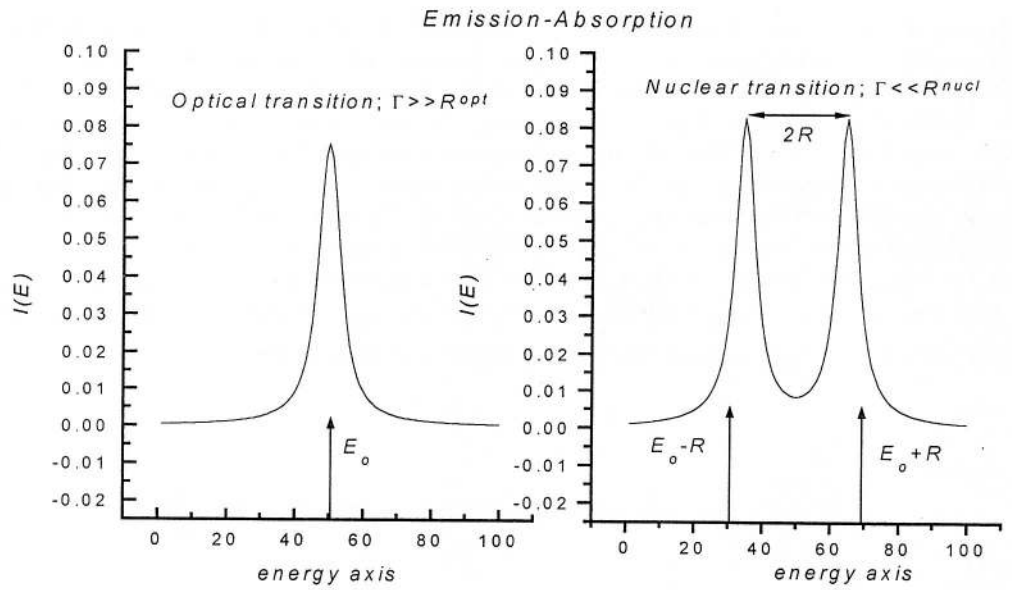

Fig. 1.2 - Emission-absorption processes for optical and nuclear transitions

Table 1.1

Energy[ev]	Optical transition	Nuclear transition
E_o	≈ 4	$\approx 10^3 \div 10^4$
Γ	$\approx 10^{-8}$	$\approx 10^{-8}$
R	$\approx 10^{-10}$	$\approx 10^{-3} \div 10^{-1}$

The nuclear resonance could be obtained if the recoil energy will be dissipated to a large mass (for example: crystals, big molecules etc.)

1.2. Mössbauer effect

Due to the vibration of the nucleus in crystal during the nuclear transition, the recoil energy, corresponding to the nuclear emission or absorption, dissipates by transfer to phonon (vibration) spectrum of the crystal. As the phonon spectrum is quantified, this transfer must occur in multiples of phonon energy and there is the probability f, that recoil energy is not transferred to crystal (Figure1.3). Classically, one shows that f probability (Mössbauer or nuclear Debye-Waller factor) will give by the thermal average of the square amplitude of oscillating emitter (Mössbauer, 1958).

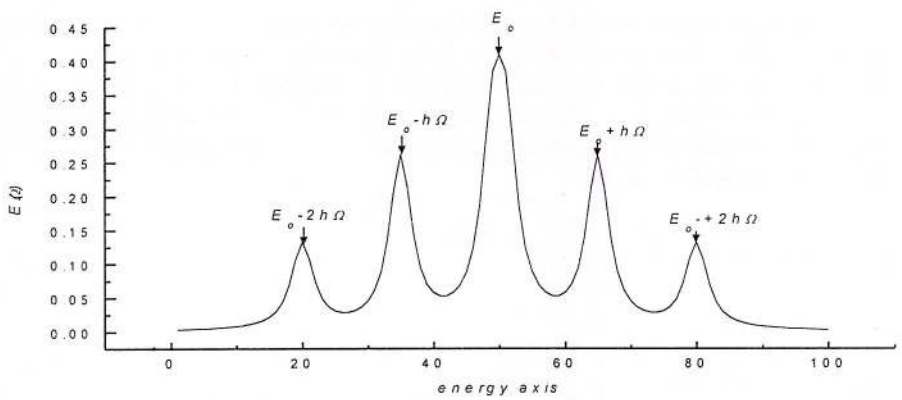

Fig. 1.3 - Classic probabilities of zero, mono, bi and so one phonon nuclear transitions.

$$\vec{A}(t) = \vec{A}_o e^{i\omega t};\ I \propto \left|\vec{A}_o\right|^2$$

$$\omega \to \omega(t) = \omega_o\left[1 + \frac{v(t)}{c}\right] \Rightarrow \vec{A}(t) = \vec{A}_o \exp\left[i\int_0^t \omega(t')dt'\right] = \vec{A}(t) = \vec{A}_o \exp(i\omega_o t)\exp\left[ikx(t)\right]$$

$$\left.\begin{aligned} & x(t) = x_o \sin\Omega t \\ & e^{ikx_o \sin\Omega t} = \sum_{n=-\infty}^{+\infty} J_n(ikx_o)e^{in\Omega t} \end{aligned}\right\} \to \vec{A}(t) = \vec{A}_o \sum_{n=-\infty}^{+\infty} J_n(ikx_o)e^{i(\omega_o + n\Omega)t} \Rightarrow I_{n=0} \propto J_o^2(kx_o) \qquad (1.3)$$

$$\left.\begin{aligned} & f = \prod_{m=1}^{3N} J_o^2(kx_{om}) \\ & J_o(kx_{om}) \cong 1 - \frac{1}{4}(kx_{om})^2 \\ & \left\langle x^2 \right\rangle = \frac{1}{2}\sum_{m=1}^{3N} x_{om}^2 \end{aligned}\right\} \to f \cong e^{-k^2\left\langle x^2\right\rangle} = e^{-\frac{k^2\left\langle u^2\right\rangle}{3}}$$

The condition to obtain the recoil free nuclear transitions is that Γ to be lower than vibrational energy $\hbar\Omega$. The Mössbauer factor depends on the recoil energy R, the crystal temperature T, and on the phonon spectrum density. The

dependencies of f factor on T and phonon spectrum density in the simplest cases of Einstein and Debye crystal models are given by the relations:

$$f = exp\left\{-\frac{2R}{3N\eta}\int_0^{\omega_{max}}\frac{1}{\omega}\left[\frac{1}{2}+n(\omega)\right]\rho(\omega)d\omega\right\};\ n(\omega)=\frac{1}{exp\left(\frac{\hbar\omega}{k_BT}\right)-1};$$

$$Einstein\ Model \rightarrow \rho(\omega)=3N\delta(\omega-\omega_E)\Rightarrow f(T,\omega_E)=exp\left[-\frac{R}{k_B\theta_E}cth\left(\frac{\hbar\omega_E}{2k_BT}\right)\right] \qquad (1.4.)$$

$$Debye\ Model \rightarrow \rho(\omega)=\begin{cases}\frac{9N}{\omega_D^3}\omega^2\ for\ \omega<\omega_D\\ 0\ for\ \omega>\omega_D\end{cases}\Rightarrow f(T,\omega_D)=exp\left\{-\frac{3R}{2\hbar\omega_D}\left[1+4\left(\frac{k_BT}{\hbar\omega_D}\right)^2\int_0^{\hbar\omega_D/k_BT}\frac{xdx}{e^x-1}\right]\right\}$$

Complete data of f factor are given in many Mössbauer data index as of Muir's (1962, 1966) and the above mentioned works.

1.3. Mössbauer line shape in transmission geometry experiment

In a standard Mössbauer experiment with a transmission geometry, the transmitted nuclear radiation is a convolution of emission and absorption intensities, $I_S(E)$, $I_A(E)$. That means it depends on the emitted and absorption Lorenz functions, Mössbauer factors and the volume concentration (abundance) of isotopes in the source f_S, c_S, and absorber f_A, c_A and the absorber thickness z. On the other hand the energies of resonance in absorber and source are in generally different, so the source is moving relative to the absorber to compensate this source-absorber energy difference. Finally the transmission function is:

$$E(v)=E_{oS}(1+v/c);\Gamma=\frac{\Gamma_S+\Gamma_A}{2};$$

$$\left.\begin{aligned}I_S(E,v)&\propto\frac{\frac{\Gamma_S}{2\pi}}{\left[E(v)-E_{oS}\right]^2+\frac{\Gamma_S^2}{4}}\\ \sigma_A(E)&\propto\sigma_o I_A(E)\end{aligned}\right\}\rightarrow T(v)\propto\int_{-v_{max}}^{+v_{max}}c_S f_S I_S(E,v)exp\left[-c_A f_A\sigma_A(E)z\right]dE \qquad (1.5)$$

The normalized experimental spectrum $\varepsilon(v)$ contains the distribution of the γ -photons relative to energy, taken in velocity units:

$$\varepsilon(v)=\frac{N_\infty-N(v)}{N_\infty}=1-\frac{T(v)}{c_S f_S}\propto c_A f_A\sigma_o z\frac{\frac{\Gamma}{2\pi}}{(v-v_o)^2+\frac{\Gamma^2}{4}} \qquad (1.6)$$

1.4. Basic Mössbauer equipment

The basic equipment for a Mössbauer spectrometer in transmission geometry is containing the driver with the source, the absorber box with the absorber and electronic controlling equipment (Figure 1.4). The driver is moving in a sinusoidal or saw-teeth mode. The absorber box is a vacuum room where the absorber is keeping to controlling temperature and/or the pressure. A computer analyzing and fitting Mössbauer spectra is attached to the spectrometer.

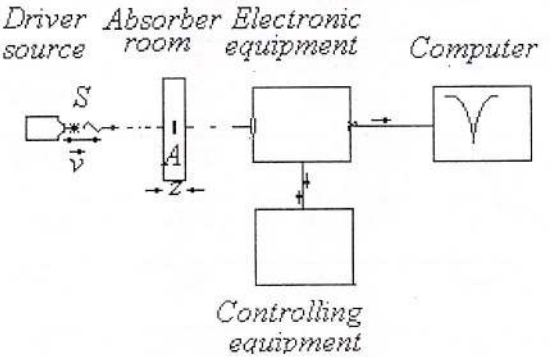

Fig. 1.4 - Basic Mössbauer equipment in transmission geometry

1.5. Computational method to fit the spectrum

To obtain correct information from the Mössbauer investigation a very careful determination of the spectral parameters is necessary by using the fitting programs. The well-known method to fit the spectra is the so-called χ^2 method. which minimizes the square of difference between the experimental points $\varepsilon_{exp}(v_i)$ of spectrum and a sum of n transmission Lorenz functions

$$\chi^2 = \frac{1}{Nr.pct - m - 1} \sum_{i=1}^{Nr.pct.} \frac{1}{\sigma_i^2} \left[f(v_i; \alpha_1, \alpha_2, \ldots \alpha_k - \varepsilon_{exp}(v_i) \right]^2 ; \qquad (1.7a)$$

$$f(v, \varepsilon_{calc}^{(1)}, v^{(1)}, \Gamma^{(1)}, \ldots) == \sum_{j=1}^{n} \varepsilon_{calc}^{(j)} \frac{(\Gamma^{(j)}/2)^2}{(v - v^{(j)})^2 + (\Gamma^{(j)}/2)^2} \qquad (1.7b)$$

where $\varepsilon^{(j)}{}_{calc}$, $v^{(j)}$ and $\Gamma^{(j)}$ are the spectral parameters of the resonance lines. The statistical errors of the spectral parameters are obtained by the inversion of errors' matrix. Finally errors' expressions are:

$$\sigma_{\varepsilon^{(j)}} = \frac{2\sqrt{2}}{\sqrt{\pi N_\infty \frac{\Gamma^{(j)}}{\Delta n_i}}}; \quad \sigma_{v^{(j)}} = \frac{\Gamma^{(j)}\sqrt{2}}{\varepsilon^{(j)}\sqrt{\pi N_\infty \frac{\Gamma^{(j)}}{\Delta n_i}}}; \quad \sigma_{\Gamma^{(j)}} = \frac{4\Gamma^{(j)}}{\varepsilon^{(j)}\sqrt{\pi N_\infty \frac{\Gamma^{(j)}}{\Delta n_i}}}; \quad \sigma_{N_\infty} = \sqrt{N_\infty} \qquad (1.8a)$$

for distinct resonance lines satisfying the relation $(v^{(j)} - v^{(i)})/\Gamma^{(j)} > 1$. N_∞ designates the spect-rum background and n_j corresponds to $\Gamma^{(j)}$ given in experimental points numbers. The line position errors have more complicated formulas and bigger values as standard ones, in the case $(v^{(j)} - v^{(i)})/\Gamma^{(j)} < 1$.

$$\Delta v^{(i)} = \frac{\varepsilon^{(j)}\Gamma^{(i)2}}{\varepsilon^{(i)}\Gamma^{(j)2}} (v^{(j)} - v^{(i)}) / \left[1 + 4\frac{(v^{(j)} - v^{(i)})^2}{\Gamma^{(j)2}} \right]^2 \qquad (1.8b)$$

Finally in this paragraph we mention that the newest and the best fitting program used for all Mössbauer isotopes is the MOSS90 (Grosse, 1992).

1.6. Characteristics of useful Mössbauer isotopes

A nucleus is a Mössbauer isotope if $R < \hbar\omega_{D,E}$ and $\hbar\omega_{D,E} > \Gamma$. There are a lot of Mössbauer nuclei, but the great majority of Mössbauer works have been done on ^{57}Fe and ^{119}Sn because at room temperature f factors are significant, their precursors are a long life-time and their natural abundance is ~%. Table 1.2 presents the Mössbauer nuclei mostly used in the mineralogical investigations (Barb, 1972, 1980).

Table 1.2. The Mössbauer nuclei mostly used in mineralogical investigations

Mössbauer nucleus	Natural abundance [%]	Transition	γ-energy [KeV]	$T_{1/2}$ of precursor	2Γ [mm/s]	Q $[10^{-24}cm^2]$	μ $[\mu_N]$
^{57}Fe	2.19	$3/2^+ \rightarrow 1/2^+$	14.4	270d	0.194	+0.187	-0.15 +0.09
^{119}Sn	8.58	$3/2^+ \rightarrow 1/2^+$	23.83	245d	0.647	-0.06	+0.69 -1.05
^{121}Sb	57.25	$7/2^+ \rightarrow 5/2^+$	37.2	50y	2.104	-0.35 -0.26	+2.48 +3.36
^{129}Xe	26.44	$1/2^+ \rightarrow 3/2^+$	80.2	$1.6 \cdot 10^7$y	7.152	-0.12	+0.69 -0.78
^{67}Zn	4.11	$1/2^- \rightarrow 5/2^-$	93.31	78h	0.0003	+0.18	+0.58 +0.88
^{197}Au	100	$1/2^+ \rightarrow 3/2^+$	77.3	65h	1.871	+0.58	+0.42 +0.14
^{186}Os	13.3	$2^+ \rightarrow 0^+$	155.03	90.65h	2.403	-1.80	+0.64

2. MÖSSBAUER SPECTRUM PARAMETERS

The linewidth of the zero-phonon process is extremely small relative to characteristic energies of interactions between the nucleus and its vicinity. The peaks in a Mössbauer spectrum are very sensitive to the extra-nuclear environment, so different compounds give different spectra and the different sites of the Mössbauer isotopes in the same compound give different subspectra, etc. The interactions between the Mössbauer nucleus and its neighbourhoods are so-called hyperfine interactions. The nuclear and extranuclear factors of the hyperfine interaction are the electric and magnetic moments of the nucleus and the electric and magnetic fields, given by the crystalline neighbourhood.

$$E^{el} = \int_{\infty} \rho(\vec{r})V(\vec{r})d\vec{r} = V(0)\int_{\infty} \rho(\vec{r})d\vec{r} + \frac{1}{2}\sum_{i,j} V_{i,j} \int_{V_{nucl.}} \rho(\vec{r})x_i x_j d\vec{r}; x_i = x,y,z;$$
$$E^{mag} = -\vec{\mu}\cdot\vec{H} = -g\beta\vec{I}\cdot\vec{H}; \beta = \frac{e\hbar}{2Mc}; \qquad (1.9)$$

The nuclear factors of the energy interactions are the electric charge density $\rho(\vec{r})$, the electric nuclear quadrupole moment $eQ_{i,j} = \int_{V_{nucl.}} \rho(\vec{r})x_i x_j d\vec{r}$ (given in barns) and the nuclear magnetic moment $\vec{\mu}(= g_I \vec{I}\beta$ where β and g_I are nuclear Bohr's magnetons and giromagnetic factor, respectively). The environment factors are the electric potential $V(\vec{r})$, the electric field gradient $V_{i,j}(\vec{r})$ and magnetic field $H(\vec{r})$ at the Mössbauer nucleus site. From the above mentioned resonance line parameters, one can determine the hyperfine interactions parameters corresponding to the surrounding electric and magnetic fields. Other important spectrum parameter is the resonance line area A given by the half-linewidth, Γ, and the resonance effect $\varepsilon(\nu_0)$.

2.1. Isomer shift parameter

The interaction between the nuclear charge density and the electric potential $V(0)$ of the electronic charge having a nonzero probability in the finite nuclear volume generates the isomer shift δ.

$$E_1^{el} = -\frac{2\pi}{3} e|\Psi(0)|^2 \int_{V_{nucl}} \rho(r)r^2 dr = -\frac{2\pi}{3} Ze^2 |\Psi(0)|^2 \langle R^2 \rangle \qquad (1.10a)$$

The effect of the presence E_1^{el} is different shifts of initial and final nuclear levels, implied in the Mössbauer transition. The isomer shift δ depends on the charge and square effective radius $<R^2>$ in initial and final nuclear states and on the probability of *ns* electrons at the nucleus in the source and absorber. δ can give information about the *ns* electrons density at nucleus volume, when the nuclear factors are known.

$$\delta_{A-S}=E_{IS}^{el}-E_{IA}^{el}=S(Z)\frac{2\pi}{3}Ze^2\left[\langle R^2\rangle_i-\langle R^2\rangle_f\right]\cdot\left[|\Psi(0)|_A^2-|\Psi(0)|_S^2\right]=cstZe^2R_{eff}^2S(Z)\frac{\Delta R}{R}\left[|\Psi(0)|_A^2-|\Psi(0)|_S^2\right];$$
$$R_{eff}\cong 1.2A^{1/3}\cdot 10^{-15}m;S(Z)\rightarrow relativistic\ effect;\Delta R\cong R_i-R_f \quad (1.10b)$$

As one can see, from the above formula, an increasing of *ns* electron probability in finite nuclear volume in absorber determines an increasing if $\Delta R>0$ (e.g. ^{119}Sn) or a decreasing if $\Delta R<0$ (e.g. ^{57}Fe) of δ_{A-S}. The isomer shift is sensitive to the number of valence electrons and consequently to chemical bonds of Mössbauer parent ion and the surrounding ions. So, if the number of 3d electrons of Fe-ion is increasing the density of 3s, 2s and 1s electrons at nucleus will decrease (due to a larger swelling of 3s electronic density)and $\delta_{Fe\text{-}S}^{1s}$, $\delta_{Fe\text{-}S}^{2s}$ and $\delta_{Fe\text{-}S}^{3s}$ are increasing. A higher density of 4s electrons will decrease $\delta_{Fe\text{-}S}^{4s}$. The two effects are in competition. In Mössbauer spectrum, the energy difference δ_{A-S}, due to the difference between *ns* electrons probabilities to the finite nuclear volume, for the source and absorber, will appear by a shift of the absorber resonance line to source one. The total shift of the resonance line will also contain a thermal shift the so-called the second order Doppler shift δ_{SODS}, $\delta_{CS}=\delta_{A-S}+\delta_{SODS}$. The second term depends on the temperature and phonon spectrum parameters. So, for the simplest crystal models this dependence is:

$$Einstein\ model\rightarrow\delta_{SODS}(T,\theta_E)=\frac{E_R k_B\theta_E}{2Mc^2}cth\left(\frac{\theta_E}{2T}\right);k_B\theta_E=\hbar\omega_E;$$
$$Debye\ model\rightarrow\delta_{SODS}(T,\theta_D)=-\frac{9k_BE_o}{16Mc^2}\left[\theta_D+8T\left(\frac{T}{\theta_D}\right)^3\int_0^{\theta_D/T}\frac{x^3dx}{e^x-1}\right];k_B\theta_D=\hbar\omega_D; \quad (1.10c)$$

2.2. Quadrupole splitting parameter

The expression of δ was derived assuming a spherical charge density, but the real nucleus has a non-spherical one, so there are possible high order interactions with a non-cubic distribution of ionic and/or electronic charges. If the nucleus has a nonzero quadrupole moment Q and a non-cubic extra-nuclear symmetry exits, the second term $E^{el}{}_2$ of the E^{el} is nonzero.

$$E_2^{el}=\frac{1}{6}\sum_{i,j=1}^{3}V_{i,j}\int_{V_{nucl.}}(3x_ix_j-r^2\delta_{i,j})\rho(r)dr=\frac{1}{6}\sum_{i,j=1}^{3}V_{i,j}Q^{i,j} \quad (1.11a)$$

The principal components $V_{i,i}$, of the electric field gradient (EFG) tensor, will determine if the electric nuclear quadrupole moments would be known for the states implied in transitions. The extra-nuclear factor EFG tensor has two contributions. The first contribution is the lattice one, generated by crystal ions $V_{i,j}^{latt}$, and the second contribution is giving by the surrounding valence electrons $V_{i,j}^{el}$ of Mössbauer parent atom.

$$V_{i,j}^{latt}=\sum_{k=1}^{Nr.ioni}\frac{q_k}{4\pi\varepsilon_o}\cdot\frac{3x_{kj}x_{ki}-r_{ki}^2\delta_{ij}}{r_{ki}^5};V_{i,j}^{el}=-e\sum_{k=1}^{Nr.electr.}p_k\left\langle\Psi_k\left|\frac{3x_jx_i-r_i^2\delta_{ij}}{r_i^5}\right|\Psi_k\right\rangle;p_k=\frac{e^{-\frac{\Delta_k}{k_BT}}}{\sum_i e^{-\frac{\Delta_i}{k_BT}}};(1.11b)$$

Here Ψ_k is the electronic wave function with the weight p_k corresponding to ionic level Δ_k.

It is important to mention when crystal field determines low or large values of Δ_k. the valence electrons realize high or low spin configurations. Figure 1.5 shows the ionic splitting of a 3d shell in different symmetry of crystal field

and the spin configurations for iron ions in crystalline fields. Magnetic electronic moment is given in electronic Bohr's magnetons.

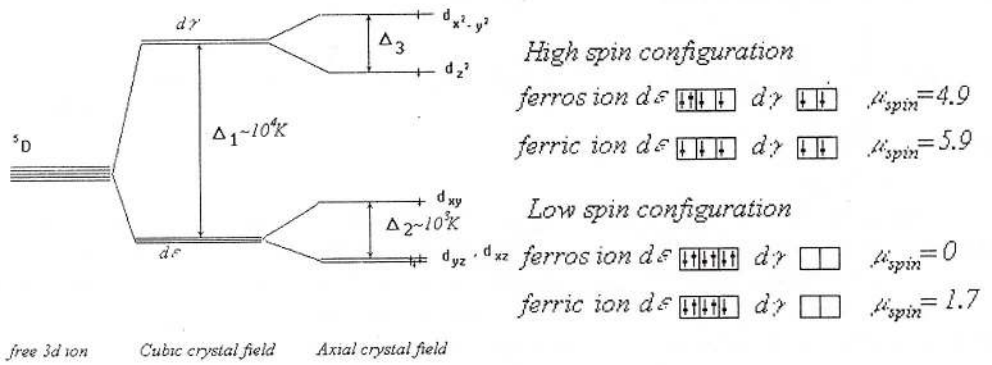

Fig. 1.5 - The ionic splitting of 3d shell in different symmetry of crystal field; and 3d spin configurations of iron ions

The contributions of p and d electrons to principal components of EFG-tensor are given in Table 1.3. The presence of the two EFG contributions will distort the inner electrons of the parent atom and as a consequence these contributions will magnify with the Sterheimer anti shielding factors γ_∞, R. The covalence factor α^2 also seems to exist in $V_{i,j}$. In the case of ^{57}Fe the Sterheimer's factors are $\gamma_\infty \approx -10.$ and $R \approx 0.32$.

$$V_{i,j} = (1-\gamma_\infty)V_{i,j}^{latt} + (1-R)\alpha^2 V_{i,j}^{el} \qquad (1.11c)$$

These two contributions are competing, having generally different signs. In the presence of hyperfine quadrupolar interactions the nuclear levels $(I>1/2)$ are splitting. So, in the axial symmetry, the energies of nuclear levels are:

$$Axial\ symmetry \Rightarrow \eta = \frac{V_{xx}-V_{yy}}{V_{zz}} = 0; E_{I,I_z} = \frac{eQV_{zz}}{4I(2I-1)}\left[3I_z^2 - I(I+1)\right] + \delta \qquad (1.11d)$$

and in the nonaxial symmetry the energies values are more complicated expressions depending on the asymmetry parameter η (see Table 1.4) (Grechishkin, 1972). The $V_{i,j}$, I and I_z are the principal components of EFG-tensor, the nuclear spin and its component on quantification axis.

Table 1.3.
The principal values of EFG-tensor components for p and d electrons

Electronic states	V_{xx} $[e\langle r^{-3}\rangle]$	V_{yy} $[e\langle r^{-3}\rangle]$	V_{zz} $[e\langle r^{-3}\rangle]$	η
p $\|x\rangle$	-4/5	+2/5	+2/5	-3
$\|y\rangle$	+2/5	-4/5	+2/5	+3
$\|z\rangle$	+2/5	+2/5	-4/5	0
d $\|xy\rangle$	-2/7	-2/7	+4/7	0
$\|yz\rangle$	+4/7	-2/7	-2/7	+3
$\|xz\rangle$	-2/7	+4/7	-2/7	-3
$\|x^2-y^2\rangle$	-2/7	-2/7	+4/7	0
$\|3z^2-r^2\rangle$	+2/7	+2/7	-4/7	0

Table 1.4.
The dependencies of nuclear levels on nuclear spin and asymmetry parameter

Nuclear Spin I	*Level k*	$E_{I,k}(I,\eta)$
1	*1,2;3;*	$\frac{eQV_{zz}}{4}(1\pm\eta);-\frac{eQV_{zz}}{2}$
3/2	*1,2;*	$\pm\frac{eQV_{zz}}{4}\sqrt{1+\frac{\eta^2}{3}};$
2	*1,2;3;4,5;*	$\pm\frac{eQV_{zz}}{4}\sqrt{1+\frac{\eta^2}{3}};\frac{eQV_{zz}}{4};-\frac{eQVzz}{8}(1\pm\eta);$
5/2	*1,2;3,4;*	$-\frac{eQV_{zz}}{10}\left(1\pm\sqrt{1+\frac{5\eta^2}{3}}\right);eQV_{zz}\left[\frac{1-\eta}{20}\pm\sqrt{\frac{6+3\eta+3\eta^2}{150}}\right];$
	5,6;7;	$eQV_{zz}\left[\frac{1+\eta}{20}\pm\sqrt{\frac{6-3\eta+3\eta^2}{150}}\right];0;$

The effect of quadrupole interaction consists of the presence of a lot of resonance lines. So in the case of nuclear transition $/E_{3/2}, 3/2> \leftrightarrow / E_{1/2}, 1/2>$, the Mössbauer spectrum will evidence two peaks at v_1 and v_2 positions. Of course the difference between the two positions depends on the nuclear factor, the nuclear quadrpole moment $Q^{n.i}$, and on the environmental factor given by electric field gradient (EFG) showing by $V_{i,i}$. The spectral parameters of such transmission spectrum are the quadrupole splitting ΔE_Q and the central shift $\delta_{C.S}$:

$$\left\langle E_{3/2},\frac{3}{2}\right| \leftrightarrow \left\langle E_{1/2},\frac{1}{2}\right| \Rightarrow \Delta E_Q=\frac{eQV_{zz}}{2}\sqrt{1+\frac{\eta^2}{3}}=v_2-v_1;\delta_{A-S}=\frac{v_2+v_1}{2} \qquad (1.11e)$$

It is important to mention that ΔE_Q cannot give the sign of V_{zz}.

2.3. Magnetic splitting parameter

The third important hyperfine interaction term corresponds to the nuclear Zeeman effect, between the nuclear magnetic momentum μ and the extranuclear magnetic field H. This interaction will occur if there is a magnetic field at the Mössbauer nucleus site. The magnetic field at the nucleus can originate from the unbalanced s-electron spin density (Fermi contact field) H_S, from the bipolar interaction between the nuclear and atomic spin moments H_D, from orbital atomic momentum if is non-zero H_L, from local H_{loc} and from external H_o field.

$$\vec{H}=\vec{H}_{loc}+\vec{H}_L+\vec{H}_S+\vec{H}_D$$
$$\vec{H}_S=-\left(\frac{16\pi}{3}\right)\mu_B\left\langle\sum_i\vec{S}_i\delta(r_i)\right\rangle;\vec{H}_L=-2\mu_B\left\langle r^{-3}\right\rangle g\langle\vec{L}\rangle=-2\mu_B\left\langle r^{-3}\right\rangle(g-2)\langle\vec{S}\rangle; \qquad (1.12a)$$
$$\vec{H}_D=-2\mu_B\left\langle\frac{3\vec{r}(\vec{s}\cdot\vec{r})}{r^5}-\frac{s}{r^3}\right\rangle\xrightarrow[axial\ symmetry]{}\vec{H}_D=-2\mu_B\left\langle r^{-3}\right\rangle(3\cos^2\vartheta-1)\langle\vec{S}\rangle;$$

The presence of H at nucleus position splits the initial and final energetic levels and consequently there are a lot of the selected transitions($\Delta I_z=0,\pm1$). When a small electric quadrupole interaction appears the splitted levels are shifted.

$$eQV_{zz} << \mu H \xrightarrow[\text{axial symmetry}]{} E_{I,I_z} = -g_I \beta H I_z + (-1)^{|I_z|+\frac{1}{2}} \frac{\Delta E_Q}{2} \cdot \frac{3\cos^2\theta - 1}{2} + \delta \quad (1.12b)$$

Here θ designates the angle between directions of H and oz-principal axis of EFG-tensor component V_{zz} (see Figure 1.6). In the Mössbauer spectrum there will appear a lot of peaks at ν_i positions. So, in the case of the nuclear transition $/E_{3/2},3/2> \leftrightarrow /E_{1/2},1/2>$, (see Figure 1.7) the magnetic, quadrupole splitting and central shift parameters are given by the relations:

$$\begin{aligned} &\delta_{CS} = \frac{1}{4}(\nu_1 + \nu_2 + \nu_5 + \nu_6); \varepsilon_Q = \frac{1}{2}(\nu_1 - \nu_2 + \nu_6 - \nu_5); \\ &\Delta_H = (3g_{3/2} - g_{1/2})\beta H \rightarrow H = \frac{\nu_6 - \nu_1}{(3g_{3/2} - g_{1/2})} = \frac{\nu_6 - \nu_1}{0.0322} \end{aligned} \quad (1.13a)$$

Here the resonance line positions for $/E_{3/2},3/2> \leftrightarrow /E_{1/2},1/2>$ transition of ^{57}Fe are:

$$\begin{aligned} &\nu_{1,6} = \delta_{CS} + \varepsilon_Q' \pm (\frac{3}{2}g_{3/2} - \frac{1}{2}g_{1/2})\beta H = \delta_{CS} + \varepsilon_Q' \pm 0.01610H; \\ &\nu_{2,5} = \delta_{CS} - \varepsilon_Q' \pm (\frac{1}{2}g_{3/2} - \frac{1}{2}g_{1/2})\beta H = \delta_{CS} - \varepsilon_Q' \pm 0.00932H; \\ &\nu_{3,4} = \delta_{CS} - \varepsilon_Q' \pm (\frac{1}{2}g_{3/2} + \frac{1}{2}g_{1/2})\beta H = \delta_{CS} - \varepsilon_Q' \pm 0.00254H; \\ &[\delta_{CS}] = [\varepsilon_Q'] = mm/s; [H] = KOe \end{aligned} \quad (1.13b)$$

It is necessary to mention that relations between the most extreme peaks at iron isotope permit to establish the sign of ε_Q relative to H:

$$\left.\begin{aligned} \nu_2 - \nu_1 &= -2\varepsilon_Q + 0.00678H; \\ \nu_6 - \nu_5 &= +2\varepsilon_Q + 0.00678H; \end{aligned}\right\} \rightarrow \begin{cases} \nu_2 - \nu_1 < \nu_6 - \nu_5 \Rightarrow \varepsilon_Q > 0 \\ \nu_2 - \nu_1 > \nu_6 - \nu_5 \Rightarrow \varepsilon_Q < 0 \end{cases} \quad (1.13c)$$

Moreover the resonance positions are satisfying controlling relations, so in the case of above mentioned isotope they are:

$$\left.\begin{aligned} \nu_2 - \nu_4 = \nu_3 - \nu_5 &= Hg_{\frac{1}{2}}\beta = -0.01186H \\ \nu_3 - \nu_2 = \nu_5 - \nu_4 &= Hg_{\frac{3}{2}}\beta = +0.00678H \end{aligned}\right\} \Rightarrow \frac{\nu_4 - \nu_2}{\nu_3 - \nu_2} = \frac{|g_{1/2}|}{|g_{3/2}|} \xrightarrow{^{57}Fe} \frac{\nu_2 - \nu_4}{\nu_3 - \nu_2} \cong 1.75 \quad (1.13d)$$

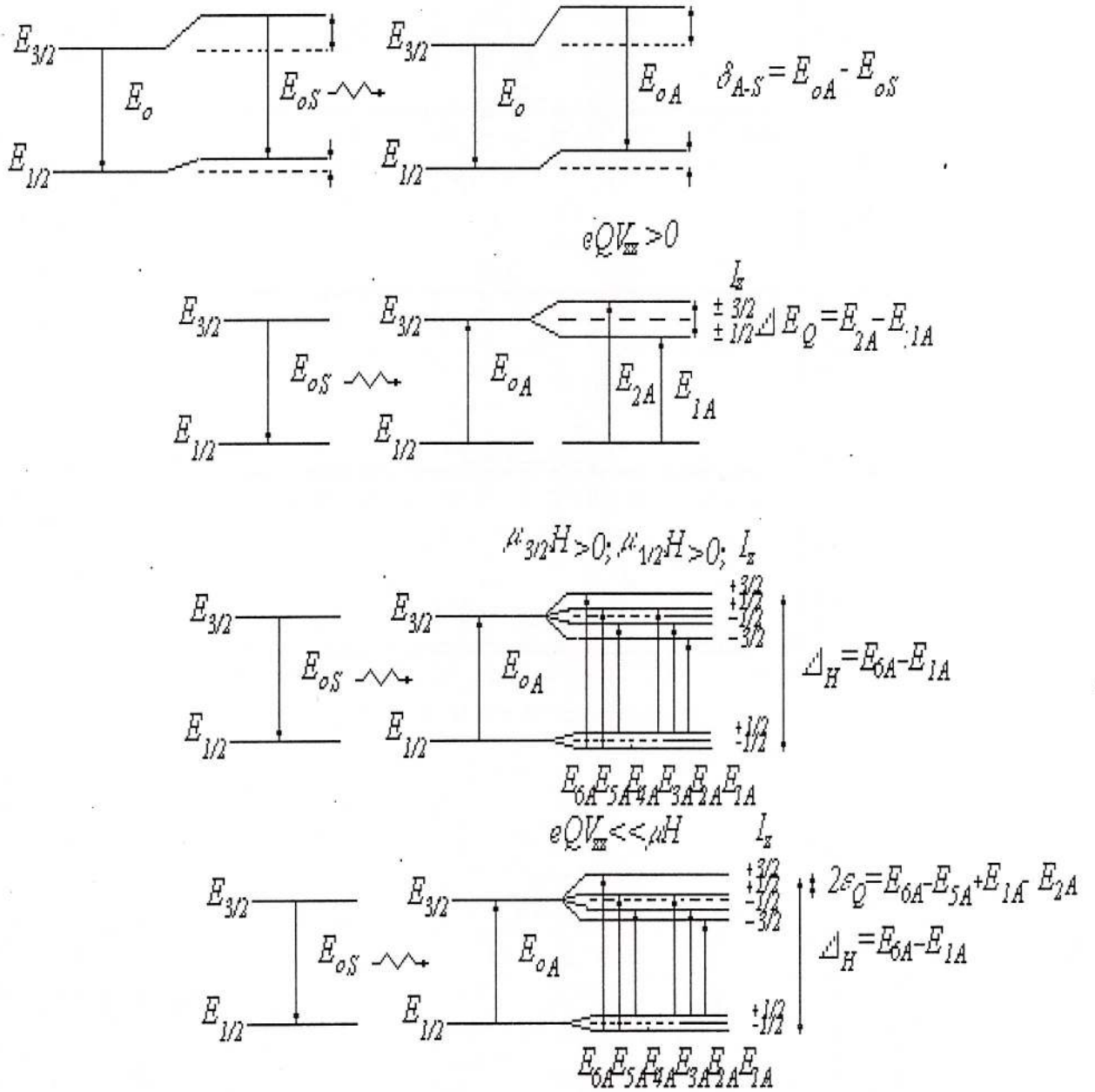

Fig. 1.6 - The splittings of nuclear levels in hyperfine fields

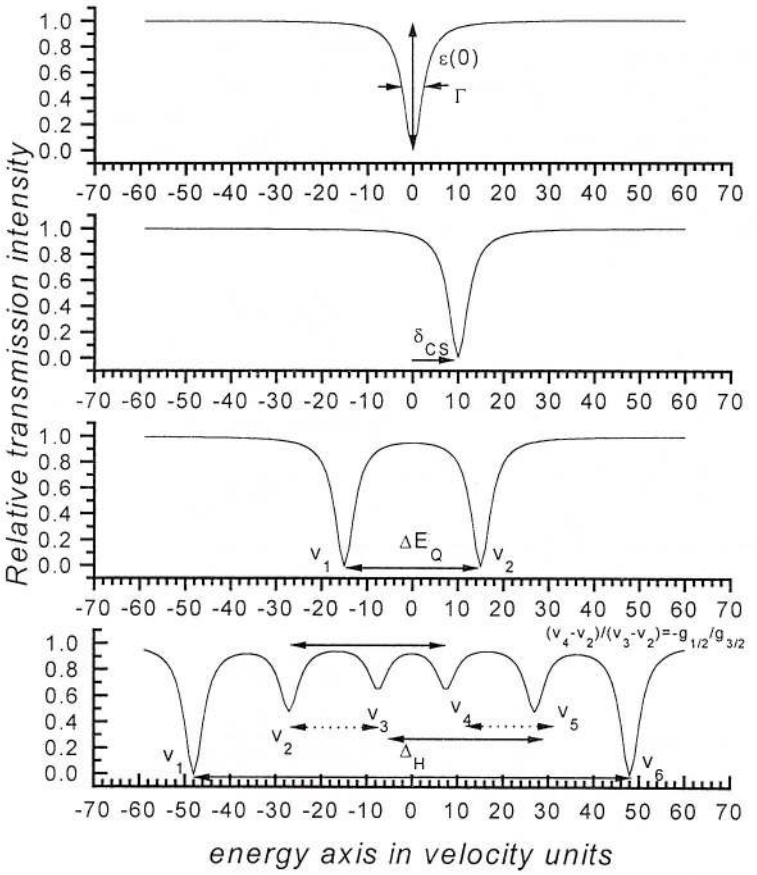

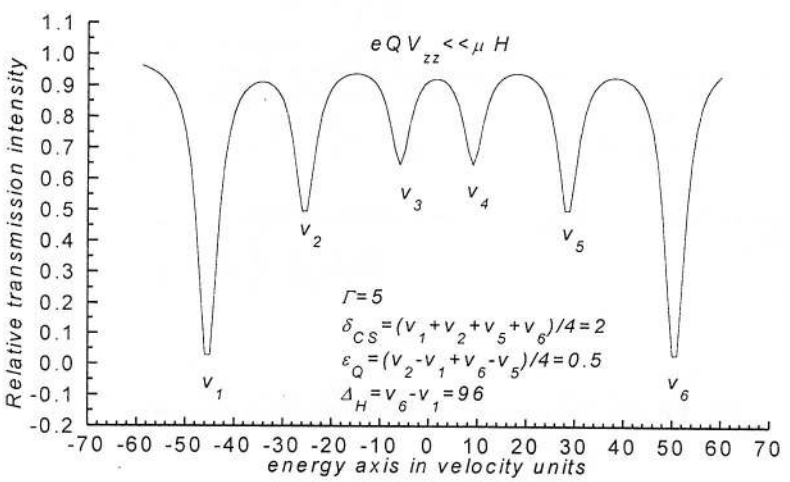

Fig. 1.7 - The spectra corresponding to the presence of hyperfine fields at Mössbauer isotope site

2.4. Resonance effect, half line-width and area parameters

The effect $\varepsilon(v_o)$ is the resonance dip at its position. The resonance effect and absorption area A under the peak are given by:

$$\varepsilon(v_o)=\frac{N_\infty - N(v)}{N_\infty}=1-\frac{T(v_o)}{c_S f_S}\propto\frac{2c_A f_A \sigma_o z}{\pi\Gamma};A=\int_{-v_{max}}^{+v_{max}}\varepsilon(v)dv\propto\varepsilon(v_o)\Gamma \qquad (1.14a)$$

and depends on the absorber f_A factor, half-linwidth $\Gamma(=\Gamma_S+\Gamma_A)$ and abundance c_A of Mössbauer parent atoms. Theoretically it is possible to determine c_A from A, but in practice there are many difficulties. The resonance area corresponds to the probability of a given nuclear transition in the hyperfine fields and this is a function of the angles between the orientations of these fields relative to the γ-ray momentum $\hbar\vec{k}_\gamma$. In the polycrystalline sample, there is not angular dependence of A values, due to the angular average. So in the case of $/E_{3/2},3/2>\leftrightarrow/E_{1/2},1/2>$ transition we have:

$$H\neq 0\rightarrow\left.\begin{array}{l}A_1=A_6\propto 3(1+\cos^2\beta);\\ A_2=A_5\propto 4\sin^2\beta;\\ A_3=A_4\propto 1+\cos^2\beta;\end{array}\right\}\rightarrow\left\{\begin{array}{l}\overline{A}_1=\overline{A}_6\propto 3\\ \overline{A}_2=\overline{A}_5\propto 2\\ \overline{A}_3=\overline{A}_4\propto 1\end{array}\right. \qquad (1.14b)$$

$$V_{zz}\neq 0\rightarrow\left.\begin{array}{l}A_1\propto 3(1+\cos^2\beta)\\ A_2\propto 2+3\sin^2\beta\end{array}\right\}\rightarrow\left\{\begin{array}{l}\overline{A}_1\propto 1\\ \overline{A}_2\propto 1\end{array}\right.$$

Finally it is important to mention that in the general case the vicinity of Mössbauer probe showed both electric hyperfine field and magnetic one so the Mössbauer spectra and their parameters are more complicated, because they are depending on the ratio $R=\Delta E_Q/\mu H$, η, θ, and φ (Barb, 1971, 1972; Constantinescu, 1980).

Acknowledgements

One of the authors is grateful to the financial supports from the Committee of CNR (Roma), Progetto Sistema Lagunare Veneziano, E.N.E.A in the framework of the Italian National Programme for Antarctic Researches, PNRA (Environmental Impact-Chemical Methodologies) and from the M.C.T. (Bucharest), Programme Orizont 2000 (The investigations of archaeological and geological materials by the techniques of resonance spectroscopies).

References

Abragam, A. (1964) L'Effect Mössbauer. Ed. Gordon and Breach. New York, 70 p.

Barb, D. (1972) Efectul Mössbauer si aplicatiile sale. Ed. Academiei R.S.R., p. 104-145.

-- **(1980)** Grundlagen und Anwendungen der Mössbauer-Spektroskopie. Akademie-Verlag, Berlin, p. 105-168.

-- , **Constantinescu, S., Tarina, D. (1971)** Polarized γ-rays transition probabilities in the case of coupled electric and magnetic hyperfine interactions. *Rev. Roum. Phys.*, 16, p. 263.

-- , **Constantinescu, S., Tarina, D. (1971)** Formulas for the relative γ-transition probabilities of the Mössbauer isotopes. *Rev. Roum. Phys.*, 16, p. 1005.

-- , **Constantinescu, S., Diamandescu, L., Tarina, D. (1972)** Contributions to the Mössbauer line shape in the coupled hyperfine interactions. *Rev. Roum. Phys.*, 17, p. 769.

Constantinescu, S. (1980) Mössbauer Investigations of Coupled Hyperfine Interactions, Ph.D. Thesis in Physics. Ed. Central Institute of Physics/Inst. Phys. Tech. Mat., 196 p., p. 7-38, Bucharest.

Fraufelder, H. (1962) The Mössbauer Effect. Ed. W.A. Benjamin, 336 p., New York.

Grechishkin, V. S. (1972) Iadernie Kvadrupolnie Vzaimodeictvie v Tverdih Telah . Ed. Nauka, p. 15-23, Moskva.

Greenwood, N. N. (1971) Mössbauer Spectroscopy. 659 p., New York, Springer-Verlag.

Gonser, U. (1975) Mössbauer Spectroscopy, 525 p., New York, Ed. Springer-Verlag.

Grosse G., (1992) MOS-90, Version 2.2. Ed. Technical University of Munich.

Gutlich, P. (1978) Mössbauer Spectroscopy. Springer-Verlag, S68, 280 p., Berlin.

Matthias, E., Shirley, D. A. (1968) Hyperfine Structure and Nuclear Radiation. Amsterdam, Ed. North-Holland Publishing Co.

Mössbauer, R. L. (1958) Kernresonanzfluoreszenz von Gammastrahlung in Ir^{191}, *Z. Physik*, 151, 124.

-- **(1959)** Kernresonanzfluoreszenz von γ-strahlung in Ir^{191}. *Z. Naturfosch*, 14, p. 211.

-- **(1963)** Nuclear resonance fluorescence of γ-radiation. (B) Recoiless nuclear resonance absorption and its applications. In Alpha, Beta and Gamma-ray Spectroscopy. Ed. by K. Siegbahn, Amsterdam, North-Holland, XXI, p. 1293.

-- , **Sharp, D. H. (1964)** General aspects of nuclear hyperfine interactions in salts of rear earths. *Rev. Mod. Phys.*, 36, p. 410.

Muir, A. H. (1962) Tables and Graphs for Computing Debye-Waller Factors in Mössbauer Studies, AI-6699, At. Int. Div., Canoga Park, California, U.S.A.

-- , **Ando, K. J., Coogan, H. M. (1966)** Mössbauer Data Index 1958-1965. Ed. Plenum Press, New York.

Wood, R.W. (1954) Physical Optics. Ed. Mc. Millan, New York.

Wertheim, G. K. (1964) Mössbauer Effect, Principles and Applications. Ed. Academic Press, 116 p., New York.

Rom. J. Mineralogy, 79, p. 49-70, Bucureşti, 1999

MÖSSBAUER SPECTROSCOPY IN MINERALOGY AND GEOCHEMISTRY PART 2 : APPLICATIONS IN MINERALOGY AND GEOCHEMISTRY

(review paper)

[1]S. CONSTANTINESCU, [2]G. UDUBAŞA [3]S. CALOGERO
[1]National Institute of Materials Physics, P.O.Box: Mg-07, Bucharest, Romania
[2] Geological Institute of Romania, 78344, Bucharest, Romania
[3]Universita Ca'Foscari di Venezia, Dipt. Chimico - Fisica, 30123, Venezia, Italy

Key words: ^{57}Fe-Mössbauer effect. Mineralogy. Geochemistry. Electronic configuration of Mössbauer ions. Resonance lines.

Abstract: The use of Mössbauer spectroscopy (MS) has developed rapidly in last decades mainly because the data given by Mössbauer spectra could not be obtained by using other techniques. Most of MS reports published contain ^{57}Fe spectra due to the wide and varying occurrence of the iron in the Earth's crust. However, spectra of ^{119}Sn; ^{197}Au etc. have been recorded. In this part we will discuss some applications of MS in mineralogy and geochemistry. The applications of MS on minerals are: (1) characterization of oxidation state and electronic configurations of Mössbauer parent ions, (2) coordination symmetry of isotope position and the distortion of its surrounding, (3) assignment of resonance lines to structurally distinctive cation positions, (4) the solid-state processes as oxidation and weathering of mineral sand rocks, (5) qualitative aspects of fingerprint applications and quantitative estimations of Mössbauer parent atoms in studied geological samples. The data below refer mainly to the ^{57}Fe MS.

2. 1. Oxidation state and electronic configuration characterisations of iron in minerals

The assignment of the oxidation state of iron, or the ratio of the oxidation states is of considerable importance to explain the colour, pleochroism, oxidation, and weathering of minerals. In addition this assignment of oxidation states may be of great importance as geothermometer or geobarometer. So, many authors have shown that Fe^{3+} is reducing to Fe^{2+} with the pressure and the ratio of these ions gives useful information about the pressure in the Earth's interior. For other minerals such as pyroxenes this ratio could be correlated to the temperature and/or pressure of formation during the crystallisation. The determination of the ratio Fe^{2+}/Fe^{3+} is not a trivial problem. The standard techniques such as X-ray crystallography cannot distinguish between the two iron ions and the chemical analyses sometimes give unreliable values. An example illustrates the success of the Mössbauer method is the tripuhyite $Fe_2Sb_2^{V}O_7$, inferring the ferrous state. The X-ray and chemical analyses suggested the formula $FeSb^{V}O_4$, inferring the presence of the ferric state. Only the Mössbauer investigations, of the above sample, indicated quadrupole spectra with $\delta_{CS} \sim 0.62$mm/s and $\Delta E_Q \sim 0.72$mm/s, corresponding to a ratio 95% ÷ 5% of the ferric to ferrous state.

The spectral parameter δ_{CS} is very sensitive to the high spin oxidation. This parameter is in the velocity range -0.6÷+2.2 for Fe^{6+} to Fe^{1+}. Fe^{2+} and Fe^{3+}, and has the characteristic values +1.44 mm/s and +0.7 mm/s respectively in the oxygen environment. These values depend on the coordination number, site symmetry and type of ligand O, S, etc. (see Fig. 2.1 and Table 2.2; Bancroft, 1973, Greenwood 1971, Gutlich, 1975).

Table 2.1.
Iron oxidation states for high spin configurations

Oxidation state	+1	+2	+3	+4	+6
δ_{CS} [mm/s] relative to NPS	~+2.2	~+1.4	~+0.7	~+0.2	~-0.6

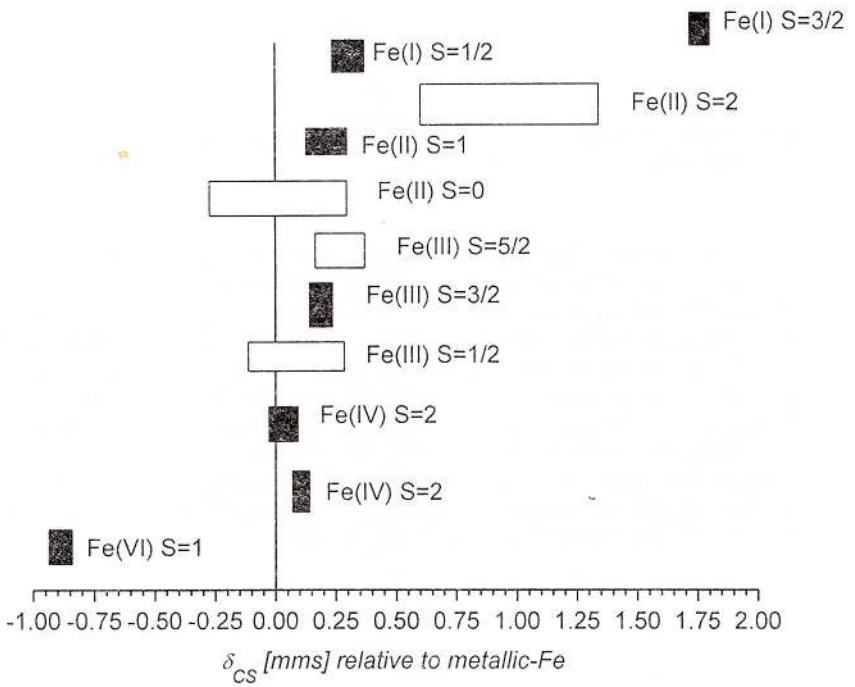

Fig. 2.1 - The central shift of iron compounds for different oxidation states and spin configurations

Many geological samples give spectra showing appreciable amounts of both Fe^{3+} and Fe^{2+}. For example, the Mössbauer spectrum of howieite consists in two qudrupolar doublets corresponding to the two iron ions (Bancroft et al., 1968), see Figure 2.2.

A transition from high to low spin of Fe^{II} configuration has been reported (Strens, 1966) for gillespite $BaFeSi_4O_{10}$ at high pressure by using Mössbauer spectroscopy.

Sometimes, the values of hyperfine magnetic field can distinguish between the two iron ions, $H(Fe^{3+}) > H(Fe^{2+})$. A classic example is the difference between H values of the α-Fe_2O_3 (hematite, H ≅515KGs) and of Fe_2SiO_4 (olivine, H ~250÷350KGs).

In sulphide minerals the oxidation states of iron can also be identified. So, in troilite FeS and pyrrhotite Fe_7S_8, δ_{CS} is of about 1.1mm/s at 300K and 1.03÷1.08 mm/s at 77K respectively. These values correspond to the Fe^{II} high spin. Generally, due to the greater covalence of the Fe-S bond the values of δ_{CS} are smaller than Fe-O one. The sulphide minerals show different values, corresponding to the different iron oxidation states, not only δ_{CS}, but also for ΔE_Q and H.

$$\Delta E_Q(Fe^{3+}) << \Delta E_Q(Fe^{2+}); H(Fe^{3+}) > H(Fe^{2+}); \qquad (2.1.)$$

The central shift values of the Fe^{II} low spin configurations in such minerals are generally much smaller than the values of the Fe^{II} high spin configurations and are comparable to Fe^{III} high spin ones.

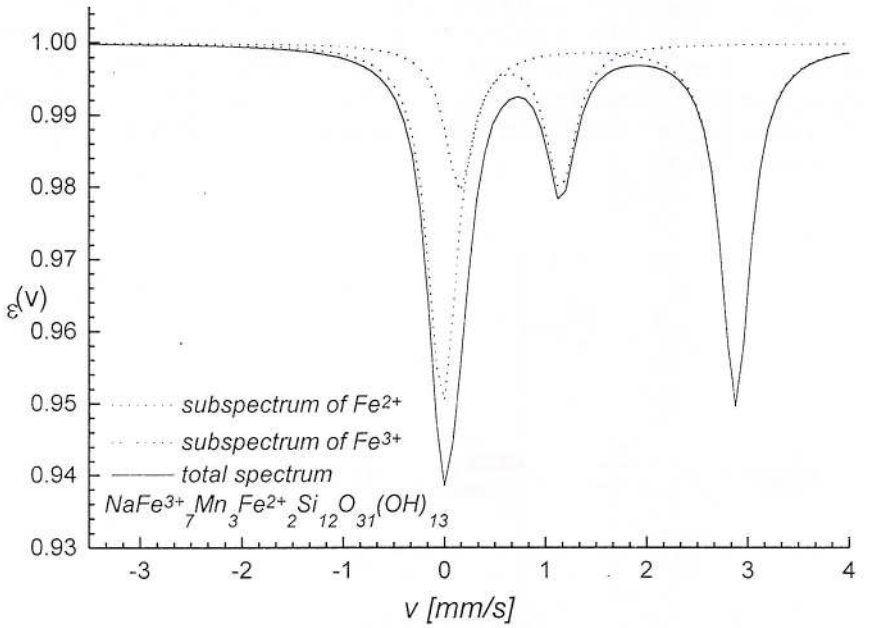

Fig. 2.2 - The Mössbauer spectrum of howieite, $Na(Fe^{2+},Mn)_{10}(Fe^{3+},Al)_2Si_{12}O_{31}(OH)_{13}$, (room temperature)

2.2. Coordination number of iron in minerals

The determination of the coordination number of the Mössbauer isotope is another problem of interest for geochemists and mineralogists. The hyperfine spectral parameters are very sensitive to that. Table 2.1 summarizes δ_{CS} values for different coordination number in oxygen surroundings. An increasing of the coordination number determines an increasing of the central shift. Moreover, in Figure 2.3 we observe the correlation between the iron ionic states ΔE_Q and δ_{CS} for different coordination numbers.

Table 2.2.

δ_{CS} for four, six and eight-coordinate sites of different iron electronic configurations in some minerals

Mineral species	δ_{CS} [mm/s]	Type of iron
Almandine garnet	1.56	8-coordination Fe^{2+}
Silicates	1.30-1.43	6-coordination Fe^{2+}
Staurolite	1.22	4-coordination Fe^{2+}
Spinels	1.07	4-coordination Fe^{2+}
Gillespite	1.01	4-coordination (square planar)Fe^{2+}
Epidote	0.61	6-coordination Fe^{3+}
Amphiboles	~ 0.65	6-coordination Fe^{3+}
$FeCl_4^-$	0.56	4-coordination Fe^{3+}
Iron orthoclase	0.72	4-coordination Fe^{3+}
$R_3Fe_2(FeO_4)_2$ R= rare earths	~0.65 ~0.45	6-coordination Fe^{3+} 4-coordination Fe^{3+}

The Mössbauer spectra of yellow and blue-green sapphirines are classic examples illustrating the determination of coordination number of the two ionic sorts of iron. The spectrum of yellow sapphirine is showing two quadrupole doublets of Fe^{3+} in the tetrahedral positions. On the other hand, the spectrum of blue-green sapphirine is evidencing two quadrupole doublets of Fe^{2+} in the octahedral positions and a doublet for Fe^{3+} in a tetrahedral position (Bancroft et al., 1968). This result confirmed the earlier suggestion that Fe^{2+} orders on six-coordinate site, while Fe^{3+} orders on four-coordinate sites (Fig. 2.4.). Mössbauer spectrum of biotite offers another exemple of the iron ions ordering in different coordinate sites. So, the spectrum is evidencing two large quadrupole doublets with big centre shift corresponding to Fe^{2+} in octahedral sites and a small quadrupole doublet with smaller center shift corresponding to Fe^{3+} in tetrahedral sites.

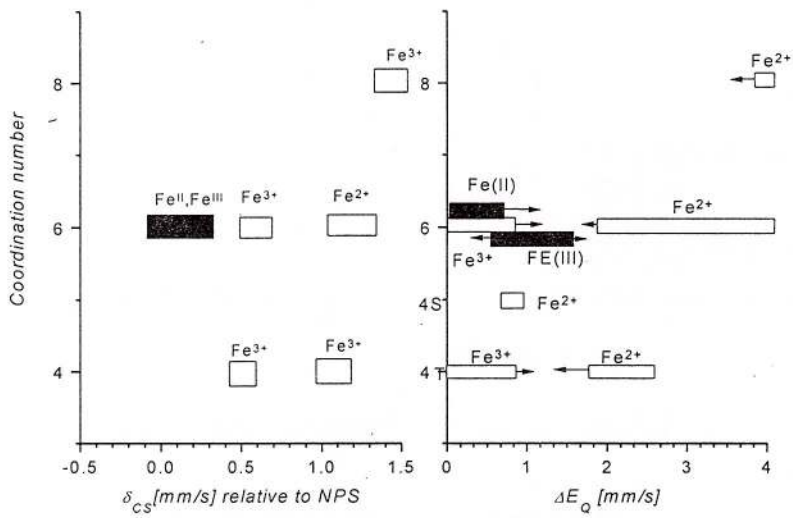

Fig. 2.3 - Coordination number of iron sites relative to δ_{CS} and ΔE_Q

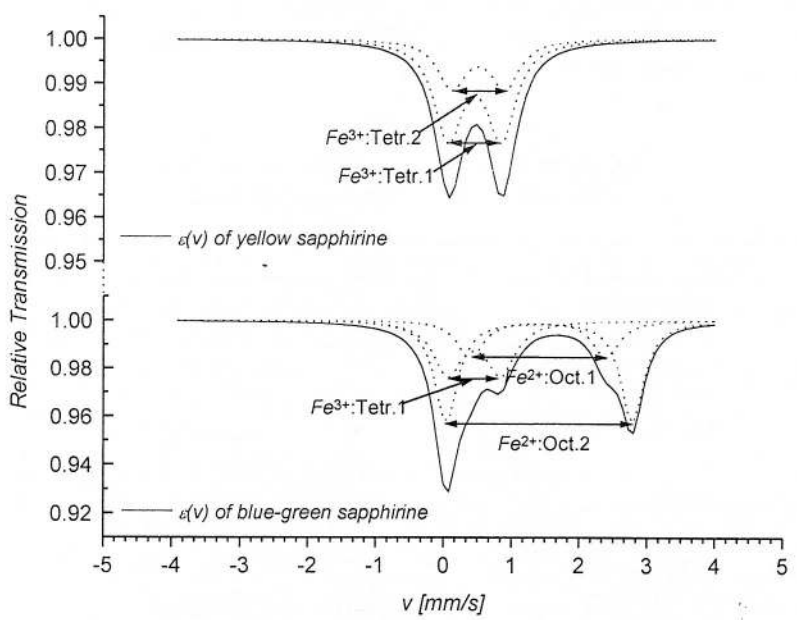

Fig. 2.4 - The Mössbauer spectra of two sapphirines $(Mg,Fe^{2+})_2(Al,Fe^{3+})_4O_6SiO_4$

2.3. Determination of distinct structural positions in complex spectra

The Mössbauer spectra of many minerals show a superposition of several simple lines or/and quadrupole subspectra or/and magnetic ones corresponding to many vicinities around Mössbauer nucleus and its different crystalline sites. Many results of the Mössbauer investigation on minerals show distinctive structural positions occupied by iron or other Mössbauer nuclei. The structural positions can be evidenced in the spectra by two or more distinctive quadrupole doublets, if the spectral parameter values could be bigger than half line-width. The ruler in iron minerals is: Fe^{2+} enters bigger volume polyhedron occupied by metallic ions $r_{Fe^{2+}} < r_{Fe-O}$ and Fe^{3+} enters smaller one $r_{Fe^{3+}} < r_{Fe-O}$. In the case of one site corresponding to the iron-oxygen distances, $r_{Fe^{3+}} < r_{Fe^{2+}} < r_{Fe-O}$, the two iron ions could occupy the same site. Let's now see some results of Mössbauer investigations on different sorts of iron containing silicates. The iron silicates are the commonest accessible materials on Earth to be investigated by this spectroscopy due to the strong affinity of silicon for oxygen and the abundance of iron and its Mössbauer isotope.

Chain silicates. Their characteristics consist of infinite chains Si-O tetrahedra linked by cations extending along the orthorhombic or monoclinic c axis.

Pyroxenes have the general chemical formula $A_2Z_2O_6$, where A = Na^+, Ca^{2+}, Mg^{2+}, Fe^{2+}, Mn^{2+},Al^{3+},Fe^{3+}, Z=Si^{4+}, ions are occupying the octahedral M_1 {}, the irregular M_2 <> (M_1:M_2=1:1) and tetrahedral sites [] respectively. The irregular sites corresponding to 6-, 7-, or 8-fold coordinated according to particular mineral. The crystalline symmetry is orthorhombic for M_2=Mg^{2+} and Fe^{2+}, or monoclinic for Na^+ and Ca^{2+}. The experimental results of Mössbauer investigations on different pyroxens have shown a correlation of the spectral parameters and the structural positions of iron ions (see Table 2.3a; Bancroft , 1973, Coey, 1984).

Table 2.3a

Assignment of structural positions occupied by iron ions in some pyroxens

Minerals	δ_{CS} [mm/s]	ΔE_Q [mm/s]	Assignment
<Ca>{Fe,Mg}[Si]$_2$ O_6	~1.45	1.9÷2.3	Fe^{2+} : M_1
*Hedenbergite, <Ca>{Fe}[Si]$_2O_6$	1.19	2.30	Fe^{2+} : M_1
<Na>{Fe,Al}[Si]$_2$ O_6	0.65	0.33	Fe^{3+} : M_1
(Fe,Mg)$_2$Si$_2$ O_6	~1.4	1.9÷2.1	Fe^{2+} : M_2
	~1.4	2.3÷2.7	Fe^{2+} : M_1
*Orthopyroxene, $Fe_2Si_2O_6$	1.17	2.48	Fe^{2+} : M_2
	1.13	1.93	Fe^{2+} : M_1
(Ca,Fe,Mg)$_2$Si$_2$ O_6	1.40	1.96	Fe^{2+} : M_2
	1.40	2.44	Fe^{2+} : M_1
	0.70	0.59	Fe^{3+} : M_1 and M_2

*Isomer shifts are relative to iron metal.

Other silicates investigated by Mössbauer technique are ***amphiboles*** with a general chemical formula $X_2Y_5Z_8O_{22}(OH)_2$ where X(=Ca^{2+},Na^+,Fe^{2+},Mg^{2+}):M_4 , Y(= Fe^{3+}, Mg^{2+} , Mn^{2+}, Al^{3+}):$M_{1,2,3}$ and Z=Si are the 10÷12, 6 and 4 fold coordinated positions. Their structures are based on double $([Si,Al]_4O_{11})_n$ tetrahedra chains that run parallel to orthorhombic or monoclinic c axis and sandwich a ribbon of octahedra. The ratio of numbers of M_1:M_2:M_3:M_4 is 2:2:1:2. The spectra have shown that M_4 positions are occupied preferentially by the larger cations as Fe^{2+}, while the positions $M_{1,2,3}$ are occupied by smaller ones such as Fe^{3+} (see Table 2.4). The Mössbauer parameters for important amphiboles are given in Table 2.3b (Bancroft, 1973; Coey, 1984) and characteristic spectra are shown in Figure 2.5. It is interesting to point out that ferrous ions are occupying M_4 sites only in cummingtonite-grunerite series and ferric ones are occupying preferentially M_2 sites. The octahedral distances r_{Fe-O} would explain these preferences (see Table 2.5, Bancroft, 1973).

Table 2.3b

Assignment of structural positions occupied by iron ions in some amphiboles

Minerals	δ_{CS} [mm/s]	ΔE_Q [mm/s]	Assignment
cummingtonite-grunerite: $(Fe,Mg)_7Si_8O_{22}(OH)_2$	~1.3	1.5÷1.7	$Fe^{2+}:M_4$
	~1.4	2.7÷2.9	$Fe^{2+}:M_{1,2,3}$
+grunerite: $<Fe>_2\{Fe\}_5[Si]_8O_{22}(OH)_2$	1.10	1.80	$Fe^{2+}:M_4$
	1.16	2.82	$Fe^{2+}:M_{1,2,3}$
anthophyllites: $(Fe,Mg)_7[Si]_8O_{22}(OH)_2$	~1.35	1.80	$Fe^{2+}:M_4$
	~1.37	2.6	$Fe^{2+}:M_{1,2,3}$
$<Ca>_2\{Fe,Mg\}_5[Si]_8O_{22}(OH)_2$	~1.4	2.89	$Fe^{2+}:M_1$
	~1.4	~1.9	$Fe^{2+}:M_2$
	~1.4	~2.4	$Fe^{2+}:M_3$
+ferroactinolite, $<Ca>_2\{Fe\}_5Si_8O_{22}(OH)_2$	1.15	2.81	$Fe^{2+}:M_{1,2}$
	1.14	1.95	$Fe^{2+}:M_3$
$Na_2(Fe^{2+}, Fe^{3+}, Mg, Al)_5Si_8O_{22}(OH)_2$	~1.4	~2.8	$Fe^{2+}:M_1$
	1.39	2.0	$Fe^{2+}:M_2$
	1.36	2.41	$Fe^{2+}:M_3$
	~0.65	~0.45	$Fe^{3+}:M_{1,2,3}$
+riebeckite, $<Na>_2\{Fe^{2+}, Mg\}_3\{Fe^{3+}\}_2Si_8O_{22}(OH)_2$	1.12	2.90	$Fe^{2+}:M_1$
	0.38	0.42	$Fe^{3+}:M_2$
	1.13	2.42	$Fe^{2+}:M_3$

+Isomer shifts are relative to metallic iron.

Table 2.4.

The sites occupied by iron ions in some amphiboles

Minerals	X:M_4	Y:$M_{1,2,3}$	Z
Grunerite	Fe_2^{2+}	Fe_5^{2+}	Si_8
Ferrogedrite	Fe_2^{2+}	$Fe_3^{2+}Al_2^{3+}$	Si_6Al_2
Ferroactinolite	Ca_2	Fe_5^{2+}	Si_6Al_2
Ferrotschermakite	Ca_2	$Fe_3^{2+}Al_2^{3+}$	Si_6Al_2
Ferroglaucophane	Na_2	$Fe_3^{2+}Al_2^{3+}$	Si_8
Riebeckite	Na_2	$Fe_3^{2+}Fe_2^{3+}$	Si_8
Magnesioriebeckite	Na_2	$Mg_3^{2+}Fe_2^{3+}$	Si_8

Table 2.5.

The mean-values of cation-oxygen lengths in amphiboles

Site	Tremolite	Actinolite	Cummingtonite	Grunerite	Glaucophane	Hornblende
M_1-$6O^{2-}$	2.075	2.104	2.098	2.126	2.087	2.075
M_2-$6O^{2-}$	2.077	2.075	2.083	2.123	1.943	2.049
M_3-$4O^{2-}$,$2(OH)^-$	2.066	2.097	2.091	2.122	2.094	2.081
M_4-$6O^{2-}$	2.419		2.305	2.299	2.398	2.435

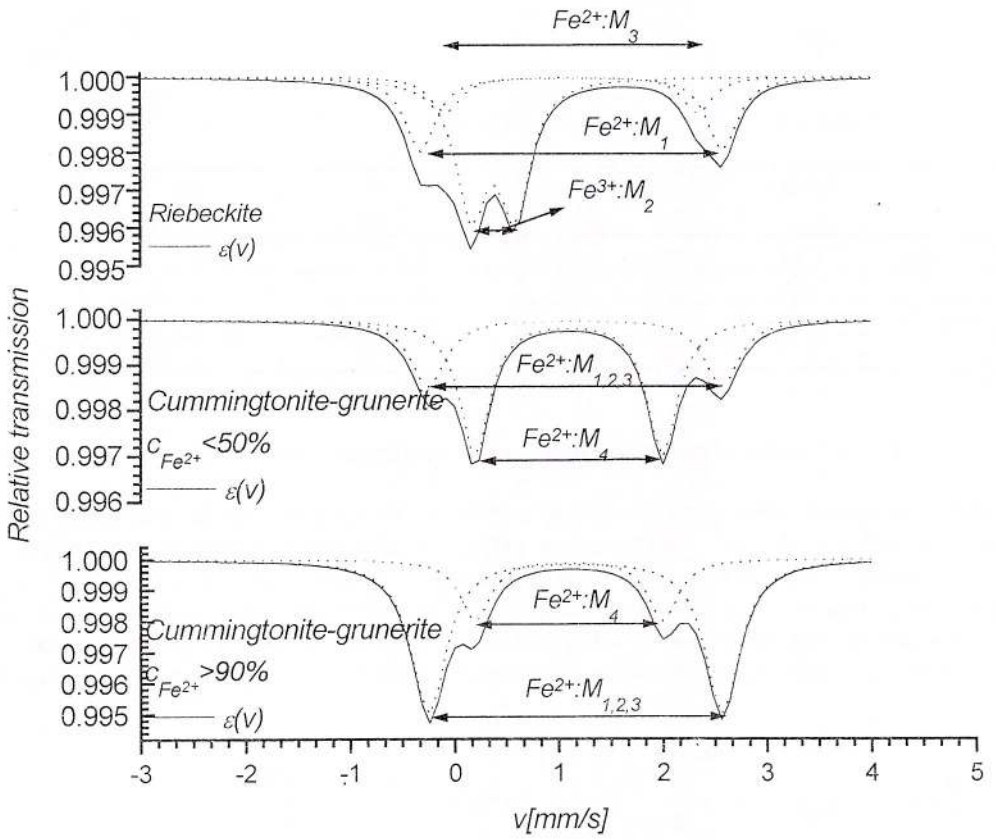

Fig. 2.5 - The iron sites in sodium and calcium amphiboles

Sheet silicates have the basic structure as a composite sheet in which a layer of Y octahedra is sandwiched between two identical layers of $(Si,Al)O_4$ linked tetrahedra.

The formula of ***micas*** is $<X>_2 \{Y\}_{4\text{-}6} [Z]_8O_{20}(OH,F)_2$, where X: K^+, Na^+, Ca^{2+} , Y sites are occupied mainly by Al^{3+}, Mg^{2+} or Fe^{2+} and Z: Si^{4+}, Al^{3+} with perhaps some Fe^{3+}, have been studied by Mössbauer spectroscopy. Micas can divide in dioctahedral and trioctahedral classes corresponding to the number 4 and 6 of Y ions. The length $r_{Y\text{-}O}$ divides the octahedral sites in larger M_1 (~2.20Å), occupied preferentially by bigger ions as Fe^{2+} , and smaller M_2 sites (~ 1.95 Å), occupied by Al, M_1:M_2=1:2. The approximated chemical formulae are given in Table 2.6.

Table 2.6.
The chemical formulae of some micas

Type	Compound	X	Y	Z
Dioctahedral	Muscovite	K_2	Al_4	Si_6Al_2
	Paragonite	Na_2	Al_4	Si_6Al_2
	Glauconite	$(K,Na)_{1,2\div2}$	$(Fe,Mg,Al)_4$	$Si_{7,\div7,6}Al_{1,\div0,4}$
Trioctahedral	Phlogopite	K_2	$(Mg,Fe)_6$	Si_6Al_2
	Biotite	K_2	$(Mg,Fe,Al)_6$	$Si_{6,\div5}Al_{2,\div3}$
	Zinnwaldite	K_2	$(Fe,Li,Al)_6$	

The Mössbauer parameters for different samples of micas are given in Table 2.7. (Bancroft, 1973). As we can see from this table, the outer quadrupole splittings can distinguish between the dioctrahedral and trioctahedral micas.

Table 2.7.
The spectral parameters for micas quadrupole doublets

Sample	%FeO	Fe^{2+}:M_2		Fe^{2+} :M_1		Fe^{3+}	
		δ_{CS}	ΔE_Q	δ_{CS}	ΔE_Q	δ_{CS}	ΔE_Q
Madacascar Muscovite	1.12	1.41	3.02	1.39	2.25	0.60	0.82
Biotite	34.6	1.38	2.56	1.36	2.18	0.63	0.74
Synthetic annite	42	1.40	2.56	1.36	2.17	0.80	0.52
Zinwaldite	5.70	1.41	2.65			0.66	0.89

2.4. Distortion of the Mössbauer isotope neighbourhood

Most of minerals are not end-members of solid solutions and the crystallographic sites become inequivalently due to different electrical and geometrical configurations giving to geometrical or/and charge competitive distortions of Mössbauer isotope neighbourhood. So, many quadrupolar, magnetic subspectra will occur in the spectra, if $\Gamma<\Delta E_Q$, ΔH. The authors considered useful to evidence how the geometrical and charge deformations of an octahedral vicinity influence the components of EFG tensor. The geometrical distortion of a configuration (Fig. 2.6) is given by Δ_{octa} and σ^2, the square relative departure of octahedral distances and angles from mean values and $\theta_o=\pi/2$ respectively.

$$\bar{r}=\frac{1}{6}\sum_{i=1}^{6} r_i;\theta_{ij}=(\hat{\vec{r}_i},\hat{\vec{r}_j});\Delta_{oct}=\frac{1}{6}\sum_{i=1}^{6}\left(\frac{r_i-\bar{r}}{\bar{r}}\right)^2;\sigma^2=\frac{1}{11}\sum_{(i,j)=1}^{11}\left(\frac{\theta_{ij}-\pi/2}{\pi/2}\right)^2 \quad (2.2)$$

Geometrical distortions can arise by the elongation/shrink on a given direction or by the shift of central Mössbauer parent ion. V_{zz} has different dependence on relative changes of distances.

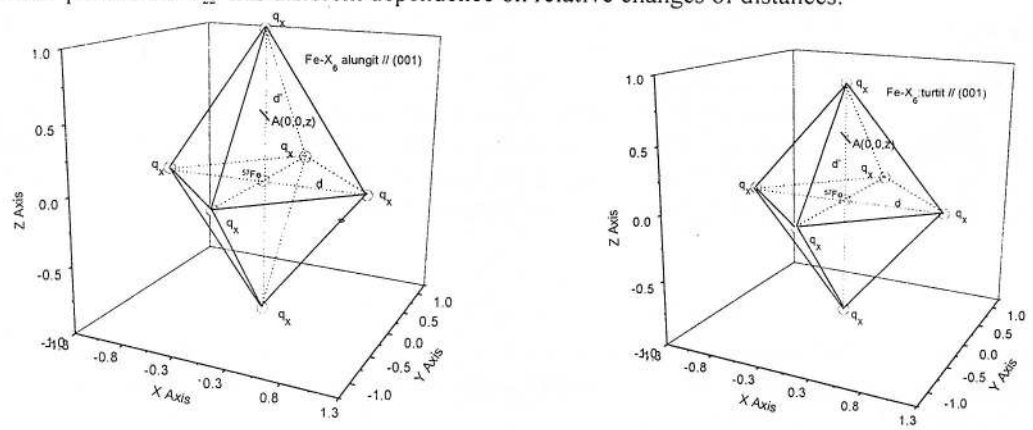

Fig. 6 - The elongated and shorted octahedron; $|\Delta d| = 0.1d$

$\underline{FeX_6}$ $\vec{r}=(\pm d,0,0),(0,\pm d,0),(0,0,\pm d')$; $\Delta d = d-d'$; $\vec{r}_o=(0,0,z)$; $\vec{r}_{Fe}=(0,0,0)$; C_3^1 possibilities

$$\bar{r}=d-\frac{\Delta d}{3d};\Delta_{oct}=\frac{2}{3}\left(\frac{\Delta d}{d}\right)^2;\sigma^2=0\rightarrow\begin{cases}\eta=0\\ \Delta E_Q^{(001)}\approx\dfrac{eQ}{8\pi\varepsilon_o}\dfrac{12q_X|\Delta d|}{d^4}\end{cases} \quad (2.3a)$$

The elongation/shrink of octahedron and the shift of central ion give a linear and square dependence of V_{zz} relative to Δd . But, generally the spectra could evidence the shift of the the Mössbauer probe too. In this last case the quadrupole splitting parameter depends on square of the shift.

$$\underline{FeX_6}\quad \vec{r} = (\pm d,0,0),(0,\pm d,0),(0,0,\pm d)\,;\,\Delta\theta = \theta - \pi/2\,;\vec{r}_o = (0,0,z);\vec{r}_{Fe} = \vec{r}_o\,;$$

$$\bar{r} = d - \frac{z}{3}\,;\Delta_{oct} = \frac{2}{3}\left(\frac{z}{d}\right)^2\,;\sigma^2 = \frac{32}{11}\cdot\left(\frac{\Delta\theta}{\pi}\right)^2 \rightarrow \begin{cases} \eta = 0 \\ \Delta E_Q \approx \dfrac{30eQq_X}{8\pi\varepsilon_o d^3}\cdot\left(\dfrac{z}{d}\right)^2 \end{cases} \qquad (2.3b)$$

It is necessary to mention that the sign of Δd cannot be determined from ΔE_Q. Figure 2.7 shows the ΔE_Q range values versus the grade of the relative distortion of oxygen octahedra (Greenwood, 1971; Bancroft, 1973; Coey, 1984).

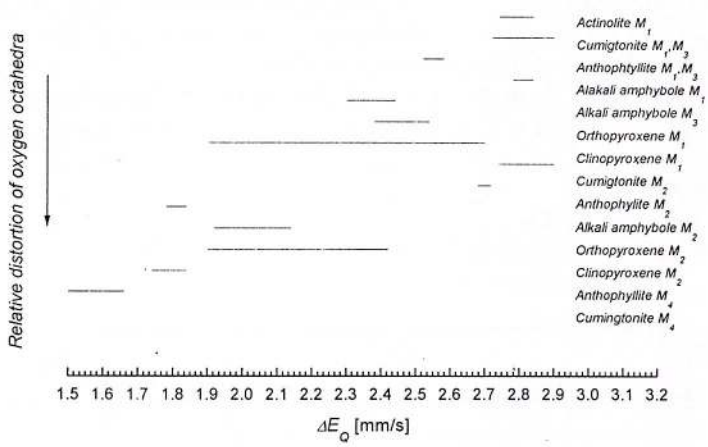

Fig. 2.7 - Quadrupole splitting versus octahedral distortion (Bancroft, 1973)

The most known charge configurations of octahedra are the cis, trans configurations (see Fig. 2.8). The calculated principal components V_{zz} of EFG tensors for the two configurations shown are as follows:

$$\underline{\text{cis}-FeX_4Y_2} \qquad\qquad \underline{\text{trans}-FeX_4Y_2}$$

$$V(0,0,z) = \frac{2q_1}{(r^2+z^2)^{1/2}} + \frac{2q_2}{(r^2+z^2)^{1/2}} + \frac{q_1}{r-z} + \frac{q_1}{r+z}\,; \qquad V(0,0,z) = \frac{4q_1}{(r^2+z^2)^{1/2}} + \frac{q_2}{r-z} + \frac{q_2}{r+z}\,;$$

$$\frac{\partial^2 V}{\partial z^2} = -\frac{2(q_1+q_2)(r^2-2z^2)}{(r^2+z^2)^{5/2}} + \frac{2q_1}{(r+z)^3} + \frac{2q_2}{(r-z)^3}\,; \qquad \frac{\partial^2 V}{\partial z^2} = -\frac{4q_1(r^2-2z^2)}{(r^2+z^2)^{5/2}} + \frac{2q_2}{(r+z)^3} + \frac{2q_2}{(r-z)^3}\,; \qquad (2.4a)$$

$$\left(\frac{\partial^2 V}{\partial z^2}\right)_{z=0}^{cis} = -\frac{2(q_2-q_1)}{r^3}\,; \qquad \left(\frac{\partial^2 V}{\partial z^2}\right)_{z=0}^{trans} = \frac{4(q_2-q_1)}{r^3} = -2\cdot\left(\frac{\partial^2 V}{\partial z^2}\right)_{z=0}^{cis}\,;$$

and as a consequence the ratio of quadrupole splitting parameters is:

$$\left|\frac{\Delta E_Q^{trans}}{\Delta E_Q^{ciss}}\right| = \left|\frac{V_{zz}^{trans}}{V_{zz}^{cis}}\right| = 2{:}1 \qquad (2.4b)$$

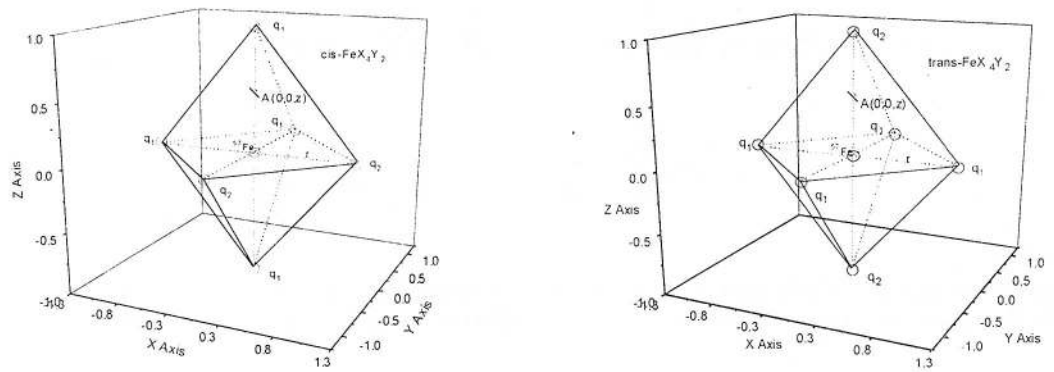

Fig. 2.8 - The cis, trans configurations

The different geometrical and/or charge configurations around Mössbauer isotope arise some additional problems in the interpretation of the spectra, which are absent for a usual mineral. The spectra will give unique hyperfine splitting parameters at each crystallographic site for end-members of solid solutions. The intermediate members have distributions of different ions, and thus there are a lot of distributions of hyperfine splitting parameters δ_{IS}, ΔE_Q and ΔH at equivalent sites. This effect is more pronounced when the neighbours are not the same charges.

Table 2.8.

The V_{zz} values and their combinatorial probabilities for different charges octahedral configurations

Configurations k ; 6-k	Probabilities C_6^k	V_{zz} $[e(q_X-q_Y)/\ 8\pi\varepsilon_0 d^3]$	η	ΔE_Q $[/eQ(q_X-q_Y)/\ 8\pi\varepsilon_0 d^3/]$
$6q_X$; $6q_Y$	1/64	0	0	0
1 $5q_X$; $1q_Y$;	6/64	-2	0	2
2a (trans) $4q_X$; $2q_Y$;	3/64	-4	0	4
2b (cis) $4q_X$; $2q_Y$;	12/64	-2	3	2
3a $3q_X$; $3q_Y$;	8/64	0	0	0
3b $3q_X$; $3q_Y$;	12/64	6	1	$2(3)^{1/2}$
4b (cis) $2q_X$; $4q_Y$;	12/64	2	3	2
4a (trans) $2q_X$; $4q_Y$;	3/64	4	0	4
5 $1q_X$; $5q_Y$;	6/64	2	0	2

Table 2.8 shows the V_{zz}, η and ΔE_Q values and their combinatorial probabilities for octahedral iron configurations of two ionic sorts q_X, q_Y. The probability $P^{(i)}$ is a sum of all combinatorial probabilities for a given $\Delta E_Q^{(i)}$ value (see Fig. 2.9) and is a measure of the corresponding quadrupole doublet area A_i. $P(\Delta E_Q^{(i)})$. In the Figure 2.2, 10 Mössbauer spectra have plotted for the above example.

$$\Delta E_Q^{(i)};\ A_i \propto P^{(i)} = P(\Delta E_Q^{(i)}) = \sum_{k_i} C_N^{k_i} \qquad (2.5a)$$

The probabilities of solid solution members for a given $\Delta E_Q^{(i)}$ value depend also on fraction $x = C_X^{oct}/N$ ($y = C_Y^{oct}/N$), where C_X^{oct} (C_Y^{oct}) is the occupancy of ionic charge q_X (q_Y) and N is the number of polyhedron corners around the Mössbauer isotope (Barb, 1995).

$$\Delta E_Q^{(k)}(x); A_k(x) \propto P_N^k(x;N,k) = C_N^k x^k (1-x)^{N-k}; \quad x+y=1; \qquad (2.5b)$$

The spectra will become more complicated if the ionic distributions of second, third, fourth etc. order vicinity would be considered.

$$\Delta E_Q^{k_1,k_2\cdots}(x_1,x_2,....); A_{N_1,N_2\cdots}^{k_1,k_2\cdots}(x_1,x_2,....) \propto P_{N_1,N_2\cdots}^{k_1,k_2\cdots}(x_1,x_2,....) = \prod_{\beta=1}^{N_S} C_{N_\beta}^{k_\beta} x_\beta^{\,k_\beta} \left(1-x_{\beta i}\right)^{N_\beta - k_\beta}$$

$$\Delta E_Q^{(i)}(x_1,x_2,....;N,k) = \sum_\alpha P_{N_1,N_2\cdots}^{k_{1\alpha},k_{2\alpha}\cdots}(x_1,x_2,....)\Delta E_Q^{k_{1\alpha},k_{2\alpha}\cdots}(x_1,x_2,....); N = \sum_{\beta=1}^{N_S} N_\beta; k = \sum_{\alpha=1}^{N_S'} k_\alpha \qquad (2.5c)$$

$$A_i(x_1,x_2,....;N,k) = \sum_\alpha A_{N_1,N_2\cdots}^{k_{1\alpha},k_{2\alpha}\cdots}(x_1,x_2,....) \propto \sum_\alpha P_{N_1,N_2\cdots}^{k_{1\alpha},k_{2\alpha}\cdots}(x_1,x_2,....)$$

Here the α and $k_{i\alpha}$ designate the shells and the number of q_X ions on the α^{th} shell contributing to $\Delta E_Q^{(i)}$ value. It is interestting to note that the probability $P(\Delta E_Q)$ for a completely random distribution of ions in shells of neighbours (case of amorfs) is (Czjzek, 1981):

$$P(\Delta E_Q) = \frac{\Delta E_Q^4 \eta (1-\eta^2)}{9\sigma^5 (1+\eta^2/3)^2 \sqrt{2}} \left[1 + f(\sigma, \Delta E_Q, \eta) e^{-\frac{\Delta E_Q}{2\sigma^2}} \right] \qquad (2.5d)$$

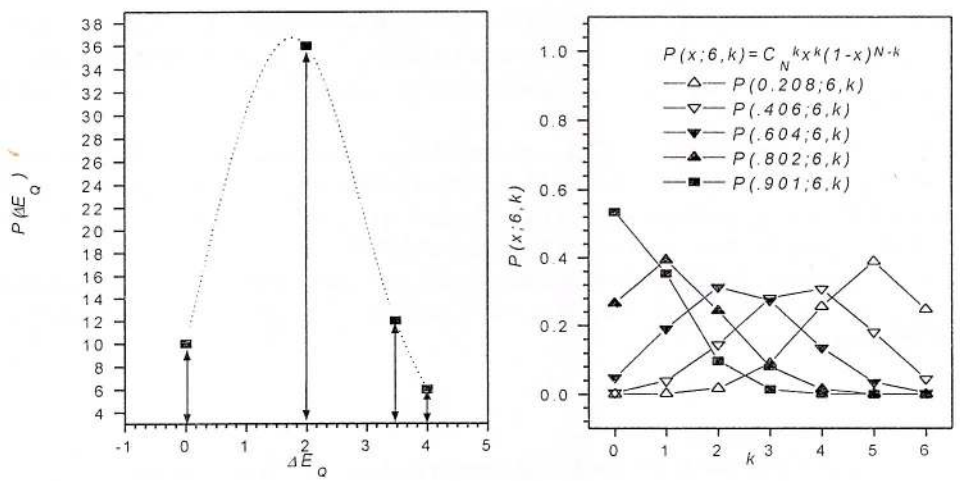

Fig. 2.9 - Plot of $P(\Delta E_Q)$ and P(x;6,k) of octahedral configurations Fe-$X_{6-k}Y_k$

The quadrupole doublets of the experimental spectra will be resolved if $\Delta E_Q^{(i)} \geq \Gamma/2$ (see Fig. 2.10). The spectra will not be resolved when $\Delta E_Q^{(i)} < \Gamma/2$.

Generally, the surrounding distortions will affect the lattice contribution of EFG tensor components, V_{ii}^{latt}. The quadrupole subspectra, corresponding to the different distortions of Mössbauer isotope neighbourhood, will be

evidenced for Mössbauer parent ions with the symmetric electronic shells (V_{ii}^{el} =0 ex.Fe^{3+}, $Sn^{2+,4+}$, Au^{+} etc.), so the quadrupole splitting is expected to increase as the surrounding distortions.

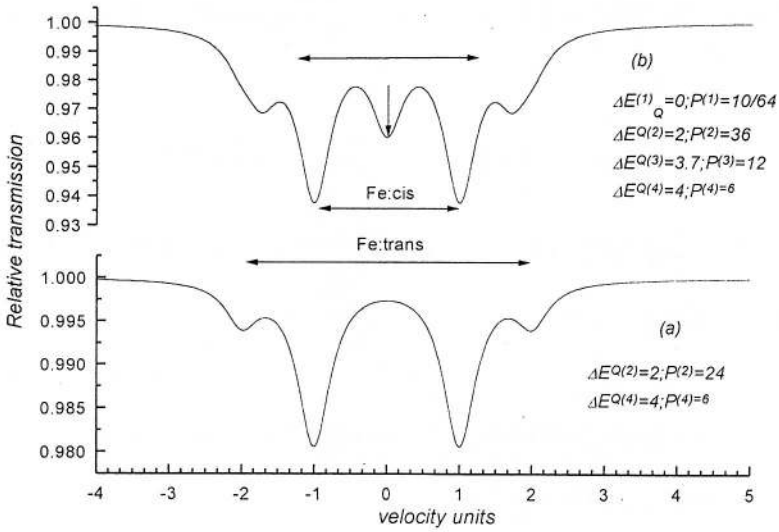

Fig. 2.10 - (a)Mössbauer spectrum of ^{57}Fe in cis and trans octahedral sites; (b)Mössbauer spectrum of ^{57}Fe surrounding by ionic $(6-k)q_X$ and kq_Y charges.ΔE_Q is given in $eQ/8\pi\varepsilon_0$ units

Many problems of assignment the subspectra to the structural variations appear for ions with nonsymmetric electronic shells (Fe^{2+}, $Sn^{1+,3+,5+}$, Au^{+}, etc.), because $V_{ii}^{el} \neq 0$. Thus, the Fe^{2+} electron valence contribution V_{ii}^{el} to V_{ii} is of about 3.7mm/s for a very small octahedral distortion. Generally, V_{ii}^{el} increases when the distortion increases, but V_{ii} decreases. That means different signs of V_{ii}^{latt} and V_{ii}^{el}.

It is important to mention that ΔE_Q depends on the ambiental temperature. This temperature dependence of ΔE_Q is directly generated both by the temperature dependencies of distances Mössbauer isotope ionic shells (surrounding distortion), giving $V_{ii}^{latt}(T)$ and $\Delta_i(T)$ ionic splittings, and indirectly by the temperature dependencies statistical weights $p_i(T)$ of ionic states.

It is interesting to mention the effect of the concentration of Mössbauer ions on the distortion of isotope neighbourhood and as consequence on ΔE_Q value. Many authors observed, a slight decreasing of $\Delta E_Q(M_1)$ and $\Delta E_Q(M_2)$ for metamorphic cumingtonite-grunerite, orthopyroxene series and also approximately the same values for M_1, M_2 sites of volcanic orthopyroxenes on iron content (Bancroft, 1967).

A careful correlation between the quadrupole splitting parameters, the electronic configuration and the distances of Mössbauer parent ion to first, second, third etc. ionic shells is necessary in order to obtain structural and compositional information on minerals.

2.5. Correlation of Mössbauer spectrum data with the structure and solid state processes

Oxidation and weathering. The mechanism of oxidation processes could be in situ transformation of Fe^{2+} to Fe^{3+} accompanied or not by the loss of protons from hydroxyl group, $(OH)^{-}$, charge transfer, or physical expulsion of iron ions from the layers in order to maintain the charge neutrality. The Mössbauer spectra of heated amosite (fibrous grunerite) evidenced spectacular changes on temperature increase (Whitefield, 1967, see Fig. 2.11).

The room temperature spectrum of an amosite with the approximate composition $(Fe_{5.5}Mg_{1.5})Si_8O_{22}(OH)_2$ is similar to that of grunerite one.

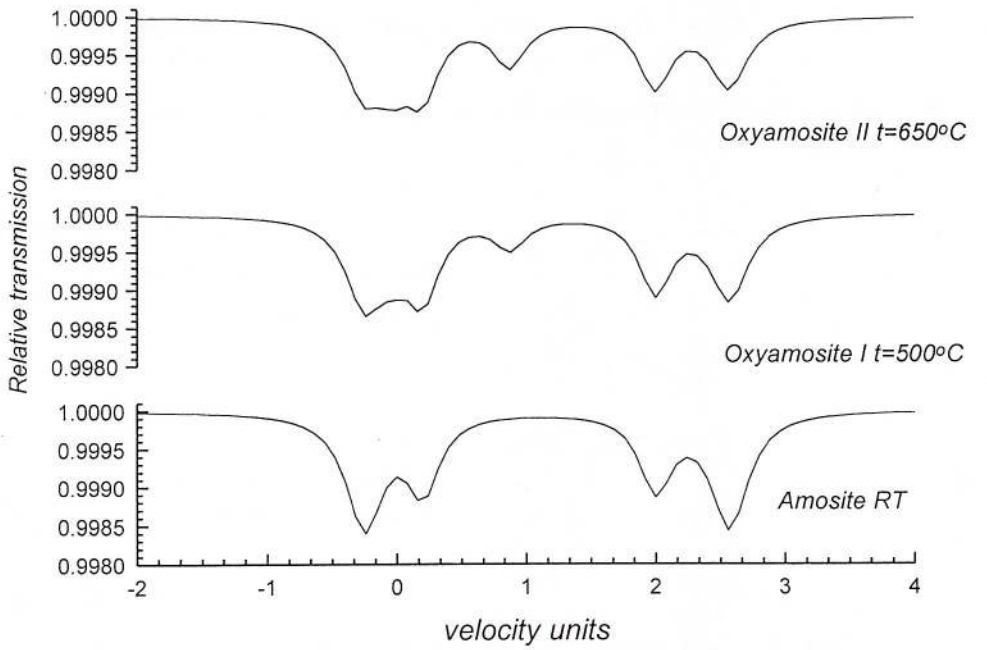

Fig. 2.11 - Mössbauer spectra of heated amosite

The inner quadrupol doublet corresponds to Fe^{2+}:M_4 and the outer one to Fe^{2+}:$M_{1,2,3}$. At 500°C a central doublet corresponding to Fe^{3+} appears and the intensity of ferrous ions in M_4 increases relative to that in $M_{1,2,3}$. The Mössbauer spectrum corresponds to that of oxyamosite of approximate composition $Fe_2^{3+}Fe_{3.5}^{2+}Mg_{1.5}Si_8O_{22}(OH)_2$. At 650°C the ferrous iron ratio is M_4/ $M_{1,2,3}$ of about 1/1 and at 900°C a doublet of pyroxene $(Fe,Mg)_2Si_2O_6$ is formed with additional hematite and spinel $(Mg,Fe^{2+})Fe_2^{3+}O_4$. The spectral parameters of amosite and oxyamosite suggested an unchanged basic structure and iron coordination. The conclusions are that Fe^{2+} : $M_{1,2,3}$ is oxidizing rather than Fe^{2+}:M_4 and electron transfer is not between cation chains.

The charge transfer, which accompanies the oxidation processes, is a spectacular solid state process observed by the color of the samples. Many silicates have mixed valence iron alkali amphiboles glaucophane-riebeckite series, oxides as $[Fe^{3+}]\{Fe^{2+},Fe^{3+}\}O_4$, vivianite $Fe_3(PO_4)_2{\cdot}8H_2O$, etc. So, the pure mineral vivianite is colourless but exposed to air the mineral becomes dark blue. That colour is atributted to the presence of the ferric ion Fe^{3+}. Generally the electronic configuration transfer $3d^6 \rightarrow 3d^5$ requires so much energy that it is necessary to be accompanied by a photon absorption. Also Mössbauer spectra evidenced the oxidation of the crocidolite $Na_2Fe^{3+}{}_4Fe^{2+}{}_{0.6}Mg_{0.4}Si_8O_{22}(OH)_2$ by a mechanism of electron transfer along the silicate chain rather across one.

The Mössbauer investigations give interesting information about of natural weathered micas especially biotite. In fresh biotite Fe^{2+} is predominant, but natural weathering processes in soil or fractured rocks oxidize ferrous ions in ferric ones. The possible mechanisms are a loss of interlayer cations (*a*), a loss of OH protons (*b*) or a loss of octahedral iron and appearance of iron hydroxide (*c*). The results of Mössbauer investigations evidenced the ferric ions in a distortioned octahedra ΔE_Q~*1.2mm/s,* corresponding to $FeO_5(OH)$ arrangement and the presence of vermiculite $(Mg,Ca)_{0.3}(Mg,Fe,Al)_3(Si,Al)_4O_{10}(OH)_2{\cdot}4H_2O$ as end product. Many authors have chosen the loss of interlayer cations as possible mechanism of oxidizing and weathering of biotite.

$$a)\quad KFe_3^{2+}Si_3AlO_{10}(OH)_2+\frac{1}{2}O_2+\frac{1}{2}H_2O\rightarrow KOH+Fe_2^{2+}Fe^{3+}Si_3AlO_{10}(OH)_2$$

$$b)\quad KFe_3^{2+}Si_3AlO_{10}(OH)_2+\frac{1}{2}O_2\rightarrow KFe^{2+}Fe_2^{3+}Si_3AlO_{10}(O)_2+H_2O \qquad (2.6)$$

$$c)\quad KFe_3^{2+}Si_3AlO_{10}(OH)_2+\frac{3}{2}O_2+\frac{1}{2}H_2O\rightarrow KFe_2^{3+}Si_3AlO_{10}(OH)_2+FeOOH$$

The Mössbauer investigations of micas have shown a more rapid weathering for trioctahedral than dioctahedral species.

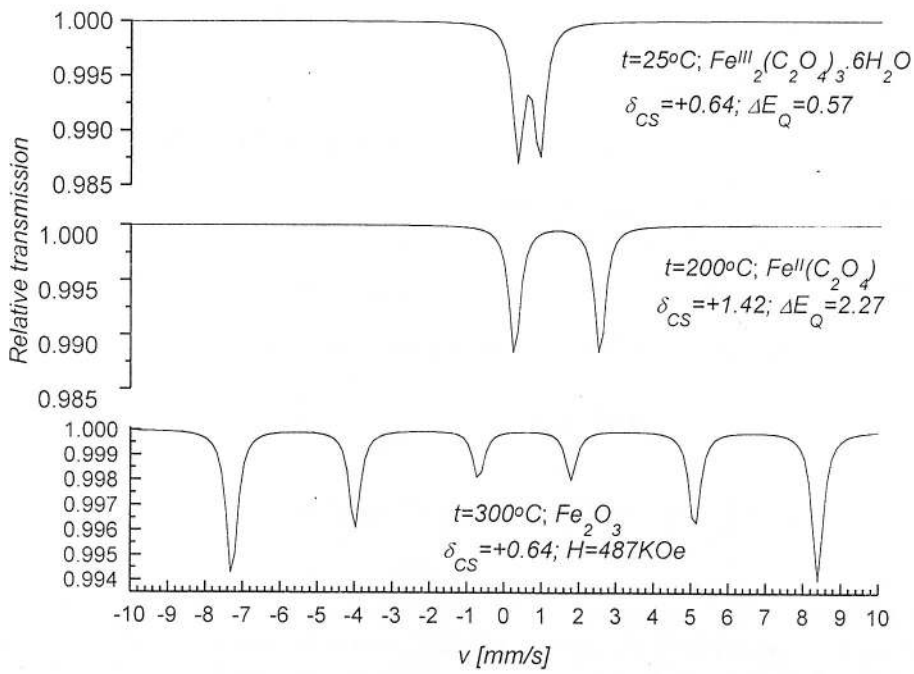

Fig. 2.12 - Mössbauer spectra for thermal decomposition of ferric oxalate

Another well-known example is of the natural weathered ilmenite $FeTiO_3$, where the spectra showed not only the characteristic quadrupole doublet ($\delta_{C.S}$ =1.35mm/s,ΔE_Q = 0.70mm/s), but a ferric specie one that was attributed to the weathering product too.

Mössbauer spectra can evidence solid ***thermal state decomposition***. A typical example is the changes of the spectrum shape given by the thermal decomposition of ferric oxalate (see Fig. 2.12). These spectra show the stages of thermal decomposition, dehydration, electron capture by iron and finally the Fe_2O_3 formation.

$$Fe_2^{III}(C_2O_4)_3\cdot 6H_2O\xrightarrow{100^oC}Fe_2^{III}(C_2O_4)_3+6H_2O$$

$$Fe_2^{III}(C_2O_4)_3\xrightarrow{200^oC}2Fe^{II}(C_2O_4)+2CO_2 \qquad (2.7)$$

$$2Fe^{II}(C_2O_4)\xrightarrow{300^oC}Fe_2O_3+2CO+CO_2$$

The effect of ***high pressure*** is known to produce changes of the ratio Fe^{3+}/Fe^{2+}, included in a large variety of iron mineral. The reduction of ferric into ferrous ion in relation to the pressure was observed in the spectra of ferric acetylacetone. The effect is reversible with some hysteresis (Drickamer, 1967). At atmospheric pressure the $Fe(AcAc)_3$ has a broad resonance line with $\delta_{C.S}$ ~0.55mm/s, at 85Kbar a high velocity shoulder appears. This shoulder is more pregnant to 165Kbar. The author assigns the shoulder to ferrous compound of $\delta_{C.S}$ ~ 1.3mm/s and ΔE_Q~1.9mm/s (see Fig. 2.13).

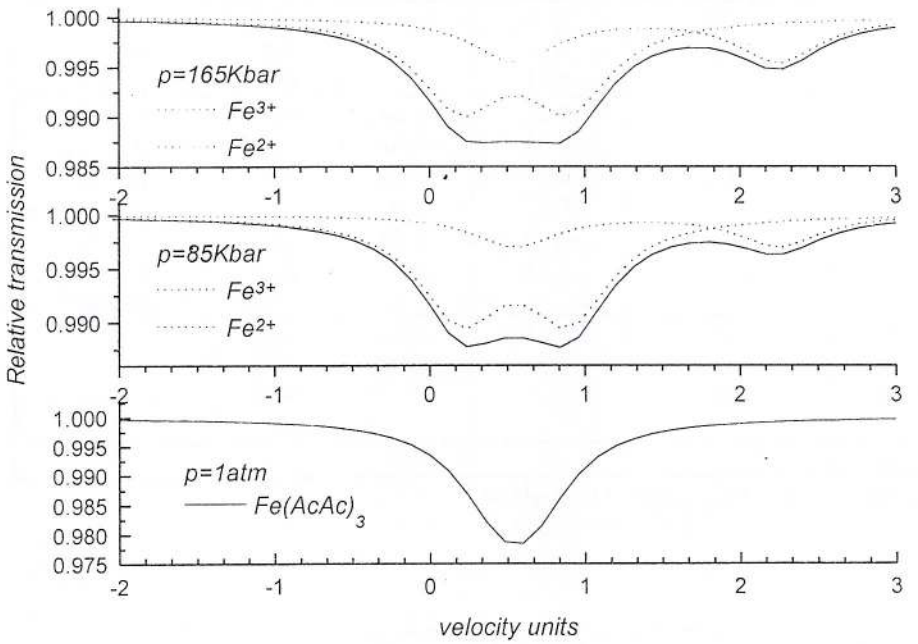

Fig. 2.13 - Mössbauer spectra of $Fe(AcAc)_3$ for different pressure conditions

2.6. Magnetic ordering

The iron oxides and iron silicates have magnetic ordering, but a few materials have this kind of ordering at room temperature. Possible reasons for low magnetic ordering of iron minerals, compared with the iron oxides, are the lower density of iron ions (especially in the solid-solution series), the weak superexchange interactions due to the bond angles Fe-O-Fe about 90° and probably the low spatial dimensionally of basic magnetic units, the octahedral sheets, ribbons or chains. Mössbauer spectra of magnetic ordered minerals can be interpreted in conjunction with the magnetic susceptibility, magnetization, neutron diffraction data. Except iron oxides the other iron minerals contain too small amount of iron for continuos magnetic superexchange path, but the iron-rich sheets, chains or group silicates show a collective magnetic behavior.

The best known iron oxides observed in the minerals are given in Table 2.9 (Greenwood, 1971).

Hematite (α-Fe_2O_3) has a crystal structure of corundum (α-Al_2O_3) with a close-packed oxygen lattice and Fe^{3+} cations in octahedral sites. Magnetically, it is antiferromagnetic at low temperature, then undergoing to weak ferrimagnetism (Morin temperature, T_M=260K), before finally becoming paramagnetic at high temperature (Neel temperature T_N=956K). Ultra-fine particle of α-Fe_2O_3 exhibits a superparamagnetism due to the decreasing relaxation time with the decreasing particle size. The Mössbauer spectra of small particle, supported on high area-silica are apparently paramagnetic spectra at room temperature. Thus based on the presence of a magnetic and paramagnetic superposed subspectra in α-Fe_2O_3 spectrum it is possible to estimate the particle size of hematite (see Fig. 2.14).

Table 2.9.
Mössbauer parameters of some iron oxides magnetically ordered

Compound	Temperature [K]	δ_{CS} [mm/s]	ε_Q [mm/s]	H [KOe]	Assignment
α-Fe_2O_3	298	+0.38	0.12*	515	
γ-Fe_2O_3	RT	0.27	-	488	Fe^{3+}:A
		0.41	-	499	Fe^{3+}:B
Fe_3O_4	RT	0.23	-0.02	491	Fe^{2+}:A
		0.64	0.00	453	$Fe^{3+,2+}$:B
	82	0.37	-0.05	511	Fe^{3+}:A
		0.77	0.50	533	Fe^{3+}:B
		0.59	-0.02	516	Fe^{3+}:B
		0.71	0.95	473	Fe^{2+}:B
		1.20	-2.62	374	Fe^{2+}:B
α-FeOOH	291	0.35	-0.15	384	
γ-FeOOH	4.2	0.30	<0.10*	460	
δ-FeOOH	80			505	Fe^{3+}:oct.
				525	Fe^{3+}:tetr.
$Fe(OH)_2$	4.2		3.06	200	

RT room temperature; $*E_Q = eQV_{ZZ}(1-3\cos^2\theta)/\delta$

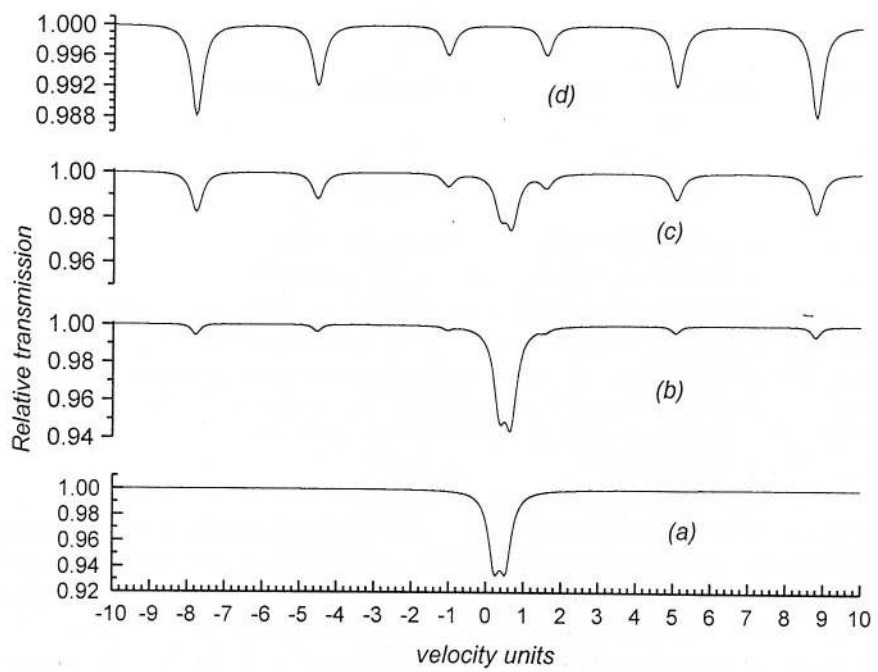

Fig. 2.14 - The Mössbauer spectra at room temperature for α-Fe_2O_3 for different particle size, a) <100Å; b)~120Å; c)~160Å; d) bulk material

The ***γ-Fe_2O_3*** has a spinel structure AB_2O_4 (A cations have a tetrahedral oxygen coordination and B cations have octahedral one). The A and B sites are insufficiently filled by ferric ions so that the stoichiometry corresponds to $Fe_{8/3}\square_{1/3}O$, where $\square$ represents a cation vacancy. The room temperature spectrum shows apparently only one magnetic sextet, so A and B cation sites are indistinguishable, that means an electronic configuration ^6S of Fe^{3+}. A magnetic external field applied permitted a partial resolution and show that all vacancies are in B sites, $[Fe]\{Fe_{10/12}\ \square_{2/12}\}_2O_4$, (Greenwood, 1971).

The ***magnetite*** $[Fe^{3+}]\{Fe^{2+}\ Fe^{3+}\}O_4$ shows at room temperature a spectrum with two magnetic sextets corresponding to A and B iron sites having 491KOe and 453KOe, respectively. The second value is lower than A sites because the fast electron hopping producing a completely averaged magnetic field. The spectrum at 77K is partially resolved, the sample having an orthorhombic symmetry and discrete valence states (Greenwood, 1971). The hyperfine magnetic field determined from the spectra is of about 508 and 480KOe and corresponds to Fe^{3+}: A and Fe^{2+}: B sites, respectively. The magnetite has Verwey transition at 110K. The spectral parameters are given in Table 2.9.

The Mössbauer spectra of many minerals aggregates or rocks show the presence of magnetic sextets corresponding to iron oxide hydroxide ***FeOOH***. The ***goethite α-FeOOH*** has the same structure as α-AlOOH with iron in a distorted octahedral environment of oxygen, below the Neel temperature ~403K, it is antiferromagnetic. Iron ions have ^6S electronic configuration, with the spins parallel to c-axis and the V_{zz} in the ab plane. ***β-FeOOH*** is similar to α-FeOOH, but clearly nonstoichiometric and contains various quantities of F^-, or Cl^-, and H_2O. It is antiferromagnetic below 295K. The extrapolated value of H is 475KOe. ***γ-FeOOH*** is similar to α-FeOOH one, but has a complex layer structure. The low temperature spectra of minerals ($10K<T<77K$) have shown the coexistence of para and antiferromagnetic phases. Finally in ***δ-FeOOH*** the iron ions are distributed in tetrahedral and octahedral sites, which are suggested in the 80K Mössbauer spectrum by two magnetic sextes corresponding to 505 and 525 KOe. The compound is a ferromagnetic and decomposes above 370K.

The helium temperature spectrum of ***iron hydroxide $Fe(OH)_2$*** exhibits an apparent four resonances of magnetic spectrum, although there are in fact eight lines present. It has a CdI_2 type hexagonal layer structure with ferrous iron, octahedrally coordinated by OH^- ions. The Neel temperature is about 34K.

More spectacular magnetic ordering is offered by the ***iron silicates*** due to the coexistence of ferrous and ferric ions in different or not octahedral sites and of low magnetic field with high EFG tensor values (see Table 2.10, Coey, 1984). In these cases the nuclear states are splitted completely but they are a weighted mixture of states with well-defined values of I_z. (so called nuclear pure states, Barb et al., 1971, 1972). The Mössbauer isotope states are characterized by energies $E_{I,k}$, obtained from a secular equation, and by the weights of pure states, $C^{I_z}_{(I,k)}$. The square absolute values of the weights will give the aria of resonance lines in spectra.

$$E_{I_g,i},\Psi_{I_e,i} = \sum_{I_z=-I_e}^{+I_e} C^{I_z}_{(I_e,i)}\Psi_{I_e,I_z} \leftrightarrow E_{I_g,j},\Psi_{I_g,j} = \sum_{I_z=-I_g}^{+I_g} C^{I_z}_{(I_g,j)}\Psi_{I_g,I_z}$$

$$A_{i,j} \propto \left|\vec{k}\cdot\int_{V_{nucl.}} \Psi_{I_e,i}\cdot\vec{J}_{nucl.}\Psi_{I_g,j}d\vec{r}\right|^2 \qquad (2.8)$$

where $\Psi_{I,k}$ are the nuclear functions. Generally, there are no analitical formulas for the nuclear energies and the weights, but in particular cases of relative orientations (see Fig. 15), there are possbile to obtaine them (see Table 2.11, for ^{57}Fe isotope, Barb et al., 1971; 1972; Grechishkin, 1972). More and detailed results for the majority of Mössbauer isotopes are given in Barb (1972) and Constantinescu (Ph.D. Thesis 1980).

Table 2.10.
The Mössbauer parameters for some silicates at 4.2K

Mineral	T_N [K]	δ [mm/s]	$eQV_{zz}/2$ [mm/s]	η	H [KOe]	θ [°]	Δ_2 [K]
Sheet-silicates							
1:1 layer silicates							
Grenalite	17	1.30	-2.96	0.0	158	90	~1000
Cronstedtite	12	1.39	-2.77	0.2	141	80	
IV		0.35	-0.13*		406		
VI		0.54	-0.14*		467		
2:1 layer silicates							
Ferropyrophilite M_2	15	0.48	0.03*		517		
Minnesatoite	28	1.35	-3.09	0.1	130	87	
Biotite M_1/M_2	7		-2.75	0.2	150	~90	1180
Chain-silicates							
Pyroxenes							
Orthoferrosilite M_1	37	1.34	-2.5	0.9	290	53	500
M_2		1.29	1.6	0.6	113	47	2000
Amphiboles							
Crocidolite M_1	30	1.31	-2.77	0.1	196	90	
M_2		0.52	0.17*		550		
M_3		1.31	-2.95	0.3	101	90	
Group-silicates							
Sorosilicates							
Ilvaite A	118	0.58	0.51*		505		
Nesosilicates							
Fayalite M_1	66		3.08	0.2	323	75	
M_2			3.02	0.2	120	0	
Laihunite M_1	~160	1.32	2.9	0.0	260	-	
M_2		0.50	0.3*		505		
Almandine		0.58	-3.45	0.1	228	90	1700

* ε_Q

The Mössbauer spectroscopy of magnetic ordered minerals has contributed substantially to the understanding of the magnetism. The spectral parameters of magnetic sextets have shown very large values of quadrupole parameter for Fe^{2+} and low magnetic fields perpendicular to V_{zz} . The information obtained from this spectroscopy corroborated with neutron diffraction data permitted to consider dominant exchange interactions in some sheet and chain silicates containing ferrous ions or a mixture of ferrous and ferric iron. For layer silicates the octahedral sheets are ferromagnetic, but the exchange coupling is antiferromagnetic between the sheets. The ratio of intraplane to the interplane coupling is 50:1, so these minerals are magnetically two dimensional.

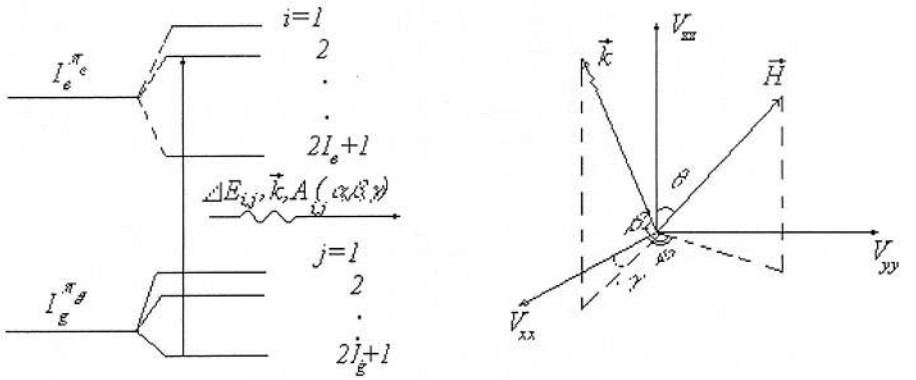

Fig. 2.15 - The splitting of Mössbauer isotope levels in coupled electric and magnetic hyperfine fields and the reltaive orientations of hyperfine magnetic field and γ- ray momentum to axes of EFG-tensor

Table 2.11.

The energy levels of I=3/2 nuclear state in the coupled hyperfine fields

Angles θ ; φ	$E_{3/2,i}(a, b, \eta, \theta, \varphi)$
0.; 0.;	$\pm 3a\sqrt{\left(1-\frac{b}{3a}\right)^2+\frac{\eta^2}{3}}-\frac{b}{2};\pm 3a\sqrt{\left(1+\frac{b}{3a}\right)^2+\frac{\eta^2}{3}}+\frac{b}{2}$
π/2; 0.;	$\pm 3a\sqrt{\left(1+\frac{b}{3a}\right)^2+\frac{1}{48}\left(\frac{b}{3a}-4\eta\right)^2}-\frac{b}{2};\pm 3a\sqrt{\left(1-\frac{b}{3a}\right)^2+\frac{1}{48}\left(\frac{b}{3a}+4\eta\right)^2}+\frac{b}{2}$
π/2; π/2;	$\pm 3a\sqrt{\left(1+\frac{b}{3a}\right)^2+\frac{1}{48}\left(\frac{b}{3a}+4\eta\right)^2}-\frac{b}{2};\pm 3a\sqrt{\left(1-\frac{b}{3a}\right)^2+\frac{1}{48}\left(\frac{b}{3a}-4\eta\right)^2}+\frac{b}{2}$

where $a= eQV_{zz}/12$ and $b=\mu H$

Many magnetic minerals show a coexistence of Fe^{2+} and Fe^{3+} ions generating the low and large values of magnetic fields. Generally the origin of ferromagnetism within the planes is a near 90° Fe^{2+}-O-Fe^{2+} superexchange bond angle, which leads to the exchange constant $J \cong 2K$ and the Fe^{2+}-O-Fe^{3+} interaction given by the electron hopping.

The dominant interaction Fe^{3+}-O-Fe^{3+} in the purely ferric sheet silicates is antiferromagneticaly within the planes. In the chain silicates the antiferromagnetic interactions are stronger than in the sheet silicates. The magnetic ordering in the group silicates is antiferromagnetic. Thus the spectra of fayalites show magnetic sextets, occurring at 66K and many authors proposed a canted magnetic structure. The transition to a collinear antiferromagnetic structure is below 20K. In the laihunite the hyperfine splitting of Fe^{3+}: M_2 appears at 160K whereas for Fe^{2+}: M1 one shows below 80K. That could be explained by the antiferromagnetic structure of M_2 site ions so that exchange interactions with the M_1 neighbours cancel each other.

The relaxation effects have been evidenced by Mössbauer spectra of the olivine-series $\{Mg_{2-x}Fe_x\}[Si]O_4$ at low temperatures. These spectra have been interpreted in terms of superpara-magnetic fluctuation of small ferrous group of about 20Å.

2.7. Occupancies and quantitative populations in silicates

As we have seen in the previous paragraphs, many minerals have two or more cation sites filled by Na^+, K^+, Ca^{2+}, Mg^{3+}, $Fe^{2+,3+}$, Al^{3+}, Si^{4+}, Ti^{4+} ions etc. Often the cation sites are of same size and energy and could be occupied by one or more sort of ions. Moreover the same ion can occupy one or more cation sites. The ***ordering process*** is a process to enter an ionic sort in one of cation positions. The ordering process might be expected to depend on the temperature and pressure conditions. As the temperature increases the cation distribution is expected to be more

random. The Mössbauer spectroscopy gives information of the ordering process using a rapid and accurate estimation of distribution on cation sites of the parent ions. The majority of the Mössbauer data of the ordering process are obtained on Fe and Sn containing minerals.

If a mineral contains two or more different types of Mössbauer parent atoms that give *non-overlapping* subspectra in the spectrum, the area of every subspectra could be related by the n_k number of k^{th} Mössbauer parent atom per formula unit:

$$\frac{a_k}{\sum_{k=1}^{nr.subsectr.} a_k} = \frac{n_k f_{Ak} \Gamma_{Ak} G(X_{Ak})}{\sum_{i=1}^{nr.subsectr.} n_i f_{Ai} \Gamma_{Ai} G(X_{Ai})} \rightarrow \frac{a_k}{a_{k'}} = Const. \frac{n_k}{n_{k'}}; Const. = \frac{f_{Ak}}{f_{Ak'}} \cdot \frac{\Gamma_{Ak}}{\Gamma_{Ak'}} \cdot \frac{G(X_{Ak})}{G(X_{Ak'})} \quad (2.9a)$$

$$X_{Ai} = n_{Ai} f_{Ai} \sigma_{0A} \rightarrow 0 \Rightarrow G \rightarrow 1 \Rightarrow \frac{a_k}{\sum_{k=1}^{nr.subsectr.} a_k} = \frac{n_k f_{Ak} \Gamma_{Ak}}{\sum_{i=1}^{nr.subsectr.} n_i f_{Ai} \Gamma_{Ai}} \rightarrow \frac{a_k}{a_{k'}} = Const.^* \frac{n_k}{n_{k'}}; Const.^* = \frac{f_{Ak}}{f_{Ak'}} \cdot \frac{\Gamma_{Ak}}{\Gamma_{Ak'}} \quad (2.9b)$$

where the saturation correction function G depends on the absorber thickness, X. The ratios of the relative subspectra areas $a_k/a_{k'}$ give the ratios of $n_k/n_{k'}$. As one can see the constant factors *Const.* and *Const**. depend on the ratios of Mössbauer factors, of half linewidths and of correction functions for each of cation sites and different parent ionic sort. In order to obtain an accurate area it is necessary to appreciate the absorber thick X_{Ak} and to estimate the f_{Ak} factors and the Γ_{Ak}. witdhs for different cation sites or for different sort of parent ionic sorts.

The estimations of areas and of site population too are not so easy to do when the resonance lines of two or more subspectra are *overlapping*. Indeed in this case an increasing of position and intensity errors and deviation of resonance line shape from the Lorenz one for superposed resonances are appearing. A very careful analysis and method have developed to determine the concentrations of n_k.

Theoretically the spectral parameter of the effect at a given velocity, $\varepsilon(v_i) = \varepsilon_i$ depends on the all n_α ($\alpha = 1,2,..N$) and the concentrations are obtained using the Kramer's ruler:

$$\varepsilon_i = \sum_{\alpha=1}^{N} \varepsilon_{i\alpha} n_j \quad i = 1,2,3...N \Rightarrow n_\alpha = \frac{D_\alpha}{D}; D = \begin{vmatrix} \varepsilon_{11} & \varepsilon_{12} & . & . & \varepsilon_{1N} \\ \varepsilon_{21} & \varepsilon_{22} & . & . & \varepsilon_{2N} \\ . & . & . & . & . \\ . & . & . & . & . \\ \varepsilon_{N1} & \varepsilon_{N2} & . & . & \varepsilon_{NN} \end{vmatrix}; D_\alpha = \begin{vmatrix} \varepsilon_{11} & . & \varepsilon_1 & . & \varepsilon_{1N} \\ \varepsilon_{21} & . & \varepsilon_2 & . & \varepsilon_{2N} \\ . & . & . & . & . \\ . & . & . & . & . \\ \varepsilon_{N1} & . & \varepsilon_N & . & \varepsilon_{NN} \end{vmatrix} \quad (2.10a)$$

$$N = 2 \Rightarrow n_1 = \frac{\varepsilon_{22}\varepsilon_1 - \varepsilon_{12}\varepsilon_2}{\varepsilon_{11}\varepsilon_{22} - \varepsilon_{12}\varepsilon_{21}}; n_2 = \frac{\varepsilon_{22}\varepsilon_2 - \varepsilon_{21}\varepsilon_1}{\varepsilon_{11}\varepsilon_{22} - \varepsilon_{12}\varepsilon_{21}};$$

where N are the number of iron compound in the investigated mineral and $\varepsilon_{i\alpha}$ are the effect of α iron compound at v_i spectral position. These effects $\varepsilon_{k\alpha}$ depend on f_{Ak}, Γ_{Ak} and X_{Ak} and can be obtained from the spectra of standard sample containing the N iron compounds. The spectra of the standard samples must be carried out under the same experimental conditions (same thickness, same background etc.) as of the investigated samples. $\varepsilon_{i\alpha}$ ($\alpha \neq k$) at resonance positions are vanished and the concentrations relative to the standard samples are:

$$n_\alpha \cong \varepsilon_\alpha / \varepsilon_{\alpha\alpha}; \alpha = 1,2,...N \quad (2.10b)$$

for a choosen velocity range of spectra, containing only almost distinct resonance lines from the iron compounds. In the case of a thick sample practically one can determine only the effects for a limited N number. Thus, for N=2 only the effects ε_I and ε_{II} can be determined:

$$\alpha = \frac{\varepsilon_{12}}{\varepsilon_{11}}; \beta = \frac{\varepsilon_{21}}{\varepsilon_{22}}; \rightarrow \left.\begin{aligned} \varepsilon_1 &= \varepsilon_I + \alpha\varepsilon_{II} \\ \varepsilon_2 &= \beta\varepsilon_I + \varepsilon_{II} \end{aligned}\right\} \Rightarrow \begin{cases} \varepsilon_I = \dfrac{\varepsilon_1 - \alpha\varepsilon_2}{1 - \alpha\beta} \propto n_I \\ \varepsilon_{II} = \dfrac{\varepsilon_2 - \beta\varepsilon_1}{1 - \alpha\beta} \propto n_{II} \end{cases} \quad (2.10c)$$

where α and β are the weigths of second/first resonance line to the first/second one at the v_{o1}/v_{o2} positions. For quantitatve site populations, it is necessary to know the total content of Mössbauer parent atoms from other experimental technique (for example chemical analysis technique).

We mention that several authors use a rough but useful approximation:

$$f_{Ak} = f\,;\Gamma_{Ak} = \Gamma\,;G(X_{Ak}) = G(X) \Rightarrow Const. = 1 \qquad (2.11)$$

Successful quantitative determinations of n_k for iron silicates minerals have been obtained in spite of these difficulties. Tables 2.12 and 2.13 (Bancroft, 1973) present the Mössbauer data of the site populations in some silicates compared with the data obtained by other techniques. The consistence of the above results evidenced the success of site population determinations by Mössbauer spectroscopy.

Table 2.12.

The iron site populations in some silicates

Minerals	Total Fe^{2+} per formula unit	Fe^{2+} site population(per formula unit) Mössbauer	X-Ray
Orthopyroxene	1.06	M_2=0.87 M_1=0.19	M_2=0.90 M_1=0.15
Glaucophane	0.61	M_3=0.28 M_1=0.33	M_2=0.29 M_1=0.32
Grunerite	6.13	M_4=1.96 $M_{1,2,3}$=4.17	M_2=1.97 $M_{1,2,3}$=4.13
Anthophyllites	1.61 1.47	M_4=1.39 $M_{1,2,3}$=0.22	 M_4=1.30 $M_{1,2,3}$=0.17
Cummingtonites	2.48 2.50	M_4=1.65 $M_{1,2,3}$=0.83	 M_4=1.74 $M_{1,2,3}$=0.58

Table 2.13.

Comparison of Mössbauer and chemical data

Minerals	$\%\{Fe^{3+}/(Fe^{2+}+Fe^{3+})\}$ Mössbauer	Chemical Analyses
Howieite	24	20
Deerite	37	37
Crocidolite	41	41
Glaucophane	28	32
Crossite	37	40

Acknowledgements

One of the authors is grateful to the financial supports from the Committee of CNR (Roma), Progetto Sistema Lagunare Veneziano, E.N.E.A in the framework of the Italian National Programme for Antarctic Researches, PNRA (Environmental Impact-Chemical Methodologies) and from the M.C.T. (Bucharest), Programme Orizont 2000 (The investigations of archeologic and geologic materials by the techniques of resonance spectroscopies).

References

Bancroft, G. M. (1973) Mössbauer spectroscopy. An introduction for inorganic chemists and gechemits. 243 p., **68**, 169, 179, 191, 206, 207, London, ed. McGRAW-HILL Book Company.

-- , **Burns, R. G., Howie, R. A. (1967)** Determination of cation distribution in orthopyroxene by Mössbauer effect. *Nature*, **213**, 1221.

-- , **Maddock, A. G., Burns, R. G. (1967)** Applications of the Mössbauer effect to silicate mineralogy. I. Iron silicates of known crystal structure. *Geochim.Cosmochim. Acta*, **31**, 2219.

Barb, D., Constantinescu, S, Tarina, D. (1971) Polarized γ-rays transition probabilities in the case of coupled electric and magnetic hyperfine interactions. *Rev. Roum. Phys.*, **16**, 263.

-- , **Constantinescu, S, Tarina, D. (1971)** Mössbauer transition probabilities in the case of coupled hyperfine interections Proc. of IV. Internationale Konferenz der sozialistischen Lander uber **Mössbauer spektrometry**, 20-25 Sept. 1971, Dresda , D.D.R., **2**, 606, Ed. Academia de Stiinte a R.D. Germane.

-- , **Constantinescu, S, Tarina, D. (1971)** Formulas for the relative γ-transition probabilities of the Mössbauer isotopes. *Rev. Roum. Phys.*, **16**, 1005.

-- , **Constantinescu, S., Diamandescu, L., Tarina, D. (1972)** Contributions to the Mössbauer line shape in the coupled hyperfine interactions. *Rev. Roum. Phys.*, **17**, 769.

-- , **Constantinescu, S., Tarina, D. (1995)** ^{57}Fe Mössbauer spectroscopy on disordred crystalline media with Ca-gallogermanate type structure. I. In the paramagnetic range. Hyperfine Interaction , **96,** 73.

Coey, J. M. D. (1975) Iron in post-glacial lake sediment core; A Mössbauer effect study. *Geochim. Cosmochim. Acta*, **39**, 401.

-- **(1980)** Clay minerals and their transformations studied with nuclear techniques : The contribution of Mössbauer spectroscopy. *At. Energy Rev.*, **18**, 73.

-- **(1984)** Mössbauer spectroscopy of silicate minerals, In: Mössbauer Spectroscopy Applied to Inorganic Chemistry New York, ed. Plenum Press, **1,** 443-509 p., 467, 472, 491, Mössbauer Spectroscopy of Silicate Minerals.

Constantinescu, S. (1980) Mössbauer Investigations of Coupled Hyperfine Interactions,198 p., 10-34, 177, Ph.D. Phys. Thesis, ed. Central Institute of Physics/Inst. Phys. Tech. Mat., Bucharest.

Czjzek, G, Fink, J., Gotz, F., Schmidt, H., Coey, J. M. D., Rebouillat, J. P., Lienard, A. (1981) Atomic coordination and the distribution of electric field gradients in amorphous solids. *Phys. Rev.*, **B23,** 2513.

Drickamer, H. J. (1967) Effect of pressure on Mössbauer resonance in potassiun ferrocyanide, potassium ferricyanide and insoluble prussian blue. *J. Chem. Phys.*, **47**, 2583.

Grechishkin, V. S. (1972) Iadernie Kvadrupolnie Vzaimodeictvie v Tverdih Telah , 263 p., 23, ed. Nauka, Moskva.

Greenwood, N. N. (1971) Mössbauer Spectroscopy, 660 p., 91, 241, 248, 251, 292, Springer-Verlag.

Gutlich, P. (1978) Mössbauer Spectroscopy, 280 p., Springer-Verlag, S68., Berlin.

Strens, R. G. (1966) Pressure-induced spin-pairing in gillespite, $BaFe^{II}$ Si_4O_{10}, *Chem. Comm.*, **21,** 777.

Whitefield, H. J., Freeman, A. G. (1967) Mössbauer study of amphiboles. *J. Inorg. Nucl. Chem.*, **29**, 903.

Rom. J. Mineralogy, 79, p. 71-84, Bucureşti, 1999

MÖSSBAUER SPECTROSCOPY IN MINERALOGY AND GEOCHEMISTRY PART 3: INVESTIGATIONS OF SOME MINERALS FROM ROMANIA

(review paper)

[1]S.CONSTANTINESCU, [2]G. UDUBAŞA, [3]S. CALOGERO
[1]National Institute of Materials Physics, P.O.Box: Mg-07, Bucharest, Romania,
[2]Geological Institute of Romania, 78344, Bucharest, Romania
[3]Universita Ca'Foscari di Venezia, Dipt. Chimico - Fisica, 30123, Venezia, Italy

Key words: ^{57}Fe-Mössbauer effect, Romanian minerals.

Abstract: Generally from a Mössbauer spectrum one intends to extract all structural information as internal fields, occupancies of different crystalline sites, ionic states of parent atoms, etc. In this part of the work, the authors want to evidence some older and newer results of Mössbauer investigations on Romanian minerals, obtained in the laboratories of different Romanian institutes.

3.1. Pyroxenes of diopside-hedenbergite-johansenite series

This work emphasized the Mössbauer investigations of the clinopyroxenes in the diopside-hedenbergite-johansenite series (<Ca>{Mg}[Si_2]O_6-<Ca>{Fe}[Si_2]O_6-$CaMnSi_2O_6$ Di.-Hed.-Joh.) obtained from the skarn deposits of Dognecea-Banat, (Ionescu et al., 1971). The structural formula of these samples and of the hedenbergite studied by Bancroft et al. (1967) are shown in Table 3.1. The sample have chemically been characterized as manganiferous ferrosalite (sample 1) and as Mn-hedenbergites (samples 2, 3).

Table 3.1.
Structural formula of investigated samples

Samples	<M_2>	{M_1}						[Z]	
	Ca	Mg	Fe^{2+}	Mn^{2+}	Fe^{3+}	Al	Ti	Si	Al
1	0.944	0.377	0.390	0.132	0.074	0.041	0.007	1.936	0.064
2	0.917	0.119	0.531	0.296	0.121	-	0.001	1.930	0.060
3	0.974	0.129	0.447	0.412	0.052	-	0.052	1.924	0.061
Hed. of Bancroft	0.950	0.180	0.850	0.020	1.530*			2.000	

* % Fe_2O_3

The spectra of the samples revealed the presence of the two ionic sorts of iron Fe^{2+}, Fe^{3+} corresponding to the two subspectra. The subspectrum, with the bigger quadrupole splitting, has assented to the Fe^{2+} in octahedral sites M_1 and the second one, with the smaller quadrupole splitting, to the Fe^{3+}:M_1 or to an other iron phase. The spectral parameters of the fitting spectra are given in Table 3.2.

The spectra of the investigated samples show different values of the quadrupole splitting parameter for Fe^{2+} corresponding to the 6-fold coordination. However, the spread of these values in a narrow range suggests that the ferrous ion occupies the same lattice positions, M_1. Moreover, one can observe the same values of $\delta_{C.S}^{exp}$ and ΔE_Q^{exp}. The observed differences can be correlated with the parameters of the crystal structure (lattice constants, mean distances M-O, angles O-M-O, cation radius, see Table 3.3) and the structural formula chemically determined see Table 3.1). The changes of lattice constants and in consequence the geometrical distortion cannot explain the changes of the ΔE_Q^{exp} values. On the other hand the increase of the M_1 cation radius causes an increase of the octahedron distortion and a decrease of the ΔE_Q^{exp} (Bancroft, 1967). In hypothesis of the presence of Fe^{3+} in M_1 sites, the absence of the nuclear qudrupole splitting, in the spectrum of the sample with a high concentration of Mn^{2+}.

suggests us a cubic symmetry of oxygen ions around these sites. So the distortion of the octahedron M_1 is in connection to the ratio Mn/Fe and the quadrupole splitting parameter of Fe^{3+} in such samples could be a measure of this ratio.

Table 3.2.
Mössbauer spectral parameters

Samples	FeO [%]	Fe_2O_3 [%]	Mol [%] Di. Hed. Joh.	Fe^{2+} $^*\delta_{CS}^{exp}$ ΔE_Q^{exp} a^{exp}/a_{tot}^{exp} [mm/s]	Fe^{3+} $^*\delta_{CS}^{exp}$ ΔE_Q^{exp} a^{exp}/a_{tot}^{exp} [mm/s]
1	11.58	2.40	40 43 17	0.989 2.178 0.970 ±0.022 ±0.022 ±0.074	-0.021 1.168 0.100 ±0.106 ±0.105 ±0.034
2	15.18	3.32	13 56 31	1.003 2.311 1.167 ±0.026 ±0.026 ±0.115	0.054 1.097 0.131 ±0.159 ±0.159 ±0.046
3	12.63	1.67	12 45 43	1.004 2.309 0.942 ±0.008 ±0.008 ±0.039	0.692 0.000 0.076 ±0.030 ±0.013
Hed. of Bancroft	25.00	1.53	15 74 11	1.250 2.150	

$^*\delta_{CS}$ is for ^{57}Co:Cu source

Table 3.3.
The lattice constants and mean distances for M_1 and M_2 site in Di-Hed-Joh

Mineral	r_m[Å]	a[Å]	b[Å]	c[Å]	β	Site	Ion (radius*)	Coord
Diopside $CaMgSi_2O_6$	2.50 2.12	9.71	8.98	5.24	105°50'	M_1 M_2	Ca^{2+}(1.12) Mg^{2+}(0.72)	8 6
Hedenbergite $CaFeSi_2O_6$		9.85	9.02	5.26	104°20'	M_1 M_2	Ca^{2+}(1.12) Fe^{2+}(0.77)$^\Delta$	8 6
Johansenite $CaMnSi_2O_6$	2.53 2.17	9.978 ±0.009	9.156 ±0.009	5.293 ±0.005	105°29'	M_1 M_2	Ca^{2+}(1.12) Mn^{2+}(0.82)$^\Delta$	8 6

* The effective radius determined with $r(^{VI}O^{2-})$=1.40[Å](Shanon et al., 1969)
$^\Delta$ The high spin configuration.

3.2. Pumpellyites

The second example is the investigations of pumpellyite samples obtained from two different mineral occurrences in the Romanian Carpathians. The pumpellyite is a membership of the group silicates, having the chemical formulas $<W>_8\{X\}_4\{Y\}_8$ $[Si]_{12}O_{56-n}(OH)_n$ and the cell parameters given in Gottardi, (1965). The differences of the spectral parameters giving the data of the iron abundance, the chemical iron-oxygen bonds, the deformation and occupancies of iron octahedra, observed at the studied samples, are discussed and correlated by the different genesis conditions of two pumpellyite-bearing occurrences (Constantinescu et al., 1997). The experimental spectrum of one sample, 15c, (Maramures Mts) shown in Figure 3.1 evidenced three quadrupole doublets characteristic of six-fold iron environment. One doublet corresponds to Fe^{2+} and other two doublets correspond to Fe^{3+}. The ferrous doublet is predominant (see Table 3.4). A numerical calculus of the ^{57}Fe quadrupole splitting parameter has been performed using a specialized program (Constantinescu, 1997) and taking into account the fractional atomic positions in the pumpellyite crystal and fractional ionic charges determined by valence summation procedure (Galli, 1969; Allmann, 1971), in order to designate the subspectra II and III to iron sorts. Table 3.5 shows both the values of ΔE_Q^{tot} and η^{tot} (asymmetry parameter) on the X and Y sites in the pumpellyite mineral calculated by the well known expressions (1.11a-d) and from table 1.4 for $I=3/2$.

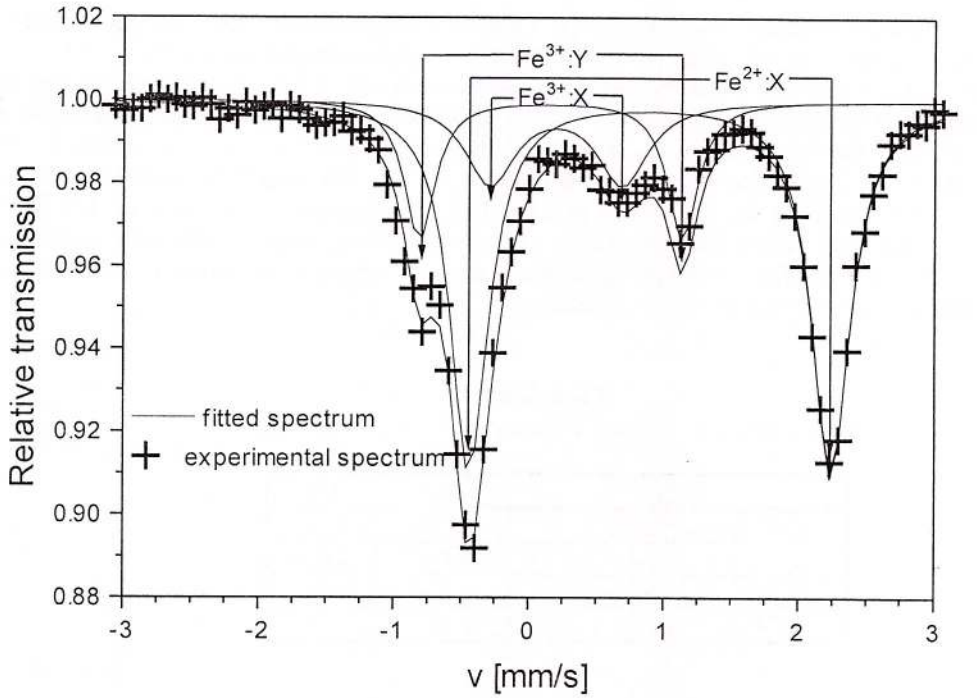

Fig. 3.1 - Mössbauer spectra of the sample 15c

Table 3.4.
The Mössbauer spectral parameters and their errors

Samples	*Qudrupole doublet*	δ_{A-Rh}^{exp} *[mm/s]*	ΔE_Q^{exp} *[mm/s]*	Γ^{exp} *[mm/s]*	$a_i^{exp} / a_{tot}^{exp}$ *[%]*
2L (Parang Mts)	*I*	0.99(2)	3.24(4)	0.48(3)	80(3)
	II	0.34(4)	1.23(8)	0.35(9)	07(5)
	III	0.26(2)	1.93(4)	0.36(5)	13(4)
15c (Maramures Mts)	*I*	0.90(2)	2.68(4)	0.34(3)	66(3)
	II	0.35(4)	1.04(6)	0.46(5)	18(4)
	III	0.26(2)	1.95(6)	0.27(4)	16(4)

Table 3.5.
The calculated ΔE_Q^A and r values for iron sites in pumpellyite lattice

Site	*Geometrical distortions* r_m; $^*\Delta_{oct}$; $^*\sigma^2$	ΔE_Q^{lat} *[mm/s]*	ΔE_Q^{el} *[mm/s]*	ΔE_Q^{tot} *[mm/s]*	η^{tot}	$\lvert\Delta E_q^{exp} - \Delta E_q^{tot}\rvert / \Gamma^{exp}$ *15c ; 2L*
$^*Fe^{2+}:X$	1.99; 9.764; 0.028	0.86(8)	3.20(4)	2.68(8)	0.10(3)	0.00(10); 1.17(10)
$Fe^{3+}:X$	1.99; 9.964; 0.028	0.86(8)	-	0.86(8)	0.60(3)	0.39(11); 1.11(14)
$Fe^{3+}:Y$	1.92;11.12; 0.022	1.91(9)	-	1.91(9)	0.47(5)	0.15(13); 0.10(12)

$Q(^{57}Fe)=0.20\cdot10^{-28}m^2$; γ_∞=-10; $^*\Delta_1$ =600(±80)cm^{-1} ,Δ_2 =2Δ_3 =20 (±5)cm^{-1}, R=0.32, α=0.9;
* *see formula 2.2*

The concordance between $\Delta E_Q^{exp}(I)$ and $\Delta E_Q^{tot}(I)$ is a good check of the high spin configuration of Fe^{2+} in X site of pumpellyite crystalline structure and also suggests a high spin configuration for Fe^{3+}. The difference between the calculated and experimental quadrupole splitting values for the *I* and *II* sublattices of 15c and 2L samples has been explained by different distortions of the X octahedra in 2L sample as the known one in this structure. The authors show that the principal responsible of geometrical distortions of X octahedra is the high pressure environment of the occurrence (Constantinescu et al., 1997). The area data furnished the relative occupances of the iron ion species in the X and Y octahedra. The used formula is 2.9 where one has taken into account the thin sample and the different recoiless *f* factor of the two iron ions in the octaheraon environment (De Grave, 1991). The different Fe^{2+}, Fe^{3+} occupancies of the octahedra suggested us different oxidation genesis conditions and thus different pressure-temperature conditions.

Table 3.6.

The occupancies of X and Y octahedra in the two samples

Ratio	2L	15c
$C_X(Fe^{3+})/C_X(Fe^{2+})$	0.100	0.167
$C_X(Fe^{3+})/C_Y(Fe^{2+})$	0.544	0.660
$C_X(Fe^{3+}+Fe^{2+})/C_Y(Fe^{2+})$	6.266	4.242
$C(Fe^{3+})/C(Fe^{2+})$	0.281	0.399

The differences in the iron abundance evidenced by the spectral parameters, the deformations and occupancies of the iron octahedra, the crystallization and the iron oxidation state of 15c and 2L samples can be explained by different conditions of two pumpellyite bearing occurrences. An important role in the genesis of the pumpellyite deposit is played by pressure-temperature conditions. High pressure and temperature could induce a large geometrical deformation of the X octahedra and a higher $C_X(Fe^{3+})$ and as a consequence a more sensitivity of the Mössbauer parameters $\Delta E_Q^{exp}(I)$, a_i^{exp} *(I)*, $\Delta E_Q^{exp}(II)$, a_i^{exp} *(II)*. On the other hand, lower pressure-temperature conditions give the possibility of the other kind of ions to enter the structure. The 2L bearing occurrence showing an iron-poor pumpellyite variety is proved thus to have been formed at lower pressure-temperature conditions as compared to the 15c one.

3.3. ^{197}Au Mössbauer investigation of Nagyagite

In spite of numerous chemical and microprobe analyses the nagyagite lacks an unequivocal formula, showing a rather continuous series of formulas from $AuPb_5Te_3SbS_5$ to $AuPb_9Te_3SbS_{11}$, but most analyses correspond to the formulas $AuPb_7Te_3Sb_{1.5}S_8$ or $AuPb_7Te_{3.5}Sb_2S_9$. The Mössbauer spectra were carried out on several nagyagite samples at 4.2K with a ^{197}Au source. In spite of wide compositional variations and non-stoichiometric compositions the nagyagite spectra show unbroadened quadrupole doublets with the same δ_{CS}^{exp} and ΔE_Q^{exp} values. The spectra of the single crystal absorbers show an axial electric field gradient at gold site corresponding to Au^{3+} in a unique site in the tetragonal unit cell (Udubaşa et al., 1993). The results of investigations have shown the same oxidation state of gold as in sylvanite, krennerite and calaverite. The antimony in nagyagite is also trivalent.

3.4. Fayalite from razoare

In the Mn-Fe Razoare deposit the coarse grained manganon fayalite is associated with rhodochrosite and apatite and is largely replaced by mangangrunerite and magnetite. The investigated samples belong to two distinct assamblages i.e.: (1) rhodochrosite dominated (sample 101); (2) rich in mangangrunerite (sample 138).

Table 3.7.
Chemical analyses in % of the two fayalite samples

Contents	Mangangrunerite assemblages	Rhodochrosite assemblages
fayalite	51.39	57.78
tephroite	39.49	37.13
forsterite	9.12	5.09
SiO_2	25.60	30.38
TiO_2	0.04	0.14
Al_2O_3	0.36	0.52
Fe_2O_3	5.79	3.72
FeO	31.76	36.19
MnO	24.10	22.96
MgO	3.16	1.79
CaO	-	0.16

Mössbauer spectra at room temperature of fayalites cannot well distinguish the two sites, but at low temperature in the magnetic phase (<66K) the separation appears to be possible to the different magnetic hyperfine splittings.Data indicate that the iron has some preference for M_2 site in volcanic olivines. The preference of Fe in M_1 sites has been observed in the samples of the low-temperature origin.

The spectral parameters of the manganon fayalites examinated and of some mangangrunerites at room temperature and ^{57}Co:Rh source are given in Table 3.8 and typical spectra are plotted in Figure 3.2.

Table 3.8.
Mössbauer spectral parameters of investigated samples

Samples	C_{FeO}/C_{MnO}	Assignment to the sites	δ_{IS}^{exp}	ΔE_Q^{exp}	$a[\%]$	${}^{*}C_{Fe^{2+}}[\%]$
138	36.7/22.5	M_1	1.028	2.674	64.36	24.41
		M_2	1.050	2.943	32.41	12.28
			0.269	-	3.23	
101	39/24	M_1	1.041	2.721	68.19	26.59
		M_2	1.059	3.013	31.81	12.40
32	22.5/13	$M_{1,2,3}$	1.075	2.873	75.25	
		M_4	0.963	1.609	24.75	

The concentrations of Fe^{2+} in octahedral sites have been obtained in the approximation of the same f factor and of the thin samples (see formula 2.9). The Mössbauer parameters of our samples exhibit two subspectra of Fe^{2+}, corresponding to M_1 and M_2 and few quantities of Fe^{3+}. Moreover, the possibility to distinguish the two Fe^{2+} subspectra could be given by the series $\{Fe_{2-x}, Mn_x\}[Si]O_4$ with very small x values. The preference of iron to occupy the M_1 suggested the low-temperature origin of the assemblage.

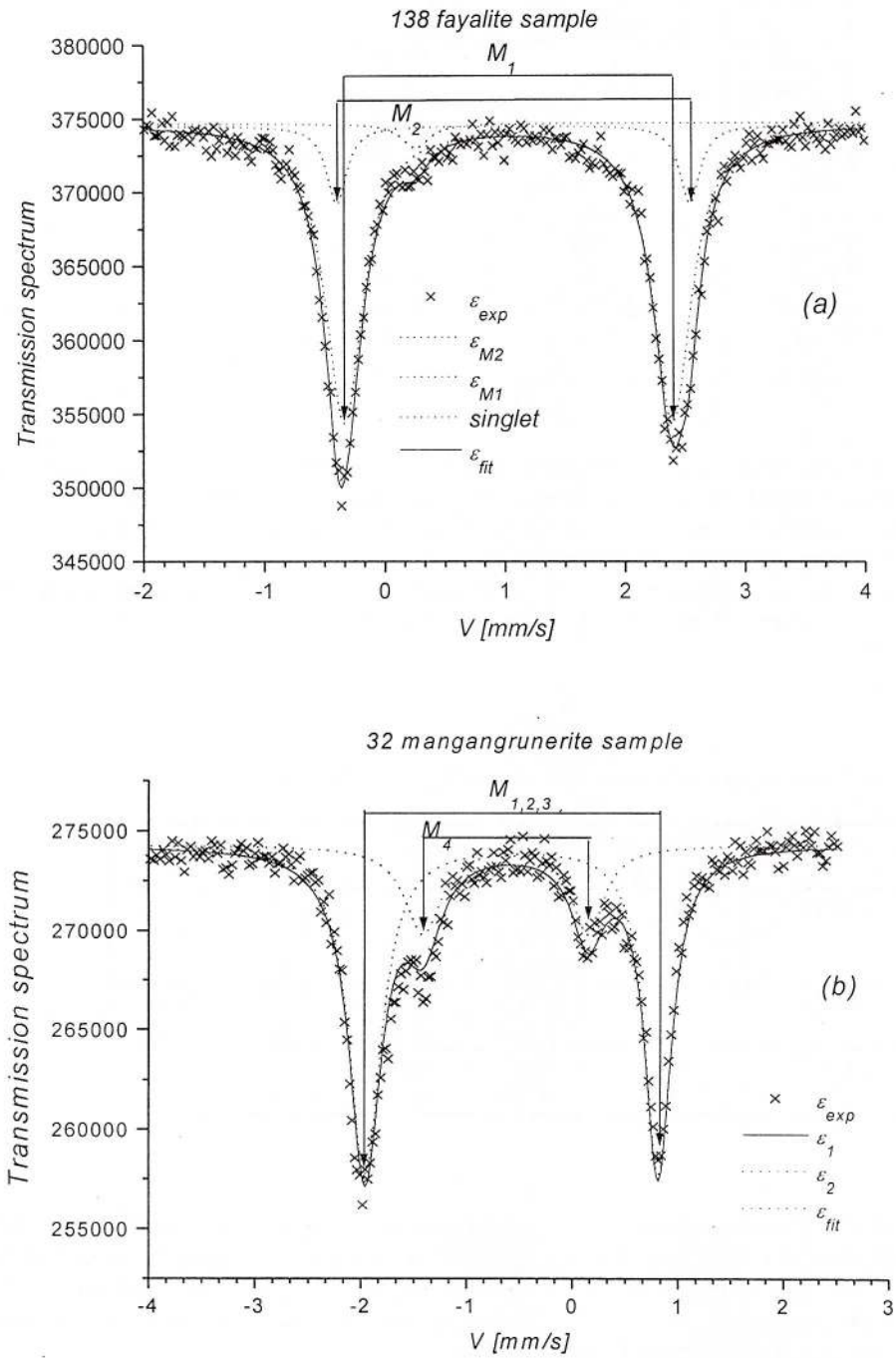

Fig. 3.2 - The spectra of 138 fayalite and of 32 mangangrunerite.

3.5. Glauconites from the Transilvanian Basin

Mössbauer investigations of Romanian glauconites include samples of Miocene age from Tihau, Salaj District. Glauconites are 2:1 sheet silicates and have the chemical formulas:

$$(K^{+}, Na^{+}, Ca^{2+})\{Mg^{2+}, Fe^{2+}, Fe^{3+}, Al^{3+}, Ti^{4+}\}_2[Si^{4+}, Al^{3+}]_4 O_{10}(OH)_2$$

The typical spectrum of a glauconite is plotted in Figure 3.3 and the values of the spectral parameters are given in Table 3.9. The spectrum evidenced the ferric and ferrous ions in the cis and trans octahedral configurations.

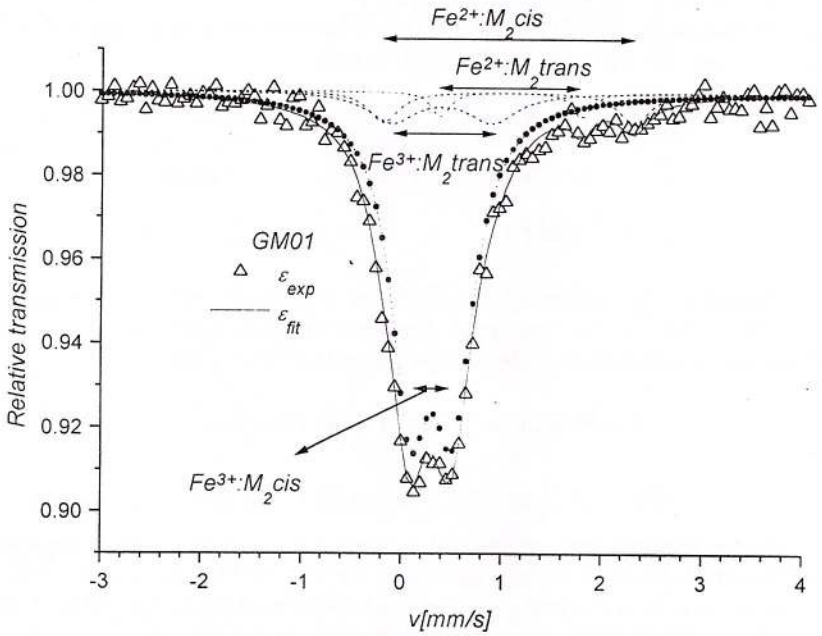

Fig. 3.3 - A typical Mössbauer spectrum of a glauconite

Table 3.9.

The values of the spectral parameters and their standard errors of the investigated glauconites

Sample	Sub-spectra	ε_{exp} [%]	δ_{CS}^{exp} [mm/s]	ΔE_q^{exp} [mm/s]	Γ [mm/s]	A^{exp}/A_{tot}^{exp} [%]	χ^2 (σ)	Assignment
GM01	I	6.9(2)	0.307(5)	0.43(2)	0.48(4)	79.6	0.993(2)	Fe^{3+}:M2(cis)
	II	0.7(4)	0.4(1)	1.04()	0.6(2)	10.5		Fe^{3+}:M1(trans)
	III	0.6(2)	1.08(3)	1.54(6)	0.22(10)	3.3		Fe^{2+}:M1(trans)
	IV	0.7(1)	1.06(4)	2.5(1)	0.4(1)	6.5		Fe^{2+}:M2(cis)
GM04	I	8.6(1)	0.296(5)	0.44(9)	0.54(1)	85.2	0.996(2)	Fe^{3+}:M2(cis)
	II	0.3(2)	0.38(8)	1.1(2)	0.22(20)	1.5		Fe^{3+}:M1(trans)
	III	0.8(1)	1.11(4)	1.7(1)	0.6(2)	8.3		Fe^{2+}:M1(trans)
	IV	0.8(1)	1.12(4)	2.7(1)	0.3(1)	5.0		Fe^{2+}:M2(cis)
GM12	I	7.7(2)	0.314(4)	0.38(1)	0.46(3)	73.7	0.995(2)	Fe^{3+}:M2(cis)
	II	1.2(3)	0.43(4)	0.95(6)	0.4(1)	10.0		Fe^{3+}:M1(trans)
	III	1.1(2)	0.9(3)	2.2(6)	0.3(1)	8.2		Fe^{2+}:M1(trans)
	IV	1.1(2)	1.1(3)	2.7(7)	0.4(1)	8.1		Fe^{2+}:M2(cis)

$\delta^{(i)}_{Fe} = \delta^{(i)}_{CS} + 0.113$mm/s

A lot of Mössbauer investigation results have been presented in many communications (Pop, 1994, 1995, 1996), but it is interesting to note the possibility to establish the geochronology of thermally undisturbed glauconites. Real crystals and in particular minerals present defects in the solid lattice. The degree of ordering in the vicinity of Mössbauer isotope is dependent on the concentration of defects. The spontaneous decrease of the number of defects arise from their migration towards the surface of the crystal. This process depends on the diffusion rate of the defects in the thermally undisturbed samples. The rate of diffusion is so slow that the ordering process around the Mössbauer isotope proceeds on the geological time scale. On the other hand the values of ΔE_Q^{exp} is a function of the number of defects which are present at a given moment in the first, second etc. coordination spheres. As a consequence a decrease of the quadrupole splitting as a function of time is expected at a rate depending on the spontaneous ordering by the diffusion mechanism. Malysheva (1975) and Danon (1977) have shown a dependence of the ferric ΔE_Q^{exp} and Γ^{exp} values of glauconites to their history (taken in 10^6 years) to exist:

$$\Delta E_Q^{exp}(t) = -0.000028t + 0.437500;$$
$$\Gamma^{exp}(t) = -0.000024t + 0.538095; \qquad (3.1.)$$
$$[t] = 10^6 \text{ years}$$

The ΔE_Q^{exp} (I) values of the glauconite spectra divide the samples in two groups. The first group of GM01, GM04 glauconites, with ΔE_Q^{exp} (I) ~ 0.43÷ 0.44 mm/s, are corresponding to the geological time 0÷500 and the second group of GM12 glauconites are corresponding to the geological time >1000.

3.6. Mössbauer study of some chlorites

The chlorites $\left\{Mg_{6-x-y}Fe_x^{2+}Al_y\right\}\left[Si_{4-x}Al_z\right]O_{10}(OH)_8$ are 2:1 layer silicates. The mineral has a structure which permits extensive isomorphic substitutions, hence it has a wide range of chemical composition. A knowledge of chemical composition of chlorites, especially the Fe/(Fe+Mg) ratio and of its influence on the distortion of iron environment and also the preference site of Mössbauer probe are particularly important in the study of phase relationships in low and medium grade metamorphic rocks and other geological assemblages. The investigated samples are representing different geological associations and are show in Table 3.10 and the Mössbauer parameters in Table 3.11.

Table 3.10.
The investigated chlorite samples

Sample	Chemical data of sample composition
A Ruschita	$\left\{Mg_{0.71}Fe_{2.53}^{2+}Mn_{0.25}^{2+}Fe_{0.61}^{3+}Al_{1.51}Ti_{0.004}^{4+}\right\}\left[Si_{2.49}Al_{1.51}\right]O_{10}(OH)_8$
B Ghelar	$\left\{Mg_{2.00}Fe_{2.19}^{2+}Mn_{0.12}^{2+}Fe_{0.54}^{3+}Al_{1.00}Ti_{0.05}^{4+}\right\}\left[Si_{2.54}Al_{1.46}\right]O_{10}(OH)_8$
C Highis Mts.	$\left\{Mg_{2.65}Fe_{1.50}^{2+}Mn_{0.03}^{2+}Fe_{0.33}^{3+}Al_{1.37}\right\}\left[Si_{2.55}Al_{1.45}\right]O_{10}(OH)_8$

Table 3.11.
The Mössbauer parameters of the investigated chlorites

Sample	Concentrations Mg	Mg/Fe	Subspectrum	Δ_{EQ}^{exp} [mm/s]	δ_{CSexp} [mm/s]	Γ^{exp} [mm/s]	Relative areas
A	0.71	0.28	I	2.66	1.05	0.35	0.5774
			II	1.96	0.92	0.56	0.2610
			III	0.48	0.03	0.68	0.1615
B	2.00	0.91	I	2.84	0.97	0.37	0.7015
			II	2.44	0.82	0.44	0.1810
			III	0.34	0.07	0.62	0.1175
C	2.65	1.75	I	2.78	0.97	0.39	0.8999
			II	0.66	0.22	0.45	0.1001

It is important to point out the results of the recent reports on chlorites (Coey, 1984).

3.7. Chemical and Mössbauer analyses of some sediment samples of the Romanian shore

The interesting investigations by Mössbauer spectroscopy in correlation to chemical data have done on the ferromanganese nodules as well as some rocks samples collected from different locations on the sea floor and respectively on shore at Constanta to 1262 m depth. The Mössbauer data of investigated samples are given in Table 3.12 (Georgescu, 1973, 1977; Barb, 1979).

Table 3.12.

Room temperature Mössbauer data of Fe-Mn nodules and rock samples of Romanian shore

Sample depth	H^{exp} [KOe]	$\Delta E_Q{}^{exp}$ [mm/s]	$\delta_{C.S}{}^{exp}$ [mm/s]	Assignment
nodule 60m	-	0.71(1)	0.30(1)	Fe^{3+}
nodule 90m	-	0.77(2)	0.61(3)	Fe^{3+}
sediment 200m	-	2.50(1)	0.85(1)	Fe^{2+}
		0.80(2)	0.70(3)	Fe^{3+}
rock 586m	517.3(3)	0.241(4)	0.128(4)	Fe_2O_3 (100%)hematite
rock 605m	492.0(3)	0.03(3)	0.01(3)	Fe_3O_4 (55.1%)
	464.0(1)	0.01(1)	0.43(2)	magnetite
	520.0(1)	0.14(2)	0.10(2)	Fe_2O_3 (23.7%) hematite
	-	2.74(2)	0.92(2)	amphiboles (21.2%)
	-	1.60(2)	0.96(2)	
rock 715m	518.0(3)	0.190(4)	0.120(4)	Fe_2O_3 (100%)hematite
rock 1262m	492.0(3)	0.05(6)	0.03(4)	Fe_3O_4 (49.5%)
	466.0(4)	0.06(4)	0.48(5)	magnetite
	520(3)	0.18(22)	0.15(23)	Fe_2O_3 (4.3%)hematite
	-	2.86(3)	0.84(2)	Amphiboles (31.2%)
	-	1.64(2)	0.86(2)	
	-	3.16(4)	0.79(3)	not identified

In the Black Sea two types of ferromanganese nodules with different degree of mineralization can be found (Barb, 1979):

a) type I- nodules with a very low degree of mineralization (~3.6% Fe_2O_3 and ~5.5% MnO_2);

b) type II- nodules with a high degree of mineralization (~26% Fe_2O_3 and ~22% MnO_2).

The spectrum of the sample 200m, belonging to the type 2, exhibits two subspectra for $Fe^{2+,3+}$. The small values of $\Delta E_Q{}^{exp}$ and $\delta_{C.S}{}^{exp}$ values prove the ferric ions to exist probably either as goethite FeOOH or $Fe_2O_3 \cdot H_2O$. The spectra of the rock samples are more complicated suggesting the presence of magnetite and hematite. One can observe amounts of amphiboles in the rocks at 615 m and 1262 m in the last one probably a member of the cummingtonite-grunerite series.

3.8. Mössbauer studies on Moci (Romania) meteorite

The spectra have been carried out for six powdered specimens in the range of high and low velocity range, at room temperature (Barb, 1982). They have shown a superposition of a lot of quadrupole doublets and magnetic sextets. The comparison of the magnetic subspectra of Moci meteorite with the Toluca meteorite, enriched in taenite, and with the Gressk one, practically consisting in only kamacite, (Malysheva, 1973) suggests the presence of these compounds. The quantities of metallic Ni have been estimated by using the following relations:

$$N = N_t + N_c = N^{Fe} + N^{Ni} = N_t^{Fe} + N_c^{Fe} + N_t^{Ni} + N_c^{Ni};$$

$$\left.\begin{aligned} A_t &\propto 2\% N_t^{Fe} = 2\% N_t \left(1 - \frac{N_t^{Ni}}{N_t}\right) \\ A_c &\propto 2\% N_c^{Fe} = 2\% N_c \left(1 - \frac{N_c^{Ni}}{N_c}\right) \end{aligned}\right\} \rightarrow N = 50 \left(\frac{A_t}{1 - \frac{N_t^{Ni}}{N_t}} + \frac{A_c}{1 - \frac{N_c^{Ni}}{N_c}} \right)$$

$$A = A_t + A_c \propto 2\% N^{Fe}$$

$$N^{Ni} = N - N^{Fe} \propto N - 50(A_c - A_t) = 50 \left(\frac{A_t \frac{N_t^{Ni}}{N_t}}{1 - \frac{N_t^{Ni}}{N_t}} + \frac{A_c \frac{N_c^{Ni}}{N_c}}{1 - \frac{N_c^{Ni}}{N_c}} \right)$$

$$\frac{N^{Ni}}{N^{Fe}} = \frac{\frac{A_t}{A} \cdot \frac{N_t^{Ni}}{N_t}}{1 - \frac{N_t^{Ni}}{N_t}} + \frac{\frac{A_c}{A} \cdot \frac{N_c^{Ni}}{N_c}}{1 - \frac{N_c^{Ni}}{N_c}} \qquad (3.2)$$

where N, N_c, N_t and A, A_c, A_t are the number of atoms and the spectral areas for the taenite, kamacite. Moreover, a magnetic phase of the troilite FeS has been detected, too. The paramagnetic phases are silicate compounds (olivines, $\{Mg,Fe\}_2\ SiO_4$, pyroxenes, $<X>\{Y\}[Si]_2O_6$ with Fe^{2+} in M_1, M_2, ilmenite, $FeTiO_3$ and cummingtonites $\{Mg,Fe\}_7[Si]_8O_{22}(OH)_2$). The spectral parameters for the indicated specimens are given in Tables 3.13.

Table 3.13a

The Mössbauer parameters of minerals from the samples of Moci meteorite at high velocity range

Specimens	ΔE_Q^{exp} [mm/s] ±0.007	δ_{Cs}^{exp} [mm/s] ±0.007	H^{exp} [KOe] ±3	a^{exp} [%] ±2	Identified mineral	Observations
A	-	0.624	308	21	troilite	stoichiometric
	-	0.174	346	14	kamacite	7at% Ni
	2.876	0.542	-	47	olivine	
	2.222	1.55	-	16	pyroxene	15%Fe:M_2
	0.837	0.384	-	6	ilmenite	
B	-	0.648	317	26	troilite	stoichiometric
	2.879	1.195	-	56	olivine	
	2.246	1.169	-	20	pyroxene	15%Fe:M_2
C	-	0.661	314	31	troilite	stoichiometric
	2.877	1.160	-	51	olivine	
	2.189	1.144	-	19	pyroxene	15%Fe:M_2
D	-	0.636	312	23	troilite	stoichiometric
	2.467	1.014	-	66	pyroxene	Fe:M_1
	1.756	0.983	-	15	Cummingtonite.	25%Fe:M_3

Table 3.13b

The Mössbauer parameters of minerals from the specimens of Moci meteorite at high and low velocity ranges

Specimens	ΔE_Q^{exp} [mm/s] ±0.007	δ_{Cs}^{exp} [mm/s] ±0.007	H^{exp} [KOe] ±3	a^{exp} [%] ±2	Identified mineral	Observations
E	-	0.525	330	8	taenite	stoichiometric
	-	0.558	314	10	troilite	stoichiometric
	-	0.151	352	5	kamacite	7at%Ni
	2.985	1.192	-	26	olivine	25%Fe:M_2
	3.089	1.209	-	9	olivine	25%Fe:M_1
	3.151	1.222	-	2	olivine	25%Fe:M_2
	2.058	1.185	-	2	pyroxene	25%Fe:M_2
	2.704	1.245	-	5	cummingtonite	Fe:$M_{1,2,3}$
	2.493	1.271	-	22	pyroxene	45%Fe:M_1
F	-	0.447	322	6	taenite	50at%Ni
	-	0.601	315	14	troilite	stoichiometric
	-	0.118	347	10	kamacite	7at%Ni
	2.950	1.174	-	26	olivine	25%Fe:M_2
	3.081	1.105	-	9	olivine	25%Fe:M_1
	3.169	1.230	-	3	olivine	Fe:M_1
	2.087	1.196	-	2	pyroxene	25%Fe:M_2
	2.677	1.267	-	6	cummingtonite	Fe:$M_{1,2,3}$
	2.267	1.284	-	36	pyroxene	45%Fe:M_1

A typical spectrum is given in Figure 3.4.

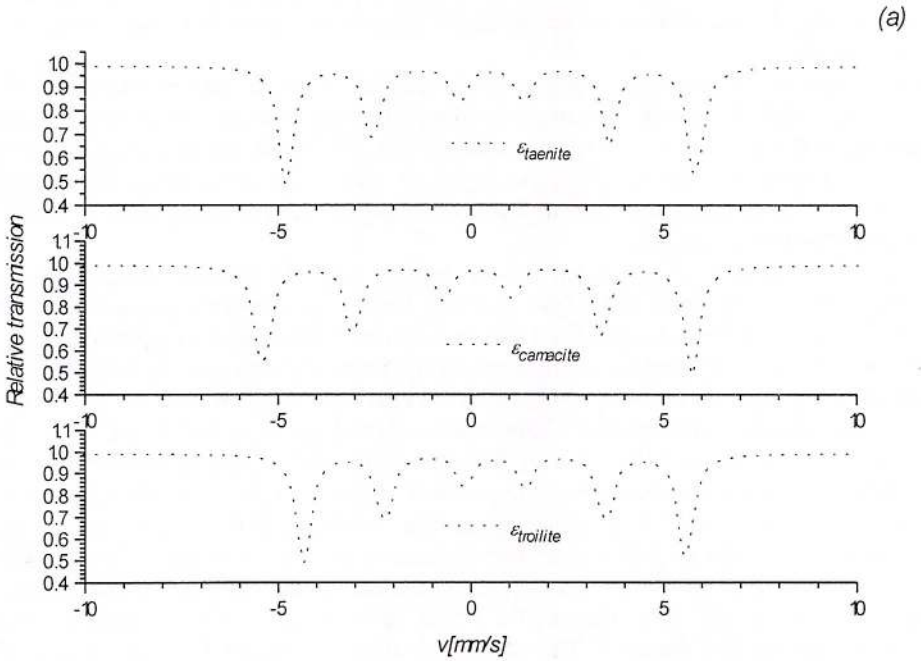

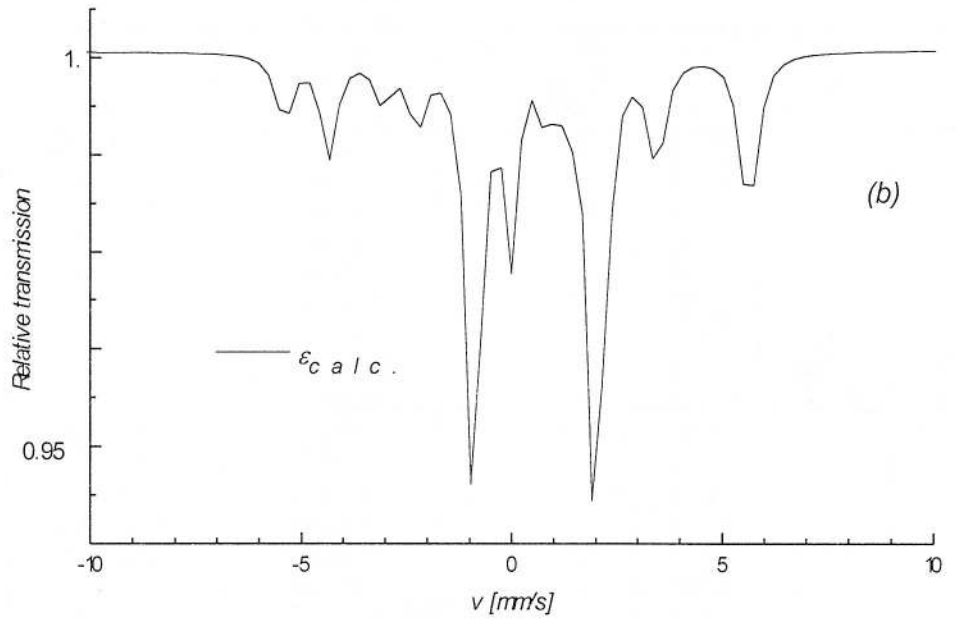

Fig. 3.4 - **(a)** The subspectra of magnetic phases for Moci meteorite; **(b)** The fitting spectrum of A specimen for Moci meteorite. The parameters are given in Table 3.13.

Conclusions

The investigations of minerals and rocks by the Mössbauer spectroscopy can be first regarded as a fingerprint technique , to help identifying the phases containing the Mössbauer isotopes in unknown mixture such as sediments, soils and mineral deposits.

The information obtained by this spectroscopy in the area of the physics and crystal chemistry of minerals are remarkable. Moreover, the Mössbauer investigations can give an unusual perspective on natural processes, associated to geochemical cycle, and on artificial transformations of minerals and their chemical compounds.

The Mössbauer spectroscopy on minerals has begun to give information about the electronic structure of inhomogeneous mixed valence compounds, about the electron hopping, relaxation phenomena, and about the filling of structural sites by Mössbauer isotopes.

The studies of magnetic order are at early stage, but the magnetic spectra , obtained at low temperature, contain much more information about the cation disorder, long range magnetic interactions in insulators, about magnetism in insulating 3d compounds, about uni and two dimensional magnetic compounds.

An important and interesting success of the minerals and rocks investigations by Mössbauer spectroscopy has been the correlation of the artificial irradiation of samples with the natural one in order to date the mineral deposits.

A fairly complete description exits now of the spectra of many minerals and rocks, especially of Fe and Sn bearing. Their interpretation includes three stages. The first stage is their decomposition into quadrupole and/or magnetic subspectra according to computer fitting procedures, which are now resonably standardized. The result of this stage is a set of δ_{CS} , ΔE_Q , ΔH, Γ, ε and a values. The main task of the second stage is the association of subspectra with the particular phases, lattice sites or environments. Sometimes this stage is not easy to do because of a strong overlapping and the departure from Lorentz line-shape of the resonance lines. Finally the third stage contains the interpretation and the correlation of the results obtained in the second stage with the chemical and physical structure of investigated minerals. The Mössbauer data should not be seen in isolation, but taken in conjunction with the data of other spectroscopies. The nuclear gamma-ray spectroscopy is not a magic wand.

The successes of Mössbauer investigations of minerals, obtained until now, claim an extension of investigations to other materials containing the Mössbauer isotopes and a correlation of spectral parameters to geological processes, to temperature-pressure conditions of geological genesis etc.

Acknowledgements

One of the authors is grateful to the financial supports from the Committee of CNR (Roma), Progetto Sistema Lagunare Veneziano, E.N.E.A in the framework of the Italian National Programme for Antarctic Researches, PNRA (Environmental Impact-Chemical Methodologies) and from the M.C.T. (Bucharest), Programme Orizont 2000 (The investigations of archeologic and geologic materials by the techniques of resonance spectroscopies).

References

Allmann, R., Donnay, G. (1971) Structural relations between pumpellyite and ardenite. *Acta.Cryst.*, B27, p. 1871-1875.

Bancroft, G. M. (1973) Quantitative site population in silicate minerals. p. 201-237.

Barb, D., Diamandescu, L., Morariu, M., Georgescu I. (1979) Mössbauer and Chemical analyses of some sediments from the Romanian shore of the Black Sea. *Journal de Physique,* 40, C2 p. 445-448.

Barb, D., Morariu, M., Diamandescu, L., Znamirovschi, V., Ciurchea, D., Motiu, A. (1982) Mössbauer studies on Moci (Romania) meteorite. *Ann. Geophys.*, 38, p. 875-879.

Coey, J. M. D. (1975) Iron in post-glacial lake sediment core; A Mössbauer effect study. *Geochim. Cosmochim. Acta,* 39, p. 401-415.

-- **(1980)** Clay minerals and their transformations studied with nuclear techniques : The contribution of Mössbauer spectroscopy. *At. Energy Rev.,* 18, p. 73-82.

-- **(1984)** Mössbauer spectroscopy of silicate minerals. In: Mössbauer Spectroscopy Applied to Inorganic Chemistry. New York, ed. Plenum Press, vol. 1, p. 443-509, Mössbauer Spectroscopy of Silicate Minerals.

Constantinescu, S., Udubasa, G., Calogero, S. (1997) Mössbauer investigation of two pumpellyites from Romania. *Rom. J. Mineralogy*, 78, p. 3-9.

-- , **Udubasa, G., Calogero, S. (1997)** Numerical calculations of the electric field gradient tensor and the Mössbauer Parameters of the distorted iron octahedra in pumpellyite crystalline structure. *Rom. J. Physics*, 42, p. 5-6, 359-369.

-- , **Calogero, S. (1997)** Program of ^{57}Fe Mössbauer quadrupole splitting parameters evaluation. *QCMP 172*, QCPE Bull. vol. 17, no.1, p. 1-3.

-- , **Udubasa, G., Calogero, S. (1997)** ^{57}Fe Mössbauer spectroscopy on two romanian Carpathian Pumpellyites. *J. Phys.*, I 7, p. 777-784.

Danon, J., Scorzelli, R., B., Pollak, H. (1977) Mössbauer spectroscopy of thermal and radiation effects in iron minerals and its applications to geochronology. Procedings of International Conference on Mössbauer Spectroscopy, 5-10 September, 1977, Bucharest, Romania, vol. 2, p. 218-228.

De Grave, E., Van Alboom, A. (1991) Evaluation of ferrous and ferric Mössbauer fractions. *Phys. Chem. Minerals*, 18, p. 337-342.

Galli, E., Alberti, A. (1969) On the crystal structure of pumpellyite. *Acta. Cryst.*, **B25**, p. 2276-2281.

Gottardi, G. (1965) Die Kristallstructur von Pumpellyite. *Tschermaks Min. Petr. Mitt.*, 3, 10, p. 115-119.

Georgescu, I., Morariu, M., Diamandescu, L. (1973) Contributions to the study of the Fe-Mn nodules from the Black-Sea by Mössbauer spectroscopy. *Rev. Roum. Phys.*, 18, p. 401-409.

-- , **Barb, D., Diamandescu, L., Morariu, M., Demetresu, M., (1977)** Chemical and Mössbauer analyses of some sediments of Romanian shore., *Thalassia Jugoslavica*, 13, p. 161.

Ionescu, J., Filotti, G., Gomolea, V. (1971) Mössbauer spectra for some pyroxenes of the diopside-hedenbergite-johansenite series. *Rev. roum. geol., geophys., geogr. (Geologie)*, 15, 1, p. 67-70.

Malysheva, T. V., Shagerev, V. D., Yermakov, A. N. (1973) Kamacite and taenite ratio in the iron meteorite Santa Catharina. *Proc. Int. Conf. Mössbauer Effect Appl.*, 3-7 September, Bratislava, 2, p. 385-388.

Pop, D., Bedelean, I., Constantinescu, S. (1994) Mössbauer analyses of glauconites from Transilvanian basin. *Anal. Univ. Bucuresti, sect. Geologie*, Supl., XLIII, p. 23-24.

-- , **Hosu, A., Daraban, I., Constantinescu, S. (1995)** Mineralogical characterization of the green clay from Rona limestone. *Rom. J. Mineralogy*, 77, Supl. I, p. 36, Abstract Volume of the 3rd Symposium on Mineralogy. Baia-Mare 25-29 August 1995.

-- , **Constantinescu, S. (1995)** Mineralogenetic assumptions based on Mössbauer spectroscopy: the case of glauconites. Abstract-Book of Symposium on Petrometallogeny, Cluj-Napoca, 21-23 August 1995, p. 100.

-- , **Weiszburg, T. G., Kuzman, E., Klencsar, Z., Constantinescu, S. (1996)** Cation exchange in glauconites from Romania. The 6th European Meeting of Petrology, Bayreuth, 9-13 Apr. 1996.

Shanon, R. D., Prewitt, C. T. (1969) Effective ionic radii in oxides and fluorides. *Acta. Cryst.* , B25, p. 925-940.

Spanu, V., Filoti, G., Ionescu, J., Medesan, A. (1977) Mössbauer study of some chlorites. Procedings of International Conference on Mössbauer Spectroscopy, 5-10 September, 1977, Bucharest, Romania, vol. 1, p. 323-324.

Udubasa, G., Wagner, F., Friedl, J. (1993) Nagyagite: Some features of its composition and Mössbauer spectra. *Rom. J. Mineralogy*, 76, Suppl. 1, p. 50-52, Bucuresti.

Rom. J. Mineralogy, 79, p. 85-90, Bucureşti, 1999

BANNISTERITE IN THE TOLOVANU Mn ORE DEPOSIT, BISTRIŢA MOUNTAINS. THE FIRST OCCURRENCE IN ROMANIA

Paulina HARTOPANU, Corina CRISTEA, Gabriela STELEA, Doina NECŞULESCU

Institutul Geologic al României. Str. Caransebeş nr. 1, 78344 Bucureşti

Key words: Bannisterite. Mn carbonate-silicate metamorphosed ore. X-ray, IR, chemical analyses. Hydrothermalism.

Abstract: Bannisterite has been found in the carbonate-silicate metamorphosed ore in the Tolovanu mine, in the Bistriţa Mountains. It forms centimetric veins almost monominerals being associated with very small amounts of quartz. Small, microscopic amounts of bannisterite are found in association with alkali pyroxene, yellow alkali amphibole, nambulite, alkali feldspar and quartz. The physical and optical properties of bannisterite, the X-ray diffractogram, the infrared spectrum and the chemistry differentiate it from the manganiferous stilpnomelane and from the ganophyllite, a mineral with which it could have been mistaken. The bannisterite genesis is hydrothermal metamorphic.

Introduction

Bannisterite has been found for the first time in the Franklin mine, New Jersey, and described as a new mineral species related to the ganophyllite and the stilpnomelane group (Smith, Frondel, 1968). Bannisterite in the Franklin mine is closely associated with baryte and calcite. It also occurs in association with: rhodonite, sphalerite, quartz, zinc amphibole, manganoan calcite and different silicates, manganese hydrates as well as bementite, caryopylite, etc. Plimer (1977) described bannisterite with a relatively high-Fe content, at Broken-Hill, New South Wales, Australia. The Australian bannisterite is found in association with: rhodonite, quartz, sphalerite, flourine, galena and apophyllite. Dunn et al. (1981) reexamined the chemical composition of bannisterite at Broken-Hill and Franklin using an electronic microprobe. On this basis it has been established that Ca plays a significant role in the composition of bannisterite; Mg and Zn are not significant for bannisterite structure; manganese is the prevailing cation; Al and (Na + K) are significant constituents of bannisterite; Fe^{+3} can substitute the bivalent cations, Al either plays an unclear role or it is still unknown. It is worth mentioning, as a general characteristic, the remarkable constance of the chemical composition of the bannisterite at Franklin and Broken-Hill. The contradictions between the predicted Al amount and that determined analytically, as well as the uncertainness concerning the role of Fe^{+3} and the possibilities of the H_2O/K substitutions determined the above-mentioned authors to state that the finesse details of the bannisterite structure remain unsolved. Bannisterite has also been found in ore deposits of volcanic affiliation in Japan (Watanabe et al., 1970).

In Romania bannisterite has been found in the carbonate-silicate metamorphosed ore in the Tolovanu mine, in the Bistriţa Mountains. The ore deposit is situated in the Tg_2 formation, mainly constituted of black quartzites in the Putna Nappe, that belongs to the crystalline-Mesozoic unit of the West Carpathians.

Physical and chemical properties

Bannisterite in the Tolovanu mine has a leafy, lamellar habitus similar to the micas. The lamellas have sizes of 1–2 cm and a glossy black colour in sample. Under the microscope the colour is brown-red after Ng and colourless yellow after Np, showing an obvious pleochroism. It displays two distinct cleavages (Pl., Figs. 1, 2) which clearly differentiate it from the micas group with which it can be optically mistaken. Bannisterite is biax negative with $2V = 0\text{-}5^0$, whereas the manganoan stilpnomelane in the Tolovanu mine has the angle of the optical axes larger than 20^0.

Table 1
X-ray powder diffraction data

sample no. BT 337		bannisterite JCPDS 21-57			ganophyllite JCPDS 17-467		
d (A)	I/I_1	d (A)	I/I_1	h k l	d (A)	I/I_1	h k l
12.22	100	12.3	100	002	12.2	100	002
		11.5	2	111			
		8.78	2	21-1	8.58	6	20-2
		8.43	2	211			
		7.95	2	202			
		7.11	4	11-3	7.09	6	11-3
		6.82	4	113	6.79	2	113
6.15	3	6.16	2	004			
		5.56	6	20-4	5.55	6	20-4
		5.20	6	40-2	5.20	16	131
4.58	5	4.59	10	22-4	4.59	20	22-4
4.25	5	4.28	6	413	4.28	10	23-3
		4.21	2	32-4			
4.099	20	4.09	16	006 040	4.07	25	006 040
3.80	4	3.79	8	333	3.78	20	333
3.56	5	3.57	6	340	3.56	10	135
3.43	20	3.44	20	-117	3.43	35	306 11-7
3.36	9	3.36	10	117	3.36	16	
		3.24	2	051			
		3.21	2	217	3.21	6	
3.074	26	3.08	12	008	3.07	30	
2.963	6	2.97	4		2.960	6	
2.795	5	2.79	8		2.789	16	
2.753	6	2.75	8		2.743	16	
2.637	15	2.64	16		2.637	50	
2.606	10	2.61	12		2.599	20	
		2.48	2		2.471	10	
2.455	6	2.46	2				
2.407	8	2.41	10		2.407	20	

Table 2
Lattice parameters (monoclinic cell)

sample no. BT 337	bannisterite JCPDS	ganophyllite JCPDS
a=22.00 Å	a=22.20 Å	a=22.24 Å
b=16.37 Å	b=16.32 Å	b=16.43 Å
c=24.67 Å	c=24.70 Å	c=24.50 Å
β=94°6′	β=94°20′	β=95°

Mineral associations of bannisterite

Bannisterite occurs in two distinct associations: (a) with little quartz and very little rhodochrosite, when it forms almost monomineral veinlets, which penetrate the tephroite or pyroxmangite ore, and (b) in association with the "alkali" paragenesis when it occurs in very small amounts, visible only under the microscope. The "alkali" paragenesis or "oxidised" paragenesis consists of alkali pyroxene of aegyrine type, yellow alkali amphibole, nambulite, alkali feldspar, quartz. In case of the last association, of oxidised medium, with high fugacity of the oxygen, bannisterite is not stable. It seems that conditions of a reduced medium, with reduced fugacities of the oxygen, as is the case of the first associations, are more favourable. In this case bannisterite intersects the manganoan ore of tephroite or pyroxmangite type, an ore characterized by reduced conditions of the environment.

X-ray analysis of bannisterite

The X-ray data obtained on the bannisterite powder at Tolovanu differ much from the manganoan stilpnomelane, with which it has been mistaken up till now. As shown in Table 1, bannisterite differs from ganophyllite, to which it is closest considering the d(A) and I/I_1 values. Bannisterite is monoclinic; the values of the primary cell are rendered in table 2 which presents a comparison with the values of the ganophyllite and bannisterite JCPDS. As shown in the two tables sample BT 337 is much closer to bannisterite than to ganophyllite .

IR data

IR spectrum has been obtained by the irradiation of a sample with a common technique (2 mg sample/800 mg KBr) using a SPECORD M 80 absorption spectometer with double fascicle and a monocromator with a diffraction network. The measured interval ranges between 3800-300 and 1200-3000 cm^{-1}. The sample was slightly impure, showing small amounts of quartz and rhodochrosite, marked with Q and R, respectively. The characteristic absorption bands for bannisterite are 3630, 3500, 3420, 1055, 1010, 960, 650, 560, 510, 445, 340 cm^{-1}. The bands 1090, 695, 464 are cummulated with the quartz ones. In the Figure the bannisterite bands are those marked with numbers, with R are the rhodochrosite bands and with Q are the quartz bands. For comparison, the stilpnomelane spectrum was taken as reference, as they are very alike, because bannisterite is a rare mineral, recently found, and has no IR spectrum until now. Plimer (1977) presented the IR spectrum of bannisterite at Broken-Hill but he did not give its image. This spectrum is characterised by a large width but with a low absorption in the area 3.500–2.200, generally indicating H_2O (loosely bonded) and OH. The peaks of intense absorption are at 1050–990 cm^{-1} and 470–400 cm^{-1}, representing the Si-O distance and the Si-O-Si bending, respectively. These peaks are quite similar to those of the bannisterite at Tolovanu.

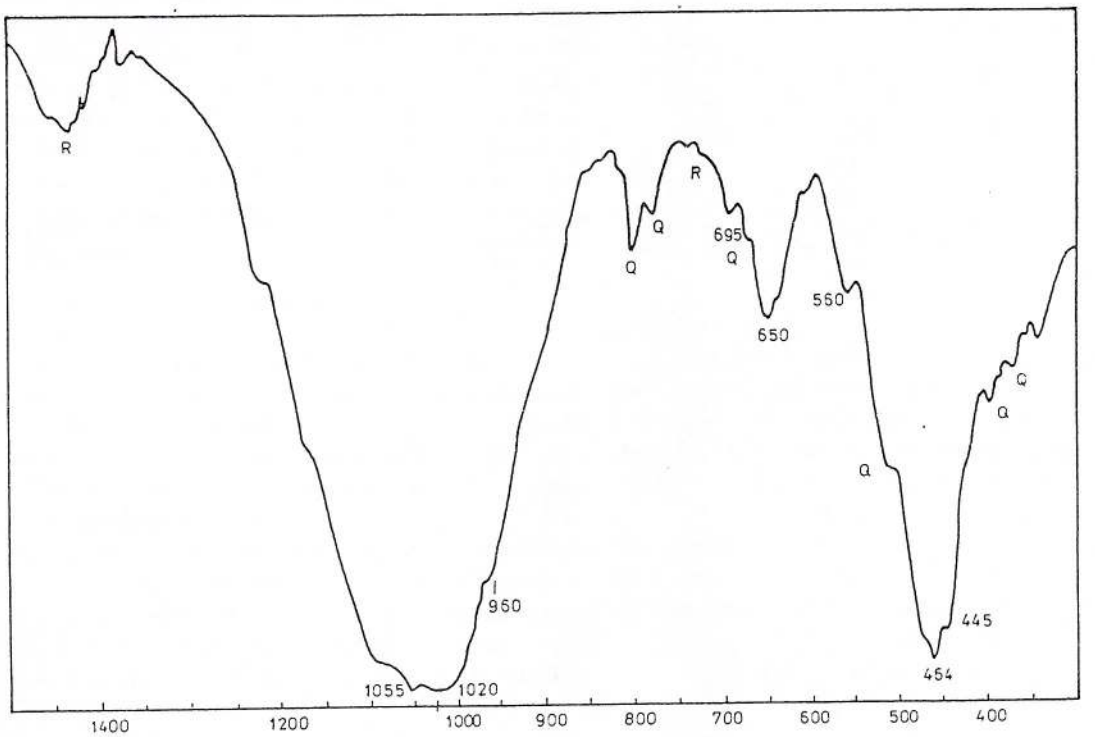

Chemical composition of bannisterite

Bannisterite crystals have been broken up to sizes of 1 cm and the cleanest grains have been selected under the binocular microscope. The chemical analysis has been effectuated using the classical method, the result being presented in Table 3. The chemical compositions of the bannisterite at Tolovanu are presented in comparison with those of the bannisterite at Franklin and Broken-Hill. A similarity between the two types of bannisterite is observed especially as regards the Fe_2O_3 content. The content in this oxide of the bannisterite at Franklin is quite low. The relatively high Fe_2O_3 content of the Romanian bannisterite could explain its presence in the "oxidised" associations rich in this oxide, such as manganoan aegirine pyroxene, manganoan magnesioriebeckite, yellow alkali amphiboles, hematite, hausmannite; "oxidised associations" specific to zones in the ore with a high oxygen fugacity. In Table 4 two chemical profiles of bannisterite from Căprăria deposit can be seen.

Table 3

Chemical composition of the bannisterite at Tolovanu Franklin and Broken-Hill

Oxides	Tolovanu	Broken-Hill	Franklin
SiO_2	47.25	45.4	46.3
TiO_2	0.11	-	-
Al_2O_3	3.46	3.84	4.2
Fe_2O_3	3.95	2.1	1.44
FeO	11.34	16.5	5.67
MgO	1.58	0.47	3.1
CaO	1.62	1.55	1.3
MnO	18.91	19.9	23.4
ZnO	0.03	0.0	4.6
K_2O	0.94	0.92	1.04
Na_2O	0.04	0.51	0.09
H_2O^+	6.53	4.00	5.00
H_2O^-	2.91	3.82	4.3
Total	98.73	99.00	100.4

From the chemical point of view, bannisterite belongs to a phyllosilicate group which forms solid solutions, whose terms have the following formulas: bannisterite: $KCa(Mn, Fe^{2+} Zn, Mg)_{21} (Si, Al)_{32} O_{46} (OH)_{16}.12 H_2O$; ganophyllite: $(K,Na)_2 (Mn,Al,Mg)_8 (Si,Al)_{12}O_{29} (OH)_{7.8-9}H_2O$; eggletonite: $(K,Na,Ca)_2 (Mn,Fe)_8(Si,Al)_{12}O_{29}(OH)_7.11H_2O$.

The empiric formula calculated from the chemical composition for bannisterite at Tolovanu, in basis 104 atoms (0.04) is, as follows $Ca_{1.14}(K_{1.19}Na_{0.01})\Sigma_{1.2}(Mn_{10.6}Fe^{+2}_{6.25}Mg_{1.55}Fe^{+3}_{1.91})\Sigma_{20.31}(Si_{31.33}Al_{2.62}\Sigma_{33.95}O_{80}(OH)_{28}.12H_2O$.

The place of bannisterite in the evolution of the manganese ore and genetic considerations

The manganese ore in the Tolovanu ore deposit evolved during three major stages: (1) the metamorphic stage, the most important one, during which the proper metamorphic ore was formed, characterized by the following association: ferriferous rhodochrosite, ferriferous tephroite, pyroxmangite, rhodonite, mangangrunerite, spessartine; (2) the metasomatosis stage, poorly represented but quite varied: Na metasomatosis (alkali pyroxene of aegirine type, yellow alkali amphiboles etc.), Li metasomatosis (nambulite formed by the substitution of Ca by Li from the rhodonite network), F metasomatosis (formation of manganoan humites at the expence of tephroite), Cl metasomatosis (formation of the minerals from the pyrosmalite group by the substitution of tephroite or rhodonite), Fe^{+3} metasomatosis (spessartine-andraite etc.) etc.; (3) the vein and hydrothermal-type stage, during which minerals such as manganoan stilpnomelane, benmentite, neotocite, baryte, hubnerite etc. were formed. Bannisterite belongs to this stage. The hydrothermalism process is not of magmatic affiliation as no magmatic bodies to which it could be related are known. In other manganese ore deposits in the world, such as in Japon, bannisterite has a certain hydrothermal origin (Watanabe et al., 1970). Plimer (1977) considered that bannisterite at Broken-Hill is the result of a retrograde metamorphism over a prograde phase, in granulitic facies, constituted of rhodonite, bustamite, pyroxmangite, hedenbergite, johannsenite, tephroite, spessartine and aboundant sulfides, such as galena, sphalerite, pyrrhotine etc. The manganese minerals formed as a result of the retrograde metamorphism in the Broken-Hill ore deposits are limited to small faults, shearing zones and transversal veinlets. In these zones beside bannisterite, pyrosmalite, inesite, sturtite, alabandine, rhodochrosite, mangangrunerite, apophyllite, Mn-calcite, kutnohorite are also found.

Conclusions

The manganese ore deposit at Tolovanu presents some mineralogical similarities with the two metamorphosed ore deposits within which bannisterite occurs: Broken-Hill and Franklin. It is also mineralogic ally related to some manganese ore deposits in Japan, including bannisterite, which are considered of magmatic affiliation. The X-ray data show that the mineral studied in this paper is bannisterite: not stilpnomelane, a mineral with which it has been mistaken up to now. The high-Fe chemical composition differentiates it from the bannisterite at Franklin, which

Table 4

Chemical profiles of bannisterite from Căprărie deposit

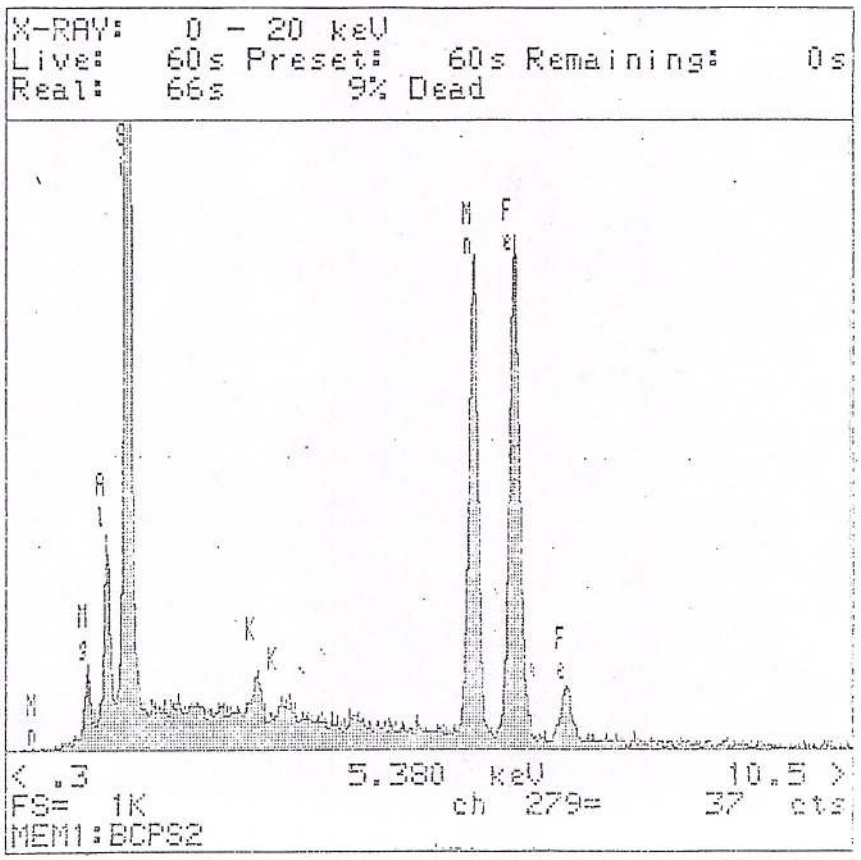

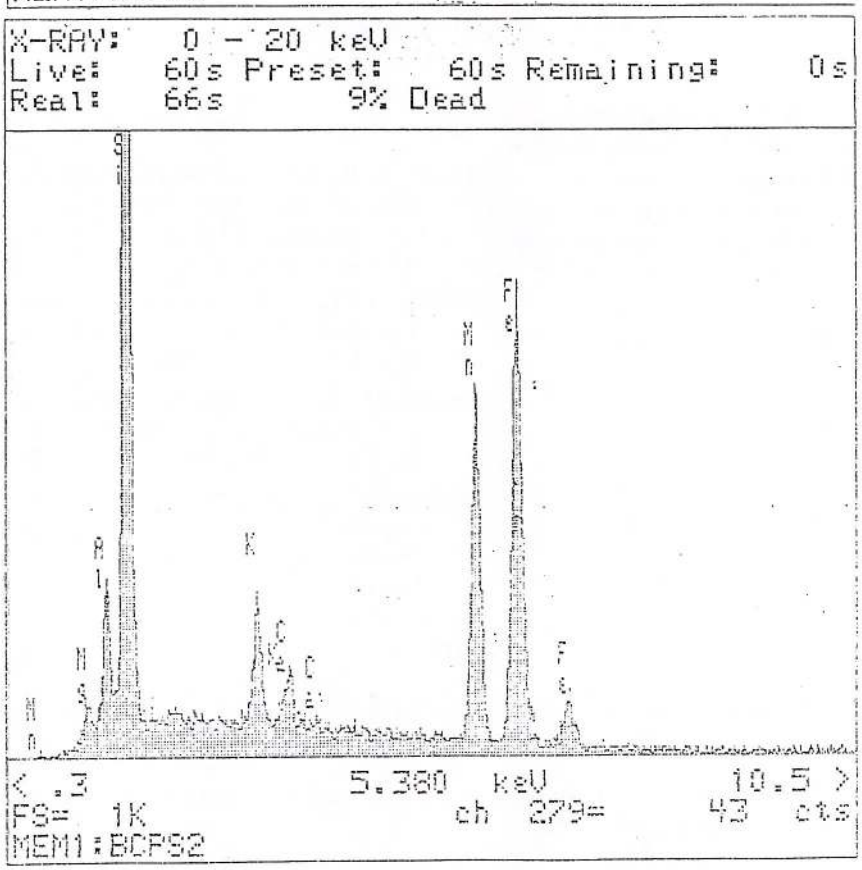

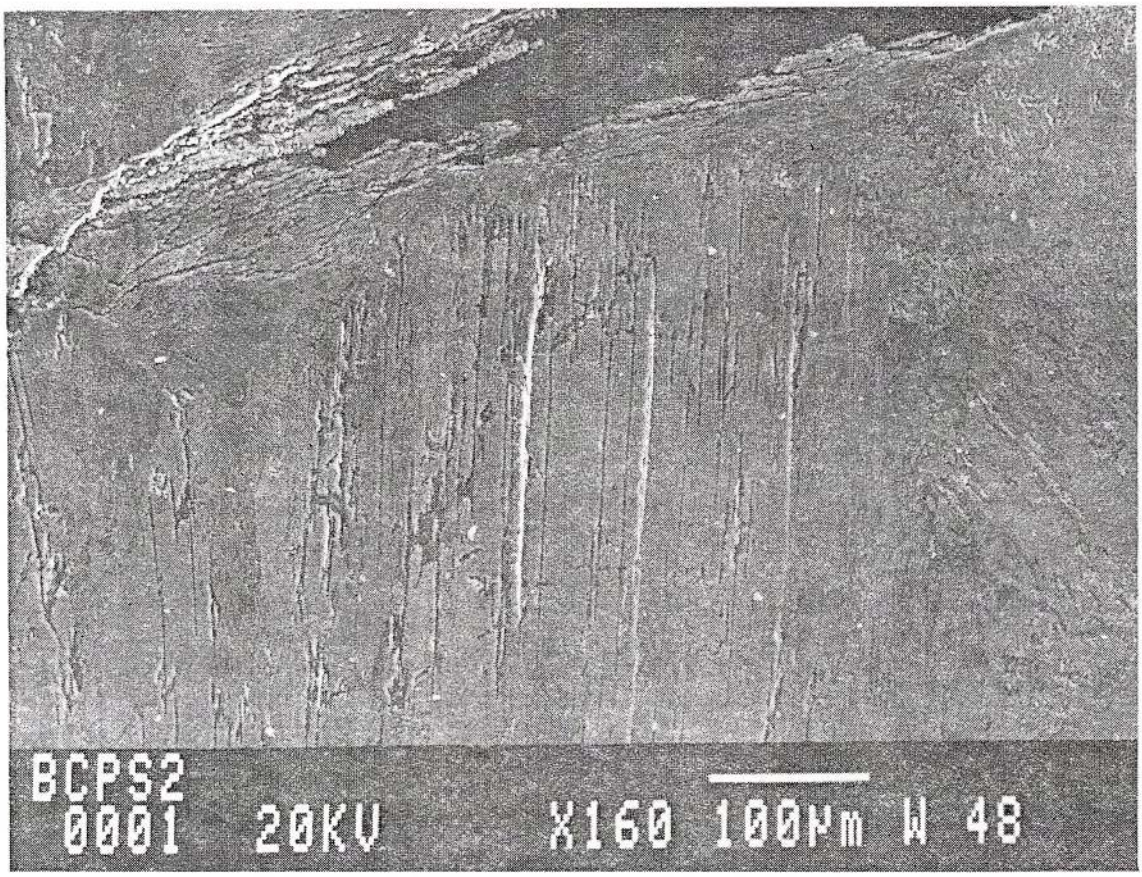

Electronic microscopical view of the bannisterite

presents a low-Fe content. It shows many similarities with the bannisterite at Broken-Hill, particularly as regards the FeO and MnO contents. Their variation is explained by the fact that bannisterite is a solid solution which varies from high-manganese species to high-iron species.

Received: January, 1998
Accepted: June, 1998

References

Dunn, J. P., Leavens, B. P., Norberg, A. J., Ramik, A. R. (1981) Bannisterite: new chemical data and empirical formulae. *American Mineralogist*, 66, p. 1063–1067.

Plimer, I. R. (1977) Bannisterite from Broken-Hill, Australia. *Neues Jahrbuch für Mineralogie Monatschefte*, p. 504–508.

Smith, M. L., Frondel, C. (1968) The related minerals ganophillite, bannisterite and stilpnomelane. *Mineralogical Magazine*, 36, p. 893–913.

Watanabe, T., Yui, S., Kato, A. (1970) Mineral deposits of volcanic affinity in volcanism and ore genesis. University of Tokio Press, 448 p., p. 128–130.

Plate

Fig. 1 – Bannisterite crystal (centre) with two cleavages on (101) and (100) pyroxmangite (high refringence, on the right) and quartz (white, on the left). Sample BT337 Tolovanu deposit, N+, x 15.

Fig. 2 – A cluster of bannisterite crystals (white) in pyroxmangite ore (grey and black high refringence). Sample BT337 Tolovanu deposit, N+, x 15.

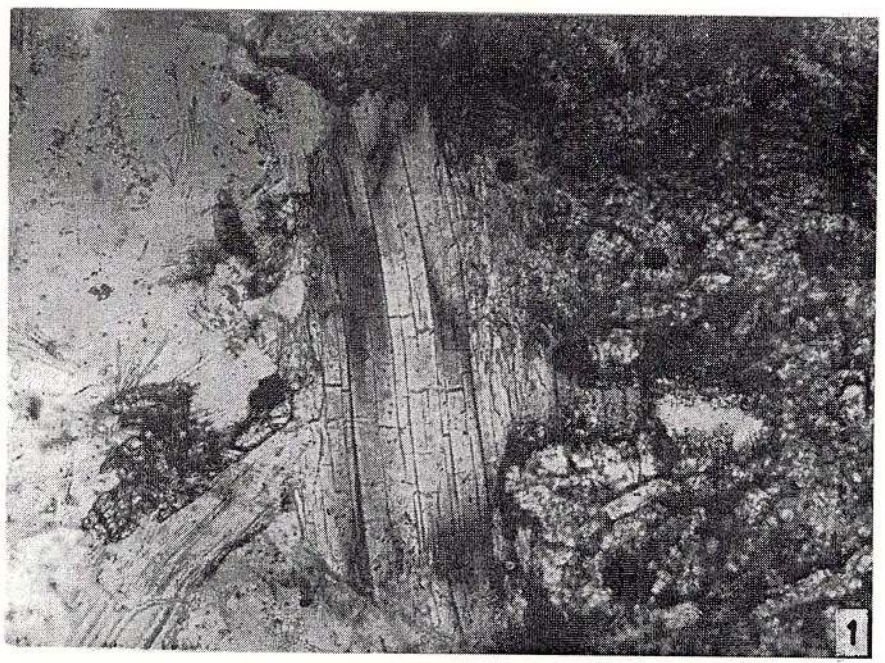

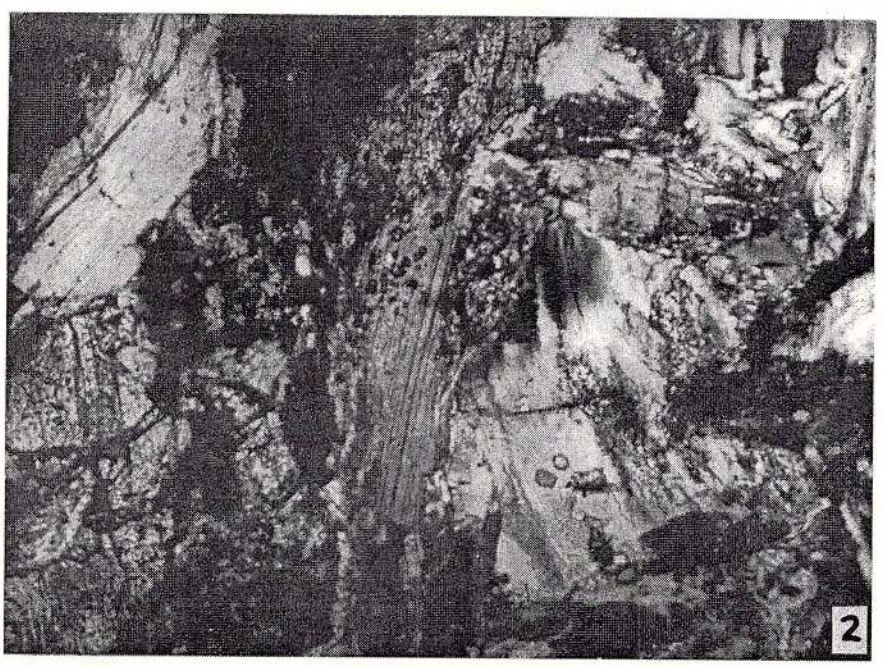

Rom. J. Mineralogy, 79, p. 91-95, Bucureşti, 1999

MANGANPYROSMALITE IN THE MANGANESE DEPOSITS OF THE BISTRIŢA MOUNTAINS: THE FIRST OCCURRENCE IN ROMANIA

Paulina HARTOPANU, Corina CRISTEA

Institutul Geologic al României. Str. Caransebeş nr. 1, 78344 Bucureşti

Key words: Manganpyrosmalite. Pyrosmalite. Tephroite ore. Chlorine metasomatosis. X-ray study. Isochemical metamorphism.

Abstract: Manganpyrosmalite occurs in the Mn metamorphosed ore in the Dadu, Oiţa, Colacu, Tolovanu, Argestru and Dealul Rusului ore deposits in the form of veinlets and nests. It is found as millimetric grains of a green-yellowish or brown-yellowish colour. The X-ray study has indicated the following cell parameters: a = 13.354Å; c = 7.169Å; V = 1107Å^3. The chemical composition of manganpyrosmalite is (%): SiO_2 = 33.13; MnO = 40.12; FeO = 10.77; MgO = 0.92; H_2O = 8.40; Cl = 5.00. The manganpyrosmalite aggregates in the manganese ore have formed by substitution of the ferriferous tephroite by solutions rich in chlorine. The source of chlorine is most likely in the initially metamorphic sediments of lagoonal-type. Thus, the presence of Na in some minerals of the manganese ore can be explained.

Introduction

Manganpyrosmalite is a mineral species relatively recently discovered, being isostructural with pyrosmalite. Pyrosmalite and friedelite recognized since the beginning of the 19th century constitute, beside shallerite, a group of phylosilicates with the formula: $(Mn^{2+}, Fe^{2+})6\ (Si_{12}\ O_{30})\ (OH, Cl)_{20}$ (Frondel, Bauer, 1953), within which pyrosmalite is the iron-rich term and friedelite is the manganese-rich term, both minerals being, therefore, the extreme terms of a solid solution. Shallerite is a variety of this group which contains As^{3+} that replaces Si^{4+}. The existence of several terms, that constitute independent minerals, of the pyrosmalite-type structure suggests the presence within this group of minerals of a polytypical series that might be similar to those between micas.

Manganpyrosmalite has been described at Sterling Hill, New Jersey, as veinlets within the franklinite ore, in association with friedelite, bementite and willemite (Frondel, Bauer, 1953). In the Broken-Hill ore deposit in New South Wales (Australia), manganpyrosmalite occurs in association with johannsenite and bustamite (Hutton, 1955). Manganpyrosmalite has also been found in some manganese mines in Japan, situated in the contact aureoles of granitic bodies (Yoshimura, 1967), where it occurs in association with rhodonite, spessartine, knebelite, dannemorite and some sulphides. Minerals of the pyrosmalite group have also been found in the Precambrian metamorphosed sulphides in Canada, which form mining fields: Matagami, Quebec (Zn-Cu-Ag-Au), Manitouwadge, Ontario (Cu-Zn-Ag-Au) and Thompson Nickel Belt, Manitoba (Ni-Au- PGE). The manganpyrosmalite occurrence in the Bistriţa Mts constitutes the fourth occurrence of this mineral, related to the metamorphic manganese ore. It is found in the Dadu, Oiţa-Colacu, Tolovanu, Argestru and Dealul Rusului ore deposits. First discovered under the microscope, manganpyrosmalite proved to be more widespread. The frequent yellow colour of the mineral ores occurring in the Bistriţa Mts is due to the preponderant presence of the minerals of the pyrosmalite group.

Occurrence

Manganpyrosmalite is found in the ore deposits in the Bistriţa Mts in the silicate-type ore and less in the carbonate-type one. In the tephroite, pyroxmangite and rhodonite ore, manganpyrosmalite forms almost monomineral centimetric veinlets (Tolovanu mine, Oiţa-Colacu), whereas in the carbonate ore it develops as relatively large crystals, with a porphyroblastic aspect, statically grown (mina Dadu) (Pl. I, Fig. 3).

The manganpyrosmalite grains have sizes up to

0.5 cm (in diameter) and a perfectly basal cleavage. The cleavage surfaces are bent, especially in case of the vein manganpyrosmalite, so that the mineral aggregates display a schistous structure (Pl. I, Figs. 1, 2). It is likely that the mineral developed in a compulsory space. The crystals are translucid, of a brown-yellowish colour, slightly greenish macroscopically and slightly yellowish-orange under the microscope. They have a slight paleochroism, from colourless to yellow, slightly orange. The birefringence is slightly lower than in case of micas and the extinction is undulatory. Optically, it is uniax negative. They resemble the micas but differ from them by lower friability and hardness.

Structure. X-ray Study

Based on the X-ray study, Frondel and Bauer (1953) pointed out the existence of the polymorphous relationships between the minerals of this group. Thus, they mentioned that the parameter a of the elementary cell is identical for these minerals, whereas the value of parameter c is always a multiple (Tab. 1).

Shallerite is a variant with two hexagonal layers, and friedelite is a variant of the structure with three rhombohedral layers, in comparison with the basal structure formed of only one layer of pyrosmalite-type hexagons. The basal configuration of the $(Si_6O_{15})^{6-}$ phylosilicates has been described by Takeuchi et al. (1969) who determined the manganopyrosmalite structure from the Kyurazawa mine, Japan. According to the researches carried out by Japanese researchers, the manganpyrosmalite structure consists of brucite-type octahedral layers in alternation with Si_6O_{15} -type tetrahedral layers. The tetrahedral layers are represented by rings formed of 6 tetrahedra with two different orientations: the oxigen atoms in the apical part of the tetrahedra rings are oriented and are connected by Mn atoms to the lower octahedral layer, whereas the tetrahedra ones with another orientation have the apical oxigen atoms connected by Mn atoms to the upper octahedral layer. The rings formed of six tetrahedra are connected together forming rings of 12 tetrahedra and rings of 4 tetrahedra, completing the planary continuity of the structure. The chlorine is preferentially located in positions occupied by (OH).

Table 1

The comparative sizes of cell parameters of -Cl, -As Mn-phyllosilicates

	a_0	c_0	Lattice type	Z
Manganpyrosmalite	13.36 A	7.16	Hexagonal	2
Pyrosmalite	13.35	7.15		
Shallerite	13.43	14.31	Hexagonal	4
Friedelite	13.40	21.43	Rhombohedral	6
Mnpy Bistriţa	13.35	7.16	Hexagonal	2

Table 2

X-ray powder diffraction data for manganpyrosmalite, sample no.BOm719

d(Å)	h k l	I/I1
7.14	001	100
6.1	101	10
3.74	211	10
3.59	002	90
3.43	102	85
2.680	401	30
2.392	003	12
2.249	402,113	16
1.843	403	15
1.670	440	10
1.523	404	10

Lattice parameters (hexagonal system):
$a_0 = 13.35$ Å $c_0 = 7.17$ Å
Analytical conditions: DRON-3 diffractometer
Radiation: Cu K α, $\lambda = 1.5418$ Å
Parameters refined by personal least-squares computer program.

Chemical Composition of Manganpyrosmalite

The chemical composition of manganopyrosmalite in the manganese ore of the Oiţa-Colacu ore deposits has been determined using the classic method for the main oxides, and chlorine has been determined by electronic microscopy in the laboratory of Cambone School of Mines in Cornwall, England. Table 3 presents the chemical composition of manganpyrosmalite in the Bistriţa Mts (A) in comparison with that of the pyrosmalite at Sterling Hill, New Jersey (Frondel, Bauer, 1953) (B) and with that at Broken-Hill, New South Walles, Australia (Hutton, 1955) (C).

Two chemical profiles of manganpyrosmalite from Dadu and Mândrileni Mn-deposits shown in the Table 4. The content of the manganpyrosmalite from Dadu (sample BDS 12A) is high, its value is arround 10% WT.

Table 3

Chemical composition of manganpyrosmalite

Oxides	A	B	C
MnO	40.12	39.09	43.44
FeO	10.77	12.43	7.65
MgO	0.92	0.74	0.89
SiO_2	35.13	34.13	34.29
Cl	5.00	3.8	undetermined
H_2O	8.40	8.18	undetermined

A - pyrosmalite from Bistriţa Mts
B - pyrosmalite from Sterle Hill (N.J.)
C - pyrosmalite from Broken Hill (N.S. Walles)

Manganpyrosmalite Genesis

Minerals of the pyrosmalite group have been found in the Fe-Mn and massive sulphides metamorphic deposits. The prograde metamorphic origin of ferropyrosmalite has been established by Vaughan (1986) for the Pegmont deposits (Australia). The manganpyrosmalite in the Geco mine (Ontario) and in the Mattagame Lake mine (Quebec) is the result of a regional metamorphism (Pan, Fleet, 1992). In the geological literature, most of the manganpyrosmalite examples are considered of a metasomatic origin, of anhydrous silicate replacement or formation of veinlets that intersect the older ore, thus emphasizing a hydrothermal origin, belonging to a late phase. Pyroxene (ferrosilite, Mn-hedenbergite, johannsenite etc.) is the most frequent mineral replaced by pyrosmalite. There follows rhodonite, whose substitution by manganpyrosmalite, in the Kyurozawa mine Japon (Watanabe, 1961), includes also the crystallization of the manganese amphiboles, quartz and Mn-calcite. In the Oiţa-Colacu mine, manganpyrosmalite formed by the metamorphic substitution of the ferriferous tephroite. Under the microscope, one has observed tephroite crystals corroded by manganpyrosmalite as well as tephroite remains in manganpyrosmalite which have some extinctions and therefore they have belong to the same crystals before the metasomatosis. In the Dadu mine the manganpyrosmalite forms porphyroblasts in the carbonatic ore without any connection with an initial anhidrous silicate or it forms veinlets that cut the tephroite, rhodonite or carbonate ore like in the other ore deposits. This occurrence as veinlets of the manganpyrosmalite - typical of all the ore deposits - indicates a hydrothermal type origin namely a metamorphic hydrotermalism. According to the Japanese authors, manganpyrosmalite formed as a result of the rhodonite reaction with H_2O and HCl, supplied by the presence of a granitic body nearby manganese ore deposits.

Conditions of Manganpyrosmalite Formation

The present thermodynamic data are not enough for an accurate estimation of the manganpyrosmalite stability. The great variation of the Fe^{2+} substitution with Mn^{2+} and of OH with Cl indicates that the minerals of the pyrosmalite group can range within a large stability field in the P and T terms. Therefore, for their formation the critical parameters are not T and P, but the composition. For the formation of the minerals from the pyrosmalitic group it is necessary a special composition of the initial rocks, of the initial premetamorphic sediments, that is of the protolith. This is proved by the fact that the minerals of this group have a restrictive spreading, being found only in the Fe-Mn deposits and the massive sulfides, both of them metamorphosed. In spite of the exclusive occurrence of these minerals in the Fe-Mn deposits and massive sulfides, there is no proof of the pyrosmalite precipitation in the hydrothermal fluids on the sea floor, and in similar actual deposits (Fe-Mn, sulfide) on the sea floor pyrosmalite has not been observed.

The chemical composition of pyrosmalite implies a relatively high activity of chlorine, but a low activity of oxygen in the surrounding fluids. Manganpyrosmalite in the ore deposits of the Bistriţa Mts is related to the minerals with a reducing character, such as magnetite, jacobsite, tephroite and some sulfides. Hematite is absent and occurs only in association with alkaline pyroxene and other Fe^{+3} - bearing minerals.

The manganpyrosmalite formation during the regional metamorphism or during the metasomatic or later hydrothermal alterations points to two possible sources for chlorine: a chlorine-rich fluid preexisting in the Fe-Mn deposits or a chlorine-rich metasomatic fluid coming from an external source. The manganpyrosmalite occurrence exclusively in Fe-Mn deposits and metamorphic massive sulfides seem to be in favour of the first source. Sayfried (1986) proved experimentally that the chlorine enrichments occur in the hydrothermal alterations on the sea floor at a high temperature (400^0 C). The chlorine enrichments in the Fe-Mn deposits could have taken place simultaneously with the deposition of Mn-carbonate, Mn-silicate or Mn-oxide sediments that formed the protolith of the presents ore. The presence of manganpyrosmalite, that preferentially includes chlorine in its structure, had a relatively high salinity during the regional metamorphism or during the metasomatic and late hydrothermal alterations. It is also likely the presence of the evaporite-type initial deposits (with NaCl predominance) among the premetamorphic sedimentary initial deposits which, by metamorphism and local existence of reducing conditions, probably led to the occurrence of manganpyrosmalite in the

Table 4

Two chemical profiles of manganpyrosmalite from Dadu and Mândrileni Mn deposits

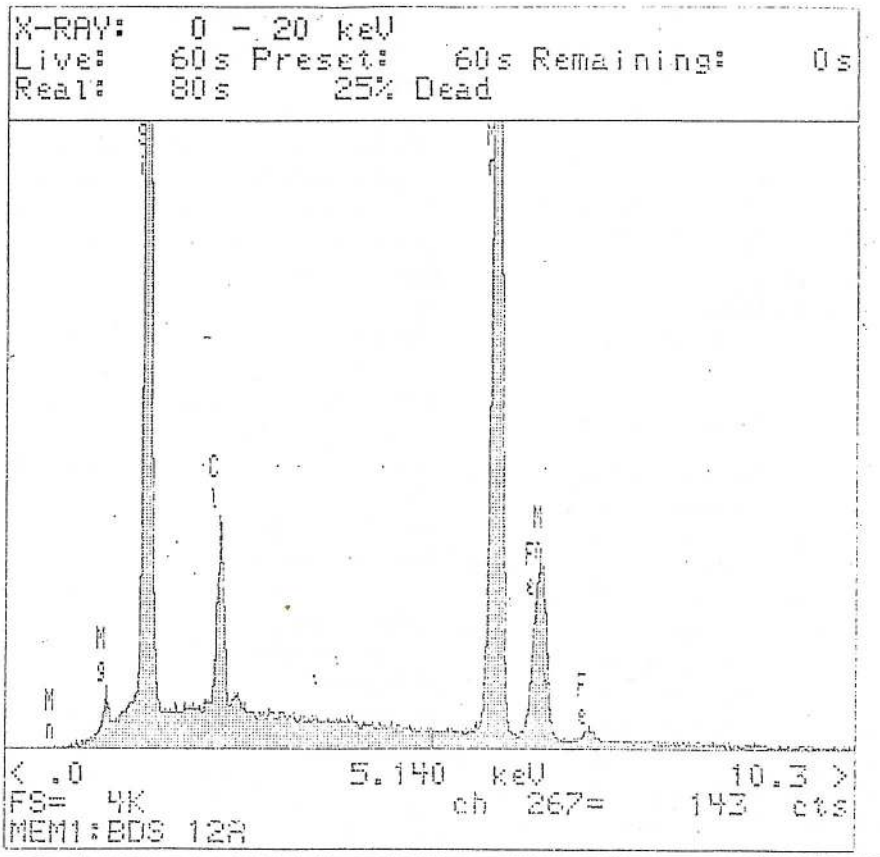

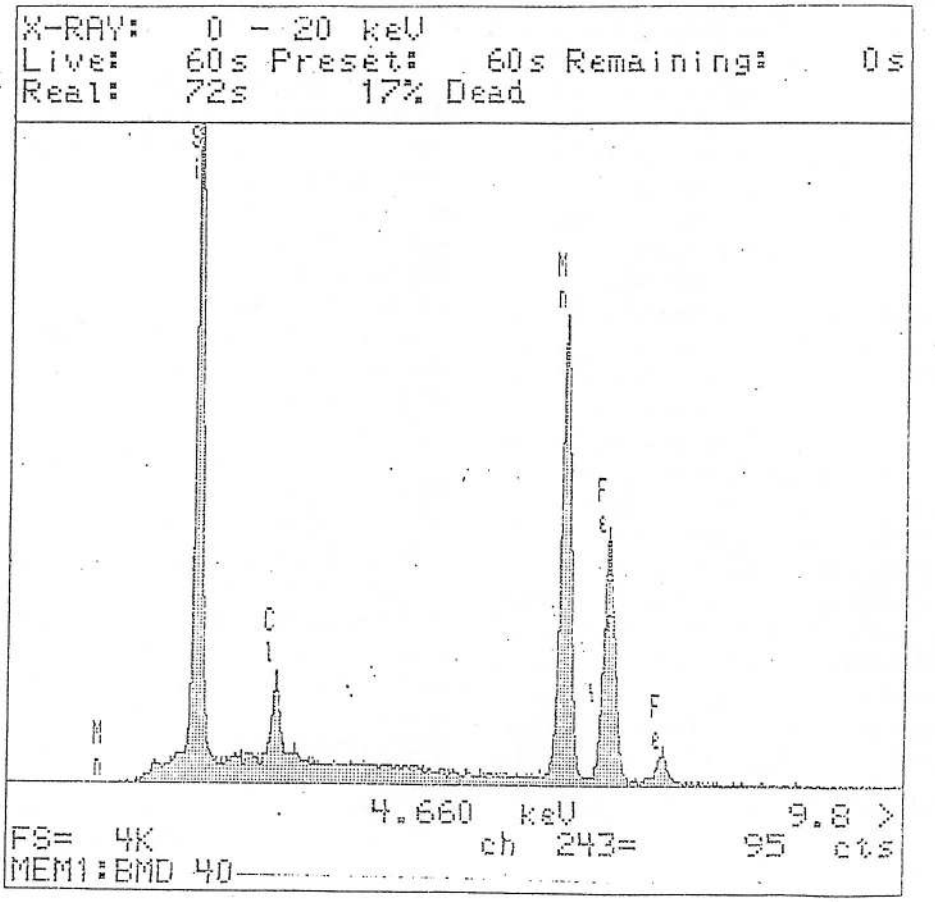

Mn ore in the Bistriţa Mts. The hypothesis of the primary source of the chlorine in the brackish lagoonal deposits would also indicate the Na source (from NaCl) from the alkaline pyroxenes and amphiboles and from albite-minerals nowadays present in the Mn ore. In this case the alteration took place in a closed system as a result of a isochemical metamorphism. The "breccious" texture shown in Figures 2 and 3 (Pl. II) is given by the "invasion" of the manganpyrosmalite which corroded the ore and broke a rectangular piece. The "rectangle" consists of small tephroite and rhodochrosite grains. At the exterior the rectangle is enveloped by the manganpyrosmalite.

The minerals enriched in chlorine, among which manganpyrosmalite, are of a great interest because they indicate the existence of some chlorine-rich fluids. Recent experimental studies established the significance of these fluids in the transport and deposition of Au and Ag, as well as of the elements from the platinum group.

Received: February, 1998
Accepted: June, 1998

References

Frondel, C., Bauer, L. H. (1953) Manganpyrosmalite and is polymorphic relation to friedelite and schallerite. *Am. Mineral.*, 38, p. 755–760.

Hutton, C. O. (1956) Manganpyrosmalite, bustamite and ferroan johannsenite from Broken Hill New South Wales. Australia. *Am. Mineral.*, 41, p. 581–591.

Pan, Yuanming, Fleet, M. E. (1992) Mineralogy and genesis of calcsilicates associated with Archean volcanogenic massive sulphide deposits at the Manitouwadge mining camp. Ontario. *Can. J. Earth. Sci.*, 29, p. 1375–1388.

Seyfried, W. E. Jr., Berndt, M. E., Janecky, D. R. (1986) Chloride depletions and enrrichements in seafloor alteration fluids: constraints from experimental basalt alteration studies. *Geochim. Cosmochim. Acta*, 50, p. 469–475.

Takeuchi, Y., Kawada, I., Irimaziri, S., Sadanga, R. (1969) The crystal structure and polytypism of manganpyrosmalite. *Mineral. J.*, 5, p. 450–467.

Vaughan, J. P. (1986) The iron end-member of the pyrosmalite series from the Pegmont lead-zinc deposits. Queensland. *Mineral. Mag.*, 50, p. 527–531.

Watanabe, T., Kato, A., Ito., J. (1961) Manganpyrosmalite from the Kyurazawa mine, Tochigi Prefecture. *Mineral. J.*, 3, p. 130–138.

Plate I

Fig. 1 – Manganpyrosmalite veinlets, with bent cleavages, in tephroite ore. Oiţa-Colacu mine. N+, x 10.

Fig. 2 – Manganpyrosmalite veinlet, with bent cleavages, in tephroite ore. Oiţa-Colacu mine. N+, x 10.

Fig. 3 – Big crystals of friedelite grown radialy. Sample BMd1, Mândrileni deposit, N+, x 20.

Fig. 4 – Manganpyrosmalite porphyroblasts (white-grey) with remains of ferriferous tephroite (black-grey, large relief). Dadu mine. NII x 20.

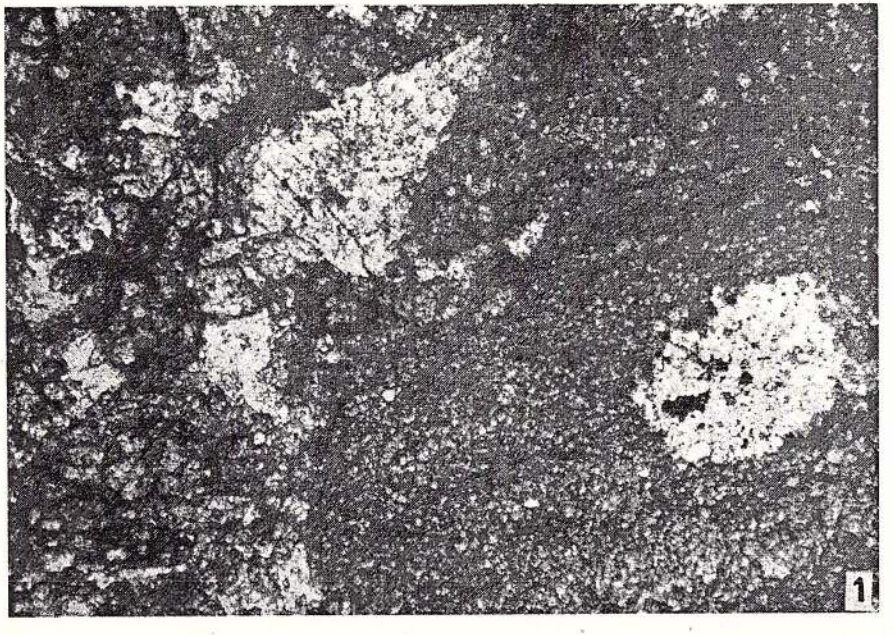

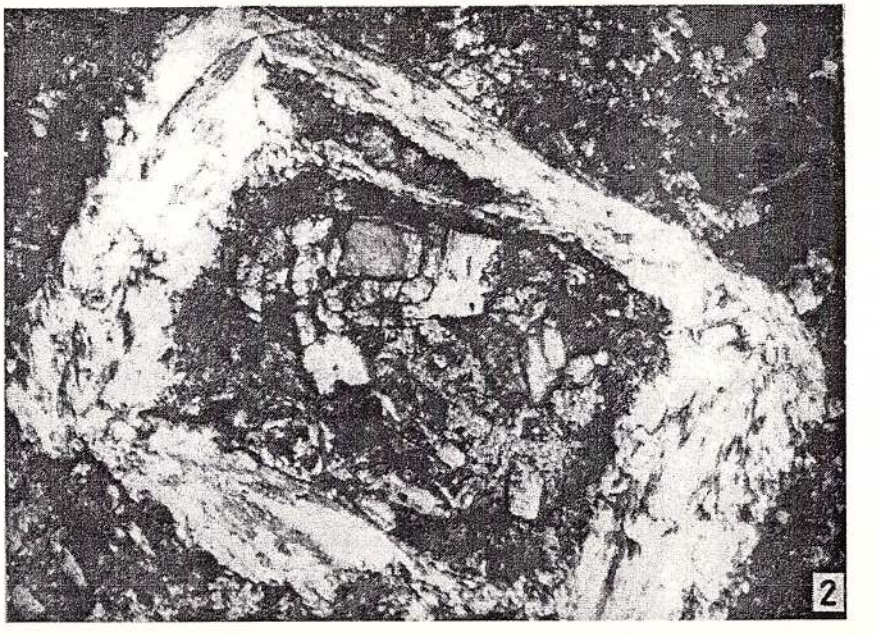

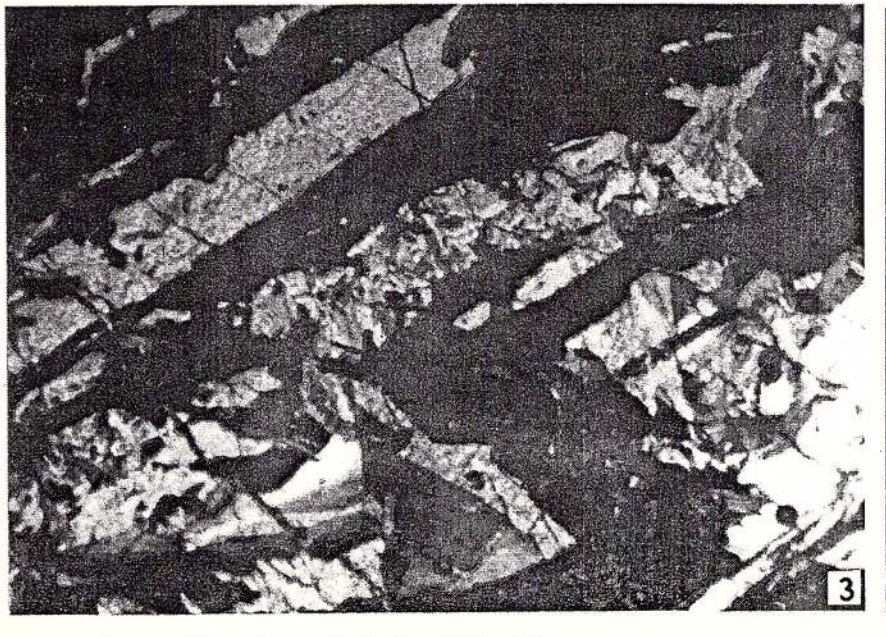

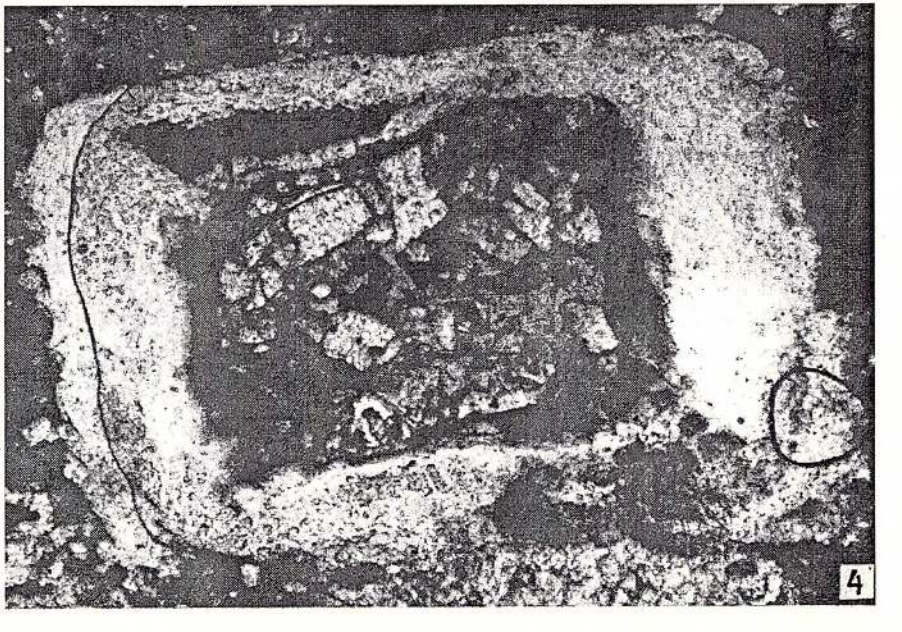

Plate II

Fig. 1 – Manganpyrosmalite porphyroblasts (white), with straight cleavages, in tephroite (triangular grain) and carbonate ore (round grains). Dadu mine. NII, x 20.

Figs. 2, 4 – "Breccious" texture formed of manganpyrosmalite (large rectangle, white-slightly grey) and tephroite, rhodonite, rhodochrosite (small rectangle in the centre), all included in a tephroite ore. Tolovanu mine. NII (Fig. 2) and N+ (Fig. 3), x 10.

Fig. 3 – Relics of pyroxmangite (black) in friedelite (white). Sample BMd1, Mândrileni deposit, N+, x 15.

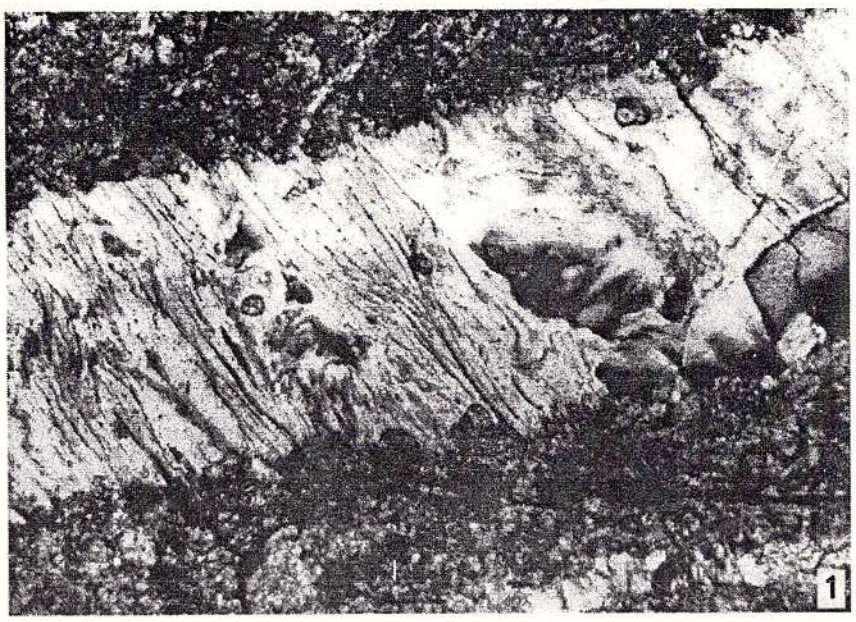

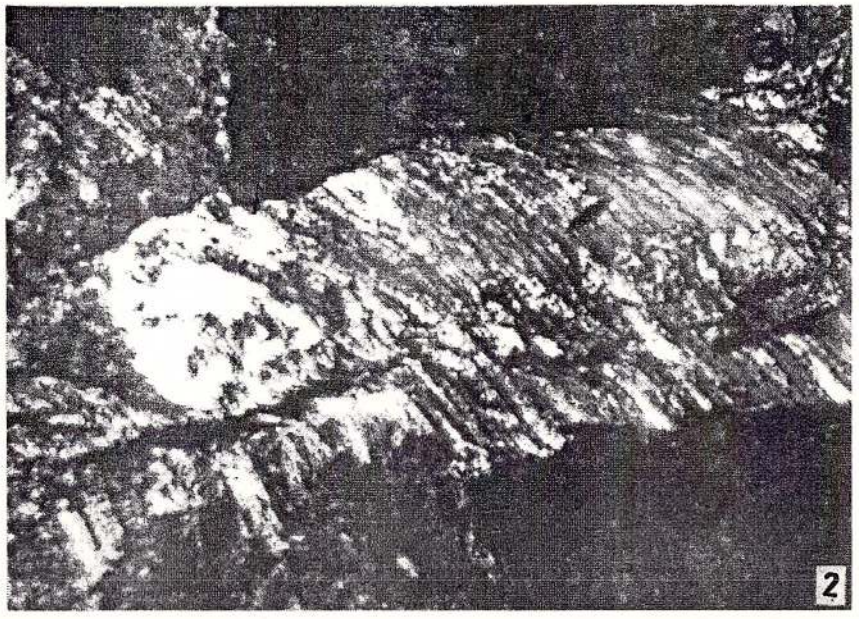

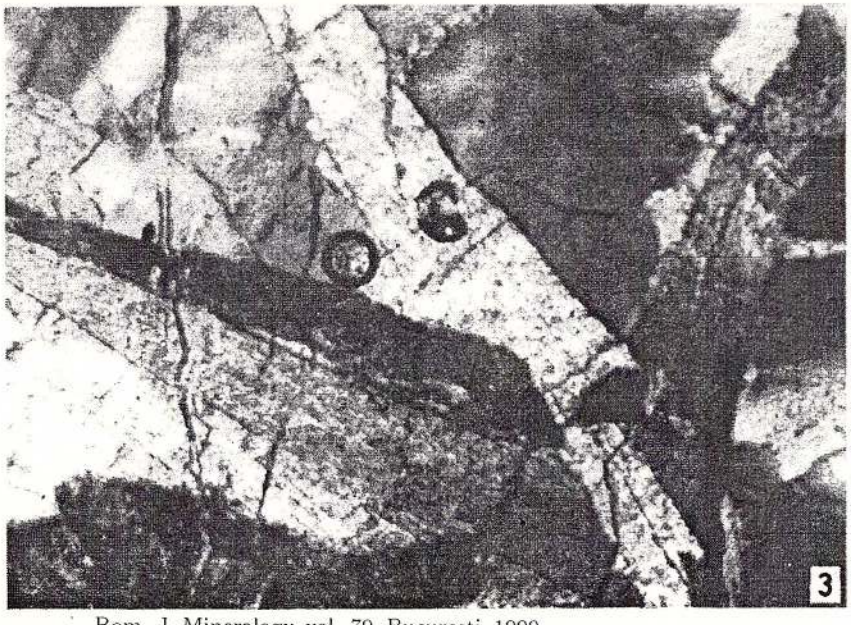

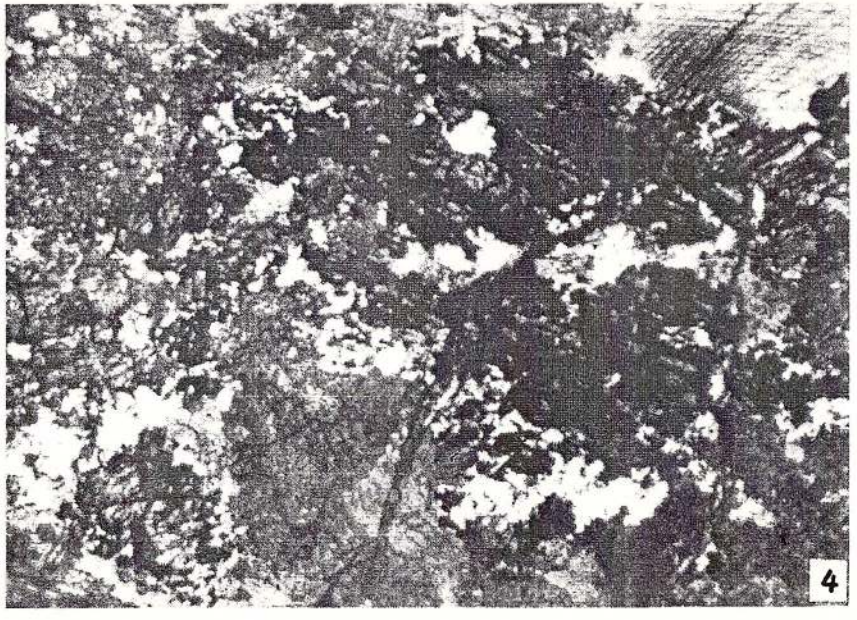

Rom. J. Mineralogy, 79, p. 97-99, Bucureşti, 1999

ON THE PRESENCE OF THE Mn-BEARING PYROXENES IN THE MANGANESE ORE OF THE SEBEŞ MOUNTAINS

Paulina HÂRTOPANU

Institutul Geologic al României. Str. Caransebeş nr. 1, 78344 Bucureşti

Key words: Tephroite ore. Spessartine ore. Green pyroxenes. Granulite facies. Brown alkali pyroxenes. Metasomatites. Vein ores.

Abstract: The manganese metamorphosed ore in the Sebeş Mts belongs to two important groups: the tephroite group (predominant) and the spessartine group. Besides the minerals known until now, our researches have pointed out the presence in this ore of numerous new minerals, among which the pyroxenes are the most widespread. They occur as two varieties with different associations and geneses. The formation of the green pyroxenes of Mn-hedenbergite-johansennite type have taken place by metamorphism under granulite facies and the brown pyroxenes seem to come from an external source infiltrated in the ore during both metasomatosis and metamorphism under amphibolites facies conditions.

The contrasting mineralogical characters of the manganese rocks, their physical and mechanical properties different from those of the adjacent rocks determined a constant synchronism between the general knowledge of the geology of the region and their knowledge. First known as a lithologic element, later on they have been studied in mineralogic and petrographic respect. Among the known researchers who studied these manganese rocks mention should be made of: Vendl (1932), Paliuc (1937), Pavelescu (1955), Savul, Ianovici (1958), Drăghici (1964), Ianovici et al.(1968), Pavelescu and Pavelescu (1968), Hârtopanu (1976, 1977, 1980, 1981).

The manganese rocks in the Sebeş Mts form two major alignments of discontinuous occurrences which cross most of the massif. The most significant geometric feature of these rocks is their alignment along the structure S_2 (Hârtopanu, Hârtopanu, 1981). Based on mineralogic, petrographic and genetic criteria Hârtopanu (1986) determined for the manganese ore in the Sebeş Mts two important groups of ores: tephroite group and spessartine group. The main difference between these groups consists in silica saturation in case of the spessartine group and silica subsaturation in case of the tephroite group. The spessartine group corresponds to the gondite rocks - rocks formed of quartz and manganese silicate (without tephroite) and devoid of manganese carbonate, spessartine and quartz being the major minerals. The tephroite group corresponds to the queluzite rocks, a name used for this type of ore deposits all over the world. These rocks are mostly formed of tephroite and rhodochrosite as major minerals and they are devoid of quartz. The tephroite group is prevailing in the Sebeş Mts and the spessartine group in the Cibin Mts. The adjacent rocks consist of paragneisses, micaschists, more rarely amphibolites and microcline gneisses. The manganese mineralogical associations display a marked individuality, so that it seems that they exclude the characteristic associations of the adjacent rocks, evolving as a closed system. The minerals described till now in the manganese associations (Hârtopanu, 1986) are, as follows: tephroite, spessartine, pyroxmangite, rhodonite, mangangrunerite, rhodochrosite, magnetite, jacobsite, vredenburgite, hematite, ilmenite, pyrophanite. Recent researches pointed out new minerals in the manganese rocks of the Sebeş Mts: spessartine-almandine, spessartine-andradite, spessartine-calderite, ferriferous tephroite, Mg-tephroite, kutnohorite, knorringite (?), Mn-fayalite, glaucochroite (?), pyroxene of johansennite type, Mn-hedenbergite, brown alkali pyroxene of Mn-aegirine type, green alkali pyroxenes of Mn-augite type, yellow alkali amphiboles of richterite type, green alkali amphiboles (of manganmagnesioriebeckite type), Mn-actinote, Mn-tremolite, Mn-biotite , Ba-phlogopite, Mn-phlogopite, brown manganese chlorite, green manganese chlorite, pennantite, neotocite, baryte, albite, friedelite, monasite, allanite, xenotim, radioactive micas, rutile, sphene. Spessartine is an omnipresent mineral in all types of manganese ore, prevailing in the spessartine group.

It also occurs in the tephroite group determining the banding of the ore. Spessartine forms several generations with different geneses. Thus, the oldest spessartine and one of the oldest minerals of the ore is (1) spessartine of metamorphic type, that forms a spessartinic mass. The limit between the grains disappeared because of the pressures it underwent. (2) Spessartine-andradite, as crystals larger than 1 cm, is specific to the metasomatosis zone, displaying a concentric zonation superposed over a sectorially radiary zonation (Pl. I, Fig. 1). It occurs in association with Mn-tremolite. (3) Spessartine-calderite is idiomorphic, clean, of a yellow colour, typical of the zones with a strong oxidation, fine-grained and associated with hematite and brown alkali pyroxenes of manganiferous Mn-aegirine type. Another paragenesis of the spessartine-calderite is with braunite, bixbyite and hematite. (4) Spessartine-almandine is the newest generation, formed on almandine with which it is associated in microschlieren (Fig.). One can notice that almandine has been rolled up and then caught in the multitude of newly formed spessartine-almandine microcrystals. The sperssatine almandine association is a disequilibrium one, as they are incompatible. The important factor which could affect the garnet composition is the oxidation state of the host rock. The stability of almandine strongly depends on the oxygen fugacity. The stability of spessartine in contrast to that of almandine is essentially independent of oxigenfugacity at least up to that defined by the magnetite-hematite buffer (Hsu, 1968). With increasing oxidation state, almandine must incorporate increasing amounts of spessartine component, in order to maintain its stability. Garnet stable under higher oxidation state must contain dominantly the spessartine component till the disappearance of the almandine component. This transformation, from almandine to spessartine happened shaply in our rocks, probably because the oxidation state has been quickly changed as it can be seen in Figure.

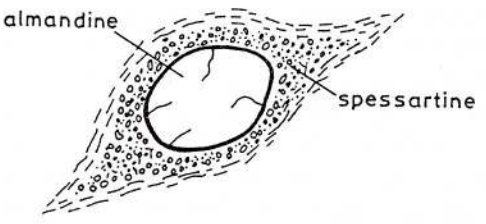

Spessartine formed at the expence of almandine

An absolute novelty for the manganese ore in the Sebeş Mts is the occurrence of the pyroxenes. They form two distinct groups: green pyroxenes of the Mn-hedenbergite-johansennite type and brown pyroxenes of Mn-aegirine type. The first group occurs in association with a spessartine type ore. The mineralogical association is: spessartine, Mn-hedenbergite green pyroxenes, Mn-apatite, quartz, magnetite. Under the microscope they show a greenish colour, with characteristic cleavages (Pl. I, Fig. 6) and a weak pleochroism with greenish-yellowish hues and -2V = ca 70^0. Also, one can observe that the green clinopyroxene (Cpx) is attacked by spessartine (Pl. II, Fig. 2). It is found in the Scorţaru and Bretan peaks.

The green pyroxenes occur as monomineral masses (Pl. II, Figs. 3, 4) on the Jigureasa Valley. The rare grains of pyroxmangite, magnetite and quartz may appear. This paragenesis with Cpx + Pxm + Gr + Mt + Q is considered by Daskupta et al. (1990) as belonging to the granulite facies in the Andhra Pradesh area. Both pyroxenes of the Jigureasa Valley and Andhra Pradesh area are of the Mn-augite-salite type.

In exchange, on the Răscoliţa Valley, the brown alkali pyroxenes occur in pyroxmangitic type rocks with which they are not in direct contact (Pl.II, Figs. 1, 2). The mineralogical association with brown alkali pyroxenes seems to invade the pyroxmangitic rock having a vein character. Besides the Mn-aegirine-pyroxene this association also includes albite, quartz, spessartine-calderite, hematite, yellow alkali amphibole. Under the microscope the brown alkali pyroxene of Mn-aegirine type has a strong yellow colour and is poorly pleochroic with yellow-orange, yellow-greenish hues. It is negative biax, with -2V = 60^0 . Both optically and by its mineralogical association it resembles the Delineşti aegirine pyroxene. As at Delineşti, the brown alkali pyroxene of Mn-aegirine type seems to be an intruding mineral coming from outside which does not belong to the associations characteristic of the ore (Pl. II, Figs. 1, 2). Both Delineşti and Sebeş Mn-aegirine pyroxene have not a zonation like that from Bistriţa.

The green clinopyroxene has probably been formed by high metamorphism. The mineral association Cpx + Grt + MnAp + Q belongs to the granulite facies. The garnet (Gr) represents solid solutions among spessartine, almandine and minor grossularite - consequently it is Fe-rich, like the clinopyroxene.

The clinopyroxene of Mn-hedenbergite-johansennite type contains appreciable Fe and Ca amounts. These compositions justify their affiliation to the first and the strongest metamorphic event in this area. Thus, in the Sebeş Mts the association dominated by clinopyroxene (Cpx) made up of Mn-hedenbergite-johansennite (Fe-rich), appears. In this association Mn-fayalite (?) may be present which, together with Cpx and quartz, forms parageneses belonging to the high grade facies (granulite facies) everywhere (in the

world) where it appears.

Other minerals determined recently in the manganese ore from the Sebeş Mts (Untul Valley) are the magnesian tephroite, kutnohorite and knorringite (?). The paragenesis MgTp + kutnohorite + knorringite (?) belongs to the granulite facies in other manganese deposits in the world .

In the Răscoala Valley the association dominated by Mn-fayalite includes much magnetite and relics of orthopyroxene and this paragenesis belongs to the granulite facies, too .

We consider that the tephroite from the Sebeş Mts, by its features as a metastable relic, was metamorphosed in the first prograde metamorphic event probably in the granulite facies. The tephroite is the oldest mineral from the ore and together with old-spessartine-calderite (?) now transformed into spessartine, spessartine-andradite, new spessartine-calderite (from "oxidation parageneses") form a paragenesis which belongs to the granulite facies.

On the Răscoliţa Valley the tephroite-type ore includes manganese olivine with a low relief and birefringence, with a low -2V, which seems to be a glaucochroite. Mn-tremolite often occurs in fibrous granular masses, as monomineral static sheaves (Pl. III, Fig. 4) or in association with zoned spessartine-grossularite (Pl. I, Fig. 1). Mn-apatite is frequently found in the ore. This is "spotted" (Pl. III, Fig. 2) probably because of the Mn^{2+} alteration from its composition in secondary manganese minerals. At least three apatite generations can be noticed in the manganese ore in the Sebeş Mts as well as in the other manganese ore deposits in Romania. They are differentiated under the microscope after the colour, pureness and relief. Among the vein-type minerals that are found both in the Semenic Mts and in the Bistriţa Mts, in the Sebeş Mts ore we have identified: baryte, green manganese chlorite, friedelite, albite, bementite, penanntite, neotocite, manganese brown chlorite. Baryte locally occurs as large crystals (Pl. III, Fig. 4) or as elongated millimetric veinlets, in association with manganese brown chlorite and neotocite (Pl. III, Fig. 6). Like in other manganese ores from Romania the affinity of baryte for the tephroite rocks is also observed (Pl. III, Fig. 3). In the pyroxmangite ore on the Răscoliţa Valley, friedelite has been identified. Under the microscope it occurs as pink-lilac to colourless leaflets, with a fibrous glassy luster and a high birefringence. It forms nests and veinlets (Pl.III, Fig. 5) in the pyroxmangitic type ore. The chlorine source in this mineral might be chlorapatite. Under the microscope, nests and veinlets of friedelite on chlorapatite have been observed. The radioactive minerals are found on all types of manganese ore, displaying a high affinity for spessartine type. In this type of ore the radioactive minerals form millimetric nests and veinlets represented by monasite, xenotim, allanite and radioactive micas. The presence of braunite is to be mentioned in an almost monomineral fragment on the Pravăţ Valley. Under the microscope, it occurs in association with bixbyite, spessartine-calderite, hematite. One can conclude that both in the Sebeş Mts and in the Lotru Mts there are predominantly oxide levels of manganese ores. The evolution of the ore toward oxide, silicate or carbonate was first of all the result of the origin of the initially premetamorphic material and secondly according to the PT of the metamorphism associated with the variations of the oxygen, CO_2, OH, F, Cl fugacities which diversified so much the manganese minerals.

References

Drăghici, C. (1964) Contribuţii la studiul silicaţilor de mangan şi fier din munţii Sebeşului. *St. tehn. econ., A*, 6, Bucureşti.

Hârtopanu, P., Hârtopanu, I. (1978) Tephroite in the Sebeş Mountains (The South Carpathians). *An. Univ. Bucureşti*, XXVII, p. 26–34, Bucureşti.

— , **Hârtopanu, I. (1981)** Relaţii microstructurale în asociaţiile manganifere din munţii Sebeş şi Cibin. *Stud. cerc. geol. geofiz. geogr., Geologie*, 26, 1, p. 35–44, Bucureşti.

— , **Udrescu, C. (1981)** Elemente urmă în mineralele manganifere din munţii Sebeş-Cibin. Semnificaţii genetice. *Stud. cerc. geol. geofiz. geogr., Geologie*, 26, 2, p. 219–232, Bucureşti.

— **(1986)** Textural relationships and their genetic significance in the manganiferous metamorphic rocks of the South Carpathians. *Teophrastus pub. S. A.* Athens, p. 605–621.

Hsu, L. C. (1968) Selected Phase Relationships on the System Al-Mn-Fe-Si-O-H: A Model for Garnet Equilibrium.

Ianovici, V., Drăghici, C., Constantinof, D., Ionescu, C., Dimitriu, Al. (1968) Geology of Manganese Deposits in Romania. *XXIII Intern. Geol. Congr.*, Praha, XIII.

Pavelescu, L. (1955) Consideraţiuni asupra unor silicaţi de fier şi mangan din munţii Sebeş. *Bul. St. Ac. R.P.R.* 2, Bucureşti.

Savul, M., Ianovici, V. (1957) Chimismul şi originea rocilor cu mangan din cristalinul Bistriţei. *Bul. Acad. R.P.R., Geol.-Geogr.*, 1/II, Bucureşti.

Vendl, A. (1932) Das Kristallin des Sebescher und Zibingebirges. *Geologica Hungarica*. IV, Bul. I.

Received: February, 1998
Accepted: June, 1998

Plate I

Fig. 1 – Spessartine-andradite, concentrically zoned and sectorially radiary in a tremolite mass. Pravăţ, N+, x 20.

Fig. 2 – Mn-hedenbergite-johansennite (white with two cleavages) in association with spessartine (isotrope) and corroded by it. Scorţaru, N+, x 20.

Figs. 3, 4 – Grain of twinned and untwinned tephroite. Sample 200 M, NII (top) and N+ (bottom), x 20.

Figs. 5, 6 – Mn-hedenbergite-johansennite (white with two cleavages) in association with spessartine (isotrope). Scorţaru, NII and N+, x 20.

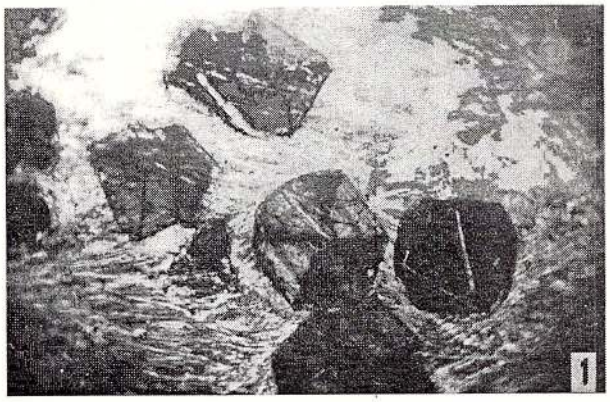
1

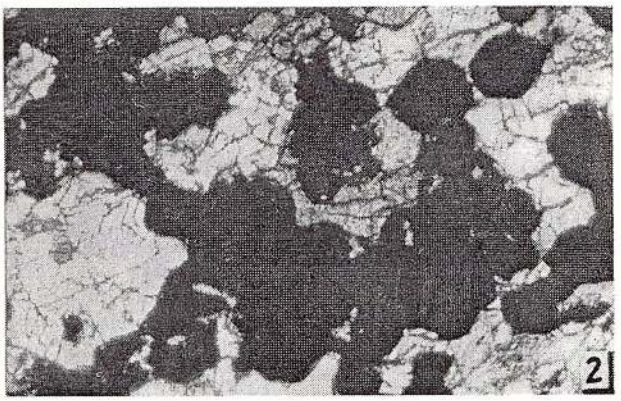
2

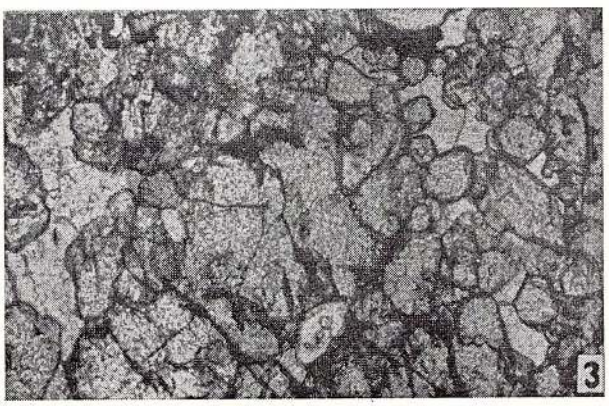
3

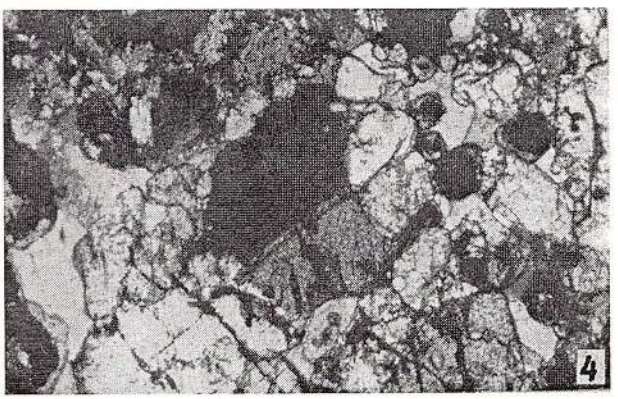
4

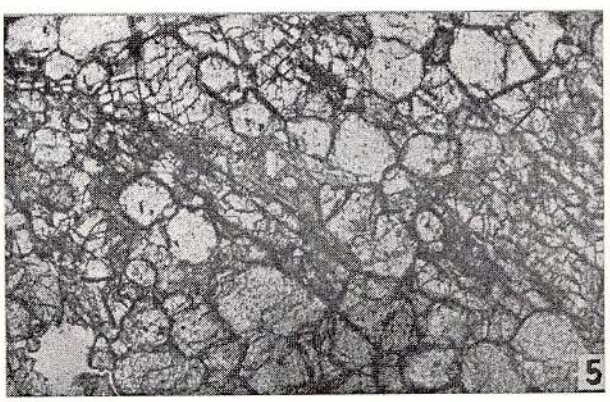
5

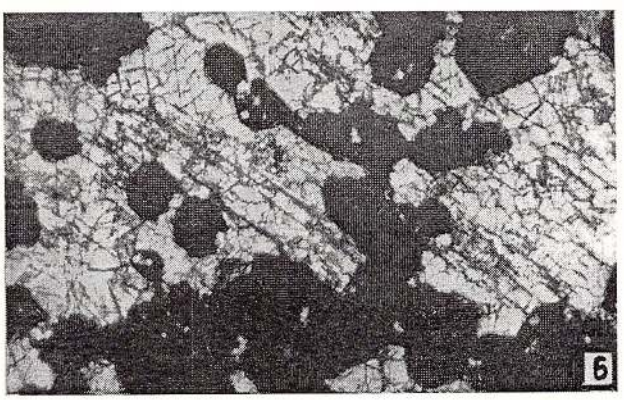
6

Plate II

Fig. 1 – Clear contact between Mn-aegirine pyroxene (top, clean white grey) and pyroxmangite (bottom, dirty grey-blackish). Sample 3, RSc, NII, x 20.

Fig. 2 – Clear contact between Mn-aegirine pyroxene + quartz + albite (top, white, vaguely grey) and pyroxmangite (bottom, altered on cleavages) .

Figs. 3, 4 – Mass of Mn-augite pyroxene. Sample 19 J, NII (top) and N+ (bottom), x 20.

Fig. 5, 6 – Mn- aegirine pyroxene in association with albite (twins) garnet (isotrope), hematite (black). Sample 10 J, NII (top) and N+ (bottom), x 20.

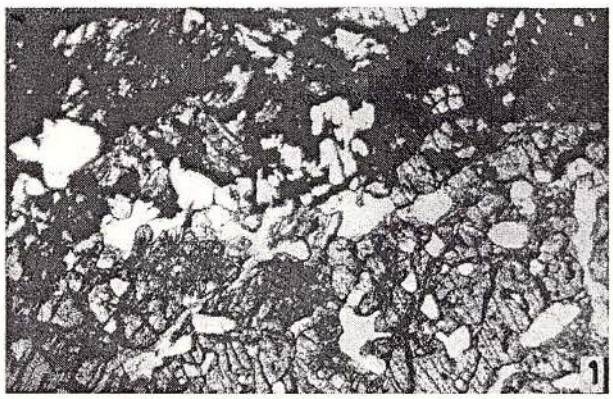

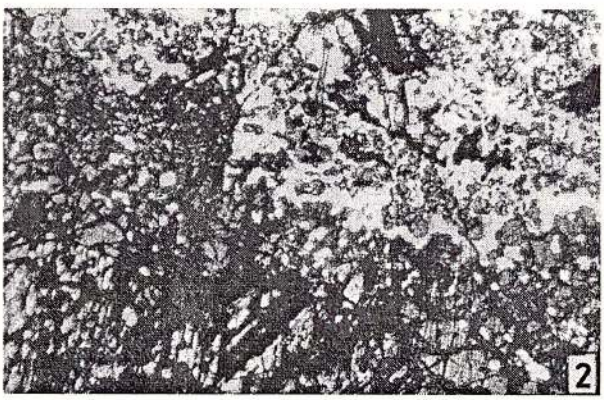

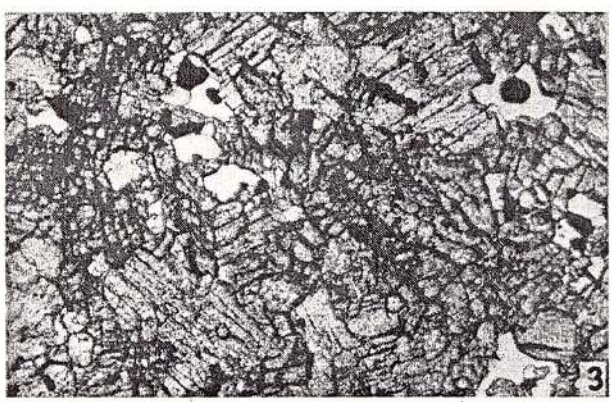

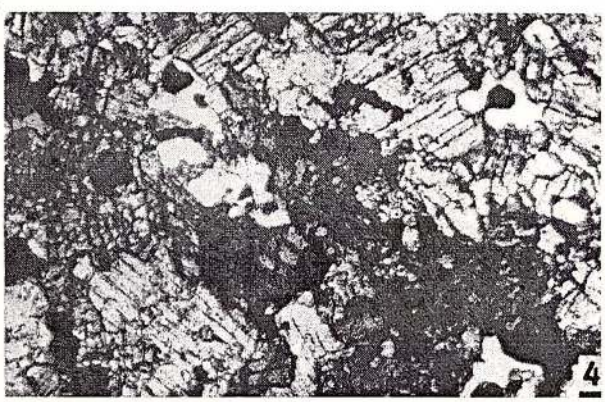

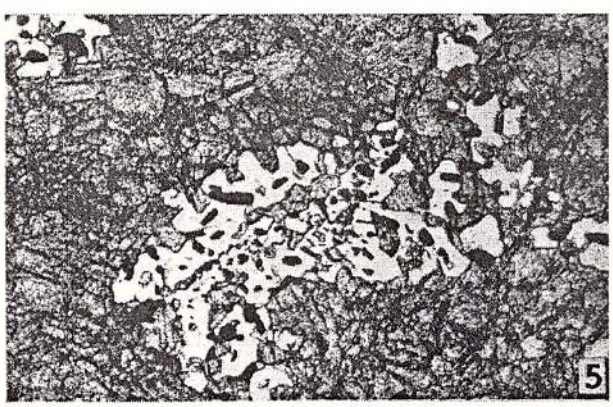

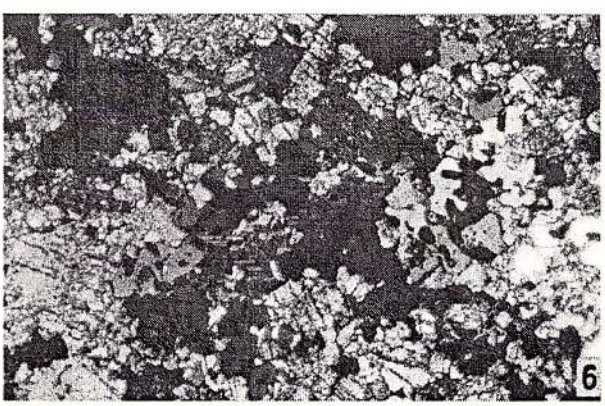

Plate III

Fig. 1 – Mn-tremolite developed statically. Sample 4 Br, N+, x 20.

Fig. 2 – Mn-apatite "spotted" + spessartine. Sample M 119, N II, x 20.

Fig. 3 – Baryte (white) + tephroite (large grey crystals with high relief). Sample 10B, NII, x 20.

Fig. 4 – Large baryte crystals. Sample 2211, NII, x 20.

Fig. 5 – Friedelite (white, fibrous, low relief) in pyroxmangite (grey, high relief). Sample 3 Rsc, NII, x 20.

Fig. 6 – Baryte-neotocite veinlet in tephroite ore. Pravăţ, NII, x 20.

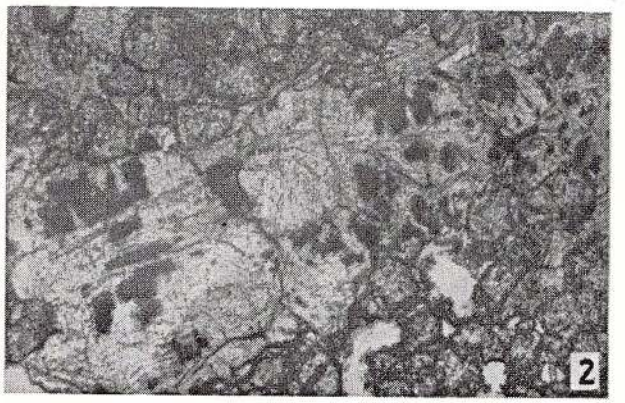

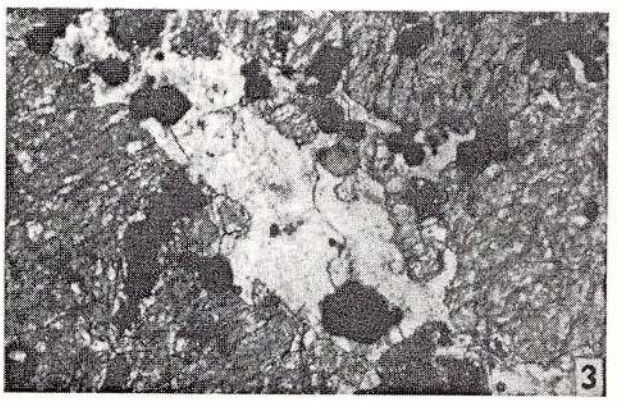

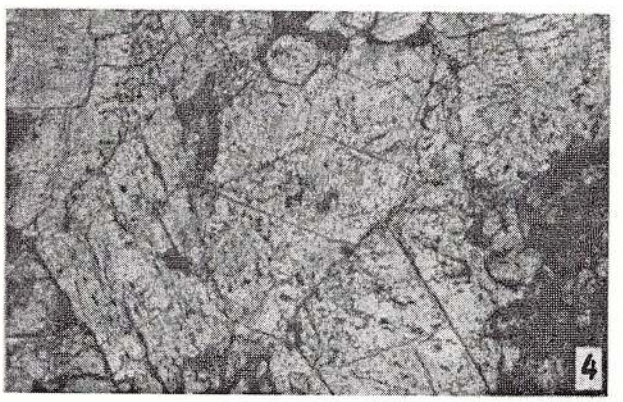

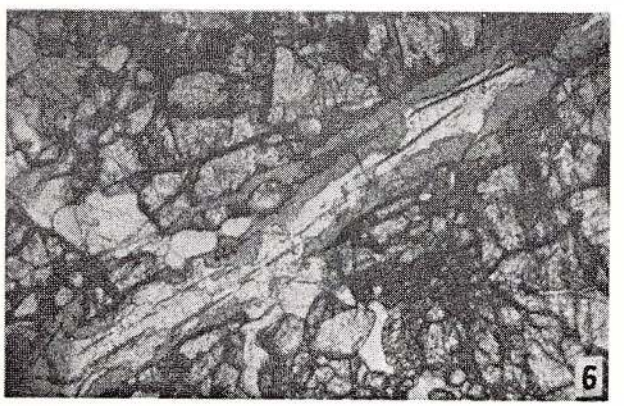

Rom. J. Mineralogy, 79, p. 101-104, Bucureşti, 1999

THE HYDROGARNETS – AN UNSOLVED PROBLEM ?

Corina IONESCU, Lucreţia GHERGARI

Universitatea "Babeş-Bolyai", Departamentul Mineralogie-Petrometalogenie

Str. M. Kogălniceanu nr. 1, 3400 Cluj-Napoca, Romania

Key words: Hydrogarnets. Hydrogarnet-type substitution.

Abstract: The water-bearing garnets are known since 1906. There are over 90 years of researches, discussions on the structure and nomenclature of this important group of minerals. A short history of the hydrogarnets is presented in this paper. Some references on the hydrogarnets state in Romania are made.

1. Introduction

The water-bearing garnets are known since 1906. There are over 90 years of researches, discussions on the structure and nomenclature of this important group of minerals. The names of hydrogarnets, some of it, rejected by IMA, are present in papers, data bases and university courses. The presence of variable amounts of hydroxil bonded in the structure of all kind of garnets is a reality.

2. History of the hydrogarnets

Hydrogrossular - the hydrous equivalent of grossular - was described for the first time by Cornu, in 1906 (fide Peters, 1965; Aines, Rossman, 1984), followed by Foshang (1920; he described hydrogrossular under the name of "plazolite"), Winchell (1933), Flint et al. (1941). In 1937 Pabst had determined the structure of hydrogrossular.

The calculation of the structural-water (McConnell, 1942-fide Deer et al., 1982) led to the acceptation of the hydrogarnets as members of the garnet group, with general formula: $X_3Y_2(ZO_4)_{3-m}(OH)_{4m}$.

In 1943 Hutton (in Deer et al., 1982) recognized hydrogrossular as a member of the $3CaO.Al_2O_3.3SiO_2$ – $3CaO.Al_2O_3.2SiO_2.2H_2O$ series, with an intermediate composition between grossular and hibschite $3CaO.Al_2O_3.6H_2O$ (Weiss et al., 1964). The minerals from this domain of composition were named *plazolite, hydrogrossular, hydrogarnet, grossularoid* and *garnetoid.*

Pabst (1942) observed a compositional zoning in a garnet, from a grossular core to a hydrogrossular rim. This was interpreted by Yoder (1950) as an indicator of a rich-water retrograde metamorphism.

The South Africa hydrogrossular IR spectrum (Frankel, 1959) shows a major absorption band at 3620 cm^{-1} and a minor band at 3660 cm^{-1}.

In 1964 Tsao found, in the Hsiaosungshan altered peridotite, a ferric hydrogarnet: the hydrougrandite. The mineral is light green, with a vitreous luster, and has an index of refraction of 1.825-1.830. The thermo-differential analysis shows three distinct characteristic thermal effects (an endothermic one at 705^{0}C and two exothermic at 440^{0}C and 900^{0}C. Tsao sustains that the hydrougrandite is distinctly different from the other known hydrogarnets (hydrogrossular, hibschite and plazolite). The chemical composition of hydrougrandite corresponds to both hydrous grossular and hydrous andradite and the mineral was named "hydrougrandite".

In 1965 Peters presented, from the Totalp (Switzerland) serpentinites, a water-bearing andradite. The IR spectrum shows a broad OH-band at 3380 cm^{-1} due to absorbed H_2O and two other bands at 3525 cm^{-1} and 3660 cm^{-1}, caused by the OH vibrations resulting from the H for Si substitution in the garnet lattice. The author considers that the similarity in the mode of occurrence and the complete solid solution between grossular and andradite make it likely that a water-bearing equivalent for andradite should also exist.

A hydrougrandite with chromium content (Cr_2O_3 - 2.20%, Fe_2O_3 - 27.79%) was described by Ford in Tasmania, in 1970.

Hsu (1980) considered that the hydrogarnet presence can be used as a temperature indicator and es-

tablished the forming of a hydrogarnet-bearing association at $< 420^0$C and 2 kbars pressures. The hydrogrossular synthesized by Hsu presents infrared absorption bands at 3620 and 3660 cm^{-1}.

After 1965, a series of papers described hydrous andradite ("hydroandradite" respectively): Onuki et al., 1982; Lager et al., 1989; Armbruster, Geiger, 1993; Armbruster, 1995).

The name "hydrougrandite" (*Miner. Mag.*, 1967, 36, p. 133) was rejected by I. M. A. Commission on New Minerals and Mineral Names but this name is frequently used in the geological literature and in geological databases.

A manganoan hydrogarnet *henritermiérite* is also known (Gaudefroy et al., 1969).

The discovery of the katoite in 1984 (Passaglia, Rinaldi), as first natural occurrence of such a garnet (with the grossular content < 50%), determined a revision of the nomenclature of the hydrogrossular group. As approved in 1985 by the IMA Commission (Dunn et al., 1985), "the name grossular should be used for the anhydrous end-member (100% Gr). Members of the series with more Gr ($50 \leq$ Gr% $<$ 100) should be named *hibschite*, leaving the alternate terms as plazolite, grossularoid, hydrogarnet, garnetoid and hydrogrossular. The name of *katoite* is adopted for members with grossular content below 50 %, including the $Ca_3Al_2(OH)_{12}$ end-member ($0 \leq$ Gr % < 50)". The IMA Commission decided also that the name hydrogrossular may still be used for members of the series with appreciable OH content but undetermined $SiO_4/(OH)_4$ ratio.

Since then (1984) many hydrogarnets occurrences, both in pyralspites and ugrandites series, were described, the most frequent being the hydroandradite. Marke de Lummen (1986) described a fluor-bearing hydorandradite in altered basalts.

The experiments were focused almost exclusively on the synthetic hydrogrossular. In a study on the water content of the pyralspites, Aines and Rossman (1984) concluded that these garnets contain two classes of hydrous component: a structural component, and an alteration-related water component. "The structural hydrous component is of great interest because: 1) the "water" contained is a record of the environment of formation or later events, and 2) the garnet structure must be changed to accommodate a hydrous component and may also change the physical properties of the garnet."

Armbruster (1995) observed that most of the hydrous andradites are characterized by Ti content; if Ti is absent, the hydrous component is very low. For the "hydroandradites" found in South Africa, the author presumes a late hydrothermal origin. These minerals show the highest degree of hydration for the andradites hitherto observed in nature.

Water contents of anhydrous garnets were detected by IR spectra, resulting that both andradite and grossular normally have about 0.148 % water content. The structural role of the water is not entirely clear, but it is believed that isolated OH^- ions take the oxygen sites, associated with empty places or substitution unbalance in cations sites (Deer et al., 1982). It is presumed that in crystalline silicates, the hydration is expressed by a hydrogarnet-type substitution $[SiO_4]^{4-} \leftrightarrow [(HO)_4]^{4-}$. The presence of this substitution, the common and preferential replacement with OH^-, is well established in the grossular - katoite ($Ca_3Al_2[SiO_4]_3$ - $Ca_3Al_2[(HO)_4]_3$) series. IR studies on natural garnets show the usual presence of minor amounts of OH^- but other substitution-types than the hydrogarnet-one are also possible (Rossman, Aines, 1991).

The substitution of Si with H was experimentally verified by Cohen-Addad et al. (1967), who showed that hydrogen is present as OH^- groups and is related with the oxygen surrounding the tetrahedral free sites. The $[SiO_4]^{4-}$ substitution with OH^- determines the increasing of the unit cell parameter (Cohen-Addad et al., 1967) (Table).

The studies of Aines and Rossman (1984) had confirmed that the so-called "hydrogarnet substitution" ($[(HO)_4]^{4-} \leftrightarrow SiO_4]^{4-}$) is common to other garnets also, not only for grossular. The hydrogarnet-type substitution is related to composition; pyralspites may contain only small amounts of water (< 5 %) reported to ugrandites (up to 20 %).

Armbruster and Lager (1989) could not establish any relation between the H site and OH^- content in the hydrogrossular series. Lager et al. (1989) presumed that the amount of OH^- is structurally controlled in garnets (the garnets with common tetrahedra edges longer than uncommon ones may include more OH^-; the pyralspites series garnets may have limited OH^- amounts). The hydrogarnets structure results by the replacement of $[SiO_4]^{4-}$ with $[(HO)_4]^{4-}$.

According to Aines and Rossman (1984), the hydrous component is not in the form of molecular H_2O. The most likely form is $[(HO)_4]^{4-}$ which substitutes $[SiO_4]^{4-}$ radical, but other substitutions, involving multiple OH^- groups, may be present. The OH^- concentration (as H_2O) is determined on the absorptivity band, in 3700–3400 cm^{-1} region.

Aines and Rossman (1984), studying OH^- – bearing pyralspites, consider that the presence of a hydrogarnet-type substitution in an end-member of a series is shown by IR Spectra in the 3500 cm^{-1} region, with up to four peaks. If the symmetry is complete, there will be two peaks. In the pyralspi-

Table

Unit-cell parameters for anhydrous and hydrous garnets

Mineral	a_0 (Å)	References
Grossular	11.85	Henmi et al., 1971
Hydrogrossular	11.94	Cohen-Addad et al., 1967
Hydrogrossular	12.11	Menzer, 1926
Katoite	12.5695	Lager et al., 1987
Katoite	12.374(6)	Schröpfer, Bartl, 1993
Andradite	12.03	Deer et al., 1982
Andradite	12.048	Skinner, 1956
Andradite	12.056	Huckenholz, Yoder, 1971
Hydroandradite-Totalp, Switzerland	12.08	Peters, 1965
Hydroandradite	12.085	Lager et al., 1989
Hydroandradite	12.106	Lager et al., 1989
Hydroandradite-South Africa	12.34	Armbruster, 1995
Hydrougrandite-China	12.063	Tsao, 1964
Hydrogarnet-Budureasa, Romania	12.07(1)	Ghergari, Ionescu, 1997

tes, the hydrogarnet-type substitution is not characteristic due to the very low level of this substitution and not to its frequency or occurrence. The difference between the Mg - O and Fe - O (in pyralspites) and Ca–O (in ugrandites) bond lengths explain the apparent lack of the hydrogarnet-type substitution in pyralspites. The Ca–O bond is shorter and is favorable for the hydrogarnet-forming in the grossular - andradite series (Aines, Rossman, 1984). The pyralspites usually contain only 0.01–0.25% hydrous component.

A correlation between the lattice constants of the hydroxylated phases and their degree of hydroxylation is observed by Schröpfer and Bartl (1993).

The last decade recorded an increasing interest for the water-bearing garnets, due to the supposition that these minerals may represent potential water - storage places in the mantle (Aines, Rossman, 1984).

3. The genesis of the hydrogarnets

There are some considerations regarding the formation of the hydrogarnets, as:

– low temperature and pressure conditions, in the presence of water (the water-bearing andradite from Totalp, Switzerland, located in ophicalcites; Peters, 1965);

– under 420^{0}C temperature and about 2 kbars pressure (Hsu, 1980);

– low-temperature hydrometasomatic genesis (Deer et al., 1982);

– late hydrothermal origin (Armbruster, 1995);

– hydro-metasomatic processes, at 300^{0}C (Ghergari, Ionescu, 1997).

4. The presence of hydrogarnets in Romania

The first remark about the presence of the hydrogarnet in Romania was made by Nedelcu and Damian (1982) but the data were quite poor. In the geodes from Măgura Uroiului (Deva) andesites, "hibschite, $Ca_3Al_3(OH)_4.(SiO_4)_2$, appears as yellow dodecahedra of 2–3 mm size".

In 1992 Marincea presumed the presence of a hydrogarnet in the metasomatites from Mraconia (Banat) but finally he concluded that the data did not confirm the supposition.

We consider that these data are not enough to prove the presence of a hydrogarnet (the lack of IR spectra, chemical data, cell parametres, even X-ray diffractometry) and the first genuine record on the presence of hydrogarnet in Romania (hydrograndite in garnet-magnetite skarns from Budureasa, Apuseni Mountains) belongs to Ghergari and Ionescu (1997).

References

Aines, R. D., Rossman, G. R. (1984) The hydrous component in garnets: pyralspites. *Am. Miner.*, 69, p. 1116–1126.

Armbruster, T. (1995) Structure refinement of hydrous andradite, $Ca_3Fe_{1.54}Mn_{0.20}Al_{0.26}(SiO_4)_{1.65}(O_4H_4)_{1.35}$, from the Wessels mine, Kalahari manganese field, South Africa. *Am. Miner.*, 80, 7–8, p. 1221–1225.

— , **Geiger, C. A. (1993)** Andradite crystal chemistry, dynamic X - site disorder and structural strain in silicate garnets. *Eur. J. Mineral.*, 5, p. 59–71, Stuttgart.

— , **Lager, G. A. (19..)** Oxygen disorder and the hydrogen position in garnet-hydrogarnet solid solutions. *Eur. J. Mineral.*, 1, p. 363–369.

Cohen-Addad, C., Ducros, P., Bertaut, E. F. (1967) Étude de la Substitution du Grouppement SiO_4 par $(OH)_4$ dans les Composés $Al_2Ca_3(OH)_{12}$ et $Al_2Ca_3(SiO_4)_{2,16}(OH)_{3,36}$ de Type Grenat. *Acta cryst.*, 23, 2, p. 220–230, Copenhagen, 1967.

Deer, W. A., Howie, R. A., Zussman, J. (1982) Rock-forming minerals. Vol.I Orthosilicates, 919 p., Garnet group, p. 467–698. J. Longmans, London.

Dunn, P. J., Fleischer, M., Langley, R. H., Shigley, J. E., Zilczer, A. Janet (1985) New mineral names. *Am. Miner.*, 70, p. 871–881.

Flint, E. P., Havord, F. M., Wells, L. S. (1941) Hydrothermal and X-ray studies of the garnet-hydrogarnet series and the relationship of the series to hydration products of Portland cement. *Jour. Res. Nat. Bur. stand.*, V, 21, p. 13–33.

Ford, R. J. (1970) A hydrogarnet from Tasmania. *Min. Mag.*, 37, p. 942–943.

Foshang, W. F. (1920) Plazolite, a new mineral. *Am. Miner.*, V, 5, p. 183–185.

Frankel, J. J. (1959) Uvarovite garnet and South Africa jade from Transvaal. *Am. Miner.*, 26, p. 565–591.

Gaudefroy, C., Orliac, M., Permingeat, F., Parfenoff, A. (1969) L'henritérmierite, une nouvelle espèce minérale. *Bull. Soc. Franç. Min. Crist.*, 92, p. 185–190.

Ghergari, L., Ionescu, C. (1997) Hydrougrandite and magnesioferrite from Budureasa (Romania). *Rom. J. Miner.*, 78, 1, Abstr. vol, 1997, p. 22–23, Bucureşti.

Hsu, L. C. (1980) Hydration and phase relation of grossular-spessartine garnets at P_{H2O} = 2kb. *Contrib. Mineral. Petrol.*, 71, p. 407–415.

Lager, G. A., Armbruster, Th., Faber, J. (1987) Neutron and X-ray diffraction study of hydrogarnet $Ca_3Al_2(O_4H_4)_3$. *Am. Miner.*, 72, p. 756–765.

— , Armbruster, Th., Rotella, F. J., Rossman, G. R. (1989) OH substitution in garnets: X-ray and neutron diffraction, infrared, and geometric-modeling studies. *Am. Miner.*, 74, p. 840–851.

Marcke de Lummen, G. van (1986) Fluor-bearing hydro-andradite from an altered basalt in the Land's End area, SW England. *Bull. Mineral.*, 109, p. 613–616.

Nedelcu, C., Damian, St. (1982) Rezervaţia geologică Măgura Uroiului (Jud. Hunedoara). In *Monumente geologice din România.* Univ. Bucureşti, 1982, p. 71–74.

Onuki, H., Akasaka, M., Takeyoshi, Y., Nedachi, M. (1982) Ti-rich hydroandradite from Sanbagawa metamorphic rocks of the Shibukawa area, Central Japan. *Contrib. Mineral. Petrol.*, 80, p. 183–188.

Pabst, A. (1937) The crystal structure of plazolite. *Am. Miner.*, V, 22, p. 861–868.

Passaglia, E., Rinaldi, R. (1984) Katoite, a new member of the $Ca_3Al_2(SiO_4)_3$ - $Ca_2Al_2(OH)_{12}$ series and a new nomenclature for the hydrogrossular group of minerals. *Bull. Miner.*, 107, p. 605–618.

Peters, T. (1964) A water-bearing andradite from the Totalp serpentine (Davos, Switzeland). *Am. Miner.*, 50, p. 1482–1486.

Rossman, G. R., Aines, R. (1991) The hydrous component in garnets: Grossular - hydrogrossular. *Am. Mineral.*, 76, p. 1153–1164.

Schröpfer, L., Bartl, H. (1993) Oriented decomposition and reconstruction of hydrogarnet, $Ca_3.Al_2(OH)_{12}$. *Eur. J. Miner.*, 5, p. 1133–1144, Stuttgart.

Tsao, Y.-L. (1964) Hydrougrandite - a new variety of hydrogarnet from Hsiaosung shan. *Acta Geol. Sinica*, 44, 2, p. 219–228.

Weiss, R., Grandjean, D., Palvin, J. L. (1964) Structure de l'aluminate tricalcique hydrate, $3CaO.Al_2O_3.6H_2O$. *Acta Cryst.*, 17, p. 1329–1330.

Winchell, A. N. (1933) Elements of Optical Mineralogy, Part II, 3-rd ed. John Wiley and Sons, New York.

Yoder, H. S. (1950) Stability relations of grossularite. *Jour. Geol.*, 58, p. 221–253.

*** * * (1967)** International Mineralogical Association: Commission on New Minerals and Mineral Names. *Min. Mag.*, 36, 133 p.

Rom. J. Mineralogy. 79, p. 105-111, Bucureşti, 1999

MINERALOGICAL AND GEOCHEMICAL CONSIDERATIONS ON THE MAGNESIO-HORNBLENDE FROM THE AMPHIBOLITES OF BUZIAŞ-SACOŞU MARE AREA

Ovidiu Gabriel IANCU

Universitatea "Al. I. Cuza", Secţia de Mineralogie şi Geochimie, B-dul Copou nr. 20 A, 6600, Iaşi, Romania

Yasunori MIURA

Yamaguchi University, Faculty of Science, 1677-1, Oaza-Yoshida, Yamaguchi, 753, Japan

Key words: Magnesio-hornblende. Amphibolites. Optical data. Electron microprobe analysis, XRD-data. Supragetic Nappes. Timiş-Boia Nappe. Lotru Lithogroup. Buziaş Hills.

Abstract: Close to Buziaş (northwest of the Semenic Mountains), nearby the Silagiu village, magnesio-hornblende was found in massive (metagabbros) and foliated amphibolites (with diablastic and nematoblastic schistosity) belonging to the Lotru Lithogroup considered to represent a supracrustal megasequence including oceanic-type metasediments and tectonic slabs of dismembered oceanic crust (Iancu, Mărunţiu, 1994). Following the modern nomenclature of the amphiboles (Leake, 1978), hornblende from six samples, representing quartz-bearing amphibolites with plagioclase (An_{19-49}) + hornblende + quartz ± epidote, biotite, apatite, sphene and ilmenite as characteristic mineralogical assemblage, was determined to be magnesio-hornblende by optical microscopy, scanning electron microscopy with energy dispersive X-ray analysis (EPMA) and X-ray powder diffractometry. In thin sections it appears as prisms with high refractive indices, moderate to strong pleochroism (variable in greens), perfect cleavage (110) and optically negative character. The cation structural positions calculated to 23 (O) from the quantitative chemical analysis on a anhydrous basis, show the following important contents: $(Ca + Na)_{M4} > 1.34$ (1.92 to 2.12), $Na_{M4} < 0.67$ (0.20 to 0.32), $(Na + K)_A < 0.5$ (0.28 to 0.40), $Mg/(Mg + Fe^{2+})$ between 0.63 and 0.68 and Si from 6.50 to 6.74 pfu. The estimation of Fe^{3+} , which places all the Na in M4 site, was based on the following stoichiometric recalculation (acc. to Spear, 1993): Si + Al + Ti + Mg + Fe + Mn + Ca + Na = 15.

1. Introduction

From the earliest days of geological research, amphiboles have played a central role in studies of metamorphic rocks because they lie in a central position in terms of the range of bulk chemistries of rocks and they can accurately transmit through colour, optical properties and chemistry, much information about their history and condition of formation. Amphiboles are especially abundant in calc-alkaline plutonic rocks and amphibolite grade metamorphic rocks where they often constitute the only ferromagnesian phase.

The first purpose of this paper is to analyse the hornblende from the amphibolites belonging to the Lotru Lithogroup of the Buziaş-Sacoşu Mare crystalline island. The main reason for that was inspired by the modern nomenclature of amphiboles (Leake, 1978), where hornblende is never used without an adjective. This nomenclature is sufficiently flexible to encompass the chemical variations within the group of amphiboles. The new classification is based largely on crystal chemistry, having as its foundation the chemical contents of the formula unit calculated to 24 (O, OH, F, Cl) or to 23 (O) equivalents when H_2O has not been determined (i.e. where EPMA analysis was used) or is thought to be unreliable (Hawthorne, 1985).

The second purpose of our work is to attempt to interpret the message recorded by hornblende regarding the conditions of metamorphism (P-T) at which the host amphibolites have formed, by using a new hornblende-plagioclase thermometer (Holland, Blundy, 1994).

2. Geological Setting

As a result of some geological prospections for iron deposits in the Buziaş-Sacoşu Mare area, Rădulescu et al. (1962) divided the mesometamorphic rocks in five petrographic complexes: 1 - the micaceous complex which consists of micaschists with garnet, muscovite and biotite; 2 - the feldspathic complex, formed of muscovite-biotite paragneisses, paragneisses with almandine, injection gneisses and pegmatites; 3 - the quartzitic complex, represented by kyanite-bearing quartzites and quartzitic schists; 4 - the amphibolic complex, characterized by amphibolites, amphibolic schists and amphibole gneisses; 5 - the limestone complex, composed mainly of limestones.

Maier (1979) divided the same rocks into two complexes: 1 - the paragneisses complex, which reminds of the Băuţar formation from Poiana Ruscă, and 2 - the micaschists complex and assigned them to the Upper Precambrian (Riphean), because of their lithological and metamorphic similarity with the Sebeş-Lotru Group from the Poiana Ruscă and Semenic Mountains. In the same author's opinion , the pre-Alpine metamorphosed formations described above were considered to be part of the Supragetic Unit.

According to Săndulescu (1984), the particular litho-stratigraphic sequence from Valeapai and Buziaş crystalline island supports the idea of considering it as a different tectonic unit, the most internal one from the Median Dacides in the South Carpathians.

Close to Buziaş, nearby the Silagiu village, on the Guranului Brook, a metamorphosed Fe-Cu-Ni mineralization was identified by Iancu (1992) in a lense-shaped amphibolite body with metagabbros and foliated amphibolites located within plagiogneisses. Taking into account the classification made by Godlevski and Lihacev (1979, fide Udubaşa et al., 1988), which is based on the Mg concentration of the host rock, the Ni: Cu ratio and the $\delta\ ^{34}S$ value of pyrrhotite, the mineralization from the Guranului Brook was assigned to the medium temperature group of the Ni-Cu magmatic deposits.

Berza et al. (1994) pointed out that the basement formations from the Buziaş Hills and those in the Tincova-Ruşchiţa-Alunu-Ghelar area from the Poiana Ruscă Mountains represent the western outcrop region of the Timiş-Boia (Laramian) Nappe, a tectonic unit of the Getic-Supragetic thrust sheets.

Iancu and Mărunţiu (1994) defined the Lotru Group as a supracrustal megasequence including oceanic-type metasediments and tectonic slabs of dismembered oceanic crust: metaperidotites and metagabbros (displaying relict cumulus structures) and acid ortho-derivates .

By palynological studies, Iancu (1995, unpublished data) found a Vendian age (Upper Riphean) for the mesometamorphic rocks of the Buziaş Hills .

Balintoni (1997) considered that toward the western part of the Poiana Ruscă Massif the overthrust plane of the Timiş-Boia Nappe is crossing Valeapai region , including the Buziaş-Sacoşu Mare crystalline island and at least in part the Serbo-Macedonean Massif.

3. Samples

To establish the mineralogical and geochemical features of magnesio-hornblende, six samples representing amphibolites (metabasites) of the amphibolite and epidote amphibolite (transitional) facies were investigated in this study and they are listed in Table 1.

The standard samples used for calibration during the quantitative electron microprobe analyses of the amphibole were synthetic oxides for Si, Al, Mg, Fe, Ti, Mn and P and natural oxides for Na, K, Ca and S (acc. to Miura and Matsumoto, 1982), and they were regularly analyzed during the analytical runs, to check on instrument stability.

4. Analytical Methods

Six polished thin sections (PTS) representing the samples presented in Table 1 were studied under the optical microscope. Quantitative chemical analyses of the magnesio-hornblende were obtained on the carbon-coated, polished thin sections by using a JSM-5400 (with JED 2001 energy dispersive X-ray analysis) scanning electron probe microanalyzer (EPMA) at the Yamaguchi University, Japan. The instrument was operated at an accelerated voltage of 15kV, a 38.5 nA beam current and 35 mm working distance. The cell parameters and density of magnesio-hornblende were determined from the X-ray diffraction pattern by using a RIGACU computer assisted diffractometer (radiation CuKα) and a non-linear least squares cell refinement computer program with regression-diagnostics (acc. to Holland, Redfern, 1997).

5. Mineralogical and Geochemical Aspects

In thin section, magnesio-hornblende appears as prism with high refractive indices, moderate to strong pleochroism (variable in greens), perfect cleavage (110) and optically negative character. The mineral was also studied under back scattered electron image (BEI) for higher magnifications (up to x 200,000) with a JEOL scanning electron microscope. The size of the mentioned amphibole in our samples ranges from 0.1 mm to 7 mm.

Table 1
Samples used in this study

Sample	Rock type	Provenance	Characteristic mineralogical assemblage	Facies
3	amphibolite	Pietrei Brook (Silagiu)	Andesine (An_{49}), Hornblende, Apatite, Titanite	Amphibolite facies
5	amphibolite	Pietrei Brook (Silagiu)	Andesine (An_{33}), Hornblende, Quartz, Apatite	Aphibolite facies
8	metagabbro	Guranului Brook (Silagiu)	Oligoclase (An_{19}), Hornblende, Quartz, Apatite, Titanite, Epidote	Epidote Amphibolite facies
9	amphibolite	Guranului Brook (Silagiu)	Andesine (An_{43}), Hornblende, Quartz, Apatite, Titanite, Biotite	Amphibolite facies
13	amphibolite	Piatra Babei Brook (Silagiu)	Andesine, Hornblende, Quartz, Apatite, Titanite, Epidote	Epidote Amphibolite facies
19	amphibolite	Quarry (Seismic Station, Buziaş)	Andesine (An_{49}), Hornblende, Quartz, Apatite, Titanite, Epidote	Epidote Amphibolite facies

Table 2
Cell dimensions of magnesio-hornblende from Buziaş-Sacoşu Mare area

Cell parameters	Samples						
	MH - 3	MH - 5	MH - 8	MH - 9	MH - 13	MH - 19	MH (IMA files)*
$a(A^0)$	9.775	9.532	9.500	9.794	9.793	9.749	9.783
$b(A^0)$	18.019	18.153	18.168	17.854	17.943	18.036	17.935
$c(A^0)$	5.301	5.322	5.305	5.329	5.313	5.299	5.297
$\beta(^0)$	104.53	103.02	102.78	104.65	104.70	104.28	104.60
$V_x(A^{03})$	903.76	897.157	893.015	901.587	903.021	902.884	899.920
$d_x(g/cm^3$	3.17	3.19	3.21	3.18	3.18	3.18	-

* After Bayliss et al., 1993

Table 3
Electron probe chemical analyses of individual magnesio-hornblende from the amphibolites of Buziaş Hills

Weight % oxides	Samples					
	MH - 3	MH - 5	MH - 8	MH - 9	MH - 13	MH - 19
SiO_2	45.57	45.95	46.71	46.66	46.38	46.13
Al_2O_3	11.93	12.40	12.53	11.67	11.92	12.13
TiO_2	0.78	0.70	0.44	0.79	0.48	0.36
FeO*	12.54	13.34	13.47	12.75	12.89	13.21
MnO	0.66	0.48	0.58	0.51	0.67	0.59
MgO	12.94	12.72	12.41	13.34	12.96	12.45
CaO	11.99	11.22	11.47	11.10	11.79	11.58
Na_2O	1.07	1.19	0.98	0.84	0.73	1.09
K_2O	0.52	0.20	0.31	0.44	0.38	0.46
LOI	2.00	1.80	1.10	1.90	1.80	1.80
TOTAL	100.00	100.00	100.00	100.00	100.00	100.00

* FeO as total iron
Analysed by O. G. Iancu

Table 4

Cation structural positions of magnesio-hornblende analyses showing range of Fe^{3+} recalculations (1) (as Spear, 1993)

Cation Structural Positions	Samples											
	MH - 3		MH - 5		MH - 8		MH - 9		MH - 13		MH - 19	
	All Fe^{2+}	$\sum Na=15$	All Fe^{2+}	$\sum Na=15$	All Fe^{2+}	$\sum Na=15$	All Fe^{2+}	$\sum Na=15$	All Fe^{2+}	$\sum Na=15$	All Fe^{2+}	$\sum Na=15$
Si (T)	6.636	6.483	6.659	6.506	6.718	6.594	6.744	6.632	6.718	6.594	6.710	6.569
Al^{IV} (T)	1.364	1.517	1.341	1.494	1.282	1.406	1.256	1.368	1.282	1.406	1.290	1.431
Al^{VI} (M2)	0.683	0.483	0.777	0.575	0.842	0.679	0.733	0.588	0.753	0.592	0.790	0.605
Ti (M2)	0.086	0.084	0.077	0.075	0.048	0.047	0.086	0.085	0.052	0.051	0.039	0.038
Fe^{3+}(M2)	-	1.056	-	1.056	-	0.844	-	0.762	-	0.843	-	0.968
Mg(2)	2.809	2.744	2.748	2.685	2.660	2.611	2.875	2.827	2.799	2.748	2.700	2.643
Fe^{2+}(2)	1.527	0.431	1.617	0.523	1.620	0.747	1.541	0.753	1.561	0.690	1.607	0.606
Mn(2)	0.081	0.079	0.059	0.058	0.071	0.070	0.063	0.062	0.082	0.080	0.073	0.071
Ca (M4)	1.870	1.827	1.742	1.702	1.767	1.734	1.719	1.690	1.829	1.795	1.805	1.767
Na (M4)	-	0.296	-	0.326	-	0.268	-	0.233	-	0.201	-	0.302
Na (A)	0.303	-	0.334	-	0.273	-	0.236	-	0.205	-	0.308	-
K (A)	0.096	0.096	0.037	0.037	0.057	0.057	0.082	0.082	0.070	0.070	0.086	0.086
Total	15.46	15.10	15.39	15.04	15.34	15.06	15.34	15.08	15.35	15.07	15.41	15.09
$Mg/(Mg+Fe^2)$	0.68		0.64		0.63		0.66		0.68		0.63	
$(Na+K)_A$	0.399		0.371		0.330		0.318		0.275		0.394	
$Al^{VI}+Fe^{3+}+Ti$	1.623		1.706		1.570		1.435		1.486		1.611	
$(Ca+Na)_{M4}$	2.123		2.028		2.002		1.923		1.996		2.069	

(1) Estimation of Fe^{3+} as of Spear (1993), based on the following stoichiometric recalculation:
Si + Al + Ti + Mg + Fe + Mn + Ca + Na = 15 (this recalculation places all the Na in M4).

(2) Mg, Fe^{2+} and Mn are distributed among the M1, M2, M3 and M4 sites according to cation site preferences.

Table 5

The formula of magnesio-hornblende from Buziaş-Sacoşu Mare Area

Sample	Calculated Formula
MH-3	$K_{0.096}(Na_{0.296}Ca_{1.827})_{2.123}(Fe^{2+}_{0.431}Mg_{2.744}Mn_{0.079})_{3.254}(Al^{VI}_{0.483}Fe^{3+}_{1.056}Ti_{0.084})_{1.623}(Si_{6.483}Al^{IV}_{1.517})_{8.00}O_{23}$
MH-5	$K_{0.037}(Na_{0.326}Ca_{1.702})_{2.028}(Fe^{2+}_{0.523}Mg_{2.685}Mn_{0.058})_{3.266}(Al^{VI}_{0.575}Fe^{3+}_{1.056}Ti_{0.075})_{1.706}(Si_{6.506}Al^{IV}_{1.494})_{8.00}O_{23}$
MH-8	$K_{0.057}(Na_{0.268}Ca_{1.734})_{2.002}(Fe^{2+}_{0.747}Mg_{2.611}Mn_{0.070})_{3.428}(Al^{VI}_{0.679}Fe^{3+}_{0.844}Ti_{0.047})_{1.570}(Si_{6.594}Al^{IV}_{1.406})_{8.00}O_{23}$
MH-9	$K_{0.082}(Na_{0.233}Ca_{1.690})_{1.923}(Fe^{2+}_{0.753}Mg_{2.827}Mn_{0.062})_{3.642}(Al^{VI}_{0.588}Fe^{3+}_{0.762}Ti_{0.085})_{1.435}(Si_{6.632}Al^{IV}_{1.368})_{8.00}O_{23}$
MH-13	$K_{0.070}(Na_{0.201}Ca_{1.795})_{1.996}(Fe^{2+}_{0.690}Mg_{2.748}Mn_{0.680})_{3.510}(Al^{VI}_{0.592}Fe^{3+}_{0.843}Ti_{0.051})_{1.486}(Si_{6.594}Al^{IV}_{1.406})_{8.00}O_{23}$
MH-19	$K_{0.086}(Na_{0.302}Ca_{1.767})_{2.069}(Fe^{2+}_{0.606}Mg_{2.643}Mn_{0.071})_{3.320}(Al^{VI}_{0.605}Fe^{3+}_{0.968}Ti_{0.038})_{1.614}(Si_{6.569}Al^{IV}_{1.431})_{8.00}O_{23}$
MH (IMA files)*	$K_{0.030}(Na_{1.060}Ca_{1.170})_{2.260}(Fe^{2+}_{0.990}Mg_{2.830}Mn_{0.000})_{3.240}(Al^{VI}_{0.720}Fe^{3+}_{0.990}Ti_{0.050})_{1.760}(Si_{7.060}Al^{IV}_{0.940})_{8.00}O_{22}(OH)_2$

* After Bayliss et al., 1993

The unit cell parameters and density of magnesio-hornblende from our samples were determined from the X-ray diffraction pattern by using a RIGAKU computer assisted diffractometer (radiation CuKα; λ = 1.5406) and a non-linear least squares cell refinement program with regression-diagnostics (Holland , Redfern, 1997). The results are in accordance with the cell dimensions of magnesio-hornblende from the IMA (International Mineralogical Association) files and are presented in Table 2 .

The quantitative chemical analyses of the magnesio-hornblende from the amphibolites of the Buziaş Hills are listed in Table 3 .

A standard amphibole formula (after Leake, 1978) is: $A_{0-1}\ B_2\ C^{VI}{}_5\ T^{VI}{}_8\ O_{22}\ (OH, F, Cl)_2$, where A = alkali site (Na, K), B = M_4 metal site (Na, Li, Ca, Mn, Fe^{2+}, Mg), C = $M_1 + M_2 + M_3$ metal sites (Mn, Fe^{2+}, Mg, Al, Fe^{3+}, Ti, Li, Zn, Cr) and T = tetrahedral site (Si, Al). As noted by Spear (1993), by far and away the best way to infer a structural formula is to measure directly the most sensitive elements by wet chemistry, Mössbauer spectroscopy and X-ray crystallography. However, electron microprobe analysis is the analytical method of choice for most petrological work, so the uncertainties inherent in calculation of a structural formula from such data must be understood and appreciated. The cation structural positions of magnesio-hornblende analyses showing range of Fe^{3+} recalculations (as of Spear, 1993) and the structural formula are presented bellow (Tables 4 and 5).

The structural values of the hornblende plotted on the $(Na+K)_A$/Si pfu diagram (acc. to Deer et al., 1992) and on the diagram representing the nomenclature of calcic amphiboles with $(Na+K)_A < 0.50$ and Ti pfu < 0.50 (after Hawthorne, 1985) as well as the contents of Si pfu, Na_{M4}, $(Ca+Na)_{M4}$, $(Na+K)_A$ and of the $Mg/(Mg+Fe^{2+})$ ratio (acc. to Leake et al., 1997), show the presence of the magnesio-hornblende in the metabasites of Buziaş-Sacoşu Mare area (Figs. 1, 2).

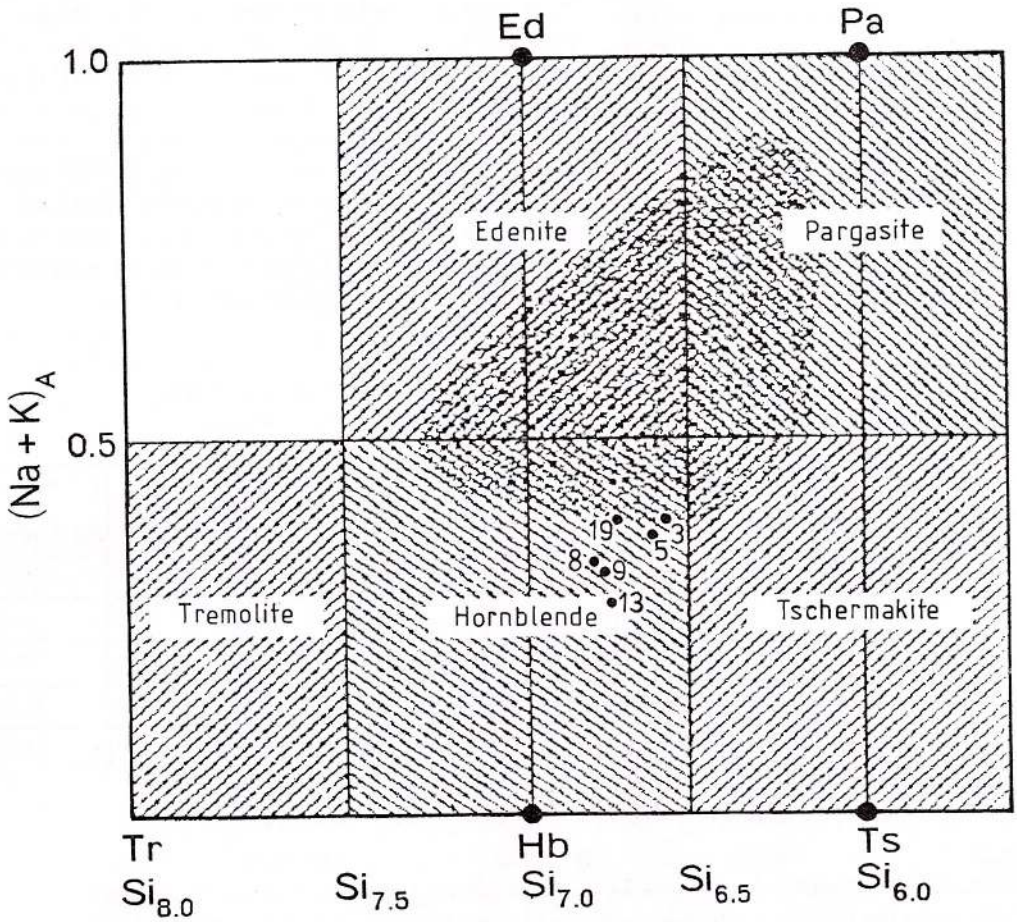

Fig. 1 – Plot of the magnesio-hornblende from the Buziaş Hills on the $Mg/Mg+Fe^{2+}$ diagram representing the nomenclature of the calcic amphiboles with $(Na+K)_A < 0.50$ and Ti < 0.50 (after Hawthorne, 1985).

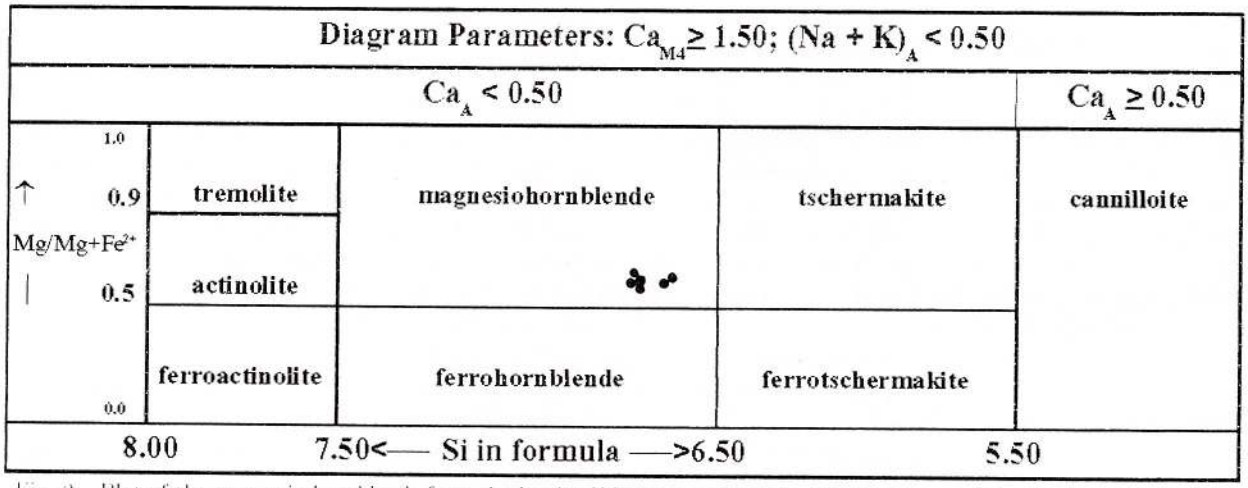

Fig. 2 - Plot of the magnesio-hornblende from the Buziaş Hills on the $(Na+K)_A$/Si pfu diagram (after Leake et al., 1997).

6. Petrologic considerations

As of Spear (1993), it has been somewhat of a "Holy Grail" to calibrate the composition of amphibole as a function of P and T so that this mineral can be used as a monitor of metamorphic grade.

A computer application for performing the thermometric calculations based on a new hornblende-plagioclase thermometer (Holland, Blundy, 1994) was used in this study to estimate the temperatures and pressures under which the amphibolites with magnesio-hornblende from the Buziaş Hills have formed and these range between 550°C - 700°C and 5 kbars (epidote amphibolite or amphibolite facies conditions). This thermometer is available under some compositional restrictions (Table 6).

The alkali site occupancy $(Na+K)_A$ is thought to reflect the relative temperature of metamorphism because the edenite exchange in amphiboles is believed to be largely temperature sensitive (Spear, 1993). Similarly, the Al^{VI} content is a measure of the amount of tschermak and glaucophane exchanges. It is generally acknowledged, all other things being equal, that at low pressure aluminium is favored in the tetrahedral site (i.e., Al^{VI}) and at high pressure aluminium is favored in the octahedral site (i.e., Al^{VI}). By plotting the values of the magnesio-hornblende analysed in this study on the $Na^{M4}/Al^{VI} + Fe^{3+} + Ti$ diagram (acc. to Laird, 1982) we can observe in which index mineral zone, the host amphibolite was formed and this is the garnet zone to the lower limit of the staurolite zone (Fig. 3).

Table 6

Calculated temperatures and pressures based on the Holland, Blundy (1994) thermometer for the amphibolites of Buziaş - Sacoşu Mare region

Sample No.	Ab content of plagioclase	An content of plagioclase	X_{ab} **	X_{an} **	$Na(M_4)$ in Hbl	Al^{VI} pfu in Hbl	Si pfu in Hbl	P (kb)	T (°C)
3	47.7	48.8	0.48	0.49	0.296	0.483	6.483	5	706
5	57.8	38.9	0.58	0.39	0.326	0.575	6.506	5	666
8	78.5	18.7	0.79	0.19	0.268	0.679	6.594	5	549
9	54.2	42.6	0.54	0.43	0.233	0.588	6.632	5	647
19	49.5	48.4	0.50	0.49	0.302	0.605	6.569	5	670

* Holland and Blundy (1994) thermometer is based on the following reaction:

$NaCa_2Mg_5(AlSi_3)Si_4O_{22}(OH)_2 + NaAlSi_3O_8 = Na(CaNa)Mg_5Si_8O_{22}(OH)_2 + CaAl_2Si_2O_8$

edenite albite richterite anorthite

The edenite-richterite thermometer can be used for assemblages with or without quartz, in the range 500 - 900 °C and under the following compositional restrictions: plagioclase feldspars must lie in the range Xan > 0.1 and < 0.9, amphiboles must have Na(M4) > 0.03, Al^{VI} < 1.8 pfu, and Si in the range 6.0 - 7.7 pfu.

** X_{ab} şi X_{an} can be obtained by dividing the Ab and An content of plagioclase with 100.

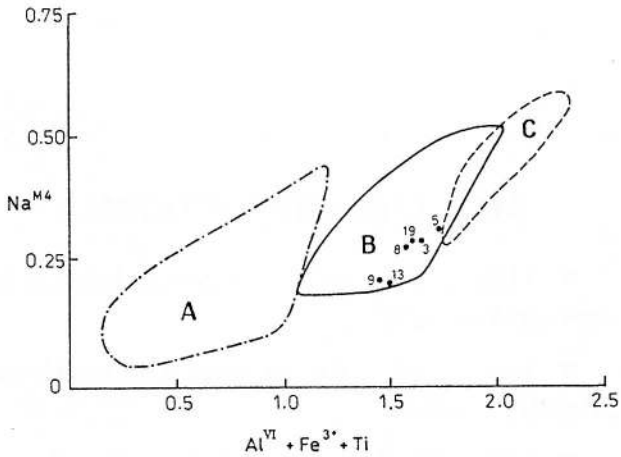

Fig. 3 Plot of the magnesio-hornblende from the Buziaş Hills on the $Na^{M4}/Al^{VI}+ Fe^{3+} +Ti$ diagram. A - Biotite zone; B - Garnet zone; C - Staurolite - Kyanite zone (A, B, C fields acc. to Laird, 1982).

7. Conclusions

Although a common mineral in metabasites, following the modern nomenclature of amphiboles, by optical microscopy, scanning electron microscopy with energy dispersive X-ray analysis (EPMA) and X-ray powder diffractometry, in this study we identified undoubtedly the presence of magnesio-hornblende as a separate mineral species, in massive (metagabbros) and foliated amphibolites (with diablastic and nematoblastic schistosity) belonging to Buziaş-Sacoşu Mare crystalline island.

Acknowledgments

Financial support was provided in part by a grant from the Japanese Ministry of Education, Science and Culture (Monbusho) to the senior author.

Received: November, 1997
Accepted: April, 1998

References

Bayliss, P., Erd, R. C., Mrose, M., Roberts, A. C., Sabina, A.P. (1993) Mineral Powder Diffraction File Databook. International Centre for Diffraction Data, 781 p., Swarthmore, Pennsylvania.

Balintoni, I. (1997) Geotectonica terenurilor metamorfice din România. Ed. Carpatica, 176 p., Cluj-Napoca.

Berza, T., Balintoni, I., Iancu, V., Seghedi, A., Hann, H. P. (1994) South Carpathians. *Rom. J. Tect. & Reg. Geol.*, 75, Suppl. 2, p. 93–103, Bucureşti.

Deer, W. A., Howie, R. A., Zussman, J. (1992) An introduction to the rock forming minerals. Longman Group UK Essex, 549 p., London.

Hawthorne, F. C. (1995) Crystal chemistry of the amphiboles. *Reviews in Mineralogy*, 9A, Mineralogical Society of America, p. 1–95, Blacksburg, Virginia.

Holland, T. J. B., Blundy, J. (1994) Non-ideal interactions in calcic amphiboles and their bearing on amphibole-plagioclase thermometry. *Contrib. Mineral. Petrol.* 116, Springer-Verlag, p. 433–447, Berlin Heidelberg .

— , **Redfern, S. A. T. (1997)** Unit cell refinement from powder diffraction data: the use of regression diagnostics. *Miner. Mag.*, 61, p. 65–77, London.

Iancu, O. G. (1992) Mineral assemblages of a metamorphosed Iron-Copper-Nickel mineralization from the Semenic Mountains. *Rom. J. Miner.*, 75, Suppl. 2, p. 15–16, Bucureşti.

Iancu, V., Mărunţiu, M. (1994) Pre-Alpine litho-tectonic units and related shear zones in the basement of the Getic-Supragetic Nappes (South Carpathians). *Rom. J. Tect. & Reg. Geol.*, 75, Suppl. 2, p. 87–92, Bucureşti.

Laird, J. (1982) Amphiboles in metamorphosed basaltic rocks: greenschist facies to amphibolite facies. *Reviews in Mineralogy*, 9B, Mineralogical Society of America, p. 113–135, Chelsea, Michigan.

Leake, B. E. et al. (1997) Nomenclature of amphiboles. Report of the Subcommittee on Amphiboles of the IMA-CNMMN. *Amer. Miner.*, 82, p. 1019–1037, Washington.

Maier, O. W. (1979) The pre-Alpine metamorphosed formations from the Supragetic Unit of Banat (Romania). *Rev. roum. géol., géophys., géogr. (Géologie)*, 23, 2, p. 137–147, Bucureşti.

Miura, Y., Matsumoto, Y. (1982) Classification of several Yamato-75 chondrite (IV). *Mem. Nat. Inst. Polar Res.*, Spec. Issue, 25, p. 1–16, Tokyo.

Rădulescu, I., Trifulescu, M., Dragomir, N., Arsenescu, V. (1962) Report, I.G.R. archives, Bucureşti.

Săndulescu, M. (1984) Geotectonica României. Ed. Tehnică, 365 p., Bucureşti.

Spear, S. F. (1993) Metamorphic Phase Equilibria and Pressure-Temperature-Time Paths. Mineralogical Society of America, 799 p., Washington.

Udubaşa G., Hârtopanu P., Hârtopanu I., Gheucă I., Dinică I. (1988) The metamorphosed Copper-Nickel mineralizations from the Vâlsan Valley, Făgăraş Mountains. *D. S. Inst. Geol. Geofiz.*, 72–73/2, p. 283–312, Bucureşti.

Russian Academy of Sciences

All-Russia Mineralogical Society

II International Mineralogical Seminar

HISTORY AND PHILOSOPHY OF MINERALOGY

October 4-8, 1999

Syktyvkar
Republic of Komi
Russia

MAIN CONFERENCE THEMES:

- History of mineralogy, interaction between mineralogical schools;
- Mineralogy in Russia, links with western and oriental countries;
- Mineralogy in former USSR and friendly countries: organization, development and results; experience of integration of research;
- Regular patterns in the origin and evolution of fundamental mineralogical ideas, change of scientific paradigms, philosophy of mineralogy;
- Archaeologic and etnographic mineralogy (special symposium).

Please, direct suggestions and requests for the First Circular to: Institute of Geology, 54 Pervomaiskaya St., Syktyvkar, 167610, Russia

Tel. +7 (8212) 42-00-37
+7 (8212) 42-51-67
Fax +7 (8212) 42-53-46
E-mail: histmin@geo.komi.ru

Mailing date of the First Circular: November 1, 1998

Rom. J. Mineralogy, 79, p. 113-122, Bucureşti, 1999

DETERMINATION OF SUBMICROSCOPIC GOLD AND SILVER IN ROMANIAN BASE-METAL ORES BY SECONDARY ION MASS SPECTROSCOPY

Nigel J. COOK

Mineralogisches Institut der Universität Würzburg Am Hubland, D-97074 Würzburg, Germany

Stephen L. CHRYSSOULIS

AMTEL, 100 Collip Circle, U.W.O. Research Park London, Ontario, Canada N6G 4X8

Key words: VMS ores. Hydrothermal ores. Baia Borşa. Herja. Nistru. Gold. Silver distribution in common sulphides.

Abstract: Preliminary investigation of Au and Ag contents in pyrite, chalcopyrite, sphalerite and arsenopyrite within samples of both metamorphosed VMS base-metal ore and Neogene hydrothermal Zn-Pb-Cu vein mineralisation from the Baia Borşa orefield, Maramureş, N-W Romania, has confirmed that the common sulphide minerals host detectable quantities of gold and silver. Furthermore, pyrite from the Herja and Nistru deposits, Gutâi Mts, Baia Mare metallogenic province, have also been determined to carry significant amounts of both gold and silver. Although of a preliminary nature, the data confirming the presence of both invisible silver and gold in several ores from northern Romania represent a valuable addition to the knowledge of precious metal distributions within these ores and have major implications for ore processing.

Introduction

The Baia Borşa Orefield is host to two distinct types of mineralisation: metamorphosed polymetallic volcanogenic massive sulphide (VMS) deposits situated within a volcano-sedimentary suite belonging to the Lower Cambrian Tulgheş Tg_3 Formation, and polymetallic epigenetic veins of Neogene age associated with the Toroioaga intrusive/subvolcanic massif. Both styles of mineralisation contain a similar range of sulphide minerals; pyrite + chalcopyrite, sphalerite, galena ± tetrahedrite-tennantite + Pb-sulphosalts (Radu, Cook, 1995; Cook, 1997b). Although the epigenetic ores contain higher values of the precious metals, the trace amounts of Au and Ag within the metamorphosed VMS ores are also of economic value and an understanding of their mineralogical distribution is essential. Knowledge of the mineralogical distribution of silver and gold in polymetallic sulphide ores is of considerable importance in choosing suitable processing technologies (Gasparrini, 1983; Chryssoulis, Cabri, 1990).

An increasing amount of data on the mineralogical distribution of the precious metals in the Baia Borşa deposits has become available in recent years through detailed microscopy and, most importantly, the application of electron probe microanalysis. Contributions include identification of the major role of galena as a silver carrier in both ore types (Cook, 1995) and the recognition that syn-metamorphic remobilisation of Au, and to a lesser extent also Ag, has had considerable effect on precious metal distributions in the metamorphosed ores (Cook, 1997b). Nevertheless, despite these advances, the mineralogical distributions for Ag and Au in the Baia Borşa ores remained poorly quantified, because previous studies have not addressed the role played by the common sulphide minerals, with the exception of galena, as precious metal carriers.

Many of the common sulphide minerals (pyrite, arsenopyrite, chalcopyrite, sphalerite), in different types of sulphide deposits, have been shown to take Au and/or Ag into their structures at concentrations well below the detection limit of conventional electron probe microanalysis (e.g. Chryssoulis et al., 1986; Chryssoulis, Surges, 1988; Cook, Chryssoulis, 1990; Cabri, 1992; Petruk, Wilson, 1993; Huston et al., 1995; Larocque et al., 1995a; b). In addition, submicroscopic ($< 1\mu m$) inclusion of Au/Ag, or minerals containing these metals, may be present within sul-

Table 1
Description and locality of samples

Sample	Locality	Ore type	Cu(%)	Zn(%)	Pb(%)	Ag(ppm)
Metamorphosed VMS ores						
BB127	Colbu Mine	Massive py ore	4.0	6.8	2.1	180
BB170	Măcârlău Mine	Massive py ore	1.1	13.6	5.1	220
BB329	Gura Băii Mine	Massive py ore	4.7	3.7	1.2	160
BB405	Dealul Bucăţii Mine	Massive py ore	-	-	-	-
BBC-1	Colbu Mine	Massive py ore	0.36	7.7	1.1	54
BBM-2	Măcârlău Mine	Remobilised cp	-	-	-	-
Hydrothermal vein-type ores						
BB191	Toroioaga Mine	Zn-Pb vein ore				
BBI-1	Ivaşcoaia Mine	Mineralised fracture				
BB372a	Colbu Mine	Mineralised fracture				

phide minerals and will not be observed during optical investigation. It is therefore imperative to take this "invisible" gold/silver into consideration when attempting to quantify the mineralogical distribution in a given deposit.

The development of advanced microbeam techniques, including secondary ion microprobe analysis (SIMS), has made it possible to measure element concentrations down to the sub-ppm level (Chryssoulis et al., 1987; 1989; Cabri, Chryssoulis, 1990; MacRae, 1995). The results of the preliminary study presented here represent the first attempt to measure invisible Au and Ag in the common sulphide within representative ore samples from Baia Borşa. Details of the sample suite are given in Table 1.

Table 2
Cameca IMS-3F ion microprobe operating conditions

Primary ions :	Cs^+
Secondary ions :	Au^- , Ag^-
Secondary matrix ions :	S^-, Fe^-, As^-
Primary ion energy :	10 kv (negative ions)
Primary current :	30 na
Crater size :	25 μm
Sputtering rates	
Arsenopyrite	13.5 $Å s^{-1}$
Chalcopyrite	11.1 $Å s^{-1}$
Pyrite	10.8 $Å s^{-1}$

Analytical

Analysis by SIMS was carried out at the laboratories of AMTEL, London, Ont. Canada on a CAMECA IMS-3f ion microprobe. Spot analyses, with a crater size of 26μm, were carried out on selected sulphide grains within carefully polished rock chip sections. Detection limits are on the order of 0.1 to 0.2 ppm, depending on mineral. Operating conditions are given in Table 2.

Results

(i) Metamorphosed VMS ores

Silver

Representative grains of pyrite, chalcopyrite and sphalerite from several ore lenses (Dealul Bucăţii, Colbu, Măcârlău, Gura Băii) were analysed. Results are given in Table 3; concentrations and distributions are presented as histograms in Figure 1.

Sphalerite is the second most abundant sulphide mineral in the metamorphosed ores, and invisible Ag was detected in all samples, with an average concentration of approximately 10 ppm (Tab. 3; Fig. 1a). The very widespread of the data indicates a heterogeneous distribution of Ag, an interpretation echoed by the identification of submicroscopic (0.1μm) inclusions of Ag-minerals in the depth profile of several grains.

Chalcopyrite. Concentrations of invisible silver in chalcopyrite display a comparably inhomogeneous distribution to sphalerite (Fig. 1b). Although two samples had mean values around 10 ppm, one sample contained appreciably higher concentrations, which significantly fall within a narrow range (BB127; 54±7 ppm). There is no evidence for submicroscopic inclusions of gold minerals and the reasons for Ag enrichment in chalcopyrite in this one sample are not clear.

Pyrite is the most abundant sulphide mineral in all samples and the presence of invisible Ag has been confirmed. The mean content of the five individual samples varies considerably (Tab. 3; Fig. 1c), but no evidence of higher concentration in Cu- or Zn-Pb rich ores is noted. The mean Ag content of 18 grains in five samples is 7.3±5.0 ppm.

Table 3
Ion microprobe analyses on mineral grains (ppm)

	Ag (ppm)	Au (ppm)
Metamorphosed VMS ores:		
BB127		
Chalcopyrite	56;57;64;51;60;58;39;49	0.14;0.06;0.12;0.12;0.08;0.05;0.08;0.18
Pyrite	5.1;3.9;8.1;7.7;11	0.26;0.26;0.50;0.39;0.34
BB170		
Sphalerite	2.8;34;30;14;7.7;17	
Pyrite	14;7.2;12;13;19	0.34;0.49;0.28;0.43;1.5
BB329		
Chalcopyrite	11;6.2;15;3.4	0.34;0.46;0.23;0.48
Pyrite	3.3;2.6	0.53;0.18
BB405		
Sphalerite	9.7;10;4.7;15	
Pyrite	11;6.9	0.37;0.44
BBC-1		
Sphalerite	31;17;9.3;2.3;9.6;3.1	
Pyrite	1.2;2.6;2.3;0.67	0.17;2.6;2.3;0.67
BBM-2		
Chalcopyrite	13;29;11;7.1;12;9.0;11	0.31;0.55;0.29;0.44;0.50;0.31;0.40
Hydrothermal vein-type ores:		
BB191		
Sphalerite	1.1;1.7;0.83;0.96;1.3;2;0.94;2.4;8.8	
Chalcopyrite	11;26;40;15;28	0.25;0.22;0.23;0.32;0.23
Pyrite	17;7;8.1;4.2;10;13;14;9.2	1.0;1.0;0.57;0.26;0.52;0.88;0.44;0.49
BB372a		
Sphalerite	0.41;0.96	
Arsenopyrite		5.7;2.6;4.9;1.1;2;20;1.2;3.6;0.52
Pyrite	3.5;6.5;9.3;7.2;11	0.45;0.34;0.84;0.41;0.53
BBI-1		
Arsenopyrite		14;32;12;89;36;56;70
Pyrite	13;24	0.65;2.2
8255 (Herja)		
Pyrite	11;15;43;29;36	10; 15;66;47;5;10;34
22N (Nistru)		
Pyrite	21;26;32;26;92;44;75;1;26	17;34;37;46;54;64;45;0.16;3.8

Gold

Pyrite grains in five samples have been analysed for Au. Concentrations are in all cases low, only exceeding 1.0 ppm in a single case (Tab. 3; Fig. 2a). No systematic variation between different sample types is noted and there is no suggestion of micro-inclusions or for inhomogeneous An distributions within individual pyrite grains.

Chalcopyrite only contains Au at levels very close to the detection limit (Tab. 3; Fig. 2b).

(ii) Hydrothermal vein ores

A small number of samples from Toroioaga mine (Caterina vein) and mineralised fractures within the Colbu and Măcârlău Mines were studied. Since the study is exploratory in nature, the sample suite cannot be considered as fully representative of the wide variety of assemblages and textures present within the vein systems.

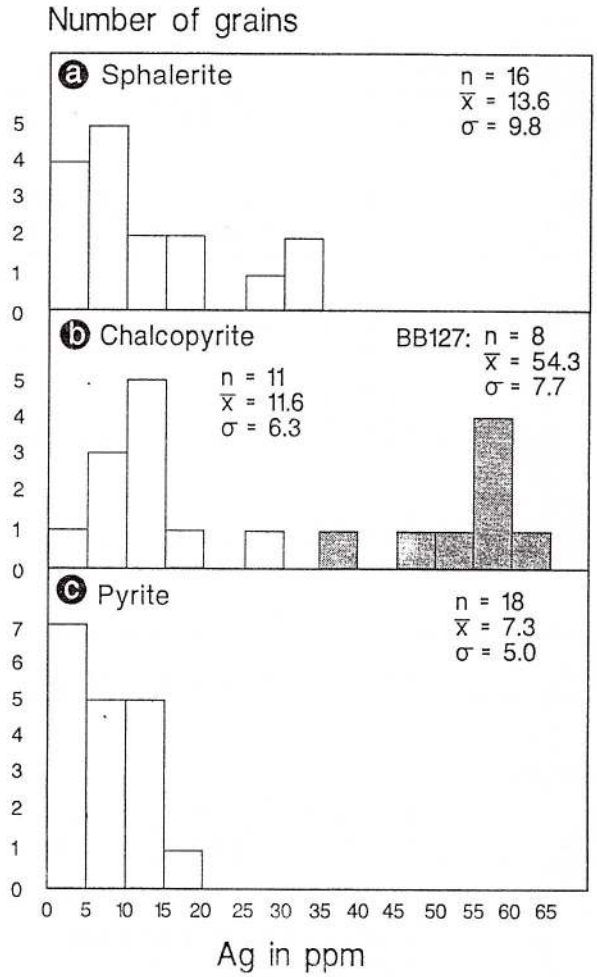

Fig. 1 – Histograms of Ag concentrations in (a) sphalerite, (b) chalcopyrite and (c) pyrite in the metamorphosed VMS ores, expressed in ppm.

Silver

Analytical results on sphalerite, chalcopyrite and pyrite are given in Table 3 and shown as histograms in Figure 3a-c.

Sphalerite. Only very low concentrations are detected (mean 2 ppm).

Chalcopyrite. Significant concentration of Ag are present in the single chalcopyrite sample measured. The silver is present as widely distributed micro-inclusions ($< 1\mu$m) throughout the chalcopyrite crystals, as shown on the two depth profiles (Fig. 4a, b).

Pyrite. Both analysed samples from the Toroioaga mineralisation contain Ag at low to moderate concentrations, in the range 4 to 24 ppm.

Gold

Analytical results for arsenopyrite and chalcopyrite are given in Table 3 and shown as hystograms in Figure 5.

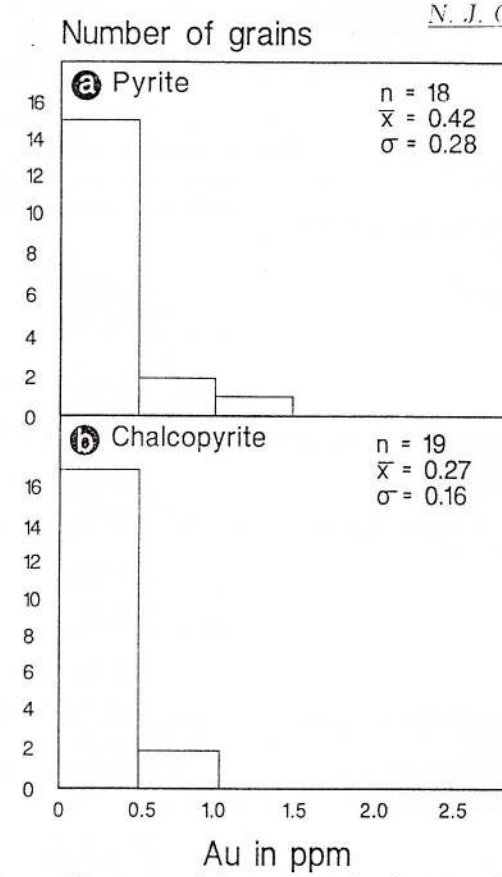

Fig. 2 – Histograms of Au concentrations in (a) pyrite and (b) chalcopyrite in the metamorphosed VMS ores, expressed in ppm.

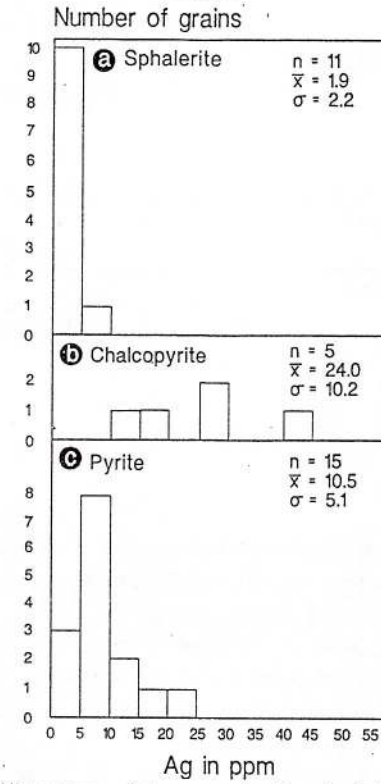

Fig. 3 – Histograms of Ag concentrations in (a) sphalerite, (b) chalcopyrite and (c) pyrite in the hydrothermal vein ores, expressed in ppm.

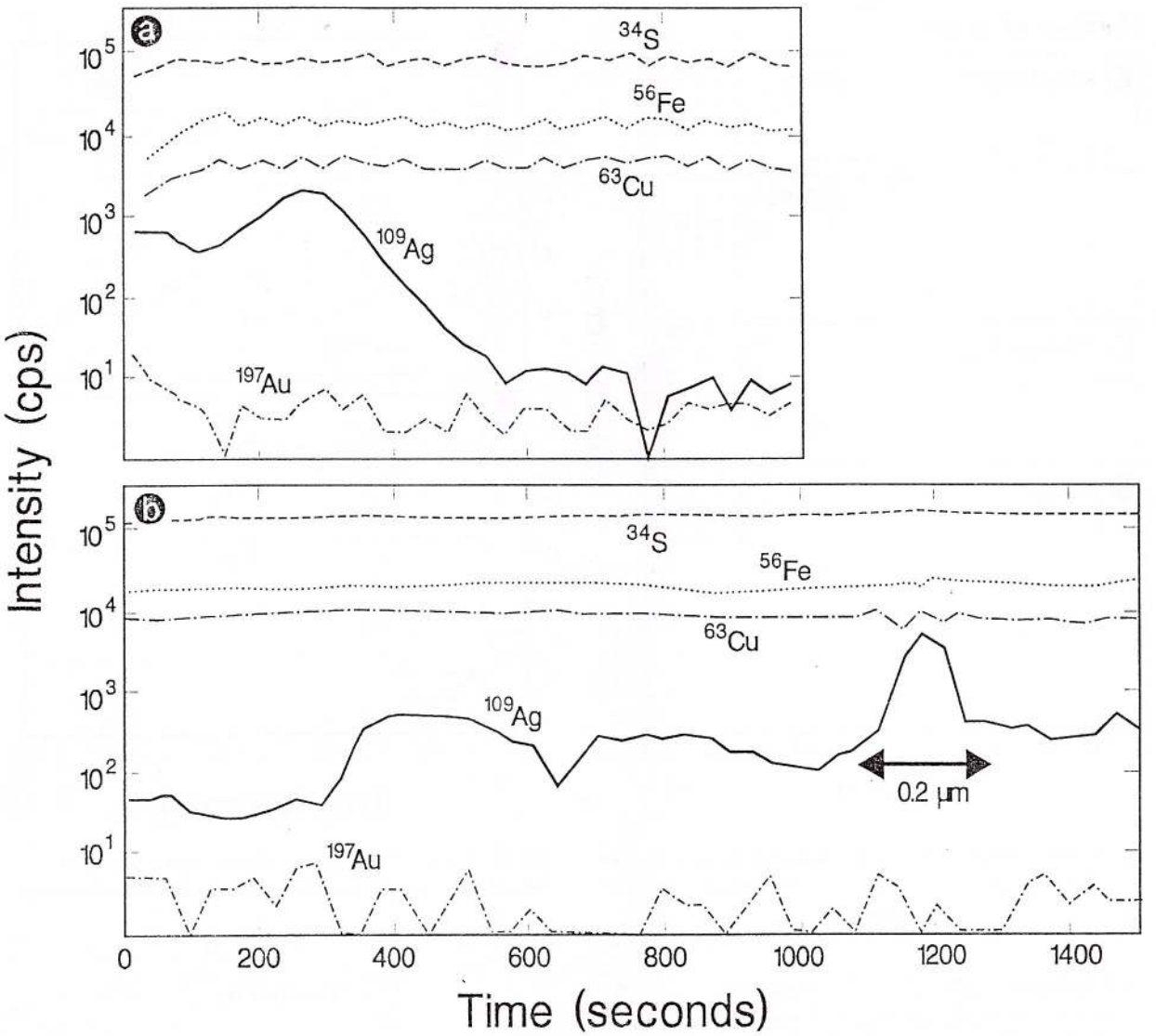

Fig. 4 – Depth profiles for two chalcopyrite grains (sample BB191), showing sub-microscopic inclusion of Ag minerals.

Arsenopyrite. Significant quantities of Au were detected in arsenopyrite from both samples, with individual analyses ranging up to as high as 89 ppm. Characteristic of the data suite is a wide range in absolute values, suggesting an erratic and inhomogeneous gold distribution; BB372a (mean 10.3, σ 17.4 ppm), BBI-1 (mean 44.1, σ 26.7 ppm). This is particularly true for sample BB372a from the Colbu occurrence where the grain size is coarser. An inhomogeneous gold distribution within individual arsenopyrite grains was shown by imaging a 150 μm area (Plate). Gold was found to be concentrated in narrow concentric rims between core and rim. In sample BBI-1, the presence of a micro-inclusion of gold was a feature of several depth profiles (Fig. 6a,b).

Pyrite within the hydrothermal vein ores is commonly arsenian. Several studies have indicated Au to be readily incorporated into As-bearing pyrite (e.g. Cook, Chryssoulis, 1990; Fleet et al., 1993; Huston et al., 1995). Microprobe analyses of pyrite within samples also analysed for Au by SIMS in the present study have indicated a strong zonation, in which As is stronly enriched (to more than 2.0 wt. %) around the grain rims (Cook, 1997b; Fig. 12). This led us to anticipate some level of Au enrichment in the arsenian pyrites. Au concentrations were determined to be low (BB191: 0.65±0.26 ppm; BB372a: 0.51±0.17 ppm), although the small sample suite (2 samples) cannot be considered to be representative. Nevertheless, we note that even these low values are well above the detection limit, and believe this to suggest that Au is tied to the As-rich parts of the grain, detailed imaging of which was beyond the scope of the present study.

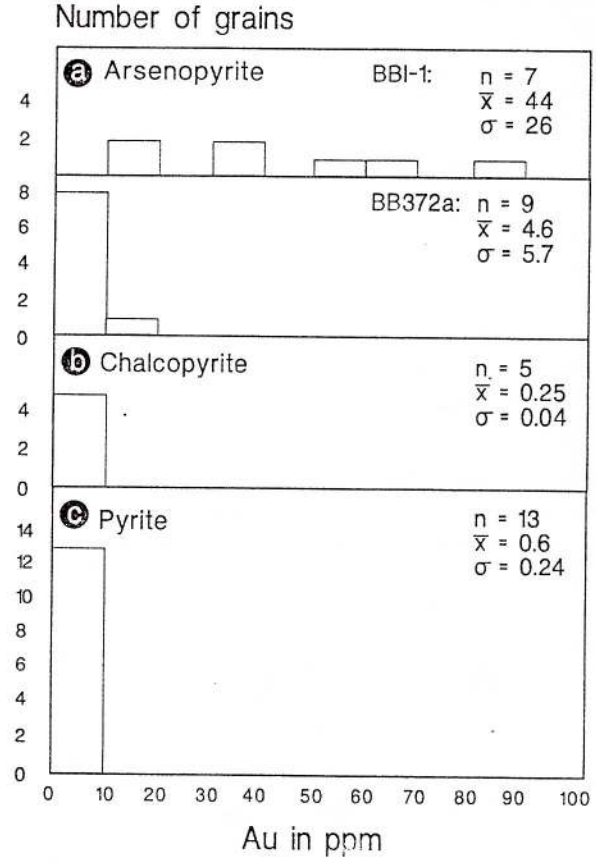

Fig. 5 – Histograms of Ag concentrations in (a) arsenopyrite, (b) chalcopyrite and (c) pyrite in hydrothermal vein ores, expressed in ppm.

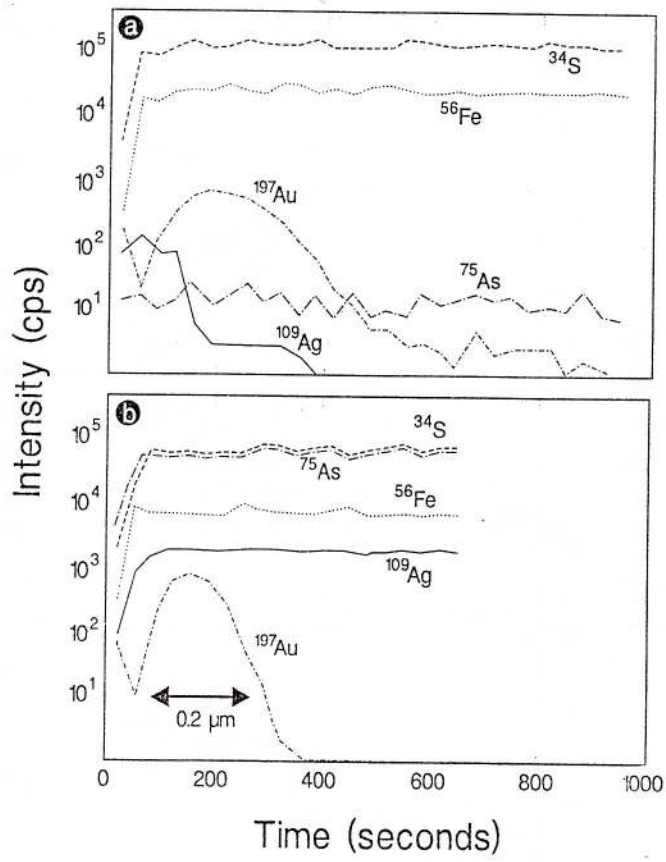

Fig. 6 – Depth profiles for two arsenopyrite grains (sample BBI-1), showing sub-microscopic inclusion of Au minerals.

Chalcopyrite (BB191; 0.25±0.04 ppm) does not contain Au at levels deemed to be significant.

(iii) Samples from Nistru and Herja Mines

In addition to the samples from the Toroioaga vein system, one sample each from the Herja (sample 8255) and Nistru (22N) deposits, Gutâi Mts, were made available to the author by Gh. Damian, Universitatea Baia Mare. Both samples are pyritic, with very minor amounts of chalcopyrite, and have been described as gold-bearing.

Silver

High mean concentrations of Ag in pyrite are recorded from both the Herja and Nistru samples (27 ± 12 and 38 ± 28 ppm respectively; Fig. 7a, b).

Gold

The pyrites in the samples from Herja and Nistru contained significant concentration of invisible Au, generally in the 20–50 ppm range, but with individual analyses up to 66 ppm (Fig. 7c, d). No evidence of inhomogeneous distributions was indicated, except for the presence of one micro-inclusion exposed in a single grain.

Discussion

Silver

In polymetallic VMS ores, Ag is generally distributed between the following four mineralogical hosts (e.g. Chryssoulis, Surges, 1988; Petruk, Wilson, 1993): (i) galena, the main sulphide host for solid solution Ag, or for sub-microscopic Ag-bearing minerals; (ii) other common sulphide minerals (pyrite, sphalerite and chalcopyrite); (iii) sulphosalts of the tetrahedrite-tennantite family and (iv) other discrete Ag-sulphosalts and other Ag carriers (e.g. electrum, tellurides, selenides, argentite-acanthite etc).

Previous data (Cook, 1995; 1997b) has indicated that galena is the most important host of Ag in the **metamorphosed VMS ores** at Baia Borşa. Galena may contain concentrations as high as 1.6 wt. % Ag, although the majority of values are closer to the mean (0.39±0.35 wt.%). Tetrahedrite plays a generally secondary role, except in Cu-rich ores containing little galena, where, on the basis of the abundance of tetra-

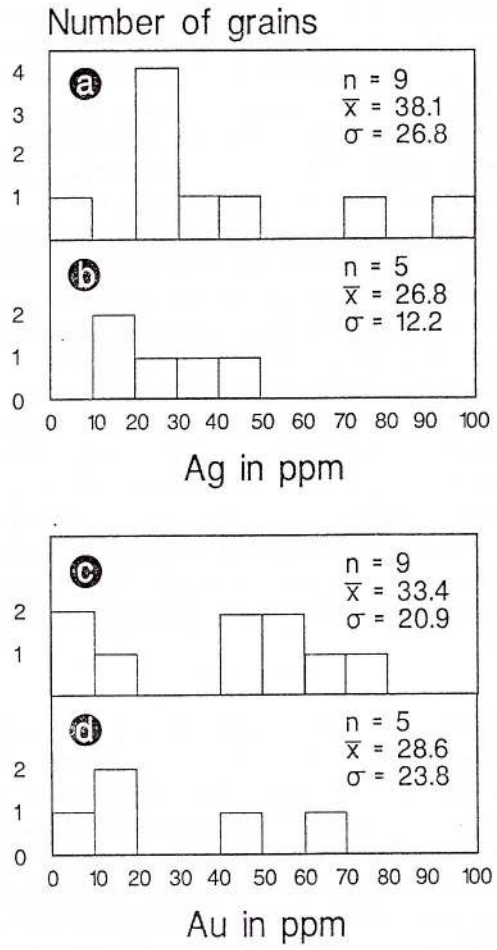

Fig. 7 – Histograms indicating concentrations of Ag in pyrite within (a) sample 22N (Nistru) and (b) sample 8255 (Herja) and Au in pyrite in (c) sample 22N (Nistru) and (d) sample 8255 (Herja).

hedrite in all studied samples, it would appear to be the dominant Ag-carrier; the tetrahedrite typically contains 12–17 wt. % Ag. Tennantite, the dominant fahlore phase in Pb-Zn rich ores contains less than 1.0 wt. % Ag. The presence of other Ag-bearing minerals, including electrum, pyrargyrite and acanthite, has been confirmed by observation and electron probe microanalysis (Cook, 1997b). However, these phases are generally rare and are considered to account for only a minor amount of Ag in the ores.

The present study addresses the concentrations of Ag within pyrite, chalcopyrite and sphalerite, which had not previously been addressed. Several studies (e.g. Harris et al., 1984; Chryssoulis, Surges, 1988; Petruk, Wilson, 1993; see also Cabri, 1992) have shown that sphalerite and chalcopyrite may contain significant Ag concentrations in VMS ores and may make a major contribution to the overall mineralogical balance of Ag in the deposit. In addition, pyrite can also contain significant concentrations of Ag (e.g. Huston et al., 1995; Larocque et al., 1995b) and may, by virtute of its abundance in most ores, also make a major contribution.

The role of invisible silver in sphalerite, chalcopyrite and pyrite in the metamorphosed ores at Baia Borşa can be assessed in terms of the mean concentrations and the proportion of each sulphide, by mode, in the sample. Given the mineralogical and geochemical diversity in the ores, only a semi-quantitative estimate may be given ; quantitative data is best obtained from millfeed or concentrates, rather than chip samples.

Ag concentrations of about 10 ppm within sphalerite, given a sphalerite content of between 8 and 15 vol. % in the investigated samples, and Ag contents in mill feed approx. 100 ppm, suggest that no more than 1 to 2 ppm of the total Ag in the ore (i.e. about 1–2 %) is present in sphalerite. However, some caution should be to this interpretation, given the small number of analysed samples and the wide range in individual analyses. For the purposes of comparison, Petruk and Wilson (1993) attribute sphalerite a greater role in studied Canadian VMS ores, accounting for 3% (Faro), 4% (Brunswick No. 12) and 19% (Trout Lake) of total silver.

The ion-probe analyses of chalcopyrite have absolute values similar to those of sphalerite. With average concentrations of about 10 ppm, and chalcopyrite contents of about 5–10 % (high grade samples), we can infer that chalcopyrite accounts for only insignificant (under 1% of total) amounts of Ag. The presence of appreciably higher concentrations in one sample may, however, infer that,in some instances, chalcopyrite does take on a more significant role as a silver carrier. However, the extent of, and an explanation for, these higher distributions is not known at present.

Despite the relatively low Ag concentrations measured in pyrite, that mineral can, by virtue of its abundance (50–80 % the ore by volume), be regarded as the third most important Ag-carrier in the ores, accounting for 2–5 % of total Ag, i.e. greater than that of sphalerite and chalcopyrite combined.

In the **hydrothermal vein ores**, the study has shown that neither sphalerite nor chalcopyrite are significant silver carriers. Pyrite, with concentrations around 10 ppm can be considered as of minor significance, accounting for a few percent of total Ag. Silver concentrations in pyrite from Herja and Nistru are appreciably higher, and suggest that pyrite should not be ignored in any subsequent detailed study of the mineralogical distribution of silver in the Neogene vein deposits.

Electron probe microanalysis (Cook, 1995;

1997a,b) has indicated galena from the Toroioaga vein system to be very Ag-rich, with the matildite ($AgBi_2$) component in galena as high as 17 mol. % in some instances (Cook, 1997a). Together with tetrahedrite and diverse Ag-bearing minerals, including freislebenite, matildite, argentite, pyrargyrite and stromeyerite (Szöke, in Szöke, Steclaci, 1962), and a range of Ag-Pb-Bi-Sb sulphosalts (Cook, 1997a), galena clearly accounts for the majority of Ag in the vein ores.

Gold

Gold concentrations in the **metamorphosed ores** are generally extremely low, well under 0.5 ppm. Although small grains of visible gold as electrum have been sporadically reported from the massive ores, they are extremely rare. The occurrence of gold within chalcopyrite-quartz mobilisates has been documented and led Cook (1997b) to propose syn-metamorphic mobilisation of gold, in which gold made available during the recrystallisation of pyrite has been relocated into the immediate wallrock. Such a model has been conclusively demonstrated by Larocque et al. (1995a) for the Mobrun VMS deposit, Quebec, Canada, by comparing the invisible gold concentrations of pyrites in different textural settings. In contrast to the Mobrun deposit, despite a comparable metamorphic history, no evidence has been found in the Baia Borşa deposits to suggest survival of primary pyrite and all pyrite would appear to have recrystallised during regional metamorphism.

Although the concentrations of invisible gold detected in pyrite are low, it can be reasonably proposed that this invisible gold, even at such low concentrations, probably accounts for a majority of the Au remaining in the massive ores after metamorphic recrystallisation and associated mobilisation. The low concentrations are in full accordance with mineralogical observations and a model of pyrite recrystallisation and reconcentration of gold in mobilised segregations.

The **hydrothermal vein ores** are characterised by enrichment in gold, yet the mineralogical distribution of gold in the deposits is poorly understood. Arsenopyrite has been demonstrated to be an important host for invisible gold in a number of ore deposits (e.g. Cathelineau et al., 1989; Cook, Chryssoulis, 1990; Cabri, 1992). Although rarely a major component in Toroioaga ores, fine-grained arsenopyrite is an abundant minor component of many of the minor hydrothermal veins and fault-related fracture fillings throughout the orefield. Locally, it may, together with sphalerite, make up the greater part of the sulphide mass, as in the fault-fill veins cross-cutting the Colbu and Ivăşcoaia massive sulphide lenses (BB 372a; BBI-1). Geochemical analysis of samples from this particular locality indicated the presence of several ppm Au, but not visible gold is observed during microscopic study, prompting the likelihood of invisible gold. Confirmation of the presence of invisible gold in arsenopyrite at significant concentrations is therefore significant, and promts a wider-ranging study of arsenopyrite within the vein ores.

Of still greater importance is the confirmation of significant concentrations of invisible gold (tens of ppm) within pyrite in the samples from Herja and Nistru. Although they do not pretend to be representative, these data suggest that the role of invisible gold within the Neogene deposits of NW Romania could be significantly greater than previously believed and warrant a much more extensive study. This is highlighted by the recent recognition (András, Ragan, 1995; András et al., 1995) that invisible gold, hosted within both arsenopyrite and pyrite, is of significance within comparable deposits (e.g. Pezinok), of similar age in the Western Carpathians, Slovakia.

Conclusions

1. Silver occurs at the ppm level in solid solution within sphalerite, chalcopyrite and pyrite in the metamorphosed VMS ores. The proportion of Ag in the ore hosted within these sulphides is, however, considered to be below 5 % of the total. There is evidence of higher Ag values in some chalcopyrites, but pyrite probably accounts for more Ag than sphalerite.

2. The major Ag-carrier in the metamorphosed ores is, as previously believed, galena, with tetrahedrite playing a subordinate role. They probably account together for more than 90 % of Ag in the ores. Neither chalcopyrite nor sphalerite are significant Ag carriers in the vein ores; a small percentage of total Ag may be present in pyrite.

3. Very little invisible gold is present within pyrite in the metamorphosed ores. This is in full accordance with the observation that all pyrite has recrystallised during metamorphism, and that gold has undergone remobilisation, being concentrated in structurally-controlled zones in the wall rock.

4. Arsenopyrite is, on the basis of the preliminary data presented here, identified as an important host for invisible gold in the vein ores, with individual grains containing up to 89 ppm. Imaging indicates an inhomogeneous Au distribution within arsenopyrite grains.

5. Although arsenian pyrite co-existing with arsenopyrite in the Toroioaga deposits does not contain significant amounts of invisible gold, significant concentrations of invisible Au were determined in pyritic samples from the Herja and Nistru deposits.

6. The confirmation of invisible silver and, especially, of gold within a number of Neogene deposits

in NW Romania represent a significant advance in the knowledge of mineralogical distributions in these economically important deposits. The data strongly suggest that a more detailed and representative investigation should be undertaken, in order to verify these findings. The data presented here are not only of considerable interest to the ore deposits geologist, but also represent information which could have important implications for the successful exploitation of the deposits.

Acknowledgements

The financial assistance allowing the author to carry out the SIMS analyses was made available by the Deutsche Forschungsgemeinschaft. The professional advice of Stephen Chryssoulis, Amtel, prior to and during the analysis run, is very much appreciated, as is operation of the ion probe by Chris Weisener. The author also wishes to thank numerous geologists in Romania (Cuarţ S.A.,Regia Autonomă Plumb şi Zinc, Univ. Baia Mare, Geological Institute of Romania) for informative discussions.

References

Andráš, P., Ragan, M. (1995) Sulfidické rudy s neviditel'ným zlatom na Slovensku. *Mineralia Slovaca*, 27, p. 57–63.

— , **Wagner, F., Ragan, M., Friedl, J., Marcoux, E., Caño, F., Nagy, G. (1995)** Gold in arsenopyrites from the Pezinok deposit (Western Carpathians, Slovakia). *Geologica Carpathica*, 46, p. 335–342.

Cabri, L. J. (1992) The distribution of trace precious metals in minerals and mineral products. *Mineralogical Magazine*, 56, p. 289–308.

— , **Chryssoulis, S. L. (1990)** Advanced methods of trace-element microbeam analyses. In: Advanced Microscopic Studies of Ore Minerals (J. L. Jambor and D. J. Vaughan eds). *Min. Assoc. Canada Short Course Notes*, 17, p. 341–377.

Cathelineau, M., Boiron, M.-C., Holliger, P., Marion, P., Denis, M. (1989) Gold in arsenopyrites: crystal chemistry, location and state, physical and chemical conditions of deposition. *Economic Geology Monograph* 6 (The geology of gold deposits - the perspective in 1988), p. 328–341.

Chryssoulis, S. L., Cabri, L. J. (1990) Significance of gold mineralogical balances in mineral processing. *Trans. Inst. Min. Metall.*, Sect. C, 99, p. 1–9.

— , **Cabri, L. J., Lennard, W. (1989)** Calibration of the ion microprobe for the quantification of precious metals in trace amounts in ore minerals. *Economic Geology*, 84, p. 1684–1689.

— , **Cabri, L. J., Salter, R. S. (1987)** Direct determination of invisible gold in refractory sulphide ores. In: Proc. Int. Symposium. Gold Metallurgy - Refractory Gold (R. S. Salter, D. M. Wyslouzil and G. W. McDonald eds.), Pergamon Press, Toronto, p. 235–244.

— , **Chauvin, W. J., Surges, L. J. (1986)** Trace element analysis by secondary ion mass spectrometry with particular reference to silver in the Brunswick sphalerite. *Can. Metall. Qurt.*, 25 p. 233–239.

— , **Surges, L. J. (1988)** Behaviour of tetrahedrite in mill circuits of Brunswick Mining and Smelting Corporation Ltd. In: Silver Exploration. Mining and Treatment. *Inst. Min. Metall.*, London, p. 205–216.

Cook, N. J. (1995) Polymetallic massive sulphide deposits at Baia Borşa, Romania. In:Mineral deposits: from their origin to their environmental impacts (J. Pašva et al. eds.) Balkema, Rotterdam, p. 851-854.

— **(1997a)** Bismuth and bismuth-antimony sulphosalts from Neogene vein mineralisation, Baia Borşa area, Maramureş, Romania. *Mineralogical Magazine*, 61, (in press).

— **(1997b)** Sulphide and sulphosalt mineralogy of Cambrian massive sulphide and superimposed Neogene mineralisation at Baia Borşa, Romania. *Mineralium Deposita* (under review).

— , **Chryssoulis, S. L. (1990)** Concentrations of "invisible gold" in the common sulfides. *Canadian Mineralogist*, 28, p. 1–16.

Fleet, M. E., Chryssoulis, S. L., Maclean, P. J., Davidson, R., Weisener, C. G. (1993) Arsenian pyrite from gold deposits: Au and As distribution investigated by SIMS and EMP, and colour staining and surface oxidation by XPS and LIMS. *Canadian Mineralogist*, 31 p. 1–17.

Gasparrini, C. (1983) The mineralogy of gold and its significance in metal extraction. *Can. Inst. Metall. Bull.*, 76, March 1983, p. 144–153.

Harris, D. C., Cabri, L. J., Nobiling, R. (1984) Silver-bearing chalcopyrite, a principal source of silver in the Izok Lake massive sulfide deposit : Confirmation of electron- and proton-microprobe analyses. *Canadian Mineralogist*, 22, p. 493–498.

Huston, D. L., Sie, S. H., Suter, G. F., Cooke, D. R., Both, R. A. (1995) Trace elements in sulfide minerals from Eastern Australian volcanic-hosted massive sulfide deposits: Part I. Proton microprobe analyses of pyrite , chalcopyrite and sphalerite ; Part II. Selenium levels in pyrite : Comparison with $\delta^{34}S$ values and implications for the source of sulfur in volcanogenic hydrothermal systems. *Economic Geology*, 90, p. 1167–1196.

Larocque, A. C. L., Hodgson, C. J., Cabri, L. J., Jackman, J. A. (1995a) Ion microprobe analysis of pyrite, chalcopyrite and pyrrhotite from the Mobrun VMS deposit in northwestern Quebec : Evidence for metamorphic remobilisation of gold. *Canadian Mineralogist*, 33, p. 373–388.

— , **Jackman, J. A., Cabri, L. J., Hodgson, C. J. (1995b)** Calibration of the ion microprobe for the determination of silver in pyrite and chalcopyrite from the Mobrun VMS deposit, Rouyn-Noranda, Quebec. *Canadian Mineralogist*, 33, p. 361–372.

MacRae, N. D. (1995) Secondary-ion mass spectrometry and geology. *Canadian Mineralogist*, 33, p. 219–236.

Petruk, W., Wilson, J. M. (1993) Silver and gold in some Canadian volcanogenic base metal deposits. In: Proc. 8th IAGOD symposium (Y. T. Maurice, ed.), E. Schweizerbart'sche, Stuttgart, p. 105–117.

Radu, D., Cook, N. J. (1995) The stratiform pyrite and base metal ore deposits hosted within the Tulgheş Series in the Baia Borşa area, Maramureş Mountains. In : 3rd Mineralogical Symposium, Excursion Guides (G. Udubaşa ed.). *Rom. J. Mineralogy*, 77, Suppl. 2, p. 79–97.

Szöke, A., Steclaci, L. (1962) Regiunea Toroioaga - Baia Borşa. Studiu geologic, petrografic, mineralogic şi geochimic. Editura Academiei Republicii Populare Române, 240p.

Plate

(a) – Reflected light photomicrograph showing pyrite (smaller grain, left) and arsenopyrite (larger grain, right) selected for imaging (sample BBI-1). Areas 'b' and 'c' are shown as elemental images in (b) and (c). Oval spot in centre of field 'b' is SIMS crater. Width of picture: 640μm.

(b) and (c) – show selected areas of the two grains. Images are shown for mass 34 (S), 75 (As) and 197 (Au). Note the clear inhomogeneous distribution of Au in both grains.

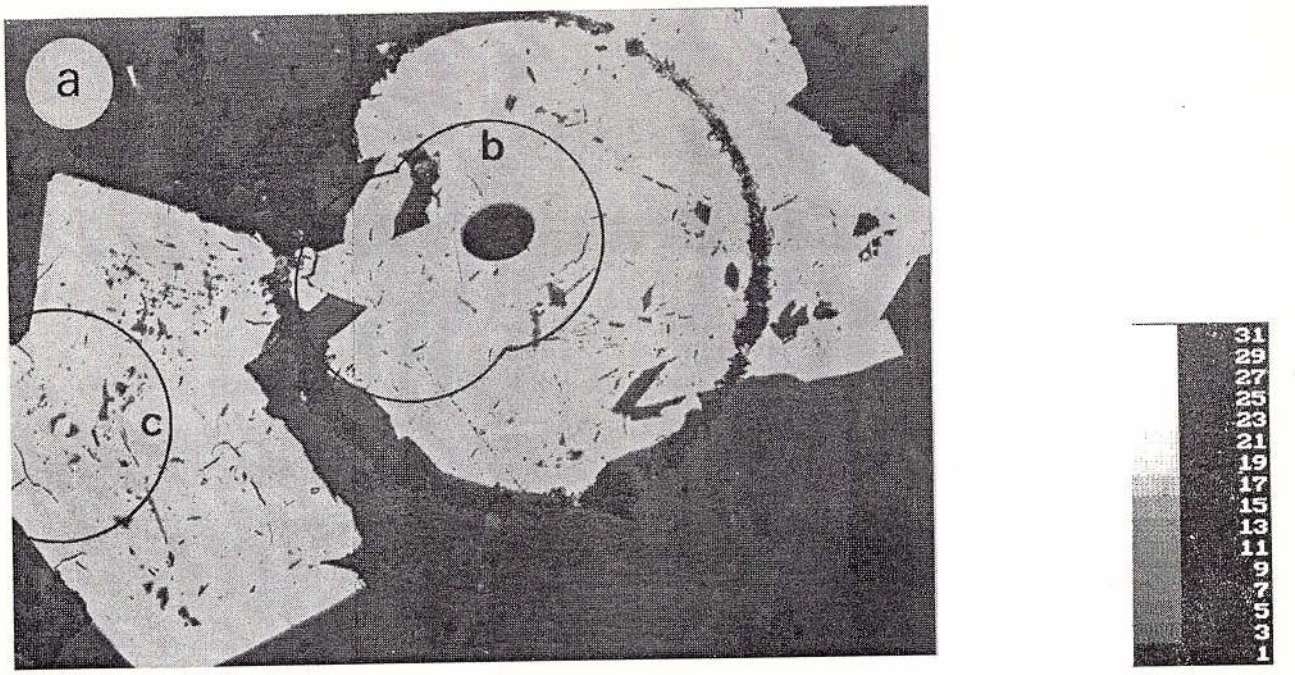

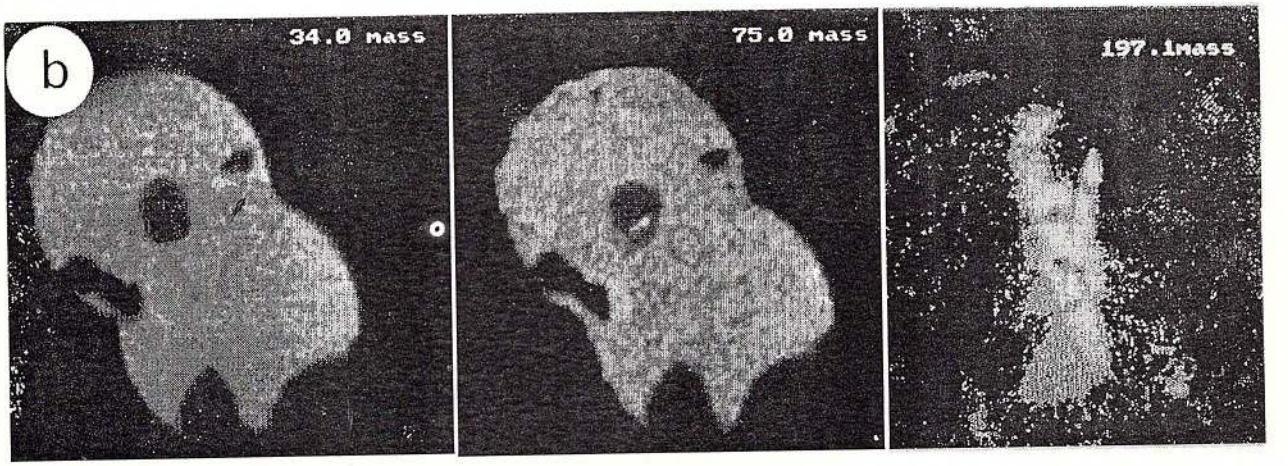

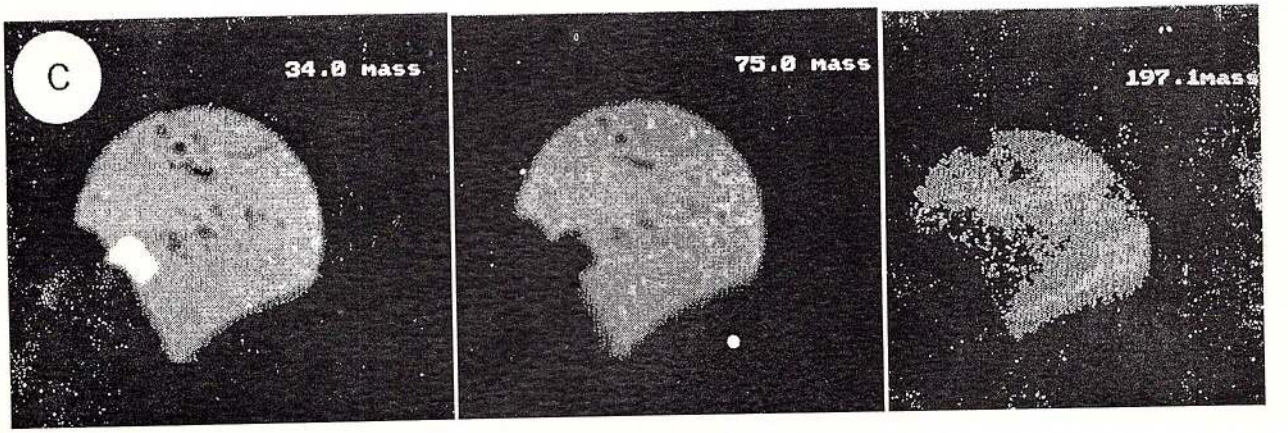

Rom. J. Mineralogy, 79, p. 123-130, Bucureşti, 1999

ACCESSORY MINERALS IN ALKALINE ROCKS FROM THE DITRĂU MASSIF (EAST CARPATHIANS), ROMANIA. PETROGENETIC IMPLICATIONS

Ion Nicolae ROBU, Lucia ROBU

Institutul Geologic al României. Str. Caransebeş nr.1, 78344, Bucureşti, Romania

Key words: Hornblendites. Syenites. Zircon. Apatite. Titanite. Magnetite. Petrogenetic Implications. Typology.

Abstract: The Ditrău alkaline massif in the East Carpathians is made up of a large variety of rock types (hornblendites, syenites, granites, diorites) and numerous dikes cross-cutting it. Accessory minerals (zircon, apatite, titanite, magnetite) from different rock types have been studied in order to establish the relationships between their mineralogical, chemical and physical properties and either chemical composition of the host rocks or geological setting. *Zircon* exhibits two crystal types pointing out a mantle origin and high concentrations of the radio-active elements in the first phases of magma evolution, preserved during its entire evolution and enriched in the final stages. *Apatite* crystals have been observed in some hornblendites and syenites with two morphological aspects, determined by the simple or complex combination of the morphological elements. The sporadic presence of the apatite crystals points out a P and H_2O deficit of the parental magma; the absence of opaque inclusions in the apatite is the result of a precocious crystallization of the apatite crystals. *Titanite* crystals have been observed in different concentrations in the studied rocks, but no differences between titanite crystals from hornblendites and syenites seem to exist. *Magnetite* is present in all studied samples, having two important morphological aspects. Frequently magnetite is substituted by hematite and goethite and sometimes it is associated with ilmenite. The sporadic presence of the ilmenite is an indirect criterion for the deep origin of the magmas that generated these alkaline rocks.

Introduction

The mineralogical, chemical and physical (color, internal structure of the crystals, morphology) characteristics of the accessory minerals selected from different rock types of the Ditrău alkaline massif have been studied for establising some connections between these minerals and the chemical composition or geological setting of their host rocks.

Geological setting

The Ditrău alkaline massif is cropping out in the East Carpathians, in the Carpian and Marisian supergroups (Kräutner, 1980) of the Bucovinian Nappe (Săndulescu, 1975); it is intruded in the crystalline formations of the Tulgheş Series, that are low-grade metamorphosed (green schists facies) and sometimes have a retrograde character (Popescu, 1971).

In the northern part, between the Ditrău valley and the Jolotca valley, the Ditrău massif is covered by the Pliocene and Quaternary deposits.

The contact between the alkaline massif and the Tulgheş crystalline schists is characterized by the mineral associations specific to the contact zones: biotite + andalusite + cordierite + corundum + spinel ± chloritoid ± alkaline amphibole bearing rocks, or the spot knot structure of rocks (Streckeisen, 1974).

Petrological and structural characters of the massif

The Ditrău alkaline massif is characterized by a large variety of mineralogical, petrographical and chemical compositions, which reflect complicated structural and textural aspects. Thus, they could have been separated (Anastasiu, Constantinescu, 1979) in: (1) foid rocks (monzonites, syenites), (2) alkali-feldspar rocks (syenites, monzonites, monzodiorites), (3) quartz-feldspar rocks (granites and diorites), (4) ultramafic rocks (hornblendites and peridotites) (Fig. 1).

The samples were selected from different kinds of

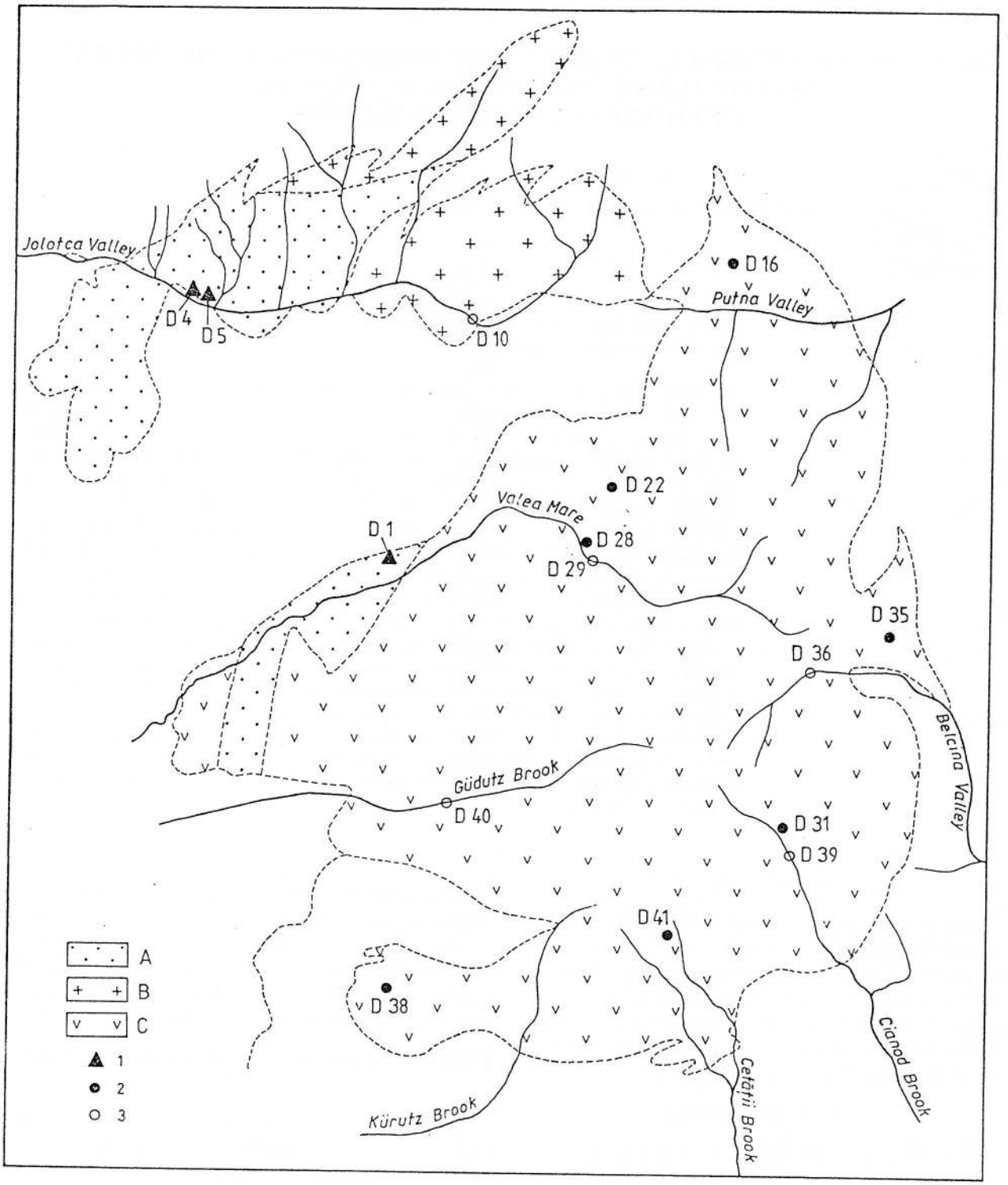

Fig. 1 - Geological sketch (after Anastasiu, Constantinescu, 1979) and location of the samples: *Geological formations*: A - hornblenditic rocks; B - syenitic rocks; C - syenitic alluviums; *Samples*: 1, hornblenditic rocks; 2, syenitic rocks; 3, syenitic alluviums.

rocks and alluviums, and they are described in Table 1.

The description of each accessory minerals is presented below:

Table 1

Rock type and the mineral assemblages of the studied samples

Sample	Rock type	Mineral assemblages
D–1	hornblendite	ho+ti ± nph ± ap+zr ± bi+mgt
D–4	hornblendite	ho+ti ± ap+zr ± bi+mgt ± il
D–5	hornblendite	ho+ti ± ap+zr ± bi+mgt ± il
D–28	nepheline syenite	nph+pgfd+kfd+bi+ti+zr+mgt+il
D–22	nepheline syenite	nph+pgfd+kfd ± bi+ti ± ap+mgt ± il+zr
D–38	nepheline syenite	nph+pgfd+kfd+bi+ti+ap+mgt+zr
D–41	alkali–feldspar syenite	pgfd+kfd+bi+ti+zr+mgt ± il
D–31	alkali–feldspar syenite	pgfd+kfd+ap+zr ± mgt
D–35	alkali–feldspar syenite	pgfd+kfd+ti+ap+ru+zr+mgt ± il
D–16	alkali–feldspar syenite	pgfd+kfd+bi+zr+mgt ± il
D–29	syenitic alluviums	ho+tu+bi+ru+ap+zr+mgt+il
D–10	syenitic alluviums	bi+ru+ru+ap+zr+ti+mgt+il
D–39	syenitic alluviums	bi+tu+ru+zr+ti+mgt+il
D–35	syenitic alluviums	bi+tu+zr+ti+mgt+il
D–40	syenitic alluviums	bi+ap+zr+ti+mgt+il

ho = hornblende; bi = biotite; amph = amphibole; pgfd = plagioclase-feldspar; kfd = alkali-feldspar; nph = nepheline; ti = titanite; ap = apatite; tu = tourmaline; zr = zircon; mgt = magnetite; il = ilmenite; ru = rutile.

Techniques of study

The rocks have been crushed under 1 mm and then separated using Frantz isodynamic magnetic separator and dense liquids (bromoform).

The crystal faces were indexed by using: (1) the abaca method (Caruba, 1975, fide Duchesne et al.) for zircon crystals, or (2) for other minerals, as apatite, titanite, magnetite, the observed faces have been compared with data from literature.

The morphology of zircon crystals had been interpreted according to original typology classification of zircon, proposed by Pupin, Turco (1972).

The optical characteristics have been observed under binocular and Jenapol microscopes. The chemical composition has been established using wet chemical method (titanite) or Geol JXA–50 microprobe analyzer for other minerals.

Mineralogical, chemical and physical properties of the accessory minerals

Zircon, *apatite*, *titanite* and *magnetite* are the accessory minerals that have an important petrogenetic semnificance and have been identified in the Ditrău alkaline massif. Table 2 indicates the sample location, rock type and the accessory minerals frequency for each studied samples.

It is to remark the same mineralogical associations and relatively the same frequency for all samples.

Zircon: Table 3 summarizes the mineralogical properties of zircons. Some common characteristics of all samples are emphasized: (1) the good development of the prism faces, (110), (100), (2) a complete absence or low–development of the (211) pyramidal one, (3) the absence or sporadical presence of the inclusions, zoning or core crystals.

Two zircon types could be separated due to: (1) the variation of prism or pyramidal face development, and (2) the optical properties:

– long prismatic crystals, with well–developed, but unequal growth of the prismatic faces [(100)> (110)] and pyramidal ones [(211) (101)]; their color varies between light and dark pink, sometimes dark brown, and they have a good transparency. The translucent, zoned and overgrown crystals are few, but a small number of them contains inclusions. This zircon type is specific to hornblendite rocks;

– short prismatic crystals, with well–developed (100) prismatic faces, and (101) pyramidal ones; the appearance of (110) prismatic and (211) pyramidal faces are sporadical. The color of this type is more homogeneous than the first zircon type (zircon from hornblendite), varying between light and dark brown. Most of zircon crystals are opaque, and only a few of them are transparent. No more inclusions, cores or zoned crystals exist. This second type of zircon is characteristic of syenitic rocks.

The morphological and the optical properties point

Table 2
Sample location, rock type and accessory mineral frequency for each sample

Sample	Sample location	Rock type	Zircon	Apatite	Titanite	Magnetite
D–1	Ditrău Valley	hornblendite	+	+	+	+
D–4	Jolotca Valley	hornblendite	+	+	+	+
D–5	Jolotca Valley	hornblendite	+	+	+	+
D–28	Ditrău Valley	nepheline syenite	+	-	+	+
D–22	Comarnic hill	nepheline syenite	+	+	+	+
D–38	Csanod Valley	nepheline syenite	+	+	+	+
D–41	Cetății Valley	alkali–feldspar syenite	+	-	+	+
D–31	Csinod Valley	alkali–feldspar syenite	+	+	-	+
D–35	Belcina Valley	alkali–feldspar syenite	+	+	+	+
D–16	Putna Valley	alkali–feldspar syenite	+	-	-	+
D–29	Ditrău Valley	syenitic alluviums	+	+	-	+
D–10	Jolotca Valley	syenitic alluviums	+	+	+	+
D–39	Belcina Valley	syenitic alluviums	+	-	+	+
D–35	Belcina Valley	syenitic alluviums	+	-	+	+
D–40	Ghidut Valley	syenitic alluviums	+	+	+	+

+ = yes; - = no.

Table 3
Mineralogical properties of zircon populations

Sample	Color	Transparency	Inclusions	Zoning	Core	Morphology
D–1	Cl, LP	yes	very rare	very rare	no	(100),(110),(101)
D–4	Cl, LP	yes	very rare	no	no	(100),(110),(101)
D–5	LP, DP	yes	no	no	no	(100),(110),(101),(211)
D–28	LP, DP	yes	no	no	no	(100),(110),(101)
D–22	DP, LB	yes, no	no	no	no	(100),(110),(101),(211)
D–38	LB, DP	yes	no	no	no	(100),(110),(101),(211)
D–41	LB, DB	yes, no	no	no	no	(100),(110),(101),(211)
D–31	Cl, LP	yes	no	no	no	(100),(110),(101)
D–35	LB, DB	yes, no	very rare	no	no	(100),(110),(101),(211)
D–16	Cl, LP	yes, no	very rare	no	no	(100),(110),(101)
D–29	Cl, LB	yes, no	no	no	no	(100),(110),(101)
D–10	Cl, DP, LB	yes, no	very rare	no	very rare	(100),(110),(101),(211)
D–39	CL, LB	yes	no	no	no	(100),(110),(101)
D–35	LP, DB	no	no	no	no	(100),(110),(101)
D–40	Cl, LP, LB	no	no	no	no	(100),(110),(101)

Cl = colorless; LP = light pink; DP = dark pink; LB = light brown; DB = dark brown.

to a common origin of the hornblendite and syenite rocks, the differences emphasized by this study being determined by the magma evolution, mainly by the content of the H_2O and radio–active elements. Thus, in the initial stage, when magma could have a low H_2O content and an important concentration of the radio–active elements (hornblenditic stage), the light color and long prismatic zircon crystals formed and had been included in the hornblenditic rocks. Later, when the degree of hydration and the radio–active elements contents increased, the short prismatic zircons had crystallized, being characteristic of the syenitic rocks (the variation of zircon habit with the magma hydration degree is demonstrated experimentally (Caruba, 1975, 1978; Caruba et al., 1975, fide Duchesne, Caruba, Iacconi, 1987). It is also known that the color variations of metamictic degree of zircons are correlated with the concentrations of the radio–active elements in the magma (Duchesne, Caruba, Iacconi, 1987).

The absence of zoned and core crystals, or their sporadical appearance in the hornblenditic and syenitic rocks, points to the same crystallization conditions, without chemical (especially Zr content) and kinetic major variations, during the zircon crystallization, and the scarcity or the absence of the assimi-

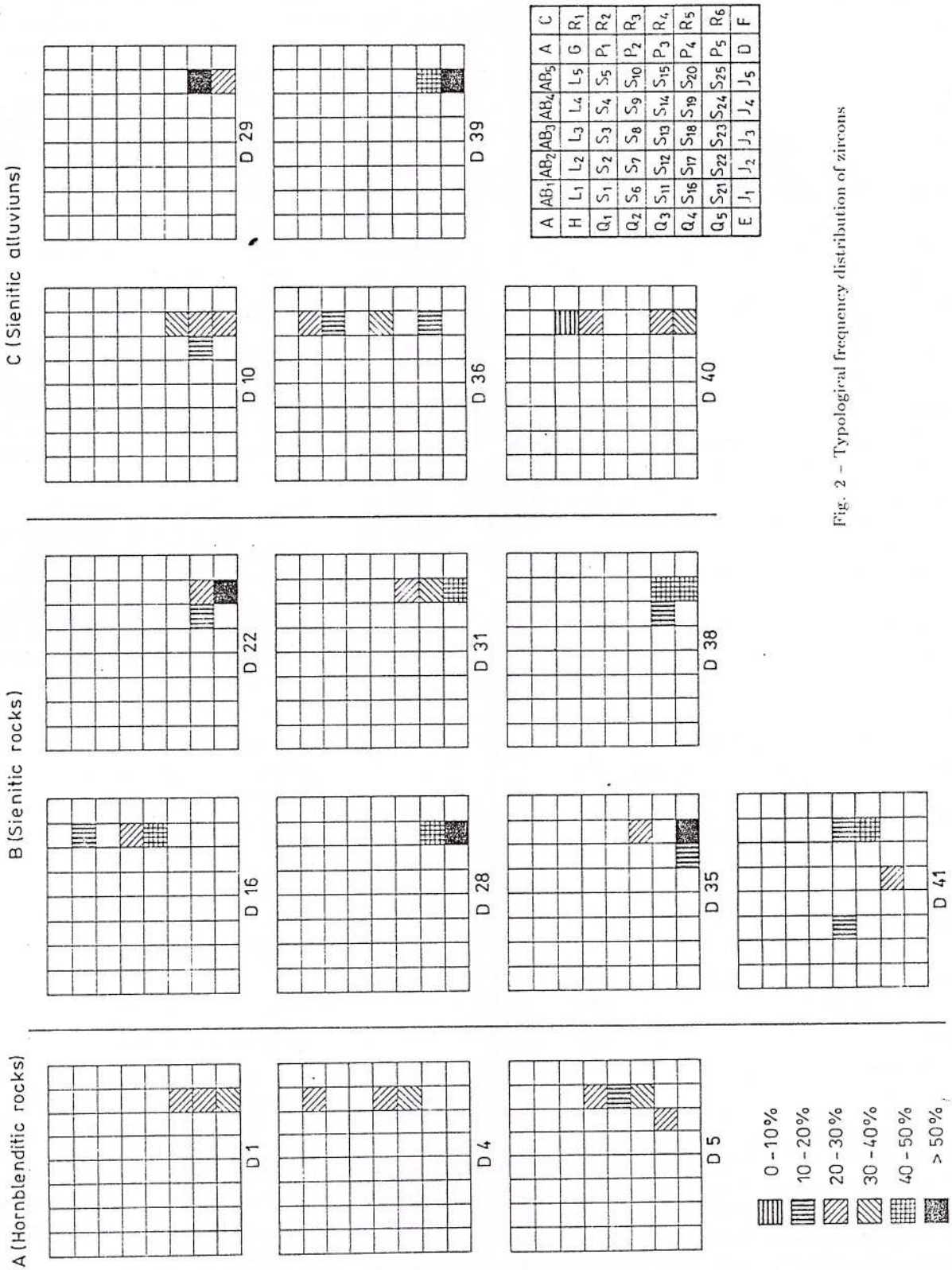

A	AB_1	AB_2	AB_3	AB_4	AB_5	A	C
H	L_1	L_2	L_3	L_4	L_5	G	R_1
Q_1	S_1	S_2	S_3	S_4	S_5	P_1	R_2
Q_2	S_6	S_7	S_8	S_9	S_{10}	P_2	R_3
Q_3	S_{11}	S_{12}	S_{13}	S_{14}	S_{15}	P_3	R_4
Q_4	S_{16}	S_{17}	S_{18}	S_{19}	S_{20}	P_4	R_5
Q_5	S_{21}	S_{22}	S_{23}	S_{24}	S_{25}	P_5	R_6
E	J_1	J_2	J_3	J_4	J_5	D	F

Fig. 2 – Typological frequency distribution of zircons

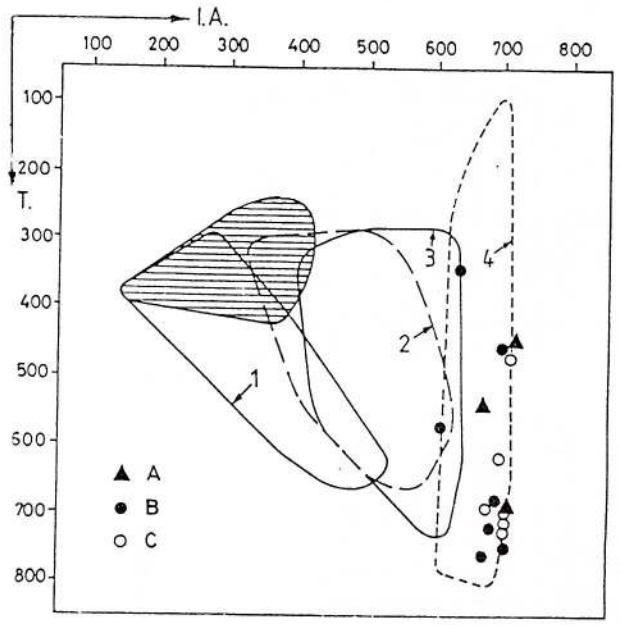

Fig. 3 - Distribution of plutonic rocks in the typological diagram: 1, diorites, quartz gabbros and tonalites; 2, granodiorites; 3, monzogranites; 4, alkaline and hyperalkaline syenite and granites; cordierite bearing rocks; A, hornblenditic rocks; B, syenitic rocks; C, syenitic alluviums.

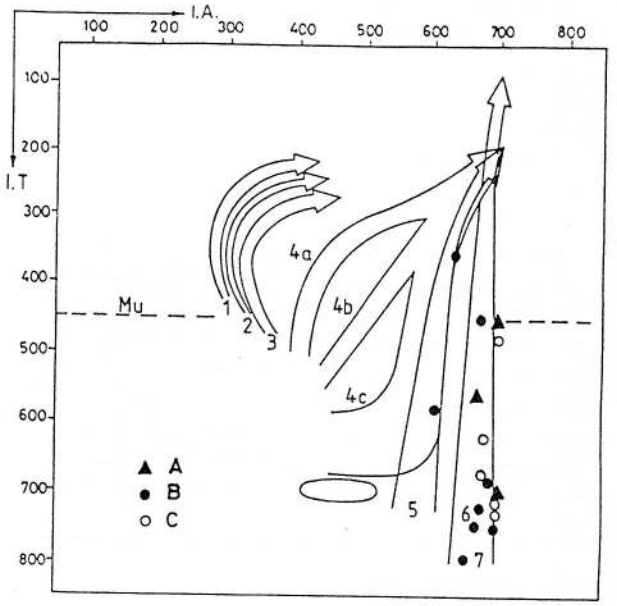

Fig. 4 - Distribution of mean points and mean T.E.T. of zircon populations (after Pupin, 1980) from: 1, aluminous leucogranites; 2, (sub) autochthonous monzogranites and granodiorites; 3, intrusive aluminous monzogranites; 4, a, b, calc–alkaline series granites (granites of crustal + mantle origin, hybrid granites); 5, sub–alkaline series granites (granites of mantle or mainly mantle origin); 6, alkaline series granites; 7, tholeiitic series granites (magmatic charnockites area); 8, Mu limit of muscovite granites; A, hornblenditic rocks; B, syenitic rocks; C, syenitic alluviums.

ıtion phenomena.

The morphological variations, especially the relation between the growth degree of two pyramidal faces, (211) and (101), emphasize the variations in magma alkalinity, during its evolution (Pupin, 1980). Thus, the morphological types observed (Fig. 2) in hornblendites and syenites are very similar, pointing to the high alkalinity degree of magma from the initial stage, until the final one.

Typological interpretation of the zircon morphological characters, according to Pupin, Turco (1972), indicates zircon crystals specific to hyperalkaline syenites and granites (Fig. 3) and a mantle, or sometimes hybrid origin (crust + mantle) for all zircon populations (Fig. 4).

Apatite: Apatite crystals have been observed in small concentrations in the hornblenditic and syenitic rocks, much more abundant in the last ones; they are colorless, transparent, without inclusions, and show hexagonal long prismatic habit, frequently without terminations.

Two morphological crystal types have been separated (Fig. 5): (1) crystals with simple termination, constituted of hexagonal prismatic faces, unequal growth (1010) > (0110), combined with pyramidal ones (1011) > (0111), and (2) complex termination crystals, with equal hexagonal prismatic faces [(1010) = (0110)], equal hexagonal pyramidal faces [(1011) = (0111)], and a [(0001)] basal pinacoid.

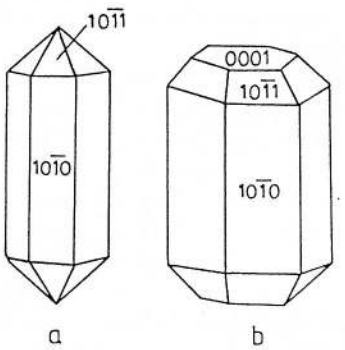

Fig. 5 - Apatite crystals

The low frequency of the apatite crystals is probably depending on the low P concentration in the parental magma; the absence of the opaque and mafic inclusions can be due to the early crystallization of apatite, before the appearance of the opaque and mafic minerals, or much later, when these are crystallized and included in other minerals.

Titanite: The abundence of titanite crystals in hornblendites and syenites is very different: high in hornblenditic rocks (20–30%) and less or none in syenitic ones. The morphology of titanite crystals is

characterized by the well developed (001) and (201) faces (Fig. 6), which are smooth and glossy. The color of titanite is yellow–brown; the crystals contain inclusions of opaque and mafic minerals, chaotically disposed.

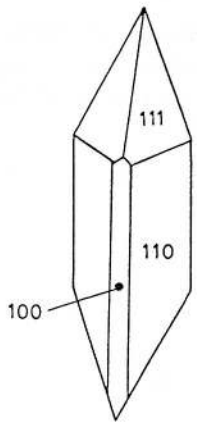

Fig. 6 Titanite crystals

The chemical composition (Tab. 4) points out a small Al content, varying from 0.38 to 2.90, and a few substitutions between Ti, O, and Al, OH, F; some reactions, suggested by the analytical data, (according to Franz, Spear, 1985) could be possible, as follows:

(1) $Ti^{4+} + O^{2-} \rightarrow Al^{3+} + OH^{-}$, (2) $Ti^{4+} + O^{2+} \rightarrow Al^{3+} + F^{-}$, (3) $Si^{4+} \rightarrow 4H^{+}$ + vacancy, but their intensity is very low.

The differences between the ideal values and ours could be determined by the presence of REE elements, some impurities, that are under detection limits in the considered samples.

The calculation of the formula for general titanite ($CaTiSiO_5$) made on the basis of five oxygens, point out a $CaTiSiO_5$ term of $CaTiO_5$ - $CaAlSiO_4(OH)$ - $CaAlSiO_4(F)$ series (Tab. 4).

The low Al content could be determined by the low H_2O and F fugacity, and high CO_2 one (according to Franz, Spear, 1983, fide Franz, Spear, 1985), and low pressure and high temperature (according to experimental studies, Holland, 1979; Franz, Spear, 1983, fide Franz, Spear, 1985).

Magnetite: Magnetite has been observed in all hornblenditic and syenitic rocks in indifferent proportions. Its crystals are dominated by two morphological aspects, the same in hornblendites and syenites: (I) octahedral crystals, with (1) smooth and glossy faces or (2) well–developed growth striae ones, disposed parallel with the edges of the crystals and (II) granular aggregates, without crystallographic faces. In reflected light, we have observed magnetite (crystals and granular aggregates) substituted by hematite and goethite. These substitutions are partial and, sometimes, total and are developed from the edge of the crystals to the central zone, or have been observed on the numerous fissures cutting them across.

Sometimes magnetite is associated with ilmenite. The sporadic presence of the ilmenite points out a deep origin, probable in the upper mantle for parental magma.

The appearance of hematite and goethite points to a high variation of the oxygen fugacity the magma evolution.

Table 4
The oxides values (%) for two titanite samples

Oxide sample number	Oxide value (%) D–38	4 a
SiO_2	35.12	24.87
TiO_2	33.68	34.87
Al_2O_3	2.90	0.38
Fe_2O_3	1.75	2.13
FeO	0.14	1.72
MnO	0.15	0.00
MgO	0.17	0.07
CaO	23.59	0.22
Na_2O	0.59	28.44
K_2O	0.75	0.23
H_2O	0.83	0.13
P_2O_5	0.30	0.45
F^-	0.04	0.10
Total	100.01	93.63
Cations (base 6, O, F)		
Si	1.100	0.885
Ti	0.799	0.920
Ca	-	1.082

Conclusions

Morphological, chemical and optical characters of the accessory minerals (zircon, apatite, titanite, magnetite) from the Ditrău alkaline massif point to:

– a common origin for hornblenditic and syenitic rocks;

– a deep origin for parental magma (probable upper mantle) which, during its evolution, maintained its initial high alkaline character, suffering (1) an increase of the radioactive elements and H_2O contents and (2) a high variation of O_2 fugacity.

References

Anastasiu, N., Constantinescu, E. (1979) Observaţii mineralogice în rocile sienitice din masivul alcalin Ditrău. *Anal. Univ. Buc.* an. XXVII, p. 77–83.

Duchesne, J. C., Caruba, R., Iacconi, I. (1987) Zircon in charnockitic rocks from Rogaland (Southwest Norway); petrogenetic implications. *Lithos*, 20, p. 357–368.

Franz, G., Spear, K. (1985) Aluminous titanite (sphene) from the eclogite zone, South-Central Tauern Window, Austria. *Chemical Geology*, 50, p. 33–46.

Popescu, C. Gh. (1971) Despre retromorfismul şisturilor cristaline din zona zăcământului Bălan; semnificaţia sa metalogenetică şi geologică. *Anal. Univ. Buc. Geol.*, XX, p. 17–31.

Pupin, J. P. (1980) Zircon and granite petrology. *Contrib. Mineral. Petrol.*, 73, p. 207–220.

Pupin, J. P., Turco, G. (1972) Une typologie originale du zircon accesoire. *Bull. Soc. Cr. Mineral. Cristallogr.*, 95, p. 348–359.

Săndulescu, M. (1975) Essai de synthèse structurale des Carpathes. *Bull. Soc. Geol. France*, (7), XVII, 3, p. 299–358, Paris.

Streckeisen, A., Hunziker, J. C. (1974) On the Origin and Age of the Nepheline Syenite Massif of Ditro. *Schw. Miner. Petr. Mitt.*, 54, 1, p. 59–78, Zurich.

Rom. J. Mineralogy, 79, p. 131-142. Bucureşti, 1999

ÉLÉMENTS MINEURS DANS LES PEGMATITES DE LA SERIE MÉTAMORPHIQUE DE SOMEŞ (MONTS GILĂU)

Dan STUMBEA

Universitatea "Al. I. Cuza", Catedra de Mineralogie - Geochimie

B-dul Copou 20A, 6600, Iaşi, România

Key words: Apuseni Mts. Gilău Mts. Geochemistry. Minor elements. Pegmatites. Muscovite. Tourmaline.

Abstract: Chemical data (spectral and those obtained using an electron probe microanalyzer) gave us the opportunity to focus our researches on two directions: the chemical characterization of pegmatite minerals and pegmatites themselves (minor elements) and the distribution of these elements in different types of pegmatites or in different occurrences of pegmatite. The study of minor elements distribution after a SW-NE direction - that means parallel with the fold axis rendered evident by different researchers - revealed some geochimical *anomalies* for barium, lead, lithium, tin, titanium - in pegmatite as total sample, respectively for tin, gallium, niobium and manganese - in muscovite and tourmaline. These *anomalies* have a qualitative significance only and they superpose each other in some spatial areas: Crişeni area, middle valleys of Şoimului and Calului rivers and upper part of Iara Valley. In our opinion anomalies pointed out by our researches superpose on some granitization zones (under ultrametamorphic conditions) in which pegmatite bodies formed by anatexis processes and not by metamorphic differentiation as in the other areas; this phenomenon made possible the development of some postpegmatite stages in the evolution scheme: pegmatite - pneumatholyte - hydrothermal processes. Finally, lithium and rubidium distribution in potassium feldspars and muscovites show that pegmatites from mesometamorphic rocks of the Gilău Mts belong to *barren pegmatites of the mica-bearing provinces*, formed at great depth in the earth's crust (7–8 to 10–11 km); after Ginsburg et al. (1979) researches these pegmatites occurred as a result of anatectic processes. On the other hand we found a geochemical trend of these pegmatites to *barren pegmatites of rare-elements provinces*.

Introduction

Généralités

Les pegmatites mises en place dans les formations mésométamorphiques de la série (groupe) de Someş appartiennent - d'après la systématisation des pegmatites de Roumanie conçue par Mârza (1980) - à la *sousprovince pegmatitique Gilău - Muntele Mare*; cette sousprovince, conjointement avec les sousprovinces Preluca, Rodna et Gétique, fait partie de la province pegmatitique Carpatique. A son tour, la sousprovince Gilău - Muntele Mare a été divisée, par le même auteur, en deux districts: le district *Someşul Rece - Valea Iara* (avec les champs pegmatitiques Muntele Rece et Valea Iara), dont les pegmatites sont mises en place dans les formations de la série de Someş; le district *Geamăna - Măzăratu*, où les corps pegmatitiques ont comme roches encaissantes les mésométamorphites de la série de Baia de Arieş. En ce qui concerne nos recherches, elles ont eu comme objet d'étude les pegmatites mises en place dans les formations mésométamorphiques du cristallin de Gilău, plus précisément les pegmatites qui se trouvent dans les métamorphites de la série ("group") du Someş situées à l'est du granite de Muntele Mare.

La série de Someş - nommée *"group"* par Dimitrescu (1988) et, plus récemment, *"lithogroup"* par Balintoni (1997) (celui-ci introduisant aussi dans cette unité structurale la formation épimétamorphique d'Arada et la soit-dite *lithozone* Botfei) - est constituée à l'est du granite de Muntele Mare par des migmatites, leptynites, gneiss, micaschistes à l'almandine, disthène, staurotide, sil-

limanite et - subordonnémment - par des quartzites, amphibolites et calcaires cristallins; ces roches sont associées à des granitoïdes. Au point de vue lithostratigraphique, les recherches menées par de nombreaux géologues (Borcoş, Borcoş, 1962; Rădulescu, Dimitrescu, 1982; Dimitrescu, 1988; Hârtopanu et al., 1982 a, b, 1986 etc.) ont mis en évidence trois formations dans la série de Someş (la formation terrigène inférieure, la formation moyenne des gneiss quartzo-feldspathiques et la formation terrigène supérieure), dont seulement les premières deux ont été trouvées à l'est du granite de Muntele Mare. Parmi les éléments de tectonique décrits par les géologues, nous considérons importante pour nos recherches l'existence d'un pli orienté SO-NE dans les formations métamorphiques de la série de Someş, pli considéré comme synclinal par Hârtopanu et al. (1982 a, b) et Hârtopanu, Hârtopanu (1986), respectivement un anticlinal - Dimitrescu (1994). Les roches encaissantes des pegmatites ont été soumises à un métamorphisme régional progressif et, ultérieurement, rétrograde, Hârtopanu et Hartopanu (1986) soulignant le caractère polycyclique de ce processus; les auteurs mentionnés trouvent les suivantes lignes isogrades intersectées de métamorphisme: staurotide - disthène/staurotide, almandine/staurotide (I^{er} cycle); sillimanite ($II^{ème}$ cycle); biotite/chlorite ($III^{ème}$ cycle - rétromorphique).

Les pegmatites apparaissent soit sous forme de corps lenticulaires (simples ou ramifiés), soit comme des filons. Les filons ont des dimensions qui varient entre des mètres, dizaines et, rarement, centaines des mètres de longueur, respectivement des épaisseurs comprises entre moins d'un centimètre jusqu'à 10–20 mètres. Les corps pegmatitiques à l'aspect lenticulaire sont moins développés: longueurs de dizaines de mètres, rarement 250 m, et épaisseurs qui varient entre 5–50 m, plus rarement 100 m. Les corps pegmatitiques les plus développés ont été trouvés dans le périmètre Crişeni - Muntele Rece et ils ont fait l'objet de l'exploitation pour le feldspath. Les corps pegmatitiques filoniens représentent généralement des corps épigénétiques par rapport aux roches encaissantes, mais nous avons trouvé aussi des corps aux contours irréguliers avec des passages gradués vers la roche métamorphique.

La minéralogie des pegmatites du cristallin de Monts Gilău est une minéralogie très simple, caractéristique aux pegmatites métamorphiques: *quartz* (plusieurs génération), *feldspaths potassique* (microcline qui domine au point de vue quantitativement l'orthoclase), *feldspaths calco - sodiques* (albite - oligoclase) et, subordonnémment, *biotite, tourmaline, grenats*. Les recherches menées par d'autres scientifiques ont mis en évidence aussi la présence du *béryl* (Stoicovici, Trif, 1963; Constantinescu et al., 1976; Mârza, 1980, 1988), *cordiérite, staurotide, sillimanite, amphiboles* (Constantinescu et al., 1976).

Au point de vue chimique, les pegmatites étudiées dans cet ouvrage sont granitiques, mais leurs genèse est métamorphique. Ce dernier aspect est soutenu et argumenté par Mârza (1980), d'après lequel les granites (le granite de Muntele Mare), les pegmatites et les migmatites de Monts Gilău sont les produits d'un processus unitaire d'anatexie - granitisation (ultramétamorphique) développé en étapes et ils ont résulté soit par différenciation magmatique (fusion complète), soit par différenciation métamorphique (fusion partiale).

Moyens analytiques

Les données analytiques utilisées pour la caractérisation des minéraux pegmatitiques et des pegmatites de la série mésométamorphique de Someş ont été obtenues soit par nous-mêmes à l'aide d'une microsonde électronique marque CAMECA SX 50, dans le Laboratoire de Pétrologie de l'Université Paris VI (France), soit ont été mises à notre disposition par l'amabilité des chercheurs de l'Institut Géologique de Roumanie; les dernières analyses ont été obtenues par voie spectrale (soit par émission, soit par absorbtion).

Considérations géochimiques sur les éléments mineurs

Eléments mineurs dans les muscovites et les tourmalines pegmatitiques

Muscovite

Manganèse. Les muscovites pegmatitiques du cristallin de Gilău sont caractérisées par une participation modeste du manganèse, comprise entre 94 et 240 ppm, avec une moyenne de 154 ppm Mn. Les données fournies par la microsonde électronique indiquent des valeurs plus élevées (217–426 ppm Mn, avec une valeur moyenne de 296 ppm Mn); cet aspect est mis par nous sur le crédit d'une pureté plus élevée des échantillons analysés par la microsonde électronique, par rapport aux échantillons analysés par voie spectrale. La comparaison des teneurs en manganèse pour les muscovites étudiées avec celles publiées pour d'autres occurrences pegmatitique de Roumanie montre des valeurs plus basses pour les muscovites des pegmatites de Gilău. La distribution du manganèse par rapport au type minéralogique de pegmatite indique une diminution de la teneur, au fur et à mesure que la participation de la muscovite dans les pegmatites encaissantes augmente et que la participation du feldspath diminue.

L'étain participe dans les muscovites étudiées avec des valeurs qui varient entre 50 et 635 ppm (moyenne de 252 ppm Sn). La participation de l'étain

est plus élevée dans les muscovites des pegmatites plagioclase-microcliniques à muscovite (277 ppm Sn) et celles des pegmatites plagioclase-muscovitiques (715 ppmSn) mises en place dans des roches granitoïdes (pegmatites magmatiques), par rapport aux teneurs obtenues pour les muscovites provenant des pegmatites du même type minéralogique, mises en place dans des roches métamorphiques: 237 ppm Sn pour les pegmatites plagioclase - microcliniques à muscovite, respectivement 332 ppm pour celles plagioclase - muscovitiques.

La distribution des corps pegmatitiques sur une aire très étendue, la variation du relief et la mise en évidence de l'anticlinal orienté SO-NE nous ont mené à l'idée de voir s'il n'y a une règle qui contrôle la distribution des éléments mineurs - l'étain, en ce cas-là dans les minéraux pegmatitiques. Ainsi, nous trouvons intéressant de souligner quelques aspects: dans le périmètre étudié, le relief est plus élève dans le secteur SO et il diminue d'après une direction SO-NE, ce qui a comme signification géologique une profondeur plus élevée pour la mise en place des pegmatites du nord-est, par rapport aux pegmatites du secteur sud-ouest; d'autre part, les conditions physiques pression-température) qui règnent sur la mise en place des pegmatites sur les flancs de l'anticlinal SO - NE diffèrent de celles qui caractérisent les pegmatites plus proches de l'axe du pli.

Vu ce qui a été dit ci-dessus, on a projeté les échantillons analysés d'après une direction SO-NE et on a construit le diagramme de la figure 1, qui révèle

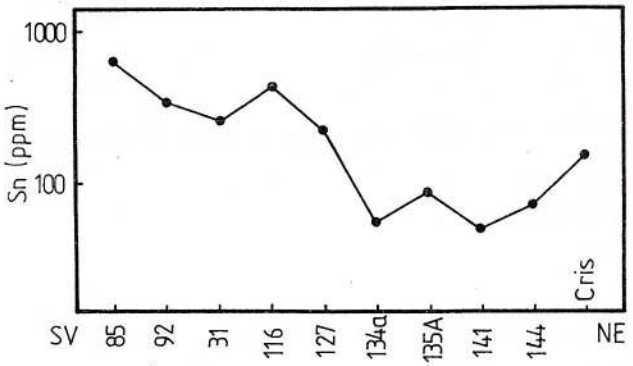

Fig. 1 - La distribution de l'étain dans les muscovites des pegmatites, d'après la direction SO-NE

d'une part la diminution de la participation de l'étain de sud-ouest vers le nord-est et, d'autre part, l'existence de quelques exceptions (échantillons 31, 116, 127, 135A et Crişeni) - nommées par nous *anomalies* positives - situées sur le cours supérieur de la vallée de la Iara (éch. 116), le cours moyen de la Vallée Şoimului (éch. 31), la Vallée Ursului (éch. 127) et le périmètre de Crişeni (fig. 2). Il faut souligner que les *anomalies* trouvées offrent seulement une information qualitative, par suite de la façon dont elles ont été mises en évidence.

Enfin, les teneurs en étain des muscovites étudiées sont beaucoup plus élevées par rapport aux données publiées pour les autres sousprovinces pegmatitiques de Roumanie.

Titane. La teneur en titane des muscovites varie entre 122 et 935 ppm, avec une valeur moyenne de 465 ppm Ti, supérieure à celle des muscovites provenant des pegmatites mises en place dans les roches métamorphiques (412 ppm Ti). De l'autre part, la participation de l'étain dans les muscovites des pegmatites des sousprovinces Preluca, Rodna et Gétique est plus élevée par rapport aux muscovites étudiées par nous.

Cuivre. Les muscovites analysées montrent une teneur en cuivre comprise dans l'intervalle < 1–16 ppm, la majeure partie des valeurs balayant le domaine < 1–4 ppm.

Plomb. Le plomb participe comme élément mineur dans les muscovites pegmatitiques des Monts Gilău dans un domaine restreint de valeurs (4,4–11,6 ppm Pb) avec une moyenne (6 ppm Pb) qui ressemble à celle trouvée pour les pegmatites des granitoïdes (5 ppm Pb). L'intervalle de fréquence maximum des teneur est compris entre 4,4 et 6,2 ppm Pb.

Le *gallium* est présent en quantités relativement importantes dans les muscovites étudiées; il est capable de pénétrer la structure de ce minéral en substituant l'aluminium, par suite de leurs rayons ioniques proches: 0,57 kX pour Al^{3+}, respectivement 0,62 kX pour Ga^{3+}.

La participation du gallium dans les muscovites des pegmatites mises en place en métamorphites (76–146 ppm Ga) a une moyenne - 95 ppm - plus basse par rapport à la teneur moyenne trouvée pour les muscovites des pegmatites magmatiques - 132 ppm Ga. La distribution du gallium dans les muscovites par rapport à la position de prélèvement - après la direction SO-NE dont on a déjà parlé - met en évidence la manifestation des *anomalies* positives pour cet élément (fig. 3) qui se superposent à peu près sur les mêmes positions spatiales que celles trouvées pour l'étain: cours supérieur de la vallée de la Iara (éch. 116), cours moyen de la Vallée Şoimului (éch. 31) et la Vallée Ursului (éch. 127) (fig. 2); on observe une légère augmentation du gallium dans le périmètre Crişeni (éch. 144, Crişeni).

Niobium. La participation du niobium dans les muscovites des pegmatites de la série de Someş varie entre 23 et 207 ppm (82 ppm Nb - moyenne). Par rapport au type minéralogique de pegmatite, on a trouvé les suivantes valeurs moyennes: 68 ppm Nb pour les muscovites des pegmatites microcliniques à structure graphique; 98 ppm Nb - pegmatites plagi-

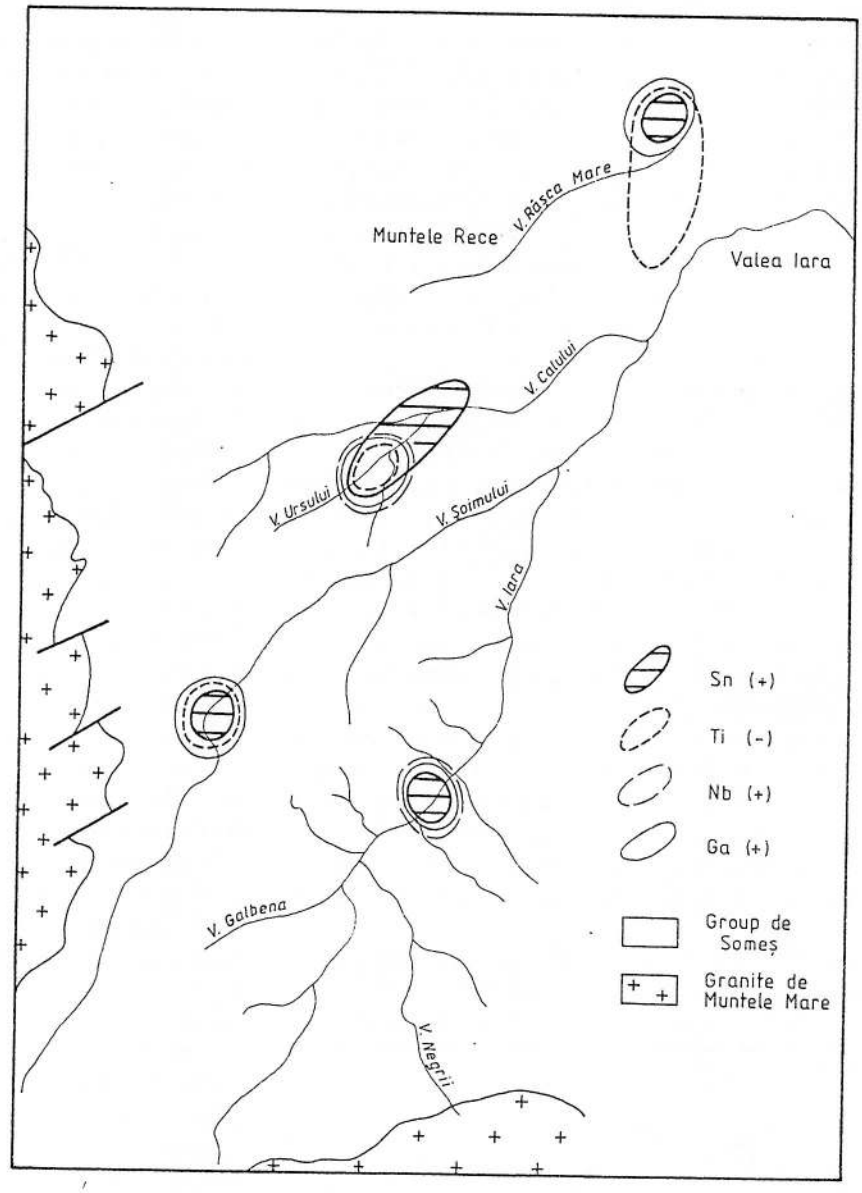

Fig. 2 – Les anomalies géochimiques qualitatives mises en évidence pour quelques éléments mineurs, dans les muscovites pegmatitiques des Monts Gilău

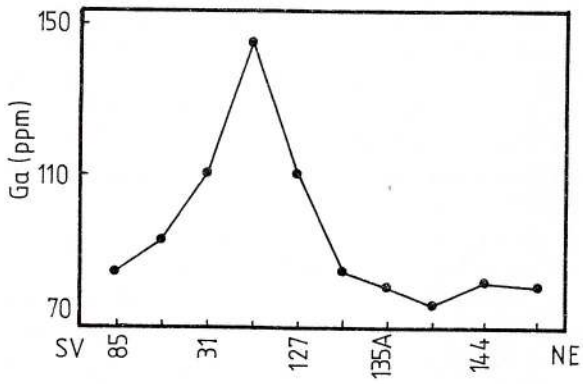

Fig. 3 - La distribution du gallium dans les muscovites des pegmatites, d'après la direction SO-NE

oclase - microcliniques à muscovite; 36 ppm Nb - pegmatites plagioclase - muscovitiques.

L'analyse de la teneur en niobium d'après la direction SO - NE révèle - encore une fois - la manifestation des zones anomales (*anomalies* positives) dans les périmètres suivants: vallée de la Iara (éch. 116), Vallée Ursului (éch. 127), Vallée Calului (éch. 135 A), Crişeni (éch. 144, Crişeni).

Lithium. La concentration du lithium comme élément mineur dans les muscovites des pegmatites étudiées est inférieure à celle mise en évidence pour les biotites; l'intervalle de variation pour cet élément est compris entre 54 et 232 ppm, avec une moyenne de 137 ppm Li. Par rapport aux muscovites pegmati-

tiques des Monts Preluca - Lăpuş et celles de la vallée Gilort, les muscovites étudiées par nous présentent une teneur plus élevée.

La distribution du lithium dans les divers types minéralogiques de pegmatite montre des teneurs de 232 ppm Li dans les pegmatites à structure graphique, 127 ppm Li dans les pegmatites plagioclase - microcliniques à muscovite et 125 ppm Li dans les pegmatites plagioclase - muscovitiques. La variation du lithium par rapport à la direction SO-NE (fig. 4) met en évidence une participation généralement constante de cet élément, avec des valeurs plus élevées (*anomales*) pour les échantillons des occurrences pegmatitiques du cours supérieur de la vallée de la Iara (éch. 116), cours moyen de la Vallée Calului (éch. 134 a), cours de la Vallée Şoimului (éch. 92) et le périmètre Crişeni (fig. 2). D'autre part, la projection des teneurs de lithium sur le diagramme de Trueman et Černý (1982) indique la disposition des échantillons dans le domaine des *pegmatites stériles mises en place dans les provinces micafères* (fig. 5); les valeurs les plus élevées passent vers le champs des *pegmatites stériles situées dans les provinces aux éléments rares*.

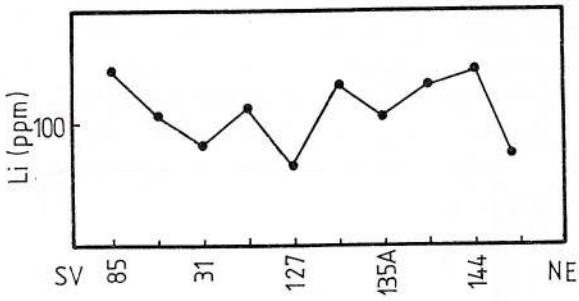

Fig. 4 – La distribution du lithium dans les muscovites des pegmatites, d'après la direction SO-NE

Rubidium. La teneur en rubidium varie dans les muscovites étudiées entre 60 et 1582 ppm, mais le nombre réduit d'analyses et la différence importante entre les deux limites ne nous a pas permis de calculer une moyenne crédible. De l'autre part, la projection des valeurs sur le diagramme de la figure 5 indique la disposition des échantillons à la limite du domaine des pegmatites stériles des provinces à mica, avec le domaine des pegmatites stériles des provinces aux éléments rares; on remarque la similitude du résultat avec celui obtenu en utilisant la teneur en lithium des muscovites.

Tourmaline

Zinc. Dans la tourmaline des pegmatites des Monts Gilău, le zinc a une participation entre 1000 et 2550 ppm, avec une teneur moyenne de 1262 ppm Zn.

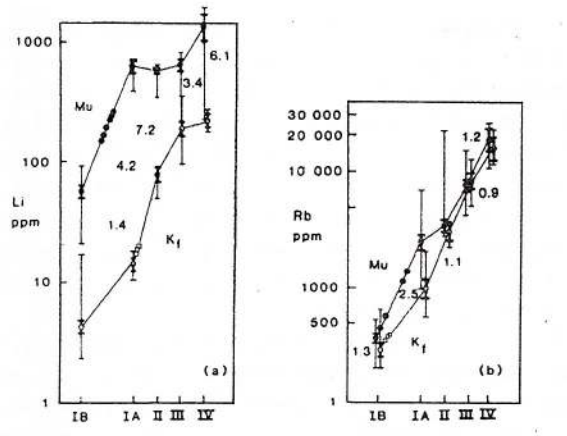

Fig. 5 – La teneur spécifique en lithium (a) et rubidium (b) dans la muscovite des pegmatites: *stériles* mises en place dans les provinces à mica (IB) et *stériles* aux éléments rares (IA); *muscovite-feldspathiques* au Be, Nb, Ta (II); *spoduméniques* au Li, Be, Ta (Nb, Sn) (III); à *spodumène et lépidolite* avec du Li, Cs, Ta, Be (Nb, Sn) (IV) (d'après Trueman, Černý, 1982)

Ces valeurs sont nettement plus élevés par rapport aux teneurs caractéristiques des tourmalines pegmatitiques des autres sousprovinces de Roumanie: 175 ppm Zn dans les tourmalines des pegmatites du massif Rodna (Murariu, 1979); 50 ppm Zn dans les tourmalines pegmatitiques de Copalnic (Murariu et Dumitrescu, 1976). D'autre part, Hann (1987) met en évidence pour les tourmalines de Muntele Mic un intervalle plus étendu de variation de la teneur en zinc (60–1150 ppm), dont la limite supérieure est comparable avec les données trouvées par nous.

Lithium. La participation du lithium dans les tourmalines pegmatitiques étudiées par nous varie entre 58 et 158 ppm (79 ppm Li - moyenne). Les données analytiques montrent une teneur de 58 ppm Li pour les tourmalines des pegmatites à structure graphique, 70 ppm Li pour les tourmalines des occurrences plagioclase - microcliniques, 95 ppm Li - tourmalines des pegmatites plagioclase - microcliniques à muscovite et 60 ppm Li - tourmalines des pegmatites plagioclase - muscovitiques.

Il est intéressant de souligner que la participation du lithium dans les tourmalines pegmatitiques des Monts Gilău est bien plus élevée par rapport aux données publiées par Murariu et Zămârca (1979) pour les occurrences de la sousprovince pegmatitique Preluca (30 ppm Li) et Hann (1987) pour les occurrences de Muntele Mic - sousprovince pegmatitique Gétique (33 ppm Li - valeur moyenne).

Gallium. La tourmaline - de pair avec la muscovite - représente le principal concentreur de gallium, par suite de la liaison de cet élément avec l'aluminium; le domaine de variation pour la teneur en gallium est

61,5-96 ppm (66,6 ppm Ga comme valeur moyenne). La participation du gallium est identique pour les tourmalines des pegmatites à structure graphique et des pegmatites plagioclase - microcliniques (80 ppm Ga); les tourmalines provenant des pegmatites plagioclase - microcliniques à muscovite présentent la teneur la plus élevée en gallium (96 ppm), tandis que dans les tourmalines des pegmatites plagioclase - muscovitiques, la participation du gallium soit la plus modeste (61,5 ppm).

La variation de la teneur en gallium des tourmalines par rapport à la position des occurrences pegmatitiques d'apres la direction SO-NE (c'est-à-dire parallèle à la direction de l'axe anticlinal) montre une corrélation négative entre les paires de valeurs *teneur en gallium/distance par rapport à un point repère (O)* situé au contact du granite de Muntele Mare avec les roches métamorphiques encaissantes (fig. 6).

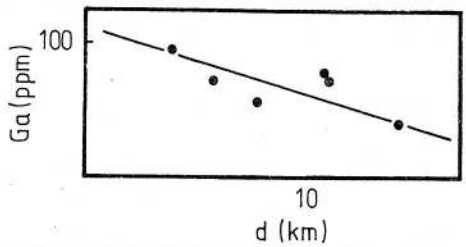

Fig. 6 – La variation de la teneur en gallium des tourmalines, d'après la direction SO-NE, par rapport le point repère O

La comparaison des données analytiques caractérisant les tourmalines pegmatitiques des Monts Gilău avec celles publiées par Constantinescu et al. (1976) pour les occurrences du massif Preluca-Lăpuş (58 ppm Ga), respectivement celles de Hann (1987) pour les occurrences de Muntele Mic (17–48 ppm Ga), montre des teneurs supérieures pour le premier cas.

Manganèse. La participation du manganèse dans les tourmalines des pegmatites étudiées varie entre 1000 et 2000 ppm, avec une moyenne de 1358 ppm Mn. Pour cet élément aussi on a mis en évidence des valeurs différentes par rapport au type minéralogique de pegmatite: 1150 ppm Mn dans les tourmalines provenant des pegmatites microcliniques à structure graphique; 1000 ppm Mn pour les tourmalines des pegmatites plagioclase - microcliniques; 1516 ppm Mn - pegmatites plagioclase - microcliniques à muscovite; 1450 ppm Mn - pegmatites plagioclase - muscovitiques.

L'étude de la distribution du manganèse d'apres la direction SO-NE (fig. 7) met aussi en évidence des valeurs *anomales* (positive) qui se superposent partiellement sur les périmètres anomaux décrits au cours de cet ouvrage (fig. 8). D'autre part, la comparaison entre la teneur en manganèse trouvée par Murariu (1979) pour un échantillon de tourmaline provenant des micaschistes de la série de Rodna et la participation du manganèse dans les tourmalines pegmatitique de Monts Gilău révèle la valeur la plus élevée du manganèse dans le deuxième cas; les seules valeurs rapprochées de celles publiées par Murariu (1979) sont les teneur qui caractérisent les tourmalines des occurrences situées dans les périmètres où on n'a pas mis en évidence de valeurs anomales pour les différents éléments mineurs. D'après Rankama et Sahama (1970), le manganèse se concentre notablement dans les étapes tardives - pegmatitique et pneumatolytique - du processus magmatique; cet aspect pourrait signifier que dans l'évolution des pegmatites des Monts Apuseni peuvent être décélés des stades tardifs (pneumatolytiques et, possiblement, hydrotermaux) qui se développent seulement dans les périmètres où l'on a pu mettre en évidence des teneurs anomales pour les éléments mineurs.

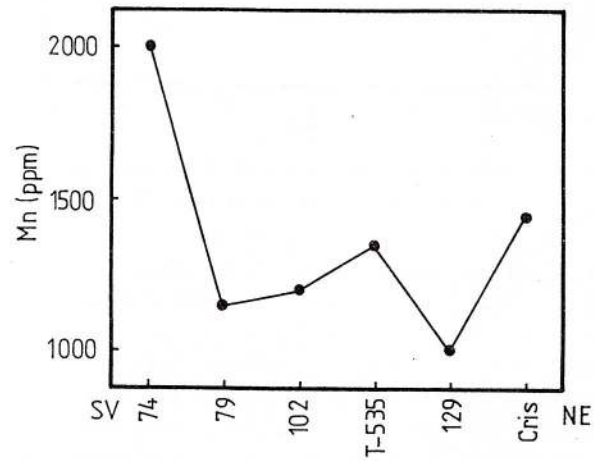

Fig. 7 – La distribution du manganèse dans les tourmalines des pegmatites, d'après la direction SO-NE

Titane. Les limites de variation du titane dans les tourmalines étudiées sont 700 et 1800 ppm; la moyenne mise en évidence par nous est de 1195 ppm Ti. La distribution du titane dans les tourmalines d'après la direction SO-NE (fig. 9) montre des valeurs anomales (*anomalies* négatives) dans les occurrences situées sur le cours supérieur de la vallée de la Iara (éch. 102), respectivement Criseni (éch. Crişeni) (fig. 8).

Plomb. La distribution du plomb dans la tourmaline des pegmatites des Monts Gilău est relativement modeste; elle est comprise entre 4,3 et 25,5 ppm, avec une moyenne de 12,6 ppm Pb. Cette donnée est comparable avec celles publiées par Murariu (1979) pour les occurrences du massif Rodna (10,8 ppm Pb), respectivement Hann (1987) pour les occurrences de Muntele Mic (8 ppm Pb).

Le *cuivre* participe dans les tourmalines étudiées dans une proportion de 1 ppm, jusqu'à 9 ppm. La

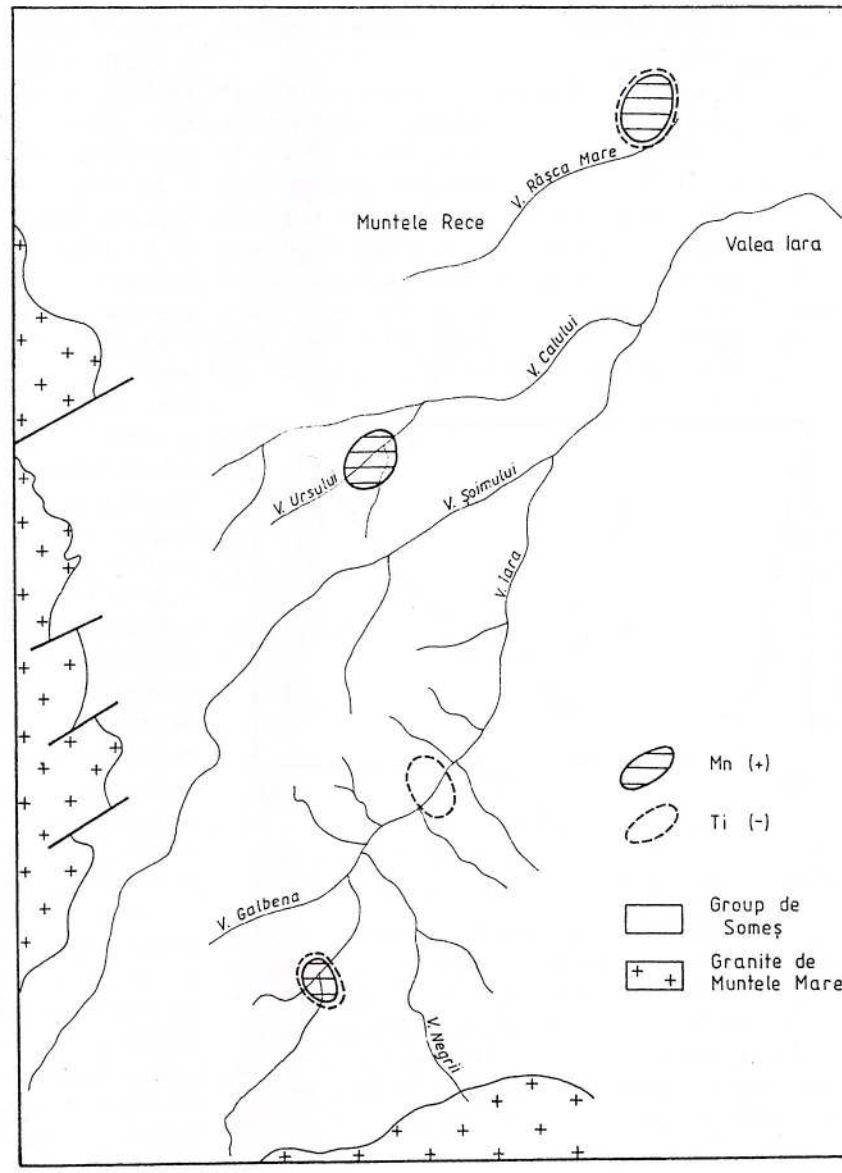

Fig. 8 – Les anomalies géochimiques qualitatives mises en évidence pour quelques éléments mineurs, dans les tourmalines pegmatitiques des Monts Gilău

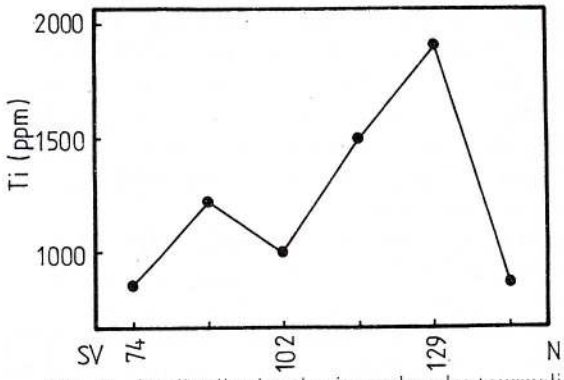

Fig. 9 - La distribution du titane dans les tourmalines des pegmatites, d'après la direction SO-NE

moyenne établie par nous est comparable à celle calculée pour les tourmalines de Muntele Mic (6 ppm Cu) - Hann (1987), mais nettement inférieure par rapport aux données de Murariu (1979), respectivement Murariu et Dumitrescu (1976) concernant les occurrences du massif Rodna (114 ppm Cu) et celles de Copalnic (130 ppm Cu).

Eléments mineurs dans les pegmatites

Baryum. Les pegmatites mises en place dans les formations métamorphiques des Monts Gilău sont caractérisées par une teneur en baryum qui varie entre 11,5 et 550 ppm avec une valeur moyenne de 112 ppm Ba, nettement inférieure à celle obtenue pour les pegmatites intragranitiques de Muntele Mare (511 ppm Ba).

Une participation plus importante du baryum a été trouvée pour les pegmatites plagioclase-microcliniques (382 ppm Ba) et celles plagioclase-muscovitiques (202 ppm Ba), tandis que la teneur

la plus réduite caractérise les pegmatites à structure graphique (21 ppm Ba).

Le diagramme de variation du baryum par rapport à la place que le corps pegmatitique occupe dans le périmètre étudié (fig. 10) - c'est-à-dire d'après la direction SO-NE révèle la variation importante de cet élément. En plus, il est intéressant de souligner que les teneurs les plus élevées sont caractéristiques aux périmètres où l'on a trouvé des valeurs anomales pour d'autres éléments mineurs, pendant cette étude: cours supérieur de la vallée de la Iara, cours moyen de la Vallée Şoimului, Vallée Ursului, le périmètre de Crişeni (fig. 11).

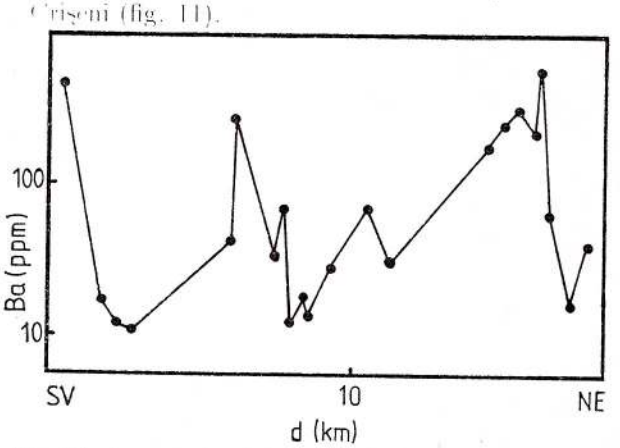

Fig. 10 – La variation de la teneur du baryum en pegmatites d'après la direction SO-NE, par rapport au point repère O

Le *strontium* participe dans les pegmatites étudiées avec des teneurs comprises entre des limites très larges: 3–155 ppm; la moyenne est 36 ppm Sr. De meme que pour le baryum, on remarque des participations plus importantes du strontium dans les pegmatites du granite de Muntele Mare (98 ppm Sr) dans lesquelles, en plus, le domaine de variation est plus restreint: 73–142 ppm Sr.

Par rapport au type minéralogique de pegmatite, la teneur la plus élevée en strontium a été trouvée dans les pegmatites plagioclase - microcliniques (100 ppm Sr), tandis que les pegmatites plagioclase - muscovitiques et celles microcliniques à structure graphique présentent pour la participation du strontium des valeurs approchées: 34 ppm Sr, respectivement 29 ppm Sr.

Plomb. La participation du plomb dans les pegmatites des Monts Gilău s'encadre dans un intervalle large de variation (3–250 ppm); la moyenne calculée par nous est de 54 ppm Pb, c'est-à-dire un peu plus basse que celle mise en évidence pour le plomb des pegmatites intragranitiques (63 ppm Pb).

En établissant les limites de variation et la moyenne des teneurs en plomb par rapport au type minéralogique de pegmatite, on a pu mettre en évidence des participations voisines pour les pegmatites plagioclase-microcliniques (30 ppm Pb), les pegmatites plagioclase - microcliniques à muscovite (32 ppm Pb) et celles plagioclase - muscovitiques (25 ppm Pb), tandis que dans les pegmatites microcliniques à structure graphique le plomb participe avec une teneur bien plus élevée (53 ppm).

La présence du plomb dans les pegmatites est due - d'après Rankama et Sahama (1970) - à sa capacité de remplacer le potassium et, subordonnémment, le calcium; cet aspect nous a mené à rédiger les diagrammes de corrélation Pb: K_2O (fig. 12) et Pb: CaO (fig. 13) qui mettent en évidence - d'une part - une population de valeurs caractérisée par des corrélations positives (a) entre les deux paires de valeurs et - de l'autre part - une population de valeurs manifestant une corrélation négative (b). Il est intéressant de souligner que les échantillons pour lesquels on a trouvé la corrélation négative proviennent de périmètres nommés par nous *anomaux* par suite de la mise en évidence des *anomalies* dont on a déjà parlé au cours de cette étude, pendant que les autre ont été prélevés du *fond* géochimique de la région. En plus, la variation de la teneur en plomb des pegmatites d'après la direction SO-NE utilisée fréquemment au cours de cette étude, suggère - une fois encore - la manifestation des *anomalies* pour l'élément dont nous parlons, dans les périmètres Crişeni, Vallée Ursului, Vallée Şoimului et le cours supérieur de la vallée Iara (fig. 11).

Cuivre. La distribution du cuivre dans les pegmatites des Monts Gilău se range dans un intervalle de variation compris entre 1 et 11 ppm. La liaison mise en évidence par nous entre la participation du cuivre et le type minéralogique de pegmatite est mise au crédit du pouvoir différent de captation manifesté par la muscovite (teneur moyenne en cuivre: 4 ppm), par rapport aux feldspaths (teneur moyenne en cuivre: < 1 ppm).

Titane. La teneur en titane des pegmatites étudiées s'encadre entre des limites très larges de variation (9–2400 ppm), avec une moyenne plutôt réduite (258 ppm Ti). La distribution du titane par rapport à la direction SO-NE met en évidence des valeurs anomales (*anomalies* négatives) pour les échantillons des périmètres Crişeni, Vallée Ursului et le cours moyen de la Vallée Şoimului.

Manganèse. Les pegmatites des Monts Gilău sont caractérisées par des teneurs en manganèse qui varient entre des limites très larges (25–3500 ppm), nos recherches mettant en évidence une distribution de la participation de cet élément par rapport au type mineralogique de pegmatite: 879 ppm Mn dans les pegmatites plagioclase-microcliniques à muscovite; 295 ppm Mn dans les pegmatites microcliniques à structure graphique; 224 ppm Mn dans les pegmatites plagioclase-microcliniques; 86 ppm Mn dans les peg-

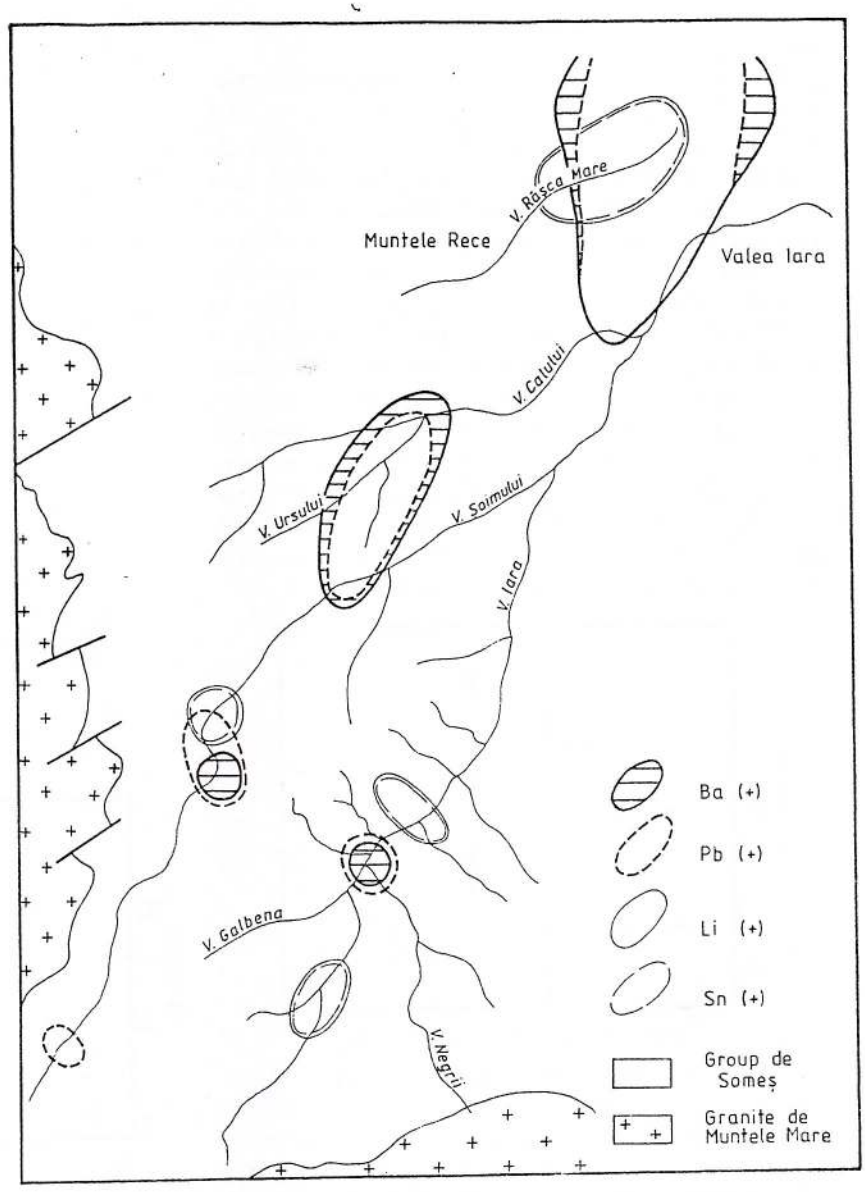

Fig. 11 – Les anomalies géochimiques qualitatives mises en évidence pour quelques éléments mineurs, dans les pegmatites des Monts Gilău

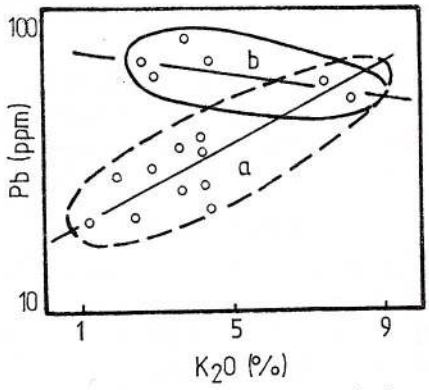

Fig. 12 – Le diagramme de corrélation Pb: K_2 pour les pegmatites des Monts Gilău. a, pegmatites du *fond* géochimique; b, pegmatites des zones *anomales*.

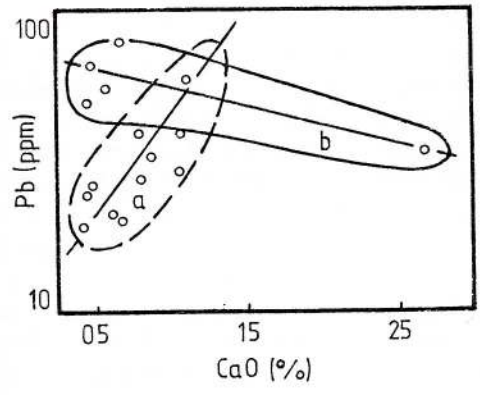

Fig. 13 – Le diagramme de corrélation Pb: CaO pour les pegmatites de Monts Gilău. a, pegmatites du *fond* géochimique; b, pegmatites des zones *anomales*.

matites microcline-muscovitiques à structure graphique.

La teneur en *lithium* des pegmatites est comprise entre 8,5 et 263, avec une valeur moyenne de 78,6 ppm Li, semblable à celle trouvée pour les pegmatites intragranitiques de Muntele Mare (75,5 ppm Li). Pour le cas du lithium aussi, on peut discuter d'un controle minéralogique de sa participation (fig. 14), contrôle soutenu en plus par le diagramme de corrélation entre la teneur en Li et la participation de la muscovite dans les associations minéralogiques des pegmatites (fig. 15). Ce dernier diagramme suggère la corrélation positive entre les deux paramètres et met en évidence la séparation des échantillons des périmètres de *fond* (a) et ceux *anomaux* (b). D'autre part, la poursuite de la teneur en lithium dans les différentes occurrences pegmatitiques d'après la direction SO-NE prouve l'existence des *anomalies* représentées dans la figure 11.

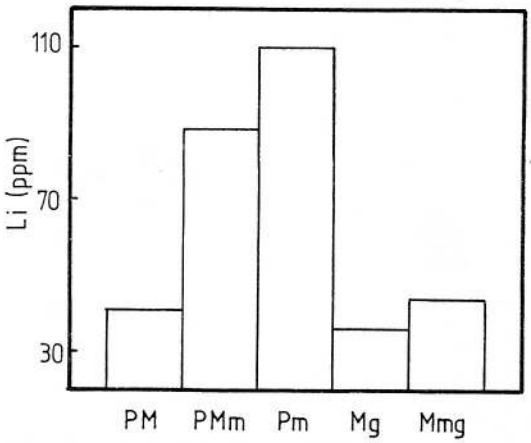

Fig. 14 – La distribution du lithium par rapport au type minéralogique de pegmatite. PM, pegmatites plagioclase-microclinique; PMm, pegmatites plagioclase-microcliniques à muscovite; Mg, pegmatites microcliniques à structure graphique; Mmg, pegmatites microcline-muscovitiques à structure graphique.

Etain. Les pegmatites mises en place dans les métamorphites de la série de Someş présentent une participation de l'étain comprise entre 1,5 et 440 ppm, avec une moyenne de 54 ppm Sn. En analysant la figure 15, on peut observer une augmentation de la teneur en cet élément en partant des échantillons de granite (7,9 ppm Sn), jusqu'à la pegmatite mise en place dans les roches métamorphiques (54 ppm Sn).

La variation de l'étain par rapport à la position des occurrences projétées sur la direction SO-NE (fig. 6) met en évidence des *anomalies* positives pour cet élément (fig. 11), superposées sur les zones anomales déjà établies à l'aide d'autres éléments mineurs.

La teneur en *bore* des pegmatites étudiées varie dans un intervalle large de valeurs (7–1900 ppm),

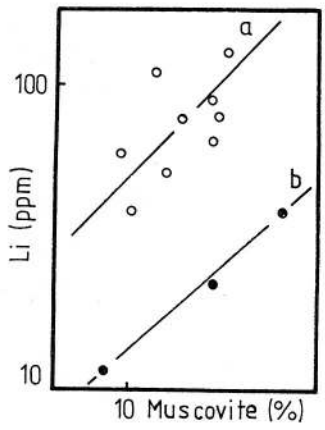

Fig. 15 – Le diagramme de corrélation entre la teneur en lithium et la participation de la muscovite dans les associations minéralogiques des pegmatites des Monts Gilău. a, pegmatite du *fond* géochimique; b, pegmatite des zones *anomales*.

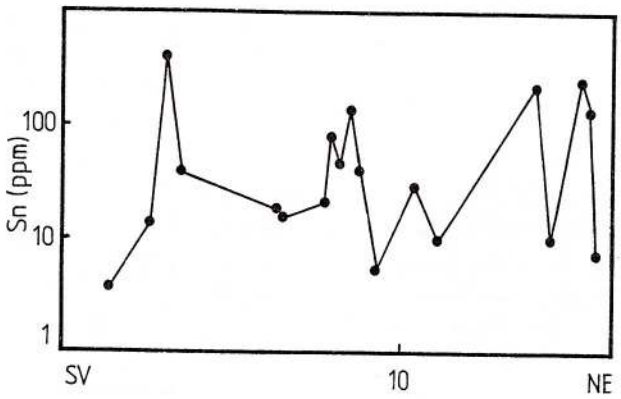

Fig. 16 – La variation de la teneur en étain en pagmatites d'après la direction SO-NE, par rapport au point repère O

avec une moyenne de 425 ppm B, supérieure à celles obtenues pour les pegmatites intragranitiques de Muntele Mare (214 ppm B), respectivement le granite même (< 83 ppm B) (fig. 17).

Conclusions

L'étude de la distribution des éléments mineurs dans les pegmatites mises en place dans les roches métamorphiques des Monts Gilău nous mène à tirer les conclusions suivantes.

Les pegmatites mises en place dans les mésométamorphites de la serie de Someş présentent les caractéristiques des pegmatites d'origine métamorphique et elles sont, généralement, semblables à celles décrites par divers auteurs dans

les autres sousprovinces pegmatitiques de Roumanie. Par contre, on a trouvé des différences nettes - au niveau des éléments mineurs - entre les pegmatites étudiées par nous et les pegmatites intragranitiques de Muntele Mare, ce qui prouve la genèse différente des deux types de pegmatites: *magmatique* pour les pegmatites intragranitiques, respectivement *métamorphique* pour les pegmatites de la série de Someş.

Le mécanisme génétique responsable de la mise en place des pegmatites du cristallin de Gilău est celui de la *différenciation métamorphique* pour la majeure partie des occurrences, mais les anomalies qualitatives superposées décrites au cours de cette étude mettent en évidence également la manifestation des *processus anatectiques* dans certains périmètres de la région, ce qui a permis le développement des stades tardifs d'évolution dans la succession pegmatitogenèse - pneumatolyse - hydrothermalisme; ces stades sont responsables de la manifestation des anomalies décrites au niveau des éléments mineurs étudiés (par exemple Li, Sn, Pb).

À notre avis, le développement des stades tardifs est en étroite relation avec la variation des paramétres *pression - température* dans le périmètre géologique étudié. Ainsi, les pegmatites du secteur sud-ouest se sont formées à des profondeurs plus réduites, c'est-à-dire à des pressions plus basses (on pourrait donc envisager des températures plus élevées) par rapport aux corps pegmatitiques du nord-est; d'une part, les pegmatites proches par rapport à l'axe anticlinal se sont formées dans les conditions d'une pression plus importante, par rapport aux pegmatites éloignées de l'axe. Ces aspects sont prouvés par nos récentes recherches (Stumbea, 1997; Stumbea, 1998) qui mettent en évidence - d'une part - des températures plus élevées pour les pegmatites du secteur sud-ouest, par rapport aux corps du nord-est et - d'autre part - une diminution des températures des pegmatites au fur et à mesure que les corps pegmatitiques occupent des positions plus proches par rapport à l'axe anticlinal.

Les anomalies sont (il faut le dire encore une fois) *qualitatives* et - par du fait du nombre plutôt réduit de données analytiques - *ponctuelles*, mais nous pouvons avancer l'hypothèse conformément à laquelle elles s'inscriveraient sur une ligne courbe allongée d'après la direction de l'axe anticlinal, parallèle donc aux isolignes de température trouvées par nous au cours des études géothermométriques (Stumbea, 1997; Stumbea 1998). Cet aspect nous porte à opiner que sur cette ligne courbe le *jeu* de la variation des paramètres évoqués (la profondeur de la mise en place, la position des corps par rapport à la charnière de l'anticlinal) produisent des conditions P-T semblables, qui permettent le développement des stades tardifs d'évolution (pneumatolyse-hydrothermalisme). En plus, cette courbe se superpose d'une manière approximative sur la limite du changement de la lithologie (faciès à gneiss/faciès à micaschistes) ce qui doit être accompagner d'une modification du chimisme de la roche au crédit de laquelle les pegmatites se sont formées.

Il faut dire, aussi, qu'on ne peut pas nier la possibilité que des résultats semblables à ceux presentés (anomalies géochimiques, isolignes de température) soient mis au crédit des éventuels bombements (apex) du granite de Muntele Mare, cachés sous les formations mésométamorphiques de la série de Someş. Quand même, une telle hypothèse devrait être prouvée - au moins - par des résultats d'investigation géophysique, de même que la première hypothèse (celle de la relation génétique entre les occurrences pegmatitiques et le pli anticlinal) devrait être prouvée - à son tour - par des recherches structurales. En plus - faut le souligner - les résultats offerts par la première hypothése ne sont que partiellement en accord avec les isogrades métamorphiques trouvées par Hârtopanu et al. (1986).

Finalement, la teneur en lithium et rubidium de la muscovite montre l'appartenance des pegmatites étudiées à un domaine de transition entre celui des *pegmatites stériles mises en place dans les provinces à muscovite* et le domaine des *pegmatites stériles mises en place dans les provinces aux métaux rares*.

Bibliografie

Balintoni, I. (1997) Geotectonica terenurilor metamorfice din România. Ed. Carpatica, 176 p., Cluj-Napoca.

Borcoş, M., Borcoş, E. (1962) Cercetări geologice şi petrografice în regiunea Runc-Segacea- V. Ierii-sat (bazinul v. Iara, Munţii Apuseni). *D. S. Com. Geol.*, XLVII, p. 131–148, Bucureşti.

Constantinescu, R., Murariu, T., Iosof, V., Tiepac, I., Mânzatu, S., Movileanu, A., Pomârleanu, V. (1976) Petrografia, mineralogia şi studiul geochimic al pegmatitelor din zona Muntelui Mare (Munţii Apuseni). Arhiva I.G.R., Bucureşti.

Dimitrescu, R. (1988) Note sur la structure du cristallin "autochtone" du Gilău du sud-ouest. *D. S. Inst. Geol. Geofiz.*, p. 75–83, Bucureşti.

— **(1994)** Structura părţii centrale a Munţilor Gilăului. *St. cerc. geologie*, 39, p. 3–6, Bucureşti.

Hann, H.P. (1987) Pegmatitele din Carpaţii Meridionali. Ed. Acad. R. S. R., p. 141, Bucureşti.

Hârtopanu, I., Borcoş, M., Boştinescu, S., Dimitrescu, R. (1982 a) Harta geologică a R. S. România, sc.: 1 : 50.000, foaia Muntele Mare, Inst. Geol. Geofiz. Bucureşti.

— **, Hârtopanu, P., Balintoni, I., Borcoş, M., Rusu, A., Lupu, M., (1982 b)** Harta geologică a R. S. România, sc.: 1 : 50.000, foaia Valea Ierii, Inst. Geol. Geofiz., Bucureşti.

— , **Hârtopanu, P. (1986)** Interesecting isograde - a possible way to find out the polymetamorphism. An example: The Someş series. *D. S. Inst. Geol. Geofiz.*, 70–71/1, p. 291–299, Bucureşti.

Mârza, I., (1980) Considération génétiques sur les pegmatites du cristallin de Gilău (Monts Apuseni) et la province pegmatitique carpatique. *An. Inst. Geol. Geofiz.*, LVII, p. 423–432, Bucureşti.

— , **Pomârleanu, E., Pomârleanu, V. (1988)** Beryl in some pegmatites in the Bondureasa valley (Apuseni Mountains). *Studia Univ. "Babeş - Bolyai", Geol.-Geogr.*, 1, p. 69–76, Cluj-Napoca.

Murariu, T., Dumitrescu, M. (1976) Contributions à la géochimie et géothermométrie des pegmatites de Copalnic (Massif de Preluca - Lăpuş). *D. S. Inst. Geol. Geofiz.*, LXII/1, p. 379–398, Bucureşti.

— **(1979)** Studiul mineralogic, geochimic şi structural al pegmatitelor din Munţii Rodnei. *St. tehn. econ., I, 15, Mineralogie-Petrografie*, p. 3–272, Bucureşti.

— , **Zămârcă, A. (1979)** Litiul în pegmatitele din Munţii Apuseni. *An. Univ. "Al. I. Cuza"*, XXV, seria II b, p. 13–20, Iaşi.

Rankama, Th., Sahama, K. (1970) Geochimia. Ed. Tehn., p. 791, Bucureşti.

Rădulescu, D., Dimitrescu, R. (1982) Petrologia endogenă a teritoriului R. S. R. Partea a-II-a. Petrologia rocilor magmatice şi metamorfice. Universitatea din Bucureşti, p. 120.

Stoicovici, E., Trif, A. (1963) Pegmatitul din Munţii Apuseni. *Rev. Minelor*, XIV/12, p. 534–545, Bucureşti.

Stumbea, D. (1997) La température d'engendrement des pegmatites des Monts Apuseni. *An. Univ. "Al. I. Cuza", XLII-XLIII (1996–1997), Geologie*, p. 77–85, Iaşi.

— **(1998)** Pegmatitele din cristalinul Gilăului (Mun[tii Apuseni). Teză de doctorat, Universitatea "Babeş - Bolyai", Cluj - Napoca.

Trueman, D. L., Černý, P. (1982) Exploration for rare-element granitic pegmatites. *Short Course Handbook*, 8, p. 463–493, Winnipeg.

Rom. J. Mineralogy, 79, p. 143-149, Bucureşti, 1999

SULFATIC FACIES IN THE NORTH-WESTERN PART OF THE TRANSYLVANIAN BASIN-MESEŞ AREA AND THEIR GENETIC SIGNIFICANCE

Ioan BEDELEAN, Nicoleta BICAN, Horea BEDELEAN

Universitatea "Babeş-Bolyai", Catedra Mineralogie-Petrometalogenie,

Str. M. Kogălniceanu Nr. 1, 3400 Cluj-Napoca, Romania

Key words: Meseş area. Sulfates. Eocene. Laminithic facies. Nodular facies. "Chicken-wire". Enterolithic facies. Clastic gypsum.

Abstract: The sulfatic accumulations from the Meseş area are situated at the level of the Foidaş Formation (Upper Lutetian) and of the Turbuţa Formation (Lower Priabonian), which represents the equivalent of the Jebuc Formation from the Gilău area (Popescu, 1984). The mineralogical and structural-textural features of the evaporitic deposits generally reflect both the depositional context, in which the separation from natural intrabasinal solutions played an essential role, and a complex of diagenetic transformations, which caused significant remobilizations and recrystallizations at the level of these evaporites. From a mineralogical point of view, they are represented by gypsum, anhydrite and subordinate celestite and barite. A complex characterisation of the typical sulfatic facies is given, i.e.: laminithic, nodular of the "chicken-wire" type, entherolithic, gypscretic and classic. The sulfatic associations as well as the mineralogy of the deposits fit in with the schema suggested by Tucker (1991).

The present study offers an analysis of sulfatic sedimentary facies occurring in the north-western part of the Transylvanian Basin, in the area of the Meseş Mountains. Actually, our study is representative for the tendency of bringing up to date certain problems closely connected to this type of deposits. From a stratigraphic point of view, all analysed sulfatic deposits are positioned on the level of the Foidaş Formation (Upper Lutetian) as well as on the level of the Turbuţa Formation (Lower Priabonian) (Fig. 1).

1. Petrographic features of facies

The morphology of facies serves as a diagnosis element for both the deciphering of genetic circumstances and the subsequent reconstitution of depositional environments, their evolution in time and space being reflected by the variation of these facies on both vertical and horizontal line.

A variation of this type can be noticed within the gypsum levels which include in most of their outcrops several successions consisting of sets of prograde parasequences representing transitions from lagoonal facies at their base to coastal Sabkha facies in the upper part.

1.1. Laminithic facies

This type of facies often occurs within the sulfatic deposits of the area. It represents a succession consisting of gypsum laminae alternating with laminae of clayey character. On the vertical line the thickness of the gypsum laminae varies from few millimetres to several centimetres. Several alternating lightly coloured bands and other darker ones may also be noticed (Pl. 1, Fig. 1).

All these variations reflect in fact the successive changes of dynamic circumstances within the sedimentary basin and they depend on the duration of the basins stable periods. The fact that these laminae might be noticed and correlated on long distances constitutes a significant specific feature indicating a uniformity of all moulding circumstances on relatively large areas.

Usually, the calcium sulfate crystals are very fine, emerging directly from the waters of a relatively deep basin, below the basic level of waves. The seasonal changes within the temperature and chemical field of water are reflected by the existence of the colour variations of laminae (varves).

The clayey intercalations causing the lamination process on various levels represent, after Popescu

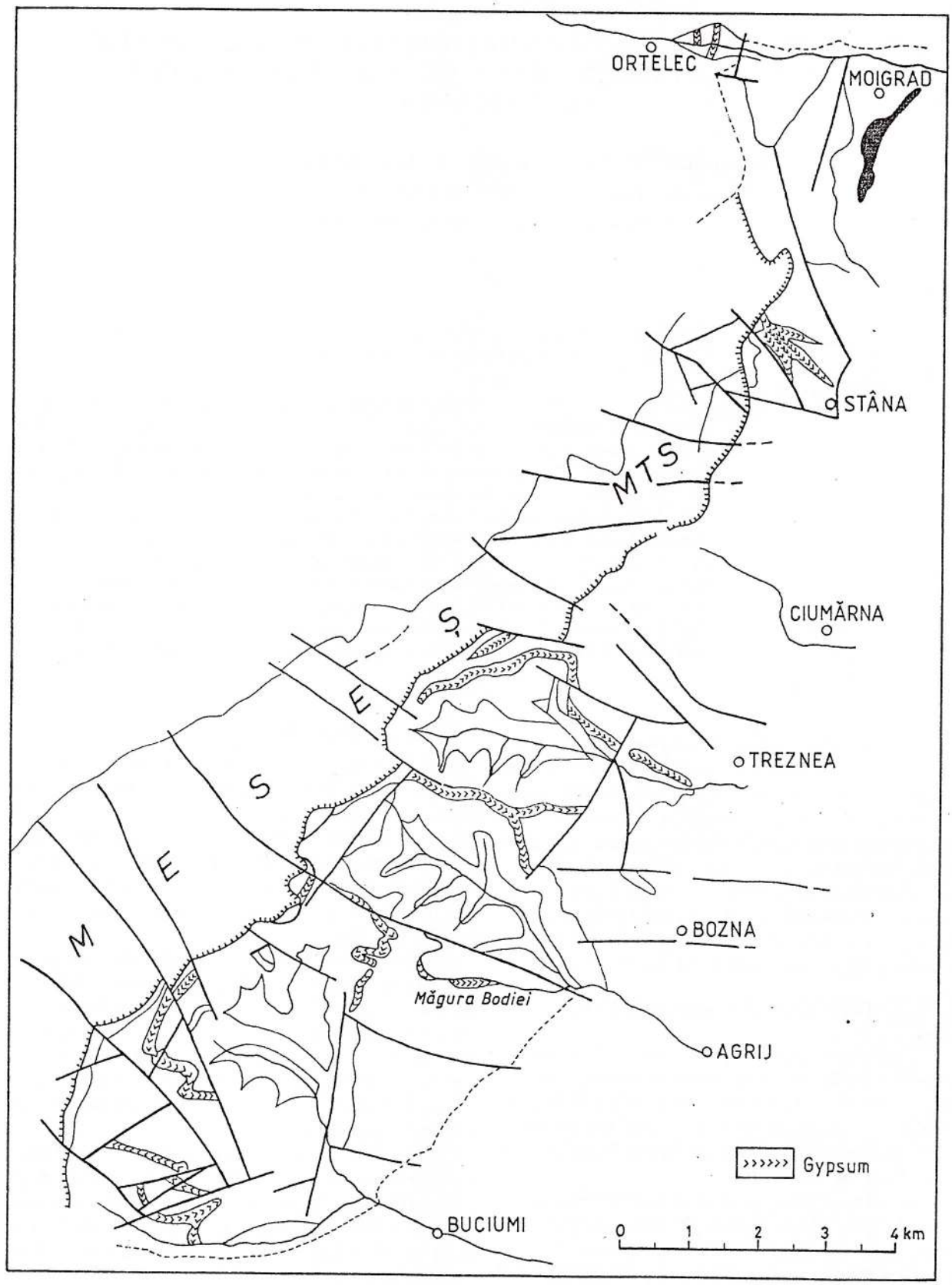

Fig. 1 – The geological sketch of the Meseş Area with the occurrences of gypsum

(1976), the products of a deposition of the material in suspension, as a result of the existence of stable evaporation conditions, with periodical influxes.

The anhydrite from the border of the Meseş crystalline occurs under the same aspect. It consists of alternating centimetric laminae of anhydrite, containing organic matter, and submillimetrical clayey laminae, also with carbonatic material. The organic matter is probably of sapropelic provenance, deriving from the phytoplankton of the photic zone.

1.2. Nodular facies

This type of facies occurs either in form of small nodules spread in the stratified levels or in form of large-sized nodules. Thus, their dimensions vary from 1-2 cm to 8 or even 10 cm. These nodules occur included in a clayey matrix usually of a grey-green colour (Pl. I, Fig. 2).

The nodular facies is specific to the Sabkha sedimentation and it has an anhydrous character (secondary gypsiferous).

Sabkha represents in fact a backshore zone periodically flooded by sea water under the circumstances of a dry climate, when a lack of poise occurs between the water share and the most important evaporation. Thus, a progressive increasing of the water salinity takes place. The anhydrite nodules (secondary gypsum) grow in the area of these swampy zones which are particularly frequent in tidal zones, in silts which can be either carbonatic or clayey. They evolve by an addition of new crystals to the pre-existing matrix and, on no account, by a further development of the already existing crystals (Shearman, 1986). The ionic share for the continental Sabkha waters which is necessary for the emergence of the crystals is supplied by the sea. This growing process causes the expulsion of the soft sediment around the nodules, followed by the constitution of the mosaic type, the "chicken-wire" type structures (Pl. I, Fig. 3). The joining of nodules takes place following the lines marked by the presence of carbonate or clay.

1.3. Enterolithic facies

The blending of anhydritic nodule series leads to the formation of strata and their continuous evolution requires a growing space. Both the effects of the lateral pressure resulting on that account and the limitation of the existing space are the causes for the sinuosity of the strata. The result is the setting up of enterolithic facies (Shearman, 1986) (Pl. I, Fig. 4).

The same type of facies is also frequent in secondary gypsiferous rocks, formed later on near to the surface by the hydration of anhydritic rocks. A comparison of the mentioned type of secondary gypsiferous stuctures with those belonging to anhydritic rocks, even to some recent sediments (coast Sabkha, Abu Dhabi), makes obvious the fact that these structures represent primary structures of growth (Shearman, 1986).

1.4. Gypsiferous crusts (gypscrete)

The gypsiferous crusts occur concomitantly with other types of facies in all outcrops, being products of the diagenesis mediated by solutions (Pl. I, Fig. 5). They represent continental facies formed as a result of the diffusion process which takes place on the ionic level, stimulated by the presence of the upwelling circulation of solutions.

1.5. Clastic gypsum

Localised only within a single outcrop (Treznea), clastic gypsum represents a reshuffled product resulted by the disintegration of a preexising deposit of the same nature. It occurs as a well individualised level, made up of an agglomeration of fragments with a flattened shape, microscopically proved to be of gypsiferous composition (Pl. I, Fig. 6).

This level might have been formed under emerse conditions, by the disintegration of the subjacent rock, followed either by a remaining on place of the material or by its transport and subsequently by its subaquatic deposition. The chaotic position of fragments within the level, their flattened shape as well as the clayey matrix in which they are included, having the same nature as the rest of clayey intercalations deposited in submerse circumstances and associated with sulfatic levels, lead us to the assumption regarding a transport following the disintegration and a subaquatic deposition .

2. Mineralogical characteristics

The mineralogical parageneses are dominated in all analysed sulfatic deposits by sulfates: gypsum, anhydrite, celestite and barite with minor non-sulfatic minerals: calcite, dolomite, smectite, illite, kaolinite, quartz and chalcedony (Tab. 1). The quasi-monomineral composition is confirmed also by the chemical analyses of the same samples of gypsum (Tab. 2).

2.1. Gypsum

The most common of sulfates and the most frequent one within sedimentary rocks, gypsum, is the prevalent mineral of the evaporitic deposits from the studied area.

Microscopically, it shows a negative relief, inferior to that af anhydrite and a poor birefringence (grey of I order). The monoclinic oblique cleavage is visible in most cases. It occurs either as hypidiomorphic crystals with a short prismatic habitus or with a porphyroblastic aspect, with a compact, irregular structure which is sometimes pseudostratified showing prints

Table 1
Chemical composition of the gypsiferous samples from Meseş Area

Occurrence	Chemical composition (%)							
	SO_3	CO_2	CaO	Al_2O_3	Fe_2O_3	MgO	H_2O	Ins HCl
Ortelec	44.55	1.95	32.51	0.33	0.12	0.49	19.25	0.80
Stâna	45.90	0.69	32.58	0.03	0.05	0.52	19.86	0.45
Treznea	46.18	1.33	32.43	0.32	0.10	0.80	18.33	0.51
Buciumi	47.09	0.17	33.04	0.37	0.75	0.45	17.49	0.91

Table 2
Mineralogical composition of the gypsiferous samples from Meseş Area

Occurrence	Mineralogical composition (%)				
	$CaSO_4 2H_2O$	$CaSO_4$	$CaCO_3$	$MgCO_3$	Residue + Fe_2O_3+Al_2O_3
Ortelec	94.32	1.18	3.35	3.35	-
Stâna	94.91	2.87	1.01	1.13	0.53
Treznea	93.04	2.76	2.48	0.92	-
Buciumi	83.71	13.87	0.22	0.38	1.85

of gypsum crystals. The texture is generally granular-lamellar, not homogeneous from a dimensional viewpoint and irregular as regarding the shape of crystals, but it might also be fine-granular, even cryptocrystalline (Pl. II, Figs. 1, 2).

Regarding gypsum, two generations could be identified. On the one hand, there are monocrystals or crystal-aggregates, usually granular, cogged ones, partly affected by corrosion processes, and on the other hand, we find a microcrystalline mass of gypsum made up of lamellar or granular microcrystals, which are sometimes prolonged, tabular. All dimensions of crystals are variable, ranging between 0.1–0.3 mm and 0.02–0.005 mm.

The aspect of interpenetration of gypsum crystals is ubiquitous. This interpenetration has been described by Truc (1986) and defined as a specific aspect of the gypsum crystals resulting from the total transformation anhydrite-gypsum.

The fibrous gypsum variety appears on the microscopic scale in form of little veins with millimetrical thicknesses. Within these veins, which usually grow on fracture lines and diaclases, the gypsum crystals have a perpendicular orientation to the walls.

2.2. Anhydrite

This mineral occurs in association with gypsum, as a relic but, at the same time, it is the main constituent of a level evidenced by some samples extracted from a drilling made on the border of the Mt. Meseş (depth 180 m).

Microscopically, all prismatic crystals with a specific orthorhombic cleavage posses a relief, which is superior to that of gypsum, stronger birefringence and straight extinction (Pl. II, Fig. 4).

The characteristic mineral within the anhydritic level occurs in form of chaotically disposed lamellae (0.1–0.25 mm), giving a lamellar textural character with some crystals of variable dimensions as well as a massive, irregular structural one. This disposing can be sometimes rosette-like, suggesting the possible primary nature of anhydrite.

We may notice within this level a gradual passing from the lower part, where some poor hydration and gypsification processes commonly occur, to the upper part, with its mass almost entirely of gypsum, the anhydrite occurring just as relics (Pl. II, Fig. 3).

As a result of these hydration processes the anhydrite lamellae become locally corroded or substituted by secondary gypsum, without being totally pseudomorphosed (gypsification process).

The anhydrite occurs in all surface deposits only in small amounts and only as relics in the gypsum mass, being evidenced diffractometrically and microscopically.

2.3. Other minerals

Celestite and barite occur entirely sporadically as hypidiomorphic crystals, corroded by gypsum, which constitutes the microcristalline mass.

By means of diffractometric, thermic and microscopic studies, there were also evidenced some other minerals occurring in association with sulfatic minerals, such as carbonates (calcite and dolomite – Pl.

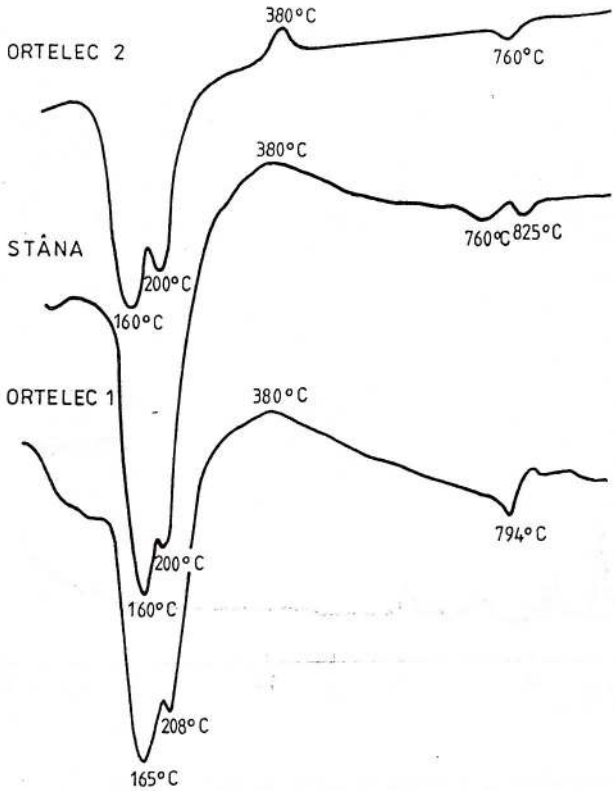

Fig. 2 – The DTA analyses of some gypsiferous samples

II, Fig. 5), clayey minerals (smectite, illite, kaolinite) and silica (qurtz, chalcedony Pl. II, Fig. 6).

The DTA analyses of some samples of gypsum, show their quasi-monomineral character. The endothermal peaks at 160^0 and 208^0 indicate the two steps of dehydration,leading to the transformation of gypsum into anhydrite and the exothermal peak at 380^0 the polymorphous transformation of $CaSO_4$ (Fig. 2).

The evidence of some carbonatic impurities (dolomite and calcite) are the endotherms at 760^0–825^0 (Fig. 2).

The X-ray analyses of the gypsum, clays and carbonatic intercalations samples prove the followings:

– the diffractograms on sulfatic samples show 2Φ values which characterise gypsum; the variable intensity of the peaks is due to the crystallinity degree (Fig. 3);

– the carbonatic intercalations are represented in the diffractograms by the peaks of dolomite and subordinated calcite (Fig. 4);

– the samples from the clay intercalations were selected ($<2\mu$) and oriented using the sedimentation method. The clay minerals assemblage consists of smectite and smectite/illite interstratification (Fig. 5), which could be formed in the alkaline environment of the sedimentary basin.

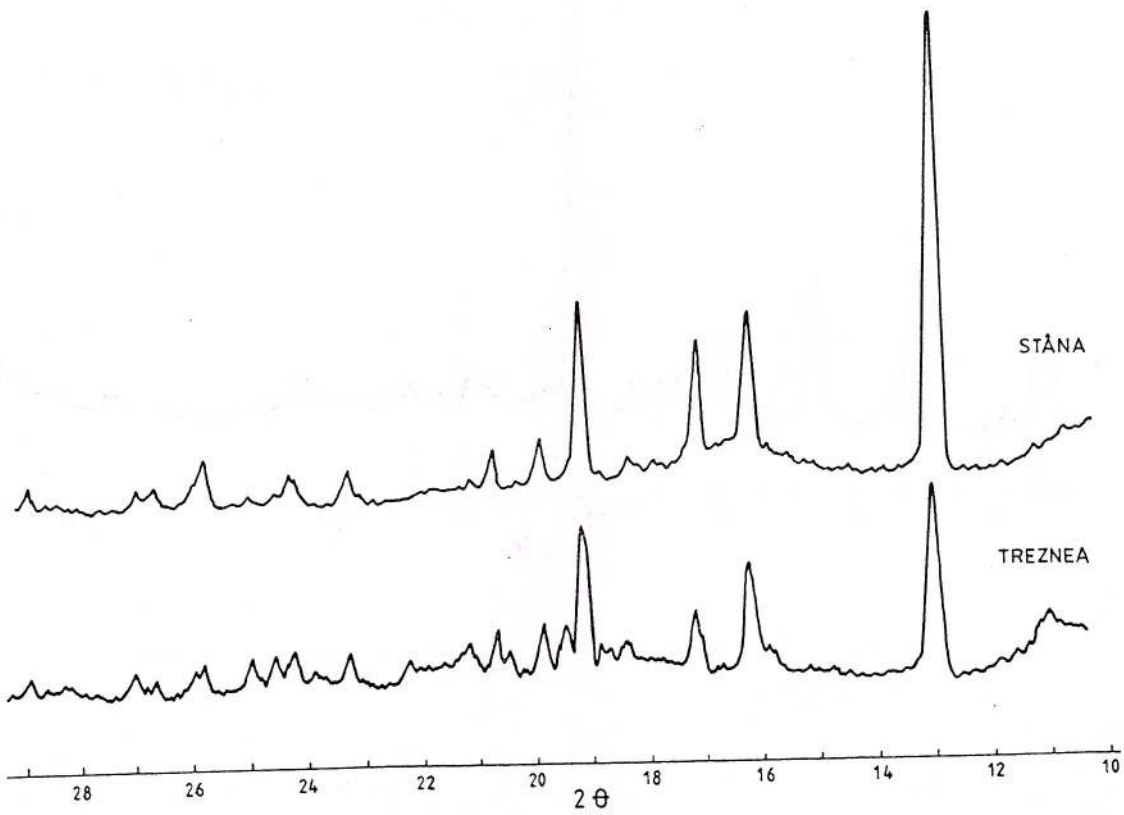

Fig. 3 – The X-ray analyses of 2 samples of gypsum

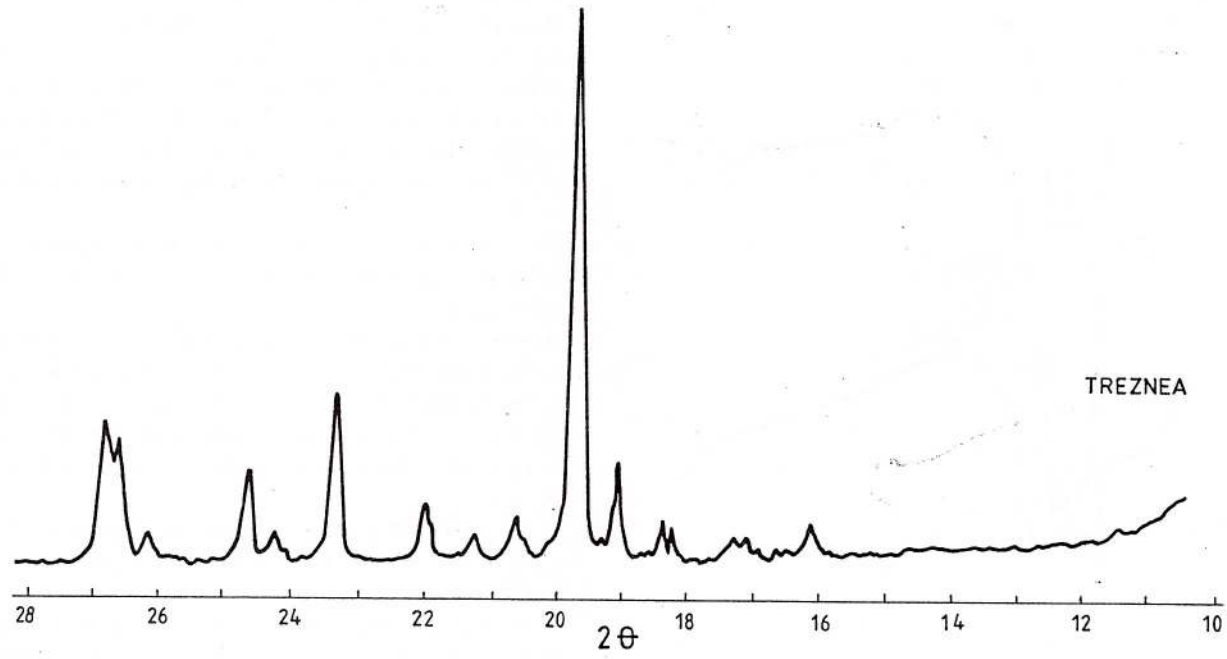

Fig. 4 – The X-ray analyses for the carbonatic impurities from gypsiferous samples (dolomite, calcite)

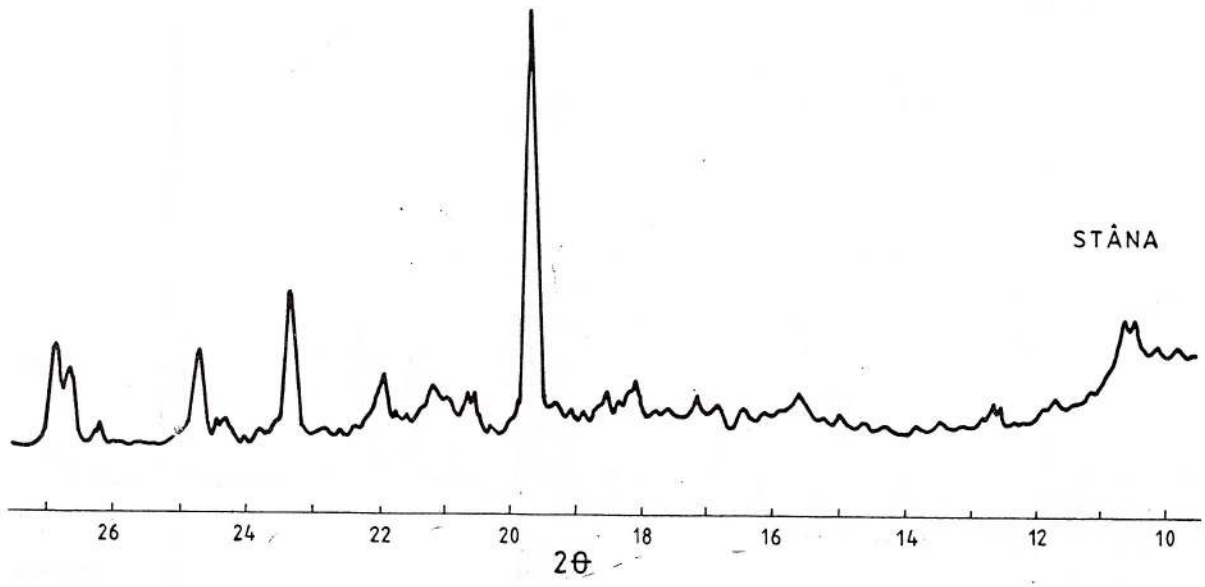

Fig. 5 – The X-ray analyses of clay intercalations from gypsiferous samples

Conclusions

This study describes from the facial view-point the Palaeogene sulfatic accumulations occurring in the Meseş area. We described in these levels the following facies: laminithic, nodular, enterolithic, clastic, gypscretic.

All limits observed at the level of transitions between these types of facies are mainly of marine flood. They delimit prograde parasequences occurring in several sets of parasequences.

On the basis of the presented material, we selected as predominant genetic models those of coastal Sabkha and of lagoon. The genetic alternatives, as regards the origin of the initial sediment, should be:

1. Anhydritic initial sediment, subsequently hydrated and converted into gypsum, its evolution following the scheme of Sabkha facies, from anhydritic nodules to enterolithic structures.

2. Gypsiferous initial sediment.

Most of the possible arguments brought in connection with this subject favour the existence of an anhydritic sediment at the origin.

At least locally, we presume the presence of a more complex transformation, starting from the stage of microcrystalline primary gypsum, which changes in the early diagenesis by recrystallization into aggregates of anhedral and, approximately equigranular crystals and subsequently into anhydrite. The development of these processes takes place having as background the dehydration of gypsum as a result of a progressive burial. Subsequently, due to the lifting of deposits the hydration of secondary anhydrite might take place, resulting in the formation of porphyroblastic gypsum (Fig. 6).

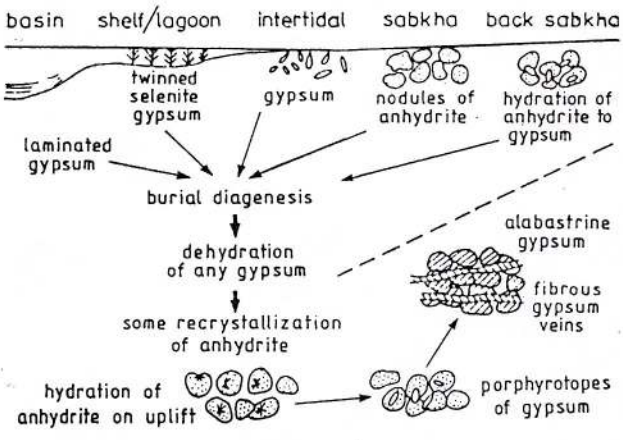

Fig. 6 – Genetic scheme for the sulfatic formations from the Meseş Area (after M. E. Tucker, 1991)

References

Anastasiu, N. (1988) Petrologie sedimentară. Edit. Tehnică, 366 p., Bucureşti.

Busson, G. (1979) Successions carbonatées anhydritiques et salifères dans le Dévonien moyen de forages du nord-est de l'Alberta (Canada occidental). Depôts évaporitiques. Edit. Technip, Paris.

— **(1986)** La synthèse des données et les évaporites fossiles. Les series à evaporites en exploration petrolière. Edit. Technip, Paris.

Cussey, R. (1985) Anhydrite diagénétique de Sabkha carbonatée dans le Tertiaire d'Irak. Depôts évaporitiques. Edit. Technip, Paris.

Mészàros, N., Moisescu, V. (1991) Bref aperçu des unités lithostratigraphiques du paléogene dans le Nord-Ouest de la Transylvanie (region Cluj-Huedin), Roumanie. *Bull. Inf. Geol. Bass.*, 28, 2, p. 31–39, Paris.

Moisescu, V. (1975) Statigrafia depozitelor paleogene şi miocen-inferioare din regiunea Cluj-Huedin-Româna şi (Nord-vestul Bazinului Transilvaniei). *An. Inst. Geol. Geof.*, p. 5–213, Bucureşti.

Popescu, B. (1976) Fomaţiunea gipsului inferior la vest de Cluj-Napoca - evaporite supratidale - aspecte petrografice şi sedimentologice. *An. Inst. Geol. Geofiz.*, XLVIII, p. 97–116, Bucureşti.

— **(1984)** Lithostratigraphy of cyclic continental to marine Eocene deposits in NW Transylvania, Romania. *Archives des Sciences*, 37, 1, p. 37–75, Geneve.

Rouchy, J. M. et al. (1986) Pétrographie descriptive des évaporites, applications sur le terrain en subsurface et au laboratoire. Les séries à evaporites en exploration petrolière. Edit. Technip, Paris.

Schreiber, B. C. (1975) Arid Shorelines and Evaporites - Sedimentary Environments and Facies. Sec. Edit., Ed. by H.G. Reading, Oxford.

Shearman, D. J. (1986) Les faciès évaporitiques de Sabkha - Depôts évaporitiques. Edit. Technip. Paris.

Todor, N. D. (1972) Analiza termică a mineralelor. Edit. Tehnică, 280 p., Bucureşti.

Tucker, E. M. (1991) Sedimentary Petrology - an introduction to the origin of sedimentary rocks. *Blackwell Scientific Publications*, 260 p., London.

Received: January 1998
Accepted: June 1998

Plate I
Petrological faciesal features

Fig. 1 – Laminithic facies (Buciumi).
Fig. 2 – Nodular facies (Stâna).
Fig. 3 – Nodular facies, "chicken-wire" type (Stâna).
Fig. 4 – Enterolithic facies (Stâna).
Fig. 5 – Crust of gypsum (Stâna).
Fig. 6 – Clastic gypsum (Treznea).

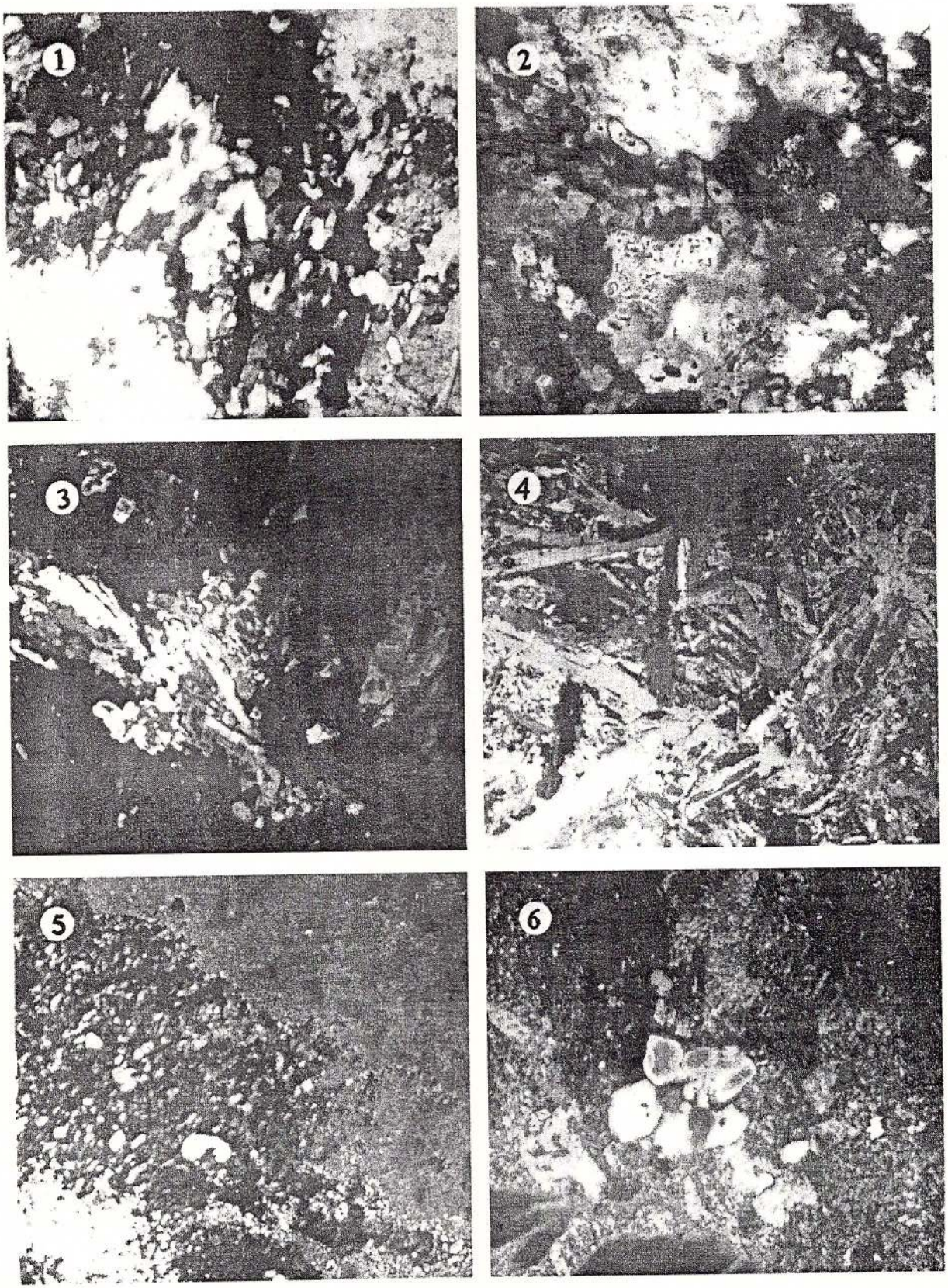

Plate II
Mineralogical features of gypsum samples

Figs. 1,2 – Large aggregates of xenomorph gypsum crystals, with distinct granulometry, partially affected by corrosion, surrounded by a microcrystalline groundmass of the same nature. Some microinclusions of anhydritic nature occur. Ortelec (1), Treznea (2), (N+ , 58 X).

Fig. 3 – Anhydritic relics irregulary shaped or rosettes as remnants of the hydration processes. Meseş Mountains-borehole. (N+ , 76 X).

Fig. 4 – Anhydrite with prismatic-lamellar aspect. Low intensity hydration and gypsum formation can be mentioned. Meseş Mountains-borehole. (N+, 76 X).

Fig. 5 – Gypsiferous microcrystalline mass associated with calcite. Stâna.(N+, 58 X).

Fig. 6 – Association consisting of cryptocrystalline silica (chalcedony), gypsum and calcite in a gypsiferous mass. Meseş Mountains- borehole. (N+, 76 X).

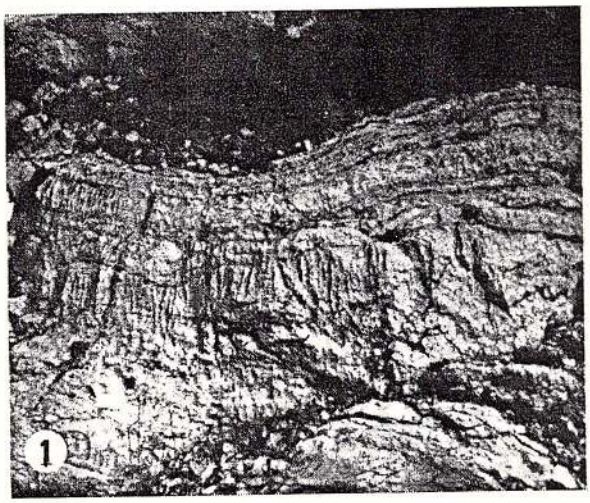

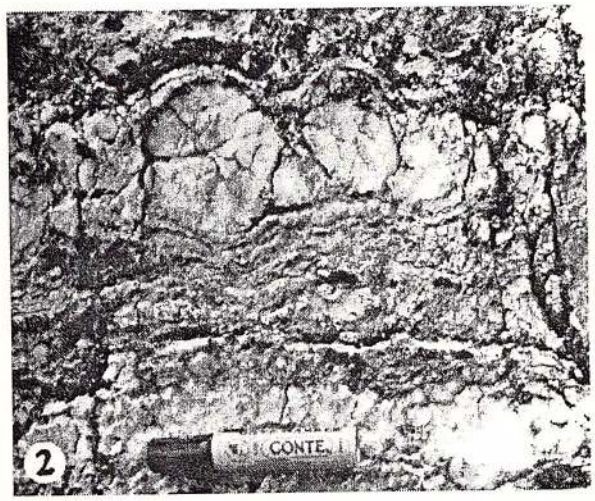

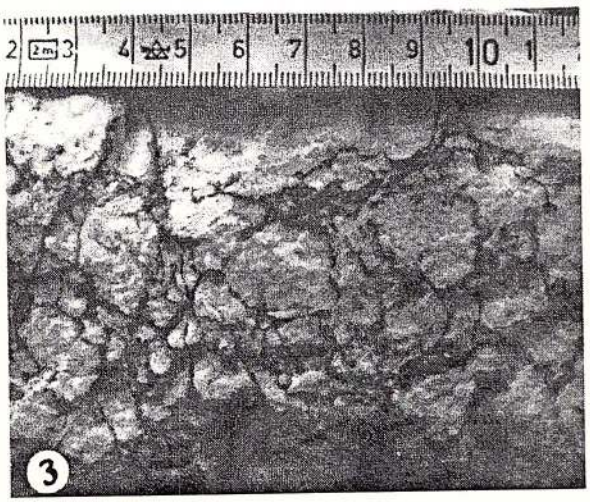

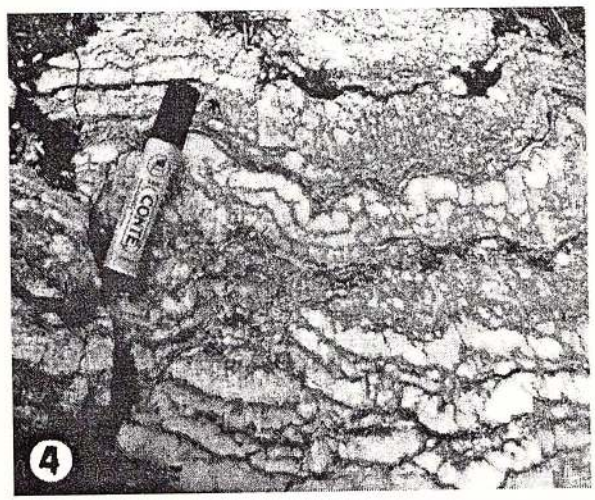

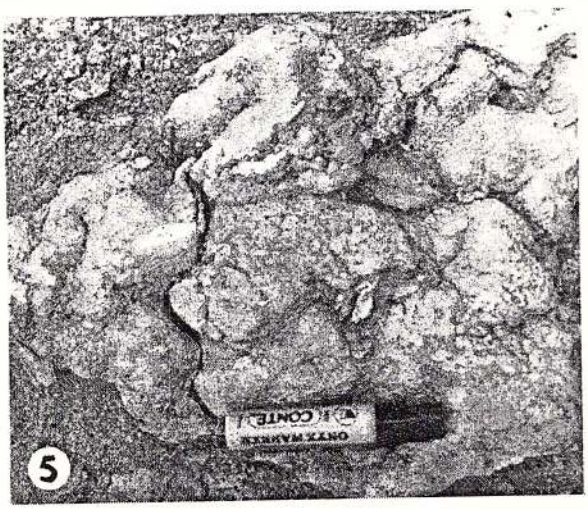

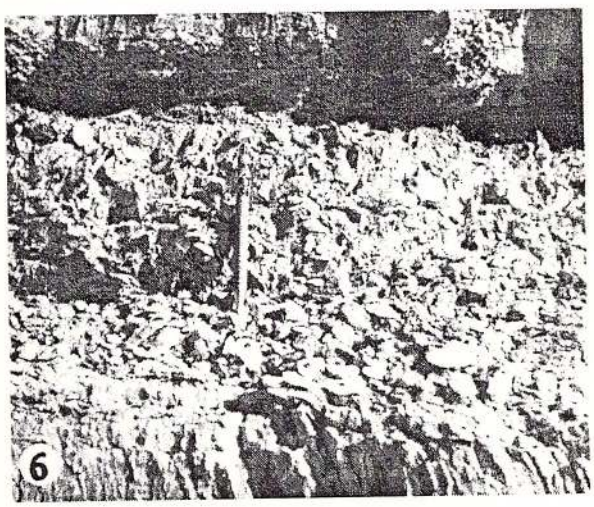

Rom. J. Mineralogy, 79, p. 151-157, Bucureşti, 1999

HUNTITE FORMED UNDER SUPERGENE CONDITIONS IN VALEA REA CAVE (BIHOR MOUNTAINS)

Lucreţia GHERGARI, Tudor TĂMAŞ

Facultatea de Biologie şi Geologie, Catedra de Mineralogie-Petrometalogenie,

Universitatea "Babeş-Bolyai", Str. M. Kogălniceanu nr. 1, RO-3400 Cluj-Napoca, Romania

Key words: Huntite. Hydromagnesite. Aragonite. Magnesian calcite. Valea Rea Cave. Bihor Mountains. Romania.

Abstract: A new huntite occurrence is presented from Valea Rea Cave (Bihor Mountains, Romania), where the mineral appears as creamy-white, thin early lamellar masses forming the filling of various fissures. Huntite from the Valea Rea Cave is associated with hydromagnesite, aragonite and magnesian calcite. Huntite has a lamellar habit with almost square shape (unit cell edges of: $a_0 = 9{,}51$ Å, $c_0 = 7{,}78$ Å) and shows two endothermic effects, at 590 ^{0}C (destruction of huntite lattice and the dissociation of $MgCO_3$), and at 860^{0}C (decomposition of calcium carbonate). The mineral association: huntite, hydromagnesite, aragonite and magnesian calcite, was formed under supergene conditions.

Introduction

Huntite, $CaMg_3(CO_3)_4$, was firstly described by Faust (1953) in Tertiary magnesite deposits from Currant Creek, Nevada. The first huntite occurrence was, however, mentioned in the Dorog mine (Hungary) by Venkovitz in 1949 (Koblencz, Nemecz, 1953), but the identification and the description of the Dorog mineral were done by Koblencz and Nemecz only in 1953. The presence of huntite was later mentioned in other parts of the world (Skinner, 1958; Kinsman, 1967; Cole, Lancucki, 1975; Hill, 1976; Hill, Forti, 1997), in connection with the weathering zone of magnesium-rich rocks. Huntite forms deposits from bicarbonate solutions close to the surface or in underground cavities (caves or mine workings). In caves, huntite was reported from coatings, crusts, *moonmilk* and flowstones (Hill, 1976; Hill, Forti, 1997). The first model for the crystal structure of huntite was proposed by Graf & Bradley (1962), on the basis of samples taken from Currant Creek. In 1986, Dollase & Reeder determined the structure of this mineral, which has the spatial group R32.

The only description of huntite in Romania belongs to Diaconu et al. (1977), who identified it in association with hydromagnesite, calcite and aragonite in a *moonmilk* deposit in Fagului Cave, Bihor Mountains.

General outlook on the geology of Valea Rea Cave region

The southern slope of the Cărligaţi - Fântâna Rece - Cornu Munţilor ridge, in the upper basin of Valea Rea valley, was investigated by Bordea & Bordea (1972), while general data on the region were synthetised by Ianovici et al. (1976), Bleahu et al. (1985), Ştefan (1980), Ştefan et al. (1988, 1992). Mineralogical studies on the cave deposits from Valea Rea Cave were done by Onac et al. (1995), Damm et al. (1996), Ghergari et al. (1998), that described until now about 29 minerals from this cave.

The Valea Rea Cave, with a mapped passage length of 18 km, is developed in Anisian dolostones and limestones belonging to the Ferice Nappe, SE of the andesitic ridge Cărligaţi - Fantana Rece (Fig. 1). In the area there also appear several microgranitic dykes, that are probably responsible for the vein mineralizations within the cave (Ghergari et al., 1997, in press).

The huntite occurrence is located in the "Pompieri II" passage from Valea Rea Cave. The passage begins at the depth of -55 m from the entrance, in the wall of a great shaft ("Marea Prăpastie") and is carved in dolomites. "Pompieri II" is a fossil, descendant canyon with phreatic morphology, lately remod-

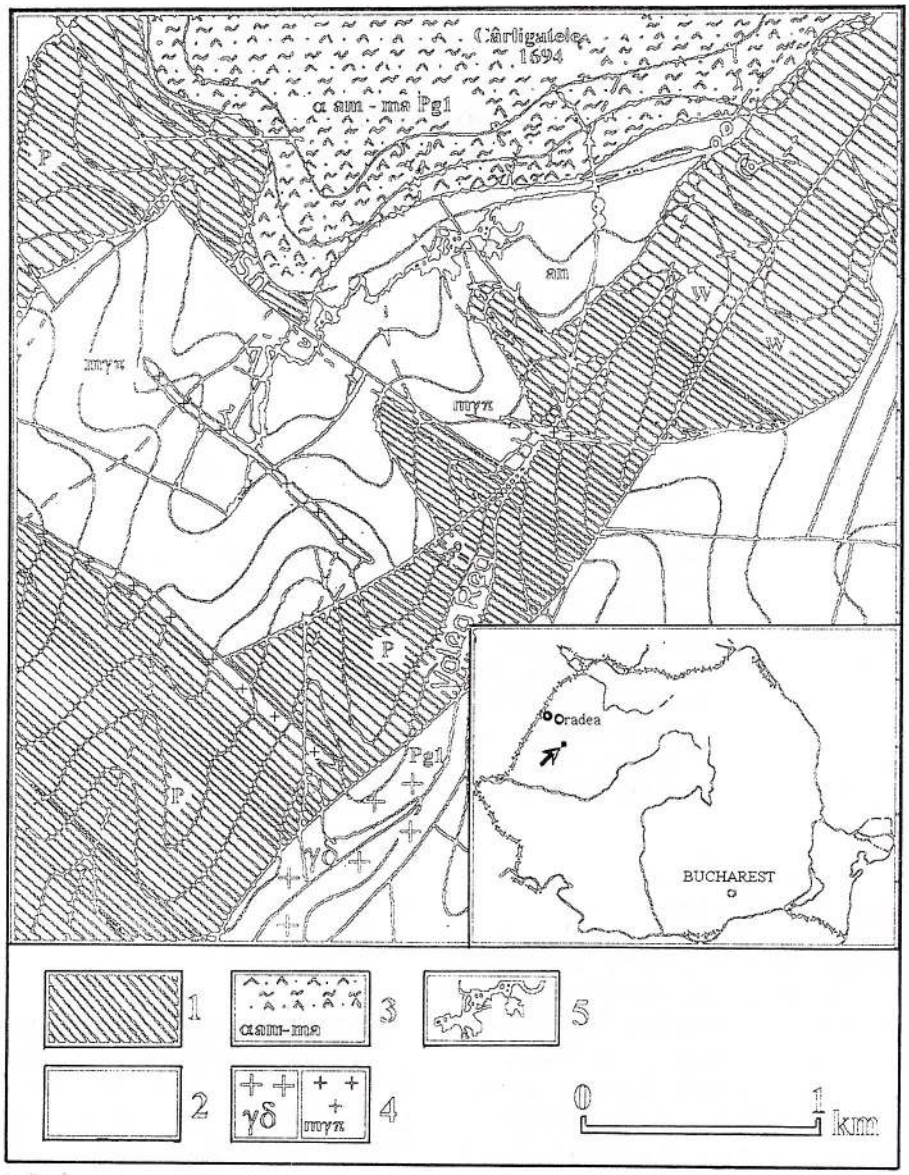

Fig. 1 – Geological map of the Valea Rea area, showing the location of the cave:
1, non-karstifiable sedimentary rocks (Permian shales and feldspar sandstones, Werfenian quartzitic sandstones); 2, karstifiable rocks (Anisian limestones and dolostones, Ladinian-Lower Norian black limestones); 3, andesites with hornblende and pyroxenes (Lower Paleogene); 4, $\gamma\delta$ - granodiorites with hornblende and biotite (Lower Paleogene); $m\gamma\pi$ - porphyry microgranites (Lower Paleogene); 5, cave (geology after Bleahu et al., 1985).

elled in vadose regime, with erosion levels, drops and whirlpools filled with a sandy material that partly resulted from the weathering of the dolomitic rock. There is a noticeable air flow through the passage, while the average temperature reaches about 8–9^{0}C. Huntite appears in a ceiling pocket at some 20 m from the beginning of the passage and forms the fillings of some fissures able with the bedding.

The carbonate rock in which the passage is carved is an inequigranular dolosparite that shows a weak thermal metamorphism; it is easy to recognise areas with lower crystallinity, included in other areas with crystals largely developed. The mineralogical constitution of the rock is attested by the X-ray diffraction recording, characteristic of dolomite (Fig. 2a). Dedolomitization is the main phenomena that may be observed in the huntite occurrence area; the process is induced by solutions seeping through fissures in the rock. X-ray diffraction pattern showed the presence of calcite and a small amount of dolomite (low dolomitic limestone), due to magnesium removal as bicarbonate (Fig. 2b).

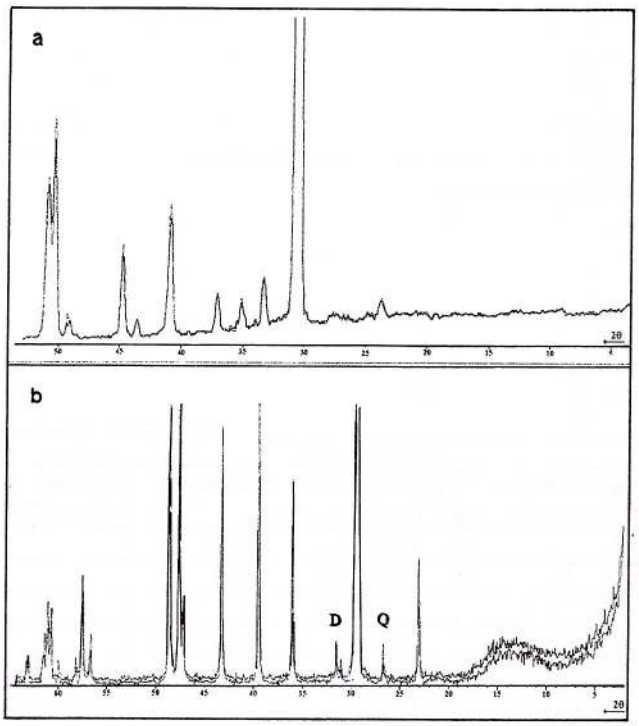

Fig. 2 – X-ray diagrams: a, dolomite; b, dolomite affected by dedolomitization (Q - quartz line; D - dolomite line; others are calcite lines).

The supergene minerals association

Huntite from Valea Rea forms consistent, creamy-white earthy masses, while hydromagnesite forms grainy, grey-white earthy loose aggregates of skeletal crystals. Even if they both appear on the fissures, the two minerals do not mix, showing different conditions of deposition. Each mineral forms aggregates with a maximum diameter of 3 to 5 cm. From a textural point of view there is a zoning in the deposition of the minerals. On the walls of the fissures, there occur porous dedolomitized carbonate rock, aragonite crystals deposit; next fluffy hydromagnesite aggregates and/or more consistent huntite earthy masses with silky aspect may appear. Huntite and hydromagnesite deposit on the surface of aragonite crystals or fill the spaces between them. In the huntite aggregates there are parallel intergrowths of small carbonate crystals (0.1–0.2 μm) with rhombohedral habit, observed under the transmission electron microscope (opaque under electron pencil), that correspond to low magnesian calcite (Pl. I, Figs. 2, 3, 4).

Huntite $CaMg_3(CO_3)_4$

Morphology. Huntite exhibits porous masses, more or less consistent, formed by small lamellar aggregates or parallel intergrowths with varied disposition (Pl. I, Figs. 1, 2). Huntite crystals have lamellar habit and rhombohedral shape, usually elongated in one direction. Lamellas are extremely thin, almost transparent under the electron pencil, frequently have curly surface and net edges. Their dimensions vary from 0.1 to 0.8 μm, rarely reaching 1 μm (Pl. II, Figs. 1, 2). Due to their submicrometric dimensions, huntite crystals were not suitable for determining optical constants. The only optical property observed was their high birefringence.

Structural characteristics. The X-ray diffraction recording obtained on pure huntite from Valea Rea (Table 1) is complete, with well represented lines and corresponds to the trigonal form, space group R32. Its calculated lattice parameters are: $a_0 = 9{,}51 \pm 0.04$ Å, $c_0 = 7{,}78 \pm 0.02$ Å.

Thermal behaviour. Huntite presents two endothermic effects, accompanied by mass losses (Fig. 3). The first endothermic effect takes place at 590°C with a loss of 39% CO_2 corresponding to the decomposition of three $MgCO_3$ molecules, while the second one appears at 860°C, with a loss of 11% CO_2 that results from the decomposition of a $CaCO_3$ molecule.

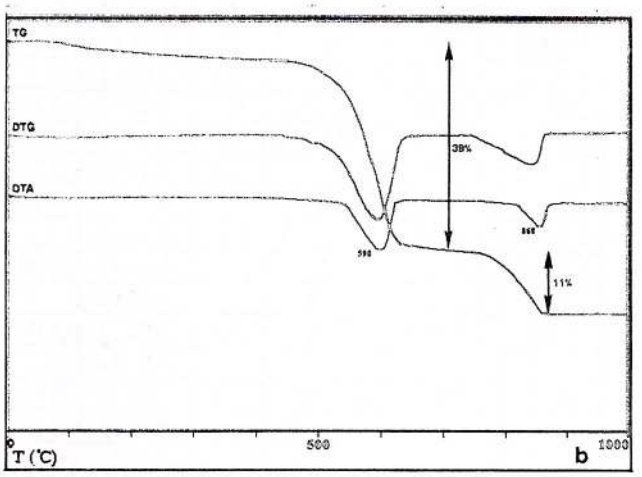

Fig. 3 – Thermal analysis of huntite (Peştera din Valea Rea)

The temperatures we obtained for the endothermic effects of huntite are lower than those obtained by Todor (1972: 635°C, respectively, 880°C), but identical to those of Koblencz and Nemecz (1953: 590°C, respectively, 860°C). The first endothermic effect recorded at lower values than the temperature of magnesite decomposition shows that the thermal stability of huntite is lower than that of magnesite; therefore we consider the first effect as being determined by the destruction of the huntite lattice, followed by the decomposition of the magnesium carbonate resulted. We do not agree with the opinion that huntite thermally behaves as being a 3:1 mixture of magnesite and calcite (Todor, 1972).

Table 1

X-ray diffraction pattern of huntite from the Valea Rea Cave, Bihor Mountains, compared with data from literature

HUNTITE, Peştera din Valea Rea, Bihor Mountains

$a_0 = 9,51 \pm 0,04$ Å, $c_0 = 7,78 \pm 0,02$ Å

Huntite (Valea Rea)				Huntite*	d (literature)				
d obs.	d calc.	hkl	I	d calc.	Faust (1953)	Koblencz & Nemecz (1953)	Skinner (1958)	Graf & Bradley (1963)	Diaconu et al. (1977)
5.6755	5.6612	101	0.81	5.6693	5.69		5.64	5.66	
				4.7513	4.81		4.73	4.75	
					4.16				
3.66	3.6432	021	1.6	3.6416	3.67	3.65	3.63	3.64	
				3.5321				3.53	
					3.15	3.145	3.12		
2.8854	2.8930	211, 12$\bar{1}$	22.4	2.8903	2.91	2.91	2.89	2.88	2.899
2.8302	2.8306	202	100	2.8346	2.838	2.829	2.830	2.83	2.840
2.7611	2.7481	300	12	2.7432	-	-	2.74	2.74	2.764
2.6016	2.5958	003	9.2	2.6071	-	2.58	2.598	2.604	2.601
2.4327	2.4329	122, 21$\bar{2}$	9.4	2.4343	2.444	2.434	2.443	2.432	2.433
2.3743	2.3799	220	8.7	2.3757	2.388	2.379	2.372	2.375	2.426
2.2802	2.2789	113, 11$\bar{3}$	4.7	2.2856	2.298	2.297	2.279	2.284	2.281
					2.204	2.203			
2.1897	2.1939	31$\bar{1}$, 131	6.2	2.1911	-	-	2.188	2.190	2.186
1.9868	1.9925	401	10.4	1.9897	1.986	1.989	1.988	1.991	
1.9681	1.9717	13$\bar{2}$, 312	23	1.9713	-	-	1.966	1.972	1.969
1.907	1.8947	104	1.2	1.9023	1.900		1.895	1.896	
				1.8898		1.888	1.888		
1.8337	1.8379	23$\bar{1}$, 321	4.5	1.8353	1.840	1.836	1.832	1.835	
				1.8208			1.818	1.821	
				1.7958	1.803		1.793	1.796	
1.7628	1.7604	024	16.7	1.7660	1,769	1.767	1.762	1.765	
1.7548	1.7542	223	14.5	1.7560	-	-	1.752	1.757	1.758
1.696	1.7013	32$\bar{2}$, 232	1.6	1.7002	1.708	1.705	1.696	1.700	
				1.6554			1.656	1.655	
				1.6106			1.608		
1.5832	1.5866	330	8.3	1.5838	1.580	1.589	1.581	1.584	
				1.5367					
1.5235	1.5277	42$\bar{1}$	1.2	1.5254	1.529	1.529	1.523	1.526	
							1.515	1.518	
				1.4849					
1.4796	1.4786	143, 14$\bar{3}$, 413, 41$\bar{3}$	4	1.4789	1.488	1.489	1.479	1.481	
				1.4622			1.462		
1.4470	1.4546	15$\bar{1}$, 511	2	1.4524	1.453	1.451	1.443	1.445	

* d values obtained from a complete powder diffraction spectrum for an elementary cell with a_0=9.50270, c=7.82120, space group R32.

Table 2

X-ray diffraction pattern of hydromagnesite from the Valea Rea Cave, Bihor Mountains

HYDROMAGNESITE, Peștera din Valea Rea; $a_0 = 18.53 \pm 0.03$ Å; $b_0 = 9.06 \pm 0.03$ Å, $c_0 = 8.42 \pm 0.01$ Å, $\beta = 90°$

No.	0	d. obs.	d.calc	I	hkl
1.	4.82	9.166	9.267	46	200
2.	6.85	6.458	6.479	20	210
3.	7.58	5.839	5.854	15	111
4.	9.59	4.623	4.633	16	400
5.	10.75	4.129	4.107	14	102
			4.125		410
6.	11.38	3.903	3.901	3	121
7.	11.57	3.840	3.819	3	[012]
			3.834		202
8.	11.90	3.735	3.735	1	411
9.	12.45	3.572		3	-
10.	12.63	3.522	3.531	4	212
11.	13.35	3.335	3.352	14	321
12.	14.09	3.163	3.177	22	511
13.	14.37	3.103	3.089	14	600
			3.116		402
14.	15.33	2.913	2.927	90	222
			2.900		601
15.	15.98	2.797	2.810	3	131
			2.808		003
16.	16.56	2.702	2.713	22	330
			2.718		231
			2.715		521
17.	17.81	2.518	2.525	16	701
			2.530		430
18.	18.08	2.481	2.491	11	602
19.	18.52	2.424	2.433	9	711
			2.401		132
					612
20.	18.99	2.367	2.367	3	123
			2.371		522
21.	19.52	2.305	2.316	100	800
			2.321		413
22.	20.04	2.247	2.248	3	140
			2.244		810
23.	20.55	2.194	2.200	18	240
24.	20.93	2.156	2.172	20	141
			2.168		811
			2.176		712
			2.173		513
			2.159		630
			2.169		432
25.	22.65	2.000	2.000		901
			2.002		214
			2.003		821
			2.009		722
			2.007		233
			2.006		523
26.	23.06	1.966	1.978	8	441
27.	23.36	1.942	1.953	8	991
			1.946		314
			1.950		242
			1.951		333
28.	23.73	1.914	1.917	5	404
29.	24.36	1.867	1.870		224
			1.874		920
			1.875		414
30.	24.74	1.840	1.838	14	830
31.	24.98	1.823	1.824	15	324
			1.830		921
			1.831		504
			1.826		640
32.	25.86	1.765	1.765	6	424
			1.771		051
			1.772		723
33.	26.15	1.747	1.740	6	604
			1.753		813
			1.756		542
			1.755		143
34.	27.37	1.675	1.678	5	105
			1.676		642
35.	28.43	1.617	1.619	20	840
			1.621		714
			1.618		434
36.	29.18	1.579	1.579	8	025
			1.579		10.30
			1.577		932
37.	29.42	1.568	1.563	19	534
			1.565		452
			1.566		
38.	30.13	1.534	1.536	9	651
			1.537		144
			1.535		814

Hydromagnesite $Mg_5[OH\ (CO_3)_2]_2 \bullet 4H_2O$

Morphology. Hydromagnesite forms earthy, sometimes loose masses with snowy aspect, less consistent when compared to huntite aggregates. The hydromagnesite mass appears as an elongated aggregate, usually consisting of skeletal crystals. In certain areas the crystals are preferentially oriented in two directions, with an angle of ca 50^0 between them. The crystals form also prisms, sometimes flattened after (100) and are ended with (021) prism faces. The crystal lengths vary from 5 μm to 40 μm - much bigger than those of huntite.

X-ray diffraction properties. The X-ray powder diffraction pattern of hydromagnesite is presented in Table 2.

Thermal behaviour. The thermal diagrams, obtained for the Valea Rea hydromagnesite (Fig. 4) are consistent with those previously recorded for this mineral. In the interval 300–600^0C, the TG and DTG, the curves reveal five reactions accompanied by mass losses. The temperatures of these reactions are given by four endothermics (336^0C, 398^0C, 492^0C, 548^0C) and one exothermic (472^0C) on the DTA curve.

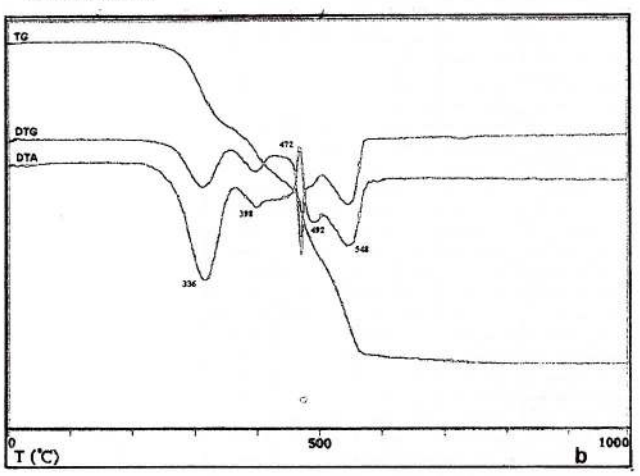

Fig. 4 – Thermal analysis of hydromagnesite (Valea Rea Cave)

Low magnesian calcite

Morphology. Low magnesian calcite associates to huntite and appears as rhombohedral crystals. It usually exhibits parallel intergrowths or crystal groups (Pl. II, Figs. 2, 3). Some of the crystals show signs of corrosion and sometimes huntite crystallises on their surfaces; in this latter case, magnesian calcite is a crystallisation support for huntite (Pl.II, Fig. 4).

X-ray diffraction. X-ray diffraction of some huntite samples shows calcite lines with $d_{(101)}$ values of 3.027, somewhat lower than that of pure calcite, due to $MgCO_3$ contents of about 2.5 to 3%.

Aragonite

Morphology. Aragonite forms aggregates of prismatic to needle-like crystals, disposed as rosettes or fans, parallel or oblique to the surface of the carbonate rock, thus resulting in small geodes. The crystals are elongated after the **c** crystallographic axis, with {110} and {100} crystallographic forms. Certain crystals exhibit the (101) prism faces. Sometimes alternate twinning can also be seen. The crystal length varies from 0.1 mm to 3 mm.

X-ray diffraction. The presence of aragonite was confirmed by X-ray powder diffraction (Fig. 5).

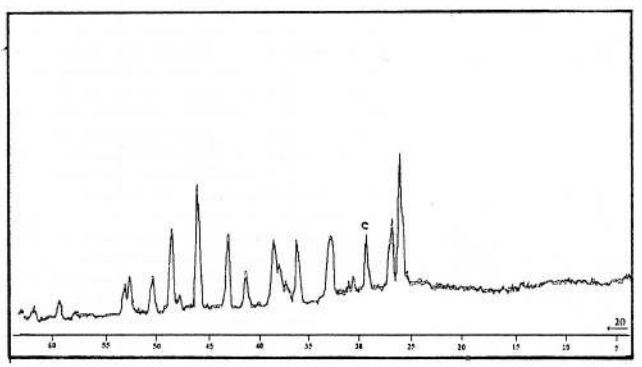

Fig. 5 – X-ray powder diffraction pattern of aragonite from Valea Rea Cave

Genetic considerations

Huntite forms under exogenous conditions, the source of magnesium being dolomite and possibly brucite formed by the hydration of periclase, the latter being a result of the fractionated decomposition of dolomite during thermal metamorphism. We did not find brucite during our study, but there were important brucite concentrations described in the neighbouring area (Ionescu, 1998). Brucite, $Mg(OH)_2$, which has been repported from caves only as a minor/trace mineral, is stable only at low CO_2 partial pressures and high pH (Hill, Forti, 1997) and in a normal cave environment it fastly reacts with CO_2, forming hydromagnesite. So, hydromagnesite deposition on fissures could be an argument for pre-existence of brucite.

The circulation of the CO_2-bearing solutions determined the partial dissolution of the carbonate rock, dedolomitization being the main phenomenon that was observed by means of optical microscopy. Dolomite dissolution occurred according to the following reaction:

$$CaMg(CO_3)_2 + 2H_2O + 2CO_2 \rightarrow Ca(HCO_3)_2 + Mg(HCO_3)_2$$

The partial dissolution of the primary dolomite has led to an increase of the rock porosity.

The bicarbonate solutions deposited prismatic aragonite microcrystals sometimes alternately twinned on the walls of the fissures, thus resulting in a Mg enrichment, which could also be determined by forming of some concentration gradients during the diffusion of the solution through the rock pores, controlled by the different mobility and solubility of Ca and Mg bicarbonates.

The different depositional conditions of calcium and magnesium carbonates are presented in Lippmann's stability diagram (1973) (Fig. 6).

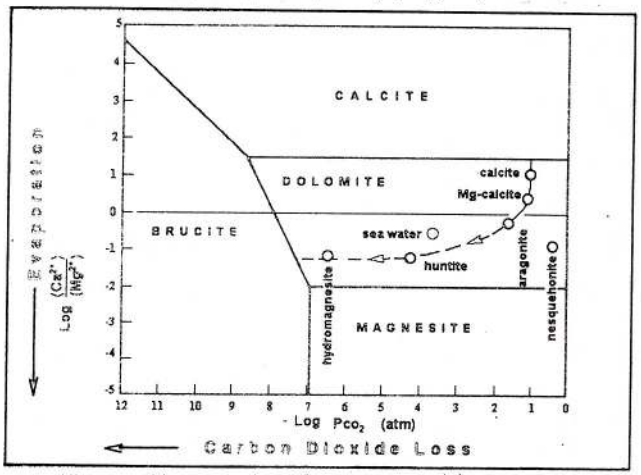

Fig. 6 - The evolution of cave water with respect to increasing evaporation and carbon dioxide loss (after Lippmann, 1973)

The increase of the Ca^{+2}/Mg^{+2} ratio, concurring with a reduced amount of the seepage water at corresponding CO_2 partial pressures, determines the deposition of magnesian calcite, aragonite, huntite and hydromagnesite. The stability diagram shows different conditions for each mineral present in the association. For huntite and hydromagnesite the Ca^{+2}/Mg^{+2} ratio is nearly the same but these two minerals form at different values of CO_2 partial pressure (smaller for hydromagnesite than for huntite). In the case of aragonite and Mg-calcite deposition, the differences in the Ca^{+2}/Mg^{+2} ratio are essential, while CO_2 partial pressures are almost the same. The presence of the four minerals in the association proves the compositional variations (Ca^{+2}/Mg^{+2}) of the solutions, as well as the variations of the CO_2 partial pressures, induced by the air flow.

Acknowledgements. The authors gratefully acknowledge the help of the anonymous referees in improving the first draft of the manuscript.

References

Bleahu, M., Bordea, S., Bordea, J., Mantea, Gh., Popescu, A., Marinescu, Fl., Cioflica, G., Ştefan, A. (1985) Harta geologică a României, scara 1:50.000, foaia Pietroasa, Ed. UGC Bucureşti.

Bordea, S., Bordea, J. (1972) Noi date stratigrafice şi structurale în nord-vestul Munţilor Bihor. *D. S. Inst. Geol. Geofiz.*, LIX/5, p. 5–13, Bucureşti.

Cole, W. F., Iancucki, C. J. (1975) Huntite from Deer Park, Victoria, Australia. *Amer. Mineral.*, 60, p. 1130–1131.

Damm, P., Perenyi, K., Pop, C., Szucs, Sz., Zih, J., (1996) Consideţii asupra Peşterii din Valea Rea (Munţii Bihor). *cerc. Speol.*, 4, pp. 21–23.

Diaconu, G., Medeşan, A., Viehmann, I. (1977) Une nouvelle paragenèse minéralogique dans la grotte "Peştera Fagului", Départment de Bihor (huntite, hydromagnésite, aragonite, calcite). *Trav. Inst. Spéol. "E. Racovitza"*, XVI, p. 203–210.

Dollase, W. A., Reeder, R. J. (1986) Crystal structure refinement of huntite, $CaMg_3(CO_3)_4$, with X-ray powder data. *Amer. Mineral.*, 71, p. 163–166.

Faust, G. T. (1953) Huntite, $Mg_3Ca(CO_3)_4$, a new mineral. *Amer. Mineral.*, 38, p. 4–23.

Ghergari, L., Tămaş, T., Damm, P., Forray, F. (1997) Hydrothermal Palaeokarst in Peştera din Valea Rea (Bihor Mountains, Romania). *Theor. Appl. Karst.*, 10, p. 115–125.

Graf, D. L., Bradley, W. F. (1962) The crystal structure of huntite, $CaMg_3(CO_3)_4$. *Acta Cryst.*, 15, p. 238–242.

Hill, C. A. (1976) Cave minerals. *Nat. Speleol. Soc.*, Huntsville, USA, 137 p.

— , **Forti, P. (1997)** Cave Minerals of the World. Second edition. *Nat. Speleol. Soc.*, Huntsville, USA, 463 p.

Ianovici, V., Borcoş, M., Bleahu, M., Patrulius, D., Lupu, M., Dimitrescu, R., Savu, H. (1976) Geologia Munţilor Apuseni. Edit. Acad. R.S.R., Bucureşti, 631 p.

Ionescu, C. (1998) Brucitul - $Mg(OH)_2$. Mineralogie şi mineralogeneză. Zăcăminte de brucit din România. Edit. Did. Pedag., Bucureşti, 150 p.

Kinsman, D. J. (1967) Huntite from a carbonate evaporite environment. *Amer. Mineral.*, 52, p. 1332–1340.

Koblencz, V., Nemecz, E. (1953) Huntit elofordulása Dorogon (Huntite from the Dorog Mine, Dorog, Hungary). *Föld. Közl.*, 83, 10–12, p. 391–395.

Lippmann, F. (1973) Sedimentary carbonate minerals. Springer-Verlag, new York, 228 p.

Onac, B. P., Bengeanu, M., Botez, M., Zih, J. (1995) Preliminary Report on the Mineralogy of Peştera din Valea Rea (Bihor Mountains, Romania). *Theor. Appl. Karst.*, 8, p. 75–79.

Skinner, B. J. (1958) Huntite from Tea Tree Gully, South Australia. *Amer. Mineral.*, 43, p. 159–162.

Ştefan, A. (1980) Studiul petrografic al părţii de est a masivului eruptiv Vlădeasa. *An. Inst. Geol. Geofiz.*, LV, p. 237–325.

— , **Lazăr, C., Berbeleac, I., Udubaşa, Gh. (1988)** Evolution of magmatism in the Apuseni Mountains and associated metallogenesis. *D. S. Inst. Geol. Geofiz.*, 72–73 (2), p. 195–213.

— , **Roşu, E., Andăr, A., Robu, L., Robu, N., Bratosin, I., Grabari, G., Stoian, M., Vâjdea, E., Colios, E. (1992)** Petrological and geochemical features of banatitic magmatites in Northern Apuseni Mountains. *Rom. J. Petrology*, 75, pp. 97–115.

Todor, D. N. (1972) Analiza termică a mineralelor. 279 p. Edit. Tehn., Bucureşti.

Plate I

SEM images on huntite and hydromagnesite samples:

Fig. 1 – Lamellar huntite aggregates.

Fig. 2 – Lammelar huntite aggregates, detail of photo 1.

Fig. 3 – Prismatic hydromagnesite aggregates.

Fig. 4 – Prismatic hydromagnesite aggregates, detail photo 3.

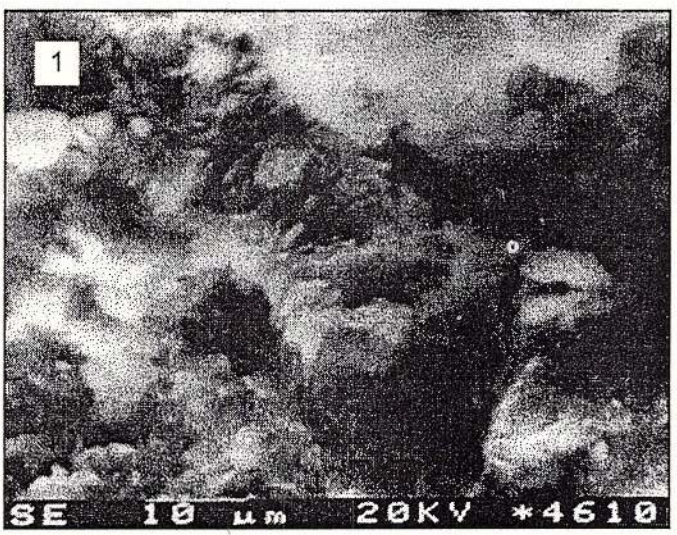

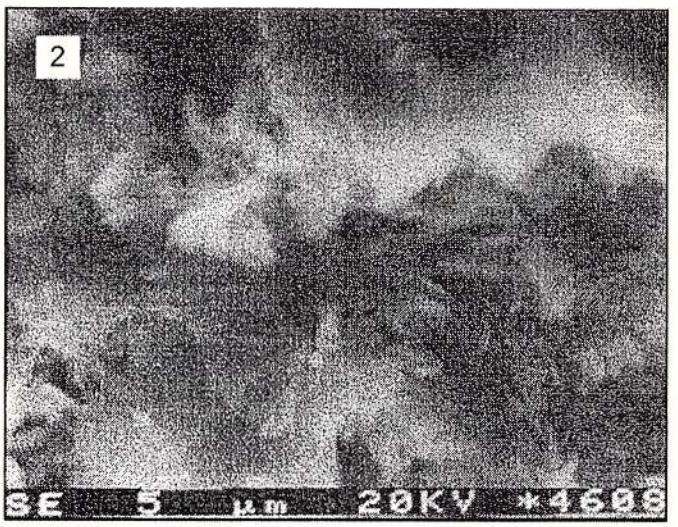

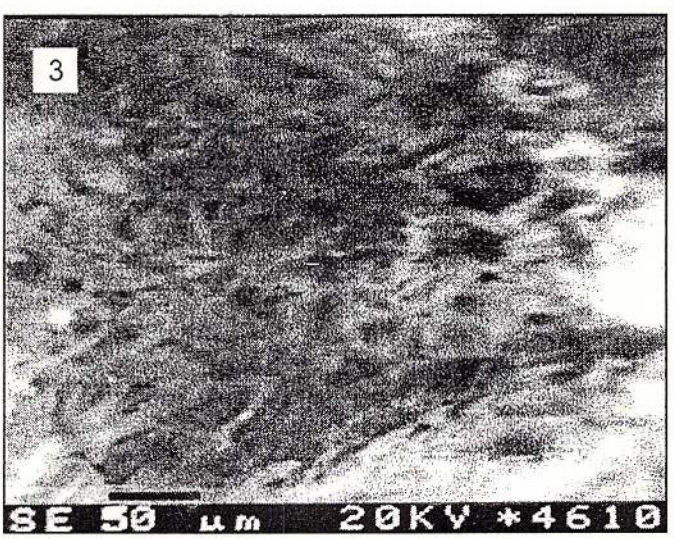

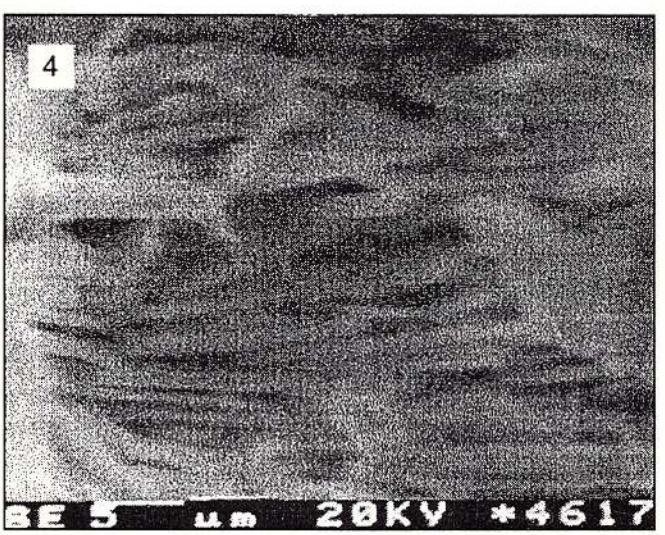

Plate II

TEM images on huntite samples:

Fig. 1 – Huntite crystals.

Fig. 2 – Huntite + magnesian calcite.

Fig. 3 – Huntite + magnesian calcite.

Fig. 4 – Detail showing huntite deposition by overgrowth on the edge of a corroded Mg-calcite crystal.

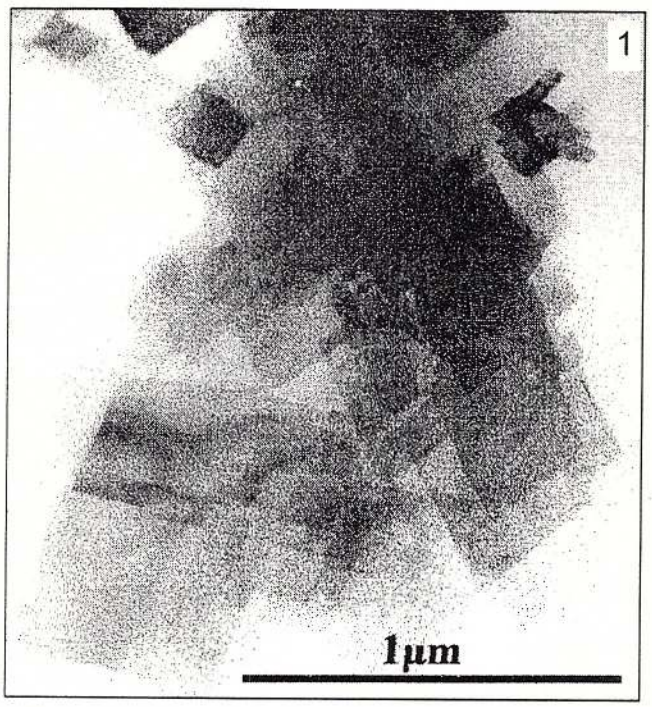

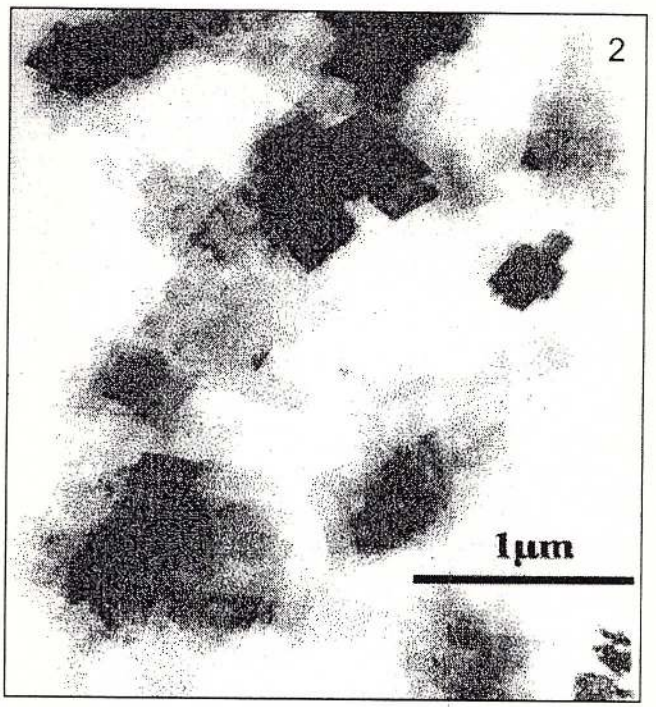

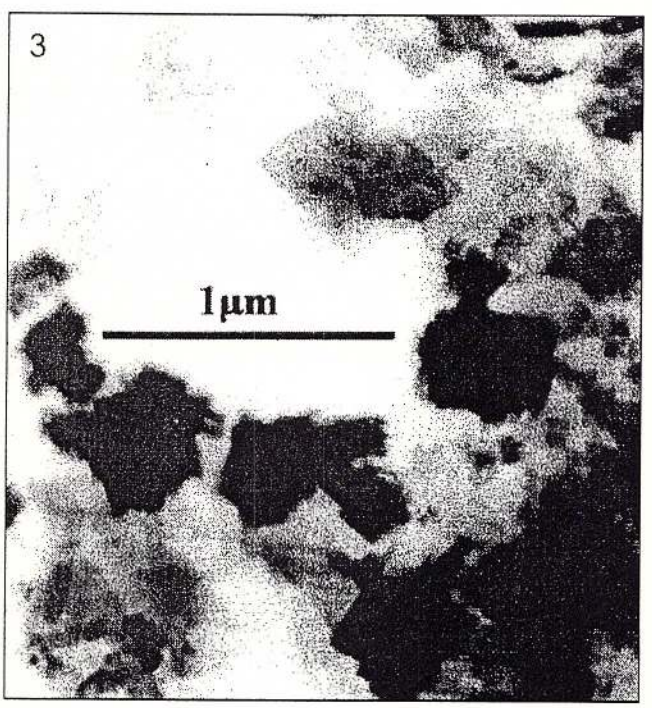

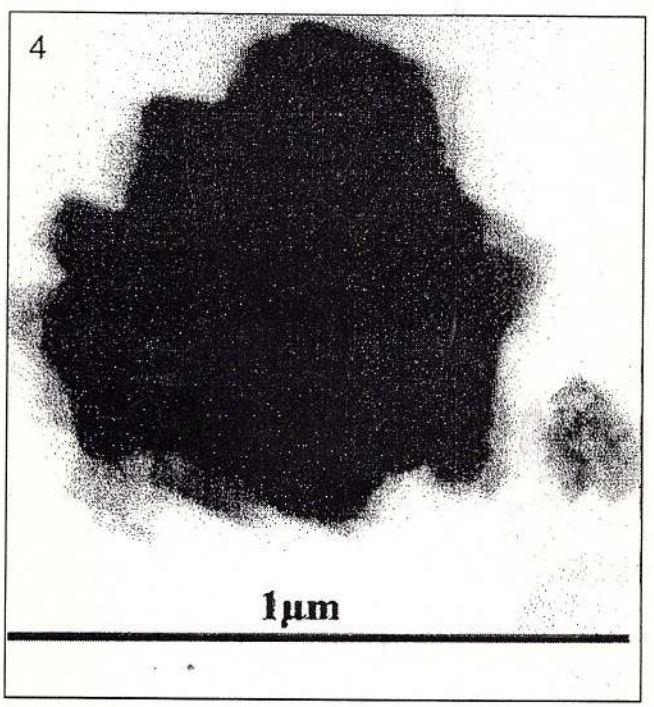

Rom. J. Mineralogy, 79, p. 159-169, Bucureşti, 1999

CHARACTERISATION OF SOME ANTARCTIC LACUSTRINE SEDIMENTS FROM NORTHERN VICTORIA LAND

L. STIEVANO, M. BERTELLE, G. LEOTTA, S. CALOGERO*

Dipartimento di Chimica Fisica, Università, I-30123 Venezia, Italy

S. CONSTANTINESCU

National Institute of Materials Physics, Bucharest, Romania

M. ODDONE

Dipartimento di Chimica Generale, Università, I-27100 Pavia, Italy

Key words: Antarctica. Lacustrine Sediments. INAA. XRD. Mössbauer Spectroscopy.

Abstract: Fifteen lacustrine sediments, sampled during the 1994-95 Austral summer in Northern Victoria Land (Antarctica), were characterised by X-ray diffraction, instrumental neutron activation analysis and ^{57}Fe Mössbauer spectroscopy. These sediments are related to the intrusive rocks from Granite Harbour, to the metamorphic rocks of the Complex of Wilson Terrane and the volcanic rocks from Mc Murdo. The samples contain quartz, alkaline feldspars, plagioclases, amphiboles, biotite, chlorite and muscovite except for the sediments of volcanic genesis that contain alkaline feldspars, plagioclases and pyroxenes. The paramagnetic components of the Mössbauer spectra have been assigned mainly to the iron sites in biotites except for those displayed from the sediments of volcanic genesis assigned mainly to pyroxenes. Mössbauer spectra at room temperature do not display magnetic ordering except for those of the sediments of volcanic genesis containing bulk magnetite, haematite and goethite. Mössbauer spectra collected at the liquid helium temperature exhibit always magnetic ordering. This spectral difference has been attributed to the different dimensions of the iron oxide particles in sediments. The scarce weathering involves a partial transformation of magnetite in haematite and goethite in the sediments of volcanic genesis. In the remaining sediments a partial hydrolysis of biotite together with a partial oxidation of iron (II) retained in silicates is present.

Introduction

In primary rocks most of the iron is located as structural iron(II) in silicates as pyroxenes, amphiboles, biotites etc. The chemical weathering of primary rocks may determine the decomposition of silicates by hydrolysis and the oxidation by atmospheric oxygen of the iron(II) structurally present in the silicates. The neo-formed iron(III) cations may be retained in silicate sites as structural iron(III) or precipitated as oxyhydroxides in different particle-sizes. In weathered soils, the iron(III) oxyhydroxides may be mobilised under anaerobic conditions by microbial reduction of the organic biomass to iron(II)-bearing species. Once mobilised the iron(II)-bearing species can be redistributed within the soil, or from a soil into a lake or sea, and they may enter in biological cycles (Coey, 1984).

This iron mobilisation is not generally observed in Antarctica since the process of formation of the sediments is at its initial stage. In fact water is generally frozen and consequently the chemical processes involved in weathering are scarcely present. However, this general statement does not take into account the chemical and mineralogical nature of the primary rocks, which might be affected by weathering in different ways.

In order to clarify some aspects of the weathering processes the study of a set of lacustrine sediments of different genesis seemed suitable. These sediments sampled in Northern Victoria Land result from the

*Author to whom correspondence should be addressed

Table 1. Details about the sampling points

Sample	Area	Geographic Coordinates
A1	Edmonson Point	74°18' S 165°04' E
A2	Skua Lake	74°42' S 164°07' E
A3	Tarn Flat	74°58' S 162°30' E
A4	Carezza Lake	74°42' S 164°03' E
A5	Inexpressible Island	74°52' S 163°43' E
A6	Camp Oasis	74°42' S 164°06' E
A7	Camp Icarus	74°41' S 164°06' E
A8	Adelie Cove South	74°37' S 164°50' E
A9	Adelie Cove North	74°37' S 164°50' E
A10	Snowy Point	74°35' S 163°49' E
A11	Cape Confusion	74°35' S 163°48' E
A12	Gondwana Lake	74°37' S 164°13' E
A13	Markham Island	74°36' S 164°56' E
A14	Teall Nunatak	74°50' S 163°33' E
A15	Vegetation Island	74°47' S 163°39' E

mechanical desegregation and the chemical weathering of volcanic rocks from Mc Murdo (dating back to Late Cenozoic), of intrusive rocks from Granite Harbour (Cambrian-Ordovician period) and of metamorphic rocks from the Complex of Wilson Terrane (Precambrian) (Armienti et al., 1991; Beccaluva et al., 1991).

These sediments were mainly characterised by X-ray diffraction analysis (XRD) and instrumental neutron activation analysis (INAA). Since iron is substantially present in sediments, their iron chemistry was investigated by ^{57}Fe Mössbauer spectroscopy. This technique can provide quantitative information about the relative population of the iron species together with specific properties of the individual iron sites as oxidation state, coordination geometry, magnetic order etc. Another advantage is that Mössbauer spectra can be collected for both crystalline and amorphous materials. So, iron hydroxides, or oxy-hydroxides, or oxides (hereafter referred to as iron oxides) can be evidenced (Hilton et al., 1987; Johnston and Lewis, 1987; Murad and Johnston, 1987).

This paper reports some chemical data concerning fifteen lacustrine samples collected in the region of Northern Victoria Land close to Skua Lake, Tarn Flat, Carezza Lake, Inexpressible Island, Camp Oasis, Snowy Point, Gondwana Lake, Teall Nunatak and Vegetation Island.

Experimental

Sampling

The sediments of lacustrine origin listed in Table 1 were sampled by the team of the Italian National Program for Antarctica Research (PNRA) during the 1994–95 Austral summer. The specimens, collected at the temperature of about -20°C, were enclosed in hermetically sealed bottles, frozen and placed in a freeze-drier. The measurements were performed on the samples without preliminary treatments.

Instrumental neutron activation analysis

Three subsamples for every sediment (after grounding, powdering <100 mesh and homogenising) were submitted to a test of homogeneity. The variance analysis, assumed as an index of the sampling variability, showed that samples of about 400 mg are quite homogeneous and representative of the material investigated. The samples were heat- sealed into polyethylene vials. Samples of about 500 mg were subjected to a first neutron irradiation for 2 h and to a second irradiation, at a thermal flux of 10^{12} n cm^{-2} s^{-1}, for 25 h in the 250 kW Triga Mark II reactor of Pavia. In the same way the standard SRM 1633a (National Institute for Sciences and Technology, USA) and another standard (prepared by adding known amounts of other elements in the reach of INAA to pure SiO_2) were irradiated. A g-ray spectrometry and a Ge(Li) detector coupled to an analyser-computer measured the induced radioactivity from 3 to 50 d after irradiation. The reliability of the procedure is confirmed by the good agreement, between found and known elemental contents, obtained for the two standards. The abundance for La, Ce, Nd, Sm, Eu, Gd, Tb, Ho, Tm, Yb, Lu, Sc, Cr, Co, Ni, Zn, As, Se, Rb, Zr, Sb, Cs, Ba, Hf, Ta, Th, U, and Fe is reported as an average of three independent determinations in Table 2.

Table 2. Elemental abundance from INAA in ppm, except for Fe in %

	A1	A2	A3	A4	A5	A6	A7	A8	A9	A10
La	94.66	82.92	31.15	82.77	84.63	88.55	131.65	53.38	44.11	83.89
Ce	177.84	155.19	58.03	152.61	169.95	186.71	266.00	104.88	91.48	160.52
Nd	73.81	62.32	21.54	62.52	70.93	75.94	128.37	45.07	42.27	66.61
Sm	13.37	11.16	4.57	12.58	12.40	13.99	23.22	8.07	7.12	13.44
Eu	3.49	2.31	0.92	2.54	2.78	2.42	4.01	1.71	1.54	2.44
Gd	11.89	10.50	5.71	13.70	14.56	17.21	16.42	6.73	7.40	10.08
Tb	2.14	1.69	1.01	1.96	2.23	2.73	2.63	1.22	1.20	1.73
Ho	2.84	2.17	1.16	2.27	2.80	3.10	3.56	1.43	1.470	2.49
Tm	1.06	0.68	0.46	0.82	1.08	0.99	1.22	0.54	0.52	0.97
Yb	5.54	3.84	2.13	4.27	1.10	4.86	7.97	3.23	2.80	5.04
Lu	0.63	0.47	0.31	0.56	3.48	0.61	0.96	0.43	0.34	0.66
Sc	7.02	9.60	8.24	15.50	13.29	14.41	20.88	10.68	9.27	16.55
Cr	16.01	37.04	20.82	61.29	89.51	84.67	77.93	49.23	41.23	92.52
Co	8.48	9.72	8.96	17.7.3	4.61	19.07	24.04	10.90	9.05	32.99
Ni	54.90	21.46	13.58	47.29	9.17	48.88	18.38	9.21	11.34	72.91
Zn	135.59	74.11	60.35	122.95	24.10	150.34	353.54	64.50	60.12	151.09
As	2.68	5.14	1.43	4.11	17.77	8.31	22.50	1.68	1.09	4.52
Se	8.92	5.52	2.35	6.92	7.87	6.65	14.51	3.60	2.76	6.56
Rb	105.89	111.64	126.73	141.97	111.31	146.24	183.35	110.75	121.23	177.42
Zr	363.92	265.65	134.59	322.32	364.79	296.82	707.71	178.64	163.56	281.82
Sb	0.23	0.25	0.14	29.91	28.68	0.34	23.00	0.00	0.00	0.24
Cs	1.66	2.69	4.38	5.45	4.46	7.97	6.34	5.59	4.33	10.98
Ba	732.52	600.19	595.95	653.17	530.27	560.73	385.03	656.54	646.65	601.77
Hf	13.33	12.61	4.36	15.05	17.93	11.61	35.02	7.64	6.10	11.90
Ta	7.95	2.01	1.16	2.58	2.50	3.79	2.55	1.36	1.16	3.58
Th	16.56	16.48	11.60	20.08	18.41	22.05	24.74	15.75	12.49	26.32
U	5.50	3.05	4.59	5.43	4.96	7.71	5.52	4.84	3.19	7.35
Fe (%)	5.50	3.29	2.46	5.28	4.99	5.80	8.28	3.01	2.79	6.56

	A11	A12	A13	A14	A15
La	66.63	59.00	39.62	71.66	130.09
Ce	130.72	118.50	74.93	94.85	239.13
Nd	54.92	48.63	38.19	42.90	87.67
Sm	10.92	10.23	7.39	9.58	15.30
Eu	2.36	1.83	2.62	2.16	2.50
Gd	8.36	6.27	9.09	9.56	12.58
Tb	1.52	1.14	1.58	1.70	1.72
Ho	2.22	1.64	2.25	5.70	2.01
Tm	0.93	0.67	0.98	0.94	0.69
Yb	4.45	4.70	2.38	2.52	3.72
Lu	0.53	0.64	0.23	0.24	0.50
Sc	10.92	8.88	21.42	20.85	10.55
Cr	47.04	53.22	76.67	75.55	26.90
Co	11.02	8.45	43.47	39.70	8.15
Ni	32.76	27.21	31.72	34.81	1.12
Zn	85.59	74.75	117.72	109.68	68.45
As	2.56	2.40	0.03	0.03	0.07
Se	5.67	3.79	3.68	3.62	4.90
Rb	110.56	108.48	29.89	134.29	150.68
Zr	281.34	213.83	184.91	194.73	305.75
Sb	0.27	0.46	0.25	0.22	0.13
Cs	3.85	4.98	0.55	4.15	8.44
Ba	541.47	539.11	321.44	387.91	880.06
Hf	13.28	7.81	5.20	5.62	11.61
Ta	3.16	2.03	3.35	1.32	1.73
Th	15.51	19.20	3.83	16.19	21.25
U	4.73	6.81	2.02	8.96	9.80
Fe (%)	3.81	3.25	10.18	2.51	2.89

Table 3. Mineralogical species detected by X-ray diffraction

	Quartz	Alkaline feldspar	Plagioclase	Pyroxene	Amphibole	Biotite	Chlorite	Muscovite
A1[a]		+	++	+				
A2[b]	+++		++					+
A3[b]	+++	+	+		+		+	+
A4[b]	+		++		+		+	
A5[c]	++	+	+		+	+	+	++
A6[b]	+++	++	++		++	+	+	+
A7[b]	+++		+++		+			+
A8[b]	+++	++	++		+	+	+	+
A9[b]	+++	+			+		+	++
A10[c]	++	+			+	+	+	++
A11[b]	++		++					+
A12[c]	+++	++	++		+	+	+	
A13[a]		++	++	+				
A14[b]	+++		++		++		+	
A15[b]	++	++	++		++	+	+	+

[a] Sediments related to lavas from Mc Murdo or Melbourne Volcano

[b] Sediments related to the intrusive rocks of Granite Harbour

[c] Sediments linked to the metamorphic rocks of the Complex of Wilson Terrane

Mössbauer Spectroscopy and XRD

The X-ray diffraction (XRD) patterns were obtained by a diffractometer operating with a CuKα/Ni radiation. The detected minerals are listed in Table 3.

The Mössbauer spectra were collected at room and at the liquid helium temperature by a 57Co/Rh source and a conventional spectrometer operating with a sinusoidal velocity waveform. Both source and absorber were kept at the same temperature. The fit of the spectra was performed by sets of appropriate Lorentzian doublets and of magnetic sextets by the software package MOS-90 (Grosse, 1992). The literature parameters for some silicates were used as input in the preliminary fits (Bancroft et al., 1967; Coey, 1984). Table 4 lists the room temperature parameters, such as the magnetic hyperfine field (B in Tesla, T), the electric quadrupole splitting (QS in mms^{-1}), the isomer shift (IS in mms^{-1}), together with the relative resonance area (A in percent of the total

Table 4. Mössbauer parameters at room temperature

Sediment	B_{hf} (Tesla)	QS (mms^{-1})	IS[a] (mms^{-1})	LW (mms^{-1})	A (%)	Site
A1	50.7	-0.19	0.37	0.30	7	haematite
	47.1	-0.02	0.26	0.30	5	magnetite
	45.8	0.00	0.66	0.30	3	magnetite
	38.9	-0.26	0.37	0.30	3	goethite
	-	2.79	1.13	0.31	14	Fe(II)
	-	1.99	1.05	0.68	48	Fe(II)
	-	0.70	0.40	0.61	20	Fe(III)
A2	-	2.64	1.11	0.34	26	Fe(II)
	-	2.04	1.13	0.38	23	Fe(II)
	-	0.78	0.33	0.49	36	Fe(III)
	-	1.22	0.65	0.85	15	Fe(III)
A3	-	2.61	1.11	0.31	20	Fe(II)
	-	2.01	1.11	0.42	23	Fe(II)
	-	0.68	0.35	0.53	44	Fe(III)
	-	1.18	0.44	0.56	13	Fe(III)
A4	-	2.68	1.10	0.29	19	Fe(II)
	-	2.06	1.13	0.39	24	Fe(II)
	-	0.79	0.30	0.43	35	Fe(III)
	-	0.93	0.53	0.61	22	Fe(III)
A5	-	2.68	1.10	0.33	23	Fe(II)
	-	2.04	1.13	0.52	25	Fe(II)
	-	0.72	0.32	0.49	41	Fe(III)
	-	0.93	0.54	0.63	11	Fe(III)
A6	-	2.64	1.10	0.31	27	Fe(II)
	-	2.06	1.14	0.40	14	Fe(II)
	-	0.81	0.33	0.52	46	Fe(III)
	-	1.18	0.51	0.47	13	Fe(III)
A7	-	2.63	1.10	0.28	17	Fe(II)
	-	2.02	1.14	0.40	24	Fe(II)
	-	0.67	0.25	0.44	43	Fe(III)
	-	1.09	0.41	0.50	16	Fe(III)
A8	-	2.62	1.11	0.33	46	Fe(II)
	-	2.04	1.10	0.41	24	Fe(II)
	-	0.78	0.36	0.65	30	Fe(III)
A9	-	2.61	1.11	0.43	45	Fe(II)
	-	2.05	1.10	0.38	26	Fe(II)
	-	0.78	0.32	0.65	29	Fe(III)
A10	-	2.67	1.08	0.32	19	Fe(II)
	-	2.26	1.04	0.59	22	Fe(II)
	-	0.55	0.37	0.39	27	Fe(III)
	-	1.10	0.40	0.42	32	Fe(III)
A11	-	2.64	1.11	0.34	30	Fe(II)
	-	2.06	1.08	0.48	30	Fe(II)
	-	0.82	0.37	0.70	40	Fe(III)
A12	-	2.60	1.10	0.34	40	Fe(II)
	-	2.06	1.05	0.40	20	Fe(II)
	-	0.78	0.35	0.62	40	Fe(III)
A13	50.2	-0.19	0.37	0.30	29	haematite
	47.6	-0.02	0.26	0.30	8	magnetite
	46.2	0.00	0.66	0.30	4	magnetite
	39.5	-0.26	0.37	0.30	2	goethite
	-	2.89	1.13	0.30	13	Fe(II)
	-	1.89	1.00	0.99	19	Fe(II)
	-	0.70	0.37	0.51	25	Fe(III)
A14	-	2.65	1.11	0.28	27	Fe(II)
	-	2.19	1.08	0.46	25	Fe(II)
	-	0.79	0.35	0.59	48	Fe(III)
A15	-	2.65	1.11	0.28	27	Fe(II)
	-	2.17	1.10	0.40	24	Fe(II)
	-	0.80	0.35	0.60	49	Fe(III)

[a] The isomer shift (IS) quoted relative to Fe metal.

Table 5. Relative resonance area (in percent) for the four fractions of the Gondwana sample A12 obtained after the magnetic separation performed by Frantz separator

	As received*	Fraction 1 (< 0.4 A)	Fraction 2 (0.4-0.8 A)	Fraction 3 (0.8-1.8 A)	Fraction 4 (Residue)
Biotite + Chlorite Fe(II) 1	40	36	36	31	21
Biotite Fe(II) 2	20	29	27	28	25
Biotite Fe(III) 1	40	6	10	11	15
Biotite Fe(III) 2	-	7	5	4	11
Amphibole Fe(II) 1	-	12	11	7	2
Amphibole Fe(II) 1	-	5	3	2	2
Amphibole Fe(III)	-	5	8	17	24

* From Table 4

iron). As reported in Appendix a selective Frantz isodynamic separator was employed for fractionating the sediments. The fractions were characterised by Mössbauer spectroscopy and XRD. The composition of the fractions for a typical sample is reported in Table 5.

Results and discussion

INAA and XRD data

The elemental abundance for main and trace elements is reported in Table 2. Even if large variations are observed among the samples, no systematic trend is apparent among sediments related to volcanic or intrusive or metamorphic rocks and their elemental composition. For comparison purposes the elemental content has been normalised to the mean sediment composition following Bowen (1979). The results are displayed on the top of Figure 1. It can be seen that the elemental contents, in particular for Se and Hf, are generally larger in the Antarctic samples than in the reference sediment. The REE content in Antarctic sediments has been normalised to NASC i.e. North American Shale Composition following Haskin et al. (1979). As displayed at the bottom of Figure 1, the REE content is generally larger in the Antarctic sediments than in NASC. In conclusion the sediments cannot be discriminated by their elemental composition and their elemental content is larger than those of the reference standards.

The sediments can be instead subdivided in two groups on the basis of the mineralogical species of Table 3 detected by XRD. The first group includes the sediments A1 and A13, collected at Edmonson Point and Markham Island, respectively. They contain alkaline feldspars, plagioclases and pyroxenes. The second group includes the sediments linked to the metamorphic and intrusive rocks. They contain variable amounts of quartz, alkaline feldspars, plagioclase, amphiboles, biotite, chlorite and muscovite.

Mössbauer Spectra

The Mössbauer spectra collected at room temperature display magnetic ordering only for the first group of sediments A1 and A13 (cf. Fig. 2). Their fit points to the presence of magnetic sextets with Mössbauer parameters listed in Table 4 close to those reported for bulk haematite (B 51.6 T, QS -0.19 mms^{-1}, IS 0.27 mms^{-1}), magnetite (B 48.6 and 45.5 T, QS -0.01 and 0.01 mms^{-1}, IS 0.17 and 0.55 mms^{-1}), goethite (B 38.0 T, QS -0.26 mms^{-1}, IS 0.37 mms^{-1}) (Murad & Johnston, 1987; Vandenberghe, 1990). The presence of magnetic sextets at room temperature shows that in the first group of sediments the iron oxides are bulk i.e. with particle-size in average larger than the 100 .On going from room temperature to liquid helium temperature, the magnetic ordering is also observed in the spectra of the remaining sediments. That is shown in Figure 3 for the representative Mössbauer spectrum of the sediment A3 from Tarn Flat indicating the presence of finely divided iron oxides in all the samples of the second group of sediments. Unfortunately the quantitative interpretation of the Mössbauer spectra at 4.2 K is complicated by the superparamagnetic relaxation of the iron(II) sites in silicates in addition to the magnetic ordering of the finely divided particles of iron oxides (Coey 1975 and 1980; Townsend et al., 1986). The fit of the spectra at 4.2 K required one (or more) magnetic sextet(s) attributable to iron oxides and one (or more) octet(s) due the iron(II) sites in silicates. An additional complication in the fitting procedure is the presence of the paramagnetic doublets due to iron(II) and iron(III) sites also at 4.2 K.

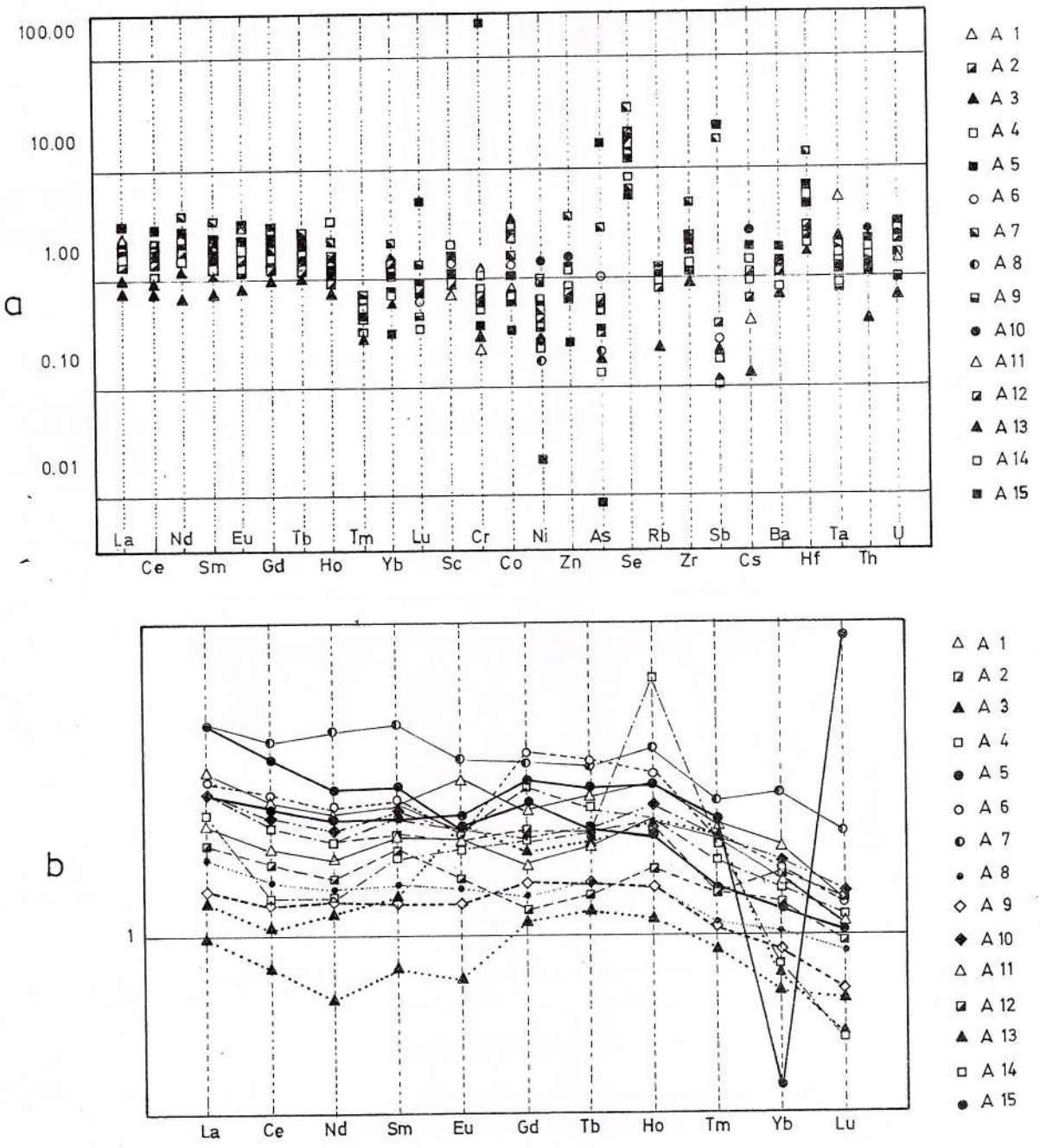

Fig. 1 – a, Trace element content of the Antarctic sediments normalised to mean sediment composition (normalising values after Bowen, 1979); b, trace REE content of the Antarctic sediments normalised to NASC, North American Shale Compposition.

Even if the typical Mössbauer spectrum collected at room temperature (Fig. 3) appears relatively simple, it may result from a large variety of spectral components attributable to the iron-containing silicates listed in Table 3. Since the assignment of a doublet to its site is not straightforward, the preliminary fits were performed by starting from the parameters reported for the silicates listed in Table 3. The final fit was performed by using three different sets of parameters.

1) The paramagnetic resonance, exhibited from the first group of sediments A1 and A13 related to volcanic rocks, has mainly been attributed to the presence of pyroxenes. Since two distinct metal sites are present in pyroxenes, the fit requires two doublets assigned to two iron(II) sites and one doublet related to iron(III) sites. The results are listed in Table 5.

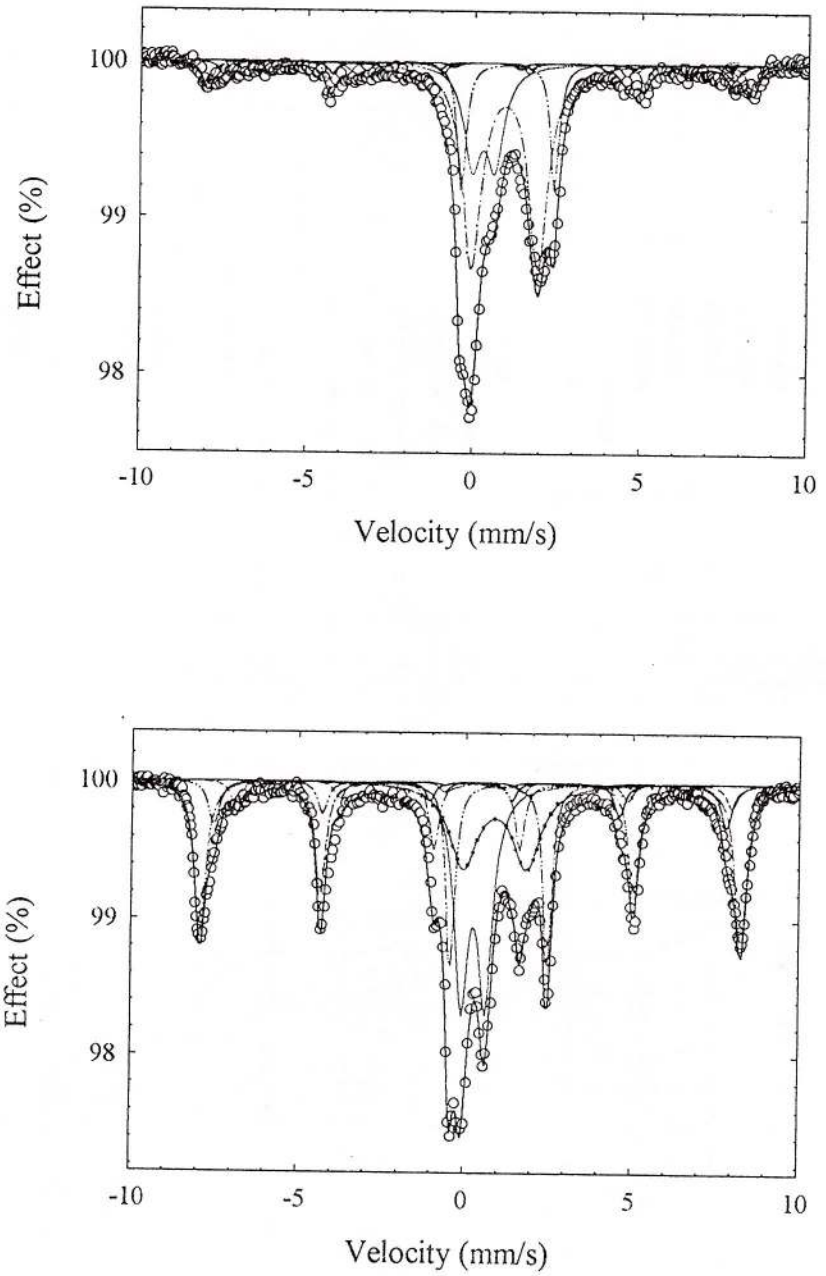

Fig. 2 – Mössbauer spectra of the sediments A1 (top) and A13 (bottom) magnetically split at room temperature

2) The spectra of part of the sediments A8, A9, A11, A12, A14 and A15 of the second group were fitted with three doublets, two attributable to iron(II) and one to the iron(III) sites. Their Mössbauer parameters reported in Table 5 are in agreement with those reported from Goodman and Wilson (1973) for biotite (Fe(II): QS 2.64, 2.19 mms^{-1}; IS 1.13, 1.11 mms^{-1}. Fe(III): QS 0.89 mms^{-1}; IS 0.34 mms^{-1}).

3) The spectra of the remaining sediments A2, A3, A4, A5, A6, A7 and A10 cannot be fitted with only three components and they require an additional component. The fit was performed by using four doublets: two for the iron(II) sites and two for the iron(III) ones. The found Mössbauer parameters in Table 5 are in rough agreement with those reported for biotite partially oxidised and altered to chlorite

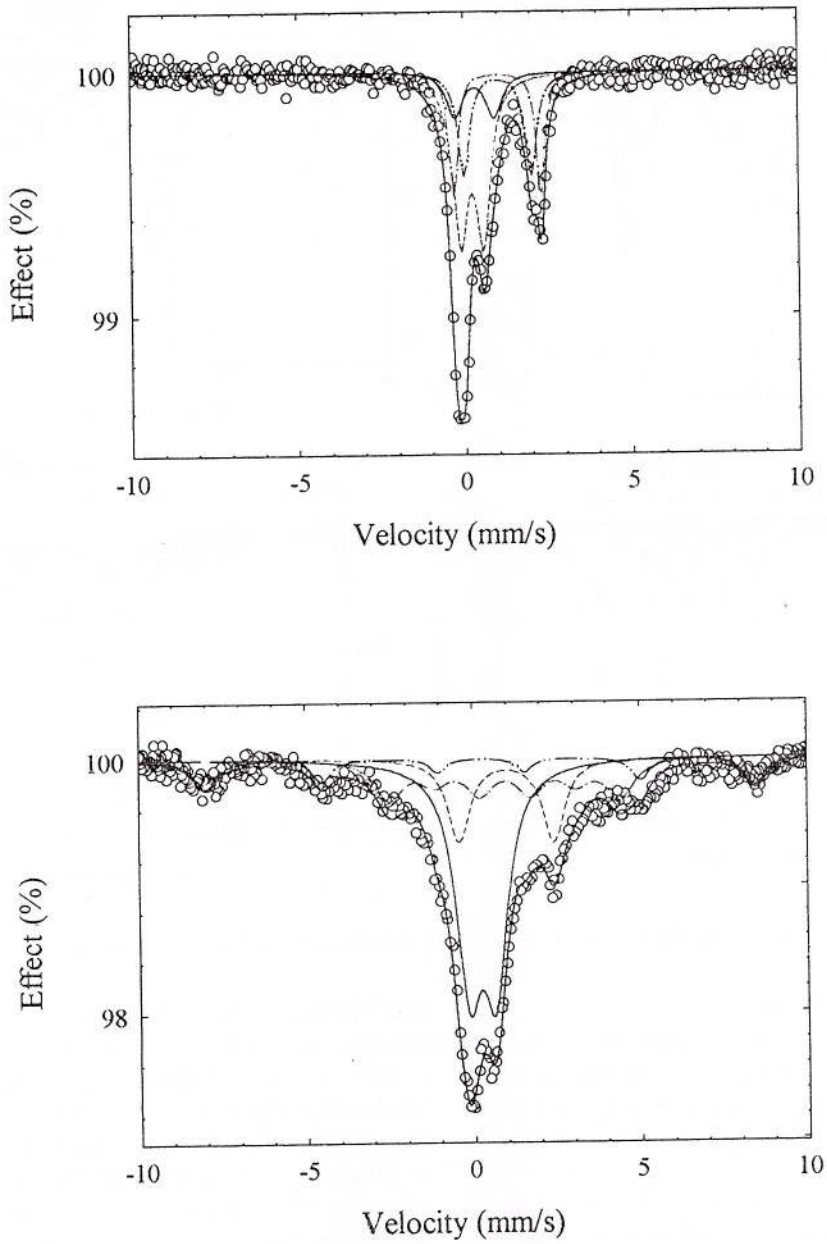

Fig. 3 – Mössbauer spectra for the sediment A3 at room (top) and the liquid helium temperature (bottom)

and muscovite (Fe(II): QS 2.66 and 2.11 mms^{-1}, IS 1.13 and 1.15 mms-1; Fe(III) QS 1.08 and 0.76 mms^{-1}; IS 0.41 and 0.34 mms^{-1} in Goodman and Wilson, 1973). It was no possible the discrimination of the spectral contributions of chlorite and muscovite since the Mössbauer parameters for chlorite (QS 2.62 mms^{-1}, IS 1.01mms^{-1}) and muscovite (iron(II): QS 2.65-2.90 mms^{-1}, IS 1.11-1.18 mms^{-1}; iron(III): QS 0.50, IS 0.34 mms^{-1} in Coey, 1984) are too close to those of biotite.

In conclusion Mössbauer spectroscopy allows a further subdivision within the second group of sediments volcanic related to intrusive or metamorphic rocks on the basis of the presence of large amounts of altered biotite.

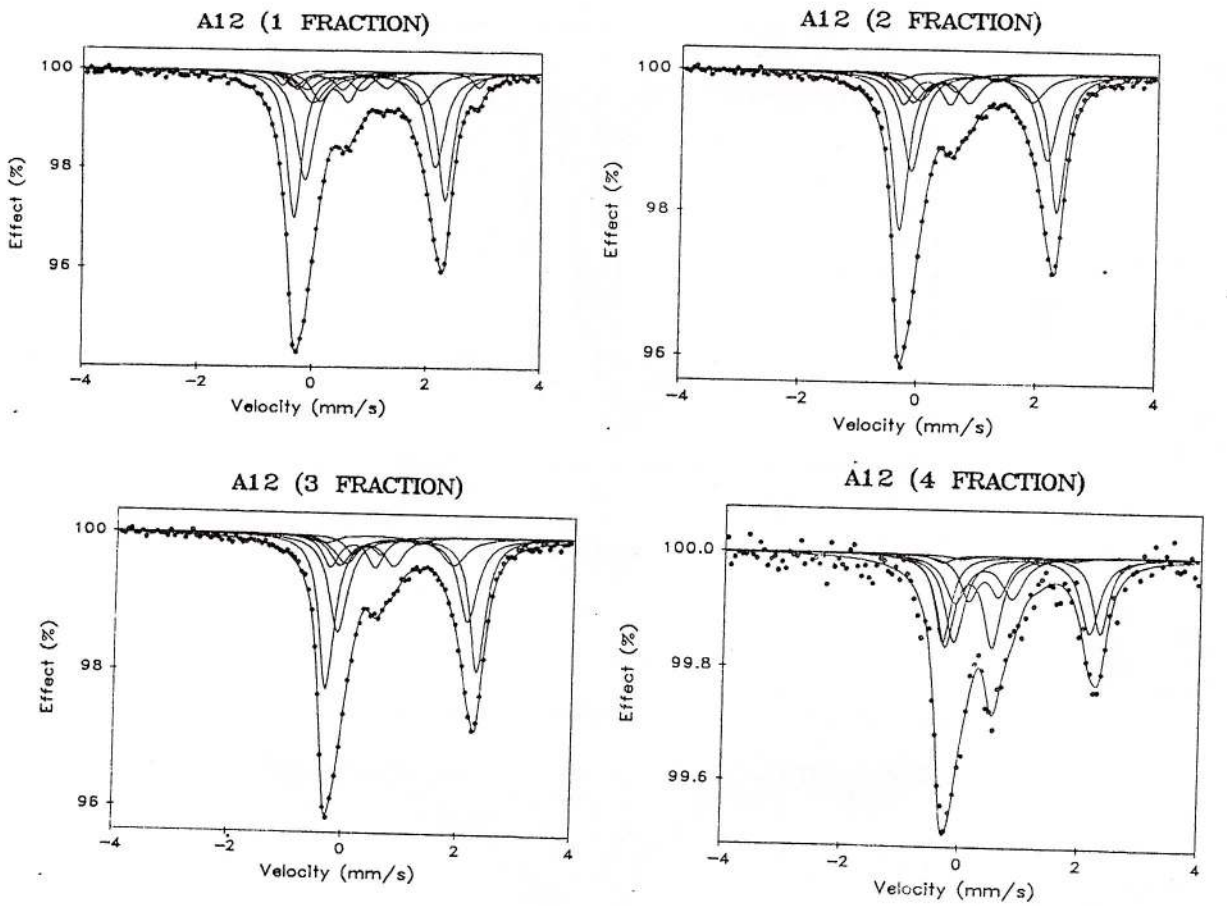

Fig. 4 – Mössbauer spectra for the four fractions obtained by Frantz separation

The chemical weathering

Some iron-bearing components present in the sediments are probably related to local oxidative and basic conditions. In fact in presence of liquid water some alterations related to the hydrolyse of silicates and to the oxidation of iron(II) are possible.

In the first group of sediments of volcanic genesis (A1 and A13) Mössbauer spectroscopy does not detect a sensible alteration of pyroxenes. On the contrary, the main alteration concerns the iron(II) present in primary magnetite in such a way that the slow oxidisation by atmospheric oxygen transforms it in haematite and goethite. The neo-formed haematite or goethite derives from the oxidation of the primary magnetite and not from oxidation, rejection and precipitation of the iron(II) present in pyroxenes.

In the second group of sediments, Mössbauer spectroscopy shows that biotite is sensibly altered by hydrolysis in such a way that the fit requires additional components in many samples. It is known in fact that biotite can partially be oxidised and transformed in other phases such as chlorite and muscovite (Goodman, Wilson, 1973). Weathering can determine not only the alteration of biotite but also an increase of Fe^{37} retained in the silicate lattices or precipitated as fine dispersed iron oxide (Schwertmann, Cornell, 1991). The alteration by hydrolysis of biotite mobilises a large number of iron(II) cations. Consequently when liquid water is suddenly available during the Austral summer, a large number of iron cations passes from silicates to solution forming many nuclei of condensation of iron oxides. The formation of a large number of fine dispersed particles explains the absence of magnetic order at room temperature observed in the Mössbauer spectra of the second group of sediments.

Appendix

In order to clarify the nature of the iron-bearing silicates present in the specimens, some sediments were fractionated by a selective Frantz isodynamic separator (-15^0 long, +20^0 lat) with magnetic fields generated by an intensity of current up to 1.8 A). The results of this procedure are shown here for the Gondwana sediment A12 for which biotite together

with chlorite and amphiboles has been detected by XRD (Table 3). The efficiency of the separation was checked performing XRD and Mössbauer spectra on the four fractions (cf. Figure 4).

A simultaneous fit with common parameters (Grosse, 1992) was performed for the Mössbauer spectra belonging to the sample after separation. In the simultaneous fit with common parameters, all parameters (except the relative resonance areas and the linewidths) are common since they are changed simultaneously in such a way that they assume the same value in all the spectra of the considered set. This means that the common parameters of all spectra are identical with each other and they may be changed only simultaneously. Common parameters were used for the paramagnetic components. The free parameters were the resonance areas and the linewidths; they are free since they concern only the spectrum they belong to and are changed in a completely free way. The simultaneous fit has been performed by writing a macro file to connect the parameters of the spectra before and after Frantz separation. The relative resonance areas (in percent) of the components present in the fractions of the sediment are listed in Table 5.

Acknowledgements

Financial support from E.N.E.A in the framework of the Italian National Programme for Antarctic Researches, PNRA (Environmental Impact-Chemical Methodologies) is gratefully acknowledged.

References

Armienti, P., Civetta, L., Innocenti, F., Manetti, P., Tripodo, A., Villari, L., Vita G. (1991) *Mem. Soc. Geol.*, 46, p. 397–424.

Bancroft, G. M., Maddock, A. G., Burns, R. G. (1967) *Geochim. Cosmochim. Acta*, 31, p. 2219–2225.

Beccaluva, L., Civetta, L., Coltorti, M., Orsi, G., Saccani, E., Siena, F. (1991) *Mem. Soc. Geol. It.*, 46, p. 383–395.

Bowen, H. J. M. (1979) In: Environmental Chemistry of the elements. Academic Press, N.Y., 42.

Bowen, L. H., De Grave, E., Vandenberghe, R. E. (1993) Mössbauer effect studies of magnetic soils and sediments. In: Mössbauer Spectroscopy Applied to Magnetism and Material Science. Long G. J. & Grandjean F. Ed., Plenum Press, N. Y., Vol. 1, p. 115–159.

Coey, J. M. D. (1975) *Geochim. Cosmochim. Acta*, 39, p. 401–415.

— **(1980)** *At. Energy Rev.*, 18, p. 73–82.

— **(1984)** Mössbauer spectroscopy of silicate minerals. In: Mössbauer Spectroscopy Applied to Inorganic Chemistry. Long G. J. & Grandjean F. Ed., Plenum Press, N. Y. Vol. 1, p. 443-509.

Goodman, B. A., Wilson, M. J. (1973) *Mineralogical Magazine*, 39, p. 448–454.

Grosse, G. (1992) MOS-90, Version 2.2, Technical University of Munich.

Haskin, L. A., Paster, T. P. (1979) Geochemistry and Mineralogy of the Rare Earths. *Handbook Phys. Chem. Rare Earths*, (North-Holland Ed., Amsterdam), Vol. 3, chap. 21.

Hilton J., Long, G. J., Chapman, J. S., Lishman, J. P. (1986) *Geochim. Cosmochim. Acta*, 50, p. 2147–2151.

Johnston, J. H., Lewis, D. G. (1987) Industrial Applications of the Mössbauer Effect, Long G. J. & Stevens J. G. Ed., Plenum Press, N. Y., p. 565–583.

Murad, E., Johnston, J. H. (1987) Iron oxides and oxyhydroxides. In: Mössbauer Spectroscopy Applied to Inorganic Chemistry. Long G. J., Ed., Plenum Press, N. Y., Vol. 2, p. 507–582.

Schwertmann, U., Cornell, R. M. (1991) Iron Oxides in the Laboratory. VCH Ed., Weinheim, Germany, p. 14–18.

Townsend, M. G., Longworth, G., Kodama, H. (1986) *Can. Mineral.*, 24, p. 105–115.

Vandenberghe, R. E., De Grave, E., Landuydt, C., Bowen, L. H. (1990) *Hyp. Inter.*, 53, p. 175–196.

ORGANISERS

University of Miskolc
Herman Ottó Museum

Co-organisers

Hungarian Geological Society
Mineralogical Society of Romania
Slovak Geological Society

ADDRESS FOR CORRESPONDENCE AND INFORMATION

"Minerals of the Carpathians" Conference
c/o Department of Mineralogy
Herman Ottó Museum
Kossuth u. 13
H-3525 Miskolc
Hungary
Phone: +36-46-326436
Fax: +36-46-367975

CONTACT PERSONS OF THE LOCAL ORGANISING COMMITTEE:

Sándor Szakáll and Béla Fehér:
e-mail: xhomin@gold.uni-miskolc.hu
and
Ferenc Mádai:
e-mail: askmf@gold.uni-miskolc.hu

Homepage:
http://www.uni-miskolc.hu/uni/dept/asvany

"MINERALS OF THE CARPATHIANS" CONFERENCE

SCOPE

From mineralogical and petrological points of view the Carpathian–Pannonian Region is one of the most interesting and complex areas of Europe.

In the last decade widening of international scientific co-operation and application of modern techniques in mineral sciences resulted in a boom of new scientific information. As a result of these activities the monograph "Minerals of the Carpathians" has been compiled by the joint work of researchers from all countries of the region.

The present meeting is intended to provide the local mineralogical community with a forum where new results and invited review papers can be presented. The other goal of the meeting is to give an insight in the state of art of mineral sciences in the Carpathian-Pannonian Region for mineralogists coming out of the region.

DATE AND PLACE

The meeting will be held in Miskolc, Hungary on March 9–10, 2000. The scientific activities will be placed in the House of Science and Technics, Miskolc.

First Circular

March 9–10, 2000
Miskolc, Hungary

SCIENTIFIC PROGRAMME

The scientific programme is planned to cover mineralogy, crystallography, petrology, geochemistry, and mineral deposits of the Carpathians in broad sense. An Open Session will also be organised depending on the demand. Contributions will be presented as invited plenary lectures and as poster sessions.

SCIENTIFIC BOARD OF THE MEETING

M. Chovan (Slovakia), V. Kvasnytsya (Ukraine), M. Novák (Czech Republic), Gh. Udubaşa (Romania), I. Viczián (Hungary)

CONFERENCE LANGUAGE

The official language of the meeting will be English.

ABSTRACTS

You are invited to submit papers in the field of the scientific programme. The abstracts are planned to be published in "Acta Mineralogica-Petrographica, Szeged".

IMPORTANT DATES

Deadline for returning the First Circular	October 15, 1999
Second Circular	November, 1999
Deadline for abstracts	January 9, 2000

The organisers try to minimise the registration and accommodation costs. Details of these fees will be communicated in the Second Circular.

Rom. J. Mineralogy, 79, p. 171-187, Bucureşti, 1999

XRD, INAA AND MÖSSBAUER CHARACTERISATION OF SOME ANTARCTIC SOIL CORES FROM WOOD BAY

M. BERTELLE, G. LEOTTA, S. CALOGERO*

Dipartimento di Chimica Fisica, Università, I-30123 Venezia, Italy

S. CONSTANTINESCU

National Institute of Materials Physics, Bucharest, Romania

M. ODDONE

Dipartimento di Chimica Generale, Università, I-27100 Pavia, Italy

Key words: Marine Soils. Lacustrine Soils. Terrestrial Soils. Mössbauer Spectroscopy. INAA. Wood Bay. Antarctica.

Abstract: Marine, lacustrine and terrestrial soil cores, sampled in a restricted area of Wood Bay in Antarctica, were characterised by X-ray diffraction, instrumental neutron activation analysis and ^{57}Fe Mössbauer spectroscopy. The soils, formed from mechanical disgregation and weathering of rocks of volcanic origin from Mt. Melbourne, consist of alkaline feldspar, olivine, augitic clinopyroxene, and iron oxides such as haematite, goethite, and magnetite. Lacustrine and terrestrial soils are richer in clinopyroxene whereas marine soils are richer in olivine. This finding shows that the soils retain a content in olivine and clinopyroxene comparable to that found in the parent lava outcropping in the Mt. Melbourne volcano. The soils appear at the initial stage of weathering. Two main weathering effects are observed: 1) atmospheric oxygen determines the oxidation of the iron(II) present in olivine and clinopyroxene and the neo-formed iron(III) is mainly retained in silicate sites as structural iron(III). 2) A part of magnetite, present as a primary constituent of the volcanic rocks, is oxidised to bulk haematite and goethite.

INTRODUCTION

Much has been reported on the volcanism of Mt. Melbourne Province in Northern Victoria Land, Antarctica, by a number of authors, inter alia Höig et al. (1991), Wörner, Viereck (1989), Viereck et al. (1989), Glasby et al.(1975, 1985). Many geochemical and petrological data concerning a wide range of volcanic rocks, sampled in the Mt. Melbourne region, have been reported by Beccaluva et al. (1991) and Armienti et al. (1991, 1994). These volcanic rocks, produced at high temperature and pressure in reducing conditions, contain mainly alkaline feldspars, olivines, clinopyroxenes, and magnetite. Their content of olivines and clinopyroxenes is variable depending on the different conditions of formation: the rocks richer in olivines were formed at lower pressure contrary to those richer in clinopyroxenes formed at relatively higher pressure (Armienti et al. 1991). Considering the soils sampled in Wood Bay, i.e. the material probably formed by mechanical disgregation and weathering of lava outcropped from Mt. Melbourne volcano, two phenomena seem prominent in the soil evolution. The first is related to the redox processes, since the iron(II)-bearing silicates may be altered and the iron(II) cations partially oxidised; the second is related to the enrichment or depauperation of some elements. Since iron, a redox probe of local variations, is substantially present in these volcanic materials, ^{57}Fe Mössbauer spectroscopy can be a useful tool because it provides quantitative information about the relative population of the iron species (Vandenberghe et al., 1990; Hilton et al., 1986). In addition Mössbauer effect, depending primarily on short-range order in solids, can detect specific properties of the individual iron sites as oxidation state, coordination symmetry, magnetic order etc. Another advan-

*Author to whom correspondence should be addressed

tage is that Mössbauer spectra can be collected for both crystalline and amorphous materials. So, poorly crystallised iron hydroxides, or oxyhydroxides, or oxides (hereafter referred to as iron oxides) can be evidenced (Johnston et al., 1987; Murad et al., 1987; Bowen et al., 1993). On the other hand, instrumental neutron activation analysis (INAA) is a reliable tool to detect the enrichment or the depauperation of many heavy elements along the depth profile of cores, or among soils belonging to different environments. These two techniques, together with X-ray diffraction (XRD), were used for studying selected marine, lacustrine, and terrestrial cores of Wood Bay and the results are here reported and discussed.

EXPERIMENTAL

Sampling

The soil cores were sampled in Wood Bay in the framework of the Italian National Program for Antarctica Research (PNRA) during the 1993–1994 Austral summer. The sampled cores were enclosed in hermetically sealed bottles. Subsequently, the cores were extruded, sectioned, frozen and placed in a freeze-drier. After sectioning the cores in layers, the pieces larger than 2mm were excluded and vegetable organisms removed. The marine core (8 MS; 74=B020' lat. S, 165=B06' long. E) was collected not too far from the shore, close to Edmonson Point. The marine core of 25 cm was sectioned in eight layers. The lacustrine core (12 LS ; $74^0$18' lat. S, $165^0$5' long. E) was sampled, at 2 m from the shore at a water-depth of 20 cm, from a small lacustrine fed by water of defrosting. The lacustrine samples derive from a core of 15 cm sectioned in eight layers. The terrestrial core (12 TS, 10x10x15h cm^3) was collected at the Wood Bay station (30 m a.s.l., 3 km North of Edmonson Point, $74^0$18' lat. S, $165^0$5' long. E) close to the Italian base of Terranova. The terrestrial core of 15 cm was sectioned in three layers of 5 cm. Subsequently the terrestrial layer 0-5 cm was fractionated in four granulometric ranges 0–50, 50–100, 100–200, and 200–2000 mm. Instrumental neutron activation analysis (INAA). Three subsamples for every specimen (after grounding, powdering < 100 mesh and homogenising) were submitted to a test of homogeneity according to Jaffrezic (1976). The variance analysis, assumed as an index of the sampling variability, showed that samples of about 400 mg are quite homogeneous and representative of the material investigated. Samples of about 500 mg were subjected to a first neutron irradiation for 2 h and to a second irradiation, at a thermal flux of 1012 n cm^{-2} s^{-1}, for 25 h in a 250 kW Triga Mark II reactor. In the same way the standard SRM 1633a from National Institute for Sciences and Technology, USA, and another standard (prepared by adding known amounts of other elements in the reach of INAA to pure SiO^2) were irradiated. A gray spectrometry and a Ge(Li) detector coupled to an analyser-computer measured induced radioactivity from 3 to 50 d after the irradiation. The reliability of the procedure is confirmed by the good agreement, between found and known elemental contents, obtained for the two standards. Major, minor, and REE abundances for La, Ce, Nd, Sm, Eu, Gd, Tb, Ho, Tm, Yb, Lu, Sc, Cr, Co, Ni, Zn, As, Se, Rb, Zr, Sb, Cs, Ba, Hf, Ta, Th, U, Fe, reported in ppm, except for Fe in %, as an average of three independent determinations, are listed in Tables 1A, 1B, and 1C for the three soil cores.

Mössbauer spectroscopy

The ^{57}Fe Mössbauer spectra were collected mainly at room temperature but also at the liquid nitrogen or liquid helium temperature with a ^{57}Co source in a rhodium matrix with a sinusoidal velocity wave form. The spectra were fitted with appropriate superposition of Lorentzian lines and of magnetic sextets using the MOS-90 software package (Grosse, 1992). The reference Mössbauer parameters for olivines and clinopyroxenes were taken from literature (Bancroft et al., 1967; Coey 1984). The resulting spectral parameters (such as the magnetic hyperfine field B in Tesla T, the electric quadrupole splitting QS in mms^{-1}, the isomer shift IS in mms^{-1}, relative to metallic iron, and the relative resonance areas A of the different components of the absorption patterns) are reported in Tables 2A, 2B and 2C. The estimated error is less than 1%. The X-ray diffraction (XRD) patterns were obtained by a diffractometer operating with a CuKa/Ni radiation.

RESULTS AND DISCUSSION

INAA and XRD data

The variation in the elemental composition listed in Tables 1A-1C is relatively scarce and depends on local environmental conditions. This dependence is displayed on comparing lacustrine soils (Table 1B) with the unfractioned terrestrial sample (last column of Table 1C): there is a depauperation in REE, Se, Rb, Ba, Hf, Th, Fe and an enrichment in Sc, Cr, Co, Ni, U, Zr, Sb. This finding may be explained considering the lacustrine soil as a collector of defrosting water, which transports detritus materials and leached elements. Therefore transport and deposition, in comparison with the terrestrial sample, alter the elemental distribution in lacustrine soils.

Comparing marine soils with the unfractioned terrestrial sample (Table 1A and last column of Table 1C) a depauperation is observed for most elements. The finding implies the presence of diffusion fluxes, (resulting from concentration gradients at the sedi-

Table 1A. Elemental abundance in ppm, (except for Fe in %) for the marine soil core vs. the depth profile

	0 - 2 cm	2 -5 cm	5 - 8 cm	8 -11 cm	11-14 cm	14-17 cm	17-23 cm	23-25 cm
La	74 (3)	74 (4)	72 (1)	68 (1)	79.5 (1)	75 (3)	77 (1)	69 (3)
Ce	142 (9)	139 (8)	136 (3)	131 (3)	150 (3)	139 (11)	141 (8)	128 (11)
Nd	61 (3)	62 (3)	61 (2)	57.1 (4)	64 (2)	58 (4)	61 (3)	56 (5)
Sm	12.4 (8)	12.6 (8)	12.2 (2)	11.5 (3)	12.6 (1)	12.1 (8)	12.5 (5)	11.3 (9)
Eu	3.2 (2)	3.3 (2)	3.1 (1)	3.1 (1)	3.07 (9)	3.2 (3)	3.3 (3)	3.2 (3)
Gd	16.2 (1)	16.0 (1)	15.3 (1)	16.5 (1)	16.3 (1)	15.4 (1)	16.3 (1)	14.6 (1)
Tb	2.69 (1)	2.78 (1)	2.89 (1)	2.75 (1)	2.82 (3)	2.46 (3)	2.58 (1)	3.0 (5)
Ho	3.35 (1)	3.41 (1)	3.44 (2)	3.35 (2)	3.46 (9)	2.78 (1)	2.87 (1)	2.88 (2)
Tm	1.12 (5)	1.02 (9)	1.1 (8)	0.94 (4)	0.95 (4)	0.94 (3)	0.79 (1)	1.0 (1)
Yb	4.6 (2)	4.5 (3)	4.3 (2)	4.17 (7)	4.4 (1)	4.4 (4)	4.5 (2)	4.2 (4)
Lu	0.55 (2)	0.54 (3)	0.54 (1)	0.50 (1)	0.56 (1)	0.52 (2)	0.56 (1)	0.51 (3)
Sc	9.4 (5)	10.7 (1)	10.2 (6)	8.7 (2)	9.9 (4)	9.7 (2)	9.9 (7)	10.2 (6)
Cr	22.9 (6)	28.8 (6)	47 (2)	28.6 (2)	29.2 (5)	18.4 (2)	29.2 (6)	38.9 (3)
Co	11.0 (3)	12.1 (1)	11.2 (1)	10.0 (1)	11.5 (2)	10.75 (5)	10.92 (5)	11.6 (4)
Ni	31.4 (1)	29.7 (2)	46.8 (3)	28 (1)	63.4 (9)	17.4 (7)	19.9 (3)	23.3 (7)
Zn	128 (2)	145 (3)	166 (3)	126 (2)	166 (2)	133 (2)	146 (2)	106 (2)
As	1.99 (5)	2.4 (1)	1.75 (3)	2.05 (2)	1.6 (1)	1.7 (3)	1.8 (.2)	1.66 (8)
Se	7.6 (1)	6.6 (5)	6.5 (2)	6.7 (2)	6.9 (3)	7.6 (4)	7.4 (3)	7.0 (3)
Rb	76.7 (7)	73 (2)	66.3 (7)	71.3 (1)	59.2 (8)	84.3 (8)	79.3 (2)	75.9 (7)
Zr	339 (5)	338 (16)	338 (12)	294 (7)	361 (21)	325 (10)	354 (3)	309.5 (1)
Sb	1.98 (2)	6.3 (2)	1.17 (1)	6 (4)	1.5 (1)	1.5 (2)	2.3 (1)	1.56 (8)
Cs	1.14 (4)	0.97 (2)	0.93 (1)	0.87 (2)	0.82 (7)	1.20 (2)	1.11 (9)	1.0 (2)
Ba	862 (28)	889 (16)	840 (15)	753 (3)	852 (23)	856 (22)	948 (5)	864 (26)
Hf	10.8 (6)	9.9 (6)	10.0 (4)	9.7 (3)	10.8 (1)	11.5 (5)	11.5 (3)	10.5 (7)
Ta	5.5 (1)	5.2 (1)	5.01 (5)	4.90 (8)	5.00 (6)	5.69 (9)	5.44 (9)	5.0 (2)
Th	11.2 (5)	10.0 (5)	9.7 (1)	10.0 (1)	9.9 (1)	11.2 (4)	10.8 (2)	9.8 (5)
U	5.6 (4)	5.0 (3)	4.8 (2)	5.02 (6)	4.9 (2)	5.1 (6)	5.4 (2)	4.7 (2)
Fe (%)	6.6 (3)	7.8 (6)	6.0 (2)	6.8 (9)	8.3 (1)	6.5 (1)	6.97 (4)	7.0 (3)

Table 1B. Elemental abundance in ppm, (except for Fe in %) for the lacustrine core vs. the depth profile

	0-2 cm	2- 4 cm	4-6 cm	6-8 cm	8-10 cm	10-12 cm	12-14 cm
La	89.1 (5)	94.8 (1)	90 (5)	88 (2)	74 (3)	87 (2)	96 (1)
Ce	166 (1)	187 (1)	178 (4)	170.5 (2)	148 (2)	157 (4)	185 (3)
Nd	69 (1)	76 (4)	78.3 (9)	67 (3)	60 (2)	65.1 (4)	80 (2)
Sm	13.4 (3)	14.6 (5)	14.8 (7)	14.2 (3)	11.8 (3)	12.5 (4)	15.4 (4)
Eu	3.95 (9)	4.3 (2)	4.23 (1)	5.1 (7)	3.3 (1)	3.7 (1)	4.1 (1)
Gd	15.4 (1)	18.3 (3)	17.8 (2)	18.2 (1)	15.2 (1)	16.3 (1)	18.4 (1)
Tb	2.49 (2)	3.03 (2)	2.87 (1)	2.71 (4)	2.68 (3)	2.79 (1)	2.93 (4)
Ho	2.84 (5)	3.6 (2)	3.57 (2)	3.46 (9)	3.46 (9)	3.6 (1)	3.54 (3)
Tm	1.24 (2)	1.36 (3)	1.11 (1)	1.1 (4)	1.2 (2)	1.25 (3)	1.16 (2)
Yb	4.96 (9)	5.3 (2)	5.12 (7)	5.3 (2)	4.3 (1)	5.0 (1)	5.5 (2)
Lu	0.59 (1)	0.63 (4)	0.59 (6)	0.58 (3)	0.50 (4)	0.56 (1)	0.65 (3)
Sc	8.30 (6)	9.8 (5)	7 (1)	7.5 (1)	5.96 (8)	8 (6)	6.7 (5)
Cr	13.1 (1)	20.3 (5)	20 (3)	20.2 (6)	14.0 (2)	40.1 (1)	20.6 (8)
Co	6.0 (3)	7.3 (2)	6.4 (2)	6.5 (1)	5.2 (4)	5.1 (2)	5.72 (8)
Ni	25 (2)	28.0 (4)	32.2 (8)	21.5 (1)	27 (3)	22 (1)	56.0 (6)
Zn	142 (6)	145.6 (3)	168 (7)	133 (8)	126.0 (1)	121 (5)	164 (3)
As	2.30 (7)	2.6 (8)	1.88 (6)	1.85 (5)	1.8 (1)	2.4 (4)	2.8 (2)
Se	8.1 (7)	9.2 (6)	8.9 (3)	9.6 (2)	6.9 (8)	7.6 (7)	9 (1)
Rb	87 (11)	102 (2)	104 (4)	107.0 (7)	82 (4)	98 (4)	121 (9)
Zr	312 (18)	361 (17)	340 (6)	308 (36)	272 (17)	326 (18)	340 (21)
Sb	2.5 (1)	19.6 (2)	1.2 (9)	8.3 (6)	8 (6)	1.15 (3)	2.2 (2)
Cs	1.37 (9)	1.3 (1)	1.4 (1)	1.65 (8)	1.20 (1)	1.4 (1)	1.47 (6)
Ba	1118 (33)	855 (13)	858 (24)	1382 (12)	683 (20)	1155 (31)	882 (28)
Hf	13.0 (7)	13.9 (7)	11 (1)	12.9 (2)	10.9 (1)	12.1 (8)	12.6 (1)
Ta	6.9 (1)	7.4 (1)	7.0 (4)	6.9 (2)	5.9 (3)	6.9 (3)	8.0 (2)
Th	14.5 (4)	15.5 (4)	14.8 (8)	14.7 (3)	12.5 (6)	14.5 (4)	16.8 (2)
U	3.6 (2)	4.51 (2)	4.6 (4)	2.8 (7)	3.9 (8)	4.5 (6)	5.1 (9)
Fe (%)	1.9 (2)	1.5 (3)	1.0 (1)	1.4 (3)	1.4 (1)	1.5 (2)	1.8 (3)

Table 1C. Elemental abundance in ppm, (except for Fe in %) for the terrestrial layer 0-5 cm vs. the granulometry

	0 - 50 μm	50 - 100 μm	100 - 200 μm	200 - 2000 μm	unfra ctioned
La	97 (5)	85 (2)	76 (6)	71 (1)	82 (5)
Ce	174 (9)	156 (3)	137 (12)	134 (5)	150 (12)
Nd	80 (1)	68.8 (9)	59 (6)	63 (3)	68 (9)
Sm	13.8 (9)	13.1 (1)	12.4 (7)	12.5 (3)	12.9 (9)
Eu	4.7 (2)	3.7 (2)	3.5 (3)	3.7 (2)	3.9 (3)
Gd	17.9 (1)	16.9 (1)	16.1 (1)	16.4 (1)	16.8 (1)
Tb	2.79 (2)	2.82 (2)	2.75 (1)	2.79 (2)	2.79 (2)
Ho	3.51 (5)	3.42 (2)	3.33 (2)	3.34 (3)	3.4 (5)
Tm	1.26 (2)	1.12 (1)	1.16 (2)	1.14 (1)	1.17 (2)
Yb	5.72 (8)	4.7 (2)	4.4 (4)	4.1 (2)	4.7 (8)
Lu	0.65 (4)	0.55 (3)	0.52 (3)	0.46 (1)	0.54 (4)
Sc	7.7 (5)	8.1 (8)	10 (2)	14.6 (9)	10.1 (8)
Cr	20.7 (1)	25 (7)	43 (1)	83.0 (8)	42.7 (7)
Co	9.4 (5)	12.5 (1)	16.0 (3)	24.8 (1)	15.7 (5)
Ni	68 (1)	28.1 (1)	27.0 (5)	36.6 (2)	39.9 (5)
Zn	146 (12)	123 (4)	159 (7)	146 (3)	143.5 (7)
As	3.27 (9)	2.36 (1)	2.17 (3)	2.6 (1)	2.6 (9)
Se	9.6 (2)	7.9 (1)	7.9 (5)	6.9 (1)	8.1 (5)
Rb	109 (7)	93 (1)	76 (1)	67.6 (1)	86.4 (7)
Zr	409 (13)	302 (13)	395 (2)	404 (4)	377 (13)
Sb	15.2 (7)	18.3 (5)	11.61 (4)	8.99 (5)	13.5 (7)
Cs	1.9 (1)	1.8 (1)	1.4 (2)	1.04 (5)	1.5 (5)
Ba	543 (24)	632 (10)	962 (32)	945 (32)	770 (32)
Hf	12.7 (9)	12.5 (6)	11.2 (3)	10.2 (3)	11.6 (9)
Ta	8.2 (1)	7.05 (2)	6.20 (5)	5.84 (4)	6.82 (5)
Th	18.3 (5)	14.4 (2)	11.5 (3)	9.5 (1)	13.4 (5)
U	5.0 (2)	4.05 (7)	5.6 (2)	4.9 (2)	4.9 (7)
Fe (%)	6.5 (4)	5.9 (6)	6.5 (5)	6.2 (4)	6.3 (5)

ment-water interface), that transport elements from the soils to the overlying seawater. This flux is compensated from another, in the opposite direction, concerning in particular Cs, Ba and Rb. In both lacustrine and marine soils, the elemental content generally increases on going from the top core to a depth of 5-10 cm. The elemental content decreases in the middle part of the core and increases again at the bottom. The influence of the physical subdivision on elemental distribution is displayed from the terrestrial layer at depth 0–5 cm fractionated in the ranges 0–50, 50–100, 100–200, and 200–2000 mm. INAA data exhibit a depauperation for REE, Ni, As, Se, Rb, Cs, Hf, Ta, Th and an enrichment for Sc, Cr, Fe, Co, Ba considering samples ordered following increasing granulometry. For comparison purposes the elemental content of Antarctic soils has been normalised to mean sediment composition (Bowen, 1979). It is displayed at the top of Figures 1A, 1B and 1C. It can be seen that the elemental content is generally larger in Antarctic soils than in the reference sediment in particular for Se. Some elements in particular As and Cs exhibit an opposite trend. The REE content in Antarctic soils has been normalised to NASC i.e. North American Shale Composition (Haskin et al., 1979). The trend, displayed at the bottom of Figures 1A, 1B and 1C, shows that the content is always larger than in NASC. Figures 1A, 1B and 1C show that the Antarctic specimens are similar among them but very different in elemental content from reference standards. Similar XRD patterns were found for marine, terrestrial, and lacustrine soils, as shown in Figure 2 for representative specimens. The major constituents are alkaline feldspars, olivines (Ol), augitic clinopyroxenes (hereafter referred to as clinopyroxene, Cpx) and iron oxides. As expected, the lacustrine soils result more amorphous than the others since less intense and numerous peaks are observed and in particular olivines are less present. It is interesting to note that the constituents present in soils

Table 2A. Mössbauer parameters at 293 K for marine layers

Layer (cm)	B (Tesla)	QS (mms^{-1})	IS[a] (mms^{-1})	A (%)	Site[b]
0 - 2	50.5	-0.19	0.37	8	Haematite
	47.7	-0.02	0.26	5	Magnetite 1
	45.9	0.00	0.66	3	Magnetite 2
	36.7	-0.26	0.37	3	Goethite
	-	2.78	1.14	42	Fe(II) Ol M2
	-	2.12	1.13	18	Fe(II) Cpx M1
	-	1.62	0.99	7	Fe(II) Cpx M2
		0.47	0.65	14	Fe(III)
2 - 5	50.5	-0.19	0.37	11	Haematite
	47.7	-0.02	0.26	6	Magnetite 1
	45.7	0.00	0.66	4	Magnetite 2
	39.4	-0.26	0.37	3	Goethite
	-	2.78	1.14	31	Fe(II) Ol M2
	-	2.08	1.14	18	Fe(II) Cpx M1
	-	1.45	1.08	8	Fe(II) Cpx M2
		0.88	0.42	19	Fe(III)
5 - 8	50.4	-0.19	0.37	9	Haematite
	47.3	-0.02	0.26	5	Magnetite 1
	45.8	0.00	0.66	4	Magnetite 2
	37.0	-0.26	0.37	3	Goethite
	-	2.77	1.14	33	Fe(II) Ol M2
	-	2.07	1.15	21	Fe(II) Cpx M1
	-	1.42	1.11	8	Fe(II) Cpx M2
		0.91	0.41	17	Fe(III)
8 - 11	50.8	-0.19	0.37	11	Haematite
	48.2	-0.02	0.26	7	Magnetite 1
	46.7	0.00	0.66	4	Magnetite 2
	37.1	-0.26	0.37	4	Goethite
	-	2.79	1.14	31	Fe(II) Ol M2
	-	2.06	1.14	20	Fe(II) Cpx M1
	-	1.26	1.14	7	Fe(II) Cpx M2
	-	0.91	0.44	16	Fe(III)
11 -14	50.7	-0.19	0.37	13	Haematite
	47.6	-0.02	0.26	7	Magnetite 1
	45.9	0.00	0.66	4	Magnetite 2
	38.5	-0.26	0.37	4	Goethite
	-	2.79	1.15	25	Fe(II) Ol M2
	-	2.06	1.13	19	Fe(II) Cpx M1
	-	1.42	1.07	8	Fe(II) Cpx M2
		0.86	0.39	20	Fe(III)
14 -17	51.1	-0.19	0.37	10	Haematite
	48.0	-0.02	0.26	5	Magnetite 1
	46.5	0.00	0.66	4	Magnetite 2
	38.4	-0.26	0.37	3	Goethite
	-	2.87	1.15	27	Fe(II) Ol M2
	-	2.36	1.13	20	Fe(II) Cpx M1
	-	1.83	1.10	14	Fe(II) Cpx M2
		0.62	0.59	17	Fe(III)
17 -23	51.4	-0.19	0.37	9	Haematite
	49.0	-0.02	0.26	5	Magnetite 1
	48.1	0.00	0.66	4	Magnetite 2
	38.4	-0.26	0.37	3	Goethite
	-	2.83	1.15	41	Fe(II) Ol M2
	-	2.10	1.14	13	Fe(II) Cpx M1
	-	1.50	1.04	7	Fe(II) Cpx M2
		0.86	0.37	18	Fe(III)
23-25	50.6	-0.19	0.37	10	Haematite
	47.7	-0.02	0.26	6	Magnetite 1
	46.1	0.00	0.66	4	Magnetite 2
	39.0	-0.26	0.37	3	Goethite
	-	2.79	1.15	34	Fe(II) Ol M2
	-	2.12	1.16	20	Fe(II) Cpx M1
	-	1.51	1.11	7	Fe(II) Cpx M2
		0.87	0.37	16	Fe(III)

[a] The isomer shift (IS) quoted relative to Fe metal.
[b] Ol = olivine, Cpx = augitic clinopyroxene

Table 2B. Mössbauer parameters at 293 K for lacustrine layers

Layer (cm)	B (Tesla)	QS (mms^{-1})	IS[a] (mms^{-1})	A (%)	Site[b]
0 - 2	51.5	-0.19	0.37	4	Haematite
	47.5	-0.02	0.26	5	Magnetite 1
	46.5	0.00	0.66	4	Magnetite 2
	39.4	-0.26	0.37	6	Goethite
	-	2.75	1.12	19	Fe(II) Ol M2
	-	2.01	1.06	26	Fe(II) Cpx M1
	-	1.38	1.02	14	Fe(II) Cpx M2
		0.83	0.36	22	Fe(III)
2 - 4	50.9	-0.19	0.37	3	Haematite
	47.9	-0.02	0.26	4	Magnetite 1
	46.3	0.00	0.66	4	Magnetite 2
	37.9	-0.26	0.37	4	Goethite
	-	2.73	1.13	22	Fe(II) Ol M2
	-	2.01	1.06	28	Fe(II) Cpx M1
	-	1.37	1.03	14	Fe(II) Cpx M2
		0.94	0.40	21	Fe(III)
4 - 6	51.7	-0.19	0.37	4	Haematite
	46.1	-0.02	0.26	5	Magnetite 1
	44.5	0.00	0.66	3	Magnetite 2
	39.4	-0.26	0.37	4	Goethite
	-	2.67	1.15	20	Fe(II) Ol M2
	-	1.94	1.09	29	Fe(II) Cpx M1
	-	1.24	1.03	13	Fe(II) Cpx M2
		1.00	0.37	22	Fe(III)
6 - 8	50.7	-0.19	0.37	4	Haematite
	46.1	-0.02	0.26	5	Magnetite 1
	44.0	0.00	0.66	3	Magnetite 2
	39.4	-0.26	0.37	4	Goethite
	-	2.73	1.09	17	Fe(II) Ol M2
	-	2.19	1.03	24	Fe(II) Cpx M1
	-	1.65	1.00	20	Fe(II) Cpx M2
		0.56	0.46	23	Fe(III)
8 - 10	52.0	-0.19	0.37	4	Haematite
	47.4	-0.02	0.26	5	Magnetite 1
	46.6	0.00	0.66	6	Magnetite 2
	39.2	-0.26	0.37	2	Goethite
	-	2.68	1.10	18	Fe(II) Ol M2
	-	2.03	1.06	27	Fe(II) Cpx M1
	-	1.44	1.00	15	Fe(II) Cpx M2
		0.84	0.39	23	Fe(III)
10 - 12	50.0	-0.19	0.37	4	Haematite
	47.0	-0.02	0.26	5	Magnetite 1
	45.6	0.00	0.66	6	Magnetite 2
	39.	-0.26	0.37	2	Goethite
	-	2.76	1.07	19	Fe(II) Ol M2
	-	2.05	1.02	30	Fe(II) Cpx M1
	-	1.38	1.00	13	Fe(II) Cpx M2
		0.41	0.46	21	Fe(III)
12 - 14	51.7	-0.19	0.37	3	Haematite
	47.8	-0.02	0.26	4	Magnetite 1
	46.8	0.00	0.66	2	Magnetite 2
	39.3	-0.26	0.37	5	Goethite
	-	2.74	1.09	18	Fe(II) Ol M2
	-	2.10	1.03	28	Fe(II) Cpx M1
	-	1.57	0.95	17	Fe(II) Cpx M2
		0.51	0.54	23	Fe(III)
14-15	51.4	-0.19	0.37	5	Haematite
	48.2	-0.02	0.26	3	Magnetite 1
	46.2	0.00	0.66	4	Magnetite 2
	36.9	-0.26	0.37	5	Goethite
	-	2.71	1.11	16	Fe(II) Ol M2
	-	2.05	1.08	26	Fe(II) Cpx M1
	-	1.43	1.03	15	Fe(II) Cpx M2
		0.88	0.38	26	Fe(III)

[a] The isomer shift (IS) quoted relative to Fe metal.

[b] Ol = olivine; Cpx = augitic clinopyroxene

Table 2C. Mössbauer parameters at 293 K for terrestrial layers

Layer (cm)	B (Tesla)	QS (mms^{-1})	IS[a] (mms^{-1})	A (%)	Site[b]
0 - 5	50.5	-0.19	0.37	6	Haematite
	47.2	-0.02	0.26	5	Magnetite 1
	45.9	0.00	0.66	5	Magnetite 2
	39.1	-0.26	0.37	4	Goethite
	-	2.82	1.14	34	Fe(II) Ol M2
	-	2.07	1.07	17	Fe(II) Cpx M1
	-	1.45	0.96	11	Fe(II) Cpx M2
		0.44	0.69	18	Fe(III)
5-10	51.3	-0.19	0.37	14	Haematite
	48.7	-0.02	0.26	5	Magnetite 1
	43.1	0.00	0.66	5	Magnetite 2
	39.1	-0.26	0.37	3	Goethite
	-	2.80	1.14	18	Fe(II) Ol M2
	-	2.00	1.08	18	Fe(II) Cpx M1
	-	1.30	1.03	10	Fe(II) Cpx M2
		0.83	0.38	27	Fe(III)
10-15	50.9	-0.19	0.37	4	Haematite
	46.9	-0.02	0.26	4	Magnetite 1
	45.6	0.00	0.66	4	Magnetite 2
	37.4	-0.26	0.37	3	Goethite
	-	2.83	1.14	34	Fe(II) Ol M2
	-	2.05	1.05	19	Fe(II) Cpx M1
	-	1.33	0.90	12	Fe(II) Cpx M2
		0.39	0.66	20	Fe(III)

[a] The isomer shift (IS) quoted relative to Fe metal.

[b] Ol = olivine; Cpx = augitic clinopyroxene

were also found in volcanic rocks of Mt. Melbourne Province according to Beccaluva et al., 1991; Armienti et al., 1994 and 1991.

The iron-bearing silicates

The representative Mössbauer spectra at 273, 80 and 4.2 K, displayed in Figures 3 and 4, show that magnetic and paramagnetic resonance is present.

The Mössbauer fit of the paramagnetic resonance was carried out on the basis of the presence of olivine and clinopyroxene, the two iron-bearing silicates detected by XRD in soils. Although two distinct metal sites (M1 and M2) are reported for natural olivines (Bragg et al., 1965) the fit of its spectrum is generally performed by only one doublet (Shinno et al., 1974). Also natural clinopyroxenes present two non-equivalent metal sites, M1 and M2 (Clark et al., 1969). The M1 site contains iron(II), together with other small cations, coordinated to six oxygen atoms in a nearly regular octahedron. The iron(II) in the M1 site gives rise to one doublet with large quadrupole splitting. Analogously the M2 site contains iron(II), together with large cations, coordinated up to eight oxygen atoms. Iron(II) in the site M2 gives rise to another doublet with quadrupole splitting smaller than that of M1. Natural olivines and clinopyroxenes may also contain in their metallic sites, M1 and M2, a variable amount of iron(III) which gives rise to another spectral component poorly split.

A complication can derive when finely divided particles of iron oxides are present. These very small particles are called superparamagnetic since the fluctuations of the electron spin direction may be so fast that the iron-nucleus can no longer follow them and the nucleus therefore senses a net zero magnetic field (Murad, Johnston, 1987). Consequently superparamagnetic iron oxides and structural iron(III) cations cannot be discriminated and only one broad spectral component is detected. As a consequence of the previous considerations, the fit of the paramagnetic subspectra was performed by using four doublets, with linewidths of about 0.3 mms^{-1}: one for olivine, two for clinopyroxene and one for both structural iron(III) and superparamagnetic iron oxide. The resulting Mössbauer parameters are listed in Tables 2A-2C together with the relative iron content for the four sites labelled as Fe(II) Ol M2, Fe(II) Cpx M1, Fe(II) Cpx M2 and Fe(III). These Mössbauer parameters are in agreement with the structural and electronic configurations assumed for the iron sites in olivines and clinopyroxenes. For instance the quadrupole splitting for iron(II) in olivine (ranging from 2.6 to 2.8 mms^{-1})

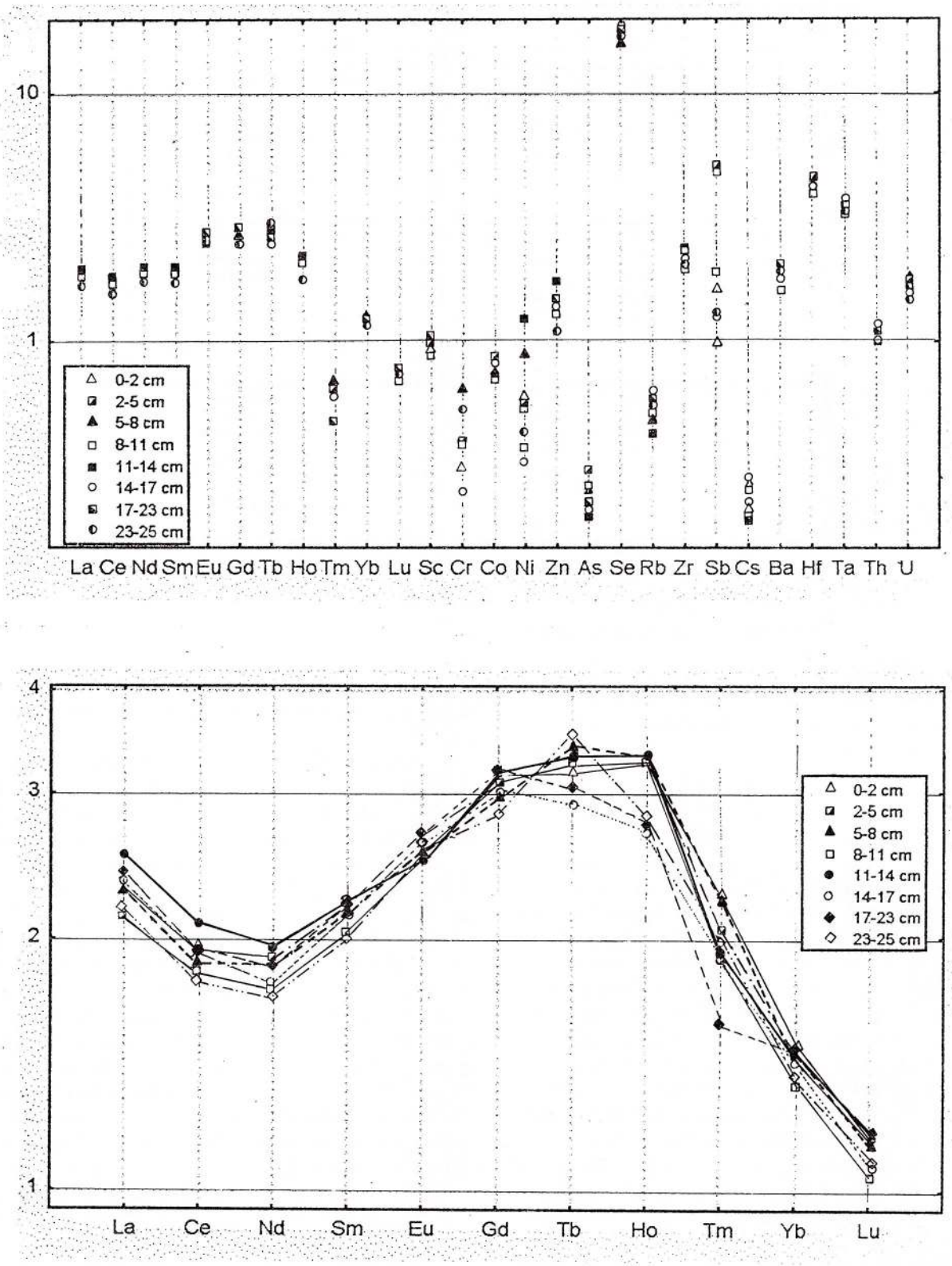

Fig. 1A – Ratio of the elemental content normalised to mean sediments composition following Bowen (top) and REE content normalised to NASC (North American Shale Composition) (bottom) for the marine specimens.

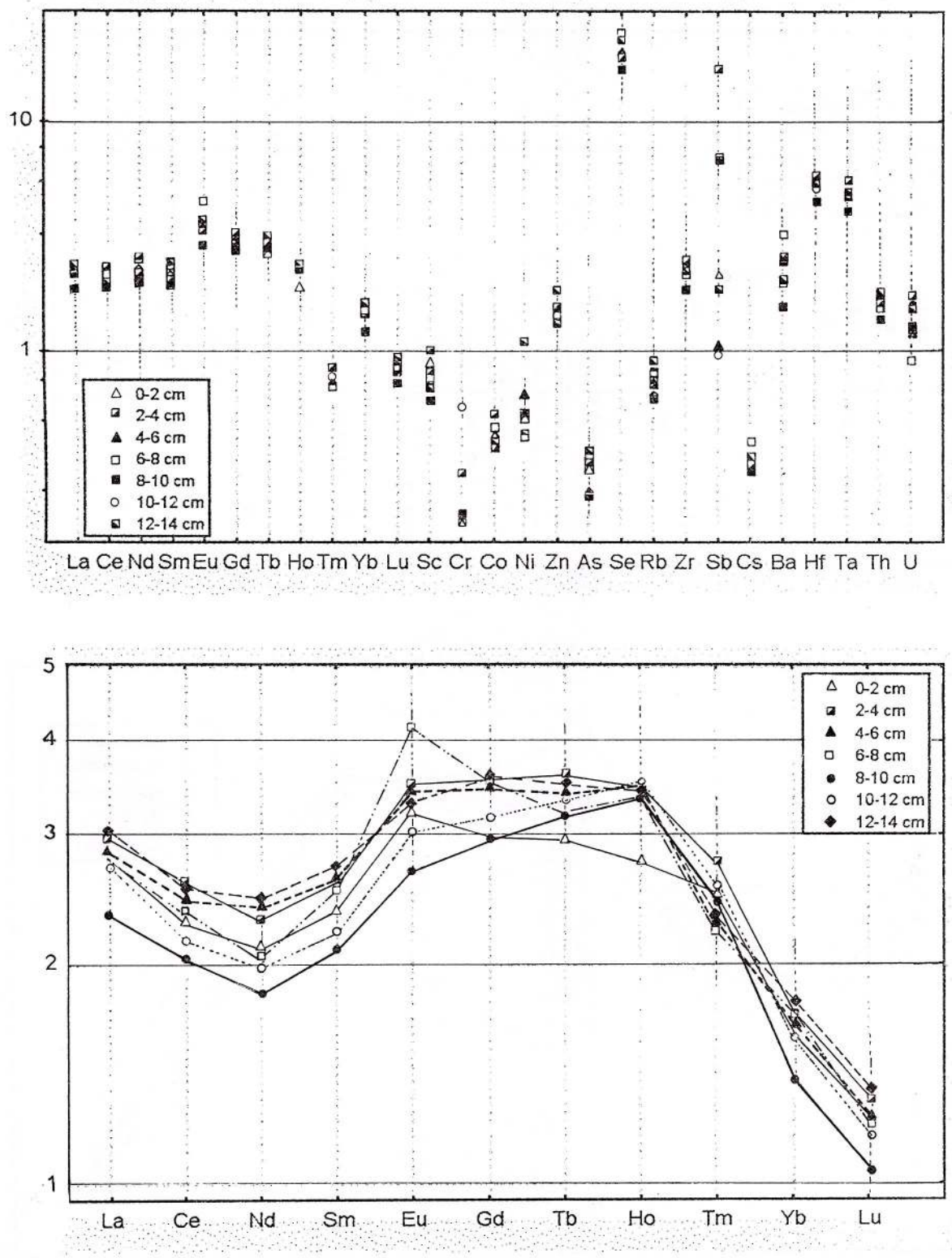

Fig. 1B – Ratio of the elemental content normalised to mean sediments composition following Bowen (top) and REE content normalised to NASC (North American Shale Composition) (bottom) for the lacustrine specimens.

34

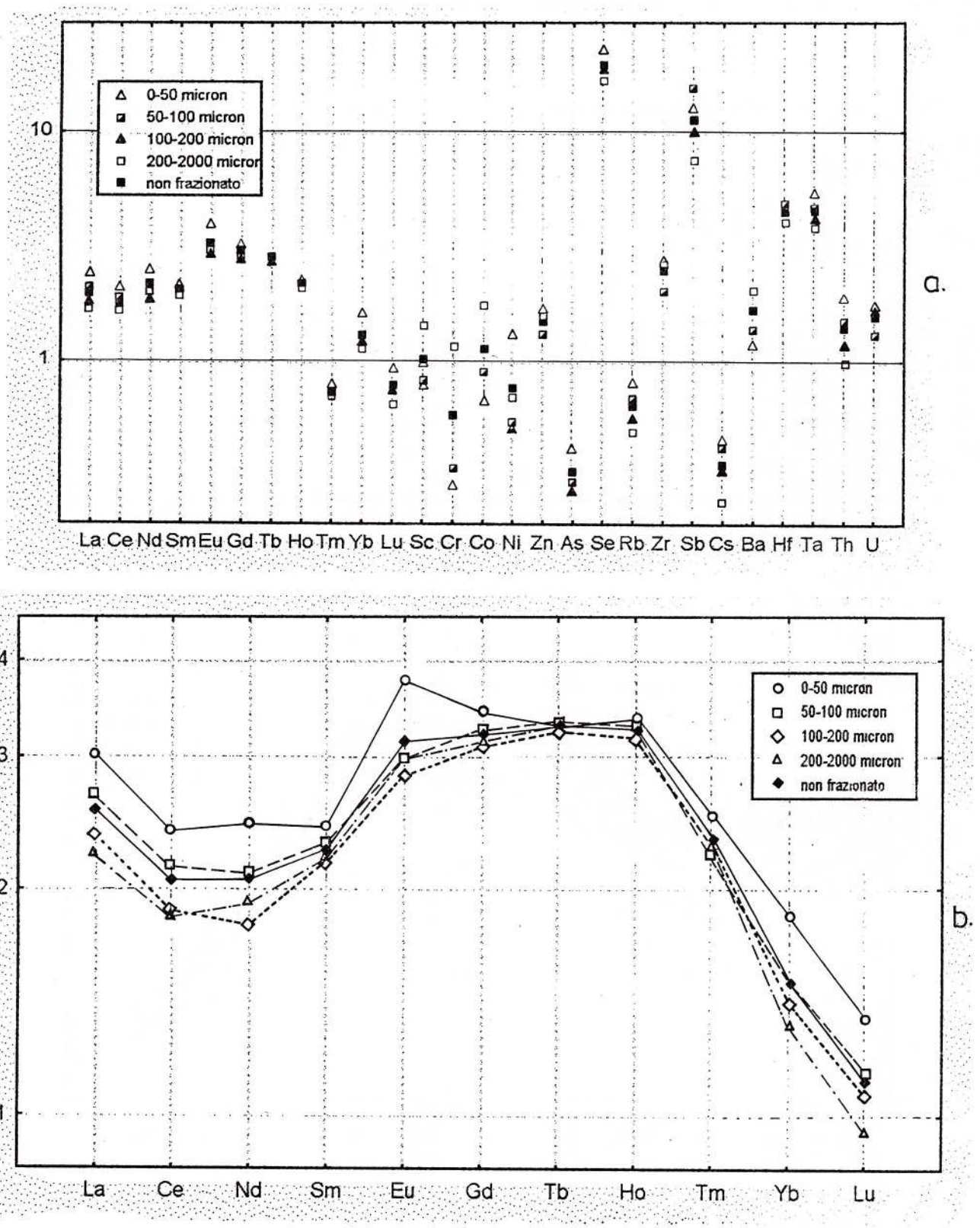

Fig. 1C – Ratio of the elemental content normalised to mean sediments composition following Bowen (top) and REE content normalised to NASC (North American Shale Composition) (bottom) for the terrestrial specimens.

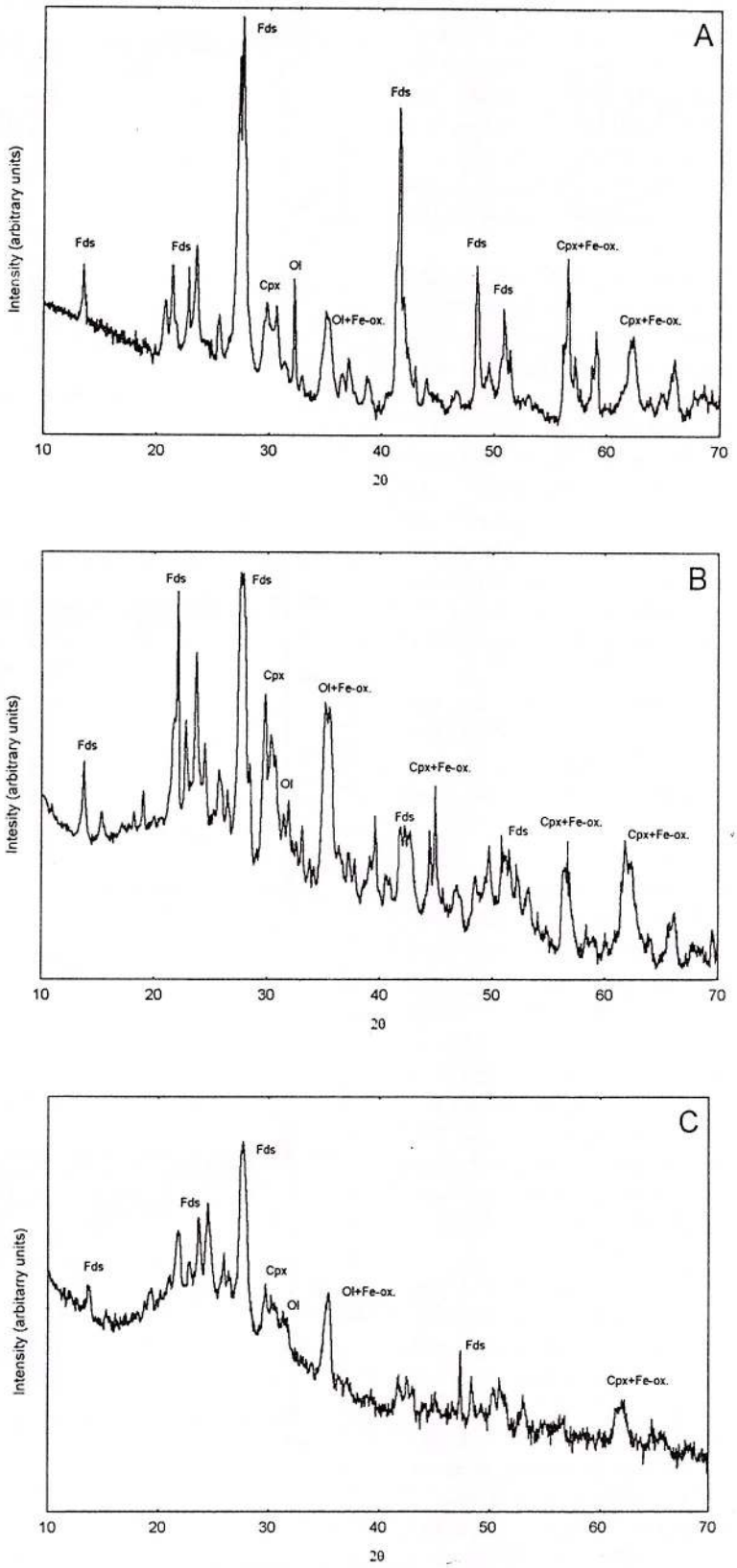

Fig. 2 – X-ray diffraction patterns for: A) the layer 0–2 cm of the marine soil; B) the layer 0–5 cm of the terrestrial soil; C) the layer 0–2 cm of the lacustrine soil. (Fds: alkali feldspar; Cpx: augitic clinopyroxene; Ol: olivine; Fe-ox:iron-oxides).

points to an enough regular site whereas its isomer shift (about 1.1 mms^{-1}) is consistent with its octahedral coordination. The same considerations can be done for the quadrupole splitting of the sites M1/M2 of clinopyroxenes, about 2.1/1.6 mms^{-1}. The isomer shift for the sites M1/M2 in marine, lacustrine, and terrestrial samples is less positive for the M2 site indicating probably that the coordination number of the site M2 is less than eight.

The broad spectral component attributed in Tables 2A-2C to iron(III) is assigned both to structural iron(III) cations in silicates and to superparamagnetic iron oxides. The presence of two spectral contributions can be inferred from the variability of the Mössbauer parameters of the doublet reported in Tables 2A-2C. The two spectral contributions cannot be separated even at the liquid helium temperature. As shown for the representative spectrum of Figure 3, all the Mössbauer spectra collected at 4.2 K exhibit the superparamagnetic relaxations for the iron(II) sites of olivine and pyroxene in addition to the magnetic ordering of the particles of iron oxides (Coey, 1975, 1980).

In conclusion the Mössbauer parameters for the iron sites remain substantially the same along the soil cores, even if olivines and clinopyroxenes contain iron and other metallic cations in their metallic sites (Coey, 1984).

The iron oxides

The possible presence of various iron oxides was taken into account in the fits of the Mössbauer spectra. The best fit required four sextets was attributed to haematite, magnetite, and goethite mainly because of the values of their magnetic fields (Murad, Johnston, 1987).

The larger six-lines subspectrum (the first reported in Tables 2A-2C) is assigned to bulk haematite i.e. with average particle-size larger than 100 = C5. In fact the Mössbauer parameters of this subspectrum agree with those reported for pure and bulk haematite: B = 51.7 T, QS = -0.19 mms^{-1}, IS = 0.37mms^{-1} (Murad, Johnston, 1987).

Two magnetic subspectra (the second and the third in Table 2A-2C) were assigned to bulk magnetite. Their Mössbauer parameters are consistent with those reported for bulk and pure magnetite: B 49 and 46 T, QS = -0.02 and 0.00 mms^{-1}, IS = 0.26 and 0.66 mms^{-1} (Murad, Johnston, 1987). Magnetite is a primary oxide in soils being already present in the parent rocks of the Mt. Melbourne volcano.

The narrow six-line subspectrum (the fourth in Tables 2A-2C) is related to goethite. Its Mössbauer parameters are in fact not far from those reported for bulk and pure goethite: B= 38.0 T, QS = -0.26 mms^{-1}, IS = 0.37 mms^{-1} (Murad, Johnston, 1987).

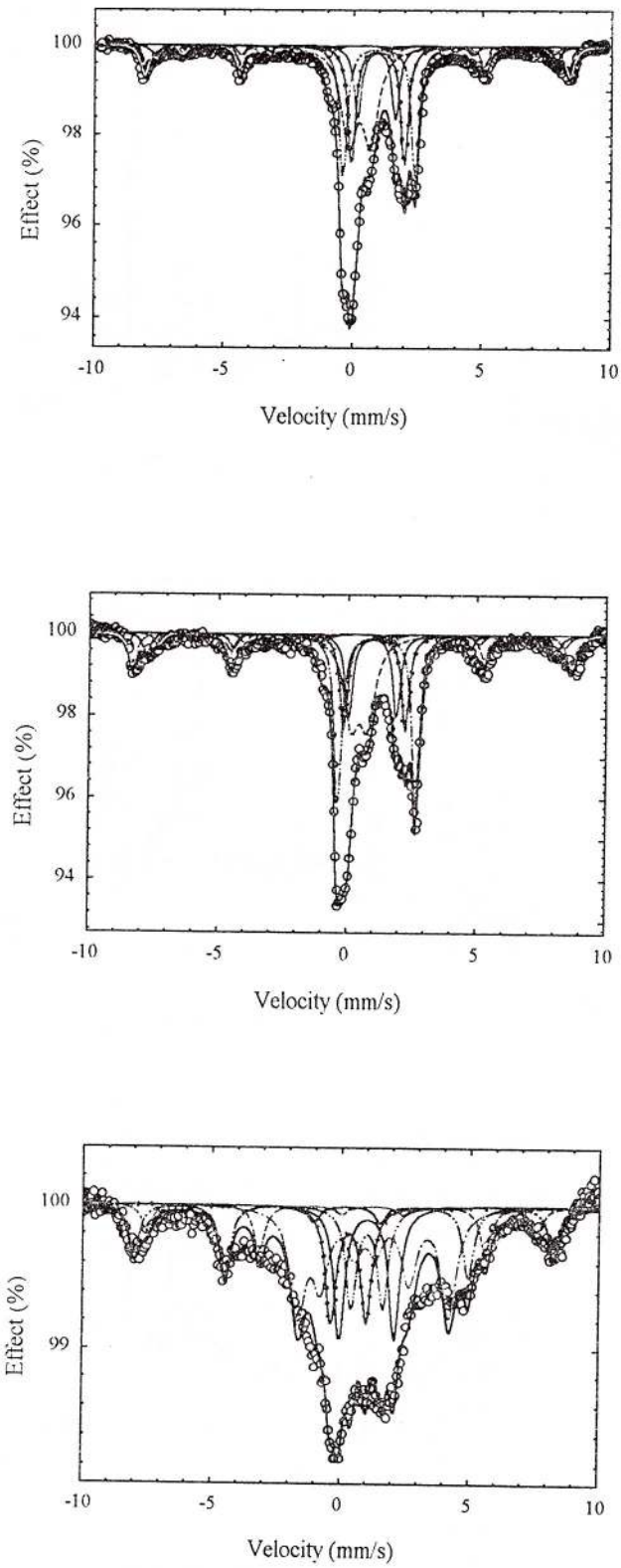

Fig. 3 – Mössbauer spectra at 293 K (top), 80 K and 4.2 K (bottom) for the layer 4–6 cm of the lacustrine soil.

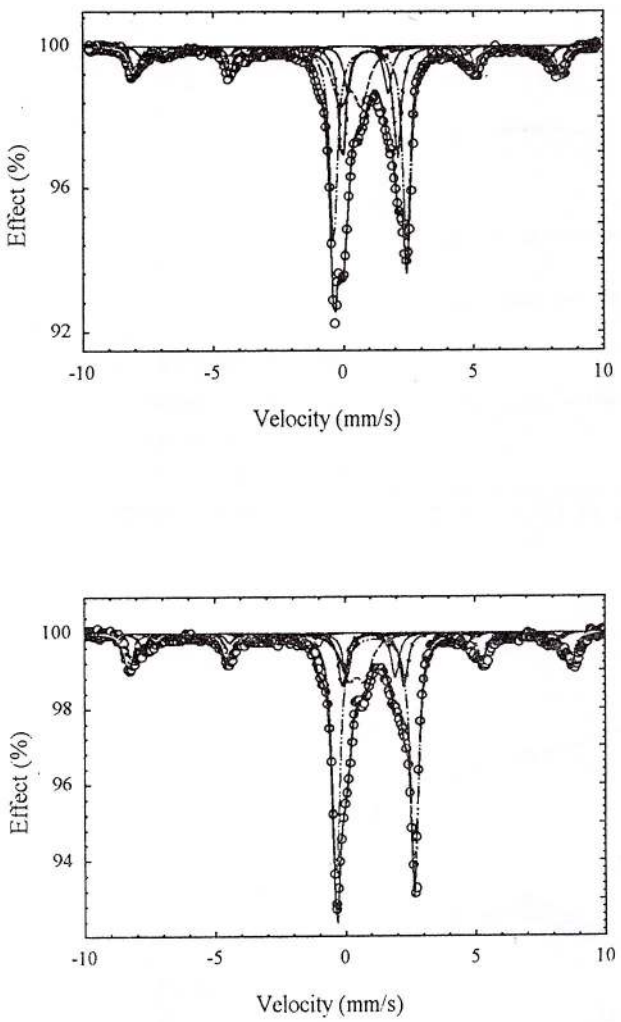

Fig. 4 – Mössbauer spectra at 293 K (top) and 80 K (bottom) for the layer 15–18 of the sea soil.

Moreover, the spectral assignment for haematite and goethite is consistent with the statement that they are thermodynamically the most stable neoformed oxides in aerobic conditions and in presence of liquid solutions (Schwertmann, Cornell, 1991; Cornell, Schwertmann, 1996). Additional evidence for the presence of goethite derives by comparing Mössbauer spectra collected at room and liquid helium temperature. The representative spectrum at the helium temperature of Figure 4 shows the expected increase in splitting, for its magnetic sextet, from the room temperature value of about 38 (Fig. 2) up to 50 T (Murad, Johnston, 1987). The spectrum of Figure 4 concerns the terrestrial layer at a depth of 0–5 cm. This spectrum is representative of a general behaviour: the presence of superparamagnetic relaxations for the iron(II) sites of olivine and pyroxene at the liquid helium temperature (Coey, 1975, 1980).

Distribution of the iron among the various sites

As shown in Figure 5, the iron content present in the various sites changes remarkably from marine to the lacustrine core. The most striking feature is the iron(II) content in olivines and clinopyroxenes. In fact in marine soils the iron(II) content is larger in olivines than in clino-pyroxenes, whereas in lacustrine soils the iron(II) content is larger in clinopyroxenes than in olivines. Since olivines are less stable than pyroxenes, the large presence of olivine in marine soils cannot be attributed to weathering but to their genesis from primary rocks. The soils retain amounts of olivines and clinopyroxenes probably comparable to that found in rocks confirming the close connection between soils of Wood Bay and rocks of Mt. Melbourne volcano: the rocks richer in olivine have been considered formed at lower pressure, contrary to those richer in clinopyroxenes formed at higher pressure (Armienti et al., 1991).

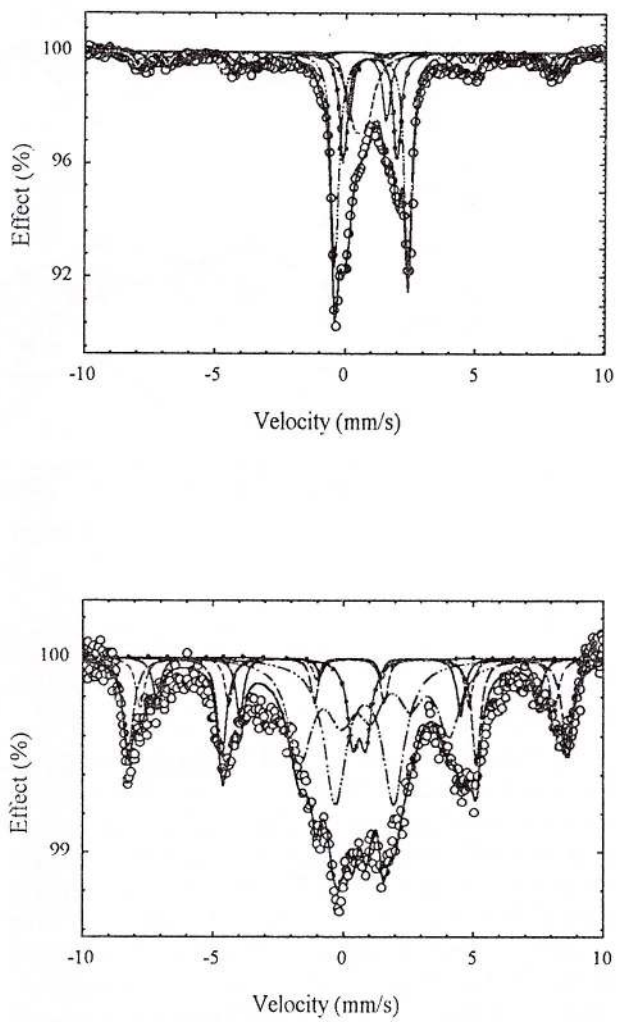

Fig. 5 – Mössbauer spectra at 293 K (top) and 4.2 K (bottom) for the layer 0–5 cm of the terrestrial soil.

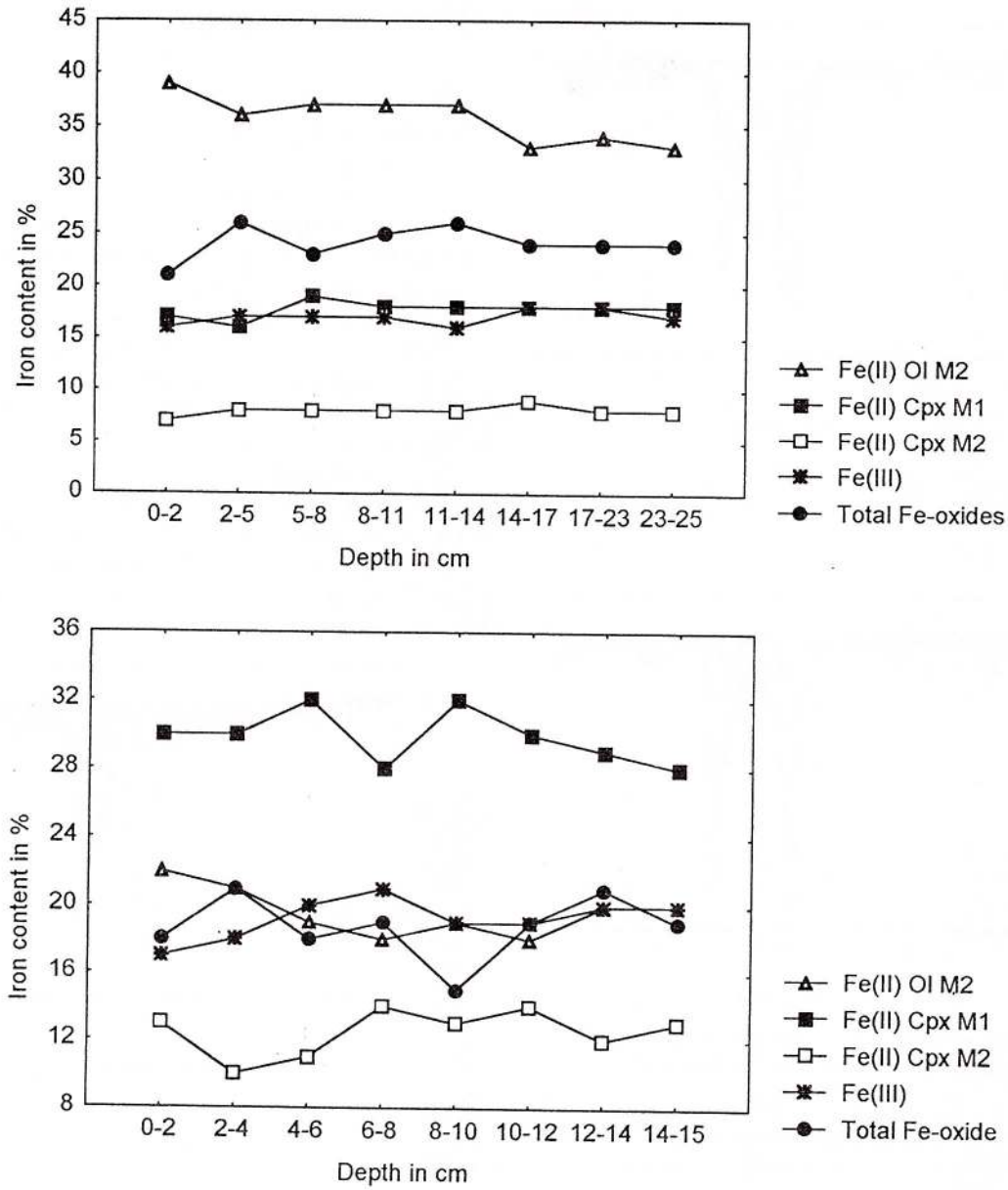

Fig. 6 - Percentage content of the iron in the various sites along the depth profile, in cm, for the marine core (top) and lacustrine core (bottom). △ = Fe(II) Ol M2; = Fe(II) Cpx M1; = Fe(II) Cpx M2; * = Fe(III); • = Total Fe-oxides

All the soils contain iron(III)-bearing species due to structural iron(III) cations in silicates and to superparamagnetic iron oxides. The content of the structural iron(III) might be due to weathering in fact, because of the prevalent reducing conditions existing during the formation of primary volcanic rocks their iron(III) content is negligible or very low (Beccaluva et al., 1991). On the contrary in soils, atmospheric oxygen determines a partial oxidation of the iron(II) content in olivines and clinopyroxenes.

A key factor for weathering

The relative percentage content of the iron in the various sites along the depth profile, displayed in Figure 6, shows that there are not large variations within the marine or lacustrine core. Taking into account the difficulty of the sampling and of the Mössbauer fitting procedure, the deviations in the amount of the various iron sites along the depth profiles shown in Figure 6 are not significant. Analogously the variations in the amount of magnetite, haematite, and

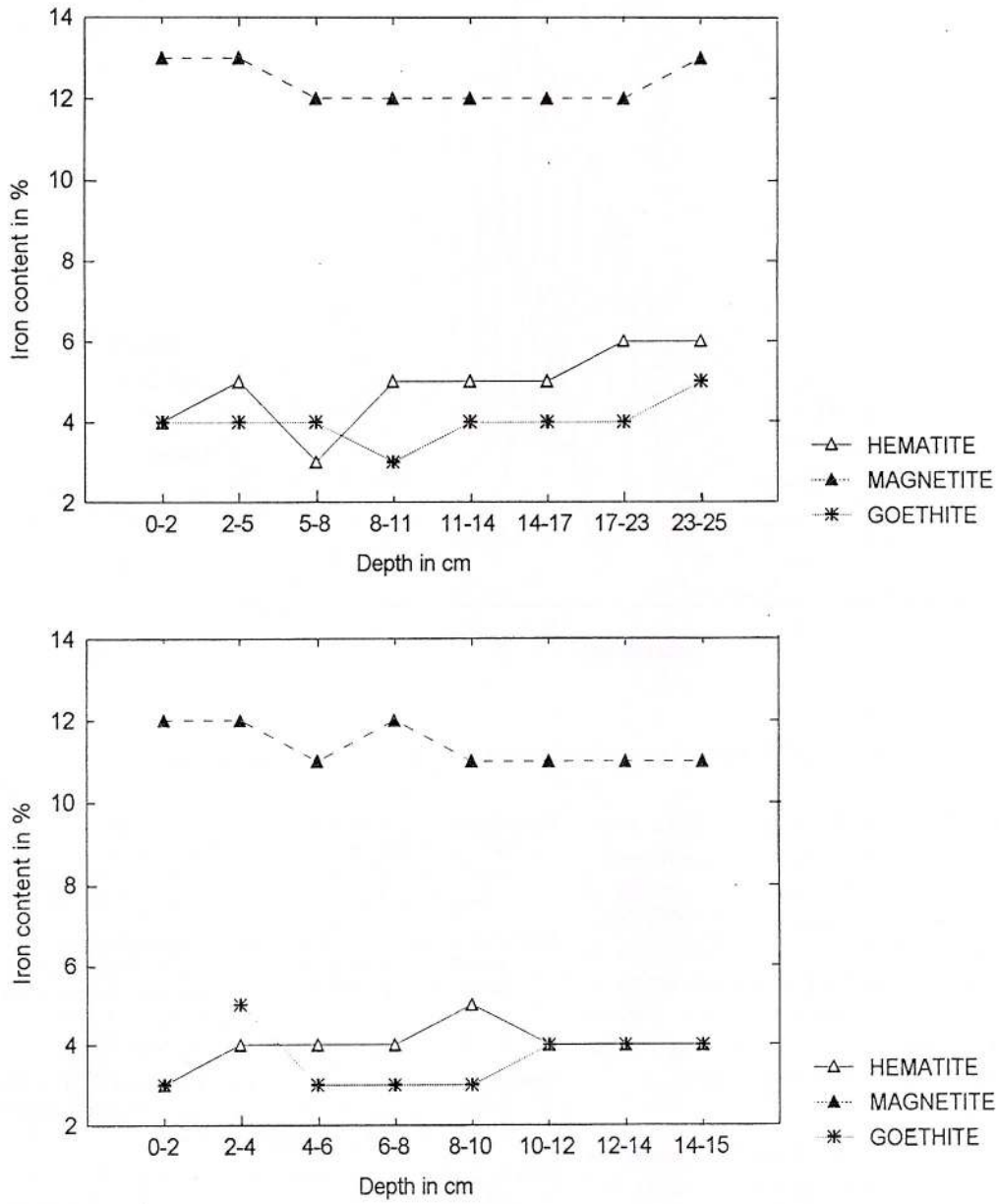

Fig. 7 – Percentage content of the iron oxides along the depth profile, in cm, for the marine core (top) and lacustrine core (bottom). △ = hematite; △ = magnetite; ∗ = goethite.

goethite within the marine or lacustrine core shown in Figure 7 are relatively small. The absence of large variations can visually be observed in Figure 8 where the envelopes obtained in the fit of the Mssbauer spectra for marine layers are reported.

The scarce variation in the content of the various iron sites along the depth profiles indicates that the same chemical processes are operative on the surface layer of the soils in Austral summer. This chemical weathering can take place only if a liquid solution is present and, since the values of pH and Eh are favourable, iron(II)-bearing materials can be oxidised. As a consequence 1) the neo- formed iron(III) is retained in the original silicates, 2) the oxidation of the iron(II) in magnetite determines the formation of bulk haematite and goethite evidenced in Mössbauer spectra (Johnston, Lewis, 1987; Schwertmann, Cornell, 1991; Murad, Schwertmann, 1980).

In conclusion the presence of different iron oxides together with the iron population in silicate sites, de-

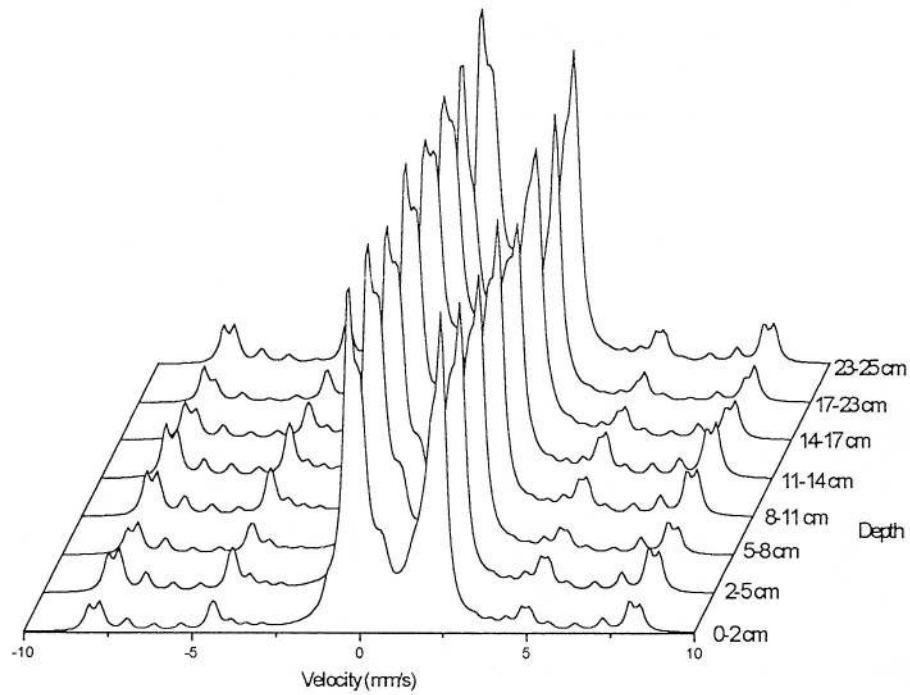

Fig. 8 - Envelops obtained by the fitted Mössbauer spectra for the marine layers

pend not only on pH and Eh but also on the temperature, a key factor for the presence of liquid solutions. Since water is generally frozen, the process of formation of the soils is at the initial stage of weathering. The silicates are in fact not altered. This is shown from the marine soils that retain a content in olivine larger than in clinopyroxenes even if olivines are less stable than pyroxenes. In addition iron is immobilised in silicate sites or in iron oxides.

Acknowledgements

Financial support from E.N.E.A in the framework of the Italian National Programme for Antarctic Researches, PNRA (Environmental Impact-Chemical Methodologies) is gratefully acknowledged.

References

Armienti, P., Civetta, L., Innocenti, F., Manetti, P., Tripodo, A., Villari, L., Vita, G. (1991) New petrological and geochemical data on Mt. Melbourne volcanic field, northern Victoria Land, Antarctica. (II Italian Antarctic expedition). *Mem. Soc. Geol. It.*, 46, p. 397-424.

— , **Francalanci, L., Salvioli, E. (1994)** Petrogenesis of the McMurdo Volcanic Group and its bearing on the recent evolution of the Crust-Mantle system in Northern Victoria Land. *Terra Antartica*, 1(3), p. 533–535.

Bancroft, G. M., Maddock, A. G., Burns, R. G. (1967) Applications of the Mössbauer effect to silicate mineralogy. I. Silicates of known crystal structure. *Geochim. Cosmochim. Acta*, 31, p. 2219–2246.

Beccaluva, L., Civetta, L., Coltorti, M., Orsi, G., Saccani, E., Siena, F. (1991) Basanite to tephrite lavas from Melbourne volcanic province, Victoria Land, Antarctica. *Mem. Soc. Geol. It.*, 46, p. 383–395.

Bowen, L. H., De Grave, E., Vandenberghe, R. E. (1993) Mössbauer effect studies of magnetic soils and sediments. In: Mössbauer Spectroscopy Applied to Magnetism and Material Science, (Long G. J. & Grandjean F. Ed., Plenum Press, N. Y.) Vol. 1, p. 115–159.

Bragg, L., Claringbull, C. F., Taylor, W. H. (1965) In: Crystal Structure of Minerals, (Cornell University Press, Ithaca, N.Y.), Vol. IV, 173.

Clark, J. R., Appleman, D. E., Papike, J. J. (1969) Crystal-chemical characterization of clinopyroxenes based on eight new structure refinements. *Mineral. Soc. Amer.*, Spec. Pap., 2, p. 31–50.

Coey, J. M. D. (1975) Iron in post-glacial lake sediment core; A Mössbauer effect study. *Geochim. Cosmochim. Acta*, 39, p. 401–415.

— **(1980)** Clay minerals and their transformations studied with nuclear techniques: The contribution of Mössbauer spectroscopy. *At. Energy Rev.*, 18, p. 73–124.

— **(1984)** Mössbauer spectroscopy of silicate minerals. In: Mössbauer Spectroscopy Applied to Inorganic Chemistry, (Long G. J. Ed., Plenum Press, N. Y.) Vol. 1, p. 443–509.

Glasby, G. P., Barrett, P. J., McDougall, J. C., McKnight, D. G. (1975) Localised variations in sedimentation characteristics in the Ross Sea and McMurdo South regions. Antarctica. *N. Z. J. Geol. Geophys.*, 18, 4, p. 605–621.

Glasby, G. P., Hunt, J. L., Renner, R. M. (1985) Trace element analyses of marine sediments from the South West Pacific. *N. Z. Soil Bur. Sci. Rep.*, 53, 62.

Grosse, G. (1992) MOS-90, Version 2.2, Technical University of Munich

Hilton, J., Long, G. J., Chapman, J. S., Lishman, J. P. (1986) Iron mineralogy in sediments. A Mössbauer study. *Geochim. Cosmochim. Acta*, 50, p. 2147–2151.

Hörnig, I. , Wörner, G., Zipfel, J. (1991) Lower crustal and mantle xenoliths from the Mt. Melbourne volcanic field, Northern Victoria Land, Antarctica. *Mem. Soc. Geol. It.*, 46, p. 337–352.

Jaffrezic, H. (1976) L'estimation de l'erreur, introduite dans le dosage des elements a l'etat de traces dans les roches liées aux caracteristiques de leur repartition. *Talanta*, 23, p. 497–501.

Johnston, J. H., Lewis, D. G. (1987) In: Industrial Applications of the Mössbauer Effect, (Long G. J. & Stevens J. G. Ed., Plenum Press, N. Y.), p. 565–583.

Murad, E., Johnston, J. H. (1987) Iron oxides and oxyhydroxides. In: Mössbauer Spectroscopy Applied to Inorganic Chemistry, (Long G. J., Ed., Plenum Press, N. Y.) Vol. 2, p. 507–582.

— , Schwertmann, U. (1980) The Mössbauer spectrum of ferrihydrite and its relations to those of other iron oxides. *Amer. Mineralogist*, 65, p. 1044–1049.

Schwertmann, U., Cornell, R. M. (1991) In: Iron Oxides in the Laboratory, (VCH Ed., Weinheim, Germany), p. 14–18.

Cornell, R. M., Schwertmann, U. (1996) In: The Iron Oxides, (VCH, Weinheim, Germany).

Shinno, I., Hayashi, M., Kuroda, Y. (1974) Mössbauer studies of natural olivines. *Mineral. J.*, 7, p. 344–358.

Vandenberghe, R. E., De Grave, E., Landuydt, C., Bowen, L. H. (1990) Some aspects concerning the characterization of iron oxides and hydroxides in soils and clays. *Hyp. Inter.*, 53, p. 175–196.

Wörner, G., Viereck, L., Hertogen, J., Niephaus, H. (1989) The Mt. Melbourne volcanic field (Victoria Land, Antarctica). II. Geochemistry and magma genesis. *Geol. Jb.*, E38, p. 395–433.

— , Viereck, L., Hertogen, J., Niephaus, H. (1989) The Mt. Melbourne volcanic field (Victoria Land, Antarctica). I. Field observations. *Geol. Jb.*, E38, p. 395–433.

Organized by the

- International Council for Applied Mineralogy (ICAM)
  President: Andrzej Szymanski (Warsaw, Poland)
  Vice-President: Robert B. Heimann (Freiberg, Germany)
  Past President: Jim Graham (Nedlands, Australia)
- German Mineralogical Society (DMG) and its Commission for Applied Mineralogy (KTM)
- Federal Institute for Geosciences and Natural Resources (BGR, Hannover)
- Geological Survey of Lower Saxony (NLfB)

Organizing Committee

General Chairman: Robert B.Heimann (Freiberg)

Scientific Program

Chairman: Horst Pentinghaus (Karlsruhe)

Correspondence

Mail: ICAM 2000 Office
BGR/NLfB
P.O.Box 510153
D-30631 Hannover
Germany

Phone: +49-511-643-2298
Fax: +49-511-643-3685
E-mail ICAM2000@bgr.de
Internet http://www.bgr.de/ICAM2000

Preliminary Deadlines

Submission of **further topics**	May	1998
Distribution of **Second Circular**	January	1999
Accommodations at reduced rates	March	1999
Submission of **abstracts**	September	1999
Notification of acceptance of paper	December	1999
Submission of **extended abstracts**	February	2000
Registration and **payment**	April	2000

General information

The "International Council for Applied Mineralogy" (ICAM) was founded in Johannesburg, S. Africa in 1981 by scientists from Australia, Canada, Germany, Poland, South Africa and the USA to provide an interdisciplinary forum for specialists in the fields of mineralogy, chemistry, mineral exploration, engineering, environment, ceramics, metallurgy, archeometry and medicine.

A further objective of ICAM is to recruit industrial participation, to highlight their current research needs, and to promote contacts to specialists in all aspects of applied mineralogy.

The previous five ICAM congresses were held in Johannesburg, S.A. (1981), Los Angeles, USA (1984), Pretoria, S.A. (1991), Perth, Australia (1993), and Warsaw, Poland (1996).

ICAM 2000 will take place in the old university town of Göttingen.

From Göttingen, it will take only 30 minutes by high speed train to the World Fair EXPO 2000 in Hannover. The EXPO 2000 has the motto

"humankind – nature – technology"

Congress Schedule

16 – 17July 2000	Workshops, excursions
18 – 20 July 2000	Conference meetings
21 – 22 July 2000	Excursions, EXPO 2000

Language

The official language of the congress will be English. No translation facilities will be provided.

Publications

A volume of all extended abstracts will be provided to the participants at ICAM 2000.

Accommodation

Due to EXPO 2000, there will be a high demand for accommodations. Therefore, early registration is recommended. About 400 rooms will be set aside until the registration deadline.

Notes

Registration fees, workshops, field trips, and scientific and commercial exhibitions will be announced in the Second Circular.

ICAM 2000

6th International Congress on Applied Mineralogy

Göttingen & Hannover, Germany

16 – 22 July 2000

First Circular, January 1998

Preliminary Topics of ICAM 2000

1 Materials
- Advanced materials
  - Biomaterials
  - Semiconductors, superconductors
  - Smart materials, sensors
  - Composites
- Glasses, glass ceramics,
- Ceramics, chemically bonded ceramics
- Building materials, cement
- Single crystal growth

2 Surfaces
- Surface and structure
- Interfaces
- Catalysts
- Coatings, thin films
- Corrosion, protective coatings
- Nanoparticles

3 Mining
- Ore deposits
- Exploration
- Mineral processing, leaching
- Beneficiation
- Tailings
- Acid rock drainage
- Industrial minerals

4 Environment
- Residues (slag, fly ash, aerosols)
- Long-term behavior, kinetics
- Landfills, repositories for hazardous waste
- Recycling
- Waste treatment
- Modeling and simulation
- Remediation, immobilization

5 Precious stones, rare minerals
- Gems
- Precious metals
- Rare earth elements

6 Cultural heritage
- Archeometry
- Weathering of artifacts
- Geochemical fingerprints
- Conservation issues
- Surface treatment

Contributions on advancements in experimental techniques in all six topics are welcome. Further suggestions are invited.

Rom. J. Mineralogy, 79, p. 189-207, Bucureşti, 1999

NEW MINERALS RECENTLY APPROVED BY THE COMMISSION ON NEW MINERALS AND MINERAL NAMES INTERNATIONAL MINERALOGICAL ASSOCIATION

The information given here is provided by the Commission on New Minerals and Mineral Names, I. M. A. for comparative purposes and as a service to mineralogists working on new species.

Each mineral is described in the following format:
IMA No. (any relationship to other minerals)
Chemical Formula
Crystal system, space group
unit cell parameters
Colour; lustre; diaphaneity.
Optical properties.
Strongest lines in the X-ray powder diffraction pattern.

The names of these approved species are considered confidential information until the authors have published their descriptions or released information themselves.

NO OTHER INFORMATION WILL BE RELEASED BY THE COMMISSION.

J. A. Mandarino, Chairman Emeritus and J. D. Grice, Chairman
Commission on New Minerals and Mineral Names
International Mineralogical Association

1994 PROPOSALS

IMA No. 94-001 The Fe^{3+}-dominant analogue of warwickite
$Mg(Fe^{3+},Fe^{2+},Al,Ti,Mg)(BO_3)O$
Orthorhombic: Pnam
a 9.258(6) b 9.351(4) c 3.081(2) Å
Black; adamantine to submetallic; subtranslucent to nearly opaque.
In reflected light: light grey, weak anisotropism, indistinct bireflectance, pleochroic from dark red to dark brown. $R_{max.}$: (9.99 %)470nm, (9.66 %)540nm, (9.29 %)589nm, (8.79 %)650nm.
6.563 (23), 4.176 (38), 2.957 (30), 2.570 (100), 2.088 (20), 1.591 (18), 1.550 (19).

IMA No. 94-002
$Mn_2SiO_3(OH)_2 \cdot H_2O$
Orthorhombic: $Pca2_1$
a 12.682(4) b 7.214(2) c 5.337(1) Å
Brown-yellowish; vitreous; transparent.
Biaxial (-), α 1.681, β 1.688, γ 1.690, 2V(meas.) 54.4°, 2V(calc.) 56.1°.
7.220 (60), 4.083 (60), 3.011 (100), 2.547 (80), 2.456 (80), 2.440 (80), 1.552 (60).

IMA No. 94-004 A member of the amphibole group.
$NaNa_2Mn^{2+}_2Mn^{3+}_3Si_8O_{24}$
Monoclinic: C2/m
a 9.89(2) b 18.04(3) c 5.29(1) Å β 104.6(1)°
Cherry red to very dark red; adamantine; transparent.
Biaxial (-), α 1.717, β 1.780, γ 1.800, 2V(meas.) 51°, 2V(calc.) 57°.
3.400 (8), 3.146 (9), 2.544 (9), 2.176 (10), 1.656 (8), 1.447 (9).

IMA No. 94-005
$(Zn,Cu)_6Zn_2(OH)_{13}[(Si,S)(O,OH)_4]_2$
Hexagonal (trigonal): $P\bar{3}$
a 8.322(1) c 7.376(1) Å
Light green; vitreous; transparent.
Uniaxial (-), ω 1.705, ϵ 1.611.
7.37 (100), 3.623 (25), 3.282 (30), 2.724 (30), 2.556 (50), 2.191 (15), 1.572 (20).

IMA No. 94-006
$(Mg_{1-x}\square_x)_2Mg_{12}(PO_4)_6(PO_3OH)_2O_6H_{6+4x}$ x = 0 to 0.3
Hexagonal: $P6_3mc$
a 12.47(1) c 5.036(6) Å
Azure blue; vitreous; transparent.
Uniaxial (-), $\bar{n} \sim 1.61$, $\Delta \sim 0.01$.
3.66 (65), 3.15 (100), 3.109 (100), 2.692 (95), 2.213 (70), 1.803 (50), 1.552 (50).

IMA No. 94-007
$Na_3(Fe^{2+},Fe^{3+})_6[Ti_2Si_{12}O_{30}(O,OH)_4](OH,O)_7 \cdot 2H_2O$
Monoclinic: P2/c
a 5.353(4) b 16.18(1) c 21.95(2) Å β 94.6(2)°
Dark brown-green; vitreous to silky; translucent.
Biaxial (-), α 1.627, β 1.667, γ 1.693, 2V(meas.) 75°, 2V(calc.) 76°.
13.00 (30), 10.94 (100), 4.44 (30), 2.728 (50), 2.641 (40), 2.547 (30), 2.480 (30).

IMA No. 94-008
$AgFeS_2$
Tetragonal: $P4_2mc$
a 5.64(1) c 10.34(3) Å
Megascopic colour not observed; metallic; opaque.
In reflected light: cream with a greyish tint, moderate anisotropism, no bireflectance, nonpleochroic. $R_{min.}$ & $R_{max.}$: (27.2, 30.1 %)470nm, (32.3, 36.4 %)546nm, (33.0, 37.1 %)589nm, (31.2, 35.3 %)650nm.
3.15 (10), 2.445 (2), 2.340 ($\leq$2), 1.910 (4), 1.692 (2).

IMA No. 94-010 A member of the milarite group.
$K(K,Na,\square)(Mn,Zr,Y)_2(Zn,Li)_3Si_{12}O_{30}$
Hexagonal: P6/mcc
a 10.196(5) c 14.284(8) Å
Dark blue, violet blue, greyish brown-blue; vitreous; transparent.
Uniaxial (-), ω 1.590, ϵ 1.586.
7.13 (30), 4.15 (45), 3.75 (50), 3.25 (100), 2.924 (39), 2.777 (32), 2.548 (520).

IMA No. 94-011
$(NH_4,K)NO_3$
Orthorhombic: Pbnm
a 7.075(5) b 7.647(5) c 5.779(5) Å
White; vitreous; transparent.
Biaxial (-), α 1.458, β 1.527, γ 1.599, 2V(meas.) ~ 90°, 2V(calc.) 87°.
3.863 (75), 3.364 (85), 3.212 (95), 3.194 (100), 2.805 (35), 2.595 (90), 2.400 (50).

IMA No. 94-012
$(Na,Mn,Fe,Al,REE)_{15}(Y,REE,Ca,Na)_2(CO_3)_9(SO_3F)Cl$
Hexagonal: P3
a 8.773(1) c 10.746(2) Å
Yellow to orange-brown; vitreous; transparent.
Uniaxial (-), ω 1.548, ϵ 1.537.
6.20 (40), 4.39 (80), 2.774 (80), 2.532 (100), 2.240 (80), 2.067 (30), 1.657 (40).

IMA No. 94-013
$Cu_2Zn[(As,Sb)O_4](OH)_3$
Hexagonal (trigonal): $P\bar{3}$
a 8.201 (1) c 7.315 (1) Å
Emerald green; adamantine; transparent.
Uniaxial (-), ω 1.801, ϵ 1.796.
2.522 (100), 2.166 (88), 1.805 (92), 1.550 (100), 1.513 (85).

IMA No. 94-014
$CuNiSb_2$
Hexagonal (trigonal): $P\bar{3}m1$
a 4.0489(2) c 5.1358(3) Å
Silver-white; metallic; opaque.
In reflected light: white with yellowish hue, distinct anisotropism, weak bireflectance, nonpleochroic. R_O & R_E: (59.3, 52.4 %)470nm, (63.0, 56.8 %)546nm, (65.5, 60.9 %)589nm, (68.6, 64.9 %)650nm.
2.901 (100), 2.572 (10), 2.074 (65), 2.023 (51), 1.660 (11), 1.284 (10).

IMA No. 94-016 The Zn-dominant analogue of högbomite-*8H*.
$(Zn,Fe^{2+})_{1-2x}Ti_xAl_2O_4$ x ~ 0.12
Hexagonal: most probably $P6_3mc$
a 5.708(4) c 18.31(2) Å
Deep brown to black; adamantine; transparent in thin sections.
Uniaxial (-), ω 1.878, ϵ 1.832.
2.85 (50), 2.60 (80), 2.42 (100), 1.592 (60), 1.550 (50), 1.470 (70), 1.425 (80).

IMA No. 94-017
$Na_8(Mn,Fe^{3+},Ti)_2Si_{10}O_{25}(OH,Cl)_4 \cdot 10H_2O$
Orthorhombic: $C222_1$
a 13.46(2) b 14.98(1) c 17.51(2) Å
Yellow to orange; vitreous; transparent.
Biaxial (+), α 1.532, β 1.540, γ 1.550, 2V(meas.) 89°, 2V(calc.) 84°.
10.049 (100), 8.823 (50), 5.025 (20), 3.806 (20), 2.718 (50).

IMA No. 94-018
$PbCa_2Al(F,OH)_9$
Monoclinic: A2, A2/m or Am
a 23.905(5) b 7.516(2) c 7.699(2) Å β 92.25(2)°
White to colourless; vitreous; transparent.
Biaxial (-), α 1.510, β 1.528, γ 1.531, 2V(meas.) 36°, 2V(calc.) 44°.
11.9 (100), 3.71 (70), 3.51 (85), 2.98 (60), 2.94 (60), 2.027 (60), 1.971 (60).

IMA No. 94-019 The cobalt-dominant member of the halotrichite group.
$(Co,Mg,Ni)Al_2(SO_4)_4 \cdot 22H_2O$
Monoclinic: $P2_1/c$
a 6.189(4) b 24.23(1) c 21.20(1) Å β 100.33(5)°
Empire rose; silky; transparent.
Biaxial (sign unknown), α 1.477, β unknown, γ 1.484, 2V unknown.
6.03 (22), 4.790 (100), 4.295 (27), 4.106 (22), 3.945 (26), 3.768 (33), 3.494 (92).

IMA No. 94-020 A member of the magnetoplumbite group.
$Pb(Zn,Fe^{3+})_3(Fe^{3+},Mn^{3+},Mn^{4+},Al,Ti)_9O_{19}$
Hexagonal: $P6_3/mmc$
a 5.854(1) c 22.882(6) Å
Black; metallic; opaque.
In reflected light: black, isotropic, no bireflectance, nonpleochroic.
R_{mean}: (23.8 %)470nm, (22.4 %)546nm, (21.7 %)589nm, (20.7 %)650nm.
11.39 (45), 3.811 (100), 2.858 (75), 2.745 (50), 2.605 (40), 2.407 (25), 1.6361 (30).

IMA No. 94-021 The gallium-dominant analogue of beudantite.
$Pb(Ga,Al,Fe)_3(AsO_4)(SO_4)(OH)_6$
Hexagonal: R3m
a 7.225(4) c 17.03(2) Å
Pale yellow; vitreous; transparent.
Uniaxial (-), ω 1.763, ϵ 1.750.
5.85 (90), 3.59 (40), 3.038 (100), 2.851 (30), 2.513 (30), 2.271 (40), 1.948 (30).

IMA No. 94-022 The F-analogue of thalenite-(Y).
$Y_3Si_3O_{10}F$
Monoclinic: $P2_1/n$
a 7.321(2) b 11.133(4) c 10.375(6) Å β 97.17(2)°
Colourless to white; adamantine; translucent.
Biaxial (-), α 1.719, β 1.739, γ 1.748, 2V(meas.) 73°, 2V(calc.) 67°.
5.60 (5), 3.81 (5), 3.12 (10), 2.828 (8), 2.253 (8), 2.187 (4), 2.131 (4).

IMA No. 94-023 The Ir-dominant analogue of isoferroplatinum.
Ir_3Fe
Cubic: Pm3m
a 3.792(5) Å
Steel black; metallic; opaque.
In reflected light: bright white with yellowish tint, isotropic, nonbireflectant, nonpleochroic. R: (66.2 %)470nm, (69.3 %)546nm, (71.1 %)589nm, (72.5 %)650nm.
2.18 (80), 1.89 (60), 1.34 (70), 1.26 (20), 1.200 (15), 1.142 (100), 1.094 (80).

IMA No. 94-024 An orthorhombic polymorph of walpurgite.
$(UO_2)Bi_4O_4(AsO_4)_2 \cdot 2H_2O$
Orthorhombic: Pbcm
a 5.492(1) b 13.324(2) c 20.685(3) Å
Yellow; adamantine; transparent.
Biaxial (-), α 1.90, β 1.99, γ 2.00 (calc.), 2V(meas.) 36°.
10.354 (94), 5.610 (40), 3.277 (56), 3.208 (100), 3.088 (76), 2.999 (50), 2.852 (46).

IMA No. 94-025
$(UO_2)_8(SO_4)(OH)_{14} \cdot 13H_2O$
Monoclinic: $P2_1/a$
a 18.553(8) b 9.276(2) c 13.532(7) Å β 125.56(2)°
Yellow; vitreous; translucent.
Biaxial (-), α 1.715, β 1.718, γ 1.720, 2V(calc.) 78°.
7.56 (100), 7.13 (48), 3.771 (34), 3.554 (20), 3.234 (10), 3.206 (13), 2.052 (8).

IMA No. 94-026
$NaCa_2[B_9O_{14}(OH)_4] \cdot 2H_2O$
Monoclinic: $P2_1/c$
a 11.4994(8) b 12.5878(9) c 10.5297(1) Å β 99.423(6)°
Colourless to light dirty-yellow and light grey; vitreous; transparent.
Biaxial (+), α 1.532, β 1.538, γ 1.564, 2V(meas.) 54°, 2V(calc.) 52°.
5.41 (66), 5.20 (57), 4.20 (56), 3.35 (89), 3.27 (59), 3.04 (100), 2.210 (59).

IMA No. 94-030
$Pb_2Bi_2(S,Se)_3$
Hexagonal (trigonal): $P\bar{3}$ or $P\bar{3}m$
a 4.191(2) c 39.60(3) Å
Silver-grey; metallic; opaque.
In reflected light: yellowish-white, distinct anisotropism, practically absent bireflectance, bluish-grey to brownish pleochroism. R_1 & R_2: (49.7, 48.5 %)470nm, (48.4, 47.4 %)546nm, (47.9, 46.8 %)589nm, (47.9, 46.2 %)650nm.
3.42 (5), 3.04 (10), 2.096 (8), 1.806 (6), 1.725 (5), 1.298 (7), 1.233 (6).

IMA No. 94-031
HgSAg(Cl,Br)
Hexagonal: $P6_2$, $P6_4$, $P6_222$ or $P6_422$
a 8.234(4) c 19.38(1) Å
Red to brownish red; adamantine; translucent.
Uniaxial (-), ω 2.3 (from polished section), ϵ could not be measured).
6.47 (20), 4.124 (30), 3.357 (60), 3.237 (30), 3.127 (50), 2.879 (100), 2.009 (50).

IMA No. 94-032
Si_3N_4
Hexagonal (trigonal): P31c
a 7.758(5) c 5.623(5) Å
Brownish red to colourless; probably adamantine; transparent.
Uniaxial (-), ω 2.03, ϵ 2.02.
2.893 (85), 2.599 (75), 2.547 (100), 2.320 (60), 1.486 (70), 1.418 (60), 1.351 (75).

IMA No. 94-033 Isostructural with the arrojadite-dickonsonite series.
$(Ba,K,Pb)Na_3(Ca,Sr)(Fe,Mg,Mn)_{14}Al(OH)_2(PO_4)_{12}$
Monoclinic: C2/c
a 16.406(5) b 9.945(3) c 24.470(5) Å β 105.73(2)°
Greenish-grey; greasy; translucent.
Biaxial (sign unknown), $n_{average}$ 1.65.
3.186 (45), 3.018 (100), 2.824 (39), 2.813 (36), 2.685 (50), 2.530 (35).

IMA No. 94-034 The magnesium-analogue of coulsonite.
$Mg(V,Cr)_2O_4$
Cubic: Fd3m
a 8.385(3) Å
Black; metallic; opaque.
In reflected light: light grey, isotropic, no bireflectance, nonpleochroic.
R: (14.0 %)470nm, (13.7 %)546nm, (13.7 %)589nm, (13.7 %)650nm.
4.84 (9), 2.52 (10), 2.093 (8), 1.612 (8), 1.482 (9), 1.092 (7), 1.048 (5).

IMA No. 94-035
$(Na,Ca,K)Cu_3(AsO_4)_2Cl\cdot 5H_2O$
Tetragonal: $P4_22_12$ or $P4_222$
a 10.085(2) c 23.836(8) Å
Intense blue to emerald green; vitreous; translucent.
Uniaxial (-), ω 1.686, ϵ 1.635.
11.90 (100), 9.29 (60), 7.132 (50), 5.043 (60), 4.641 (40), 3.098 (80), 3.061 (70).

IMA No. 94-036
$Hg_6^{1+}Hg^{2+}[Cl,(OH)]_2O_3$
Orthorhombic: Pbma
a 11.790(3) b 13.881(4) c 6.450(2) Å
Black to very dark brown; metallic; opaque.
In reflected light: white, strong anisotropism, moderate bireflectance, pleochroic from white to a higher reflecting blue-white. R_1 & R_2: (22.8, 29.6 %)470nm, (20.7, 25.7 %)546nm, (20.3, 24.6 %)589nm, (20.2, 23.2 %)650nm.
5.25 (80), 3.164 (60), 3.053 (100), 2.954 (70), 2.681 (50), 2.411 (50).

IMA No. 94-038
$Ag(Cd,Pb)AsS_3$
Tetragonal: I4/amd
a 5.499(5) c 33.91(4) Å
Grey; metallic; opaque.
In reflected light: greyish white with bluish tint; anisotropism, bireflectance and pleochroism not observed. R_O: (31.3 %)470nm, (30.4 %)543nm, (29.3 %)587nm, (27.1 %)657nm.
3.19 (50), 2.77 (100), 1.960 (80), 1.679 (70), 1.598 (70), 1.274 (60).

IMA No. 94-043
$Cu_3^{2+}Te^{6+}O_6 \cdot 2H_2O$
Monoclinic: $P2_1/n$
a 9.204(2) b 9.170(2) c 7.584(1) Å β 102.32(3)°
Emerald green; adamantine; transparent.
Biaxial (sign unknown), n 1.91 - 1.92.
6.428 (100), 3.217 (70), 2.601 (40), 2.530 (50), 2.144 (35), 1.750 (35).

IMA No. 94-045
$Fe^{3+}(Mn,Fe^{2+},Mg)(PO_4)O$
Monoclinic: I2/a
a 9.977(2) b 6.339(2) c 11.836(3) Å β 105.77(3)°
Black; weakly submetallic; opaque.
Optical properties could not be measured due to the opaque nature of the mineral.
3.256 (23), 2.970 (100), 2.861 (35), 2.810 (98), 2.064 (25), 1.778 (22).

IMA No. 94-046 A member of the amphibole group.
$(K,Na)Ca_2(Mg,Fe^{2+},Al,Fe^{3+},Ti)_5(Si,Al)_8O_{22}[(OH),F,O]_2$
Monoclinic: C2/m
a 9.9199(4) b 18.0591(8) c 5.3180(3) Å β 105.36(1)°
Black; vitreous; opaque, but translucent in thin splinters.
Biaxial (-), α 1.654, β 1.664, γ 1.670, 2V(meas.) = 79°, 2V(calc.) = 75°.
8.45 (95), 3.283 (45), 3.140 (100), 2.707 (35), 2.344 (70), 2.018 (35), 1.652 (40).

IMA No. 94-047
(Cu,Fe)(Sn,Sb)
Tetragonal: space group unknown
a 4.22(1) c 5.10(3) Å
Megascopic colour was not observed; metallic; opaque.
In reflected light: pinkish-white, distinct anisotropism, distinct bireflectance, pleochroic from light pink to pinkish-white. $R_{max.}$ & $R_{min.}$: (72.6, 64.8 %)470nm, (77.4, 68.2 %)546nm, (78.5, 68.9 %)589nm, (79.0, 69.0 %)650nm.
2.96 (9), 2.10 (10), 1.72 (3), 1.488 (3), 1.214 (4), 1.092 (4).

IMA No. 94-048 A member of the epidote group.
$(Mn^{2+},Ca)(La,Ce,Ca)(Al,Mn^{3+},Mn^{2+})_3(Si_3O_{11})O(OH)$
Monoclinic: $P2_1/m$
a 8.891(3) b 5.704(3) c 10.107(8) Å β 113.99(2)°
Brown-red; vitreous; transparent.
Because of the small grain size, most of the optical properties could not be determined.
2.897 (100), 2.857 (45), 2.707 (60), 2.615 (60), 2.178 (60), 2.145 (60).

IMA No. 94-049
$Mn_3(Nb,Ta)_3(Nb,Mn)_2W_2O_{20}$
Monoclinic: $P2_1$
a 24.73(2) b 5.056(3) c 5.760(3) Å β 103.50(7)°
Red to brown-red; metallic; opaque.
In reflected light: light grey, weak anisotropism, weak bireflectance, nonpleochroic. $R_{max.}$ & $R_{min.}$: (19.2, 18.0 %)470nm, (18.5, 17.5 %)546nm, (19.3, 18.5 %)589nm, (16.5, 16.0 %)650nm.
6.0 (5), 3.74 (8), 3.69 (8), 2.98 (10), 1.783 (5), 1.744 (6), 1.732 (7), 1.456 (5).

IMA No. 94-050 An F-dominant, triclinic polymorph of canasite, with additional H_2O.
$K_3Na_3Ca_5(Si_{12}O_{30})(F_3OH)\cdot H_2O$
Triclinic: P1
a 10.0941(3) b 12.6913(2) c 7.2405(1) Å
α 90.00(2)° β 111.02(2)° γ 110.20(2)°
Lilac-grey, blue-grey, rarely greenish; vitreous; translucent.
Biaxial (-), α 1.536, β 1.539, γ 1.542, 2V(meas.) = 70°, 2V(calc.) = 89.8°.
5.88 (37), 4.70 (54), 4.21 (40), 3.01 (25), 2.915 (100), 2.354 (30), 2.307 (21).

IMA No. 94-051
$Pb_2Bi_2Te_2S_3$
Hexagonal: space group unknown
a 4.230(4) c 33.43(2) Å
Dark grey to black; metallic; opaque.
In reflected light: greyish-white with a slight pinkish tint, very faint anisotropism, very weak bireflectance, nonpleochroic. R_O & R_E: (40.4, 39.3 %)470nm, (42.1, 40.8 %)546nm, (41.3, 40.8 %)589nm, (41.9, 40.9 %)650nm.
3.35 (40), 3.06 (100), 2.22 (25), 2.115 (50), 1.311 (25), 1.213 (25).

IMA No. 94-052
$K_2Na_4Ca_3Ti_2Be_4Si_{12}O_{38}$
Orthorhombic: Fddd
a 12.778(4) b 14.343(3) c 33.69(1) Å
Pink, dark red, seldom white; vitreous; transparent.
Biaxial (+), α 1.630, β 1.644(calc.), γ 1.675, 2V(meas.) = 70°.
9.23 (9), 4.15 (10), 3.30 (10), 3.16 (10), 2.53 (10), 2.42 (10), 1.582 (9).

IMA No. 94-053
$Na_2C_2O_4$
Monoclinic: $P2_1/a$
a 10.426(9) b 5.255(5) c 3.479(3) Å β 93.14(8)°
Pale yellow; vitreous; transparent.
Biaxial (-), α 1.415, β 1.524, γ 1.592, 2V(meas.) = 72°, 2V(calc.) = 72°.
5.203 (13), 2.898 (27), 2.826 (100), 2.602 (56), 2.334 (33), 2.177 (13), 2.041 (14).

IMA No. 94-054 A member of the zeolite group.
$Na_3Mg_3Ca_5Al_{19}Si_{117}O_{272}\cdot 93H_2O$
Orthorhombic: Cmca
a 13.698(2) b 25.213(3) c 22.660(2) Å
Colourless to light straw; vitreous; transparent.
Biaxial (-), α 1.480, β 1.485, γ 1.486, 2V(meas.) < 60°, 2V(calc.) 48°.
11.34 (100), 10.64 (31), 4.64 (35), 4.37 (79), 4.01 (57), 3.938 (36), 3.282 (68).

IMA No. 94-055 A member of the cuprorivaite group.
$SrCuSi_4O_{10}$
Tetragonal: P4/ncc
a 7.366(1) c 15.574(3) Å
Colour; vitreous; transparent.
Uniaxial (-), ω 1.630, ϵ 1.590.
7.79 (35), 3.444 (40), 3.330 (100), 3.119 (55), 3.033 (50), 2.605 (30), 2.322 (30).

IMA No. 94-056
$Ag_{24}HgAs_5S_{20}$
Hexagonal: space group unknown
a 15.00(1) c 15.46(3) Å
Wine-red to violet; metallic; opaque.
In reflected light: grey, weak to moderate anisotropism, very low bireflec
pleochroism. $R_{max.}$ & $R_{min.}$: (31.0, 30.3 %)470nm, (29.2, 27.6 %)546nm,
(27.6, 26.0 %)589nm, (24.6, 23.9 %)650nm.
3.17 (6), 3.091 (10), 2.998 (4), 2.755 (3), 1.878 (8).

IMA No. 94-057 A member of the crichtonite group.
$(Sr,Pb)(Y,U)(Ti,Fe^{3+})_{20}O_{38}$
Hexagonal (rhombohedral): $R\bar{3}$
a 9.197(1) α 68.75(2)°
Black; metallic; opaque.
In reflected light: ash-grey with pale bluish tones, weak anisotropism, low bireflectance,
very weak pleochroism. R_1 & R_2: (17.73, 17.22 %)470nm, (17.14, 16.50 %)546nm,
(16.54, 16.11 %)589nm, (16.48, 16.00 %)650nm.
3.412 (m), 2.902 (m), 2.846 (mw), 2.499 (mw), 1.916 (mw), 1.603 (m), 1.441 (m).

IMA No. 94-058 The Ba-analogue of hennomartinite.
$BaMn_2^{3+}[Si_2O_7](OH)_2\cdot H_2O$
Orthorhombic: Cmcm (?)
a 6.325(1) b 9.120(1) c 13.618(1) Å
Dark brown; earthy to brilliant; translucent to transparent.
Biaxial (-), α 1.82, β 1.845 (calc.), γ 1.85, 2V(meas.) 46°.
4.85 (100), 4.557 (50), 4.322 (59), 3.416 (77), 2.869 (80), 2.729 (82).

IMA No. 94-059 A member of the amphibole group.
$(Na,K)(Ca,Na,Fe^{2+})_2Mg_5(Si,Al)_8O_{22}(F,O,OH)_2$
Monoclinic: C2/m
a 9.893(4) b 18.015(5) c 5.279(3) Å β 104.61(4)°
Grey to black; vitreous; opaque, but thin fragments are transparent.
Biaxial (-), α 1.603, β 1.613, γ 1.623, 2V(meas.) 90°, 2V(calc.) 89°.
9.06 (6), 8.46 (8), 3.282 (9), 3.140 (10), 2.703 (6), 1.443 (7).

1995 PROPOSALS

IMA No. 95-001 A member of the crandallite group.
$SrFe^{3+}{}_3(PO_4)_2(OH,H_2O)_6$
Hexagonal (trigonal): R$\bar{3}$m
a 7.28 c 16.85 Å
Yellow, brown; vitreous to resinous; transparent to translucent.
Uniaxial (-), ω 1.872, ϵ 1.862
5.88 (10), 3.65 (6), 3.06 (9), 2.96 (5), 2.81 (5), 2.53 (5), 2.25 (6), 1.969 (5), 1.820 (5).

IMA No. 95-002 The Mn^{2+} and (O,F) analogue of paulkerrite.
$(H_2O,K)_2Ti(Mn^{2+},Fe^{2+})_2(Fe^{3+},Ti^{4+})_2(PO_4)_4(O,F)_2 \cdot 14H_2O$
Orthorhombic: Pbca
a 10.561 b 20.858 c 12.516 Å
Greenish-yellow, sometimes light brown; vitreous; transparent.
Biaxial (+), α 1.612, β 1.621, γ 1.649, 2V(calc.) 59.9°.
10.40 (90), 7.50 (80), 6.28 (100), 5.22 (40), 3.97 (40), 3.77 (50), 3.13 (100), 2.88 (40).

IMA No. 95-003
$Cu(Pt,Ir)_2S_4$
Cubic: Fd3m
a 9.940 Å
Steel grey; metallic; opaque.
In reflected light: white with greenish tint, isotropic, no bireflectance or pleochroism. R: (37.3 %)470nm, (37.7 %)546nm, (38.1 %)589nm, (38.6 %)650nm.
5.72 (4), 2.98 (6), 2.48 (5), 1.90 (7), 1.75 (10), 1.29 (5), 1.014 (5).

IMA No. 95-005 The strontium end-member of the cryptomelane group.
$(Sr,Ba,K)Mn_8O_{16}$
Monoclinic: $P2_1/n$
a 10.00 b 5.758 c 9.88 Å β 90.64°
Black; submetallic; opaque.
In reflected light: grey, strong anisotropism, grey-blue to white bireflectance, pleochroism strong. $R_{max.}$ & $R_{min.}$: (34.2, 26.0 %)470nm, (31.7, 24.4 %)546nm, (30.6, 23.4 %)589nm, (27.9, 22.3 %)650nm.
3.15 (100), 3.13 (80), 2.409 (80), 2.229 (40), 2.170 (60), 2.170 (60), 1.556 (50).

IMA No. 95-006 The silver analogue of roquesite in the chalcopyrite group.
$AgInS_2$
Tetragonal: $I\bar{4}2d$
a 5.880 c 11.21 Å
Havana brown; metallic; opaque.
In reflected light: brownish grey; abundant red internal reflections; strong anisotropism in oil from red brick with orange tint to bluish-grey and purplish; pleochroism weak, brown to clear brown-grey in oil. $R_{max.}$ & $R_{min.}$: (29.3, 27.8 %)460nm, (27.5, 25.9 %)540nm, (27.65, 25.6 %)580nm, (27.4, 27.5 %)660nm.
3.351 (100), 2.941 (80), 2.082 (75), 2.030 (75), 1.767 (80), 1.188 (40).

IMA No. 95-007 Probably belongs to the marcasite group.
CoSbAs
Orthorhombic: space group unknown
a 3.304 b 6.092 c 10.26 Å
White; metallic; opaque.
In reflected light: silver-white, weak to distinct anisotropism, weak bireflectance, nonpleochroic. R_2 & R_1: (58.2, 55.5 %)470nm, (56.8, 55.6 %)546nm, (55.8, 55.5 %)589nm, (55.0, 55.5 %)650nm.
2.63 (10), 2.53 (8), 1.942 (10), 1.730 (4), 1.640 (4), 1.3963 (4), 1.1182 (8).

IMA No. 95-009 The natural analogue of synthetic $PtSe_2$.
$PtSe_2$
Hexagonal (trigonal): $P\bar{3}m1$
a 3.730 c 5.024 Å
Silvery lead grey; metallic; opaque.
In reflected light: white; anisotropism moderate to strong with tints from pinkish-yellow to dark-grey-lilac; strong bireflectance; pleochroism: R_{max} light-yellow, R_{min} light-lilac. $R_{max.}$ & $R_{min.}$: (48.4, 35.1 %)470nm, (48.3, 35.0 %)546nm, (49.1, 35.3 %)589nm, (50.8, 36.5 %)650nm.
5.04 (3), 2.72 (10), 1.983 (5), 1.859 (5), 1.747 (3), 1.360 (4).

IMA No. 95-011
$Cu(Mg,Cu,Fe,Zn)_2Te^{6+}O_6 \cdot 6H_2O$
Hexagonal (trigonal): P3
a 5.305 c 9.693 Å
Pale yellow to pale orange-yellow; vitreous; transparent to somewhat translucent.
Uniaxial (-), ω 1.803, ϵ 1.581 (calc.).
9.70 (100), 4.834 (80), 4.604 (60), 2.655 (60), 2.556 (70), 2.326 (70), 1.789 (40).

IMA No. 95-012
$Cu[AsO_3OH] \cdot 2H_2O$
Triclinic: $P\bar{1}$
a 6.020 b 7.632 c 11.168 Å α 74.43° β 89.32° γ 86.55°
Turquoise blue; vitreous; transparent.
Biaxial (-), α 1.615, β 1.660, γ 1.700, 2V(meas.) 82°, 2V(calc.) 84°.
7.35 (100), 5.239 (50), 4.440 (60), 3.936 (60), 3.302 (40), 3.008 (50), 2.840 (35).

IMA No. 95-013 The zinc analogue of arsenbrackebuschite.
$Pb_2(Zn,Fe)[(As,S)O_4]_2 \cdot H_2O$
Monoclinic: $P2_1$ or $P2_1/m$
a 8.973 b 5.955 c 7.766 Å β 112.20°
Pale olive green with streaks of white; adamantine; transparent.
In reflected light: pale brownish grey; abundant colourless to very pale yellow internal reflections; anisotropism not detectable by eye; bireflectance measurable but not noticeable by the eye; nonpleochroic. $R_{min.}$ & $R_{max.}$: (11.2, 11.5 %)470nm, (10.8, 10.9 %)546nm, (10.7, 10.8 %)589nm, (10.7, 10.8 %)650nm.
4.85 (50), 3.659 (30), 3.246 (100), 2.988 (60), 2.769 (60), 2.293 (30), 2.107 (50), 1.889 (30).

IMA No. 95-014
$Ca_2FeCl[B_9O_{13}(OH)_6] \cdot 4H_2O$
Monoclinic: $P2_1$
a 11.64 b 9.38 c 8.735 Å β 98.40°
Pale yellow; vitreous; transparent.
Biaxial (+-), α 1.550, β 1.554, γ 1.592, 2V(meas.) 36.6°, 2V(calc.) 32.6°.
8.65 (3), 7.29 (10), 5.32 (2), 4.50 (2), 2.958 (3), 2.744 (2), 2.113 (3).

IMA No. 95-015
$Ca_5(SiO_4)_2SO_4$
Orthorhombic: Pnma
a 6.863 b 15.387 c 10.181 Å
Bright blue; vitreous; transparent.
Biaxial (-), α 1.630, β 1.637, γ 1.640, 2V(meas.) 63.3°, 2V(calc.) 66.2°.
3.198 (27), 3.042 (32), 2.853 (40), 2.830 (100), 2.617 (32), 2.565 (57), 1.9612 (26), 1.8924 (27).

IMA No. 95-016
$Mn_2V(V,As)O_7 \cdot 2H_2O$
Monoclinic: $P2_1/n$
a 7.809 b 14.554 c 6.705 Å β 93.25°
Orange-red; vitreous; transparent.
Biaxial mean n 1.82, 2V small.
5.32 (80), 3.436 (50), 3.260 (50), 3.039 (100), 2.723 (60), 2.573 (50b), 2.441 (50), 1.592 (60).

IMA No. 95-017 The natural analogue of synthetic $FeNb_3S_6$.
$FeNb_3S_6$
Hexagonal: $P6_322$
a 5.771 c 12.190 Å
Dark grey to black; metallic; opaque.
In reflected light: grey; distinct to strong anisotropism from blue-grey to dark-brown; distinct bireflectance; pleochroism, light grey to grey. $R_{max.}$ & $R_{min.}$: (36.3, 29.5 %)470nm, (36.6, 29.4 %)546nm, (36.1, 28.9 %)589nm, (34.7, 28.1 %)650nm.
6.11 (8), 3.04 (6), 2.88 (5), 2.606 (8), 2.096 (10), 1.665 (8), 1.524 (6).

IMA No. 95-018 A member of the mica group (compare 95-019).
$K(Fe^{2+},Mg)(Fe^{3+},Al)Si_4O_{10}(OH)_2$
Monoclinic: C2/m
a 5.270 b 9.106 c 10.125 Å β 100.27°
Blue green; earthy; translucent in thin section.
Complete optical data could not be measured, mean n 1.640.
3.65 (52), 3.358 (86), 3.321 (100), 3.090 (60), 2.584 (50).

IMA No. 95-019 A member of the mica group (compare 95-018).
$K(Fe^{2+},Mg)(Al,Fe^{3+})Si_4O_{10}(OH)_2$
Monoclinic: C2/m
a 5.270 b 9.106 c 10.125 Å β 100.27°
Blue green; earthy; translucent in thin section.
Complete optical data could not be measured, mean n 1.625.
3.65 (52), 3.358 (86), 3.321 (100), 3.090 (60), 2.584 (50).

NOTE: The minerals represented by 95-018 and 95-019 occur intimately mixed, have the same unit cell parameters, and give the same X-ray powder diffraction data. They differ in chemical composition.

IMA No. 95-020
$CaB_3O_4(OH)_3$
Monoclinic: Pc
a 7.234 b 8.130 c 8.378 Å β 98.22°
Colourless to white; vitreous; transparent to translucent.
Biaxial (-), α 1.580, β 1.605, γ 1.623, 2V(meas.) 63°, 2V(calc.) 80°.
4.30 (64), 3.379 (100), 3.169 (25), 3.122 (31), 2.151 (20), 1.919 (20), 1.846 (45).

IMA No. 95-021 The natural analogue of synthetic $PbSb_2O_6$.
$PbSb_2O_6$
Hexagonal (trigonal): P31m
a 5.295 c 5.372 Å
Colourless to pale yellow; resinous; transparent.
Uniaxial (-), ω 2.092, ε 1.920
3.49 (VS), 2.648 (M), 2.110 (W), 1.887 (W), 1.651 (W), 1.531 (W).

IMA No. 95-022
$KFe^{3+}_8(PO_4)_6(OH)_7 \cdot 8H_2O$
Monoclinic: C2, Cm or C2/m
a 29.52 b 5.249 c 18.56 Å β 109.27°
Yellowish brown, pale yellow, cream to white; vitreous to silky; translucent.
Biaxial (+), α 1.780, β 1.785, γ 1.800, 2V(calc.) 60°.
9.41 (60), 4.84 (90), 4.32 (70), 4.25 (50), 3.470 (60), 3.216 (100), 3.116 (80).

IMA No. 95-023
$Sr_3Na(La,Ce)(PO_4)_3(F,OH)$
Hexagonal (trigonal): P3
a 9.647(1) c 7.170(1) Å
Bright yellow to greenish-yellow; vitreous; transparent.
Uniaxial (-), ω 1.653, ε 1.635.
3.59 (87), 3.30 (65), 3.17 (32), 2.897 (100), 2.884 (100), 2.790 (54), 1.910 (36), 1.796 (36).

IMA No. 95-024 The cubic polymorph of lueshite and natroniobite.
$NaNbO_3$
Cubic: $Pm\bar{3}$ or P23
a 3.911 Å
Brownish-black; adamantine; opaque.
In reflected light: bluish; reddish-brown internal reflections; isotropic; nonpleochroic. R: (15.75 %)480nm, (15.00 %)540nm, (14.70 %)580nm, (14.35 %)660nm.
3.915 (35), 2.765 (100), 1.953 (53), 1.747 (8), 1.594 (30), 1.380 (22), 1.234 (7).

IMA No. 95-025
$[Zn_{8-x}Al_x(OH)_{16}][(SO_4)_{x/2-y/2}Na_y(H_2O)_6]$
Hexagonal (trigonal) : $P\bar{3}$
a 3.082 c 11.116 Å
Pale blue; vitreous to waxy, translucent.
Uniaxial (sign unknown), ω 1.532, ε unknown.
11.12 (100), 5.549 (24), 3.704 (15), 2.595 (6), 2.408 (6), 2.167 (4), 1.926 (4).

IMA No. 95-026 A member of the zeolite group.
$NaCaAl_3Si_{17}O_{40}\cdot 7H_2O$
Orthorhombic: Cmcm
a 9.747 b 23.880 c 20.068 Å
Colourless; vitreous; transparent.
Biaxial (+), α 1.476, β 1.478, γ 1.483, 2V(meas.) 65°, 2V(calc.) 65°.
11.94 (40), 9.04 (33), 8.23 (29), 7.69 (29), 3.79 (100), 3.61 (40).

IMA No. 95-027
$Cu_5(VO_4)_2O_2\cdot n(Cs,Rb,K)Cl$
Hexagonal (trigonal): P3
a 6.375 c 8.399 Å
Black; resinous-metallic; opaque.
Reflectance measurements could not be made because the material is too fine grained.
3.43 (7), 2.810 (4), 2.315 (10), 2.131 (3), 1.598 (4).

IMA No. 95-028 An hexagonal polymorph of alabandite.
MnS
Hexagonal: $P6_3mc$
a 3.9817 c 6.4447 Å
Dark brown to black; resinous; opaque.
In reflected light: steel- grey; brown-red internal reflections; anisotropism, 2.62 to 2.77; bireflectance, 0.15; nonpleochroic. $R_{max.}$ & $R_{min.}$: (24.5, 22.1 %)470nm, (22.6, 20.5 %)546nm, (22.1, 20.0 %)589nm, (21.6, 19.6 %)650nm.
3.445 (89), 3.217 (72), 3.036 (66), 1.988 (82), 1.820 (100), 1.691 (63).

IMA No. 95-029 The Mn-analogue of berthierite.
$MnSb_2S_4$
Orthorhombic: Pnam
a 11.47 b 14.36 c 3.81 Å
Black; submetallic; opaque.
In reflected light: light grey; distinct anisotropism; faint bireflectance; nonpleochroic. $R_{max.}$ & $R_{min.}$: (35.0, 24.0 %)470nm, (36.1, 23.9 %)546nm, (36.9, 24.9 %)589nm, (35.6, 25.7 %)650nm.
4.46 (40), 3.69 (90), 3.23 (70), 3.05 (40), 2.90 (80), 2.65 (100), 2.18 (40), 1.906 (40), 1.813 (50).

IMA No. 95-030
$Zn_3Cu_2(SO_4)_2(OH)_6 \cdot 4H_2O$
Triclinic: P1
a 5.415 b 6.338 c 10.475 Å α 94.38° β 90.08° γ 90.24°
Greenish blue; vitreous; transparent.
Biaxial (+), α 1.629, β 1.630, γ 1.637, 2V(meas.) 60°, 2V(calc.) 42°.
10.459 (61), 5.230 (74), 3.486 (40), 3.157 (6), 2.728 (6), 2.493 (7), 2.355 (7), 1.743 (9).

IMA No. 95-031
$(K,Na)_2(Nb,Ti)_2Si_4O_{12}(O,OH)_2 \cdot 4H_2O$
Monoclinic: Cm
a 14.692 b 14.164 c 7.859 Å β 117.87°
White; vitreous; translucent.
Biaxial (+), α 1.649, β 1.655, γ 1.759, 2V(meas.) 20°, 2V(calc.) 28°.
7.10 (9), 4.98 (6), 3.262 (10), 3.151 (8b), 2.956 (6), 2.549 (4), 1.723 (4), 1.591 (4b), 1.451 (4b).

IMA No. 95-032
(Fe,Os,Ru,Ir)
Hexagonal: $P6_3/mmc$
a 2.591 c 4.168 Å
Megascopic colour unknown; metallic; opaque.
In reflected light: white; weak anisotropism. R: (57.4 %)470nm, (53.4 %)546nm, (53.3 %)589nm, (54.4 %)650nm.
2.246 (5), 2.087 (6), 1.976 (10), 1.297 (6b), 1.180 (6b), 1.100 (5b).

IMA No. 95-033
$Na_6Mn(Ti,Nb)Si_{10}(O,OH)_{28}\cdot 4H_2O$
Monoclinic: I2/m
a 13.033 b 18.717 c 12.264 Å β 99.62°
Yellow, pinkish-yellow or pink; vitreous to greasy; translucent to transparent.
Biaxial (-), α 1.536, β 1.545, γ 1.553, 2V(meas.) 87°, 2V(calc.) 86°.
10.56 (100), 6.38 (50), 5.55 (45), 4.78 (40), 4.253 (40), 3.196 (80), 2.608 (50).

IMA No. 95-034
$Na_5(Y,Dy,Gd)(Ti,Nb)Si_6O_{18}\cdot 6H_2O$
Hexagonal (trigonal): R32
a 10.696 c 15.728 Å
Colourless; vitreous; transparent or cloudy.
Uniaxial (-), ω 1.612, ε 1.607.
5.99 (60), 3.21 (100), 3.093 (40), 2.990 (85), 2.61 (40), 1.998 (55),
1.481 (44b).

IMA No. 95-035
(Nb,Ta)C
Cubic: Fm3m
a 4.45 Å
Bronze-yellow; metallic; opaque.
In reflected light: yellowish- to rose-cream; no anisotropism, bireflectance or pleochroism. R: (33.9 %)480nm, (38.5 %)540nm, (45.1 %)580nm, (52.8 %)660nm.
2.56 (10), 2.22 (9), 1.574 (8), 1.343 (8), 1.289 (7), 1.115 (3).

IMA No. 95-036 The calcium-dominant analogue of belovite-(Ce).
$Na(Ca,Sr)_3Ce(PO_4)_3F$
Hexagonal (trigonal): P3
a 9.51 c 7.01 Å
Bright yellow; vitreous; transparent.
Uniaxial (-), ω 1.682, ε 1.660.
3.51 (30), 3.12 (40), 2.84 (100b), 2.753 (40), 1.967 (30), 1.870 (30).

IMA No. 95-037 The natural analogue of synthetic $Fe_3^{3+}PO_7$.
$Fe_3^{3+}PO_7$
Hexagonal (trigonal): R3m
a 7.994 c 6.855 Å
Brown to red brown; greasy; non-translucent.
Optical data could not be obtained because of the small size of the domains.
4.86 (10), 3.09 (100), 2.446 (16), 2.078 (20), 1.997 (13), 1.845 (11),
1.623 (23), 1.545 (12), 1.440 (16).

IMA No. 95-038 The natural analogue of synthetic $Fe^{3+}PO_4$.
$Fe^{3+}PO_4$
Hexagonal (trigonal): $P3_121$
a 5.048 c 11.215 Å
Brown to red-brown; greasy; non-translucent.
Optical data could not be obtained because of the small size of the domains.
4.360 (19), 3.445 (100), 2.518 (7), 2.362 (14), 2.298 (7), 2.180 (10), 1.8846 (12), 1.5814 (8), 1.4214 (10).

IMA No. 95-039
$Cu_5Zn_3(Te^{6+}O_4)_4(OH)_8 \cdot 7H_2O$
Triclinic: P1 or $P\bar{1}$
a 8.794 b 9.996 c 5.660 Å α 104.10° β 90.07° γ 96.34°
Pale blue to deeper blue-green; vitreous to pearly; transparent to translucent.
In reflected light: very pale light brown; light emerald green internal reflections; anisotropism unknown; slight bireflectance. R values could not be measured with certainty.
9.638 (100), 8.736 (50), 4.841 (100), 2.747 (60), 2.600 (45).

IMA No. 95-040
$Ba_2Ce(CO_3)_3F$
Monoclinic: $P2_1/m$ or $P2_1$
a 13.396 b 5.067 c 6.701 Å β 106.58°
Yellow; vitreous; transparent.
Biaxial (-), α 1.584, β 1.724, γ 1.728, 2V(meas.) 16°, 2V(calc.) 18°.
4.000 (10), 3.269 (100), 2.535 (20), 2.140 (40), 2.003 (40), 1.635 (10), 1.373 (10).

IMA No. 95-041
In_2Pt
Cubic: $Fm\bar{3}m$, $F4\bar{3}2$ or $F4\bar{3}m$
a 6.364 Å
Bright white; metallic; opaque.
In reflected light: bright white with yellowish tint; no anisotropism, bireflectance or pleochroism. R: (49.3 %)470nm, (60.6 %)550nm, (68.5 %)590nm, (80.1 %)650nm.
2.25 (100), 1.92 (60), 1.59 (60), 1.299 (80), 1.125 (60), 1.076 (60), 1.006 (60).

IMA No. 95-042
$InPt_3$
Cubic: $Pm\bar{3}m$
a 3.988 Å
Bright white; metallic; opaque.
In reflected light: bright white with yellowish tint; no anisotropism, bireflectance or pleochroism. R: (56.1 %)470nm, (62.5 %)550nm, (65.7 %)590nm, (71.3 %)650nm.
2.30 (100), 1.99 (60), 1.411 (40), 1.203 (80), 1.151 (40), 0.997 (20).

IMA No. 95-043
$Fe_2(Ta,Nb)$
Hexagonal: $P6_3/mmc$, $P6_3mc$ or $P\bar{6}2c$
a 4.87 c 7.76 Å
Greyish-yellow; metallic; opaque.
In reflected light: greyish white; no anisotropism, bireflectance or pleochroism.
R: (55.4 %)460nm, (60.8 %)540nm, (65.7 %)590nm, (71.3 %)660nm.
2.84 (7), 2.46 (6), 2.22 (9), 2.00 (3), 1.92 (4), 1.41 (3), 1.34 (8).

IMA No. 95-044 The natural analogue of synthetic $Bi_{16}CrO_{27}$.
$Bi_{16}CrO_{27}$
Tetragonal: I4, $I\bar{4}$ or I4/m
a 8.649 c 17.24 Å
Orange-brown; adamantine; translucent.
Uniaxial (+), ω 2.50, ε 2.55.
In reflected light: greyish white to light orange; orange internal reflections; weak anisotropism; weak bireflectance; very weak pleochroism. R_E & R_O:
(21.46, 19.40 %)470nm, (27.46, 25.22 %)546nm, (29.80, 26.22 %)589nm,
(29.98, 25.96 %)650nm.
3.19 (100), 2.730 (40), 1.980 (40), 1.715 (30), 1.655 (55), 1.124 (25),
1.054 (25).

IMA No. 95-045 A member of the amphibole group.
$Li_2(Mg,Fe^{2+})_3Fe_2^{3+}Si_8O_{22}(OH)_2$
Monoclinic: C2/m
a 9.474 b 17.858 c 5.268 Å β 101.88°
Black; vitreous; translucent.
Biaxial (+), α 1.699, β 1.703, γ 1.708, 2V(meas.) 72°, 2V(calc.) 84°.
8.222 (61), 4.458 (19), 3.044 (100), 2.741 (53), 2.712 (14), 2.341 (14),
1.433 (46), 1.392 (14).

IMA No. 95-046
$Na_2(Sr,Ba)_{14}Na_2Al_{12}F_{64}(F,OH)_4$
Monoclinic: C2/m
a 16.046 b 10.971 c 7.281 Å β 101.734°
Colourless to white; vitreous; translucent.
Biaxial (-), α 1.436, β 1.442, γ 1.442, 2V(meas.) 0-5°, 2V(calc.) 0°.
7.844 (8), 3.643 (9), 3.453 (10), 3.193 (10), 3.112 (9), 2.989 (9), 2.220 (8),
2.173 (9), 2.001 (8).

IMA No. 95-047
IrBiS
Cubic: $P2_13$
a 6.164 Å
Steel black; metallic; opaque.
In reflected light: bright white with yellowish tint, isotropic.
R: (46.2 %)470nm, (47.2 %)550nm, (47.6 %)590nm, (47.4 %)650nm.
2.75 (70), 2.51 (60), 1.860 (100), 1.090 (50), 1.090 (50).

IMA No. 95-048 A polymorph of geminite.
$Cu^{2+}(AsO_3OH)\cdot H_2O$
Triclinic: P1 or $P\bar{1}$
a 6.435 b 11.257 c 18.662 Å α 79.40° β 86.48° γ 83.59°
Very light green to colourless; vitreous; transparent.
Biaxial (+), α 1.602, β 1.642, γ 1.725, 2V(meas.) 70°, 2V(calc.) 73°.
18.3 (25), 11.00 (100), 3.171 (30), 2.952 (50), 2.920 (60), 2.816 (50), 2.492 (25).

IMA No. 95-049 The Pt-dominant analogue of taimyrite.
$(Pt,Pd,Cu)_9Cu_3Sn_4$
Orthorhombic: Pmmm, Pmm2 or P222
a 7.89 b 4.07 c 7.73 Å
Pinkish lilac; metallic; opaque.
In reflected light: pinkish lilac, distinct to moderate anisotropism, weak to distinct bireflectance, pleochroic from brownish pink to pinkish lilac. $R_{max.}$ & $R_{min.}$: (44.1, 42.8 %)470nm, (50.0, 49.5 %)546nm, (54.6, 51.8 %)589nm, (56.8, 55.6 %)650nm.
2.283 (10), 2.163 (4), 2.030 (2), 1.369 (3), 1.218 (2), 1.143 (2).

IMA No. 95-050 The vanadium analogue of atelestite.
$Bi_2O(OH)VO_4$
Monoclinic: $P2_1/c$
a 6.973 b 7.539 c 10.881 Å β 107.00°
Light brown; adamantine; transparent to translucent.
Biaxial (+), α 2.26, β 2.27, γ 2.30, 2V(meas.) 65°, 2V(calc.) 61°.
6.667 (23), 6.102 (22), 4.279 (38), 3.267 (100+), 3.150 (62), 2.734 (36), 2.549 (21), 1.889 (21).

IMA No. 95-051 A member of the zeolite group.
$Ca_4(Ca,Sr,K,Ba)_3Cu_3Al_{12}Si_{12}O_{48}(OH)_8\cdot\sim H_2O$
Cubic: Fm3m
a 31.62 Å
Light blue; vitreous; transparent.
Isotropic: n 1.505.
18.34 (100), 15.82 (50), 9.69 (5), 4.43 (5), 3.87 (5), 3.47 (5).

IMA No. 95-052 A member of the mica group; the Cr-dominant analogue of muscovite.
$KCr_2[AlSi_3O_{10}](OH,F)_2$
Monoclinic: C2/c
a 5.32 b 9.07 c 20.20 Å β 95.6°
Emerald green; vitreous; transparent.
Biaxial (-), α 1.619, β 1.669, γ 1.673, 2V(meas.) 31°, 2V(calc.) 31°.
9.94 (6), 4.52 (8), 2.60 (10), 2.40 (6), 2.15 (6), 1.519 (10).

IMA No. 95-053 The lanthanum-dominant analogue of ancylite-(Ce).
$SrLa(CO_3)_2(OH)\cdot H_2O$
Orthorhombic: Pmcn
a 5.072 b 8.589 c 7.276 Å
Light yellow to yellowish brown; vitreous; transparent.
Biaxial (+), α 1.640, β 1.668 (calc.), γ 1.731, 2V(meas.) 70°.
4.36 (92), 3.738 (88), 3.705 (90), 2.955 (100), 2.664 (89), 2.358 (87), 2.092 (80).

Rom. J. Mineralogy, 79, p. 208-209, Bucureşti, 1999

RECENZII - BOOK REVIEWS - BUCHBESPRECHUNG - ANALYSE D'OUVRAGES

Editura F. Enke din Stuttgart, Germania, a scos pe piaţa în ultimele luni mai multe cărţi de geologie, care arată interesul tradiţional al editurii pentru Ştiinţele Pământului şi faptul că geologia în general reprezinta încă un domeniu în care publicarea ideilor, conceptelor şi realizărilor merită să fie menţionată. Cele trei cărţi prezentate mai jos "atacă" domenii deosebite, dar la fel de interesante. În ordinea prezentării acestea sunt: (1) - un dicţionar geologic, binevenit într-o perioadă în care apar numeroşi termeni noi, se redefinesc concepte etc.; (2) - un îndreptar pentru observaţii de teren, extrem de util celor care încep dificila meserie de geolog şi (3) - un ghid geologic pentru o zonă interesantă, care ar trebui să servească drept model pentru popularizarea geologiei, încă o "cenuşăreasă", cunoscută doar accidental şi incomplet, în multe ţări europene.

HANS MURAWSKI, WILHELM MEYER – Geologisches Wörterbuch (Dicţionar geologic).
Editura F. Enke, Stuttgart, 1998, 278 p., 82 fig., 7 tab., format 12x19 cm, 24.80 DM.

Este a zecea ediţie a acestui dicţionar, prima ediţie datând din 1937 (autor C. Chr. Beringer). Începand cu 1957 au apărut mai multe ediţii realizate de H. Murawski.

Faţă de ultima ediţie (1992, a 9-a) sunt introduse numeroase date noi, prof. W. Meyer apelând la specialişti din alte domenii pentru aducerea la zi şi organizarea nivelului ştiinţific al noţiunilor şi termenilor.

Un aspect care trebuie subliniat în mod deosebit este strădania autorului actualei ediţii (W. Meyer) de a stabili paternitatea diverselor noţiuni, chiar dacă sensul actual al acestora s-a modificat într-o măsura sau alta. În cazurile în care paternitatea rămâne necunoscută s-a menţionat autorul care a utilizat pentru prima data în lucrări o noţiune sau un termen anume. Interesant este, de asemenea, demersul pentru a stabili etimologia principalilor termeni (latină, greacă) sau derivarea acestora de la denumiri de localităţi tip, de exemplu denumirea etajelor: Aalenian de la localitatea Aalen din Germania, Maastrichtian de la localitatea Maastricht din Olanda, Permian de la regiunea Perm din Urali, Dacian de la Dacia etc.

Sunt puţine lipsuri, dar ele pot fi totuşi remarcate: nu se vorbeşte nimic despre fractali, care au o importanţă deosebită în evaluarea corectă a porozităţii rocilor sedimentare, în explicarea cristalizării dendritice sau scheletice etc.; nu este amintită anomalia de Ir de la limita Cretacic/Terţiar, mult discutată în legătură cu extincţia dinozaurilor, "mixing" şi "mingling" etc.

Valoarea dicţionarului este însă indiscutabilă; într-un volum redus sunt incluse numeroase noţiuni, sunt explicaţi termeni mai puţin cunoscuţi, sunt prezentate scheme şi clasificări extrem de utile geologilor începători şi nu numai lor. Cartea merită să fie achiziţionată de orice bibliotecă de geologie sau de Ştiinţele Pământului în general.

MARTIN KLEIN – Geologie im Gelände (Geologia pe teren)
Editura F. Enke, Stuttgart, 1999, 119 p., numeroase figuri şi tabele, format 15,5x23 cm, 23.80 DM.

O apariţie inedită, care pune la îndemâna geologilor începători un excelent ghid, în care sunt prezentate toate "cheile" pentru înregistrarea completă şi sistematică a datelor oferite de teren. Sunt incluse numeroase sugestii pentru asigurarea unui echipament corespunzător, "unelte" elementare pentru determinări expeditive pe teren (plăcuţa de porţelan, un magnet, sticluţa cu acid, lupa etc.), scheme generale pentru recunoaşterea diverselor tipuri de roci şi pentru descrierea lor, sugestii pentru măsurarea elementelor tectonice, un tabel cu culorile mineralelor şi cu proprietăţile principale ale celor mai răspândite minerale, elemente esenţiale pentru recunoaşterea grupelor de organisme fosile, scara stratigrafică până la nivelul etajelor, un extrem de util îndreptar pentru evaluarea participării procentuale a componenţilor, modele de legendă pentru hărţi etc.

Pentru Germania (dar nu numai) sunt date adrese utile ale instituţiilor geologice. Nu lipseşte o bibliografie adecvată, un index de termeni şi, în final, modele pentru carnetele de teren, cu exemple de înregistrare a observaţiilor.

Pentru geologii cu experienţă, cartea d-lui Klein este un prilej de comparare a stilurilor proprii de achiziţionare a datelor de pe teren, iar pentru geologii începători - un model adecvat şi demn de preluat. Oricum, o asemenea carte, într-un format potrivit pentru teren, este recomandată oricărui geolog "boboc" pentru maximizarea observaţiilor de teren.

CHRISTOPH HEBESTREIT – Wutach und Feldberg region. Ein geologischer Führer (Regiunea Wutach şi Feldberg. Un ghid geologic).

Editura F. Enke prin Georg Thieme Verlag, Stuttgart - New York, 1999, 136 p., 44 fig. (inclusiv fotografii), format 12x19 cm, 29.90 DM.

Partea de sud a masivului Pădurea Neagră (Schwarzwald) conţine formaţiuni geologice de vârste extrem de diferite, acoperind intervale de timp de la Paleozoic la Cuaternar. Acest motiv prilejuieşte autorului o prezentare succesivă a caracteristicilor perioadelor geologice care pot fi examinate în aceasta zonă. Sunt localizate exact locurile cel mai bine reprezentate pentru principalele entităţi cronostratigrafice care sunt ilustrate prin schiţe şi secţiuni geologice, fotografii şi bloc diagrame. În egală măsură interesantă pentru specialişti şi amatori, cartea oferă o informare completă asupra geologiei zonelor Wutach şi Feldberg, după principiul unui ghid geologic elaborat de un cunoscător al regiunii. Adrese utile, "de sprijin" pentru vizitatori, precum şi un glosar de termeni, adresat în special amatorilor, completează în mod fericit această "interfaţă" între o lucrare de specialitate şi una de popularizare. Stilul prietenos al textului uşurează accesul spre tărâmul încă puţin explorat al celor care vor să ştie mai mult despre trecutul Pământului.

Prof. Dr. Gheorghe Udubaşa
Institutul Geologic al României

Rom. J. Mineralogy, vol. 79, p. 210, Bucureşti, 1999

OANA PETREUŞ, ION PETREUŞ – Materiale compozite
Editura Gh. Asachi, Iaşi, 1999, 183 p.

Colaborarea dintre un chimist (O.P.) şi un mineralog (I.P.) a produs un unicat, perfect miscibilizat. Unicat din punctul de vedere al noutăţii pe piaţa românească a cărţii, unicat prin omogenizarea limbajului chimic şi al ştiinţei materialelor, cartea oferă cititorului interesat o introducere elegantă în încă prea puţin cunoscuta lume a materialelor avansate.

Interesul pentru materialele compozite (MC) rezidă atât în performanţele lor, care depăşesc deseori materialele clasice, monocomponente sau monofazice, cât şi în faptul că uneori ele sunt mai ieftine decât cele clasice. Realizarea acestor materiale implică un efort deosebit de inovare, un "consum" ridicat de inteligenţă, în scopul de a reuni componente relativ banale şi cu proprietăţi modeste în materiale noi, cu rezistenţă nebănuită, utilizabile în ramuri industriale care implică deseori condiţii extreme (de temperatură, presiune, frecare etc.).

Pornind de la exemplul cel mai banal (şi probabil cel mai vechi ?) de material compozit, chirpiciul, (matrice argiloasă şi fire de paie), autorii prezintă diferitele tipuri de materiale compozite moderne, relativ numeroase, cu domeniile lor de utilizare.

După definiţii ("combinarea inteligentă a două materiale distincte cu proprietăţi mai bune decât materialele iniţiale în parte") şi clasificări (MC cu particule, cu fibre, cu structuri/lamele), sunt prezentate cele mai importante compozite, în care atât matricea, cât şi "armătura" (ranfortul) sunt variabile.

Textul lucrării este foarte condensat, astfel că, în loc de un rezumat, am optat pentru enumerarea materialelor compozite descrise de autori: compozite cu matrice metalică ranforsată cu fibre (de bor, de grafit, de carbură de siliciu etc.), compozite cu matrice ceramică (cu fibre de carbon, cu whiskeri de SiC etc.), compozite cu matrice de carbon ranforsată cu fibre, compozite cu matrice polimerică ranforsată cu fibre, compozite hibride etc. Urmează o introducere în tehnologiile de fabricaţie (difuzie, pulberi, de turnare, fabricaţie "in situ"), prezentarea proprietăţilor MC cu fibre, utilizările acestora, compozitele laminare, MC structurale naturale, compozitele ortopedice etc.

Spre încheiere sunt amintite domeniile de perpectivă în domeniul MC ortopedice (cu fibre de carbon acoperite cu material bioceramic în matrice polimerică; matrici polimere biodegradabile, ranforsate cu fibre de hidroxiapatit), calitatea esenţială a multor MC şi anume aceea de a fi biodegradabile şi, în final, necesitatea cooperării între specialişti, care să-şi dezvolte "o nouă structură de gândire".

Cartea ar trebui să fie prezentă practic în orice bibliotecă (din păcate tirajul n-a putut fi decât la nivel... provocativ, suportat de autori), fiind probabil necesar ca în curând să apară o nouă ediţie.

* * *

Deşi reprezintă un domeniu colateral al preocupărilor mele, aş recomanda călduros şi cartea "Materiale polimerice" de Oana Petreuş, apărută în acelaşi an la Editura Cermi din Iaşi, 293 p., în care una dintre componentele importante ale materialelor compozite, polimerii, este prezentată în detaliu. Această carte aduce un supliment de informaţii faţă de prima lucrare, bine venit pentru cei interesaţi de ambele domenii.

Prof. dr. **G. Udubaşa**
M.c. al Academiei Române

Rom. J. Mineralogy, vol. 79, p. 211, Bucureşti, 1999

R. P. C. MORGAN – Eroziunea şi conservarea solului (Bodenerosion und Bodenerhaltung). Enke/Georg Thieme, Stuttgart, 236 p., 61 fig., 45 tabele. Apărută 1999. Preţ: Euro 50.62.

După două cărţi de bază în domeniul pedologiei (Chimia solului / Bodenchemie de G. Sposito şi Tratat de Pedologie de Scheffer / Schachtschebel, ambele publicate in 1998) editura Georg Thieme din grupul Enke continuă seria cărţilor care tratează solul, de această dată cu o carte care întruneste două aspecte aparent contradictorii, eroziunea şi conservarea solului ! "Ofensiva pedologică" a editurii G. Thieme este binevenită, întrucât solul, ca şi apa, este un element esenţial pentru menţinerea vieţii la un nivel acceptabil.

Cartea prof. Morgan, de la colegiul Silsoe al Universităţii Cranfield, Bedford, Anglia, în traducerea a doi specialişti germani, H. H. Becher şi Susanne Witt, este un tratat cuprinzător, care se adresează, în egală măsură pedologilor, geologilor, inginerilor de mediu, celor care se ocupă de utilizarea terenurilor. Un text cu mare densitate de informaţii, cu o bibliografie iniţială de cca 30 pagini, la care se adaugă literatura germană în domeniu, suplimentată de traducători şi un index de subiecte abordate în cuprinsul cărţii. Toate acestea recomandă cu căldură această apariţie editorială tuturor celor care, direct sau indirect, se ocupă de sol, "atacă" sau conservă solul, fac planificări strategice sau tactice privind producţia agricolă, extinderea diverselor construcţii etc.

Structura cărţii cuprinde 11 capitole, prezentate într-o ordine logică, în felul următor:

1. Răspândirea fenomenelor de eroziune a solului;
2. Procesele şi mecanismele de eroziune (bazele hidrologice, eroziunea propriu-zisă produsă de factori diverşi, de la torenţi la vânt);
3. Factorii care influenţează eroziunea (inclusiv rolul păturii vegetale);
4. Evaluarea riscurilor de eroziune;
5. Modelarea eroziunii (modele, validarea acestora, selectarea unui model acceptabil/previzibil);
6. Măsurarea eroziunii solului (pe teren şi în laborator);
7. Strategii pentru controlul eroziunii (toleranţa de pierdere a solului, principii de conservare şi planificare a acesteia);
8. Metode de stabilizare a solurilor;
9. Valorificarea/utilizarea solurilor;
10. Procedee tehnice de control al eroziunii;
11. Punerea în aplicare a acestora (elemente socio-economice, condiţii politice locale, organisme responsabile, cadrul juridic de aplicare etc.).

Numeroase tabele, schiţe, diagrame, modele matematice de evaluare a eroziunii, hărţi exemplificative privind modalitatea de cartare a proceselor de eroziune etc. completează textul saturat de informaţii. Un avantaj evident al acestei cărţi este oferit de acoperirea globală a proceselor erozionale, diferenţiate în funcţie de condiţiile fizico-geografice, de existenţa unor organisme locale sau regionale de studiu, supraveghere şi aplicare a unor metode de stopare sau diminuare a eroziunii solului. Exemplele date sunt din toată lumea.

În final, o carte necesară oricărei instituţii de profil, de la ştiinţe naturale la ingineria mediului, de la lucrări publice la agricultură.

Prof. dr. **G. Ududbaşa**
M.c. al Academiei Române

Rom. J. Mineralogy, vol. 79, p. 212, Bucureşti, 1999

O. WAGENBRETH – Istoria Geologiei în Germania (Geschichte der Geologie in Deutschland). Enke im Georg Thieme Verlag, Stuttgart, 264 p., 123 figuri, 1999, Preţ: DM 128.

Cartea prof. Wagenbreth de la Universitatea Tehnică a Academiei de Mine din Freiberg, Germania, se situează la graniţa dintre geologie şi istorie, fiind la fel de interesantă atât pentru geologi, cât şi pentru istorici.

Structurată în 5 capitole, cartea începe cu un interesant demers (Cap. 1, Introducere) privind definirea ştiinţei şi a legilor evoluţiei, situaţia geologiei, în general, şi în Germania şi influenţa complexităţii geologice asupra dezvoltării Ştiinţelor Pământului, exemplificate de Germania, în special prin Saxonia şi, mai ales, prin Munţii Metaliferi ai Saxoniei.

Cap. 2. "Preistoria geologiei ca ştiinţă" cuprinde informaţii asupra concepţiilor din antichitate şi Evul Mediu asupra dezvoltării ştiinţelor naturii, rolul perioadelor Renaşterii (evidenţiindu-se G. Agricola, considerat părintele mineralogiei moderne) şi Iluminismul (N. Steno, A. Kircher) în crearea fundamentelor geologiei moderne.

Cap. 3. "Formarea Geologiei ca Ştiinţă" numeşte pe J. Hutton (Scoţia) şi A. G. Werner (Germania) ca fondatori ai geologiei, deşi împărtăşeau concepţii opuse privind originea rocilor (plutonist şi neptunist). Interesante sunt datele privind preocupările lui Goethe în geologie (şi fizică, mai ales optică) şi moştenirea ştiinţifică lăsată de Werner numeroaselor sale generaţii de studenţi la faimoasa Academie de Mine din Freiberg.

Cap. 4. "Geologia ca ştiinţă naturală clasică a secolului al XIX-lea în Germania" se extinde pe aproape 100 de pagini şi cuprinde toate contribuţiile germane la dezvoltarea geologiei. Sunt menţionate universitaţile germane în care ştiinţele geologice erau deja diferenţiate, personalităţile cu realizări deosebite (L.V. Buch, E. Suess, C.F. von Gümbel, F. Zirkel, H. Rosenbrusch, B.V. Cotta, C. Ochseuins etc.), devenite clasici ai geologiei în general.

Cap. 5. "Geologia în Germania în secolul al XX-lea" cuprinde realizări germane în diversele domenii ale geologiei, instituţiile proeminente şi profesorii acestora, asociaţiile profesionale şi revistele de specialitate. H. Stille, A. Wegener, H. Cloos, P. Ramdohr sunt câţiva titani ai geologiei mondiale din acest secol, ale căror lucrări constituie încă pietre de hotar în gândirea geologică actuală.

Un index util de persoane şi unul de subiecte încheie această carte, incitantă, care ar trebui să fie tradusă şi în alte limbi, pentru ca rolul geologiei germane şi al geologilor germani să fie mai bine cunoscut.

Prof. Dr. **G. Ududbaşa**
M.c. al Academiei Române

Rom. J. Mineralogy, vol. 79, p. 213–214, Bucureşti, 1999

JACQUES-MARIE BARDINTZEFF: Vulcanologie (Vulkanologie).
Traducere în limba germană de Sven Lewerenz. Enke/Georg Thieme, Stuttgart, 1999, 280 p., 150 fig.

Autorul "Vulcanologiei", Jacques-Marie Bardintzeff, Profesor la Universitatea Paris-Sud, este o figură binecunoscută în toată lumea vulcanologilor contemporani, neobosit globe-trotter în căutarea "evenimentelor" vulcanice fierbinţi, oriunde s-ar desfăşura acestea, nelipsit de la majoritatea manifestărilor ştiinţifice din domeniu, unul dintre cei mai buni cunoscători ai fenomenului vulcanic. Cercetător dedicat şi cu rezultate notabile, recunoscute pe plan internaţional, este în aceeaşi măsură şi un redutabil "popularizator" al ştiinţei vulcanologiei, autor al aproximativ unei duzine de cărţi despre vulcani.

Cartea de faţă, scrisă într-un stil sobru, accesibil în acelaşi timp, se adresează unui cerc larg de specialişti, geologi şi geofizicieni, nu neapărat vulcanologi, reprezentând o excelentă Introducere în Vulcanologia zilelor noastre. In cele 280 de pagini ale sale, cartea oferă cititorului, fie el om al catedrei, student, cercetător sau geolog dedicat aplicaţiilor practice, o imagine clară şi comprehensivă, la nivelul cercetărilor zilei, asupra ştiinţei interdisciplinare a vulcanologiei. Ilustraţia bogată (peste 50 de fotografii, marea lor majoritate color şi executate de autor) conferă cărţii o valoare suplimentară.

Vulcanologia Profesorului Bardintzeff este structurată în trei părţi (cu 16 capitole în total), dintre care prima ("De la manta la camera magmatică") reprezintă introducerea absolut necesară pentru înţelegerea fenomenului vulcanic. Ea se referă la procesele premergătoare erupţiilor vulcanice, ce au loc în manta şi crustă, de la formarea magmelor prin topirea parţială a fenomenelor binecunoscute de cristalizare fracţionată, contaminare şi amestec de magme. Se accentuează, pe bună dreptate, rolul apei şi al fluidelor din magmă, factor esenţial în determinarea explozivităţii, respectiv, a stilului erupţiilor vulcanice.

Cu partea a două a cărţii ("ajungerea magmei la suprafaţă şi tipurile de erupţie") se ajunge, de fapt, în domeniul propriu-zis al vulcanologiei. Renunţând la nomenclatura greoaie şi oarecum subiectivă a tipurilor de erupţie practicată în deceniile trecute, mai ales în urma lucrărilor lui Rittman şi Tazieff (tipul hawaiian, strombolian etc.), autorul preferă o prezentare după criterii fenomenologice a activităţii eruptive a vulcanilor în următoarea ordine: erupţii de lavă (curgeri de lavă, lacuri de lavă, domuri de lavă şi intruziuni), căderi piroclastice (cu digresiuni utile privind morfologia conurilor vulcanice, craterele şi calderele), curgeri piroclastice (incluzând şi fenomenul de val piroclastic, pe lângă procesele de tip "nuée ardente" şi erupţiile de ignimbrite), hidrovulcanismul (interacţiunea dintre magmă şi apă în mediu terestru) şi vulcanismul submarin. În mod surprinzător, procese secundare în raport cu erupţiile vulcanice, cum sunt laharurile, sunt tratate în subcapitolul "Curgeri piroclastice", în timp ce alte procese secundare, cum sunt de pildă avalanşele de debrite, nu sunt prezentate defel în capitolele referitoare la fenomenologia vulcanică. Procesele eruptive abordate sunt tratate succint cu accent pe relevarea aspectelor esenţiale în înţelegerea fenomenelor respective. Ultimele două capitole ale părţii a doua a cărţii se referă, pe scurt, la produsele activităţii vulcanice şi la contextul geodinamic al vulcanismului, capitol care, în majoritatea manualelor de vulcanologie îşi găseşte locul privilegiat la începutul tratatelor sau, concluziv, la sfârşitul lor.

Cea de-a treia parte a Vulcanologiei, intitulată "Vulcanii şi omul" se ocupă, în principal, cu cele două laturi ale prezenţei vulcanilor în mediul ambiant al omului, (1) permanenta ameninţare a vulcanilor activi asupra comunităţilor umane ce trăiesc în apropierea lor, tipurile de hazard vulcanic şi tehnicile de evaluare a riscului, şi (2) latura benefică a relaţiei vulcan-om (vulcanii ca resursă de energie şi vulcanii ca resursă de prosperitate, recreere şi agrement). Anul 1979 a intrat în analele vulcanologiei ca un exemplu de nereuşită în "managementul" unei crize vulcanice majore, şi pe care autorul l-a trăit, de altfel, din plin, pe propria sa piele în calitate de membru al echipei de supraveghere a vulcanului. Adresându-se cititorului de limbă germană, traducerea Vulcanologiei de Jacques-Marie Bardintzeff se încheie cu un scurt capitol în care se prezintă, în doar câteva pagini, vulcanismul alcalin intracontinental de tip monogenetic de vârstă Pleistocenă din Germania (zonele Eifel, Vogelsberg şi Kaiserstuhl), al cărui studiu a stat în decursul mai multor secole, la originea unor progrese remarcabile ale vulcanologiei moderne.

Cartea Profesorului Bardintzeff se înscrie meritoriu, prin originalitatea abordării, caracterul deosebit de clar şi didactic al prezentării şi calitatea deosebită a ilustraţiei, originală şi ea în cea mai mare parte, pe lista tratatelor de vulcanologie modernă care au văzut lumina tiparului în ultimul deceniu al mileniului al 2-lea, şi, nu în ultimul rand, pe lista tot mai lungă şi mai prestigioasă a lucrărilor autorului însuşi. Am sublinia faptul că pe piaţa cărţii de vulcanologie, dominată covârşitor în ultimii ani de autorii anglo-americani, apariţia tratatelor de vulcanologie în limba franceză ale lui Jacques-Marie Bardintzeff, şi a traducerilor acestora în limba germană, vine în întâmpinarea unei nevoi reale a comunităţilor ştiinţifice şi universitare în multe ţări ale lumii. Traducerea în limba română a cărţii, alături de alte tratate de vulcanologie din literatura engleză, cu abordare diferită a tematicii, ar fi binevenită.

Alexandru Szakàcs, Gheorghe Udubaşa

INSTRUCTIONS TO AUTHORS

ROMANIAN JOURNAL OF MINERALOGY publishes original scientific contributions dealing with any subject of this field.

Only papers presenting concisely and clearly new information will be accepted. The manuscript will be submitted for critical lecture to one or several advisers. Papers will be definitely rejected after a second unsatisfactory revision by the authors. The manuscripts will not be returned to the authors even if rejected.

Manuscripts are prefered in English or French. Manuscripts submitted in Romanian will be accompanied by an abstract in English or French (maximum 10 per cent of the manuscript volume).

Papers should be submitted on diskette and typed text in duplicate to the secretary of the Editorial Board, including the reproduction ready original figures. The manuscript should comprise: text (with a title page which is the first page of it), references, key words, abstract, illustrations, captions and a summary for technical purposes.

Author(s) should add a separate sheet with a short title (colontitle) of maximum 60 strokes and a summary indicating the hierarchy of headings from the text listed in decimal classification (1; 1.1; 1.1.1) but not exceeding four categories.

Text should be on diskette, format ASCII and 2 copies, holding an empty place of 3 cm on the left side of the page. The text cannot exceed 10 typewritten pages (including references and figures).

Front page (first page of the text) should comprise: a) title of the paper (concise but informative) with an empty space of 8 cm above it; b) full name(s) of the author(s); c) institution(s) and address(es) for each author or group of authors; d) text.

Footnotes should be numbered consequtively.

Citations in the text should include the name of the author and the publication year. Example: Ionescu (1970) or (Ionescu, 1970). For two authors: Ionescu, Popescu (1969) or (Ionescu, Popescu, 1969). For more than two authors: Ionescu et al. (1980) or (Ionescu et al., 1980). For papers which are in course of print the publication year will be replaced by "in press". Unpublished papers or reports will be cited in the text like the published ones.

Abstract, of maximum 20 lines (on separate sheet), must be in English, summarizing the main results and conclusions (not a simple listing of topics).

Key words (max. 10 items), in English or French, following the language used in the text (or the Resumé if the text is in Romanian), given in succession from general to specific, should be typed on the abstract page.

References should be typed in double-line spacing, listed in alphabetical order and chronological order for authors with more than one reference. Abbreviations of journals or publishing houses should be in accordance with the recommendations of the respective publications or with the international practice.

Examples:

a) journals:

Giuşcă, D. (1952) Contributions à l'étude cristallochimique des niobates. *An. Com. Geol.*, XXIII, p. 259–268, Bucureşti.

– , Pavelescu, L. (1954) Contribuţii la studiul mineralogic al zăcămîntului de la Muşca. *Comm. Acad. Rom.*, IV, 11–12, p. 658–991, Bucureşti.

b) special issues:

Strand, T. (1972) The Norwegian Caledonides. p. 1–20. In: Kulling, O., Strand, T. (eds.) Scandinavian Caledonides, 560 p., Interscience Publishers.

c) books:

Bălan, M. (1976) Zăcămintele manganifere de la Iacobeni. Ed. Acad. Rom., 132 p., Bucureşti.

d) maps:

Ionescu, I., Popescu, P., Georgescu, G. (1990) Geological Map of Romania, scale 1:50,000, sheet Cîmpulung. Inst. Geol. Geofiz., Bucureşti.

e) unpublished papers or reports:

Dumitrescu, D., Ionescu, I., Moldoveanu, M. (1987) Report. Arch. Inst. Geol. Geofiz., Bucureşti.

Papers or books published in Russian, Bulgarian or Serbian etc. should be mentioned in the references transliterating the name and titles. Example:

Krasheninnikov, V. A., Basov, I. A. (1968) Stratigrafiya kainozoia. Trudy GIN, 410, 208 p., Nauka, Moskow.

Illustrations (figures and plates) must be numbered and submitted as originals on separate sheets (tracing papers), ready for reproduction. The thickness of the lines, lettering and symbols on figures should be large enough to be easily read after size-reduction. The original size should not extend beyond the print area of the page: column width 8 cm, page width 16.5 cm, page length 23 cm for figures; the width of line drawings should not extend over a single (16.5/23) or double (23/33 cm) page area and must be selfexplanatory (including title, authors, legend etc.). The graphic scale is obligatory.

Photographic illustrations (black-and-white only) must be of high quality and should be grouped into plates 16/23 cm in size. Each plate should have the photos numbered, i.e. Pl. I, Fig. 1; Pl. II, Fig. 1.

Tables should be numbered and entitled. Original size of the tables should correspond to the above mentioned (8/16.5 or 16.5/23) dimensions of the printing area.

Author(s) will receive only one set of preprint proofs which must be returned, with corrections, 10 days after receiving them. Only printing errors should be corrected, no changes in the text can be accepted.

Thirty offprints of each paper are supplied to the author(s) free of charge.

Editorial Board

Editat cu sprijinul Agenţiei Naţionale pentru Ştiinţă, Tehnologie şi Inovare – Colegiul Consultativ pentru Cercetare Ştiinţifică şi Dezvoltare Tehnologică

Edited with the support of the National Agency for Science, Tehnology and Innovation – Advisory Board for Scientific Research and Technologic Development

Translation and language review by:
Adriana Năstase, Mariana Borcoş

Editorial Staff:
Gabriela Ioane, Petruţa Cuciureanu

Illustration:
Paraschiv Toader

Printing:
G. Bădulescu, D. Gavril, N. Păleanu, S. Iacoblovici, F. Dumitru

(Contents continued from front cover)